FACULDADE DE ENGENHARIA DA UNIVERSIDADE DO PORTO

Performance-Based Seismic Design and Assessment of Steel Moment Frame Buildings

Luís Augusto Ferreira Rodrigues de Macedo

Doctoral Program in Civil Engineering

Supervisor: Dr José Miguel de Freitas Castro

January 24, 2017

Performance-Based Seismic Design and Assessment of Steel Moment Frame Buildings

Luís Augusto Ferreira Rodrigues de Macedo

Doctoral Program in Civil Engineering

Thesis Examining Committee :

President: **Dr Rui Artur Bártolo Calçada** (by delegation of the Dean of the University of Porto), Full Professor at the Civil Engineering Department of the Faculty of Engineering of the University of Porto, Porto, Portugal.

Examiner: **Dr Mario D'Aniello**, Assistant Professor at the University of Naples "Federico II", Naples, Italy.

Examiner: **Dr Carlos Alberto da Silva Rebelo**, Associate Professor at the Civil Engineering Department of the Faculty of Science and Technology of the University of Coimbra, Coimbra, Portugal.

Examiner: **Dr João Paulo Sousa Costa de Miranda Guedes**, Assistant Professor at the Civil Engineering Department of the Faculty of Engineering of the University of Porto, Porto, Portugal.

Examiner: **Dr Xavier das Neves Romão**, Assistant Professor at the Civil Engineering Department of the Faculty of Engineering of the University of Porto, Porto, Portugal.

Supervisor: **Dr José Miguel de Freitas Castro**, Assistant Professor at the Civil Engineering Department of the Faculty of Engineering of the University of Porto, Porto, Portugal.

January 24, 2017

Abstract

The main objective of the research documented in this thesis is to contribute to a better understanding of the behaviour and performance of steel moment-resisting frames designed according to the current version of Eurocode 8 (EC8), the European seismic code. To this end, the existing design requirements of Part 1 of Eurocode 8 are applied to an extensive number of building archetypes, both highlighting the difficulties associated with their design process and also potential improvements that can either suppress or minimise those difficulties. Most notably, a more rational and consistent definition of the adopted behaviour factor for the design to EC8, according to the so-called Improved Force-Based Design (IFBD) methodology, as well as a more efficient criterion for the design of panel zones, are thoroughly detailed and validated.

The seismic performance of the archetypes is assessed through advanced nonlinear structural analysis considering current code-defined performance levels. Several contributions are made, namely regarding the numerical consideration of hysteretic strength and stiffness deterioration of European open-section steel profiles, the design of the panel zone, and, finally, the selection and scaling of representative ground motion records. In particular, a comprehensive definition of a novel and fully integrated frameworks is shown, namely for: i) the calibration of hysteretic models that consider both stiffness and strength deterioration, based on the actual structural response of steel members, obtained whether from experimental testing or from detailed finite element models, and ii) the optimized selection and scaling of ground motion records for code-based and probabilistic-based seismic performance assessments.

The FEMA P695 methodology is adopted in order to define the archetypes considered in this research study, as well as to provide the basis for a reliable evaluation of the seismic performance factors of steel MRFs designed according to the requirements of EC8 and the IFBD methodology. Furthermore, the fully probabilistic Performance-Based Earthquake Engineering (PBEE) framework proposed by the Pacific Earthquake Engineering Research (PEER) Center is implemented and applied to compute the expected economic

losses (and their disaggregation) of the buildings considered within this research study. Moreover, the economic losses are also evaluated for the design seismic intensity levels, thus allowing for the characterization of the performance of code-designed steel buildings with improved seismic performance metrics, a valuable input for stakeholders. Important contributions to the design and numerical modelling of steel MRFs, as well as to the reliable selection of ground-motion records, are made.

The findings contained within the various parts of this research work allow for an improved understanding of the current design approach of EC8 for steel MRFs and corresponding influence on building seismic performance and associated safety levels. Most notably, the results obtained allow extracting the following conclusions: i) steel MRFs designed to EC8 exhibit a seismic performance, which, in many cases, is not fully consistent with the design assumptions, particularly in terms of the target ductility levels, ii) the application of the IFBD methodology to the seismic design of steel MRFs can result in relevant material savings with no significant detriment on the seismic performance, and iii) steel MRFs designed according to EC8 comply with the no-collapse performance requirement defined in the European code, however, the considerable level of losses observed may prove to be unacceptable.

Resumo

Esta dissertação tem como objetivo principal contribuir para uma melhor compreensão do comportamento e desempenho sísmico de pórticos metálicos simples (ligações rígidas) dimensionados de acordo com a versão atual do Eurocódigo 8, a norma Europeia aplicável ao dimensionamento sísmico de estruturas. Deste modo, os requisitos atuais de dimensionamento da Parte 1 do Eurocódigo 8 (EC8) são aplicados a um conjunto abrangente de arquétipos estruturais, evidenciando não só as dificuldades associadas ao processo de dimensionamento, como também identificando potenciais aspetos passíveis de melhoria da norma tendo em vista a minimização dessas dificuldades. Em particular, uma definição mais racional e consistente do coeficiente de comportamento adotado durante o processo de dimensionamento de acordo com o EC8, seguindo a metodologia *Improved Force-Based Design* (IFBD), assim como um critério mais eficaz para o dimensionamento do painel da alma, são detalhados e validados.

O desempenho sísmico dos arquétipos é avaliado para os níveis de desempenho propostos pelo Eurocódigo 8 com recurso a análises não-lineares. Neste contexto, são efetuadas várias contribuições, nomeadamente no que diz respeito i) à definição dos parâmetros de deterioração cíclica de resistência e rigidez nos modelos histeréticos de plasticidade concentrada utilizados na simulação de perfis Europeus de secção aberta, ii) ao dimensionamento do painel da alma, e iii) à seleção de grupos de acelerogramas reais consistentes com a sismicidade da localização dos edifícios. Em particular, salienta-se a construção de duas ferramentas computacionais que permitem: i) a calibração otimizada de modelos histeréticos com a inclusão de efeitos de deterioração de resistência e de rigidez, recorrendo a resultados provenientes de ensaios experimentais ou de modelos avançados de elementos finitos, e ii) a seleção e escalamento otimizado de acelerogramas reais para avaliação do desempenho sísmico em contexto regulamentar ou probabilístico.

A metodologia proposta no documento FEMA P695 é utilizada na definição dos arquétipos considerados neste estudo, assim como na avaliação dos parâmetros de desempenho e resposta sísmica (coeficiente de comportamento e sobre-resistência), dimen-

sionados de acordo com o EC8 e com a metodologia IFBD. Finalmente, a metodologia probabilística *Performance-Based Earthquake Engineering* (PBEE), proposta pelo *Pacific Earthquake Engineering Research* (PEER) Center, é implementada e aplicada para calcular as perdas económicas expectáveis (e correspondente desagregação) nos edifícios considerados neste estudo. As perdas são avaliadas para níveis de intensidade sísmica consistentes com o dimensionamento, permitindo assim a caracterização do desempenho sísmico de acordo com métricas melhoradas, um contributo relevante para apoio à tomada de decisão.

As conclusões apresentadas nas diversas partes desta tese permitem uma melhor compreensão do dimensionamento sísmico de pórticos simples de acordo com o EC8 e correspondente influência no desempenho sísmico dos edifícios e níveis de segurança associados. Dos resultados obtidos salientam-se as seguintes conclusões: i) a aplicação do EC8 a pórticos metálicos simples conduz a soluções estruturais cujo desempenho sísmico não é totalmente consistente com os pressupostos de cálculo, nomeadamente no que diz respeito ao nível de ductilidade imposto à estrutura pelo sismo de dimensionamento, ii) a aplicação da metodologia IFBD no processo de dimensionamento pode conduzir a poupanças relevantes de material, sem que com isso se verifique uma redução significativa do desempenho sísmico das estruturas, e iii) pórticos metálicos simples dimensionados de acordo com o EC8 cumprem com os critérios de limitação de dano e de não-colapso, no entanto apresentam níveis de perdas expectáveis que podem revelar-se inaceitáveis.

Acknowledgements

The completion of this thesis would not have been possible without the help and friendship of several people. Therefore, I would like to express my sincere gratitude to those who have contributed, in any way, to this achievement.

Firstly, I would like to express my sincere gratitude to my supervisor, Prof. Miguel Castro, for his unconditional support and friendship. The long and vibrant talks, always with a unique enthusiasm and an enormous willingness to speak about science and life.

Special thanks to Prof. Mota Freitas, for the words of encouragement and persuading me to conduct the PhD.

I would like to thank to Prof. Rui Pinho for the opportunity of attending several courses at ROSE School.

I would also like to thank to Prof. László Gergely Vigh and Dr. Adam Zsarnoczay for the research opportunity in Budapeste.

I also thank the Portuguese Foundation for Science and Technology for supporting this research through the PhD grant SFRH/BD/60796/2009.

To Prof. Xavier Romão and Prof. João Paulo Miranda Guedes for their friendship.

I would also like to thank to Prof. Fernando Ferreira, Prof. Armando Vilaça and Prof. Jorge Justo for theirs support and encouragement.

A special thanks to Nuno Pereira and António Silva, for their friendship and help. Their opinions, encouragement and optimism were fundamental during this journey.

To my friends Joana Delgado, João Sousa Dias, Nuno Gonçalves, Bruno Pereira, Gonçalo Bagulho, José Barros and to so many other that in one way or the other, contributed for the successful completion of my studies.

To my colleagues: Alexandre Costa, Andreia Meixedo, André Monteiro, Bruno Quelhas, Cristiana Bonifácio, Jiang Yadong, João Rocha, Joel Malveiro, Mário Marques, Miguel Araújo, Miriam López, Ricardo Monteiro, Rui Barros and Sérgio Neves.

To my parents-in-law for their support. To my nephews, specially to Bia for her drawings.

To my grandparents, for all the love and role model. They know how much I love them.

Last but not least, to my parents and Ana, to whom I dedicate this thesis. My parents for all their love and unconditional support. To my wife Ana for her dedication and love. Her contagious happiness, her kindness, willpower, patience and encouragement were fundamental to the success of this PhD journey.

January 24th, 2017

Luís Macedo

"O valor das coisas não está no tempo que elas duram,
mas na intensidade com que acontecem.
Por isso, existem momentos inesquecíveis,
coisas inexplicáveis e pessoas incomparáveis."

Fernando Pessoa

Contents

List of Figures

List of Tables

Chapter 1

Introduction

1.1 Motivation

The devastating effect of natural disasters has become increasingly noticeable over the past decades. The socio-economic effects of such events are significant and may take decades to overcome. Figure 1.1 shows the losses due to natural disasters since the beginning of the last century. As one may infer from the data shown, a significant escalation of the amount of losses was observed since the 80's. Whilst numerous reasons may justify this trend, it is consensual that some circumstances play a decisive role (Guin and Saxena, 2000): i) the increase of the population density in already highly populated cities located in areas of high hazard, ii) the increase of the standards of living, with the corresponding increase of property values and infrastructures, and iii) the lack of adequate preparedness and resilience to deal with the consequences of disasters.

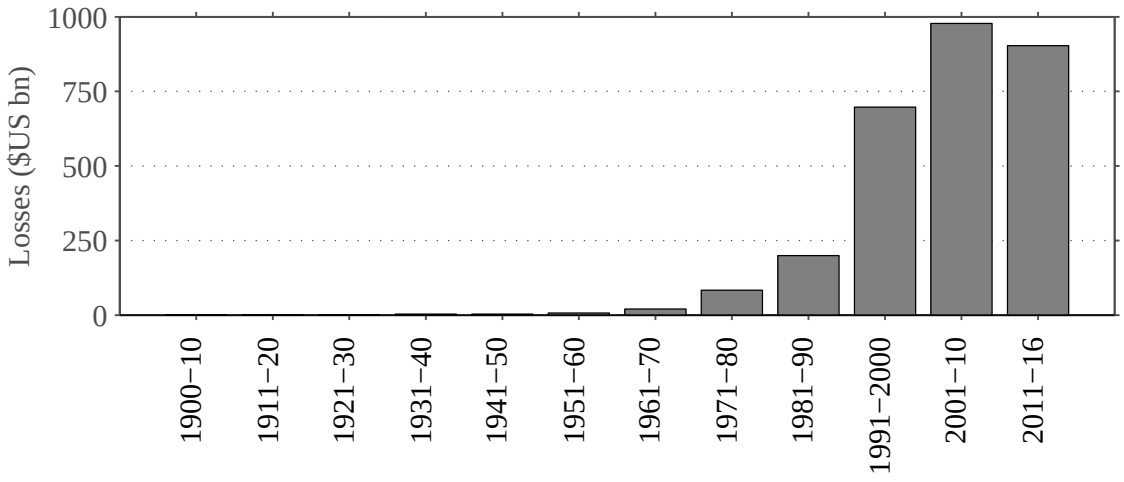

Figure 1.1: Losses due to natural disasters from 1900-2016 (source: http://www.emdat.be/).

Among the typologies of natural disasters, earthquakes are, perhaps, one of the most destructive, with significant economic, environmental and cultural consequences. Figure 1.2 shows the groups of costliest and deadliest events worldwide in the last few decades.

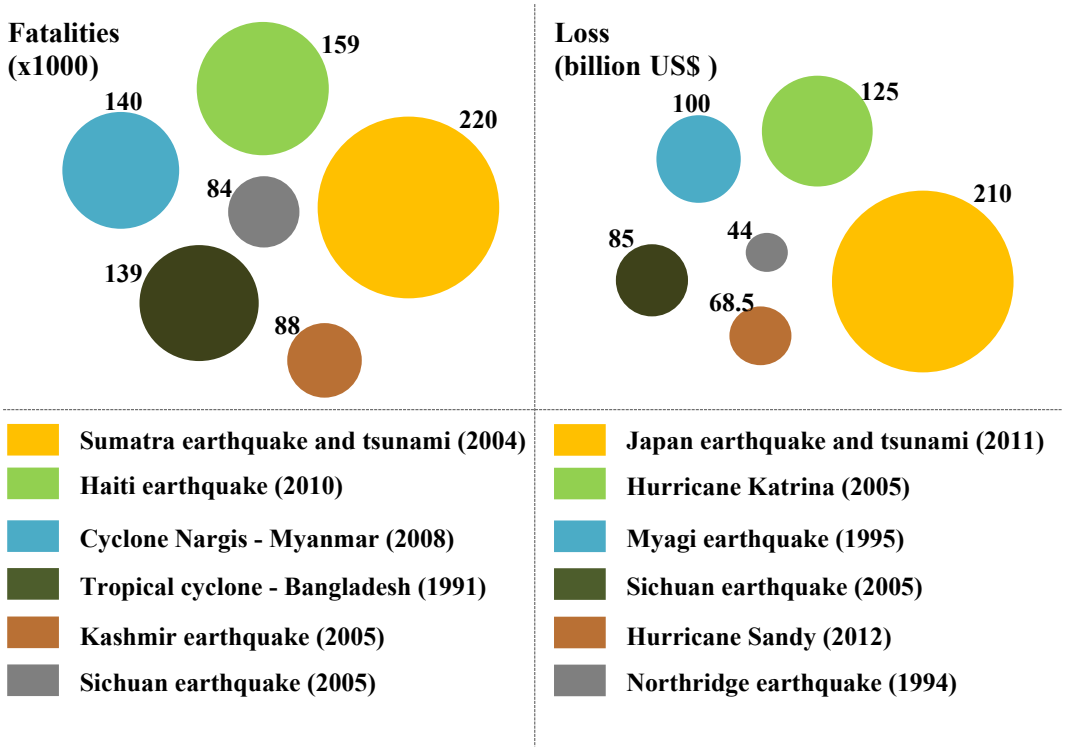

Figure 1.2: Losses due to natural disasters from 1900-2016 (source: http://www.emdat.be/).

As it can be concluded from Figure 1.2, earthquakes have, within the various types of natural disasters, a remarkable importance regarding the number of fatalities and immediate economic losses. Moreover, there seems to be no direct correlation between the events with the highest tolls to human life and to the economy, as no natural disaster is repeated in both of the groups shown in Figure 1.2. In fact, these two parameters are closely linked to the socio-economic characteristics and level of development of the affected areas. For example, the 2010 Haiti earthquake was responsible for a significant number of deaths that may be justified by the lack of adequate earthquake-resistant design practices, and also by the inadequate quality of the building stock (Romão, 2012; Miranda, 2014). Such large and densely populated urban areas in developing countries imposed an accelerated growth of buildings and infrastructures, that, generally, exhibited inappropriate levels of quality and safety. Moreover, the absence of preparedness to the challenges associated with post-earthquake scenarios in developing countries are also a vital issue concerning the number of fatalities observed. Regarding the earthquakes that caused significant amounts of economic losses (e.g. 2011 Tōhoku, Japan, 1995 Kobe, Japan, 1994 Northridge, USA, 2010 Chile, 2011 Christchurch, New Zealand), the losses were largely associated to business disruption. Although most of the structures behaved as expected, namely to what concerns the safeguarding of life-safety (as per the design requirements), the significant levels of damage (mainly in the non-structural elements) caused considerable repair times and, in several cases, uneconomical repair costs (Elwood et al., 2014). Consequently, normative design requirements existing at the time,

which mainly focused on the prevention of structural collapse, were called into question (Elwood et al., 2014; Boroschek et al., 2014). For example, during the 2010 Chile earthquake, a substantial number of hospitals (15), within a distance of 500 km to the epicentre, were required to stop operating due to significant non-structural damage (Boroschek et al., 2014).

Regarding earthquakes occurred in Europe, two recent seismic events exposed the significant consequences of this natural hazard. The 2009 L'Aquila Earthquake in Italy was responsible for 295 human fatalities, and direct economic losses of around US$2.5 billion. Field observations raised three issues that current code regulations do not address explicitly: i) near-source effects, ii) non-structural damage, and iii) repairability (Iervolino et al., 2014). Moreover, the 2012 Emilia Romagna earthquake, also in Italy, precipitated 24 human casualties and losses of US$15.8 billion, the latter mainly due to earthquake-induced downtime of facilities. Concerning Portugal, a recent study conducted by Aon Benfield (2012) regarding the seismic risk of the country, an estimated loss of €5.5 billion for a 1 in 250 years return period earthquake, and €13 billion for a 1 in 500 years return period event. The opportunity to observe the effects of earthquakes has continuously constituted, and still constitutes, a valuable source of information for the evolution of seismic design codes. In the examples and data presented before, a significant amount of the earthquake losses resulted from the inadequate behaviour of constructions. It is therefore consensual that modern seismic design codes should ensure that constructions exhibit controlled and adequate behaviour. It is from this perception that the concept of performance-based earthquake engineering emerges.

Over the last few decades, steel structures have become a robust alternative to traditional reinforced concrete solutions. The increasing consciousness regarding environmental sustainability, associated with better strength and ductility characteristics, as well as more rapid construction processes, highlighted the advantages of this structural solution, with attractive and adequate characteristics from a seismic resistant viewpoint (Castro, 2006; Elghazouli, 2009). It is, however, important to note that the use of ductile materials does not necessarily lead to ductile structures, and that reliable design requirements, that allow the exploitation of all the material's capacity, need to be defined. The damage levels observed in steel structures after the Northridge (USA, America, 1994, 6.7 Mw) and Kobe (Japan, Asia, 1995, 6.9 Mw) earthquakes triggered the development of research studies and experimental campaigns targeting the improvement of standards and recommendations for the seismic design of steel structures (Miller, 1998; Mahin, 1998; Nakashima et al., 1998; Kuwamura, 1998; Krawinkler and Al-Ali, 1996). In Europe, seismic design of steel structures has become an increasing research trend, particularly since the early 90's.

From the discussion made in the previous paragraphs, it becomes clear the importance of developing improved design rules, which allow for a reliable prediction of the performance of structures under seismic loads.

1.2 Research objectives and contributions

The main objective of this thesis is to contribute to a better understanding of the seismic behaviour and performance of current code-based designed steel moment-resisting frames, which can provide important guidance for a future revision of Eurocode 8 (EC8) (CEN, 2005c). Within this objective, the current design requirements defined by Eurocode 8 are applied to a large number of structural archetypes, highlighting the difficulties and discussing possible improvements to the code. The seismic performance of the structures are evaluated considering the current code defined performance levels and the fully probabilistic framework proposed by the Pacific Earthquake Engineering Research (PEER) Center (Porter, 2003), so-called Performance-Based Earthquake Engineering (PBEE). However, a fully consistent application of these performance evaluation techniques involves addressing two major requirements: i) an accurate numerical modelling strategy and ii) an accurate definition of the seismic input. Therefore, several contributions are presented in this thesis regarding the modelling incorporation of strength and stiffness deterioration of the European open-section steel profiles, the panel zone design and ground motion record selection.

The main objectives of this thesis can therefore be summarised as:

1. Critical analysis of the EC8 requirements for the seismic design of steel moment-resisting frames and assessment of the influence of adopting a more rational selection of the behaviour factor.
2. Calibration of the strength and stiffness deterioration parameters of the Ibarra et al. (2005) hysteretic model for European open-section steel profiles.
3. Comparison of the effectiveness of different seismic design criteria for panel zones, followed by the proposal and validation of a more efficient design criterion.
4. Development of a novel and fully integrated framework for ground motion record selection and scaling, that allows not only code-based ground motion record selection but also obtaining the Conditional Mean Spectrum (CMS) for the European territory.
5. Assessment of the influence of the behaviour factors on the collapse performance of steel moment-resisting frames using the methodology proposed in FEMA P695 (FEMA, 2009).
6. Evaluation of economic losses and its disaggregation in steel moment-resisting frames designed according to Eurocode 8.

1.3 Outline of the thesis

Although there is a main goal in the thesis, the chapters have been written in such a way that each one is devoted to a specific subject and can be read independently. Throughout each chapter, references to other chapters are made, if necessary. The thesis consists of eight chapters that are outlined in the following paragraphs (Figure 1.3).

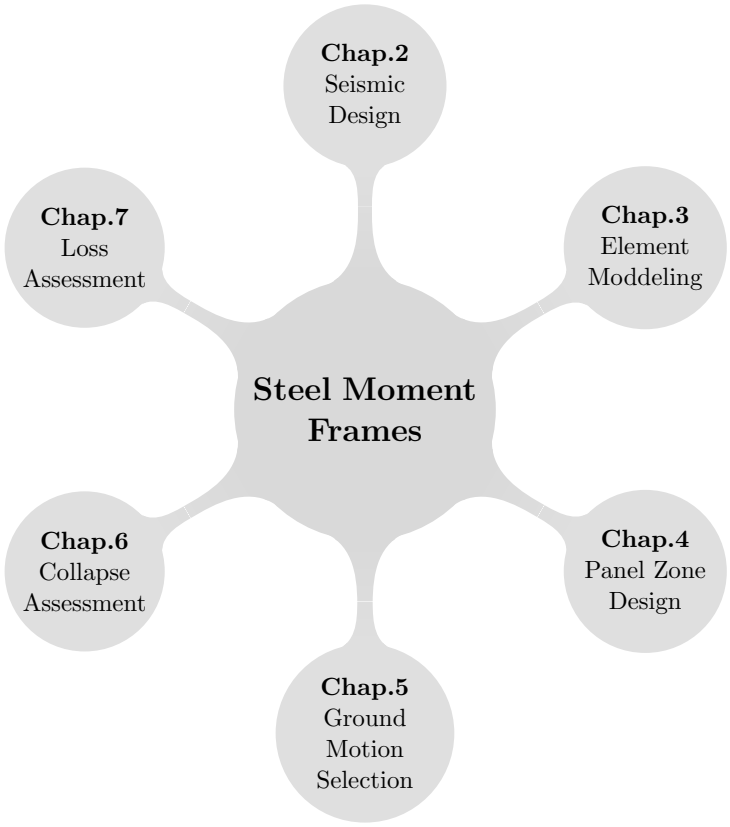

Figure 1.3: Outline of thesis.

Chapter 1 consists of an introductory presentation of the various topics addressed in this thesis, as well as the main objectives of the research.

Chapter 2 presents a general overview of the Eurocode 8 design provisions for steel moment-resisting frames (MRFs) and discusses the influence of a more rational selection of the behaviour factor in detriment of the use of code-prescribed values. To this end, a large number of steel MRFs are designed for three site locations. The seismic performance of the buildings is then evaluated through nonlinear static and response-history analyses, allowing to demonstrate the limitations and consequences of designing steel MRF buildings with the code-prescribed behaviour factors.

Chapter 3 provides an overview of the available nonlinear modelling techniques for steel members. A reliable seismic performance assessment of a steel building depends on the accuracy of the numerical models adopted and their ability to capture the expected level of degradation. Existing hysteretic models that incorporate strength and stiffness degradation of members, such as the one proposed by Ibarra et al. (2005), have taken a step further in providing more realistic collapse assessments of steel structures. A procedure employing optimisation algorithms is proposed for the calibration of strength and stiffness deterioration parameters of the Ibarra et al. (2005) hysteretic model using detailed FE results. The validation of the procedure is performed through the simulation of a full-scale test of a steel moment-resisting frame. Having established the calibration

methodology, the calibration of strength and stiffness deterioration parameters of the Ibarra et al. (2005) hysteretic model for European open-section steel profiles is performed.

Chapter 4 discusses the implications of adopting different criteria in the design of panel zones in steel MRFs. Panel zone design procedures differ mainly on the consideration of energy dissipation in this component. The European provisions are firstly reviewed and the inconsistencies between different parts of the Eurocodes is identified. The numerical modelling of the panel zone is validated against experimental results and several panel zone design criteria are then applied to the buildings designed in Chapter 2. Based on the European and American standards and guidelines, a new procedure is proposed and evaluated. The results demonstrate the advantages of its use.

Chapter 5 presents SelEQ, a novel and fully integrated framework for ground motion record selection and scaling. In addition to typical record selection procedures, SelEQ allows obtaining the Conditional Mean Spectrum (CMS) for the European territory, the latter making use of the open source platform OpenQuake and the recently proposed SHARE seismic hazard model. SelEQ incorporates a number of features that simplify preliminary record selection (e.g. disaggregation for a specific site) and allow advanced selection criteria (e.g. control of mismatch of individual ground motion records). The framework makes use of the Adaptive Harmony Search meta-heuristic optimisation algorithm in order to significantly minimise computational cost and analysis time, whilst still meeting the imposed selection constraints.

In Chapter 6 the performance factors used in the design of frames described in Chapter 2 are assessed using the methodology proposed in FEMA (2009). The methodology allows not only to evaluate if the adopted behaviour factor is adequate but also if it provides sufficient margins against collapse under maximum considered earthquake (MCE) ground motions. The seismic performance assessment of the structures is carried out through nonlinear static and response-history analyses, which allowed for the evaluation of the seismic performance factors.

In Chapter 7 the PEER-PBEE methodology, with the improvements proposed by Ramirez and Miranda (2012), is implemented and used to assess the expected economic losses of buildings designed in Chapter 2. The expected economic losses and corresponding disaggregation were assessed for the seismic intensity levels considered at the design stage, thus allowing for the characterisation of the performance with improved seismic-performance metrics that can help stakeholders and building owners. The expected annual losses (EAL) and expected present value (PV) of life-cycle losses are also computed for each buildings. The results obtained are then discussed and relevant conclusions are highlighted.

Finally, Chapter 8 presents a summary of the main conclusions and findings of the conducted research, alongside recommendations for future research on the topics addressed in this thesis.

In Appendix B a sensitivity study is conducted to evaluate the performance of several variants of the Harmony Search algorithm. A variance-based global sensitivity analysis of the algorithms is performed to assess the sensitivity of the algorithms regarding the choice of input parameters, and demonstrates the importance of the interaction between the algorithms parameters.

1.4 Code-based vs performance-based design earthquake engineering

The first design requirements for seismic-resistant structures arose after the devastating 1755 Lisbon Earthquake, in southern Europe's Portugal, with an estimated magnitude between 8.5 and 9.0 on the moment-magnitude scale (Mw). During the reconstruction of the city, a set of constructive recommendations were defined according to building typologies. Close to a half-century later, the events of Messina (Italy, Europe, 1908, 7.1 Mw) and Kantō (Japan, Asia, 1923, 7.9 Mw) triggered the development of the first seismic design rules that prescribed that buildings should be designed for horizontal forces equivalent to a percentage (10%) of the building's weight. Back in 1927, in the USA, the first building code with specific provisions for seismic design was published, namely the Uniform Building Code (UBC) (ICBO, 1927). The main intent of the document was to avoid the collapse of buildings as a consequence of earthquake events, whilst also avoiding the falling hazards related to non-structural elements coming down from the buildings to the streets. In its Introduction, it was even stated that the code intended to give the structures adequate resistance to withstand earthquake ground motions, without any reference, at the time, to structural dynamic behaviour or to the concept of ductility.

> "The design of buildings for earthquake shocks is a moot question but the following provisions will provide adequate additional strength when applied in the design of buildings or structures." (in 1927 UBC - Lateral Bracing Appendix (ICBO, 1927))

Later in the 60's, the work of Cornell (1968) on seismic hazard, combined with research studies on the nonlinear material and structural behaviour, provided a significant contribution to a better understanding of the seismic action and on its effects on structures. Furthermore, it was also during this period that the concept of ductility was first introduced. In 1966, the Structural Engineers Association of California (SEAOC) published a set of recommendations (Committee et al., 1959), in which the concept of seismic performance came into view to the Earthquake Engineering community. Recognising that damage cannot be avoided under major earthquakes, the following seismic design recommendations were made (Fardis, 2009):

> "Structures should, in general, be able to:
>
> - Resist a minor level of earthquake ground motion without damage;
> - Resist a moderate level of earthquake ground motion without structural damage, but possibly experience some non-structural damage;
> - Resist a major level of earthquake ground motion having an intensity equal to the strongest either experienced or forecast for the building site, without collapse, but possibly with some structural as well as non-structural damage."

As it can be noted, these were the first recommendations in which the concept of design towards the achievement of performance levels was employed.

The major earthquakes that occurred in 1989 (Loma Prieta, USA), 1994 (Northridge, USA) and 1995 (Kobe, Japan) were a turning point in the evolution of Earthquake Engineering. All these events caused relatively small number of casualties, but considerable damage to property and economic losses due to downtime. After these events, the perception that designing structures to avoid collapse or accounting for direct life-safety may be insufficient in modern societies. As a consequence, the SEAOC "Vision 2000" document was published in 1995, pioneering the concept of Performance-Based Earthquake Engineering (PBEE) (Vision, 1995). In Performance-Based Seismic Design, the structure is designed to meet pre-defined damage levels (acceptable performance) for pre-defined earthquake design levels which are based on the occupancy or expected consequences of its failure. Figure 1.4 shows the performance objectives matrix, which summarises the minimum recommended performance levels for each earthquake design intensity level and for various performance objectives. It is important to note that PBEE not only considers the performance based on the damage to structural components, but also to non-structural components.

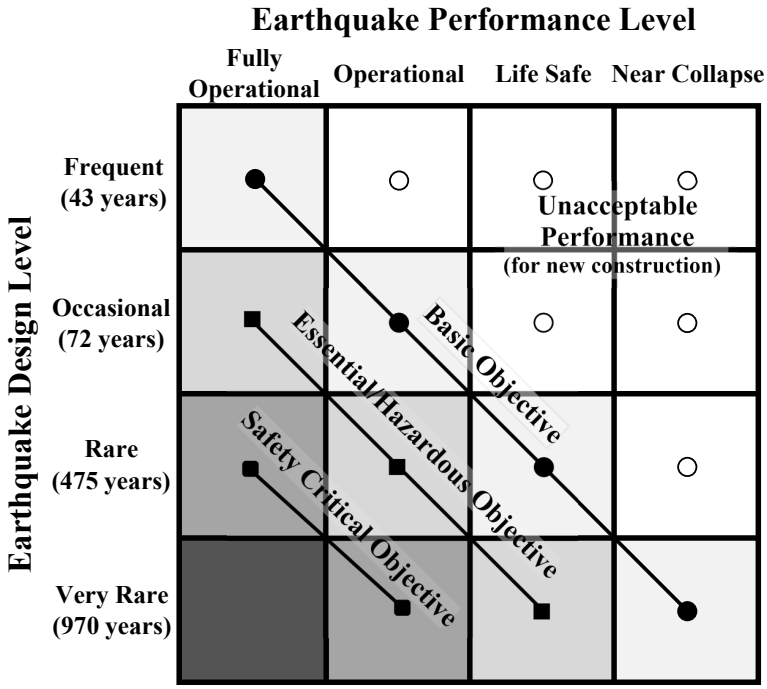

Figure 1.4: Performance objectives for buildings defined in Vision 2000 (Vision, 1995).

Typically, the acceptable levels of damage (or performance levels), are defined as a function of the deformation of the structural elements (e.g. curvature, rotation, displacement). In addition to the performance levels, this first-generation of performance-based methods defined several analytical procedures that could be used to simulate the seismic response of buildings (FEMA, 2006).

Despite the significant progress that first-generation performance-based design procedures ensured, it is undeniable that they provided a fully deterministic and ambiguous measure of the

buildings' performance, which most of the times is not meaningful for stakeholders. Consequently, several research studies (Ramirez and Miranda, 2012; Hwang et al., 2015; Tzimas et al., 2016; Karavasilis et al., 2015) proposed more explicit and improved seismic performance metrics (e.g. casualties, economic losses associated with repair/replacement, downtime) which can help stakeholders in their decision making process (Cornell and Krawinkler, 2000). To this end, the Pacific Earthquake Engineering Research (PEER) Center proposed the so-called Performance-Based Earthquake Engineering (PBEE), that is a fully probabilistic framework that can be used to evaluate damage and economic losses resulting from an earthquake (Cornell and Krawinkler, 2000; Porter, 2003; Ramirez and Miranda, 2009). The PEER-PBEE has since become the reference procedure to evaluate damage and economic losses resulting from an earthquake. Figure 1.5 illustrates the framework behind the PEER-PBEE methodology, which comprises four main steps: i) hazard analysis, ii) demand or structural analysis, iii) fragility or damage analysis, and iv) loss analysis.

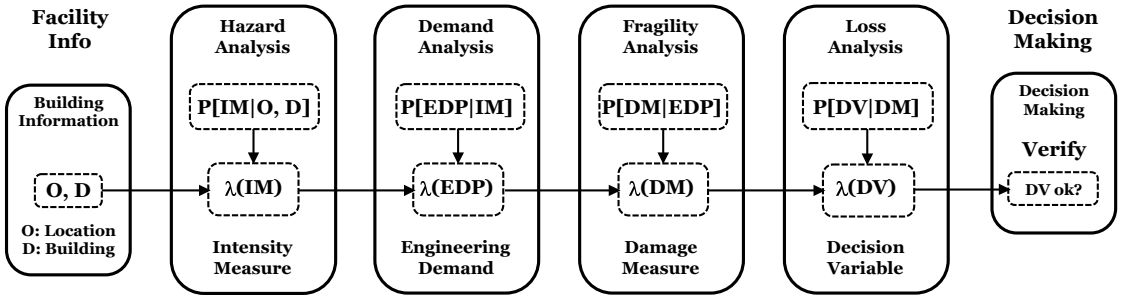

Figure 1.5: PEER-PBEE methodology (Porter, 2003).

The first step of the methodology consists on the conduction of a probabilistic seismic hazard analysis (PSHA) to obtain the seismic hazard for the site under consideration, which describes the annual frequency of exceedance (or the probability of exceedance within a certain time frame, or the return period) of a given ground motion intensity measure or IM (e.g. PGA, PGV, $Sa(T_1)$). This stage may also include the selection of hazard consistent ground motion records to use in the second step of the methodology, namely the analysis of the response of the structure (Porter, 2003). In the second step, response-history analysis is performed for several intensity levels of the same IM, in order to compute the desired engineering demand parameters or EDPs (e.g. inter - storey drift, residual inter-storey drift, peak floor accelerations). The third step (fragility analysis) correlates the EDPs to the probability of equalling or exceeding particular levels of damage, producing damage measures (DMs). Finally, in the fourth step, the probabilistic estimation of the structural performance conditioned on damage is performed. The structural performance is quantified via decision variables (DVs) that could be, for example, the repair cost, downtime, loss of life or other metrics that allow stakeholders and building owners to perform their decisions. In mathematical terms, the PEER-PBEE methodology is expressed by Equation 1.1, in terms of the mean annual occurrence rate of the decision variable, $\lambda(DV)$ (Cornell and Krawinkler, 2000; Porter,

2003). Modifications of the original PEER formulation have also been proposed in recent years. Aslani and Miranda (2005) introduced a procedure that explicitly takes into account the variation of dispersion of the structural response with changes in the intensity level, whilst Ramirez and Miranda (2012) incorporated the irrepairability conditions due to excessive residual deformations. Figure 1.6 shows a comparison between the first-generation and the PEER performance-based earthquake engineering proposals. More details about the implementation and application of the PEER-PBBE methodology can be found in Chapter 2.

$$\lambda(DV) = \int\int\int G(DV \mid DM)\, dG(DM \mid EDP)\, dG(EDP \mid IM)\, |\, d\lambda(IM)\, | \tag{1.1}$$

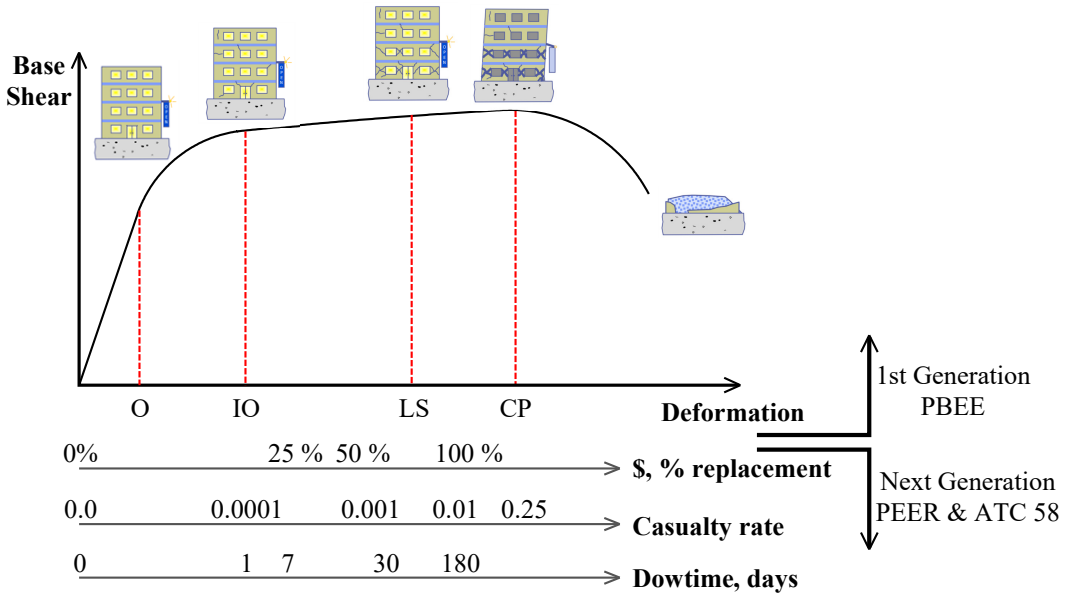

Figure 1.6: Illustration of performance-based earthquake engineering (FEMA, 2012a).

Although the framework itself is well defined and a series of recent guidelines and companion tools have been made available aimed at the promotion of its use among the community (FEMA, 2012a,b), its application by practitioners proved to be difficult. This is due to the complexity of the modelling techniques, analysis procedures, hazard analysis and ground motion record selection (issues address in Chapter 3, 4 and 5). Furthermore, this new design philosophy has been steadily introduced in modern seismic design codes. The concept of performance level is already present in Part 1 of Eurocode 8 (EC8), which is designated by limit state. Two limit states are considered in EC8: i) no- local- collapse, termed as Ultimate Limit State (ULS), which aims to protect human life under rare earthquake events by avoiding collapse of any structural member, and ii) damage limitation, termed as Serviceability Limit State (SLS), which targets the control of damage mainly in non-structural elements under more frequent seismic events. The design process involved in the verification of these limit states is straightforward and follows well-established force-based

design procedures. For the SLS, the designer should demonstrate that the building deformations (inter-storey drift ratios) for reduced seismic intensity levels comply with code-prescribed limits, which are function of the ductility of the adopted non-structural elements. Regarding the ULS, the first step of the design procedure concerns the definition of the level of ductility that the designer expects from the structure, followed by the selection of a code-recommended behaviour factor (Chapter 2 addresses this issue). This is a crucial step in the design process since the ductility demands and detailing specifications of dissipative members are governed by that choice. Moreover, the assessment of the building's sensitivity to second-order effects is also function of the adopted behaviour factor for the evaluation of the inelastic displacement. Although not explicitly mentioned, EC8 tries to address the no-global collapse limit state through the application of capacity design procedures. This concept imposes a clear hierarchy of strengths between structural elements, aiming to control the energy dissipation mechanism (Paulay and Priestley, 1992; Fardis, 2009). The capacity design approach establishes which members are expected to dissipate energy (dissipative components) and which members should remain elastic (non-dissipative components). Additionally, the code defines the design rules for each component type. As one may infer, the evaluation of the building's performance based on code specifications may prove to be difficult to accomplish. Consequently, several methodologies have been developed aiming at a better assessment of the seismic performance of buildings. Examples of such methodologies are: i) the N2 method recommended in EC8, ii) the Capacity Spectrum Method (CSM) specified in ATC40 (ATC, 1996), or iii) the Adaptive Capacity Spectrum Method (ACSM) proposed by Casarotti and Pinho (2007).

Furthermore, regarding the ULS, the Federal Emergency Management Agency (FEMA) proposed the FEMA P695 (FEMA, 2009) framework for the calibration of building seismic performance factors such as behaviour and overstrength factors. The proposed validation procedure ensures that structures exhibit adequate margins against collapse. In brief terms, this methodology evaluates the safety margin against collapse of an earthquake load resisting system designed with a specific behaviour factor, and then compares it with an admissible limit. The latter depends on an acceptable probability of collapse and the uncertainty associated to such probability (Zareian et al., 2010). This methodology has been applied to a wide range of structural systems, from masonry shear wall structures to buckling-restrained steel braced frames. Zareian et al. (2010) applied the FEMA P695 methodology to assess the seismic collapse performance of special MRFs designed in accordance with ASCE 7-10 (ASCE/SEI, 2005) and AISC 341-05 (ANSI, 2005). However, that research study considered a reduced number of structural configurations and adopted the seismic performance factors defined in the American provisions, which are different from those proposed in the European seismic code. Figure 1.6 shows the FEMA P695 application diagram (FEMA, 2009).

In the last two decades, a new generation of design procedures has been developed aiming to provide designers with better control of the seismic performance of structures. The remarkable advantage of these promising methods is the ability to define and control the performance objective for each structure. These emerging methods are the so-called displacement-based design

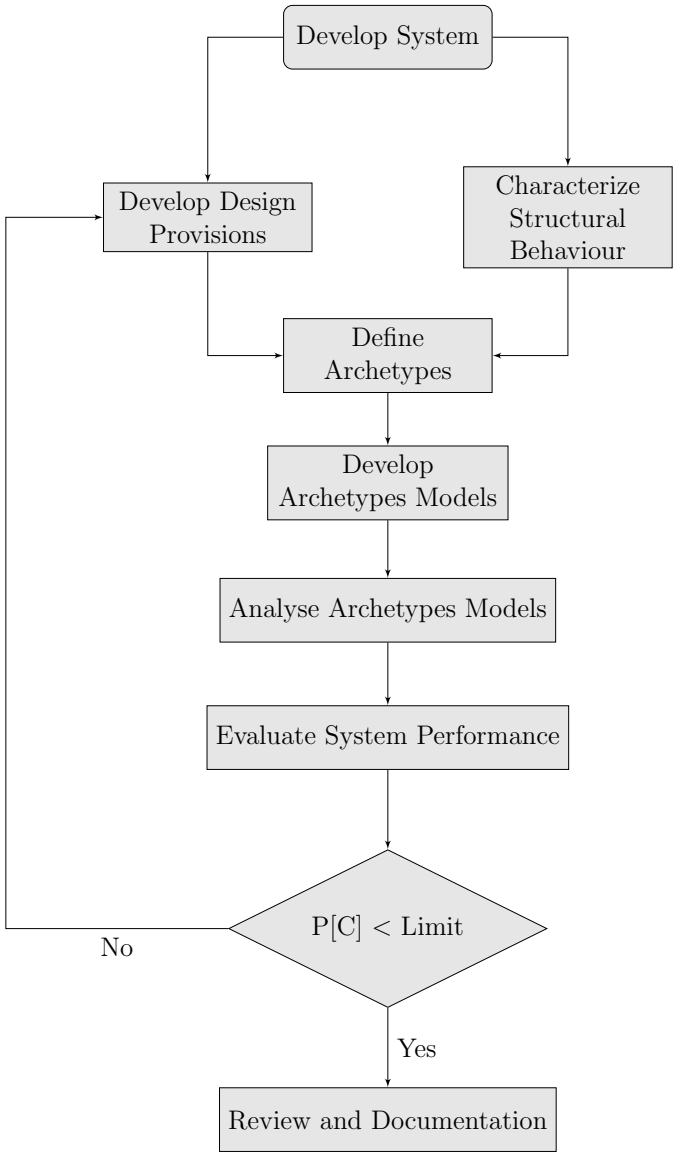

Figure 1.7: FEMA P695 application diagram (FEMA, 2009).

methods and, as mentioned before, aim for a more reliable control of the inelastic deformations, and hence of the amount of damage that the structure will experience. Examples of displacement-based design methods are the Direct Displacement-Based Design (DDBD) proposed by Priestley et al. (2007), and the yield point spectra (YPS) proposed by Aschheim and Black (2000). Both methods are based on the transformation of multi-degree- into single-degree-of-freedom systems, and have, has the starting point of the design process, the definition of the target displacement. This parameter is often related with the performance level required for the structure. The YPS method is based on the initial stiffness of the structure and resorts to the inelastic response spectra to obtain the required base shear. On the other hand, the DDBD is based on the substitute structure approach (Shibata and Sozen, 1976) and uses the secant stiffness associated with the elastic re-

sponse spectra, whilst introducing the equivalent viscous damping concept. A review of the most prominent displacement-based design procedures applied to reinforced concrete structures can be found in Sullivan (2002).

The scope of this research study is to not only contribute to a better understanding of the behaviour of steel moment-resisting frames, but also to present viable proposals intended for the improvement of current design procedures, whilst also providing the adequate tools and frameworks to assess the seismic performance of steel buildings, within the scope of performance-based design.

Chapter 2

A more rational selection of the behaviour factor for seismic design according to Eurocode 8

2.1 Introduction

Moment-resisting frames (MRFs) are one of the many possible frame typologies, simply defined as rectilinear assemblages of rigidly connected beams and columns, with its lateral strength mainly being attained by the development of bending moments and shear forces in the members and joints. To what concerns the steel MRF variety, the existing practical and scientific knowledge can be considered to be quite extensive, often acknowledging the high ductility of these structures when subjected to seismic excitation.

From an European design perspective, Eurocode 3 – Part 1-1 (EC3-1-1) (CEN, 2005a) provides the methodologies for the determination of the capacity of steel members under various loading conditions. Specifically concerning the design for earthquake resistance, the requirements of the European seismic design code (Eurocode 8 – Part 1 (EC8) (CEN, 2005c)) must be followed. The main intent of EC8 is to ensure the development of a controlled plastic mechanism under seismic loading through the application of capacity design principles. According to such approach, strategic dissipative regions are defined to undergo inelastic behaviour during the occurrence of a seismic event. In the case of steel MRFs, the code allows for the designer to fully exhaust material elasticity, taking advantage of the inelastic behaviour at the end regions of the beams, at the base of the first-floor columns and at the top end of the columns located in the top storey. The remaining structural members must then be designed to remain elastic.

One relevant aspect to consider in the seismic design according to the European code is the adopted value for the behaviour factor, q, which directly correlates to the energy dissipation capacity of the structure. EC8 prescribes an upper limit of q depending on the structural system and on the ductility class. The prescribed values of q are not specific to any given structure, but

rather upper values to take into consideration in the structural design stage. Thus, the determination of the adopted value should not be taken lightly as misconceptions might occur during the design process. The assumption that the use of an high value of q will lead to lower equivalent seismic forces (given that the seismic forces obtained with the use of the seismic design spectrum are proportional to q), and thus lead to savings in steel weight, may prove to be erroneous. Elghazouli (2009); Peres and Castro (2010) demonstrated that the adoption of high values of the behaviour factor can result in stiffer structures. This is due to the need to comply with the limits specified in EC8 for the inter-storey drift sensitivity coefficient (θ), which is used to control the level of second-order (P-Δ) effects in the structure. The need for a more stiff structure may lead to oversized dissipative members that impose high values of system overstrength, Ω. Additionally, the use of an incorrectly estimated behaviour factor may even lead to a structure that will remain elastic throughout the seismic event, disregarding the intent of the code when taking into consideration the inelastic behaviour of the dissipative regions. In order to provide an improvement to the force-based design procedure of EC8, Villani et al. (2009) proposed a methodology for the rational determination of the adopted value of the behaviour factor. This Improved Force-Based Design (IFBD) methodology consists of a simple reordering of the design steps, yet it is fully compliant with the design requirements of EC8. Whilst aiming to achieve structural design solutions that perform more consistently with the requirements prescribed in performance-based guidelines, IFBD considers the adoption of a behaviour factor based on the actual properties of the structure, targeting the minimization of the Ω parameter as defined in EC8. The application of this improved design methodology to MRF structures is usually reflected in relevant material savings.

The purpose of this Chapter is to evaluate the consequences of adoption of EC8 recommended behaviour factor and to present a more rational methodology for the selection of a behaviour factor as a function of the structure and the level of seismic action at the site. To this end, an extensive study of 360 steel MRFs is conducted considering different behaviour factors. A detailed comparison of the seismic performance of the MRFs is conducted through response-history analysis. The results indicate that, within the context of the current version of EC8, a more rational selection of the behaviour factor in seismic design can lead to substantial material savings without compromising safety.

2.2 Seismic design of steel moment resisting frames to EC8

In this section, the force-based design methodology of EC8 concerning the design of earthquake-resistant steel moment-resisting frames is detailed. The background behind the purpose of the behaviour factor is presented, and its importance is discussed. Finally, the IFBD methodology is described in detail, and the arguments that support its use are discussed.

2.2.1 Behaviour factor

In order to resist vertical or wind loads, structures are designed according to a set of pre-defined loads, mainly taking advantage of the elastic behaviour of the members. However, to assume the

same design strategy (i.e. a structural response fully in the elastic material range) for seismic actions would be unfeasible, especially for high intensity levels. Structural members would be required to have considerable (sectional) proportions, which would be both expensive and aesthetically unappealing. Therefore, taking advantage of the material inelasticity proves to be advantageous, being not only a tool for the dissipation of the energy induced in the structure by the earthquake event, but also a way for the equivalent forces to be lower than those obtained elastically.

In order to take the non-linear behaviour into account during the design stage, force reduction coefficients or behaviour factors (R or q) were introduced. These parameters aim to facilitate the consideration of the non-linear deformation and energy dissipation capacity of the structure with the use of an elastic analysis. The structure will experience deformations in the inelastic material range which, in turn, will induce damage in the structural members, as well as in non-structural components. Focusing on the former, they must be adequately defined by ensuring that the deformation capacity will not be exhausted. Moreover, certain criteria must be met in order to ensure that the global ductility intended for the structure is attainable, namely by avoiding the development of premature unstable plastic mechanisms (e.g. soft-storey). This is achieved by the application of capacity design principles (Paulay and Priestley, 1992).

According to Ferraioli et al. (2014), the behaviour factor is directly related to the parameters that define the energy dissipation capacity of the structure, namely structural ductility, viscous damping, redundancy and member overstrength. Based on this, it is possible to define q as shown in Equation 2.1, where q_μ is associated to the ductility of the structure (i.e. the capacity of the structure to hysteretically dissipate energy), q_ξ to the damping (taken as 1.0 since it is assumed that the viscous damping coefficient is the same in both the linear and non-linear structural response). The overstrength components, q_ρ and q_Ω, are related with the redundancy of the structure (defined in EC8 though the α_u/α_1 coefficient) due to material hardening, plastic hinge formation sequence throughout the structure or non-structural elements contributions and with the excessive strength of the structural members in comparison to the internal induced loads (due to lateral stiffness requirements to meet second-order effects and damage limitations performance requirements). It is important to note that this overstrength of the structure is highly susceptible to the ratio between gravity and seismic loads, which may result in significant strength reserves, particularly in structures located in low seismicity areas.

$$q = \Omega \times q_\mu \times q_\xi = q_\rho \times q_\Omega \times q_\mu \times q_\xi \tag{2.1}$$

Figure 2.1 shows the typical lateral behaviour curve of steel MRFs, in which the physical meaning of the behaviour factor is illustrated.

EC8 specifies upper (or reference) values of the behaviour factor for a number of structural systems and different ductility classes. To what concerns steel MRFs EC8 prescribes different limits to the medium (DCM) and high (DCH) ductility classes, in accordance with Table 2.1.

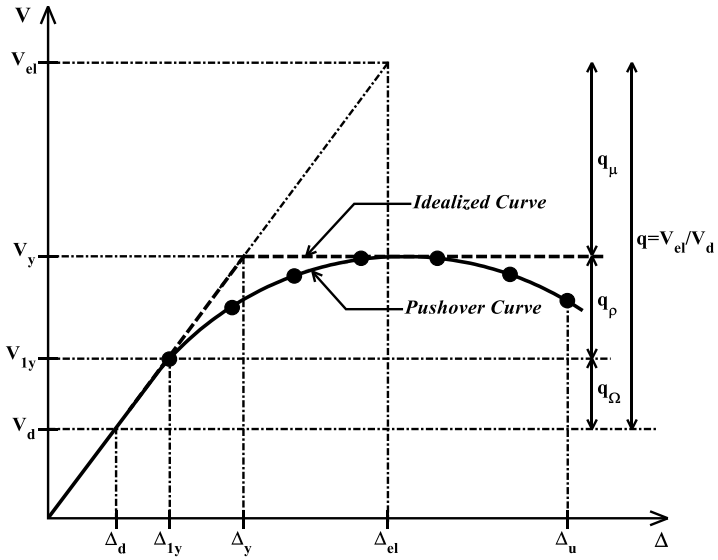

Figure 2.1: Typical lateral behaviour curve of steel MRFs.

Table 2.1: Cross-sectional requirements for local ductility of steel elements

Structural ductility class	Range of the reference values of q	Required cross-sectional class
DCM (medium)	1.5 <q <2.0	Class 1, 2 or 3
	2.0 <q <4.0	Class 1 or 2
DCH (high)	q >4.0	Class 1

2.2.2 Requirements of EC8 for steel MRFs

The seismic design methodology of EC8 regarding steel MRFs is aimed at ensuring global ductile behaviour, by imposing that the yielding of the dissipative elements occurs before damage and premature failure of the remaining members, in accordance with a capacity design approach.

Regarding its main considerations, the code prescribes a no-collapse requirement (in order to avoid local or global collapse) and a damage limitation requirement (in order to avoid the occurrence of excessive damage for low intensity earthquakes), prescribing different probabilities of occurrence for the seismic action associated with each requirement. The seismic action is defined in EC8 through the use of an elastic response spectrum, with two spectrum types being considered (types 1 and 2, referring to a seismic event higher and lower than 5.5 in magnitude, respectively). Applicable elastic analysis methods (equivalent lateral force method or modal response spectrum method) and behaviour factors (reference values reduced values) are considered to be a function of height and plan regularity.

For the verification of the damage limitation requirement, EC8 limits the inter-storey drifts of the structure in accordance to Equation 2.2, where: d_r is the design inter-storey drift; ν is a

reduction coefficient to take into account the lower return period of the seismic action associated with this requirement (recommended values of 0.4 or 0.5, depending on the importance of the structure); ψ concerns the type of non-structural elements (recommended values of 0.5% for brittle materials, 0.75% for ductile elements and 0.1% if the non-structural elements do not exist or are fixed in way as to not interfere with structural deformations); h is the storey height.

$$d_r \times \nu = \psi \times h \tag{2.2}$$

According to the European code, if second-order (P-Δ) effects are not incorporated in the analysis, then they must be taken into account in the design process. EC8 prescribes a simplified procedure to determine the sensitivity of the structure to P-Δ effects, by calculating a drift sensitivity coefficient, θ, for each storey, as shown in Equation 2.3. In each storey, P_{tot} is the total axial load installed in the columns of that storey, d_r is the design inter-storey drift, V_{tot} is the total shear load and h is the storey height. Whilst the code does not allow θ to be higher than 0.3, if lower than 0.1 than there is no need to consider second-order effects in the design, and if between 0.1 and 0.2, the influence of the P-Δ effects may be taken into account by amplifying the seismic lateral forces by $1/(1-\theta)$.

$$\theta = (P_{tot} \times d_r)/(V_{tot} \times h) \tag{2.3}$$

As previously stated, EC8 tries to ensure that MRFs are designed so that plastic hinges form in the beams (or in the connections to the columns), but not in the columns. However, this requirement may be waived at the base of the frame, at the top level of a multi-storey building and for a single storey building.

For plastic hinges in the beams, ensuring that the full plastic moment of resistance and rotation capacity are not decreased by compression and shear forces is mandatory. As such, for members of cross-sectional classes 1 and 2, Equation 2.4 through Equation 2.6 should be met at the location plastic hinge formation is expected to occur. In the expressions, N_{Ed} is the design axial force, M_{Ed} is the design bending moment and V_{Ed} is the design shear force (sum of the design value of the shear force due to the non-seismic actions, $V_{Ed,G}$, and the design value of the shear force due to the development of the plastic moment of the cross-section with opposite signs at the end sections of the beam, $V_{Ed,M}$), $N_{pl,Rd}$, $M_{pl,Rd}$ and $V_{pl,Rd}$ are the design resistance calculated in accordance with EC3-1-1 (CEN, 2005a). For members with cross-sectional class 3, Equation 2.4 through Equation 2.6 should be checked replacing the design plastic resistances with the elastic (yield) values.

$$N_{Ed}/N_{pl,Rd} \leq 0.15 \tag{2.4}$$

$$M_{Ed}/M_{pl,Rd} \leq 1.00 \tag{2.5}$$

$$V_{Ed}/V_{pl,Rd} = (V_{Ed,G}+V_{Ed,M})/V_{pl,Rd} \leq 0.50 \tag{2.6}$$

EC8 also allows for the design of dissipative semi-rigid and/or partial strength beam to column connections, providing that a number of requirements are verified: the connections have a rotation capacity consistent with the global deformations; members framing into the connections are demonstrated to be stable at the ultimate limit state; the effect of connection deformation on global drift is taken into account using non-linear static (pushover) or time history analysis. The connection design should be such that the rotation capacity of the plastic hinge region or θ_p (as defined in Equation 2.7, where δ is the beam deflection at midspan and L is the beam span), is not less than 35mrad or 25mrad for DCH or DCM structures, respectively. According to the European code, the column web panel shear deformation should not contribute to more than 30% of θ_p.

$$\theta_p = \delta/0.5L \tag{2.7}$$

Non-dissipative members should be verified in compression considering the most unfavourable combination of the axial force and bending moments. The design forces are calculated according to Equation 2.8, where $N_{Ed,G}(M_{Ed,G},V_{Ed,G})$ are the compression force (respectively the bending moment and shear force) in the member due to the non-seismic actions included in the combination of actions for the seismic design situation, $N_{Ed,E}(M_{Ed,E},V_{Ed,E})$ are the compression force (respectively the bending moment and shear force) due to design seismic action, γ_{ov} is the overstrength factor (1.25) and Ω is the minimum overstrength value of all beams in which dissipative zones are located.

$$N_{Ed}(M_{Ed},\, V_{Ed}) = N_{Ed,G}(M_{Ed,G},V_{Ed,G}) + 1.1 \times \gamma_{ov} \times \Omega \times N_{Ed,E}(M_{Ed,E},V_{Ed,E}) \tag{2.8}$$

It is important to note that EC8 defines Ω, for each beam, as the ratio between the design value of the plastic moment of resistance in beam i, $M_{pl,Rd,i}$, and the design value, $M_{Ed,i}$. However, Elghazouli and Castro (2009) concluded about the importance of considering the effect of gravity loads in this calculation, in accordance with Equation 2.9.

$$\Omega = \left(\frac{M_{pl,Rd,i}-M_{Ed,G,i}}{M_{Ed,E,i}}\right)_{min} \tag{2.9}$$

In order to avoid soft-storey collapse mechanisms (as such a mechanism might entail excessive local ductility demands in the columns of the soft storey), EC8 states that a minimum value of bending resistance of the columns should be guaranteed at all joints of primary or secondary seismic beams with primary seismic columns, regarding the ratio between the sum of design moments of resistance of the columns, $\sum M_{Rc}$, and beams, $\sum M_{Rb}$, framing the joint, following the "weak beam-strong column" criterion of Equation 2.10.

$$\sum M_{Rc} \geq 1.3 \times \sum M_{Rb} \tag{2.10}$$

2.2.3 Improved Force-Based Design

One of the most important aspects to take into consideration in the seismic design according to EC8 is the behaviour factor adopted. This factor is directly related to the level of ductility intended (during the design) for the structure, which may even not be explored under the correct conditions. As already mentioned, the use of an incorrectly estimated value of q may lead to a structure that will remain elastic throughout the design seismic event, without exploring the inelastic behaviour of the dissipative regions (despite aiming to do so in the design stage).

Aimed at an improvement upon the force-based design procedure of EC8, Villani et al. (2009) proposed a methodology for the rational selection of the adopted value of the behaviour factor, instead of using the upper bound reference values proposed by the design code. The authors were able to identify that steel MRFs exhibited lateral resistances much greater than the estimated design values. This was due to a number of reasons, namely the verification of the requirements related to second-order effects (θ limitation) and the overstrength of the structure itself (Ω). Thus, a methodology was developed to estimate a behaviour factor that leads to more consistent structural design solutions, whilst relying on simple elastic analysis.

In simple terms, Villani et al. (2009) proposed that the definition of the behaviour factor value should be established by ensuring that the design base shear, V_d,is equal to the base shear that would lead to the formation of the first plastic hinge in the structure, V_{1y}. Thus, q is defined as:

$$q = \frac{V_{el}}{V_d} = \frac{V_{el}}{V_{1y}} \tag{2.11}$$

This Improved Force-Based Design (IFBD) methodology consists of a simple reordering of the design steps, namely through the consideration of the serviceability deformation checks at the beginning of the design process, and complies with the design requirements of EC8. Whilst aiming to achieve structural design solutions that perform more consistently with the requirements prescribed in performance-based guidelines, IFBD allows for the adoption of a behaviour factor based on the actual properties of the structure and on the seismicity of the building location, leading to minimum Ω values of 1.0, which is valuable for the design of non-dissipative members. The reordering of the design steps consists of: 1) estimate the elastic seismic forces based on the dynamic characteristics of the structure design to gravity and wind loads; 2) perform the verification of damage limitation (Equation 2.2), in which an increase in members dimension might be necessary to comply; 3) estimate q by calculating the base shear that would lead to yielding of the first structural element; 4) calculate the design base shear (elastic value divided by the behaviour factor) and the associated seismic forces according to EC8; 5) perform an elastic analysis and verify the θ limitation (Equation 2.3), in which an increase in members dimension might be necessary to comply; 6) perform the resistance verification of dissipative and non-dissipative members/components.

According to the authors, the adoption of a behaviour factor specific for each structure and for the level of seismic action, allows for a considerable reduction of the cost of the structure

(in comparison to a scenario in which q is overestimated), whilst also permitting the use of the available structural ductility without any reduction in safety.

2.3 Parametric seismic design study

In order to assess the influence of considering different behaviour factors in seismic design according to EC8 (e.g. code-prescribed values, IFBD), an extensive parametric design study was devised. A total of 360 steel MRF configurations (number and length of bays, number of storeys) were considered, each designed with different levels of q. In the following sections the parametric study is described in detail, and the obtained design solutions are compared in terms of structural weight.

2.3.1 Definition of the parametric design study

As mentioned before, an extensive parametric study was defined in the context of this research study, intended to quantify the influence of different behaviour factors in the seismic design of steel MRFs to EC8. A number of parameters were considered, namely: building plan configuration (number of bays and bay width), number of storeys, seismic location and behaviour factor.

Regarding the building configurations, six cases were defined by varying both the number (3, 4 or 5) and the span of the bays (equal and different between bays) in the main frame direction, as well as only the number (2, 3 or 4) of the bays in the orthogonal direction. Figure 2.2 shows the elevation and plan views of building configuration 3, in which the direction (x-z plane orientation) and the type (internal) of the frames considered in this study is identified. As one may infer from the figure, building configuration 3 has three and four frames in the y-z and x-z planes, respectively, the former with two 6m bays and the latter with three bays (6m+8m+6m). Every building configuration was assumed to have a first storey with 4.5m in height, with the storeys above it with 3.5m. The properties of the remaining building configurations are shown in Table 2.2.

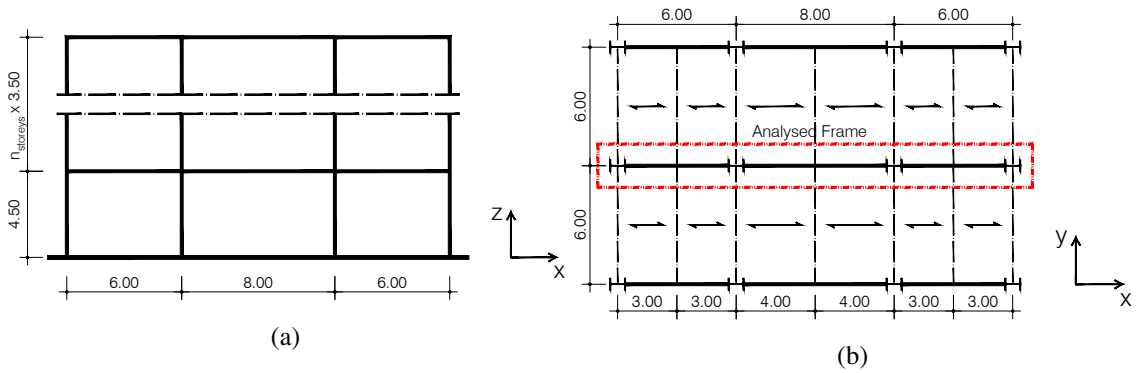

Figure 2.2: Building configuration 2: a) Elevation view, b) Plan view.

Table 2.2: Building configurations and geometrical properties

Config.	x-z plane		y-z plane		h_1 [m]	h_{others} [m]
	N. of frames	Bays [m]	N. of frames	Bays [m]		
1	3	6+6+6	4	6+6	4.5	3.5
2	3	6+8+6	4	6+6		
3	3	8+8+8	4	8+8		
4	4	6+6+6+6	5	6+6+6		
5	3	8+6+8	4	6+6		
6	5	8+8+8+8+8	6	8+8+8+8		

For all configurations shown in Table 2.2, buildings with 2, 3, 4, 5, and 8 storeys, corresponding to low to medium rise buildings, were considered. Additionally, four seismic intensities were defined by considering three locations in Portugal, namely Porto (low seismicity), Lisbon (moderate seismicity) and Lagos (moderate-to-high seismicity) with soil Type B, and one location (Lagos) with soil type C.

Regarding the structural design of the archetypes, the frames were firstly designed for gravity loads in accordance with the provisions of EC3-1-1 for sectional resistance, stability checks and serviceability deflection limits. European steel open sections with H (HE) or I (IPE) shape were adopted for the beams and columns, respectively. The steel grade considered for all members was S275. Seismic design was performed in accordance with the current provisions of EC8, considering two ductility classes defined in the code, namely high or DCH (q=6.5) and moderate (q=4) ductility classes. Additionally, a behaviour factor obtained with the IFBD methodology was also considered. Table 2.3 shows a summary of the parametric seismic design study. As one may infer from the table, a total of 360 steel MRFs were considered in this research study.

A summary of the vertical distributed loading is shown in Table 2.4, where g_k and q_k are the permanent and the imposed loads, respectively. The transmission of vertical loads to the central frame was considered as point loads at each storey level, in accordance with the positioning of the secondary beams. Additionally, and in order to calculate the storey masses for seismic design, load combination $g_k + 0.3q_k$ was considered for the intermediate storeys and $g_k + 0.0q_k$ for the top storey, in accordance with the EC8 design requirements. The slabs are considered to act as rigid diaphragms, thus, each storey mass can be equally distributed by the frames in the x-z plane.

The parameters required for the definition of the elastic response spectra (for each seismic load level considered) that are specified in the Portuguese National Annex of EC8 (CEN, 2010) are shown in Table 2.5.

Figure 2.3 shows the EC8 response spectra for the four site locations. Furthermore, the fundamental period of the buildings are also depicted. As one may infer from the figure, the large

Table 2.3: Parametric design study summary

Configuration	N. of Storeys	Seismic Load Level	Behaviour Factor
1	2	Porto (soil type B)	IFBD
2	3	Lisbon (soil type B)	4
3	4	Lagos (soil type B)	6.5
4	5	Lagos (soil type C)	
5	8		
6			

Table 2.4: Vertical distributed loads

Storey	Load type	Load $[kN/m^2]$
Top Storey	g_k	4.75
	q_k	1.00
Other Storeys	g_k	5.75
	q_k	2.00

Table 2.5: Elastic response spectra parameters

Location	Soil Type	Spectrum Type	a_g $[m/s^2]$	S	T_B [s]	T_C [s]	T_D [s]
Porto	B	1	0.35	1.35	0.10	0.60	2.00
		2	0.80	1.35		0.25	2.00
Lisbon		1	1.50	1.29		0.60	2.00
		2	1.70	1.27		0.25	2.00
Lagos		1	2.50	1.18		0.60	2.00
		2	1.70	1.27		0.25	2.00
Lagos	C	1	2.50	1.30		0.60	2.00
		2	1.70	1.46		0.25	2.00

majority of the frames is positioned on the constant velocity branch of the spectrum of the EC8, with fundamental periods higher than 0.5s.

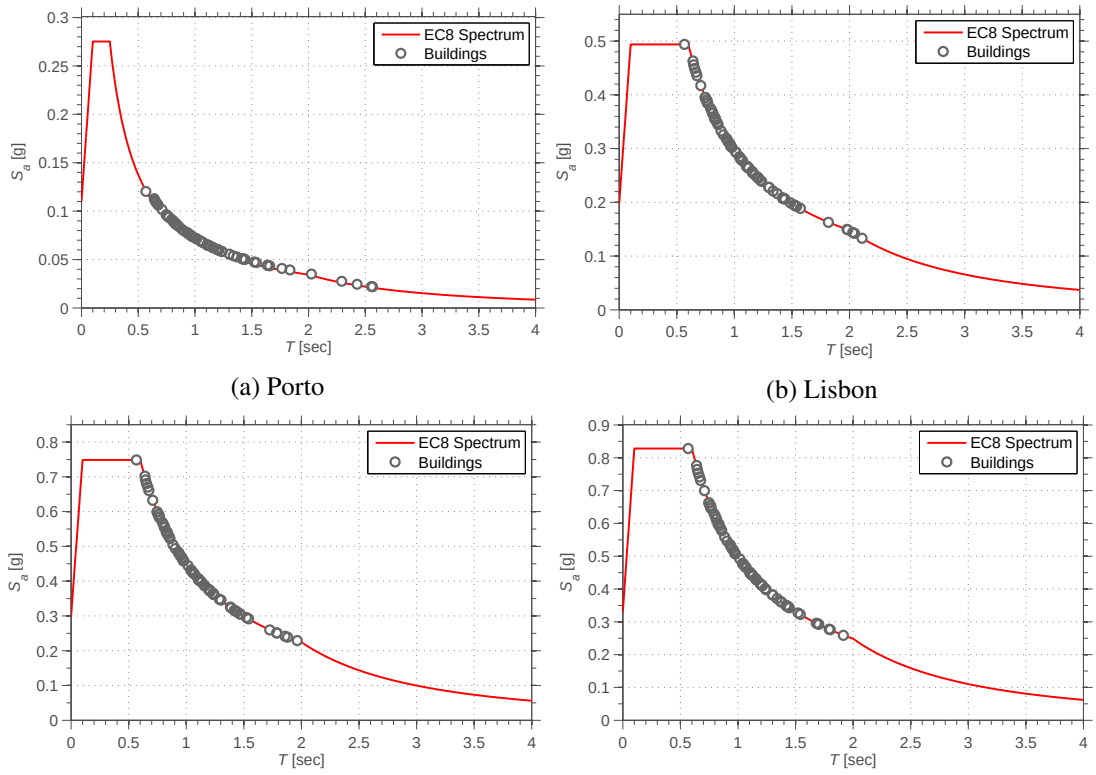

(a) Porto

(b) Lisbon

(c) Lagos (soil type B)

(d) Lagos (soil type C)

Figure 2.3: EC8 response spectra.

Seismic design was performed taking into account second-order effects (P-Δ effects), by limiting the maximum value of the interstorey drift sensitivity coefficient to 0.2. The EC8 capacity design beam-column joint requirement $\sum M_{Rc} \geq \sum 1.3 M_{Rb}$ was also taken into account in the design of all frames. Moreover, the damage limitation performance requirement was considered in the seismic design by limiting the inter-storey drift to $d_r \nu \geq 0.01h$. All frames were designed based on the equivalent lateral force analysis method.

2.3.2 Comparison of the design solutions

The solutions obtained using the different ductility design criteria are now compared in terms of steel weight. Additionally, the governing design criteria, as well as the main difficulties faced during the design process are identified. In Figure 7.7, the steel weight of the lateral load resisting system of each design solution is shown, for the location of Porto. In the figure, bar plots summarizing the design solution's weights are shown for the six building configurations, five frame heights (2, 3, 4, 5 and 8 storeys) and three behaviour factors considered ($q = IFBD$, $q = 4$ and $q = 6.5$).

As one may infer from the results shown in Figure 7.7, among the design solutions for all building configurations, the ones with the lowest steel weight are those designed using a lower behaviour factor (IFBD). This observation may seem contradictory, the reason being that the use of

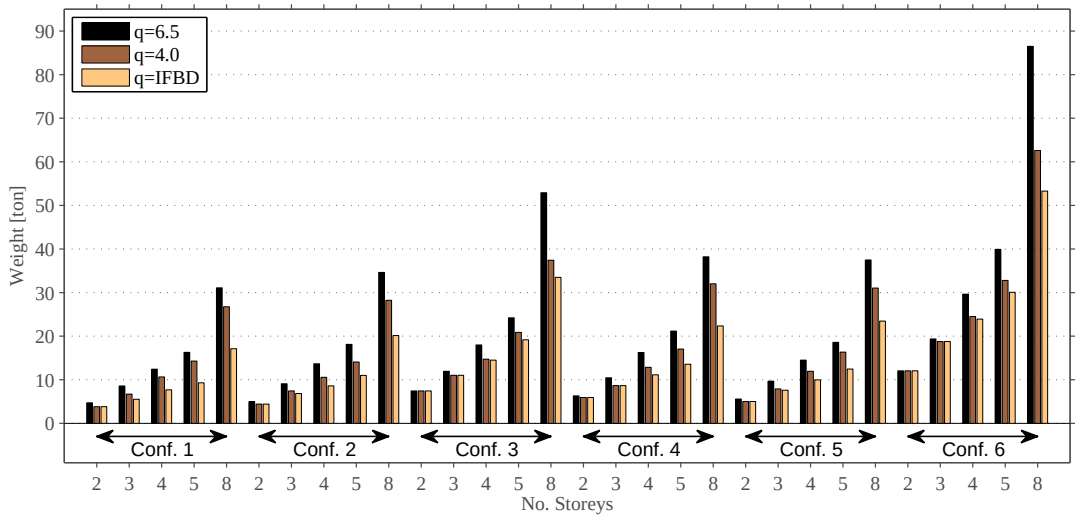

Figure 2.4: Steel weight comparison of the various building configurations, for Porto.

a high behaviour factor may be sometimes associated with savings in element sizes (and therefore material quantities), as the seismic forces are directly reduced by this parameter. However, if stiffness related criteria are the governing factor in the design, then what matters is to ensure sufficient lateral stiffness to the structure rather than controlling ductility demand through the reduction of lateral seismic force demands. This point will be further discussed in the following paragraphs. It is important to note that the trends obtained for Porto are identical to those obtained for the remaining seismic locations (Lisbon and the two soil type scenarios of Lagos).

As previously mentioned, according to EC8, second order effects are quantified on the basis of the inter-storey drift sensitivity coefficient, also designated by stability coefficient, θ, which is calculated for each storey of the structure in accordance with Equation 2.3, where the value of d_r is the displacement between floors for the storey under analysis. According to the recommendations of the code, this displacement is obtained using the equal displacements rule, assuming that the displacements factor, q_d, adopts the same value of the behaviour factor, q. Equation 2.3 can thus be rewritten as:

$$\theta = \frac{P_{tot} \times d_r}{V_{tot} \times h} \leq 0.2 \Leftrightarrow \frac{P_{tot} \times \frac{d_{el}}{q} \times q_d}{\frac{V_{tot,el}}{q} \times h} \leq 0.2 \Leftrightarrow \frac{P_{tot} \times d_{el}}{V_{tot,el} \times h} \times q \leq 0.2 \Leftrightarrow K_e \geq \frac{P_{tot} \times q}{0.2 \times h} \quad (2.12)$$

As shown in Equation 2.12, a condition of minimum elastic lateral stiffness is "indirectly" imposed by the code. From the decomposition of the aforementioned expression, it is possible to conclude that the minimum lateral stiffness is directly proportional to the behaviour factor adopted. In this sense, the use of high values of the behaviour factor for flexible structures, such as moment-resisting frame systems, will implicitly lead to more demanding requirements of lateral stiffness, and consequently to a heavier structural solution. This methodology for the evaluation of P-Δ effects has been studied by Peres and Castro (2010), in which the authors concluded that the non-

verification of the code requirements for second-order effects, in its current formulation, does not imply that the building is sensitive to second-order effects. More importantly, it has been shown that the θ coefficient does not adequately reflect the susceptibility of the structure to second-order effects. Moreover, this approach adopted by the European code is not fully aligned with other design codes. For example, although the American code ASCE 41-13 (ASCE/SEI, 2013) defines the same Equation for the stability coefficient, the behaviour and displacement coefficients factors are different, resulting in comparatively lower values of θ (Villani et al., 2009; Peres and Castro, 2010). Although this limitation has been recognized, no alternative methodology has been proposed as of yet.

By analysing the entire set of results, some observations may be withdrawn regarding the influence of IFBD on the total steel weight of the design solutions. Figure 2.5 show the ratio between material quantities obtained with the use of IFBD in comparison to the cases for wich a behaviour factor equal to 6.5 has been adopted. The savings can reach 45% for taller buildings and are consistently greater than 20-25% for buildings with more than three storeys. A comparison with a lower behaviour factor (q=4) leads to similar conclusions, i.e., material savings of up to 35% and, on average, of about 15%. It is important to note that, for the two-storey frames, as well as for some three-storey designs, the design was usually governed by strength requirements, resulting in similar structural solutions, independently of the adopted behaviour factor.

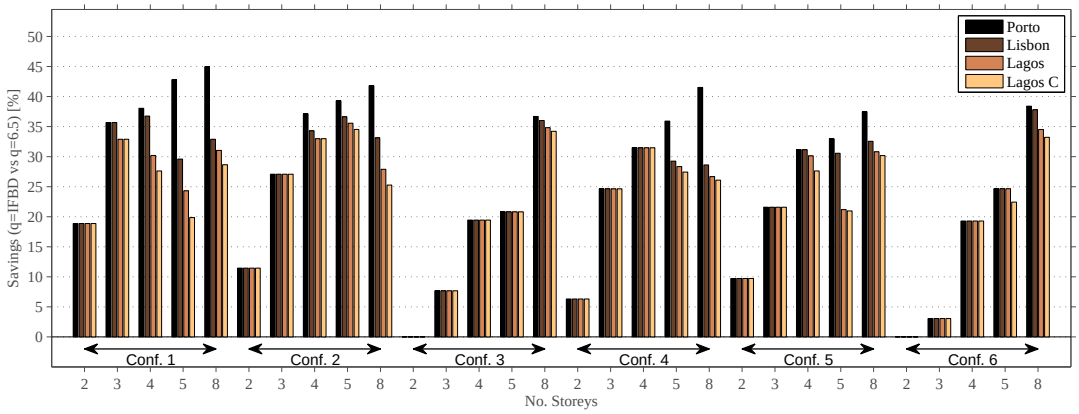

Figure 2.5: Influence of the use of IFBD on the total weight of the design solution.

Since the majority of the designs conducted with the recommended behaviour factors specified in EC8 were governed by lateral stiffness requirements, mainly related with the control of second-order effects, this resulted in structural solutions that are the same for all four studied locations. As an example, the obtained structural solution for Porto (low seismicity zone) was the same as the one obtained for Lagos with soil type C (moderate-to-high seismicity zone) (see Figure 2.6). In these cases, sufficient lateral stiffness needed to be provided to the structure during the design process, which is, as discussed before, dependent on the behaviour factor adopted. Conversely, for the frames designed using IFBD, there is an adequacy between the site's seismicity level and the structural solution, as shown in Figure 2.7.

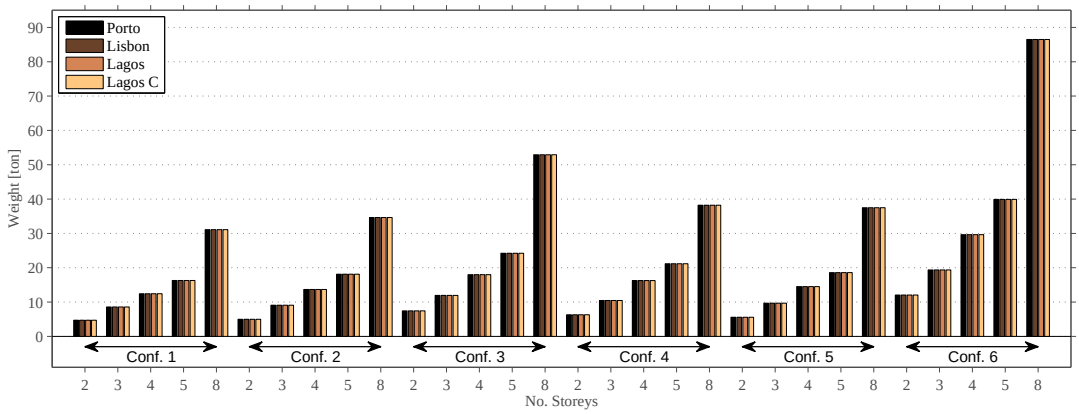

Figure 2.6: Non-sensitivity of the weight of the design solution to the seismicity level, with the use of EC8-prescribed upper bound behaviour factor (6.5).

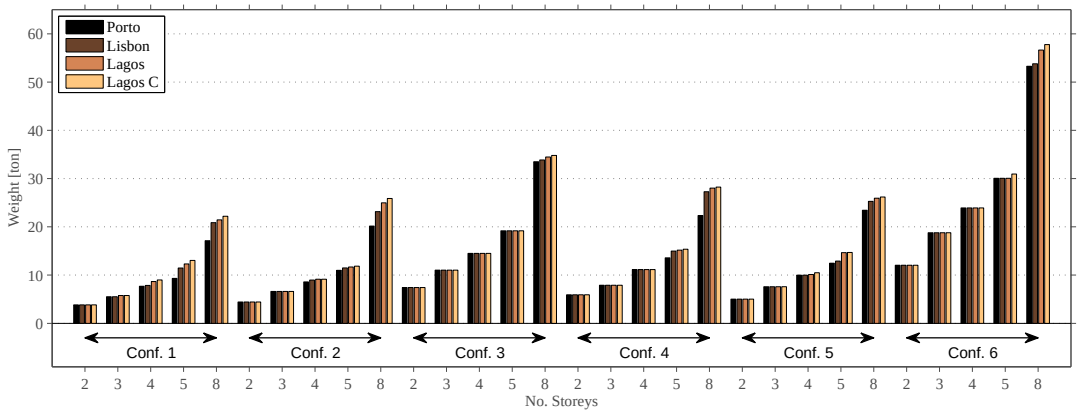

Figure 2.7: Sensitivity of the weight of the design solution to the seismicity level, with the use of IFBD.

Based on the results shown before, it is possible to conclude that a careful selection of the behaviour coefficient allows for lighter lateral load-resisting structural solutions that still fully meet the design requirements of EC8. This conclusion cannot be dissociated from the fact that steel moment-resisting frames are eminently flexible structures in which the code requirements for the damage limitations and for the verification of second-order effects are often the governing criteria in their design. The most interesting and attractive aspect of the IFBD methodology is the fact that the selection of the behaviour factor is made based on the actual properties of the structure and on the seismicity level of the site in which building is located.

2.4 Seismic performance assessment

In order to assess the effect of designing the steel frames for different ductility conditions (i.e., behaviour factors), the seismic performance of the structures was evaluated through nonlinear static

and response-history analyses. Moreover, it was possible to assess if the buildings designed using IFBD have adequate seismic performance, in addition to the advantages in material savings shown thus far. Given the large number of structures to be analysed, only the most relevant response parameters will be presented and discussed.

2.4.1 Numerical modelling

The numerical seismic assessment of the structures was carried out the nonlinear finite element analysis program OpenSees (McKenna, 2011) . Material nonlinearity was considered through a concentrated plasticity approach, considering both strength and stiffness deterioration effects (Lignos and Krawinkler, 2010; Araújo and Castro, 2013). Figure 3.2 illustrates the monotonic backbone curve, as well as the comparison between the "exact" and numerical hysteresis of an European steel open cross-section HEB300, according to the aforementioned proposals. The effect of the axial load on the flexural capacity of the columns was taken into account in an approximate manner: 1) a preliminary pushover analysis was conducted to evaluate the expected average axial force under the combined actions of gravity and lateral loading ($P_{grav} + 0.5 \times P_E^{max}$, where P_{grav} and P_E^{max} are the axial load due to gravity loads and the maximum axial force due to lateral loading, respectively) (Zareian et al., 2010); 2) the backbone curve is modified by reducing the bending moment strength according to the $N - M$ interaction equations proposed in EC3-1-1, whilst no modification of the stiffness and deterioration parameters is performed.

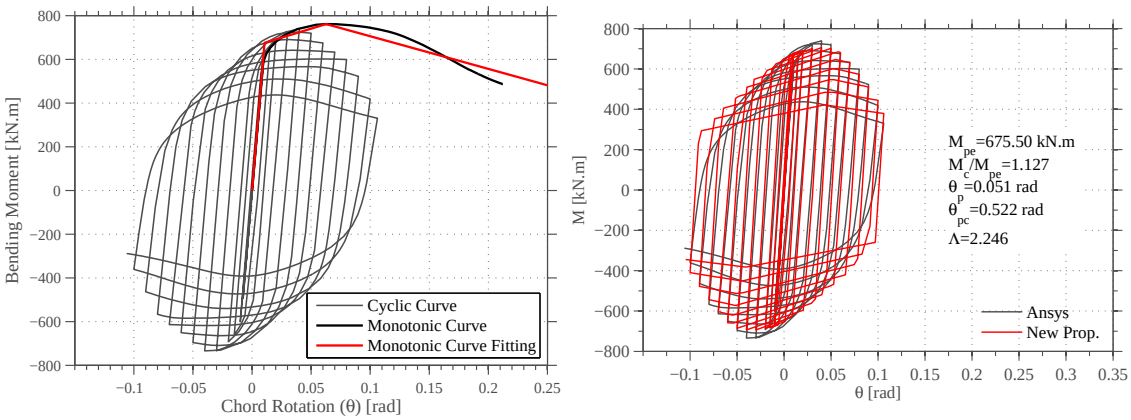

(a) (b)

Figure 2.8: Example of the calibration/modelling procedure of a HEB300 steel profile: a) calculation of strength and stiffness degradation parameters; b) Cyclic flexural behaviour of the member with the calibrated degradation parameters.

The panel zones of the steel frames were simulated with a beam-column joint element that is available in OpenSees. For the panel zone, the Krawinkler (1978) tri-linear moment-distortion relation was adopted. Furthermore, the design of the panel zones was attained with a "balanced" design methodology (Castro et al., 2008), and no strength degradation was considered. Figure 2.9 illustrates the adopted modelling strategy for the panel zones.

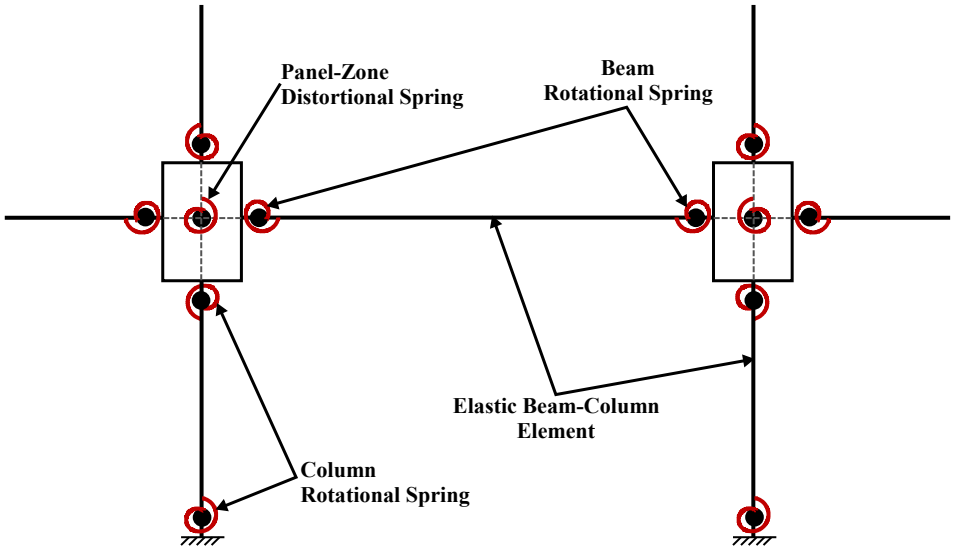

Figure 2.9: Numerical modelling illustration of the structural elements and panel zones.

2.4.2 Nonlinear static analysis

Nonlinear static pushover analysis was performed on each building considering a lateral load pattern proportional to the first-mode of vibration, following Equation 2.13, where F_i is the horizontal force acting at the floor i, λ is the load factor, m_i is the mass at floor i, $\phi_{(1,i)}$ is the ordinate of the fundamental mode at floor i, and N is the number of storeys.

$$F_i = \lambda \frac{m_i \phi_{1,i}}{\sum_1^N m_i \phi_{1,i}} \tag{2.13}$$

Figure 2.10 shows the lateral capacity curves for a building, located in Lisbon, designed using different values for the behaviour factor. In the figure, the grey circle displayed in the figures represents the formation of the first plastic hinge in the structure, V_{1y}. Also shown in the plots are the design (V_{design}) and elastic ($V_{elastic}$) base shears.

A first observation that can be extracted from Figure 2.10 is that the buildings designed for different ductility levels exhibit, as expected, different lateral resistances. However, the building that shows greater lateral capacity is the one designed with a higher behaviour factor. This observation is contradictory with the design philosophy, according to which, the adoption of an higher value of behaviour factor assumes a greater exploration of the nonlinear response and hence should result in a weaker lateral load resisting system. For the example presented in Figure 2.10, the design base shears considered for the buildings designed with the code recommended behaviour factors, 4 (DCM) and 6.5 (DCH), were much lower than the base shear corresponding to the formation of the first plastic hinge in the frame. This means that the structure would remain elastic for the design seismic intensity level defined in the code, which directly goes against the design assumptions. On the other hand, the building designed using IFBD (q=2.41) exhibits a behaviour that closely

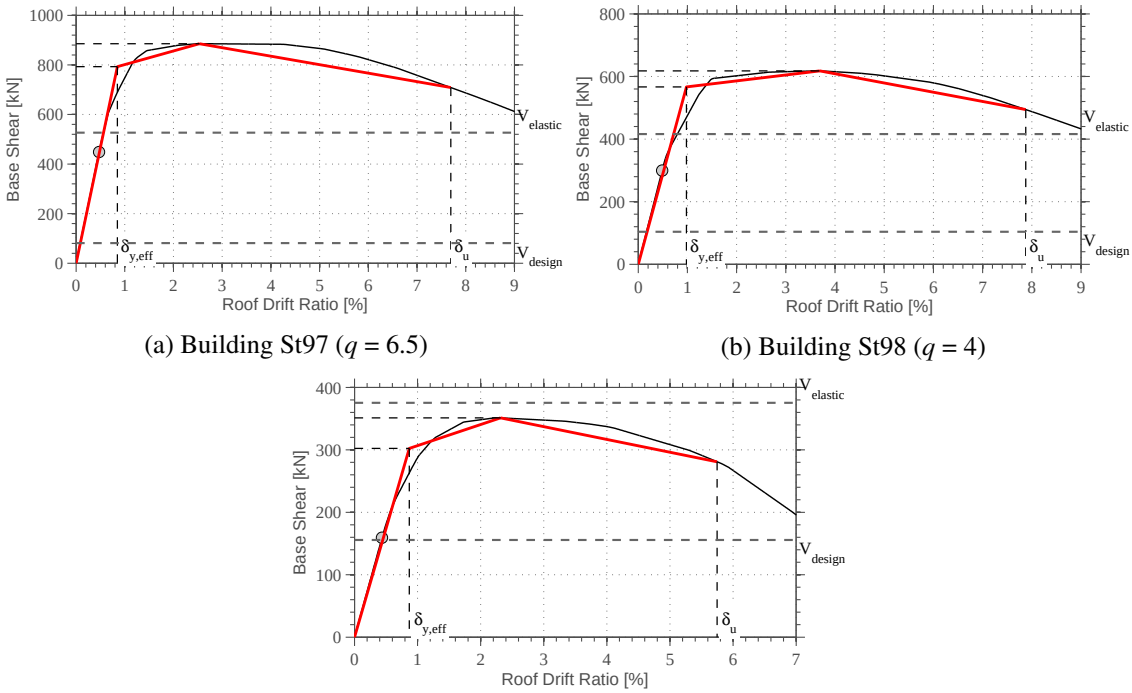

(a) Building St97 (q = 6.5)

(b) Building St98 (q = 4)

(c) Building St99 (IFBD)

Figure 2.10: Nonlinear static pushover results for configuration 1 buildings located in Lisbon.

matches the design considerations, i.e., the design base shear force is similar to base shear associated to the formation of the first plastic hinge in the structure. Moreover, despite the building being designed with a lower behaviour factor, a more consistent exploration of ductility is observed in comparison to the other scenarios. Two parameters with special interest can be derived from the capacity curves shown in the plots, namely the overstrength, Ω, and the building ductility, μ. Using the concepts introduced by Uang (1991), the overstrength factor is defined as the ratio of the maximum base shear resistance, V_{max}, and the design base shear, V_d, whereas the frame ductility is defined as the ratio of ultimate roof drift displacement, δ_u, to the effective yield roof drift displacement, $\delta_{y,eff}$. The ultimate roof drift displacement is herein defined as the displacement that occurs at a 20% reduction in strength after the peak lateral force is achieved. In order to find the effective yield roof drift displacement, the bilinearization of the capacity curve is performed according to the methodology prescribed in ASCE 41-13 (ASCE/SEI, 2013). Figure 2.11 shows the relation between the ductility of the building and the overstrength factor for all buildings.

As one may infer from Figure 2.11, the distributions of ductility values were consistently higher than 4.0. Due to the stiffness requirements imposed by the European seismic code, the frames designed with the recommended behaviour factors exhibit very high overstrength (i.e., a significant difference between the design base shear and the maximum base shear capacity) and higher available ductility. For buildings designed with the highest behaviour factor (q=6.5), values of overstrength between 6 to 10 were observed. On the other hand, for buildings designed with a lower prescribed value (q=4.0), the value of Ω varied between 3 and 6. Finally, for buildings

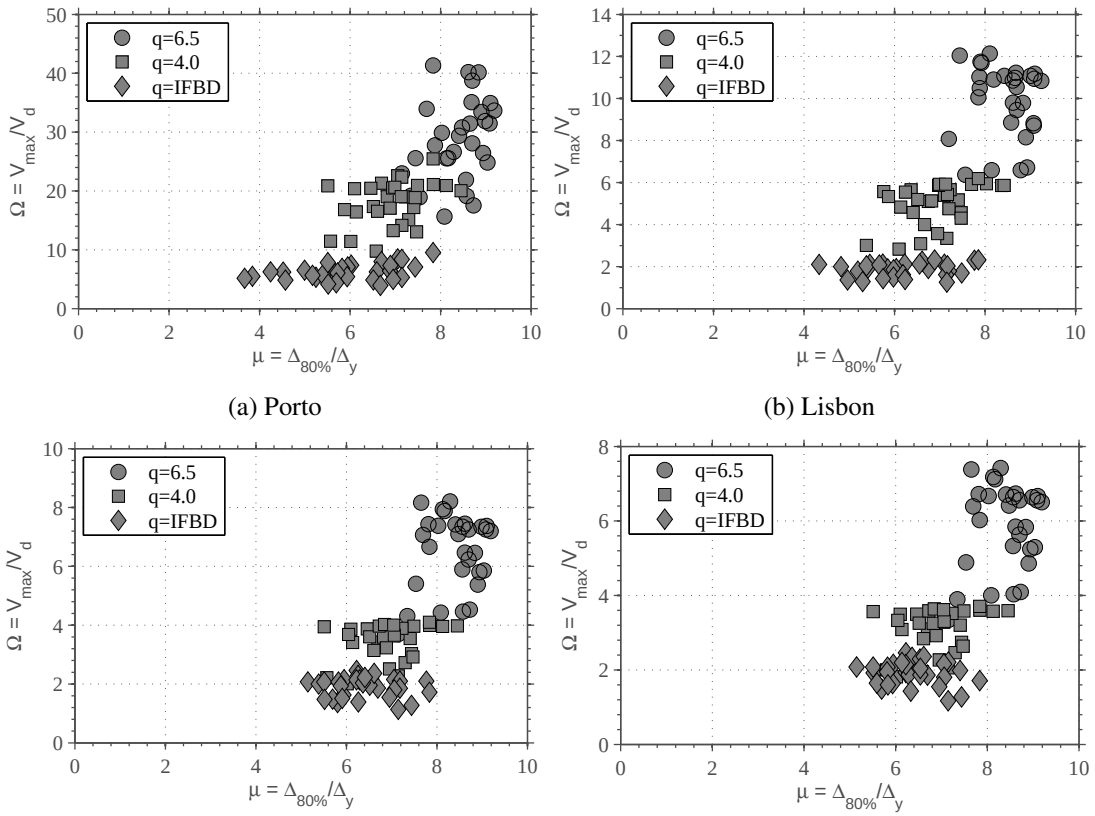

(a) Porto

(b) Lisbon

(c) Lagos (soil type B)

(d) Lagos (soil type C)

Figure 2.11: Building ductility vs. overstrength.

designed with the IFBD procedure, the overstrength was, on average, around 2, whilst always greater than 1. The overstrength observed for buildings located in Porto was fully conditioned by the stiffness requirements due to second-order effects, since lower seismic forces are acting in the structure compared to its capacity.

Another interesting aspect is related to the overstrength ratio (α_u/α_1) defined in EC8. According to the code the value of α_u/α_1 can be explicit determined using pushover analysis or alternatively recommended values for each lateral resistance structural system adopted. Moreover, EC8 specifies that the maximum value of α_u/α_1 that may be used in the design is equal to 1.6, even when non-linear static analysis was used. For steel MRFs a value of 1.3 for the α_u/α_1 is specified. Figure 2.12 the overstrength ratio (α_u/α_1) evaluated from the lateral capacity curves is shown, for all building locations.

As shown by the figure, the values of α_u/α_1 are independent of the behaviour factor adopted in the design and are always greater than the upper limit of 1.6 defined in the code. Additionally, it can be concluded that the value is practically insensitive to the number of storeys and building configuration. Importantly, the buildings designed using the IFBD procedure exhibit similar values of α_u/α_1 to those recorded in buildings designed with q equal to 4 and 6.5, indicating therefore similar levels of moment redistribution capacity.

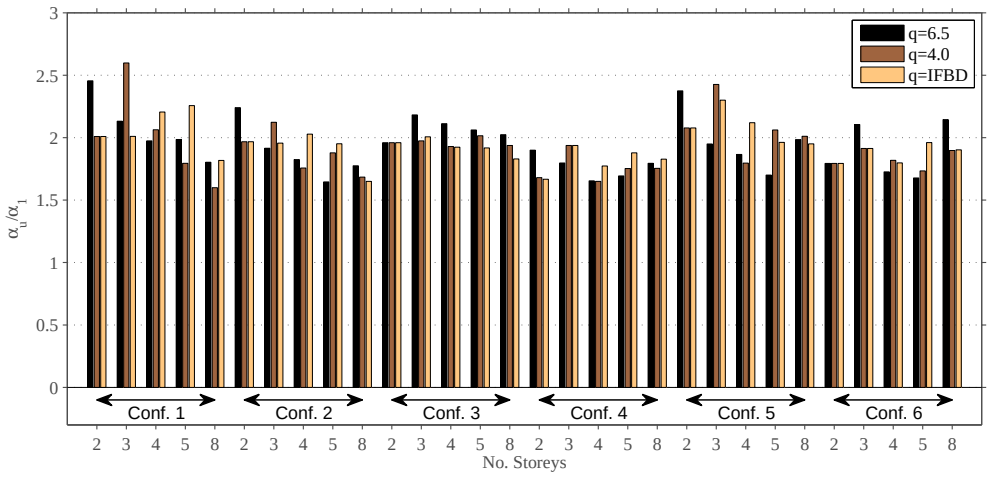

Figure 2.12: Building overstrength ratio (α_u/α_1) vs. q., for Lisbon.

2.4.3 Nonlinear response-history analysis

A more detailed and accurate seismic performance assessment requires the use of response-history analyses. These mainly consist of subjecting the numerical model of the structure to a suite of ground motion records that have been previously selected in accordance to code requirements, site location and other seismological parameters. EC8 establishes that a minimum number of three ground motion records must be used, in which the structural response parameter should be taken equal to the maximum value obtained from the analyses performed with the three ground motion records. Alternatively, if seven ground motion records or more are considered, the value of the structural response parameter can be computed as the average response value obtained for the set of ground motion records. Recently, Araújo et al. (2016) showed that a more accurate estimation of the average structural response parameter is obtained if ten ground motion records are used, whilst also implementing additional criteria to control, in the record selection process, the level of mismatch of each individual record in relation to the target spectrum.

In this research study, a suite of 40 ground motion records was selected for each site location using the SelEQ tool (Chapter 5), an advanced ground motion record selection and scaling framework, that allows the user to not only obtain the ground motion selection but also features the possibility to conduct probabilistic seismic hazard analysis (PSHA) for the European territory. Figure 2.13 shows the response spectra of the selected ground motion records for the site locations under study, as well as the corresponding mean and median response spectra. In general, a fairly good matching between the mean spectra of the selected ground motions and the code spectra was achieved.

Inherent viscous damping was considered through the adoption of Rayleigh damping, considering a damping ratio of 2.0% assigned to the first two fundamental periods of vibration. Following the recommendation and coefficient modifications proposed by Zareian and Medina (2010), initial stiffness proportional damping was assigned to the elements that remain elastic, and mass pro-

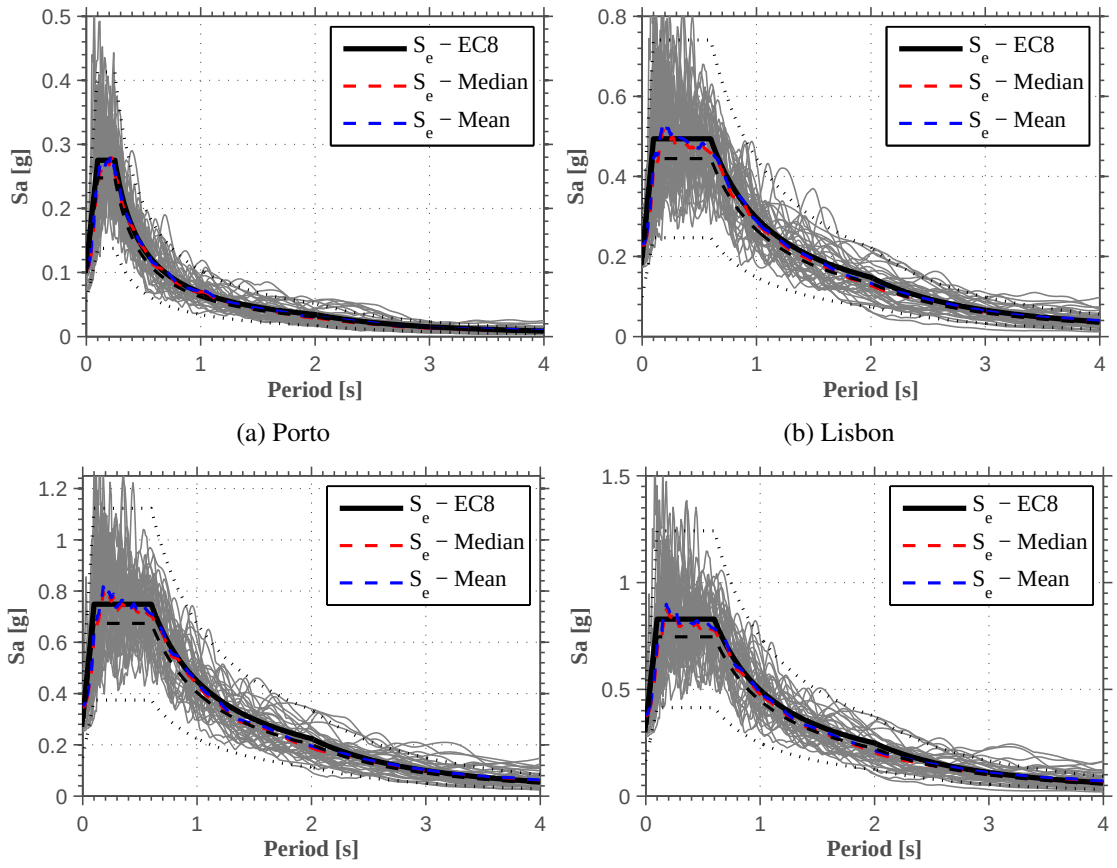

(a) Porto (b) Lisbon

(c) Lagos (d) Lagos (soil type C)

Figure 2.13: Response spectra of selected ground motion records and EC8.

portional damping to the nodes where the masses are lumped. Regarding the maximum time step used in the analysis, a sensitivity study was conducted for multiple engineering demand parameters, and a maximum value of 0.005s was defined. Additionally, in case of non-convergence during the analysis, a procedure was implemented that reduces the time step down to a value of 0.002s. Similar conclusions were drawn by the work of Barbosa et al. (2017), in which the authors pointed out that a time step of 0.002s produces negligible errors in the evaluation of the roof acceleration time-history response.

Response-history analyses were performed for two seismic intensity levels: frequent earthquake corresponding to the damage limitation limit state (SLS) and design earthquake corresponding to the non-collapse performance requirement (ULS). The performance evaluation of buildings was conducted for a set of structural response parameters that characterize both their local and global behaviour. For damage limitation, the structural response parameter considered was the distribution of maximum inter-storey drifts. Regarding the non-collapse requirement, the following structural response parameters were considered: i) distribution of maximum inter-storey drifts, ii) distribution of maximum floor accelerations, iii) ductility demands in the structural elements and iv) distribution of the inter-storey drift sensitivity coefficient, θ. Among the previously de-

fined structural response parameters, the maximum inter-storey drift pattern allows for an overall evaluation of the structural behaviour namely, the identification of undesirable plastic mechanisms. Moreover, the distribution of maximum floor accelerations is an important parameter in the evaluation of the performance, since non-structural components represent a significant fraction of building costs of repair in post-seismic scenarios, and damage observed in this components is usually well correlated to floor accelerations.

2.4.3.1 Damage limitation intensity level (SLS)

Regarding the evaluation of the seismic response for the damage limitation intensity level, Figure 2.14 shows the maximum inter-storey drift ratios for the structures located in Lisbon. In Figure 2.14, the distribution of inter-storey drift ratios (ISDR) along the height of the frames is shown, for the different behaviour factors considered. The results and observations obtained from the designs for Lisbon are representative of the remaining seismic zones. Thus, only the results for the structures located in Lisbon are shown herein.

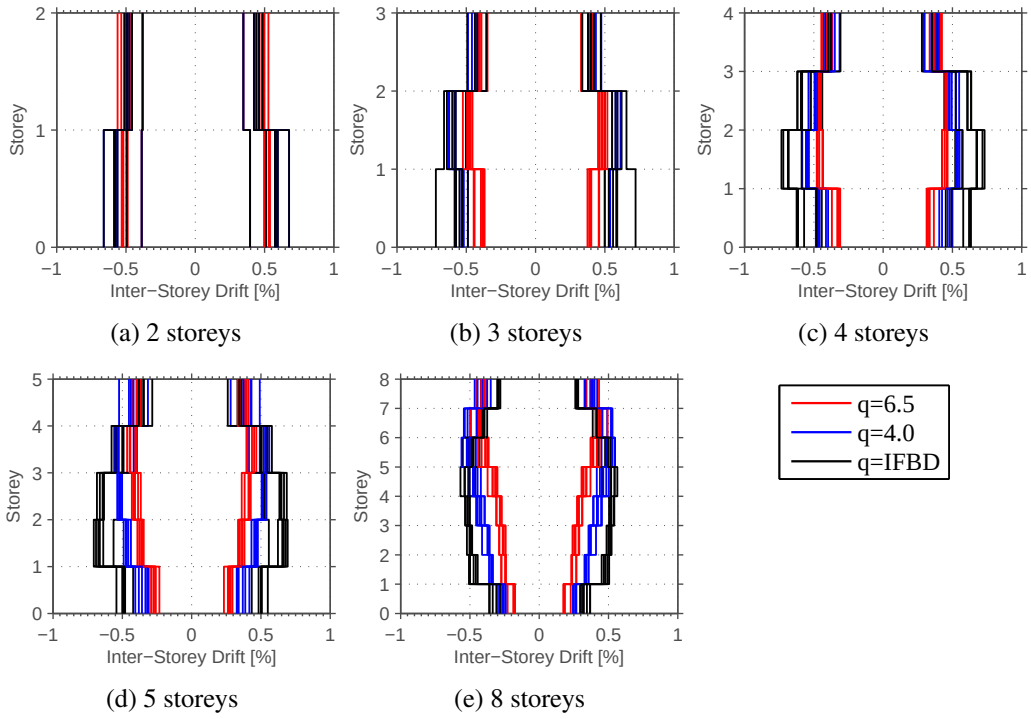

(a) 2 storeys (b) 3 storeys (c) 4 storeys

(d) 5 storeys (e) 8 storeys

Figure 2.14: Maximum inter-storey drift ratio at the damage limitation limit state for the structures located in Lisbon.

A careful inspection of the figure reveals that all buildings fulfil the damage limitation criteria considered at the design stage (ISDR<1%). Nevertheless, for buildings with more than three storeys, the designs using the EC8 recommended behaviour factors clearly exhibited lower inter-storey drifts in comparison to those designed with the IFBD procedure. This observation is in agreement with the results obtained at the design stage, where the taller configurations were often

governed by stiffness requirements related to the consideration of second-order effects. In contrast, the low-rise configurations were usually controlled by member strength requirements, leading to the same structural solution, regardless of the behaviour factor adopted and, for this reason, the differences in the ISDR are not so pronounced. Another important conclusion from the results shown in Figure 2.14 is the expected low inelastic demand in buildings for the serviceability seismic intensity level, since for these values of ISDR the frames are close to the value of first plastic hinge formation observed in the pushover analyses.

2.4.3.2 Non-collapse intensity level (ULS)

Regarding the seismic response for the non-collapse seismic intensity level (ULS), Figure 2.15 shows the maximum inter-storey drift ratios for the structures designed for Lagos (soil type C).

As expected, the inter-storey drifts observed for the buildings designed with the IFBD procedure are higher than those recorded in the buildings designed with EC8 prescribed behaviour factors. Nevertheless, there was no evident concentration of deformation over the building height, which indicated the absence of undesirable soft-storey mechanisms. Moreover, the ISDR in the IFBD-designed buildings exhibited a uniform distribution over the building height, which reflects a uniform distribution of plasticity. In addition, it should be noted that the maximum ISDR were always below the 2.0-2.5% limit that is typically prescribed in performance-based assessment guidelines (e. g. ASCE 41-13 (ASCE/SEI, 2013)).

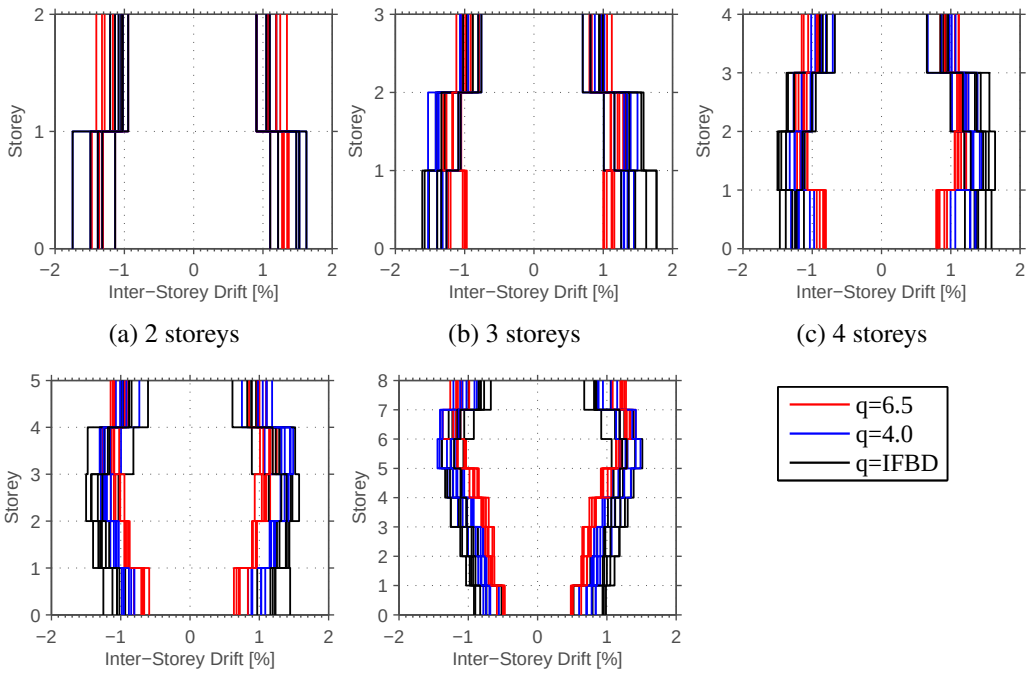

(a) 2 storeys (b) 3 storeys (c) 4 storeys

(d) 5 storeys (e) 8 storeys

Figure 2.15: Maximum inter-storey drift ratio at ULS for the structures located in Lagos (soil type C).

The maximum floor accelerations recorded for the ULS are shown in Figure 2.16, and the maximum inter-storey drift sensitivity coefficients, θ, obtained during the response-history analysis and computed according Equation 2.3, are shown in Figure 2.17. In both figures, only the results obtained for the structures designed for Lagos (soil type C) are shown, since the results and observations for the remaining structures were similar.

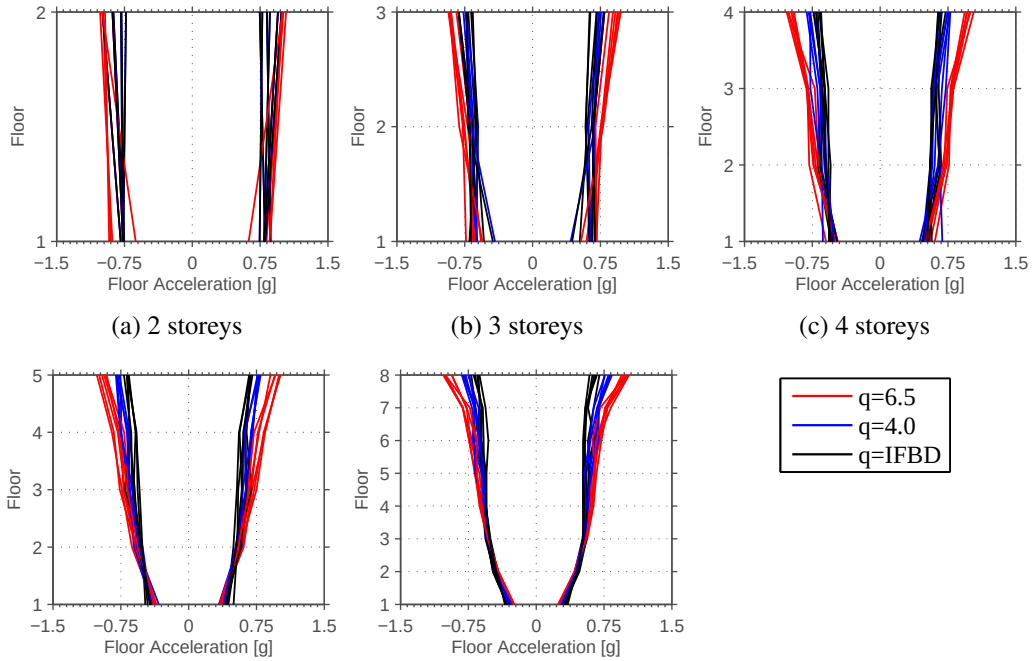

(a) 2 storeys (b) 3 storeys (c) 4 storeys

(d) 5 storeys (e) 8 storeys

Figure 2.16: Maximum peak floor acceleration at ULS for the structures located in Lagos (soil type C).

The analysis of the results shown in Figure 2.16 allows concluding that the IFBD designs exhibited lower levels of floor acceleration for all configurations and heights. This difference is even more pronounced in buildings with more than three storeys. As previously mentioned, lower floor accelerations are often associated with less damage to non-structural acceleration sensitive components. Nevertheless, higher ISDR values are an indicator of higher levels of damage to non-structural drift-sensitive components. If this balance allows for similar "overall" damage levels, the option for the lighter structural solution could mean significant economic savings, and thus be a preferable one. Finally, from Figure 2.17 one is able to infer that buildings designed with the EC8-prescribed behaviour factors are consistently associated to very low values of θ, not consistent with the values obtained at the design stage, which were close to 0.2. Since the design of these buildings was often controlled by stiffness requirements related to the control of second-order effects, it is clear that the inaccurate evaluation of the θ coefficient has severe implications in the final structural solution.

Another important parameter to evaluate concerns the ductility demands observed in the beams, for the same seismic intensity level. Figure 2.18 shows the results obtained for the 3-storey and

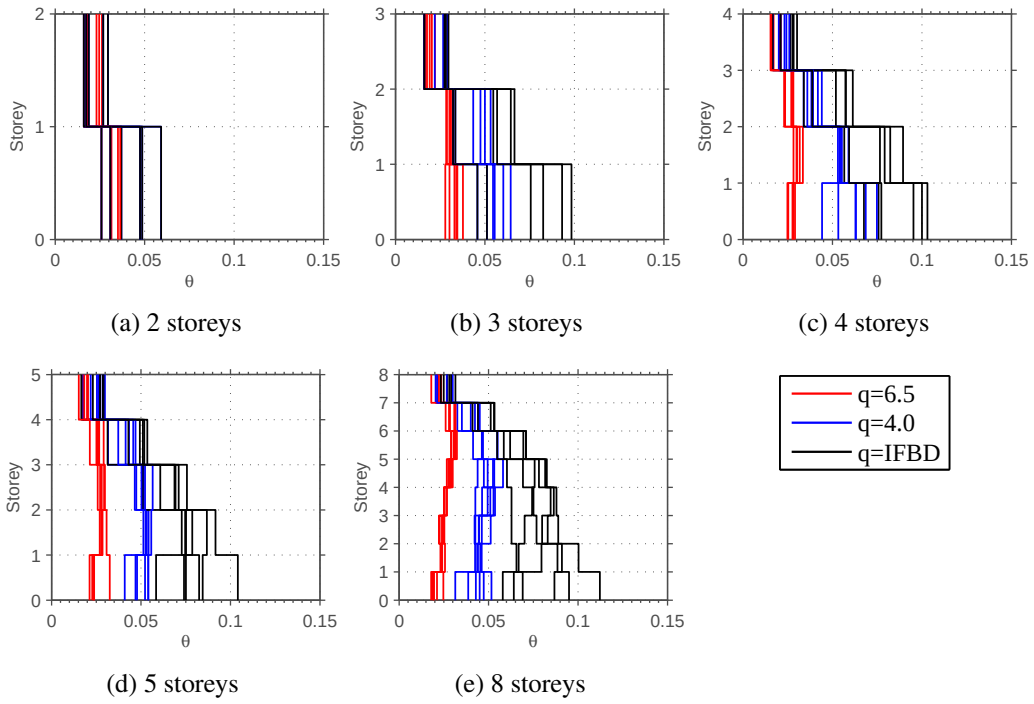

(a) 2 storeys (b) 3 storeys (c) 4 storeys

(d) 5 storeys (e) 8 storeys

Figure 2.17: Stability coefficient (θ) at ULS for the structures located in Lagos (soil type C).

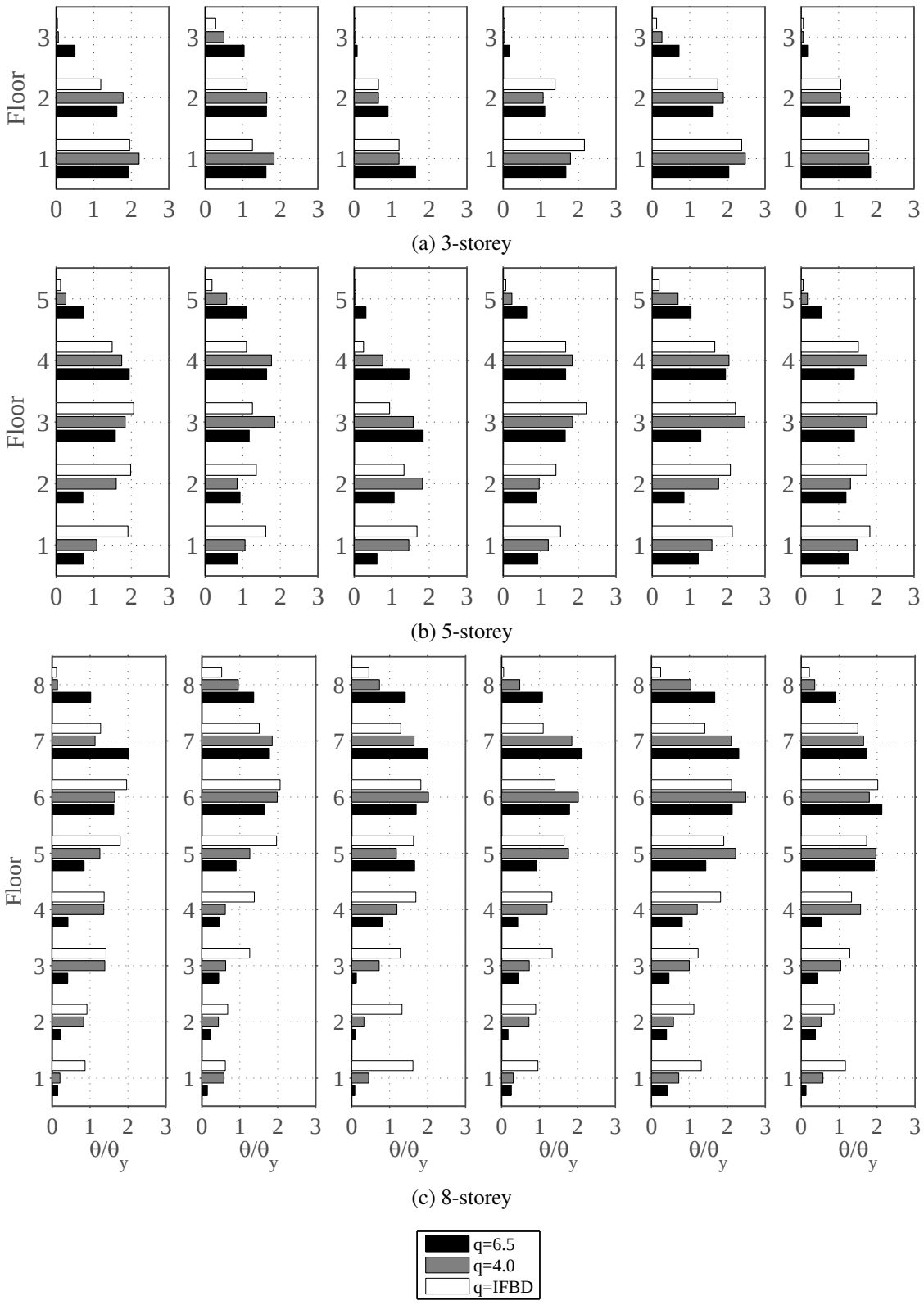

Figure 2.18: Beam ductility demands at ULS for the structures located in Lagos (soil type C).

8-storey structures designed for Lagos (soil type C).

As one may infer from Figure 2.18, despite the assumption of a medium or high level of ductility demand at the design stage, the buildings designed with the EC8-recommended behaviour factors generally exhibit the lowest levels of ductility demand in the beams. On the other hand, the buildings designed with the IFBD procedure were consistent with the design assumptions. This strengthens the already pointed-out observation that the IFBD-designed buildings show a more predictable and consistent behaviour with the design assumptions. Additionally, as already identified in the ISDR results, the distribution of plasticity demands along the height of the building is more uniform for the IFBD-designed structures, with the other buildings showing concentration of plastic demands in the upper storeys. These results clearly demonstrate the advantages of using the IFBD procedure for the selection of the behaviour factor in comparison with the use of the code-recommended behaviour factors. As for the ductility demands in the columns, the first storey columns consistently showed ductility demands greater than one, indicating that no plastic hinges would occur in columns at higher storeys. Therefore, it can be concluded that there are no undesirable soft-storey column-mechanism developing in the buildings.

The results shown thus far allow concluding that the use of the IFBD methodology for the definition of the behaviour factor allows not only to obtain lighter structural solutions but also structures with a more predictable and consistent behaviour with the design assumptions. Through the nonlinear response-history analysis, it was possible to confirm that the all buildings comply with the code requirements, exhibiting adequate lateral stiffness and strength. Additionally, there was no evidence of the formation of undesirable soft-storey mechanisms in the structures, regardless of the behaviour factor adopted.

2.4.4 Collapse risk assessment

The collapse assessment of the buildings is now performed through the conduction of incremental dynamic analysis (IDA) (Vamvatsikos and Cornell, 2002). The first mode spectral acceleration, $S_a(T_1)$, was considered as the seismic intensity measure, IM, and the maximum inter-storey drift as the engineering demand parameter, EDP. In each analysis, the sidesway collapse was defined as the instant in which dynamic instability occurs, that is, the point where a significant increase of displacements is observed without a relevant increase of lateral inertia forces (Karavasilis et al., 2015; Ramirez and Miranda, 2012; Hwang and Lignos, 2017). In the evaluation of the collapse fragility curve of each building, aleatory or record-to-record variability, β_{RTR}, and epistemic or modelling uncertainty, β_{MDL}, were taken into account. The total uncertainty, β_{TOT}, was computed using Equation 2.14, assuming that both uncertainties are independent and lognormally distributed (Liel et al., 2009; Tzimas et al., 2016).

$$\beta_{TOT} = \sqrt{\beta_{RTR}^2 + \beta_{MDL}^2} \tag{2.14}$$

Following the FEMA 695 recommendations (FEMA, 2009), record-to-record variability and modelling uncertainty were taken as 0.40 and 0.35, respectively, resulting in a value of total system

uncertainty equal to 0.53. The median collapse capacity was adjusted to account for the spectral shape effect according to Method 2 proposed by Haselton et al. (2009). Figure 2.19 shows the IDA curves and the corresponding collapse fragility curves before spectral shape adjustment.

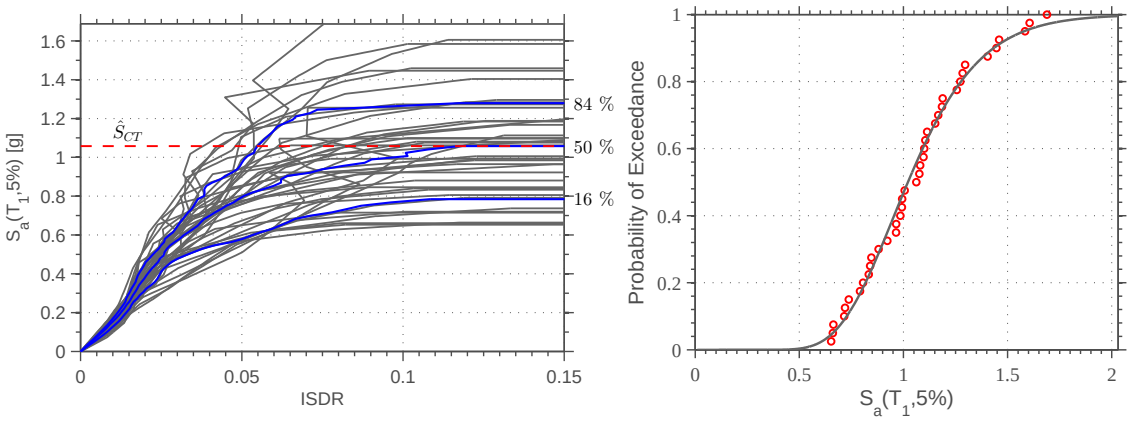

(a) IDA (b)

Figure 2.19: IDA curves and collapse fragility curves for building St99 (configuration 1, 4 storeys, q=IFBD) located in Lisbon.

Figure 2.20 show the collapse fragility curves of all the buildings. The seismic intensity measure, $S_a(T_1)$, was normalized by the design spectral acceleration at the fundamental period of the building in order to simplify the identification of the collapse probability. Inspection of the plots shown in the figures reveals that, for the seismic design intensity level, all buildings exhibit a probability of global collapse lower than 5%, indicating therefore the presence of significant reserves of lateral strength. This allows concluding that, regardless of the behaviour factor adopted, all buildings meet the non-collapse performance requirement. However, as previously established in this research study, frames designed with the IFBD procedure are associated to significant material savings in comparison to equivalent designs with the EC8-recommended behaviour factors, whilst being in full compliance with the code requirements.

Despite the acceptable performance identified in the fragility curves analysed for the seismic design intensity level, the effectiveness of each building's structural solution is better assessed on the basis of the evaluation of the mean annual frequency of collapse or seismic risk. This takes into consideration all possible levels of seismic intensity, weighted by the corresponding probabilities of occurrence. Computation of the seismic risk was performed by integrating the collapse fragility curve of the structure over the seismic hazard curve at the site (Eads et al., 2013) as:

$$\lambda_C = \int_0^\infty P(C|IM)d\lambda(IM) = \int_0^\infty P(C|IM)\left|\frac{d\lambda(IM)}{dIM}\right|dIM \tag{2.15}$$

where $P(C|IM)$ is the probability that the structure will collapse given that the ground motion intensity is $IM = im$, $d\lambda(IM)$ is the mean annual frequency of the ground motion intensity and $|d\lambda(IM)/d(IM)|$ is the derivative of the seismic hazard curve.

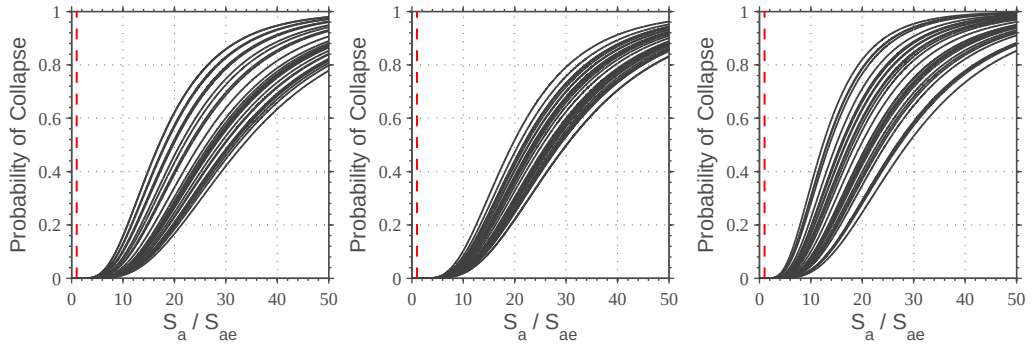

(a) Porto - q=6.5 (b) Porto - q=4.0 (c) Porto - q=IFBD

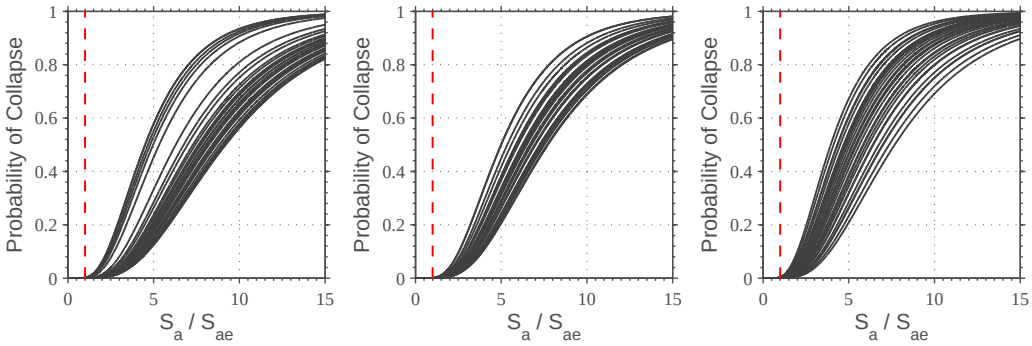

(d) Lisbon - q=6.5 (e) Lisbon - q=4.0 (f) Lisbon - q=IFBD

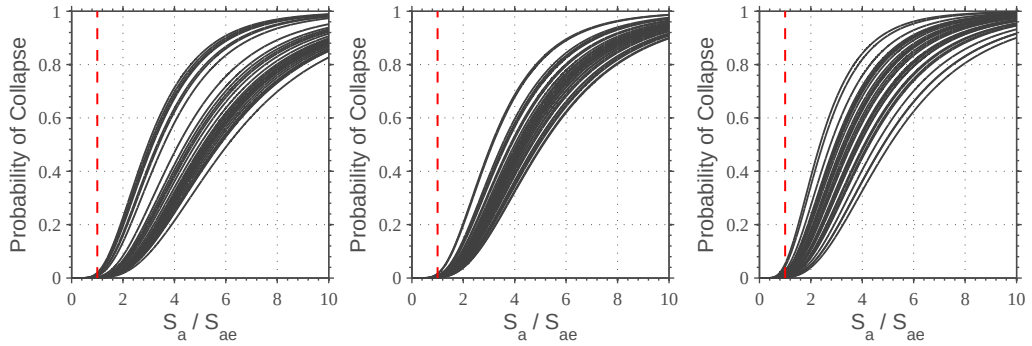

(g) Lagos B - q=6.5 (h) Lagos B - q=4.0 (i) Lagos B - q=IFBD

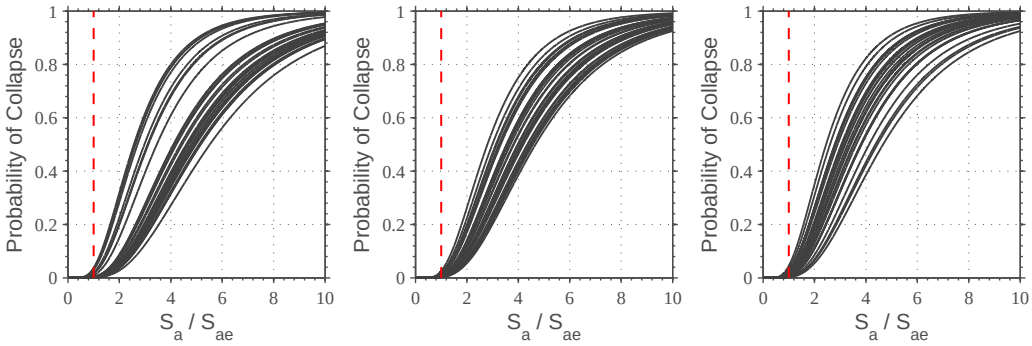

(j) Lagos C - q=6.5 (k) Lagos C - q=4.0 (l) Lagos C - q=IFBD

Figure 2.20: Collapse fragility curves of all buildings.

The site hazard curves for all buildings in the Portuguese territory were computed through PSHA using the open source software OpenQuake (Pagani et al., 2014) and the seismic hazard models developed in the SHARE project (Woessner et al., 2015). It should be noted that, for the Portuguese territory, the seismic hazard models developed in the SHARE project were implemented, but with the inclusion of additional hazard sources (Vilanova and Fonseca, 2007) and using the ground motion prediction equations from Atkinson and Boore (2006) and Akkar and Bommer (2010), with a weight of 70% and 30%, respectively (Silva et al., 2015). Figure 2.21 shows the hazard curves associated to four buildings located in Lisbon and Lagos.

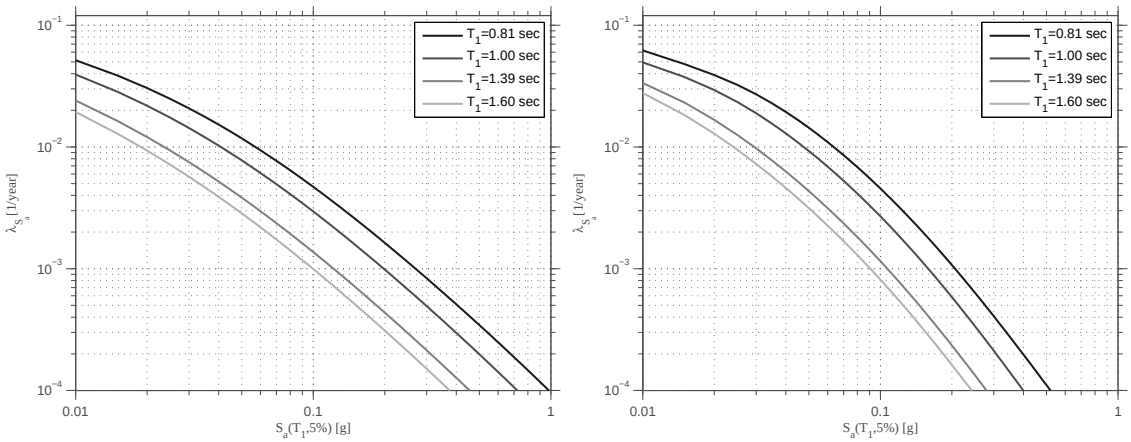

(a) Lisbon (b) Lagos

Figure 2.21: Seismic hazard curves.

Figure 2.22 shows the mean annual frequency of collapse (seismic risk) for all buildings. It is possible to conclude that, in general, the IFBD-designed buildings are characterized by higher seismic risk, in comparison to the other buildings considered in the study. However, the differences observed can only be assessed by considering a reference value of acceptable seismic risk, which is not usually specified by seismic codes. Following the approach proposed by Pinto and Franchin (2014), a maximum value of the mean annual frequency of exceedance of the non-collapse limit state of 0.0047 was adopted. As shown in the figures, all buildings comply with this limit.

Another useful seismic metric is the probability of collapse over the buildings lifetime, which, for a common building, is set at 50 years. Based on the Poisson assumption, the probability of collapse over the building lifetime can be computed as shown in Equation 2.16, where λ_c is the mean annual frequency of collapse.

$$P(Collapse\ in\ 50\ years) = 1 - e^{-\lambda_C \times 50} \tag{2.16}$$

Table 2.6 shows the maximum and minimum probabilities of collapse in 50 years for each site location.

As one may conclude from Table 2.6, the highest values of probability of collapse in 50 years were consistently associated with the buildings designed according to the IFBD procedure. How-

Table 2.6: Probabilities of collapse in 50 years (%)

Location	q=6.5		q=4.0		q=IFBD	
	max	min	max	min	max	min
Porto	0.02	0.003	0.013	0.004	0.03	0.004
Lisbon	0.27	0.05	0.20	0.07	0.31	0.07
Lagos (soil type B)	0.07	0.007	0.06	0.01	0.11	0.01
Lagos (soil type C)	0.21	0.01	0.17	0.02	0.22	0.02

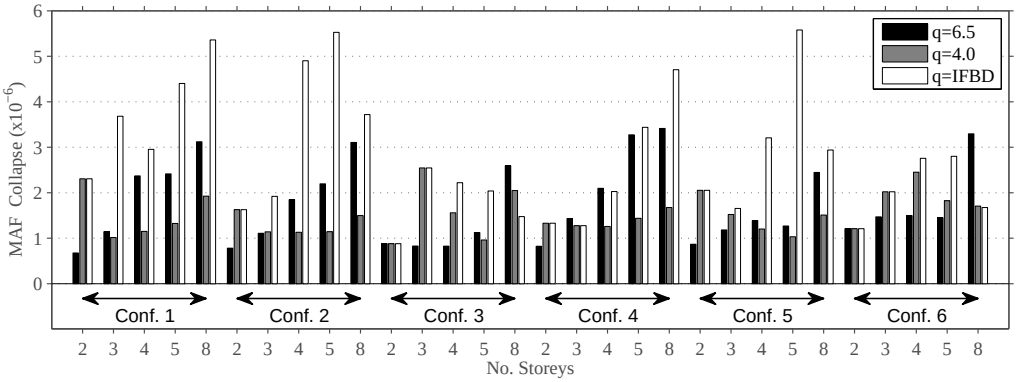

(a) Porto

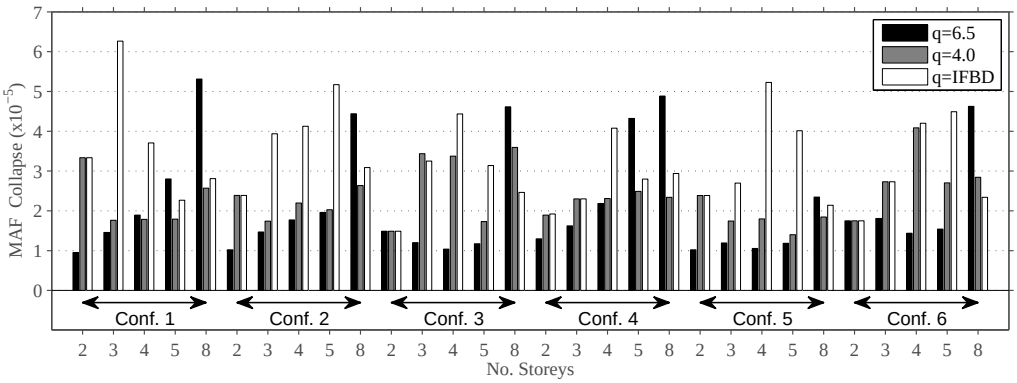

(b) Lisbon

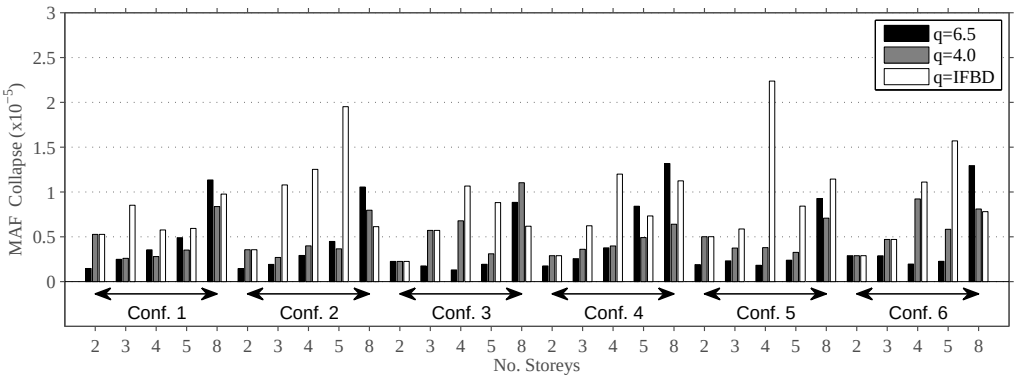

(c) Lagos

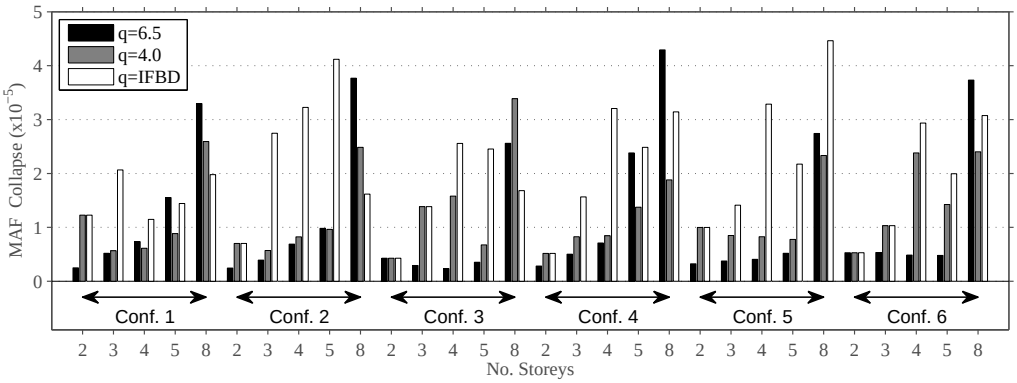

(d) Lagos (soil type C).

Figure 2.22: Mean annual frequency of collapse for all buildings.

ever, even for this scenario, the results clearly demonstrate the very low probabilities of collapse of all buildings over the building lifetime, regardless of the value of behaviour factor considered in the design.

2.5 Conclusions

In this Chapter, current European seismic design provisions for steel moment-resisting frames, considering different ductility classes, were investigated. A set of 360 buildings, located in 4 different locations, were designed considering code-recommended behaviour factors and a recent proposal for the definition of the behaviour factor (Villani et al., 2009), designated as Improved Force-Based Design (IFBD), that fully complies with the requirements of EC8. This procedure defines the behaviour factor whilst taking into account the actual properties of the structure and site location of the building. From the analysis of the obtained results, the following conclusions can be withdrawn:

- The seismic design of steel moment-resisting frames using code-recommended behaviour factors are typically controlled by stiffness requirements due to second-order effects, with the exception of low-rise buildings, in which member-strength requirements may govern the design. Current code provisions related to the control of second-order effects can be interpreted as a requirement of storey lateral elastic stiffness that is directly proportional to the value adopted for the behaviour factor, leading in this way to heavier structural solutions;
- The application of the IFBD procedure allows the designer to achieve significant material savings, whilst the structural solutions obtained are in full compliance with the requirements of the European seismic design code;
- A comparison of the designs based on the results from nonlinear static analyses clearly demonstrated the discrepancy between the design assumptions and the obtained structural solution when code recommended behaviour factors are used. The significant difference between the design base shear and the capacity of the buildings leads to structural solutions that, in many cases, will remain elastic for the seismic design intensity level. On the other hand, buildings designed with a behaviour factor evaluated according to the IFBD procedure are more consistent in this aspect, and take advantage form the available ductility;
- Response-history analyses showed that the IFBD buildings comply with code requirements at both damage limitation and non-collapse limit states, exhibiting adequate stiffness and strength. Concerning ductility demands, the IFBD-designed buildings exhibited more uniform inelastic demands over the building height and ductility values compatible with the design assumptions. Conversely, buildings designed considering medium and high ductility classes as defined in EC8, do not take advantage of the available ductility, exhibiting ductility demands similar or lower to those observed in the IFBD-designed buildings. Additionally, it should be mentioned that there was no evidence of the formation of an undesirable soft-storey column-mechanism in any of the buildings considered in this study;

- In line with the conclusions extracted in previous studies regarding the evaluation of second-order effects in seismic design of buildings according to EC8 (Peres and Castro, 2010), the results obtained in this study highlight the inconsistency between the value of the inter-storey drift sensitivity coefficient parameter, θ, evaluated at the design stage and the values recorded in the response-history analyses;
- The mean annual frequency of collapse, or seismic risk, was evaluated for all buildings considered in the study. Despite the higher values observed for the buildings designed with the IFBD procedure, all structures comply with the limit proposed by (Pinto and Franchin, 2014). Additionally, the values of probability of collapse in 50 years were computed, with all buildings showing fairly low probabilities of collapse over the building lifetime.

Apart from the considerable savings of material that can be achieved with the application of the IFBD procedure for the evaluation of the behaviour factor to adopt in seismic design, a more rational selection of the behaviour factor provides practitioners with a more realistic and accurate prediction of the structural response, and, consequently, of the expected inelastic demands. The proposed IFBD procedure can therefore be extended for other materials and structural systems, in order to provide engineers with a more realist idea of the expected seismic behaviour of the structures being designed.

Chapter 3

Calibration of strength and stiffness deterioration parameters for European steel open-sections

3.1 Introduction

Nonlinear dynamic analysis has become the reference procedure to assess the seismic performance of earthquake resistant buildings. For an accurate evaluation of the behaviour of steel buildings under seismic loads, two important requirements usually stand-out: (i) an accurate numerical modelling strategy; (ii) an accurate definition of the seismic input. Focusing on the former, it is well established that modelling-related issues assume a prominent role in the assessment of the seismic behaviour of steel structures (Liel et al., 2009). Phenomena such as local buckling, member strength and stiffness deterioration (Lignos and Krawinkler, 2010, 2012) can have a significant influence on both local and global structural responses.

Generally speaking, nonlinearity in the response of beam-column elements can be simulated with two different approaches, namely concentrated and distributed plasticity. Considering the former, inelasticity is lumped at critical member regions through nonlinear springs, generally associated to the locations where plastic hinges are expected to occur. These concentrated plasticity springs will play a dominant role on the inelastic response of the member, since the remaining portion of the member is simulated through fully elastic finite elements. To what concerns the latter modelling approach (i.e. distributed plasticity), inelastic behaviour can occur at any given location along the element (Fragiadakis and Papadrakakis, 2008). This is attained via explicit simulation of the member's cross-section along its length, trough the coupled use of fibre discretization and a given material constitutive behaviour. Both modelling approaches encompass advantages and disadvantages. For example, distributed plasticity models account for the interaction between axial force and bending moment (N-M) and take into consideration the spread of plasticity along the length of the member. However, current distributed plasticity models fail to capture deterioration-related phenomena, such as local buckling and lateral torsional buckling.

Furthermore, localization phenomena (i.e. a numerically-related issue in which damage is incorrectly concentrated in a single "infinitesimal" position of the member) can occur, particularly when dealing with reinforced concrete members. In turn, concentrated plasticity models can simulate strength and stiffness deterioration phenomena, being generally regarded as more computationally efficient. Notwithstanding, this type of models are associated to the inability to account for N-M interaction effects, an aspect that can play a crucial role in the response of columns under significant and variable axial compression. In the context of concentrated plasticity springs for flexural response, a moment–rotation relationship must be defined in the numerical model. This process can be considered to be somewhat more challenging than the distributed plasticity counterpart (e.g. fibre discretization coupled with uniaxial stress-strain constituive model), and hence may carry added levels of complexity to the model definition. Given the relevance of cyclic strength and stiffness degradation effects in steel beam-column elements, as denoted in the previous paragraph, this research study fully focuses on modelling aspects associated to the concentrated plasticity approach.

Recently, Lignos and Krawinkler (2010, 2012), proposed several moment-rotation relationships intended for concentrated plasticity models, aiming at a realistic representation of the behaviour of steel beam-column elements. The base hysteretic model (proposed by Ibarra et al. (2005)) has the ability to incorporate cyclic strength and stiffness deterioration, which the authors have calibrated against the behaviour of typical American steel profiles, on the basis of an extensive database with more than 350 experimental tests. In the European context, however, in which the profiles available in the steel industry differ from the American counterparts, no information is currently available in the literature. Furthermore, although recent studies have shown the influence of the axial load on the deformation capacity of deep wide-flange steel members (Elkady and Lignos, 2015), these parameters have yet to be calibrated to account for this effect.

Given the background provided in previous paragraphs, the present study aims at the calibration of the parameters of the Ibarra et al. (2005) hysteretic model based on the behaviour of European open-section steel profiles (e.g. "I"-shape or IPE, "H"-shapes HEA, HEB and HEM), on the basis of detailed and simplified finite element analyses under uniaxial bending. In order to conduct the calibration of these degradation parameters, a robust optimization methodology, based on the Harmony Search optimization algorithm (Macedo et al., 2013), was employed. The proposed numerical modelling procedure was validated against experimental data from a recent full-scale test conducted on a steel moment-resisting frame (Ryu et al., 2011) subjected to cyclic lateral loading. A comprehensive database of European steel open-section profiles was defined, being used for application of the aforementioned optimized calibration framework. The database of results obtained in this context, assembled under the form of regression-fitted equations, can be used by both researchers and practitioners when dealing with the seismic performance and collapse assessment of steel structures built with European steel open-sections.

3.2 Detailed finite element model

In order to establish an accurate and reliable model to simulate the flexural behaviour of steel open-section members, a finite element (FE) model was calibrated against existing experimental data (Araújo et al., 2017). The specimens tested by D'Aniello et al. (2012) under monotonic and cyclic loading conditions were modelled using the numerical modelling software ANSYS (ANSYS, 2013). The specimens consist of a set of steel cantilever columns, made with European commercial hot-rolled steel open-sections (HEB240, HEA160 and IPE300), with a height of 1.885m.

Regarding the numerical model, the SHELL181 thin-walled finite element available in the software was used, considering five Gauss points across the plate thickness. A fairly refined mesh of 0.02×0.02 m was adopted for the first third of the length of the member, in order to adequately simulate the development of local buckling, whilst elements with double the size were adopted for the remaining portion of the member. A mesh sensitivity study was conducted to support the adopted meshing solution. In order to accurately replicate the cyclic and monotonic behaviour of the members, two distinct material models were used. The monotonic behaviour was simulated considering a multi-linear kinematic material model with hardening. In this case, the engineering stress-strain relationships obtained from the material characterisation of the specimens were converted into true stress-strain relationships and introduced directly in the FE models. Moreover, it was observed that the inclusion of local geometrical imperfections in the model, according to the tolerances specified for fabrication in EN 10034 (CEN, 1993), is of critical importance to accurately capture the experimental results (Araújo and Castro, 2013). Regarding the cyclic behaviour of steel members, this was modelled using a nonlinear kinematic material model with hardening (Chaboche, 2008), combined with a nonlinear isotropic hardening model. Both parameters of the model, i.e. the initial hardening modulus, C_i, and the rate at which the hardening modulus decreases with increasing plastic strain, γ_i, (Chaboche, 2008), were calibrated on the basis of the experimental data so as to provide a good agreement between the numerical and experimental results. The loading was imposed laterally at the top of the member and the AISC (ANSI, 2005) loading protocol was adopted. The boundary conditions were defined so that no flexural-torsional instabilities would occur (D'Aniello et al., 2012).

Regarding the comparison between the experimental and numerical results obtained with the model described above, Figure 3.1 illustrates the ability of the FE model to represent the local instabilities that develop in the member. In particular, the coupled in-plane and out-of-plane instability mechanism observed more clearly in the IPE300 member (Figure 3.1 b) is well simulated, despite the presence of torsional restraints at both ends. Figure 3.2 depicts the comparison of monotonic and cyclic moment-rotation behaviours of all tested specimens. As shown, the FE models are able to accurately capture the onset of local buckling, i.e. the point from which the deterioration of the member initiates, as well as the actual strength deterioration of the member. Although the Bauschinger component of the hysteretic behaviour and the unloading stiffness deterioration (Jiao et al., 2011) were not completely reproduced in the HEB240 member, resulting in

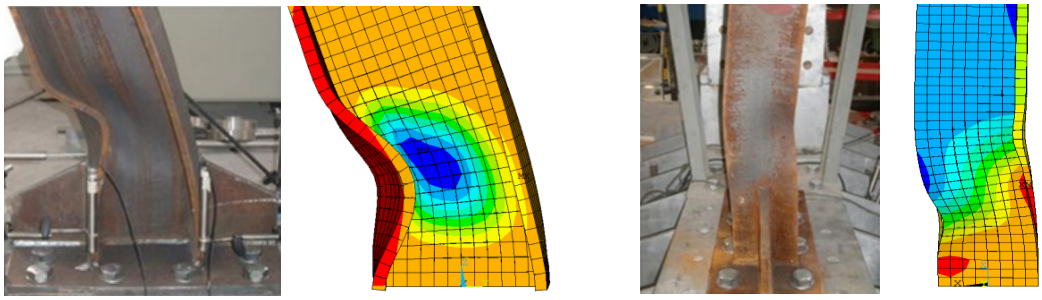

(a) (b)

Figure 3.1: Experimental and numerical deformation modes of two steel members: a) instability mechanism of an HEB240 specimen; b) coupled in-plane and out-of-plane instability mechanism of an IPE300 specimen.

slightly "fatter" hysteretic loops and higher energy dissipation levels, the prediction of the strength deterioration of the member with the number and amplitude of cycles was not affected. In the case of the IPE300 member, the numerical model was equally able to accurately capture the unloading stiffness deterioration resulting from the coupled buckling mechanism illustrated in Figure 3.1 b.

Based on the comparisons shown above, it can be concluded that the detailed numerical modelling approach adopted leads to fairly accurate and reliable response estimates, regarding both local deformation modes and global moment-rotation behaviours.

3.3 Calibration of Ibarra et al. (2005) strength and stiffness deterioration hysteretic model using optimization algorithms

As previously stated, a number of modelling strategies can be adopted to simulate the nonlinear response of steel members (Macedo et al., 2015). Whereas distributed plasticity models are known to better capture yielding and the interaction between bending and the axial load, concentrated plasticity models can capture, in a more empirical manner, strength and stiffness degradation effects and are more consistent with the common limit state checks prescribed in current building codes (ATC, 2010). In fact, strength and stiffness deterioration is a key behaviour characteristic of steel members, which is triggered by local and torsional instability phenomena, as shown in Figure 3.1. Thus, concentrated plasticity models are typically a preferable option for modelling the behaviour of this type of members when subjected to earthquake loads.

Amongst the proposals available in the literature, the Ibarra et al. (2005) hysteretic model stands out as a concentrated plasticity model that accounts for deterioration effects of the flexural response. This model is based on the following three concepts: (i) a backbone curve that sets the bounds within which the hysteretic behaviour of the member is confined. In the absence of monotonic-to-cyclic deterioration, the cyclic backbone curve is similar to the monotonic behaviour of the member, and is referred to as the initial or monotonic backbone curve. As soon as cyclic deterioration sets in, the backbone curve starts moving towards the origin and is continuously

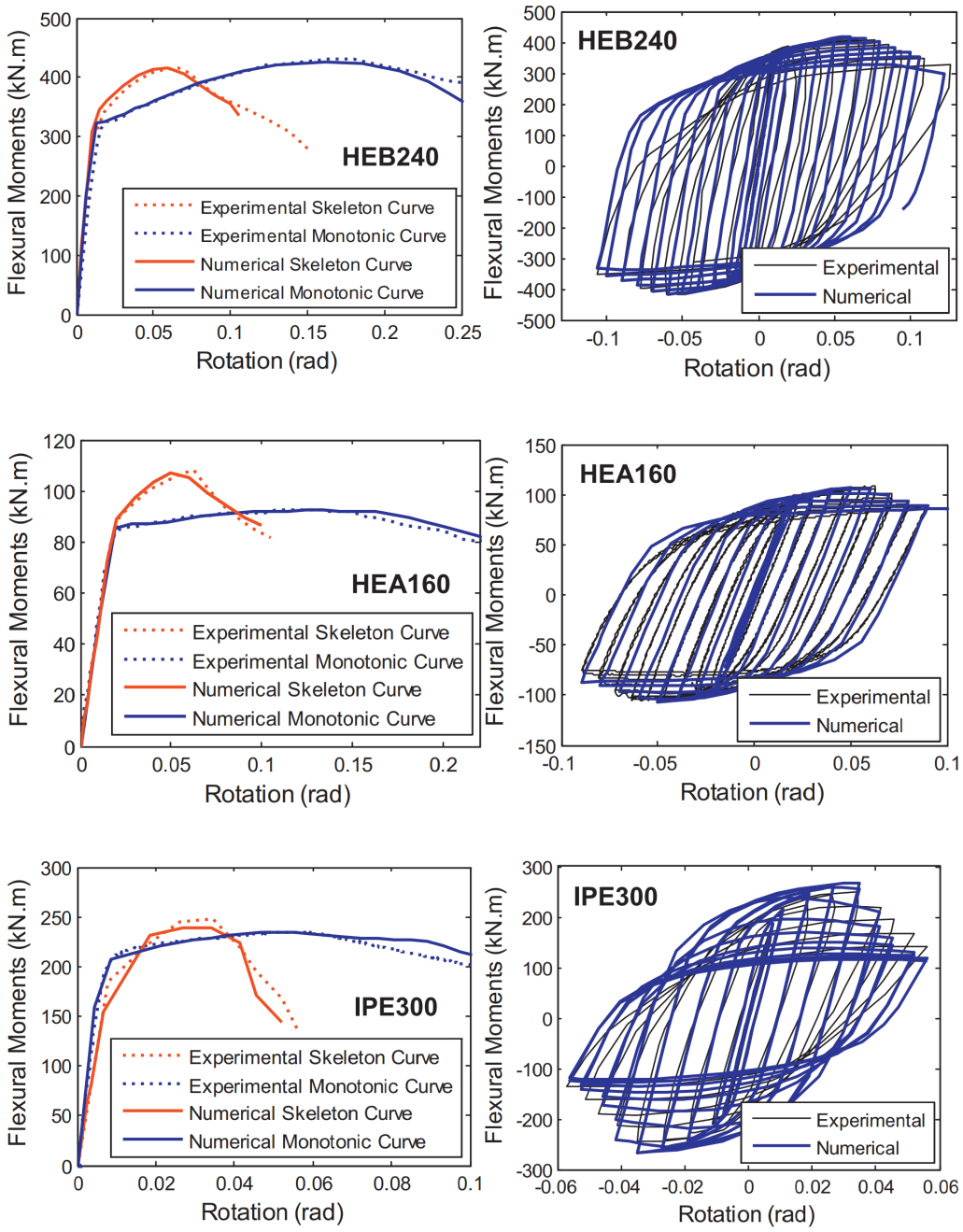

Figure 3.2: Experimental and numerical behaviour of specimens (Araújo et al., 2017).

updated, being designated as the cyclic backbone curve; (ii) a number of rules that characterise the hysteretic behaviour between the bounds of the backbone curve; (iii) a number of rules that define the various deterioration modes with respect to the backbone curve.

The monotonic backbone curve is usually close to, but not necessarily identical to, the curve that characterises the monotonic behaviour of the member. Generally speaking, it might account for an average effect of cyclic hardening, which can be quite significant for steel members. Hence,

in order to account for this average cyclic hardening effect in the definition of the monotonic backbone curve, the monotonic analyses of the set of members considered in this study were conducted with the use of the nonlinear kinematic material model with hardening, previously used to capture the cyclic behaviour of the experimental tests. A comparison between the experimental monotonic curve of the IPE300 profile tested by D'Aniello et al. (D'Aniello et al., 2012) and the numerical monotonic curve obtained from ANSYS (ANSYS, 2013) which includes the average cyclic hardening effect is shown in Figure 3.3.

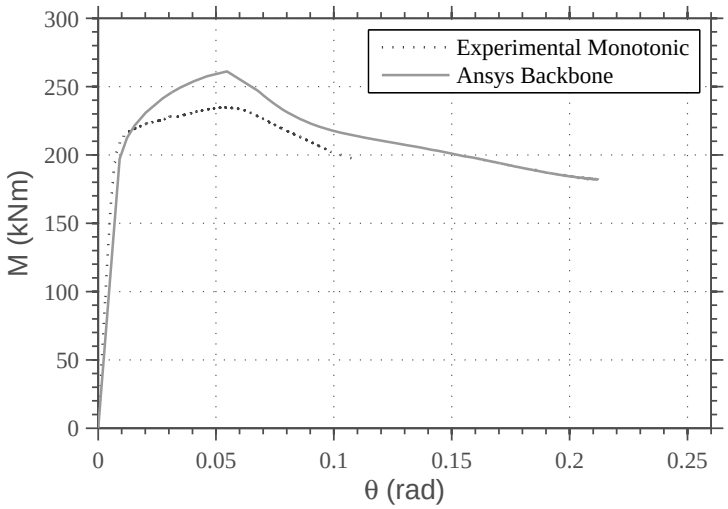

Figure 3.3: Comparison between the experimental and numerical monotonic curves for an IPE300 profile.

It is important to underline that the use of the aforementioned hysteretic model involves the computation of the "exact" monotonic behaviour of the member, whether it comes from experimental evidence or from a reliable advanced numerical model. Resorting to Figure 3.4, the concentrated modelling approach is detailed in the following paragraphs. As shown in Figure 3.4, the numerical monotonic curve obtained from ANSYS (ANSYS, 2013) was used to calibrate the Ibarra et al. (2005) monotonic backbone curve. The monotonic backbone curve is characterized by four key points: (i) the effective yield point, M_{pe} and θ_y, obtained from the monotonic curve provided by ANSYS and considering a bilinear idealisation based on the equivalent energy before strength deterioration sets in; (ii) the capping strength point, M_c and θ_c, which defines the onset of strength deterioration and is defined by the pre-capping plastic rotation, $\theta_p = \theta_c - \theta_y$; (iii) the residual strength point, M_r and θ_r, that represents the stabilization of the hysteretic response of steel members at large inelastic deformations and is suggested by Lignos and Krawinkler (2010) to occur at $0.4 \times M_{pe}$; (iv) the ultimate deformation point, θ_u, characterized by the post-capping plastic rotation, $\theta_{pc} = \theta_u - \theta_c$. Frequently fracture may occur before the member strength stabilizes at a residual value, leading to an ultimate deformation capacity smaller than the deformation at which M_r is reached (Araújo and Castro, 2017). The 20% drop in the peak strength, 80% M_c, is also represented and was used to define the post-capping plastic rotation.

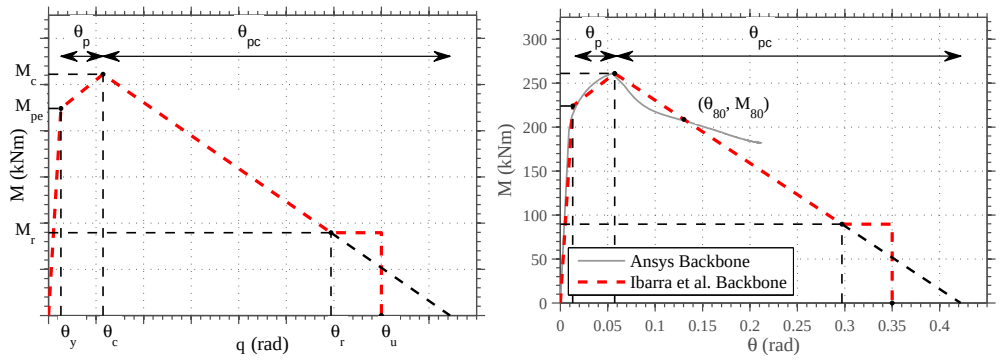

(a) (b)

Figure 3.4: Ibarra et al. (2005) monotonic backbone curve.

The cyclic loading typically causes four modes of deterioration that may be classified as: (i) strength deterioration, defined by a cumulative plastic rotation capacity Λ_s; (ii) post-capping strength deterioration, defined by the Λ_c parameter; (iii) accelerated reloading stiffness deterioration, defined by a cumulative plastic rotation capacity parameter, Λ_a; (iv) unloading stiffness deterioration, defined by the Λ_k parameter. Ibarra et al. (2005) accounted for all deterioration modes in a single parameter, β_i, which is given by Equation 3.1.

$$\beta_i = \left(\frac{E_i}{E_t - \sum_{j=1}^{i} E_j} \right)^c \tag{3.1}$$

where, E_i is the hysteretic energy dissipated in inelastic excursion i, E_t is the reference hysteretic energy dissipation capacity, given by $E_t = \Lambda M_y$, $\sum E_j$ is the hysteretic energy dissipated in all previous inelastic excursions, and c is the exponent defining the rate of deterioration, typically set equal to 1 for simplicity (Lignos and Krawinkler, 2010).

According to Lignos and Krawinkler (2010), it is assumed that every member has a reference value of E_t, which is an inherent property of the member, regardless of the loading history applied. The effect on the hysteretic behaviour of the Λ values associated to each deterioration mode is shown in Figure 3.5.

The analysis of the results shown in Figure 3.5 allows concluding about the fairly significant effect of the majority of the deterioration parameters in the hysteresis of the member. Those related with strength, post-capping strength and unloading stiffness deterioration have the ability to lead to radically different moment-rotation behaviours. Given the importance of peak and residual strengths on seismic performance and collapse assessment methodologies, the first two parameters (Figure 3.5 a and Figure 3.5 b) appear to be highly relevant. Also, the results shown in the figure seem to indicate that the parameter related with the accelerated reloading stiffness deterioration has a negligible effect on the hysteretic response. By employing different values of each parameter, optimum comparisons between the "exact" behaviour (e.g. experiment, FE model) and the

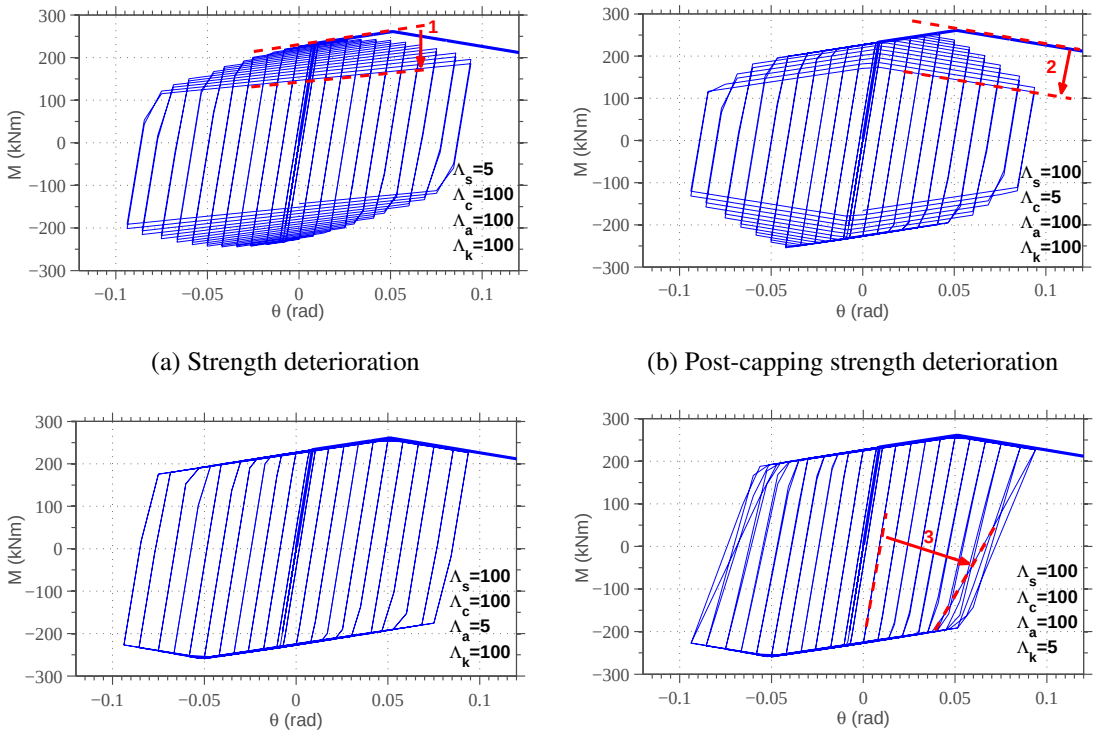

(a) Strength deterioration

(b) Post-capping strength deterioration

(c) Accelerated reloading stiffness deterioration

(d) Unloading stiffness deterioration

Figure 3.5: Sensitivity of the hysteretic response to the numerical deterioration parameters.

hysteretic model may be achieved for the IPE300 profile, as shown in Figure 3.6.

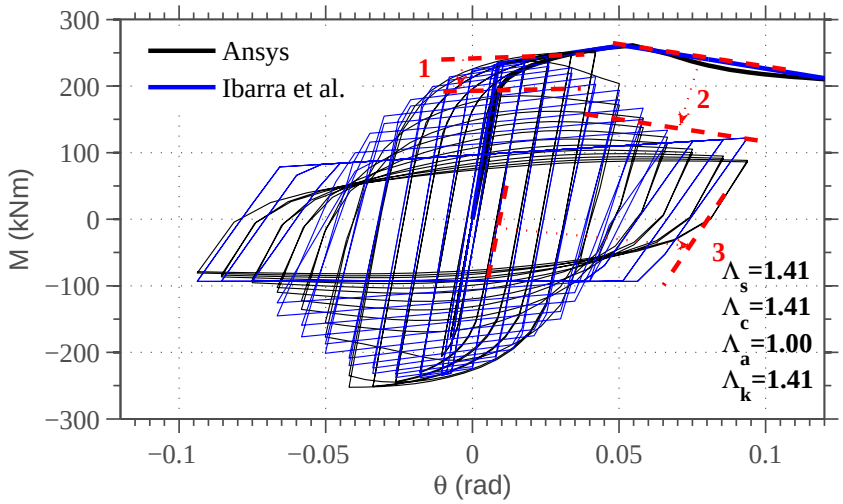

Figure 3.6: "Exact" and calibrated hysteretic response for IPE300 profile.

Although the results shown in Figure 3.6 may be accomplished, the process is usually associated with a trial and error approach: "manual" procedures are defined, in which the user tries

multiple combinations of the parameters that influence the problem at hand, until the best solution appears. This, however, may be lacking in both efficiency and consistency, particularly for complex numerical models, in which the sensitivity of the response to the defining parameters of the model is not clear beforehand. Furthermore, if the quality assessment of the "best" parameter combination is not defined on a solid basis (e.g. visual-based match criterion), the level of ambiguity of the solution may be considerable.

An efficient calibration of any numerical model requires the user to resort to hundreds, if not thousands, of iterative analyses that are time-consuming and may not necessarily lead to the most optimized solution. A number of meta-heuristic optimization methods are available that allow overcoming these difficulties, namely to significantly minimise computational effort, whilst still meeting the constraints of the problem. Recently, Macedo et al. (2013) applied the Harmony Search (HS) algorithm for earthquake record selection and scaling. The same framework is now employed for this study, in order to calibrate the deterioration parameters of the Ibarra et al. (2005) model, assuming the response obtained with the detailed model in ANSYS to be the "exact" one. Figure 3.7 shows an overview of the procedure adopted in the proposed optimized calibration framework. The calibration process initiates with the definition of a steel section and the corresponding material properties. Two ANSYS (ANSYS, 2013) models are generated, and a monotonic and a cyclic analyses are conducted. The results of the monotonic analysis are used to obtain the parameters of the Ibarra et al. (Ibarra et al., 2005)) monotonic backbone curve, whilst the cyclic results are stored for later use in the calibration framework. Taking the parameters of the Ibarra et al. (Ibarra et al., 2005)) monotonic backbone curve, an OpenSees (McKenna, 2011) model of a cantilever element subjected to a cyclic lateral displacement at the top is generated, and an optimization process is launched to obtain the steel section's strength and stiffness deterioration parameters.

To what concerns the meta-heuristic Harmony Search (HS) optimization algorithm (Geem et al., 2001), its formulation is based on the jazz music improvisation, wherein a set of music players are looking for combinations that are more aesthetically pleasing, through an extemporaneously process of memorization. In this process, improvisational musicians always look to produce a piece of music in perfect harmony. More details of the HS optimization algorithm can be found in Chapter 5.

In order to attain a solution for the optimization problem, an objective function, $f(x)$, needs to be defined. To what concerns the calibration of an hysteretic model, the objective function is aimed at minimizing the difference between the responses of the member obtained either with experimental testing or with detailed FE analysis and with OpenSees, the latter using the aforementioned hysteretic model. Since the history of loading displacements computed in both analyses is the same, the objective function is defined as the difference between the history of bending moments at the base of the cantilever. Moreover, the differences in the cumulative energy dissipation

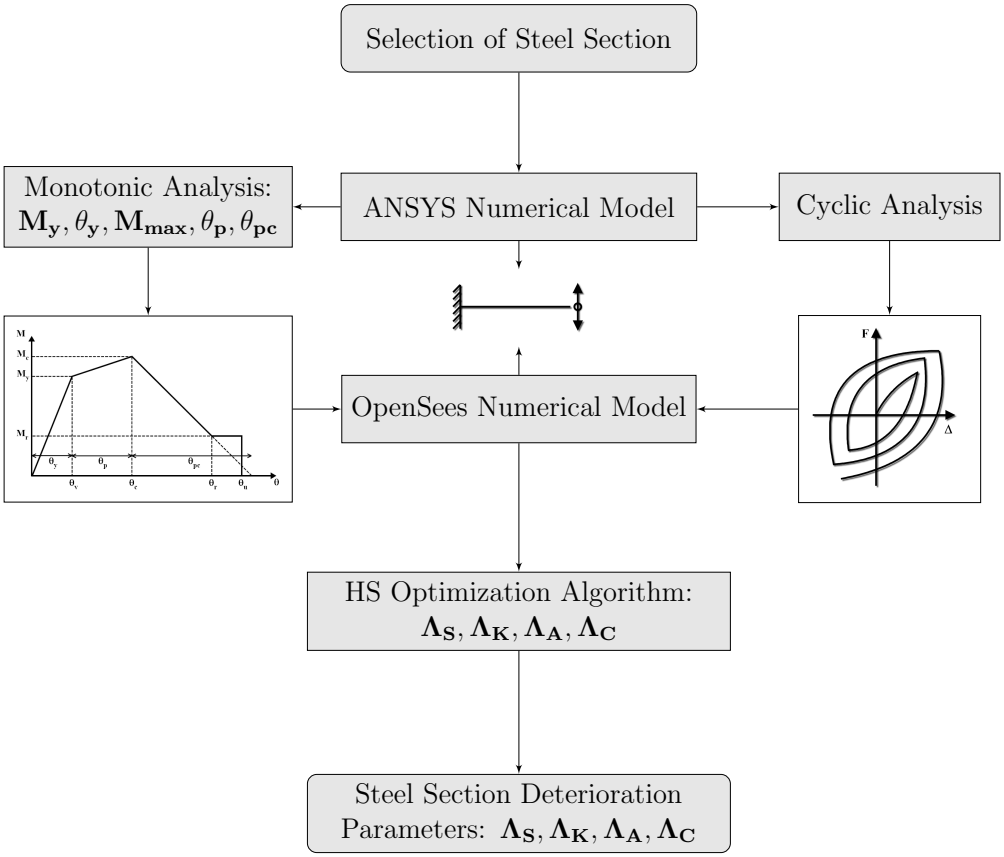

Figure 3.7: Parameter calibration procedure.

are also considered in the objective function (Equation 3.2).

$$f(x) = \frac{\sqrt{\sum_{i=1}^{n_P}\left(M_{exp}(i) - M_{OpenSees}(i)\right)^2}}{\sqrt{\sum_{i=1}^{n_P}\left(M_{exp}(i)\right)^2}} + w \times \frac{\sqrt{\sum_{i=1}^{n_P}\left(E_{exp}(i) - E_{OpenSees}(i)\right)^2}}{\sqrt{\sum_{i=1}^{n_P}\left(E_{exp}(i)\right)^2}} \tag{3.2}$$

where n_P is the total number of points, $M_{exp}(i)$ and $E_{exp}(i)$ are the bending moment and cumulative energy in the experimental or detailed FE model, respectively. $M_{OpenSees}(i)$ and $E_{OpenSees}(i)$ are the bending moment and cumulative energy in the OpenSees model, respectively. w is a weighting factor indicating the relative importance of the errors in the bending moment and the cumulative energy dissipation.

To enable the use and dissemination of the calibration framework, a graphical user interface (GUI) was developed. CalTool (Advanced Calibration Tool) follows a modular and extensible development approach, currently reflecting the procedures detailed previously. Figure 3.8 shows the CalTool GUI.

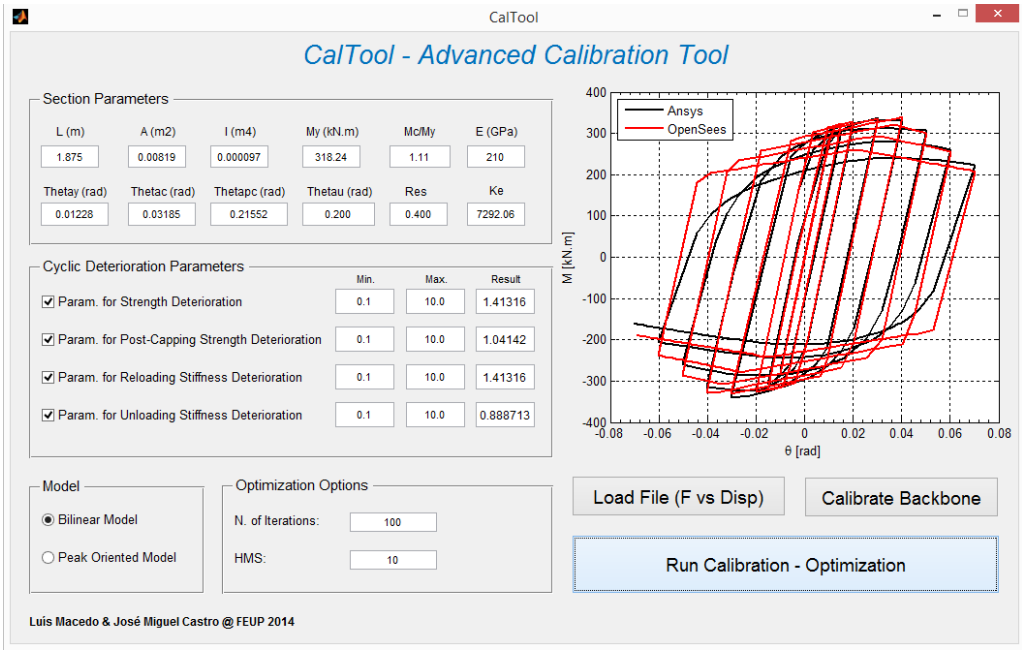

Figure 3.8: CalTool Interface.

3.3.1 Validation of the optimized calibration framework

In order to validate the optimized calibration framework previously described, a full-scale experimental test of a steel moment-resisting frame is used (Ryu et al., 2011). The selected test specimen is shown in Figure 3.9, having a beam span of 5.4 m and a column height of 2.4m. The beam and column sections are BH426x280x12x16 and BH390x300x10x16, respectively. The yield strength of the steel in the beams and columns is equal to 279 MPa and 335 MPa, respectively, and the measured Young's Modulus is equal to 209 GPa. A detailed description of the test can be found in Ryu et al. (2011).

The tested frame was firstly modelled using the structural analysis software package ANSYS, following the same modelling approach discussed previously. The initial hardening modulus, C_i, and the rate at which the hardening modulus decreases with increasing plastic strain, γ_i, were calibrated from experimental data so as to provide a good agreement between the numerical and experimental results, and values of 4500 N/mm2 and 50 were obtained, respectively. The loading, as well as the boundary conditions, were imposed according to the information provided in Ryu et al. (2011). Figure 3.10 and Figure 3.11 show a comparison, between the experimental results and the numerical analysis, of the local deformation modes and the global hysteretic response, respectively.

As shown in the figures, the developed FE model accurately captures all the deformation mode patterns oberved during the test at the main critical sections, as well as the lateral response of the tested steel frame. Both the cyclic and deteriorating behaviour is well captured, thus leading to results consistent with the experimental evidence. Having established that the detailed model in

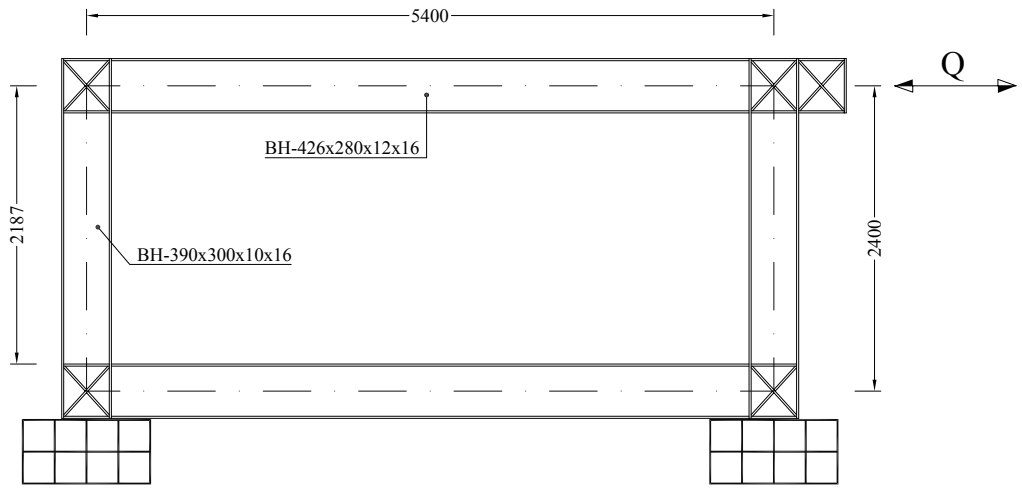

Figure 3.9: Test setup.

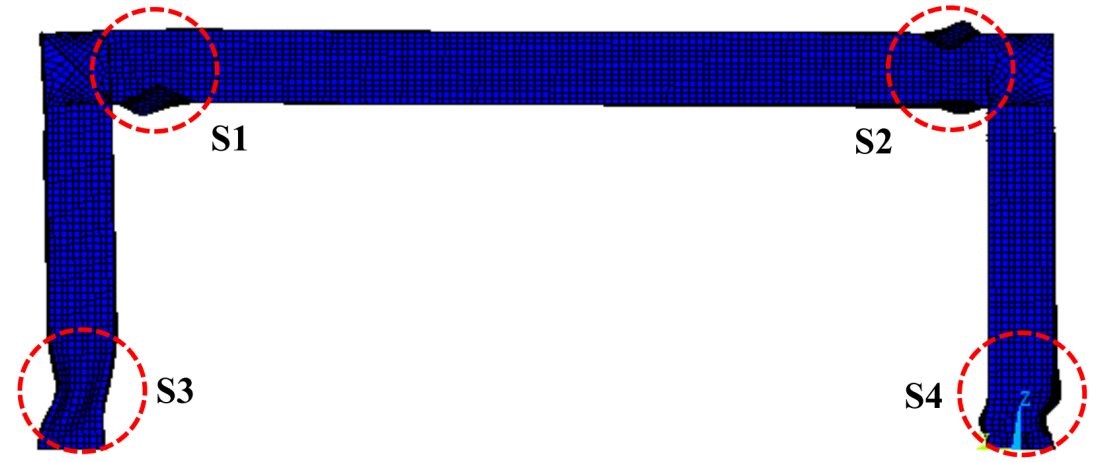

(a) Section S1 (b) Section S2 (c) Section S3 (d) Section S4

Figure 3.10: Comparison between the experimental and numerical (ANSYS) local deformation modes of the steel frame test.

ANSYS (ANSYS, 2013) accurately simulates the experimental response of the steel structure, the monotonic and cyclic responses of the column and beam sections of the specimen were individually assessed using the same FE modelling approach. Then, assuming this response to be "exact", the optimized calibration framework discussed before was applied. Figure 3.12 shows a comparison between the full hysteretic response obtained with ANSYS with the proposal by Lignos and

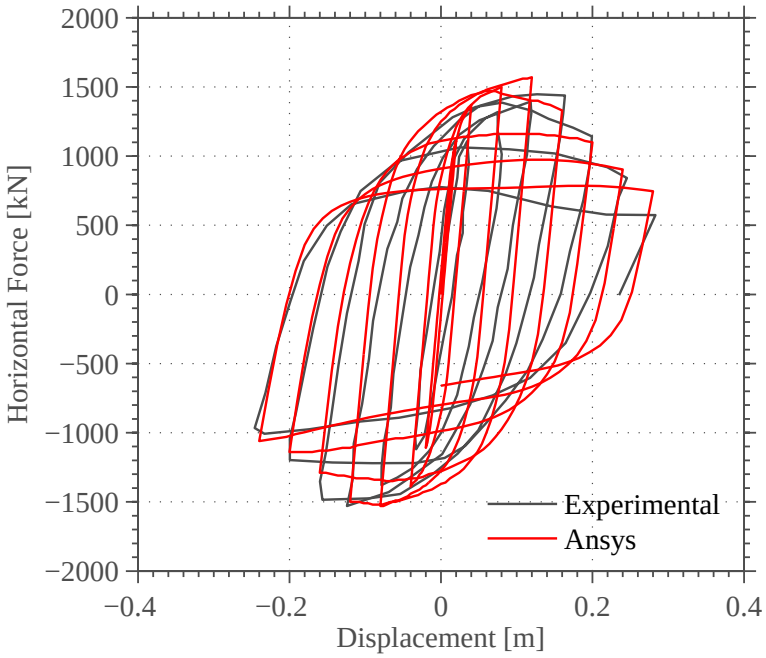

Figure 3.11: Comparison between the experimental and numerical (ANSYS) global hysteretic response of the steel frame test.

Krawinkler (2010) and the optimization calibrated solution.

The analysis of the results shown in Figure 3.12 allows concluding that the model based on the optimized calibrated parameters provides more accurate results in comparison with the results obtained using the parameters available in the literature. A quick inspection of the results indicates that the adopted procedure leads to more accurate and reliable estimates of the member responses. Hence, for each member, the deterioration parameters of the hysteretic model were obtained and used to model the whole structural system, the response of which was compared afterwards with the experimental results obtained by Ryu et al. (2011), as shown in Figure 3.13. For comparison purposes, the proposal by Lignos and Krawinkler (2010) is also shown in the figure.

As shown in Figure 3.13, the comparison between the numerical results and the experimental data for the existing concentrated plasticity models (Figure 3.13) leads to less accurate predictions of the lateral response of the steel frame. The results indicate a clear underestimation of the peak lateral strength and residual lateral capacity of the frame. Conversely, the numerical model with the optimized calibrated deterioration parameters (Figure 3.13) is able to simulate reasonably well the hysteretic behaviour of the frame and leads to good estimates of the peak lateral strength and residual lateral capacity. However, the model is not able to simulate with good accuracy the unloading stiffness deterioration process, with no significant improvements over the concentrated plasticity model with deterioration parameters defined according to existing proposals. Nevertheless, the optimized calibrated approach seems to lead to fairly reasonable comparisons to the experimental evidence, and is thus positively validated.

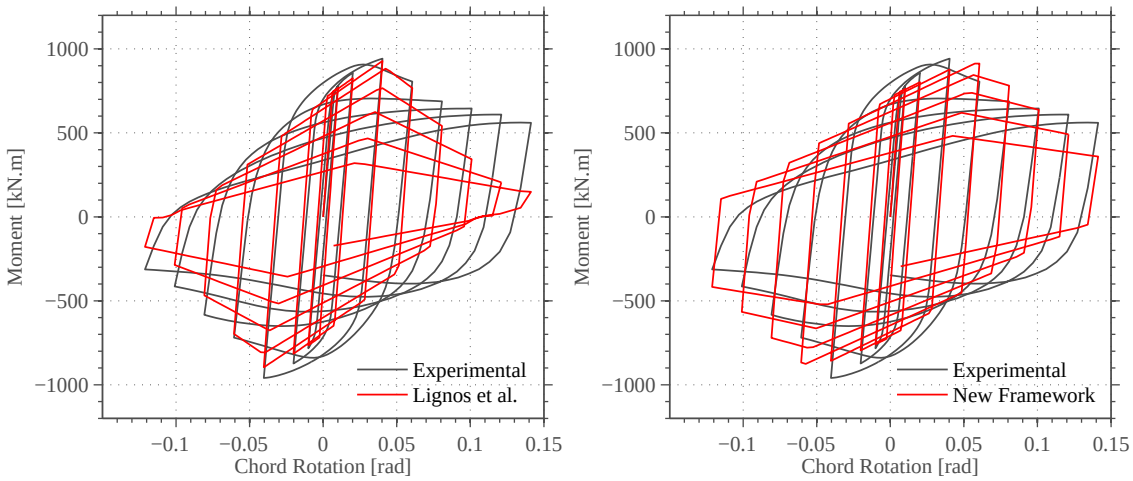

(a) Column - Lignos and Krawinkler (2012)

(b) Column - Proposed framework

(c) Beam - Lignos and Krawinkler (2012)

(d) Beam - Proposed framework

Figure 3.12: Comparison between the experimental and two numerical hysteretic responses of the column and beam sections of the tested steel frame.

The results obtained in the simulation of the full-scale experimental test of a steel moment-resisting frame clearly show the efficiency of the proposed calibration procedure in obtaining the deterioration parameters of steel open-sections.

3.4 Proposed deterioration parameters for European steel profiles

Although it has been shown that the use of optimization procedures to obtain calibrated deterioration parameters, leads to fairly accurate comparisons to the "exact" hysteretic response of the structural member, the entire process is computationally heavy. This, however, may be avoided if expressions or tabulated data is available, relating the properties of a given steel section with the optimum deterioration parameters to adopt in a concentrated plasticity model. To this end, a comprehensive set of European steel profiles with open-sections is adopted, and the framework

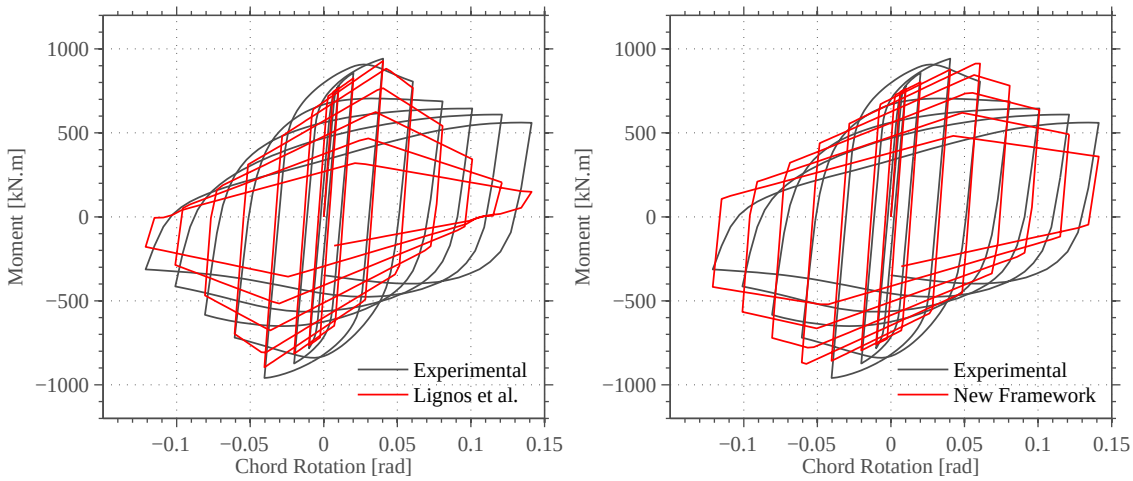

(a) Lignos and Krawinkler (2012) (b) Proposed framework

Figure 3.13: Comparison between the experimental and two numerical hysteretic global responses of the tested steel frame.

detailed and validated in this study is applied. In the following paragraphs, the preliminary observations concerning the monotonic and cyclic flexural behaviour of the members are discussed. Moreover, the database of numerical results is used to propose regression-fitted expressions for the deterioration parameters of the Ibarra et al. (2005) model for the considered scope of steel members.

3.4.1 Behaviour of steel open-section members

As previously mentioned, a comprehensive set of steel beam-column members with typical IPE (270 to 600), HEA, HEB and HEM (240 to 1000) cross-section profiles was numerically evaluated in ANSYS, following the same modelling assumptions described before in this chapter. Cantilever lengths were set to 1.885 m, and a power law was fitted to the stress-strain data of every member tested by D'Aniello et al. (2012), as presented in the work of Araújo and Castro (2017). This provided the basis for the calibration of the multilinear kinematic material model with hardening used in the monotonic analyses. Mean values of $C_i = 11333\ N/mm^2$ and $\gamma_{i,mean} = 123$ of those obtained from the initial calibration of the HEB240, IPE300 and HEA160 members were adopted in the nonlinear kinematic material model with hardening. Figure 3.14 and Figure 3.15 show a comparison, for four European open-section steel profiles, between the full hysteretic response obtained with the proposal by Lignos and Krawinkler (2012) and the optimization framework developed in this research study. In the figures, the set of deterioration parameters obtained with both methodologies is also shown. It is important to underline that both modelling approaches are based on the hysteretic model proposed by Ibarra et al. (2005).

As shown in Figure 3.14 and Figure 3.15, the calibration of the cyclic responses obtained with ANSYS using the HS algorithm provides very consistent optimum Λ parameters, which accurately

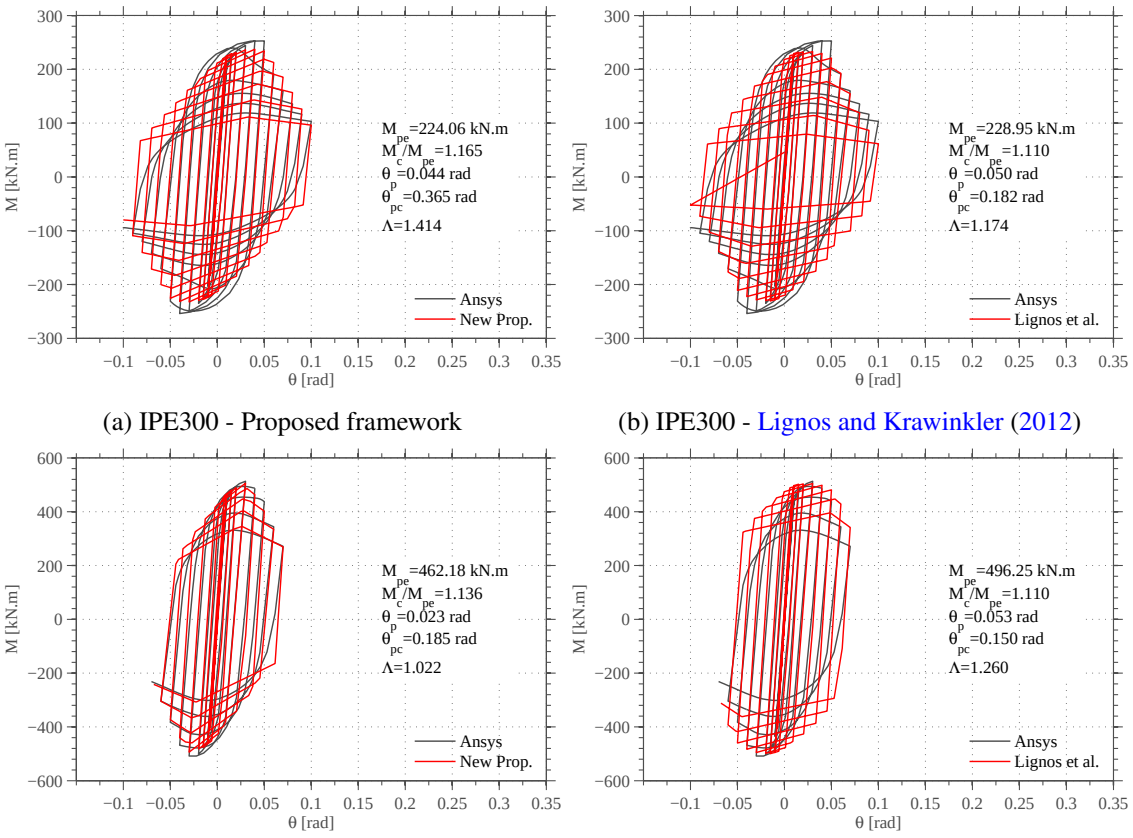

(a) IPE300 - Proposed framework

(b) IPE300 - Lignos and Krawinkler (2012)

(c) HEA300 - Proposed framework

(d) HEA300 - Lignos and Krawinkler (2012)

Figure 3.14: Calibration using the HS algorithm and prediction using the expressions proposed by Lignos and Krawinkler (2012).

capture the strength, post-capping and stiffness modes of deterioration of the steel members. Although the expressions proposed by Lignos and Krawinkler (2012) lead to reasonable results, for some European steel open-section the observed behaviour seems to be clearly less accurate. Despite this indication, it is important to note that the proposal was developed based on regressions made on experimental data from American steel profiles. No demonstration has been made yet regarding the applicability of the proposal to European profiles. Thus, its applicability and accuracy to European steel profiles is not necessarily guaranteed.

Given both the randomness of the generated Λ and the inherent learning mechanism (convergence) of the HS algorithm, it is important to evaluate the stability of the algorithm for multiple runs. Essentially, this might provide some indication of how consistent is the optimized Λ across multiple runs. Figure 3.16 shows the "behaviour" of Λ for a total of 20 runs, each with the same number improvisations (20000).

The analysis of the results shown in Figure 3.16 points to the high stability of the calibrated deterioration parameters. As it can be observed, across multiple runs, the obtained Λ-values are roughly the same, with coefficients of variation (CoV) lower than 0.012. This clearly indicates that the framework developed has the ability to achieve the representative optimized solution resorting

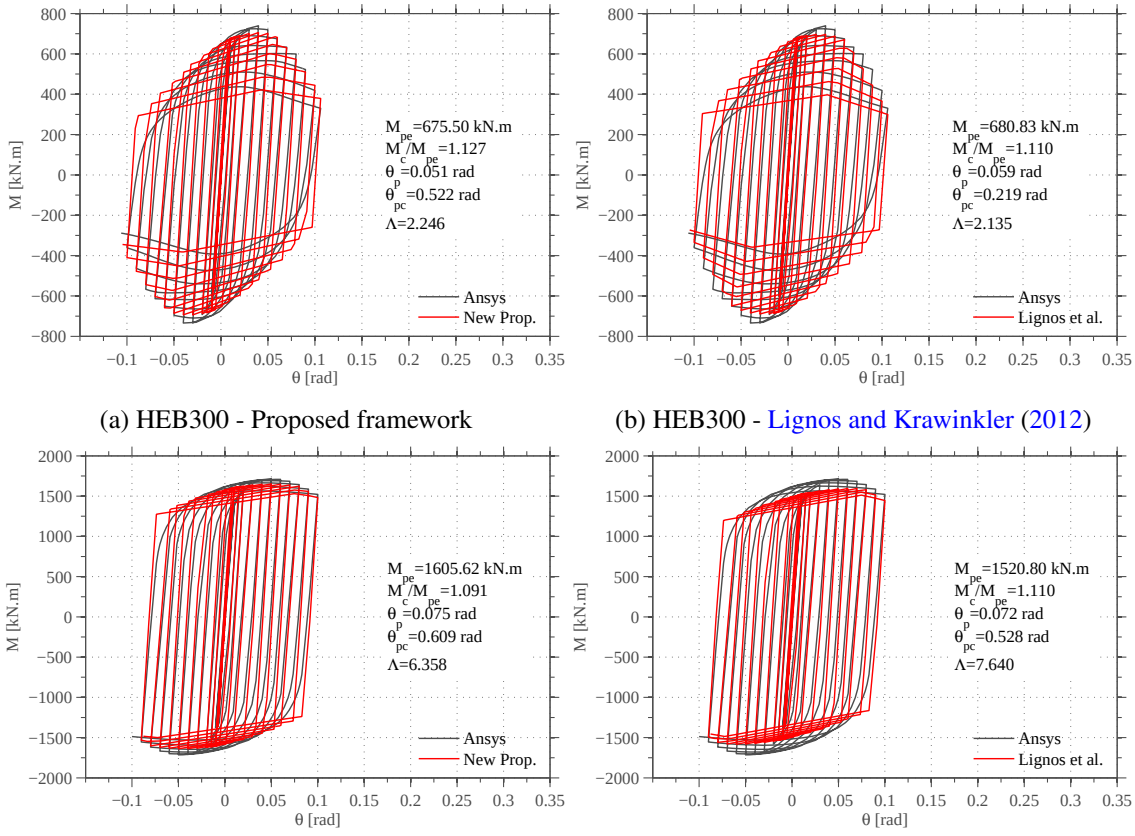

(a) HEB300 - Proposed framework

(b) HEB300 - Lignos and Krawinkler (2012)

(c) HEM300 - Proposed framework

(d) HEM300 - Lignos and Krawinkler (2012)

Figure 3.15: Calibration using the HS algorithm and prediction using the expressions proposed by Lignos and Krawinkler (2012).

to a single run.

Tables 3.1, 3.2, 3.3 and 3.4 show the obtained values of Ibarra et al. (2005) parameters for European steel open-sections.

Table 3.1: Hysteretic model parameters for IPE profiles according to Ibarra et al. (2005) .

	λ_w	λ_f	M_{pe}	M_c	M_y/M_{pe}	M_c/M_{pe}	θ_p	θ_{pc}	Λ
IPE 270	37.82	6.62	176.31	202.76	1.22	1.15	0.0640	0.4970	1.8150
IPE 300	39.24	7.01	224.06	261.11	1.19	1.17	0.0443	0.3649	1.4140
IPE 330	40.93	6.96	285.24	327.69	1.20	1.15	0.0393	0.2832	1.2320
IPE 360	41.83	6.69	371.31	418.29	1.22	1.13	0.0412	0.2450	1.2550
IPE 400	43.37	6.67	467.45	529.62	1.21	1.13	0.0360	0.2283	1.4270
IPE 450	44.77	6.51	620.29	691.55	1.22	1.11	0.0369	0.1999	1.2594
IPE 500	45.88	6.25	780.35	894.80	1.18	1.15	0.0307	0.2129	1.1520
IPE 550	46.45	6.10	997.84	1127.58	1.20	1.13	0.0310	0.1916	1.0727
IPE 600	46.83	5.79	1288.04	1430.13	1.22	1.11	0.0337	0.2048	1.0671

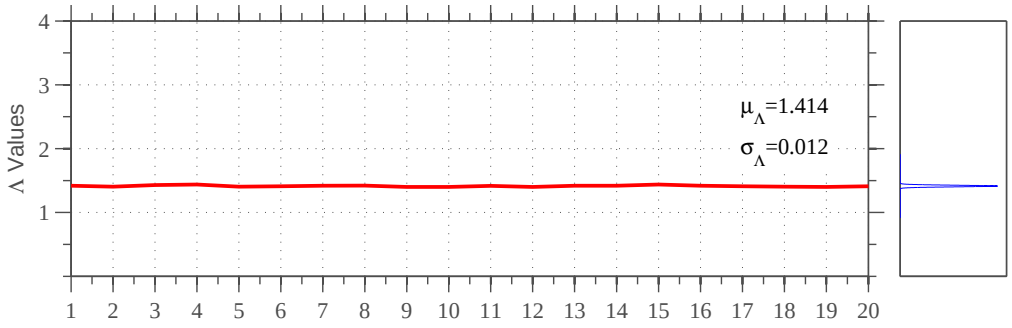

(a) IPE300

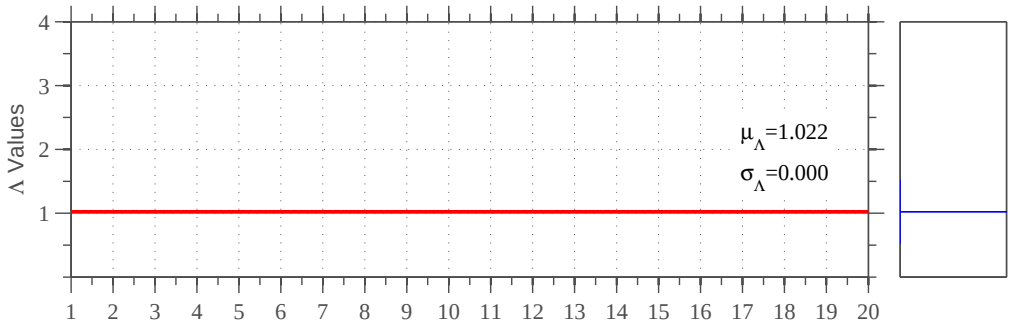

(b) HEA300

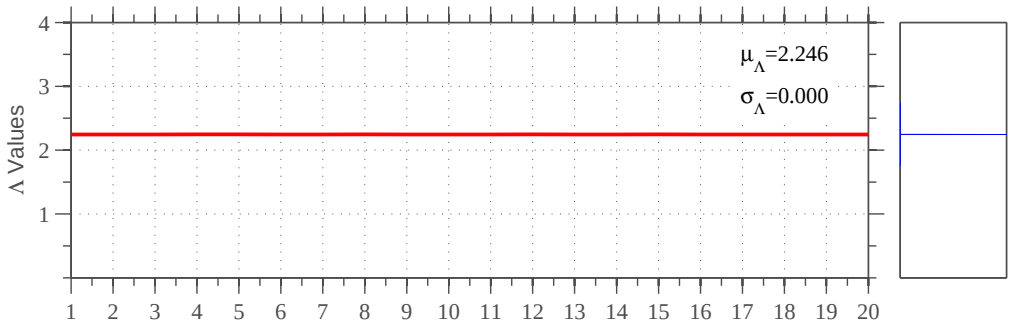

(c) HEB300

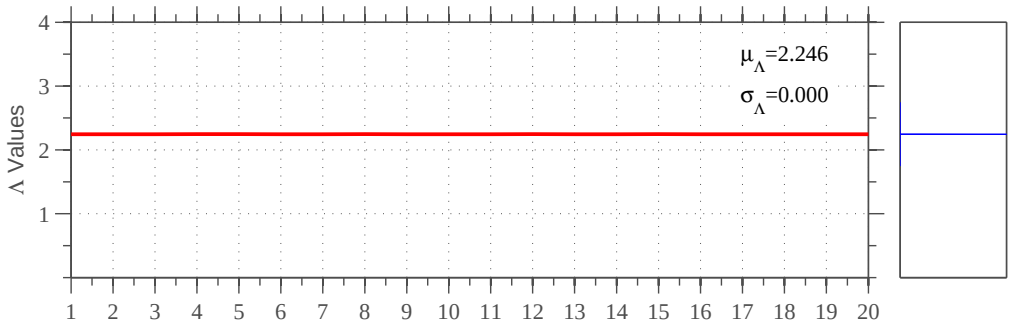

(d) HEM300

Figure 3.16: Stability of the calibrated deterioration parameters.

Despite the the consistency of the obtained strength and stiffness deterioration parameters, it is worth mentioning that only one steel material was considered in this study and that all the parameters have been derived for the same element length. Extension of the current work should

Table 3.2: HEA Ibarra et al. (2005) hysteretic model parameters.

	λ_w	λ_f	M_{pe}	M_c	M_y/M_{pe}	M_c/M_{pe}	θ_p	θ_{pc}	Λ
HE 240 A	27.47	10.00	258.41	292.18	1.18	1.13	0.0384	0.2486	1.3707
HE 260 A	30.00	10.40	305.85	351.45	1.14	1.15	0.0283	0.2191	1.0514
HE 280 A	30.50	10.77	370.06	422.54	1.13	1.14	0.0226	0.1896	1.0690
HE 300 A	30.82	10.71	462.18	525.05	1.14	1.14	0.0226	0.1845	1.0220
HE 320 A	31.00	9.68	556.98	638.06	1.16	1.15	0.0283	0.2200	0.9980
HE 340 A	31.26	9.09	647.74	731.42	1.18	1.13	0.0347	0.2147	0.9910
HE 360 A	31.50	8.57	755.34	841.35	1.22	1.11	0.0446	0.2529	1.0350
HE 400 A	32.00	7.89	941.77	1047.89	1.23	1.11	0.0505	0.4309	1.1043
HE 450 A	34.61	7.14	1193.23	1307.28	1.24	1.10	0.0462	0.4137	1.4340
HE 500 A	37.00	6.52	1445.01	1602.32	1.22	1.11	0.0384	0.4718	1.4270
HE 550 A	39.36	6.25	1723.70	1866.80	1.24	1.08	0.0412	0.4111	0.9920
HE 600 A	41.54	6.00	1932.44	2156.03	1.19	1.12	0.0277	0.4450	1.0430
HE 650 A	43.56	5.77	2207.54	2472.38	1.19	1.12	0.0309	0.3986	1.0590
HE 700 A	43.86	5.56	2570.50	2834.63	1.20	1.10	0.0332	0.3736	1.1809
HE 800 A	48.93	5.36	3091.68	3458.56	1.17	1.12	0.0269	0.3401	1.1481
HE 900 A	51.88	5.00	3846.40	4271.43	1.17	1.11	0.0269	0.3005	1.2165

consider variation of the material properties, element length and uncertainties related with the cross-section dimensions.

Table 3.3: Hysteretic model parameters for IPE profiles according to Ibarra et al. (2005) .

	λ_w	λ_f	M_{pe}	M_c	M_y/M_{pe}	M_c/M_{pe}	θ_p	θ_{pc}	Λ
HE 240 B	20.60	7.06	392.68	439.03	1.24	1.12	0.0780	0.8147	2.7787
HE 260 B	22.50	7.43	463.76	526.92	1.21	1.14	0.0589	0.7159	2.4880
HE 280 B	23.24	7.78	563.13	629.34	1.23	1.12	0.0589	0.5838	2.3910
HE 300 B	23.82	7.89	675.50	761.39	1.21	1.13	0.0505	0.5216	2.2457
HE 320 B	24.26	7.32	796.11	884.11	1.24	1.11	0.0627	0.7430	2.4022
HE 340 B	24.75	6.98	899.85	994.57	1.25	1.11	0.0621	0.8313	2.7059
HE 360 B	25.20	6.67	1011.87	1109.59	1.26	1.10	0.0623	0.7798	2.6131
HE 400 B	26.07	6.25	1210.75	1340.24	1.25	1.11	0.0532	0.8628	3.3430
HE 450 B	28.43	5.77	1491.04	1645.58	1.24	1.10	0.0462	0.7125	3.3037
HE 500 B	30.62	5.36	1834.26	1978.11	1.26	1.08	0.0490	0.5008	2.7470
HE 550 B	32.80	5.17	2102.50	2286.31	1.24	1.09	0.0471	0.4007	2.7630
HE 600 B	34.84	5.00	2316.63	2621.30	1.19	1.13	0.0304	0.4249	3.0555
HE 650 B	36.75	4.84	2625.90	2975.13	1.18	1.13	0.0276	0.3872	2.6913
HE 700 B	37.41	4.69	3034.95	3392.19	1.19	1.12	0.0314	0.3812	2.2475
HE 800 B	41.94	4.55	3716.85	4106.76	1.19	1.10	0.0323	0.2918	1.8810
HE 900 B	44.86	4.29	4572.73	5010.66	1.19	1.10	0.0323	0.2530	1.7910
HE 1000 B	48.84	4.17	5283.48	5866.82	1.16	1.11	0.0277	0.2600	1.9140

Table 3.4: Hysteretic model parameters for HEM profiles according to Ibarra et al. (2005) .

	λ_w	λ_f	M_{pe}	M_c	M_y/M_{pe}	M_c/M_{pe}	θ_p	θ_{pc}	Λ
HE 240 M	11.44	3.88	858.60	932.22	1.33	1.09	0.1352	0.5995	7.5720
HE 260 M	12.50	4.06	1026.24	1112.18	1.32	1.08	0.1113	0.7720	6.6980
HE 280 M	12.84	4.36	1179.53	1286.31	1.30	1.09	0.0917	0.7451	6.4550
HE 300 M	12.48	3.97	1605.62	1752.32	1.29	1.09	0.0754	0.6087	6.3580
HE 320 M	13.29	3.86	1694.14	1900.62	1.25	1.12	0.0668	0.5643	9.9470
HE 340 M	14.14	3.86	1846.41	2017.53	1.28	1.09	0.0772	0.4743	5.6750
HE 360 M	15.00	3.85	1962.68	2129.28	1.29	1.08	0.0719	0.4590	4.5320
HE 400 M	16.76	3.84	2164.36	2367.06	1.27	1.09	0.0560	0.4770	5.8510
HE 450 M	18.95	3.84	2425.67	2676.50	1.26	1.10	0.0538	0.4055	5.7920
HE 500 M	21.14	3.83	2731.73	2983.11	1.26	1.09	0.0538	0.3523	3.9050
HE 550 M	23.43	3.83	2961.02	3316.26	1.22	1.12	0.0396	0.3837	6.5770
HE 600 M	25.71	3.81	3255.38	3648.35	1.21	1.12	0.0370	0.3599	6.4170
HE 650 M	28.00	3.81	3642.61	3994.03	1.23	1.10	0.0403	0.3029	4.9840
HE 700 M	30.29	3.80	3982.75	4333.14	1.23	1.09	0.0403	0.2754	3.5300
HE 800 M	34.95	3.79	4485.21	5061.42	1.17	1.13	0.0261	0.3036	4.1570
HE 900 M	39.52	3.78	5181.31	5798.12	1.17	1.12	0.0269	0.2739	1.7910
HE 1000 M	44.19	3.78	5965.50	6578.85	1.17	1.10	0.0301	0.2447	2.5080

3.4.2 Fitting of nonlinear regression models

On the basis of the numerical data summarized in the previous section, empirical equations for predicting the Λ-values of the Ibarra et al. (2005) hysteretic model for European steel open cross-section profiles are derived by means of nonlinear regression analyses Lignos and Krawinkler (2010), and assuming the flange and web slenderness as predictor variables. The nonlinear model used to predict the capacity of the members, R_c, is given by Equation 3.3.

$$R_c = a_1 \times \left(\frac{b_f}{2 \times t_f}\right)^{a_2} \times \left(\frac{h}{t_w}\right)^{a_3} \tag{3.3}$$

where a_1, a_2 and a_3 are the regression coefficients, b_f and t_f denote the width and thickness of the flange and h and t_w refer to the depth and thickness of the web. Figure 3.17 shows a fitting example of the nonlinear regression model to the numerical strength and stiffness deterioration parameters results obtained for the range of IPE profiles considered. Regarding the fitting for the different

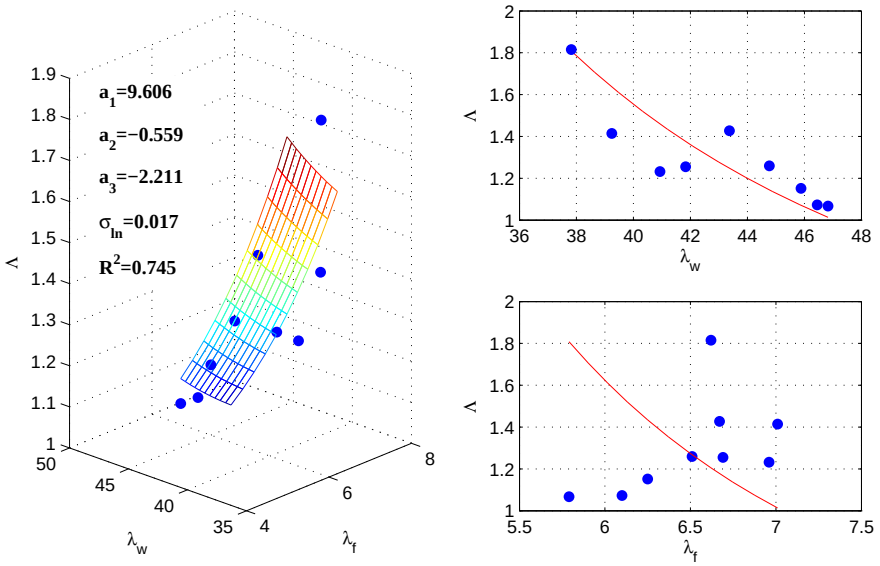

Figure 3.17: Fitting example of the nonlinear regression model to the numerical strength and stiffness deterioration parameters results obtained for the range of IPE profiles considered.

cross-section families, it is important to emphasize that only for the IPE and HEM profiles it was possible to derive an empirical equation for entire set of members with reasonable goodness-of-fit coefficients (e.g. R^2). However, for the HEA and HEB profiles, two sub-sets were created and the associated empirical equations were determined. Table 3.5 summarizes the values of a_1, a_2 and a_3, as well as the goodness-of-fit coefficient R^2 and the residuals standard deviation σ_{ln}, estimated for the strength and stiffness deterioration parameters for the families of steel profiles considered in this study.

Table 3.5: Summary of the Nonlinear regression model parameters.

	IPE	HEA HEA240 to HEA450	HEA HEA500 to HEA900	HEB HEB240 to HEB500	HEB HEB550 to HEB1000	HEM
a_1	9.606	7.092	8.132	5.069	-4.069	5.844
a_2	-0.559	-1.176	-2.285	-1.507	2.556	-1.33
a_3	-2.211	-1.016	-1.074	-0.363	0.259	-0.806
R^2	0.745	0.866	0.958	0.896	0.775	0.626
σ_{ln}	0.017	0.002	0.009	0.001	0.024	0.001

3.5 Conclusions

In this Chapter, a research study was conducted to evaluate the strength and stiffness deterioration parameters of the Ibarra et al. (2005) hysteretic model for laterally-restrained steel elements, made with standard European open-section profiles. Lignos and Krawinkler (2010) proposed several moment-rotation relationships obtained from calibration of an extensive database with more than 350 experimental tests conducted on American steel profiles. However, standard European cross sections exhibit different web and flange slenderness levels, parameters that a relevant influence on the strength and stiffness deterioration parameters.

Thus, an advanced numerical FE model was developed to simulate the behaviour of steel sections under monotonic and cyclic flexural loading. The model was firstly validated against the experimental tests carried out by D'Aniello et al. (2012). A calibration procedure was then implemented to obtain the strength and deterioration parameters of the Ibarra et al. (2005) hysteretic model. The procedure makes use of the Harmony Search meta-heuristic optimization algorithm in order to significantly reduce the computational effort associated with conventional optimization schemes. Moreover, the calibration procedure was validated by simulating a full scale test of a steel frame.

Finally, the calibration procedure was applied to a wide range of European steel open-section profiles, allowing to obtain the strength and deterioration parameters of the Ibarra et al. (2005) hysteretic model. A set of nonlinear regression-based prediction equations for these parameters were proposed, having particular interest for numerical modelling of steel elements with a concentrated plasticity approach.

Chapter 4

Panel zone design in steel moment frames

4.1 Introduction

The panel zone in moment-resisting frames connections is defined as the column web portion delimited by the beam continuity plates and the column flanges, as shown in Figure 4.1.

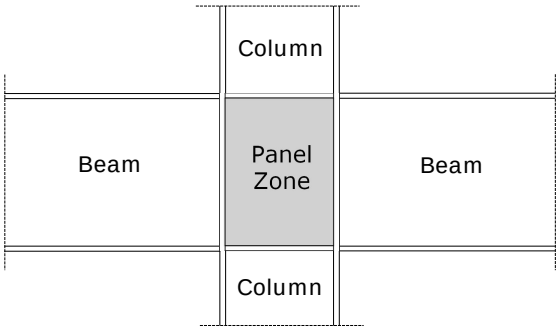

Figure 4.1: Panel zone.

The panel zone of a steel joint is known to play an important role both on the lateral stiffness and capacity of a steel frame. As demonstrated by Schneider and Amidi (1998), neglecting the deformation of the panel zone in the numerical models of steel moment-resisting frames generally leads to inaccurate estimates of structural deformation (underestimation up to 10% in drift) and load capacity (overestimation up to 30% of the base shear). It has become apparent that an inadequate design of the panel zone can lead to a significant reduction in the resistance capacity of the joint, which can be controlled by a premature yielding of the panel zones (Gupta and Krawinkler, 2000).

Whilst the design of the panel zone to gravity loads is perfectly established in current design codes, the situation is rather different when seismic design is considered. For the latter, current methodologies generally classify the panel zone in terms of strength, as weak, balanced or

strong (Popov, 1987; El-Tawil et al., 1999; El-Tawil, 2000). This classification is based on the ratio between the strength of the panel zone and the flexural capacity of the connecting beams. The difference between these three approaches is found on the level of energy dissipation that is capable of occurring on the panel zone (Bertero et al., 1973; Castro et al., 2008). Strong panel zones are designed to remain elastic during a seismic event, and, in this case, the component does not dissipate energy through inelastic response. Conversely, if weak panel zones are considered, most of the energy dissipation during an earthquake will occur on these components. Since the early '70s, many studies have been conducted and different approaches for panel zone design have been proposed. Early experimental studies have shown that panel zones exhibit stable hysteretic behaviour and are able to withstand significant levels of shear deformation (Krawinkler, 1971; Fielding and Huang, 1971; Bertero et al., 1972). Based on those experimental observations, the research community agreed that the panel zone could provide an important contribution to the inelastic behaviour of moment-resisting frames (MRFs). As a result, new panel zone design rules were introduced in the 1988 version of the Uniform Building Code (ICBO, 1988), in which the strength requirements concerning panel zones were relaxed. However, during the 1994 Northridge earthquake, significant damage was observed in steel joints. Consequently, an extensive experimental campaign was carried out with the objective of identifying the reasons for the observed damage, and also to develop alternative design procedures that could mitigate future damage on both new and existing joints. It was found was that one of the factors that contributed to that damage was the excessive inelastic deformations that developed on panel zones (Tremblay et al., 1995; El-Tawil, 2000). These conclusions resulted in the proposal of a new design approach for panel zones that established the concept of a balanced panel zone (FEMA, 2000). In this design approach, the panel zone is proportioned in such a way that the initiation of yielding occurs almost simultaneously with the formation of plastic hinges in the connecting beams.

It is important to note that it has been recently reported that the application of the aforementioned design approach to new structures is not necessarily reflected in a reliable participation of the panel zones to the inelastic response (Jin and El-Tawil, 2005). This observation points out to a possible limitation in the panel zone design approach which may be related with the evaluation of the strength demands on this component. Castro et al. (2008) evaluated the influence of the gravity loads on the ductility demands of the beams and concluded that, for high levels of gravity loading, the location of plastic hinges in the beams can occur away from the joint region. This introduces different design demands for the panel zone. Despite the reduced participation of the panel zone in the inelastic response, this allows for the reduction of deformation demands in other structural components, namely in the beams.

El-Tawil et al. (1999) compared different panel zone design criteria and concluded that "weak" panel zones allow for lower plastic deformation on beams. However, for large rotation demands, the development of shear stresses is such that it can lead to brittle failure of the panel zones. Recently, a comparison of the American (ANSI, 2010) and European (CEN, 2005b) code provisions for the design of the panel zone (Brandonisio et al., 2011, 2012) allowed concluding that the criteria defined in the American code avoids shear buckling of the panel zone. On the other hand, it was

found that the requirements of the European code are unsafe and do not ensure the stability of the panel zone under large inelastic deformations. Consequently, it was recommended that the non-dimensional slenderness, $\overline{\lambda}_w$, of the panel zone should be lower than 0.3 for commonly adopted aspect ratios corresponding to a panel zone slenderness, b/t, lower than 50ε, where t and b are the panel zone width and thickness, respectively. ε is coefficient depending on f_y, $\varepsilon = \sqrt{235/f_y}$.

This chapter provides a critical overview of the seismic design criteria for panel zones. The influence of the procedure adopted for panel zone design on the local and global behaviour of steel moment frames is assessed. Emphasis is placed on the definition of a consistent and reliable criterion for the panel zone design. To this end, a parametric study involving several steel moment-resisting frames is carried out, in which the panel zones are designed according to different approaches. The assessment of the structures is performed with both non-linear static and response-history analyses.

4.2 Panel zone design

Code provisions and guidelines for the design of panel zones have been subjected to numerous changes over the years. The reader is referred to Castro et al. (2005) and Davila-Arbona (2007) for an extensive description of the evolution of the design criteria of panel zones since the '70s.

Experimental studies conducted by Fielding and Huang (1971), Bertero et al. (1972) and Krawinkler (1978) concluded that even after yielding, a panel zone develops stable and ductile behaviour. The main conclusions of these studies were then included in the ICBO (1988). These code provisions allowed yielding of the panel zone to occur. However, during the 1994 Northridge earthquake, significant damage in the welded zones of joints was observed and later attributed to high levels of panel zone distortion. As a consequence, new design guidelines (FEMA, 2000) were proposed and established a criterion in which the beams and the panel of zone should yield simultaneously. The following sections summarize both the European and American design rules for panel zones.

4.2.1 American code provisions and design guidelines

4.2.1.1 FEMA350 (FEMA, 2000)

After the 1994 Northridge earthquake, and due to the significant damages that occurred in steel joints, an extensive research campaign was carried out aiming at the development of new guidelines and standards for the design, assessment and retrofit of steel buildings in seismic zones. Within the research campaign, a large number of experimental tests of steel joints were conducted. It was concluded that a more stable and ductile behaviour of the joints was obtained when the yielding of the panel zone occurred simultaneously with the yielding of the connecting beams (i.e. a "balanced" panel zone approach). Thus, the guidelines of FEMA 350 (FEMA, 2000)

proposed the use of "balanced" panel zones, where the required panel zone thickness is given by:

$$t \geq \frac{C_y \times M_c \times \left(\frac{H-d_b}{H}\right)}{0.9 \times 0.6 \times f_{yc} \times R_{yc} \times d_c \times (d_b - t_{bf})} \tag{4.1}$$

where t is the equivalent panel zone thickness (including doubler plates), $C_y \times M_c$ is the sum of the beam yielding moments, H is the average storey height, d_c is the column depth, d_b is the beam depth, f_{yc} is the column yield strength and R_{yc} is the ratio between the expected and the nominal yield strength of the column.

4.2.1.2 AISC 2010 (ANSI, 2010)

To what concerns AISC-2010 (ANSI, 2010), the document specifies that the panel zone must be reinforced when the required force for Load and Resistance Factor Design (LRFD), $\sum R_u$, exceeds the panel zone strength, $\phi_v \times R_n$ as shown in:

$$\sum R_u \leq \phi_v \times R_n \tag{4.2}$$

where ϕ_v is the resistance factor for the panel zone strength, taken as $\phi_v = 1.0$ for LRFD design.

The required shear strength for the panel zone is calculated as follows:

$$\sum R_u = \frac{M_{f1}}{d_{b1}} + \frac{M_{f2}}{d_{b2}} - V_{col} \tag{4.3}$$

$$V_{col} = \frac{(M_{f1} + M_{f2})}{H} \tag{4.4}$$

where $M_{f1} = M_{f1L} + M_{f1G}$ is the sum of bending moments due to factored lateral loads, M_{f1L}, and the bending moments due to factored gravity loads, M_{f1G}; $M_{f2} = M_{f2L} - M_{f2G}$ is the difference between the bending moments due to factored lateral loads, M_{f2L}, and the bending moments due to factored gravity loads, M_{f2G}; d_{b1} and d_{b2} are the beams depth; V_{col} is the column shear and H is the average storey height above and below the joint.

The nominal panel zone shear strength depends on whether or not the shear deformation of the panel zone is considered in the analysis. If not considered, the nominal panel zone shear strength should be determined as:

$$For \quad P_r \leq 0.4 \times P_c : \qquad R_n = 0.60 \times f_{yc} \times d_c \times t_p \tag{4.5}$$

$$For \quad P_r > 0.4 \times P_c : \qquad R_n = 0.60 \times f_{yc} \times d_c \times t_p \times (1.4 - P_r/P_c) \tag{4.6}$$

where P_r is the axial design capacity, P_c is $0.6 \times P_y$ (P_y is the axial yield strength of the column), f_{yc} is the minimum specified yield stress of the column, d_c is the column depth and t_p is the panel zone thickness.

When frame stability (including plastic panel zone deformation) is considered in the analysis, the nominal shear strength of the panel zone is given by:

$$For \quad P_r \leq 0.75 \times P_c : \quad R_n = 0.60 \times f_{yc} \times d_c \times t_p \times \left(1 + \frac{3 \times b_{cf} \times t_{cf}^2}{d_b \times d_c \times t_w}\right) \tag{4.7}$$

$$For \quad P_r > 0.75 \times P_c : \quad R_n = 0.60 \times f_{yc} \times d_c \times t_p \times \left(1 + \frac{3 \times b_{cf} \times t_{cf}^2}{d_b \times d_c \times t_w}\right) \times \left(1.9 - \frac{1.2 \times P_r}{P_c}\right) \tag{4.8}$$

where b_{cf} is the column flange width; t_{cf} the column flange thickness; d_b the beam depth and t_w is the panel zone thickness.

Finally, a minimum panel zone thickness condition is established to avoid local buckling of the column web, according to:

$$t \geq \frac{d_z + w_z}{90} \tag{4.9}$$

where t is the thickness of the column web including doubler plates, d_z is the depth of the panel zone between continuity plates and w_z is the width of panel zone between column flanges.

4.2.1.3 ASCE 41-13 (ASCE/SEI, 2013)

ASCE 41-13 (ASCE/SEI, 2013) is one of the most recent guidelines for the seismic evaluation and retrofit of existing buildings. According to the document, the shear demand of the panel zone should be determined at the development of a hinge at the critical location of the connection as follows:

$$V_{PZ} = \frac{\sum M_{b,pl}}{d_b} \times \left(\frac{L}{L - d_c}\right) \times \left(\frac{H - d_b}{H}\right) \tag{4.10}$$

where $\sum M_{b,pl}$ is the sum of the yield moments of the connecting beams, d_b the depth of beam, L is the length of beam between the centreline of the columns, d_c is the column depth and H is the average storey height of columns.

Additionally, the expected shear strength of the panel zone is defined as:

$$V_y = 0.55 \times f_{ye} \times d_c \times t_p \tag{4.11}$$

where f_{ye} is the expected yield strength of the column and t_p is the total thickness of panel zone, including doubler plates.

4.2.2 European standards - Eurocodes

The verification of the panel zone in the seismic design situation according to Eurocode 8 (EC8) (CEN, 2005b) should be performed by ensuring that the shear force demand, $V_{wp,Ed}$, is lower than the shear strength, $V_{wp,Rd}$, according to:

$$\frac{V_{wp,Ed}}{V_{wp,Rd}} \leq 1.0 \tag{4.12}$$

The resulting shear force, $V_{wp,Ed}$, on the panel zone should be calculated according to Part 1-8 of Eurocode 3 (EC3-1-8) (CEN, 2005b), as:

$$V_{wp,Ed} = \frac{M_{b1,Ed} - M_{b2,Ed}}{z} - \frac{V_{c1,Ed} - V_{c2,Ed}}{2} \tag{4.13}$$

where $M_{b1,Ed}$ and $M_{b2,Ed}$ are the bending moments at the column faces; $V_{c1,Ed}$ and $V_{c2,Ed}$ are the column shear forces (see Figure 4.2) and z is the lever arm, taken as the difference between the beam depth, d_b, and the flange thickness, t_{fb}. It is important to note that, according to the European seismic code (CEN, 2005c), the design shear force in the panel zone, $V_{wp,Ed}$, should take into account the plastic resistance of the adjacent dissipative zones in the beams or connections. Therefore, for welded beam-column connections, the design shear force must be calculated assuming the plastic bending moment resistance of the connecting beams.

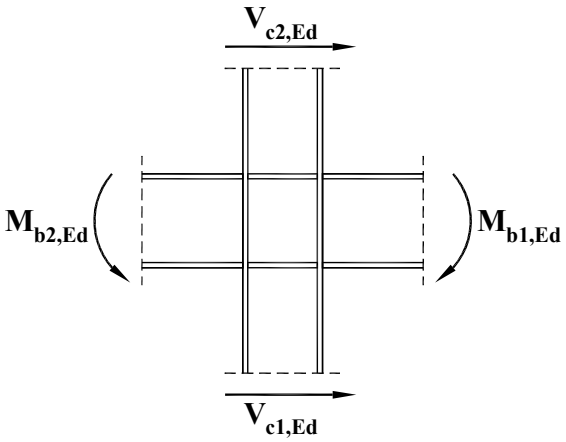

Figure 4.2: Shear forces and bending moments acting on the joint.

According to EC3-1-8 (CEN, 2005b), for panel zones with slenderness, d/t_w, lower than 69ε (where ε is coefficient depending on f_y, $\varepsilon = \sqrt{235/f_y}$), the plastic shear resistance, $V_{wp,Rd}$, of an unstiffened column panel zone, should be obtained using:

$$V_{wp,Rd} = \frac{0.9 \times f_{y,wc} \times A_{vc}}{\sqrt{3} \times \gamma_{M0}} \tag{4.14}$$

where $f_{y,wc}$ is the yield strength of the column web, A_{vc} is the shear area of the column and

γ_{M0} is the partial safety factor. The shear area, A_{vc}, should be calculated according to EN 1993-1-1 (CEN, 2005a). The reduction factor, 0.9, used in the expression intends to consider the reduction in the shear strength due to axial loads. However, EC8 clearly states that it is not required to take into account the effect of the axial force and bending moment on the plastic resistance in shear.

If transverse web stiffeners are used in both the compression and tension zone, the plastic shear resistance of the panel zone, $V_{wp,Rd}$, may be increased by $V_{wp,add,Rd}$ as:

$$V_{wp,add,Rd} = \frac{4 \times M_{pl,fc,Rd}}{d_s} \quad but \quad V_{wp,add,Rd} \leq \frac{2 \times M_{pl,fc,Rd} + 2 \times M_{pl,st,Rd}}{d_s} \tag{4.15}$$

where d_s is the distance between the centrelines of stiffeners and $M_{pl,fc,Rd}$ and $M_{pl,st,Rd}$ are the design plastic bending moment resistance of a column flange and stiffener, respectively. Figure 4.3 shows the typical monotonic zone behaviour curve of a panel zone, where the above-mentioned shear resistances are identified.

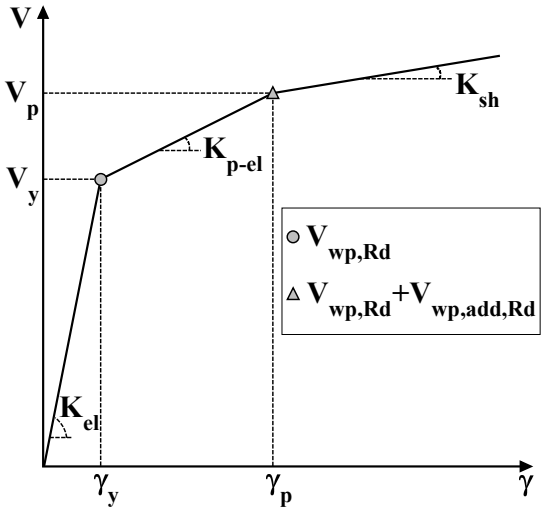

Figure 4.3: Monotonic behaviour of a panel zone .

The shear strength of the panel zone can be increased by adding supplementary web plates. Nevertheless, EC3-1-8 (CEN, 2005b) defines a set of requirements that should be fulfilled for this to be allowed: 1) the thickness, t_s, of the supplementary web plate should be not less than the column web thickness, t_{wc}; 2) when the column web is reinforced by adding a supplementary web plate, the shear area, A_{vc}, may be increased by $b_s \times t_{wc}$. If further supplementary web plate is added on the other side of the web, no further increase of the shear area should be made; 3) the steel grade of the supplementary web plate should be equal to that of the column. The fulfilment of these code requirements implies that the panel zone can only be reinforced with one supplementary web plate, with a thickness equal to that of the column web. However, for seismic design situations, these criteria are extremely restrictive. The consequence for the designer is that if plates with additional thickness are required, the designer is forced to change the column's section profile. For example, if the structure is designed to dissipate energy in the beams, the connections of the beams to the

columns should be designed for the required level of overstrength, taking into account the plastic bending moment resistance, $M_{pl,Rd}$, and the shear force, $(V_{Ed,G} + V_{Ed,M})$. Notwithstanding, the code is not explicit in defining if the capacity design criterion should be applied for the connection and panel zone, since the design criteria and strength capacity indicate that the dissipative behaviour of the panel zone could be considered. Specifically, if capacity design of the panel zone is required, this will be characterized by higher demands which may lead to the adoption of stronger columns due to limitation of the supplementary web plate thickness. Eurocode 8 also allows for the use of semi-rigid and/or partial strength connections. For such case, the following requirements for the panel zone should be met: 1) the connections have a rotation capacity consistent with the global deformations; 2) the effect of connection deformation on global drift is taken into account using non-linear static (pushover) global analysis or non-linear response-history analysis. Additionally, the design of the connection should be such that the rotation capacity of the plastic hinge region, θ_p, is not less than 35 mrad and 25 mrad, for structures of ductility class DCH and DCM (with $q > 2$), respectively. The shear resistance of the panel zone should comply with Equation 4.12, and the shear deformation of the column's web panel should not contribute to more than 30% of the plastic rotation capacity of the joint, θ_p. The practical implementation of these criteria may prove difficult to attain, since engineers typically resort to elastic numerical models in the design, in which the assessment of plastic rotation of connection components is unfeasible. Therefore, it is necessary to establish a design criterion that automatically incorporates and satisfies the previous requirements. Regarding the European standard for the assessment and retrofitting of buildings for earthquake resistance, EN 1998-3 (CEN, 2005e), the code states that the panel zone at beam-column connections should remain elastic at the damage limitation limit state. Moreover, the thickness of the column panel zone (including the doubler plate), t_w, should satisfy the following equation, to prevent premature local buckling under large inelastic shear deformations:

$$t_w \geq \frac{d_{pz} + w_{pz}}{90} \tag{4.16}$$

where d_{pz} and w_{pz} are the panel zone depth and width, respectively.

Continuity plates with thickness not less than that of beam flanges should be placed symmetrically on both sides of the column web to ensure satisfactory performance at all limit states.

The required strength of the panel zone is given by:

$$d_c \times t_w \times \tau_y \geq \frac{\sum M_{pl,b}}{d_b} \times \left(\frac{L}{L - d_c}\right) \times \left(\frac{H - d_b}{H}\right) \tag{4.17}$$

where d_c and t_w are the column depth and panel zone thickness, respectively, d_b is the beam depth, τ_y is the yield shear strength and H and L are the average storey height and distance between the column centrelines, respectively. As one may infer from the previous equations, this methodology is similar to that of AISC 2010 (ANSI, 2010) and ASCE/SEI 41-13 (ASCE/SEI, 2013) (see Equation 4.9 and 4.10).

4.3 Panel zone modelling

4.3.1 Cruciform beam-column sub-assemblages

Typically, the study of the behaviour of joints/connections in moment-resisting frames is carried out using a cruciform sub-assemblage structure, which is assumed to be representative of the behaviour of a moment-resisting frame (see Figure 4.4). Under lateral loads the inflection points are assumed to occur at the mid-height of the columns and at the mid-span of the beams.

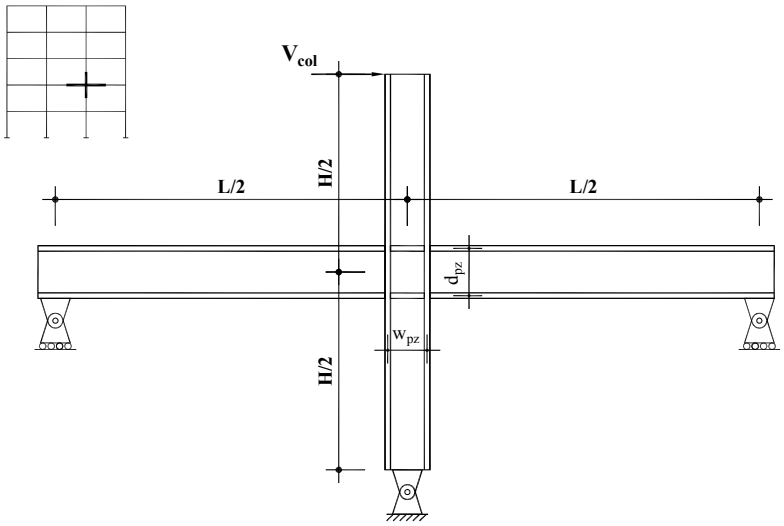

Figure 4.4: Cruciform beam-column sub-assemblages.

Making use of equilibrium equations for the simplified cruciform structure, it is possible to define the shear demand of the panel zone as a function of the bending moments of the beams and the shear forces of the columns, as:

$$V_{PZ} = \frac{M_{b,L}}{d_{pz}} + \frac{M_{b,R}}{d_{pz}} - V_{col} \tag{4.18}$$

For a symmetric structure, the bending moments in the beams are equal and can be related with the column shear force as follows:

$$M_{b,L} = M_{b,R} = R_{Beam} \times \left(\frac{L}{2} - \frac{w_{pz}}{2}\right) \tag{4.19}$$

$$V_{col} \times H = R_{Beam} \times L \tag{4.20}$$

$$M_{b,L} = M_{b,R} = V_{col} \times \frac{H}{L} \times \left(\frac{L}{2} - \frac{w_{pz}}{2}\right) \tag{4.21}$$

Substituting Equation 4.21 into Equation 4.18, Equation 4.22 is obtained, which is the shear demand of the panel zone for a given bending moment of the beam.

$$V_{PZ} = 2 \times M_b \times \left[\frac{1}{d_{pz}} - \frac{1}{(L - w_{pz})} \times \left(\frac{L}{H} \right) \right] \tag{4.22}$$

Assuming that the formation of plastic hinges in the beams will occur, one can calculate the shear demand of the panel zone when the yield moment develops by replacing M_b by $M_{pl,b}$ (yield moment of the beam) in the previous equation (Equation 4.22).

Castro et al. (2008) defined a ratio of capacity to demand, β, as the ratio between the first yield shear force, $V_{y,pz}$, of the panel zone and the shear force that develops the plastic capacity of the connecting beams, as:

$$\beta = \frac{V_{y,pz}}{V_{pl,pz}} \tag{4.23}$$

For simultaneous yielding of the panel zone and the connecting beams, the β parameter should be equal to one, corresponding to a "balanced" panel zone design. In a similar manner, a β value smaller than 1.0 indicates a "weak" panel zone, in which the yielding of the panel zone occurs before yielding of the beams. Conversely, β greater than 1.0 implies a "strong" panel zone, in which the yielding of beams occurs before the yielding of the panel zone. Equation 4.23 can thus be rewritten with the inclusion of β, and an equation to obtain the thickness of the panel zone depending on the design criterion can be written as:

$$t_{pz} = \beta \times \frac{\sum M_{pl,b}}{w_{pz} \times \tau_y} \times \left[\frac{1}{d_{pz}} - \frac{1}{(L - w_{pz})} \times \left(\frac{L}{H} \right) \right] \tag{4.24}$$

It is important to note that the aforementioned derivation assumes that the shear stress in the panel zone is constant over the depth of the component and that, once the yield shear stress is reached, all the panel has yielded.

4.3.2 Analytical model

Different analytical models for the panel zone have been proposed in the literature in the last fifty years. The most relevant proposals are summarized in Figure 4.5. Fielding and Huang (1971) suggested a bi-linear model to reproduce the behaviour of the panel zone. A few years later, Krawinkler (1978) proposed a tri-linear model and, more recently, Kim and Engelhardt (2002) suggested a quadri-linear analytical model. All proposals have similar behaviour in the elastic range, but are significantly different for the inelastic range. Among them, the tri-linear model proposed by Krawinkler (1978) is the most used approach due to its simplicity and robustness, being able to accurately simulate both the elastic and inelastic behaviour of a panel zone. As such, this model was implemented in this research study.

Castro et al. (2005) derived the analytical model parameters of Krawinkler (1978) for the elastic range, which can be obtained based on the application of simple concepts of mechanics of

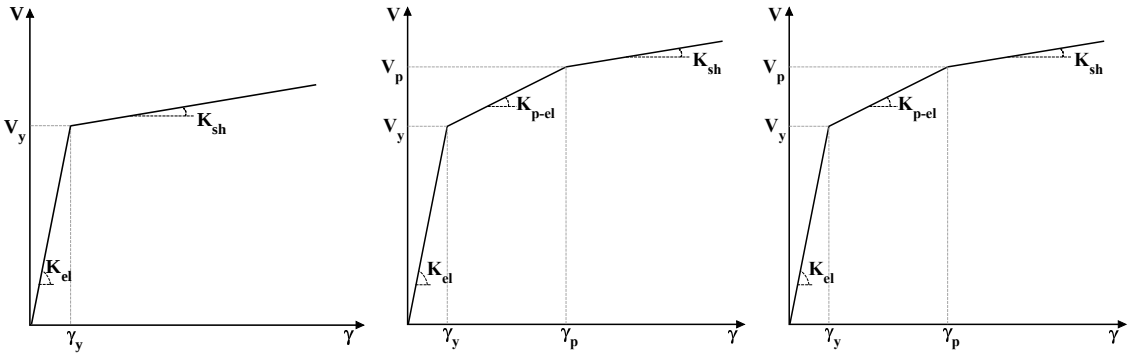

(a) Fielding and Huang (1971) (b) Krawinkler (1978) (c) Kim and Engelhardt (2002)

Figure 4.5: Panel zone analytical models.

materials, as follows:

$$V_y = \frac{f_y}{\sqrt{3}} \times A_v \tag{4.25}$$

$$\tau = G_s \times \gamma \tag{4.26}$$

$$\gamma_y = \frac{\tau_y}{G_s} = \frac{f_y}{\sqrt{3} \times G_s} \tag{4.27}$$

where V_y and γ_y are the yield shear force and yield distortion, respectively, τ is the shear stress, f_y is the panel zone yield strength, A_{vc} is the shear area, G_s is the elastic shear modulus of the steel material and γ is the panel zone distortion.

It is important to note that different definitions of the effective shear area, A_v have been proposed. Fielding and Huang (1971) proposed that the effective shear area shouild be taken as $A_v = d_c \times t_{wc}$ (where d_c is the column depth and t_{wc} is the column web thickness), Krawinkler (1978) defined $A_v = (d_c - t_{cf}) \times t_{wc}$ (where t_{cf} is the column flange thickness) while Wang (1988) considered the effective shear area equal to $A_v = (d_c - 2 \times t_{cf}) \times t_{wc}$.

The shear force demand in the panel zone can be determined as a function of the bending moment transferred by the beam, as follows:

$$V = \frac{M}{d_{pz}} \tag{4.28}$$

where d_{pz} is the distance between the mod-plane of the beam flanges and M the beam bending moment.

By rewriting the previous equations one can get:

$$M = G_s \times \gamma \times A_v \times d_{pz} \tag{4.29}$$

The yield moment and the elastic stiffness of the panel zone are given by:

$$M_{y,pz} = A_v \times d_{pz} \times \tau_y \tag{4.30}$$

$$K_{el} = \frac{M_{y,pz}}{\gamma_y} = A_v \times d_{pz} \times G_s \tag{4.31}$$

After yielding, the panel zone distortion is followed by bending of the column flanges. This phenomenon provides additional strength to the panel zone. Additionally, the continuity plates also contribute to in-plane additional stiffness. Krawinkler (1978) proposed an empirical expression for the post-elastic stiffness based on experimental results (see Equation 4.32).

$$K_{p-el} = \frac{4 \times E_s \times b_c \times t_{cf}^2}{10} = 1.04 \times G_s \times b_c \times t_{cf}^2 \tag{4.32}$$

According to Krawinkler (1978), the strain hardening starts at a distortion equal to four times the yield distortion and, consequently, the post yield strength can be calculated as:

$$M_{y,p-el} = M_{y,pz} + 3.12 \times \tau_y \times b_c \times t_{cf}^2 = A_v \times d_{pz} \times \tau_y \times \left(1 + \frac{3.12 \times b_c \times t_{cf}^2}{A_v \times d_{pz}}\right) \tag{4.33}$$

After yielding, the increase of strength is just due to strain hardening of the material. The strain hardening stiffness is usually defined as the elastic stiffness multiplied by a strain hardening parameter, μ, as:

$$K_{sh} = \mu \times K_{el} \tag{4.34}$$

4.3.3 Numerical model and validation

Several numerical models have been proposed in the past in order to simulate the behaviour of a panel zone. Among them, the Krawinkler and the Scissors (Charney and Downs, 2004) models have been widely used in the modelling of moment-resisting frames (Figure 4.6).

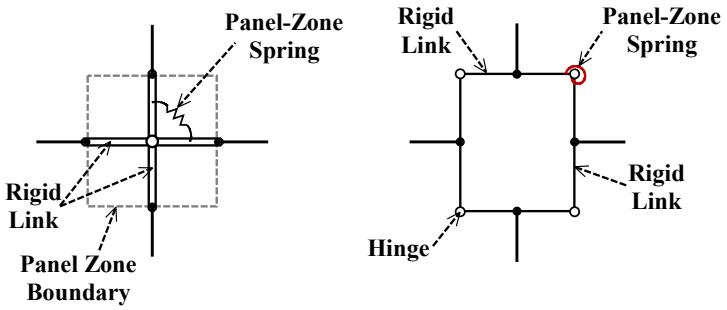

Figure 4.6: Panel zone mechanical models: Scissors model and Krawinkler model.

More recently, Altoontash (2004) developed a joint element that consists of five rotational springs, as shown in Figure 4.7. The four external nodes define the link of the beam and column elements connecting to the joint. Moment-rotation relationships can be assigned to each of these four nodes. The central node simulates the behaviour of the panel zone based on a moment-distortion relationship specified by the user. This joint element, "JOINT2D", has been implemented in the non-linear finite element analysis program OpenSees (McKenna, 2011).

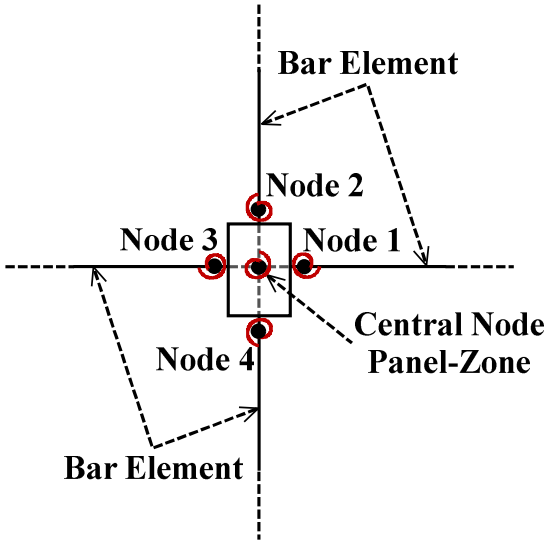

Figure 4.7: "JOINT2D" element implemented in OpenSees (McKenna, 2011).

The "JOINT2D" element was used in the numerical analyses carried out in this research study. Since frames with welded connections were considered, the springs of the four external nodes were assigned a rigid behaviour.

In order to evaluate the accuracy of the analytical and numerical models previously described, several monotonic and cyclic experimental tests were simulated and the experimental and numeric model results compared. The experimental tests conducted by Krawinkler (1971), Krawinkler and Bertero (1975) and Lee et al. (2002) were selected for this validation. All the tests were conducted in simplified cruciform sub-assemblage structures. The geometrical and material properties of the specimens are listed in Table 4.1.

Figure 4.9 and Figure 4.10 show a comparison of the results for two experimental tests under monotonic loading whereas Figure 4.11, Figure 4.12 and Figure 4.13 illustrate the results of three experimental tests under cyclic loading. The loading protocol considered in the cyclic experimental tests is shown in Figure 4.8. The tri-linear analytical model proposed by Krawinkler (1978) and the joint element "JOINT2D" were used in the comparisons. Moreover, it should be mentioned that several types of panel zone typologies (with and without additional plates, with and without continuity plates) were compared to cover the range of application of the analytical and joint element model.

Table 4.1: Experimental test data.

Model	Beam	Column	E	f_{yc}	f_{yb}	μ	L	H
			GPa	*MPa*	*MPa*	%	*m*	*m*
A1	10B15	8WF24	208	279	286	2.185	8.128	2.032
B1	14B22	8WF24	205.5	293	265	2.685	8.128	2.032
CR1	$W24\times94$	$W14\times283$	194.4/195.1/205.8	349.6	348.9	2.260	7.112	4.343
CR2	$W24\times94$	$W14\times193$	205.4/195.1/204.4	345.4	348.9	1.920	7.112	4.343
CR3	$W24\times94$	$W14\times176$	205.4/195.1/203.3	344.4	374.4	1.920	7.112	4.343

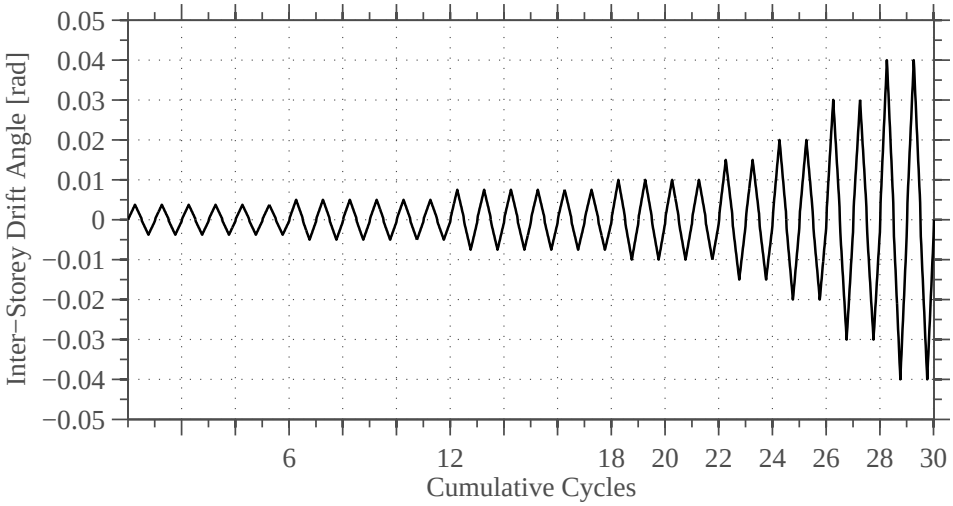

Figure 4.8: Loading protocol.

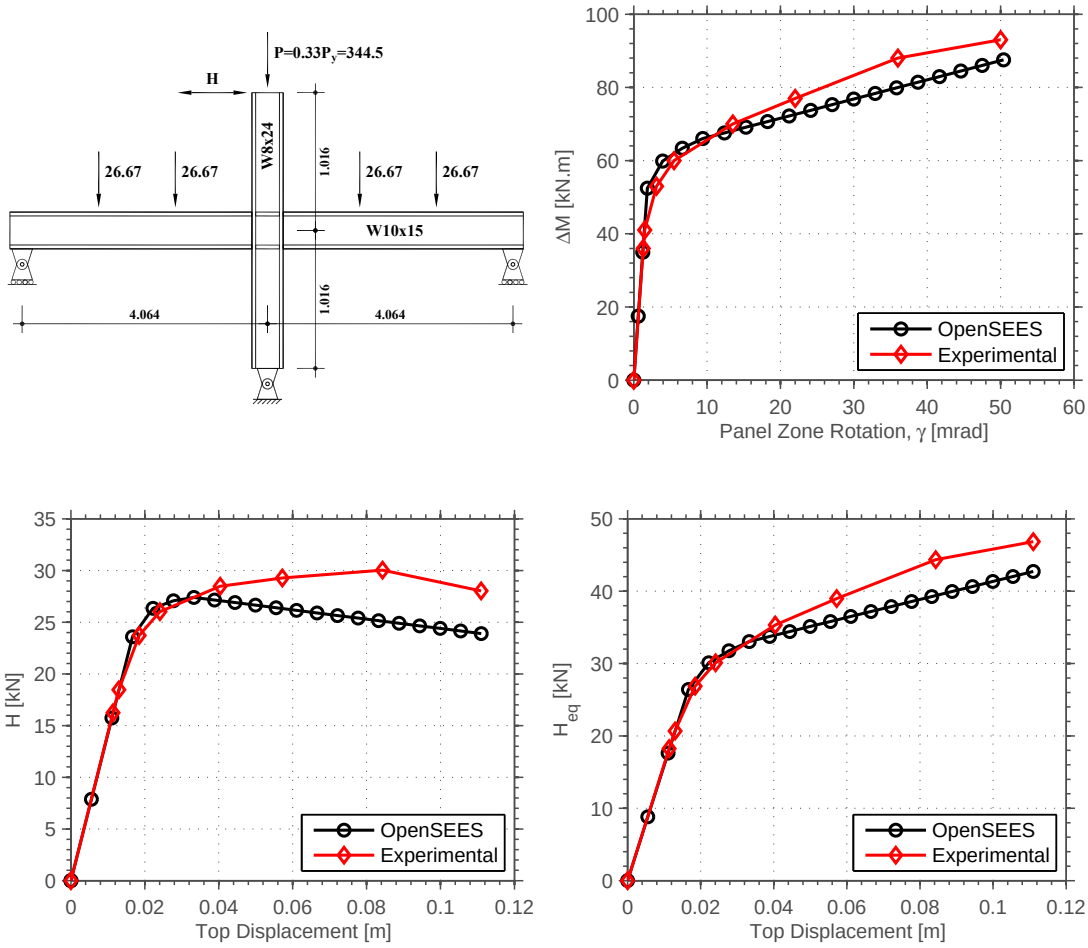

Figure 4.9: Validation of the numerical model for test A1 (Krawinkler, 1978).

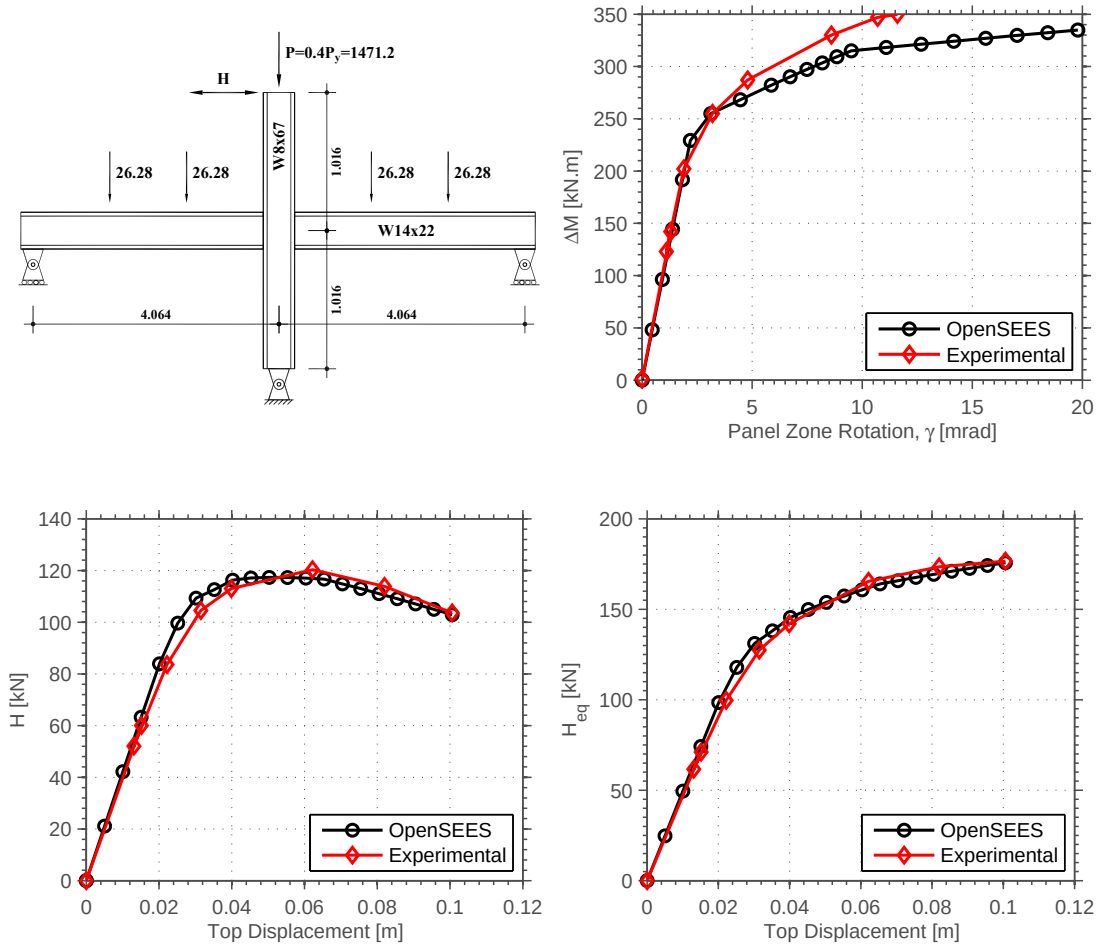

Figure 4.10: Validation of the numerical model for test B1 (Krawinkler, 1978).

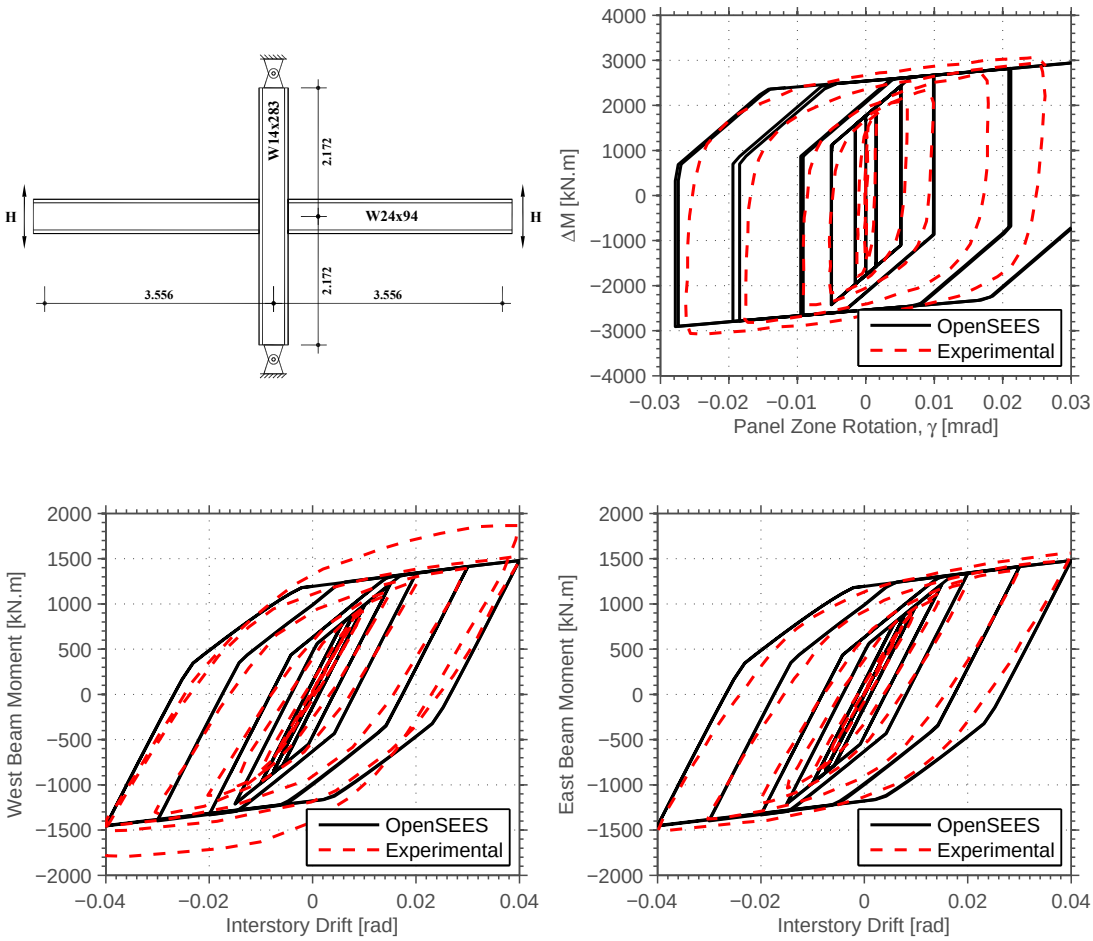

Figure 4.11: Validation of the numerical model for test CR1 (Lee et al., 2002).

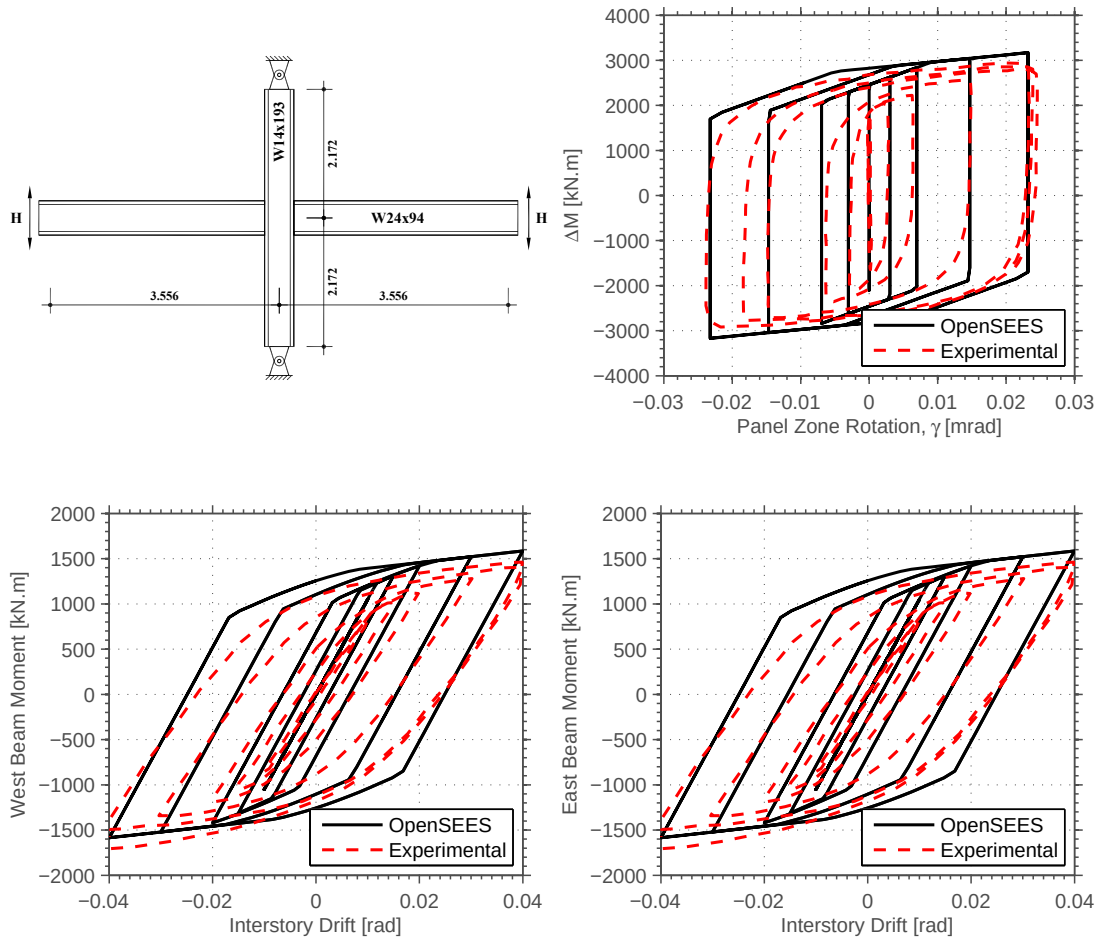

Figure 4.12: Validation of the numerical model for test CR2 (Lee et al., 2002).

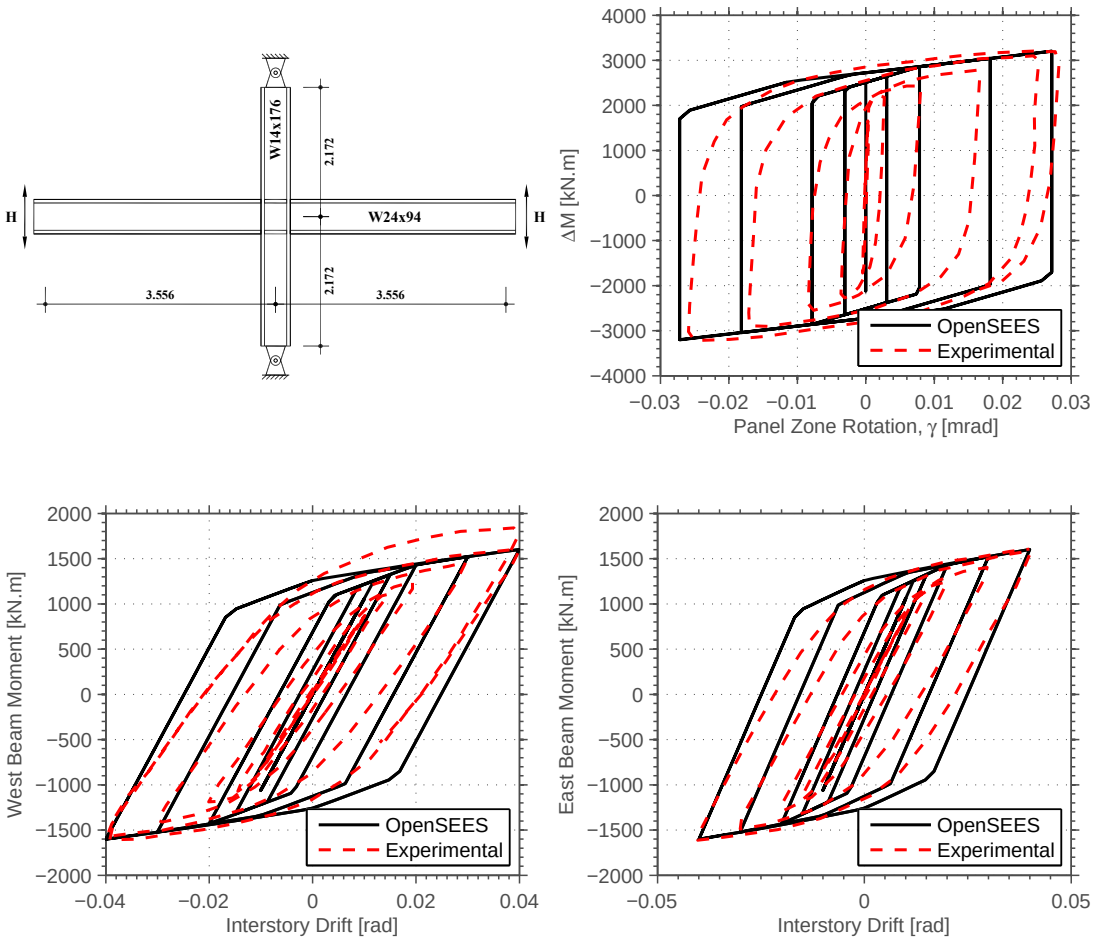

Figure 4.13: Validation of the numerical model for test CR3 (Lee et al., 2002).

The analysis of the results allows concluding that the Krawinkler (1978) tri-linear model can adequately simulate the behaviour of the cruciform structures. Additionally, the behaviour of the panel zones was also accurately captured. A good agreement between the experimental and numerical results for global and panel zone behaviour can be seen from the figures. Furthermore, this good correlation was obtained for all panel zone typologies.

4.4 Parametric study

In order to assess the influence of the panel zone design procedure on the lateral behaviour and seismic performance of moment-resisting frames, a detailed parametric study consisting of three different building configuration structures with different heights (2, 3, 4, 5 and 8 storey steel residential buildings) was defined. Figure 4.14 shows the elevation and plan views of one of the building configurations, whilst also identifying the analysed frame. It should be mentioned that in all the configurations, the resistance to seismic loads is provided by the MRFs in the longitudinal direction (x direction) and by a bracing system in the transversal direction (y direction). In this research study, only the longitudinal internal frames were subject of investigation. Table 4.2 shows a detailed definition of each building configuration.

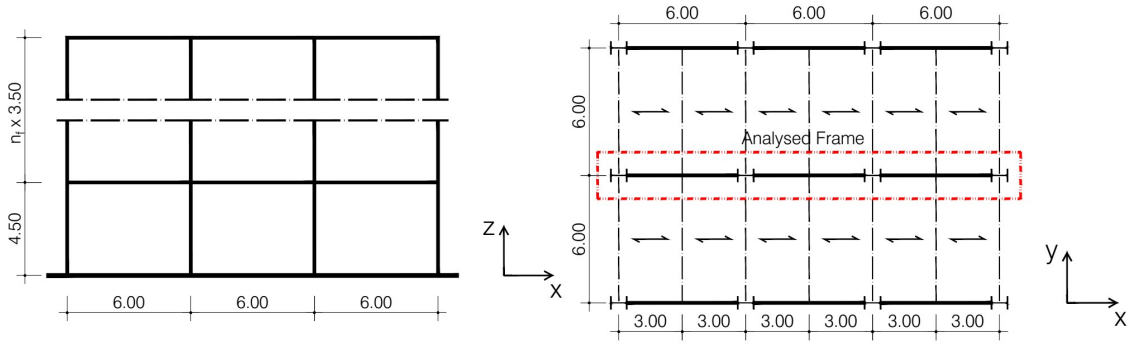

Figure 4.14: Building configuration 1: a) Elevation view, b) Plan view.

Table 4.2: Building configurations and geometrical properties

Config.	x-z plane		y-z plane		h_1 [m]	h_{others} [m]
	N. of frames	Bays[m]	N. of frames	Bays [m]		
1	3	6+6+6	4	6+6	4.5	3.5
2	3	8+8+8	4	8+8		
3	4	6+6+6+6	5	6+6+6		

A single geographic location in Portugal was defined for all buildings, namely Lisbon which is characterized as a moderate seismicity region.

4.4.1 Building design

Regarding the structural design, the buildings were firstly designed for gravity loads in accordance with the provisions of Eurocode 3 (CEN, 2005a) for the ultimate limit state (sectional and stability resistance checks) as well as for the serviceability limit state (deformation control). European steel HE sections were adopted for the columns and steel IPE sections for the beams. The seismic design was performed in accordance with the Improved Forced Based Design (IFBD) procedure discussed by Chapter 2. This design method essentially consists of a re-organization of the design steps proposed in EC8, whilst incorporating a more realistic procedure for the selection of the behaviour factor. The serviceability inter-storey drift ratio (IDR) was limited to 1% and the inter-storey drift sensitivity coefficient, θ, as defined in EC8, was limited to 0.2. The capacity design of the non-dissipative members was conducted according to the EC8 criteria with the modifications proposed by Elghazouli (2009). All frames were designed based on the equivalent lateral force analysis method. Further details about the buildings design and obtained design solutions can be found in Chapter 2.

4.4.2 Panel zone design

As previously discussed in this document, the design and verification of the panel zone according to European standards is ambiguous and inconsistent. Furthermore, there is an evident conflict between the different Eurocode parts. Therefore, the definition of a consistent and reliable procedure for the design of the panel zone under seismic actions is needed. The proposed procedure is based on a set of criteria proposed in both the European and American standards and guidelines, mainly consisting of:

1. definition of the thickness of the panel zone in accordance with Equation 4.24;
2. the slenderness of the panel zone, w_{pz}/t_{pz} , should be lower than 50ε to avoid shear buckling;
3. the thickness of the panel zone should satisfy the requirement shown in Equation 4.16, to prevent premature local buckling under large inelastic shear deformations.

Moreover, it should be noted that the requirements of Part 1-8 of Eurocode 3 (EC3-1-8) regarding supplementary web plates, namely that its thickness should be not less than the column's web thickness and not greater than column's web thickness, are extremely demanding for seismic design situations. Moreover, there are no analogous requirements in other seismic standards and guidelines. Consequently, the verification of this requirement was waived in this study. This assumption is even more acceptable when there is no evident justification for the imposed requirement, apart from possible construction issues.

As discussed by El-Tawil et al. (1999) and Popov (1987), there are three main philosophies for the seismic design of steel panel zones. These design philosophies essentially differ on the expected dissipative behaviour of panel zone. In the first approach, the panel zones remain elastic (i.e. strong panel zones) and all the plastic deformation occurs in the beams. Conversely, the panel zones could be designed to concentrate all the plastic deformation and beams remain elastic (i.e. weak panel zones). As noted by El-Tawil et al. (1999), the concentration of all inelastic deformation in the panel zones can induce adverse effects in the joints. Finally, the third design procedure seeks to distribute the plasticity between the beams and panel zone (i.e. balanced panel zone). Following the above mentioned design procedure and recognizing the limitations of weak panel zones, four different panel zone design provisions were considered in this study (each building was designed according to each of the four cases). In the first case, the buildings were assumed to have strong panel zones. In the second case, a procedure which aims to achieve balanced panel zones was used. For this case Equation 4.24 was applied to evaluate the required panel zone thickness, t_{pz}. In the third case, the panel zones were designed according to the 1988 version of ICBO (1988). In this design procedure the objective is to proportion the panel zone to resist the shear demand resulting from the development of 80% of the plastic moment capacities of the framing beams. The 20% reduction of the shear demand was proposed in UBC to account for the 'favourable' effect of the gravity moments. However, El-Tawil et al. (1999) concluded that this 20% reduction could significantly overestimate the effective reduction due to gravity-induced bending moments. Additionally, the use of a discretionary reduction factor when the gravity bending moments were calculated during the design process is arguable El-Tawil et al. (1999). Moreover, it is clear that the UBC procedure can only be considered for internal panel zones. This limitation has already been pointed out by El-Tawil et al. (1999). In order to overcome this limitation, an additional case is considered in this study in which the proposed procedure in the 1988 version of UBC is applied to internal zones and the external panel zones, according to a balanced panel zone criterion. A summary of the four design cases along with the values of the parameter β to use in Equation 4.24 is shown in Table 4.3.

Table 4.3: Panel zone design cases.

Case	Description	β - Internal Joints	β - External Joints
1	"Strong" panel zones	1.3	1.3
2	"Balanced" panel zones	1.0	1.0
3	ICBO (1988)	0.8	0.8
4	Modified ICBO (1988) for external panel zones	0.8	1.0

The adoption of a value of β equal to 1.3 in the definition of "strong" panel zones is related to the capacity design beam-column joint requirement specified in EC8. Moreover, if the panel zone is taken as a non-dissipative component, it should be designed with the appropriate overstrength

factors ($1.1 \times \gamma_{ov}$). However, EC8 does not clearly state that the panel zone should be considered as a non-dissipative component. The contribution of plastic deformation of the panel zone to the joint's plastic rotation is mentioned, and the panel zone shear resistance includes the contribution of column flanges, which implies the development of inelastic deformations. Figure 4.15 shows the effect of the panel zone modelling strategy on the fundamental period of vibration of the buildings.

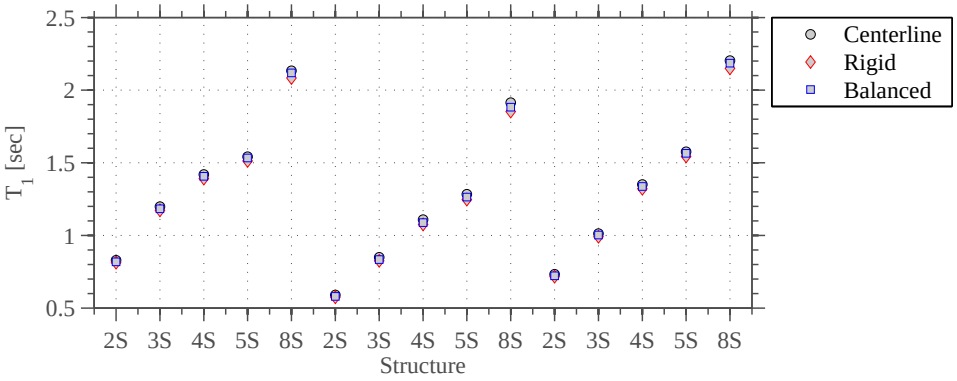

Figure 4.15: Building fundamental period of vibration for different modelling strategies.

The results shown in Figure 4.15 point to the low influence of the panel zone properties on the fundamental period of vibration of the buildings. These results confirm that the use of the centreline model approach to evaluate the modal properties of the buildings, thus computing the corresponding seismic loads, is appropriate and does not lead to unreasonable results. Such conclusion was already reached by Krawinkler and Mohasseb (1987). In order to have a consistent methodology for the analysis of the results, these will be presented for several joints identified in accordance with Figure 4.16.

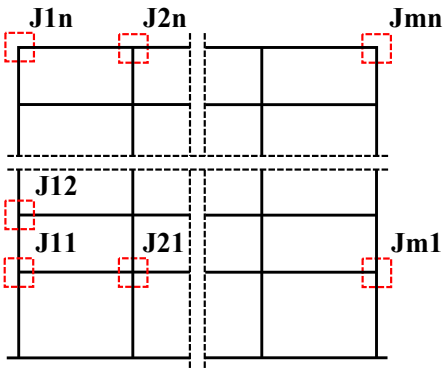

Figure 4.16: Joint identification.

Figure 4.17 shows the panel zone to column web thickness ratio. A ratio of 2 would be the maximum acceptable value according to the requirements of EC3-1-8 (CEN, 2005b). However, as it is possible to conclude from the results shown, this requirement would impose the use of larger

columns if non-dissipative or balanced panel zones are adopted. Nevertheless, the ratios exhibited by joints designed to have balanced behaviour are between 1.5 and 2.5, suggesting that the thickness of the additional plate is close to that of the column web. On the other hand, rigid/non-dissipative panel zones require significant plate thicknesses.

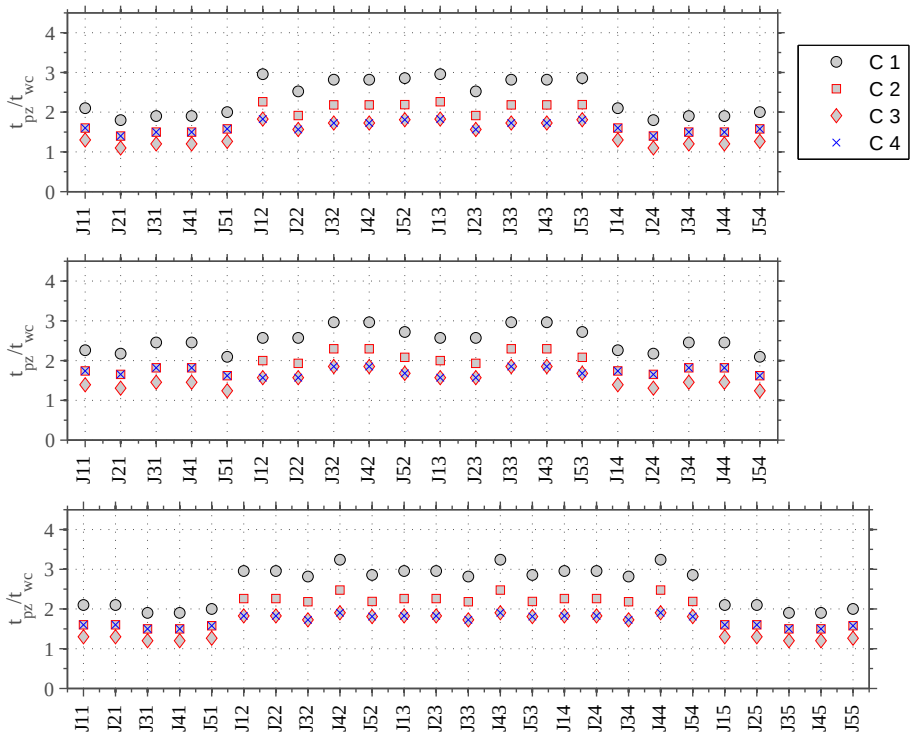

Figure 4.17: Panel zone to column web thickness ratio for the 5-storey buildings.

Regarding Case 3 and Case 4, the thickness of the additional plates is always lower than the column web thickness. Equally important are the slenderness requirements to avoid shear buckling. Figure 4.18 and Figure 4.19 show that, independently of the adopted design criterion, all panel zones comply with the slenderness requirement.

4.5 Nonlinear structural analysis

4.5.1 Numerical modelling

The assessment of the structures was carried out through non-linear static and response-history analyses conducted with the non-linear finite element analysis program OpenSees (McKenna, 2011). The material non-linear behaviour was considered through a concentrated plasticity approach considering strength, stiffness, and deterioration effects (Lignos and Krawinkler, 2010; Araújo and Castro, 2013). Figure 4.20a illustrates the calibrated cyclic flexural behaviour for a steel HEB300 profile. The effect of the axial load on the flexural capacity of the columns was taken into account in a simplified manner: 1) a preliminary pushover analysis was conducted to

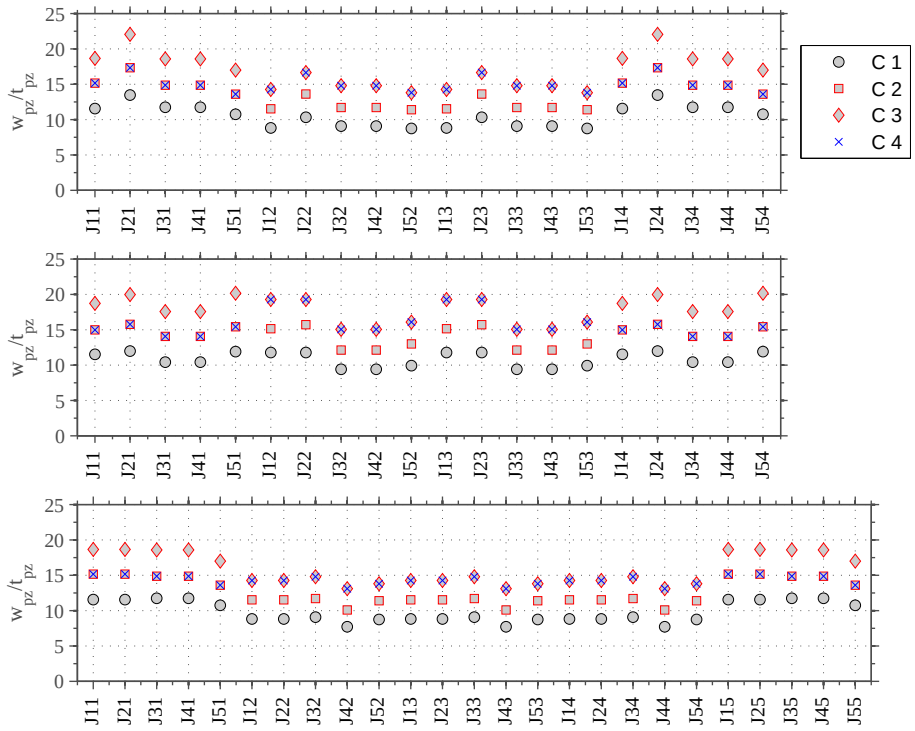

Figure 4.18: Panel zone slenderness for the 5-storey buildings.

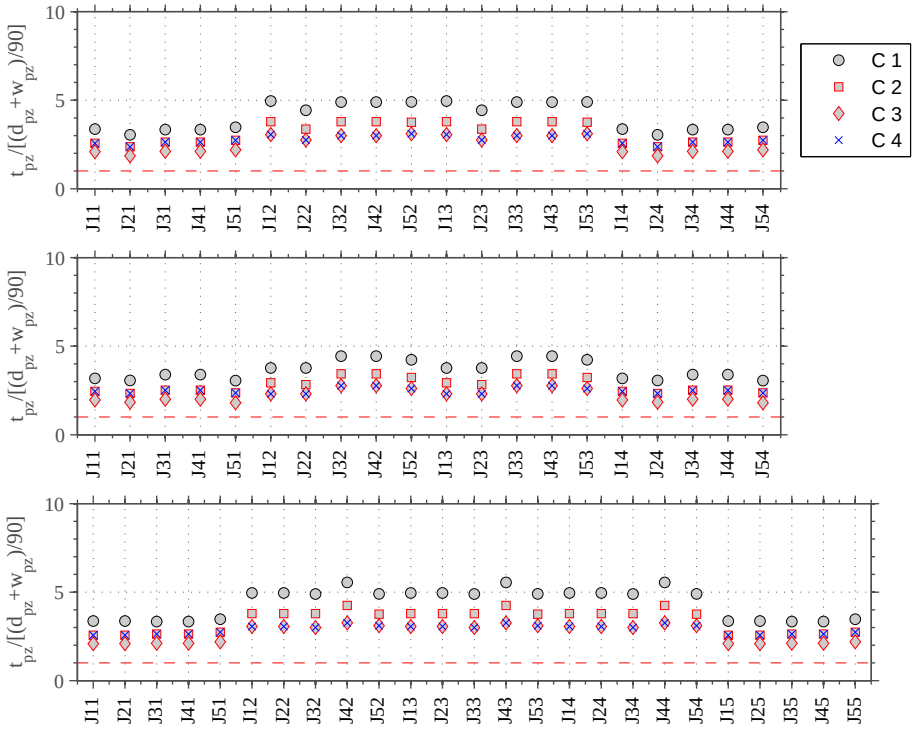

Figure 4.19: Panel zone Equation 4.16 condition for the 5-storey buildings.

evaluate the expected average axial force under the combined actions of gravity and lateral loading ($P_{grav} + 0.5 \times P_E^m ax$, where P_{grav} and $P_E^m ax$ are the axial load due to gravity loads and the maximum axial force due to lateral loading, respectively) (Zareian et al., 2010); 2) the backbone curve is adapted reducing the bending moment strength according to the axial force-bending moment interaction equations proposed in Part 1-1 of EC3 (CEN, 2005a). No modification of the stiffness and deterioration parameters is done. The panel zones were represented with a beam-column joint element, "JOINT2D", that is available in OpenSees. For the panel zone, the Krawinkler (1978) tri-linear moment-distortion relation was adopted. Furthermore, no degradation effects were considered in the panel zone. Figure 4.20b illustrates the adopted modelling strategy for the seismic performance assessment.

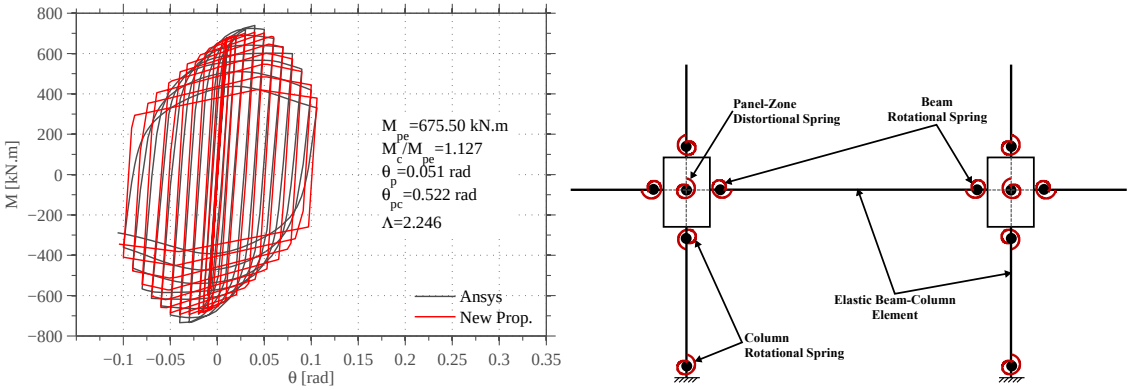

(a) (b)

Figure 4.20: Numerical modelling: a) cyclic flexural behaviour of an HEB300 and b) overview of the beams/columns elements and panel zones.

4.5.2 Nonlinear static analysis

Nonlinear static pushover analyses were performed on each building considering a first-mode proportional lateral load pattern, following Equation 4.35:

$$F_i = \lambda \frac{m_i \phi_{i,1}}{\sum_i^N m_i \phi_{i,1}} \tag{4.35}$$

where F_i is the horizontal force acting at floor i, λ is the load factorm m_i is the mass at floor i, $\phi_{1,i}$ is the ordinate of the fundamental mode at floor i and N is the number of storeys.

4.5.2.1 Global lateral behaviour

In order to evaluate the influence of the detailing of the panel zone on the lateral capacity of the buildings, a first comparison was conducted considering a building without additional panel zone plates and a building with the panel zones designed to have a balanced behaviour (Case 2), as shown in Figure 4.21. As expected, the buildings with balanced panel zones (Case 2) exhibit higher lateral capacity (+20/25%) in comparison with buildings with panel zones without any

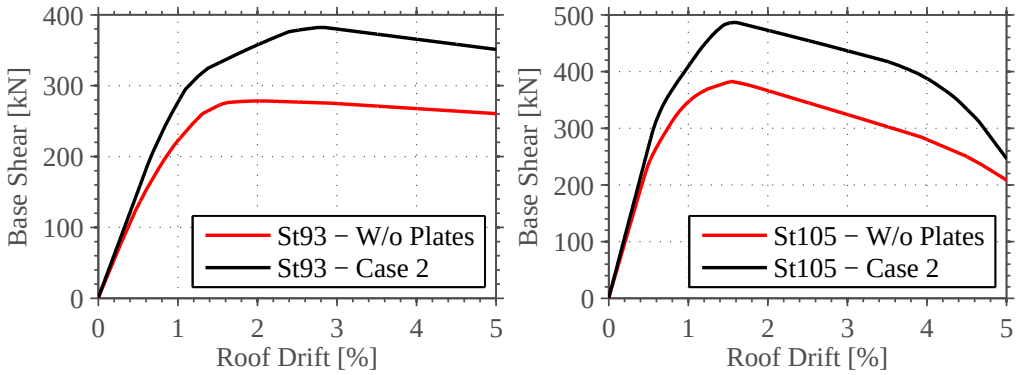

(a) (b)

Figure 4.21: Comparison of the lateral capacity of the buildings with and without additional panel zone plates.

doubler plates. The lateral behaviour of the buildings designed with different criteria for the panel zone is shown in Figure 4.22.

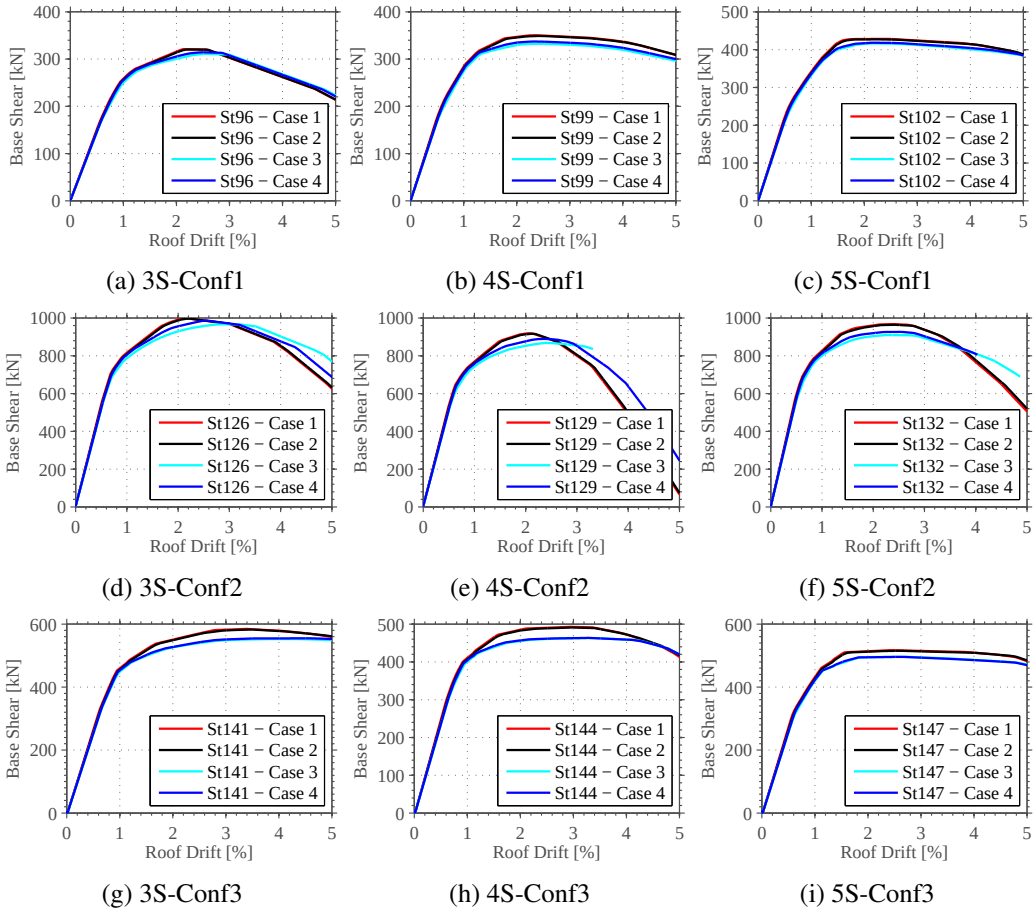

(a) 3S-Conf1 (b) 4S-Conf1 (c) 5S-Conf1

(d) 3S-Conf2 (e) 4S-Conf2 (f) 5S-Conf2

(g) 3S-Conf3 (h) 4S-Conf3 (i) 5S-Conf3

Figure 4.22: Pushover curves for buildings with 3, 4 and 5 storeys.

As expected, the frames designed to have strong panel zones (Case 1) show the highest lateral

capacity. Conversely, the frames designed according to the UBC approach (Case 3) exhibit the lowest lateral strength due to the presence of weaker panel zones. Nevertheless, the differences between the buildings designed with different panel zone conditions are not significant. Moreover, the ductility is similar for all the designed cases, indicating that although the buildings have different dissipation zones, the global lateral behaviour is identical.

4.5.2.2 Shear demand on the panel zones

The typical procedure to evaluate the shear demand on a panel zone is based on idealised assumptions, such as those considered in the derivation of Equation 4.18. However, the internal force distribution in a real frame does not necessarily follow such idealised scenario. It is therefore of interest to compare the actual shear demands imposed on the panel zones, as observed in the analysis, with those obtained assuming idealised conditions, where inflection points are assumed to form at the mid-span of the beams and at mid-height of the columns. The comparisons were established for both external and internal panel zones. The differences between the analytical and the actual shear demands on two external panel zones are depicted in Figure 4.23.

As one may infer from the results shown in Figure 4.23, the analytical shear demands imposed on the panel zones located at joints J11 and J21 (see Figure 4.16) were higher than the shear demands developing in the numerical model. This overestimation of the shear demand leads to a higher strength requirement for that panel zone, which is sufficient to change the strength ratio between the beam and the panel zone. Hence, the participation of the two components to the inelastic response is also different. However, it is important to note that there is not a constant pattern in terms of the differences between the analytical and the actual shear demands. Another important observation is that the overestimations at the yield displacement of the buildings ($\approx$1%) seem to be independent of the approach adopted for the panel zone design.

4.5.2.3 Plastic demands on beams and panel zones

The criteria adopted for the panel zone design has a significant influence on the plastic demands imposed on the structural components. Figure 4.24 shows the beam plastic rotation demands as well as the panel zone distortion demands. As expected, buildings designed to develop strong panel zones (Case 1) exhibit the highest beam plastic rotations and the lowest panel zone distortions. Conversely, buildings in which the panel zones were designed according to Case 3 and Case 4 displayed larger deformations in the panel zone. Designs according to Case 2 showed an intermediate and more desirable behaviour, where both the beam and the panel zone contribute to the joint plastic rotation. The results clearly point to the advantages of adopting balanced panel zones. The concentration of beam plastic rotations exhibited by Case 1 and the large panel zone distortions observed in Cases 3 and 4 indicate that the most adequate behaviour was achieved when both the beams and panel zones contribute to the inelastic response. However, it is important to note that the participation of the panel zone in Case 2 appears to be lower in comparison with the participation of the beam. This effect can be attributed to the analytical overestimation of the shear

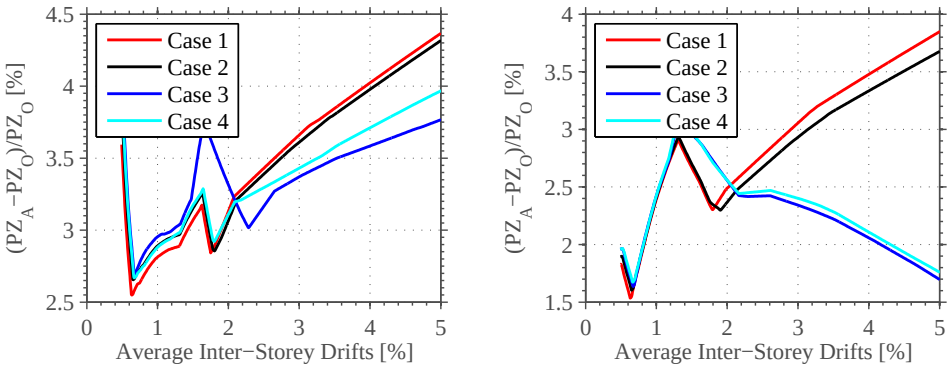

(a) *Conf 1 - J11* (b) *Conf 1 - J21*

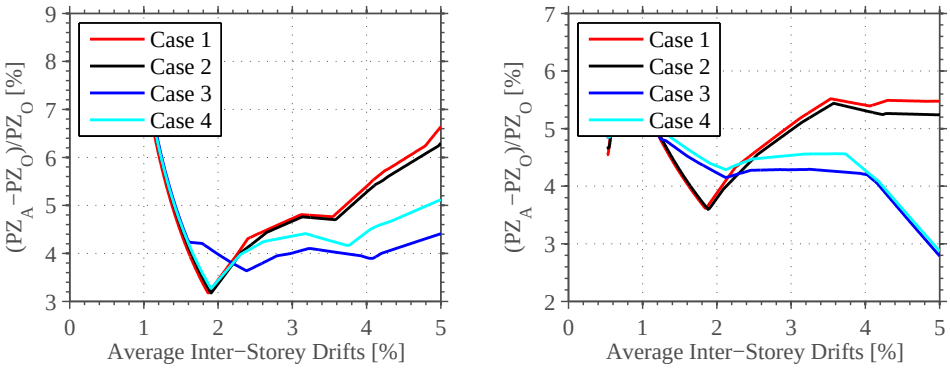

(c) *Conf 2 - J11* (d) *Conf 2 - J21*

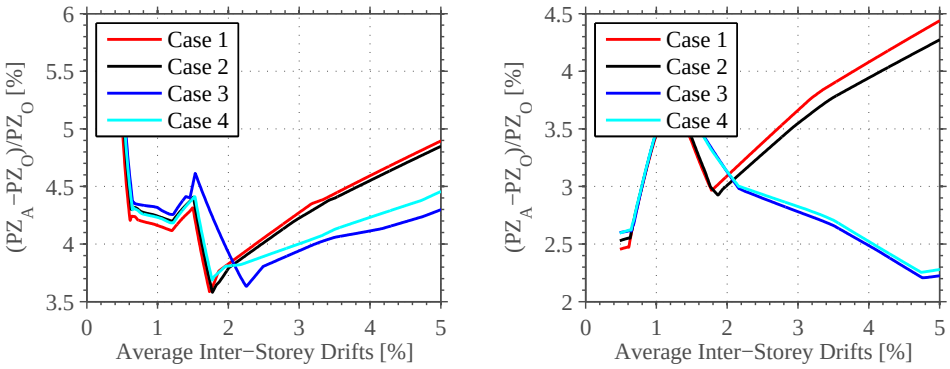

(e) *Conf 3 - J11* (f) *Conf 3 - J21*

Figure 4.23: Comparison of shear demands on panel zones on the 5-storey buildings.

demand imposed on the panel zone, which resulted in higher strengthening than that required to achieve a fully balanced panel zone. Finally, the effect of the gravity loads on the joint plastic mechanism is shown in Figure 4.24. As expected, for the external joints, the joint on the right (J41) yields earlier (for an ISDR of 0.8%). Additionally, for the internal joints, it was observed that the connecting beams yield at different deformation levels, causing the yielding of the panel zone after large lateral deformations (≈2%).

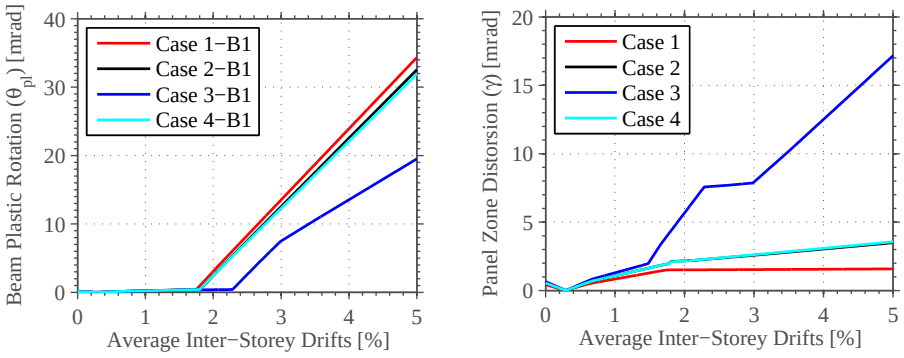

(a) *J11*

(b) *J11*

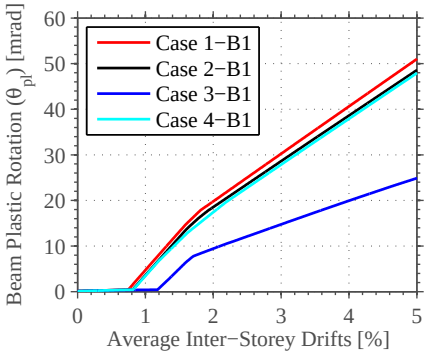

(c) *J41*

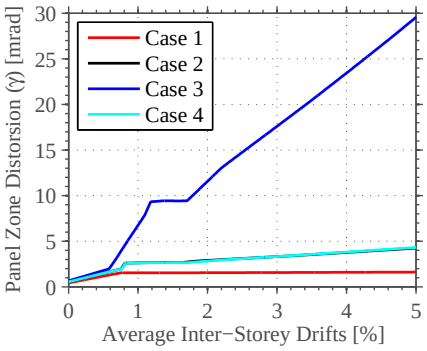

(d) *J41*

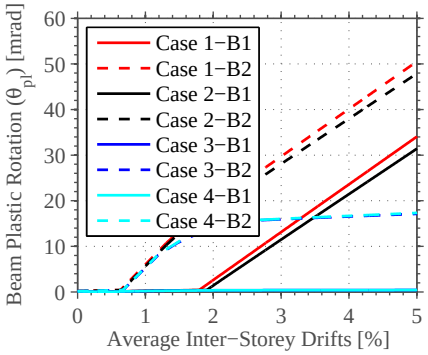

(e) *J21*

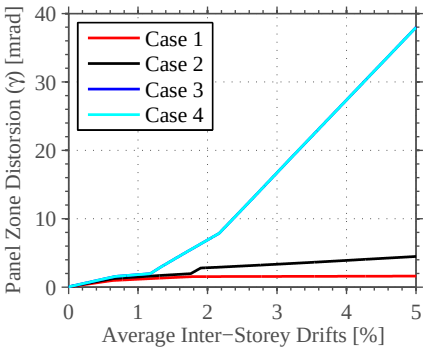

(f) *J21*

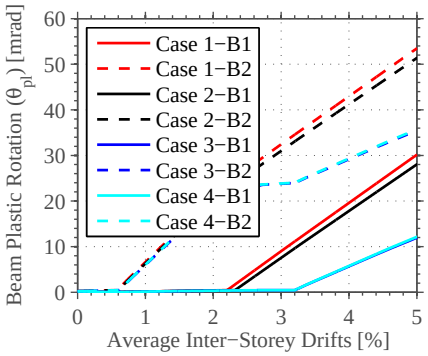

(g) *J22*

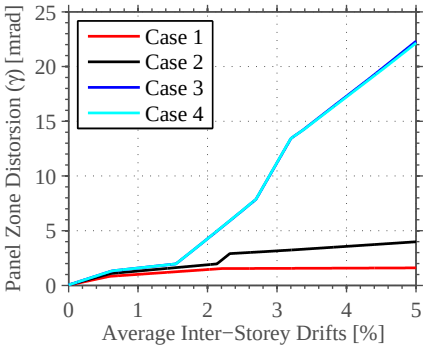

(h) *J22*

Figure 4.24: Comparison of plastic demands on joints (Conf. 1 - 5-storey building).

4.5.2.4 Moment distribution at the joints

The influence of the panel zone design criterion on the bending moment distributions at a joint is shown in Figure 4.25, for three different joints.

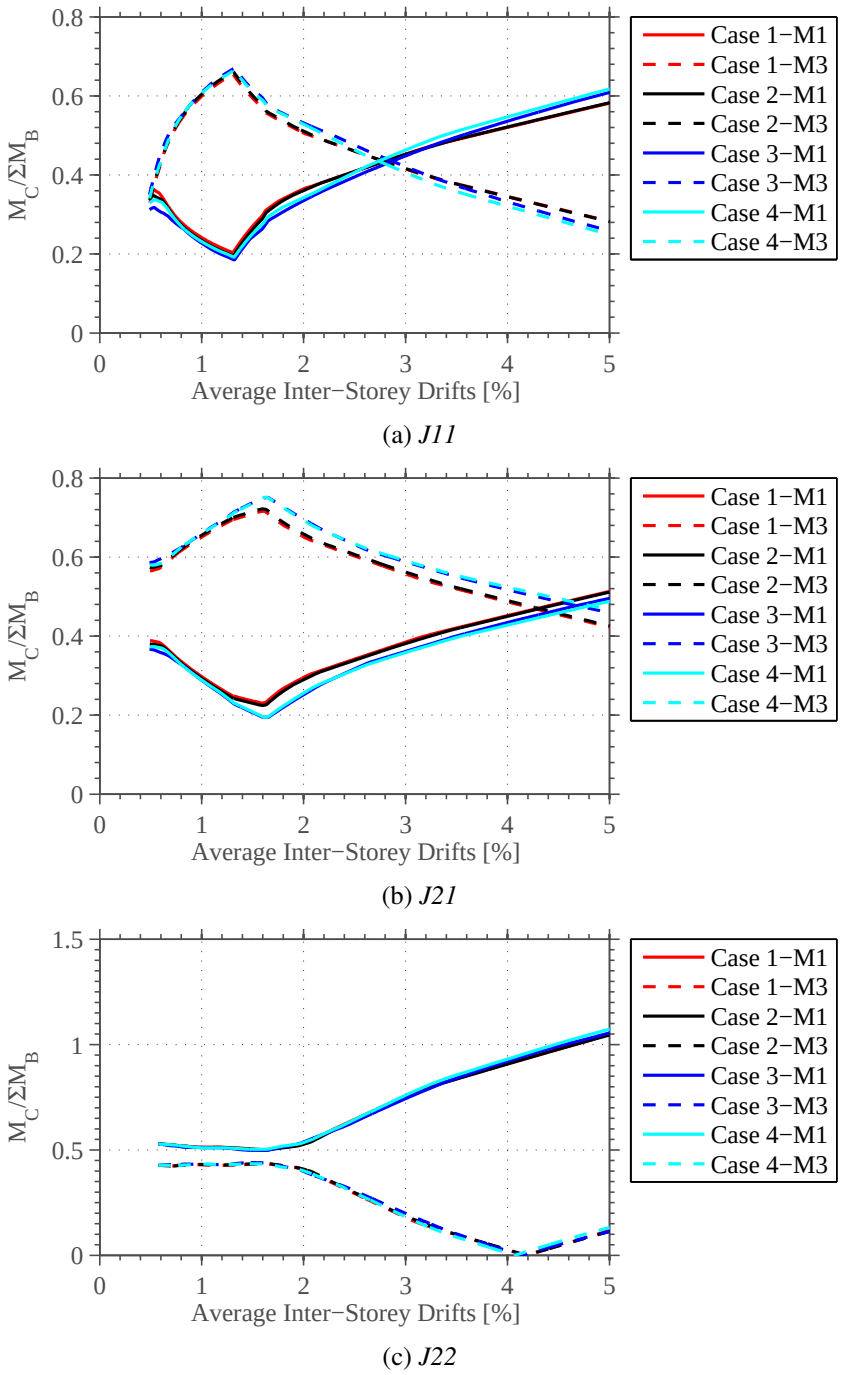

(a) *J11*

(b) *J21*

(c) *J22*

Figure 4.25: Moment distribution at several joints J11, J21 and J22.

Close inspection of the results shown in Figure 4.25 reveals that the criterion adopted for the panel zone design plays a minor role on the moment distribution. This observation is important to

clarify that the application of the capacity design criterion does not need to take into account the decisions taken concerning the design of the panel zones.

4.5.3 Response-history analysis results

The seismic performance assessment of the buildings was then conducted through the use of response-history analyses. A suite of forty ground motion records was selected following the disaggregation of the site hazard from PSHA conducted in Chapter 2 and the recent recommendations proposed by Araújo et al. (2016). The SelEQ framework (Chapter 5) was employed for the selection and scaling of the ground motions. Figure 4.26 shows the response spectra of the selected ground motion records for the site location under study, as well as the corresponding mean and median response spectra. A good matching between mean spectra of the selected ground motions and the code spectra was obtained, as one may infer from the figure.

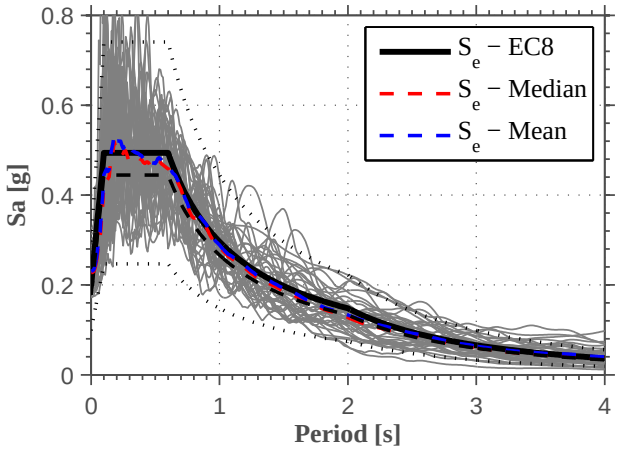

Figure 4.26: Response spectra of the selected ground motion records and EC8 elastic response spectrum.

Inherent damping was included using Rayleigh damping matrix, considering a damping coefficient equal to 2% assigned to the first two fundamental periods of vibration. Following the recommendation and coefficient modifications proposed by Zareian and Medina (2010), initial stiffness proportional damping is assigned to the elements that remain elastic, and mass proportional damping is assigned to the nodes where the masses are lumped. Regarding the maximum time step used in the analysis, a sensitivity analysis was conducted for multiple engineering demand parameters, and a maximum value of 0.005s was defined. Additionally, in case of non-convergence during analysis, a procedure was implemented that reduces the time step up to a value of 0.002s. Similar conclusions were drawn by Barbosa et al. (2017), where the author mentioned that a time step of 0.002s produces negligible errors in the evaluation of the roof acceleration response-history.

Response-history analyses were performed for two intensity levels: 10% in 50 years earthquake, corresponding to the no-collapse performance requirement (ULS) and 2% in 50 years earthquake, corresponding to the near-collapse (CLS) performance requirement. The performance

evaluation of the buildings was conducted for a set of structural response parameters that characterize their global behaviour and local ductility demands. The inter-storey drift ratio (ISDR) and the peak floor acceleration (PFA) were used to compare the global behaviour of the building and the beams and panel zones ductility demands to evaluate the contribution of these components to the energy dissipation.

4.5.3.1 Global lateral behavior

The maximum inter-storey drift ratio and the maximum peak floor acceleration for the non-collapse seismic intensity level (ULS) for all buildings are plotted in Figure 4.27 and Figure 4.28, respectively. As shown in Figure 4.27 and Figure 4.28, all buildings exhibited similar perfor-

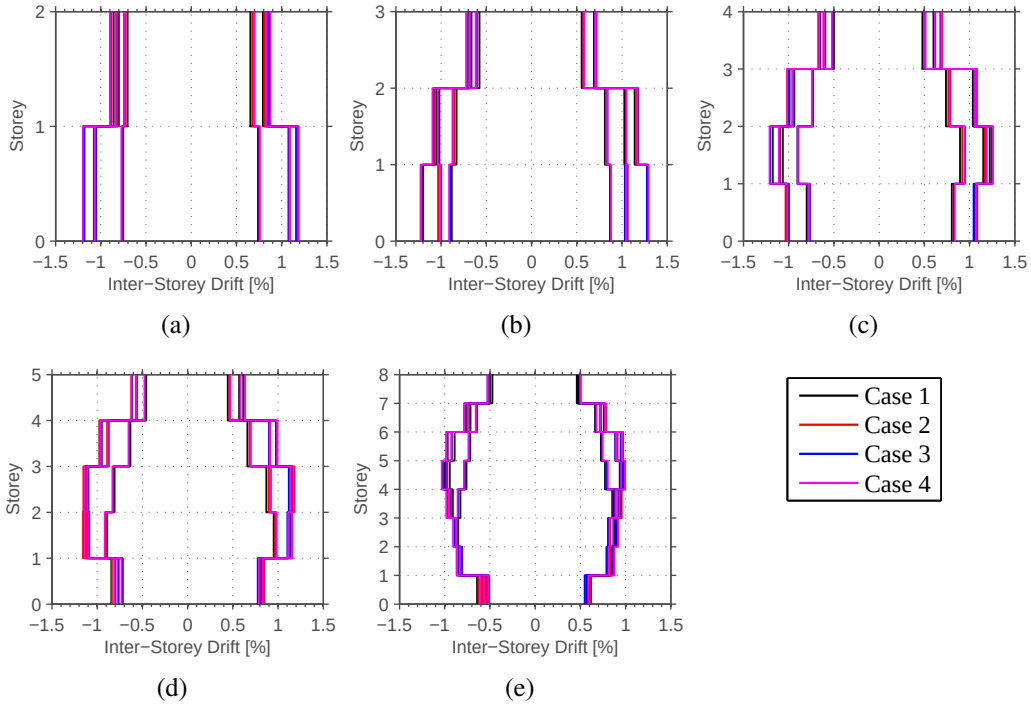

Figure 4.27: Maximum inter-storey drift ratio at ULS for buildings: a) 2-storeys, b) 3-storeys, c) 4-storeys, d) 5-storeys and e) 8-storeys.

mance, regardless of the adopted panel zone design criterion. Moreover, the maximum inter-storey drift ratios observed in all buildings were around 1% and consequently it is not expected a significant level of inelastic behaviour in the buildings.

4.5.3.2 Plastic demands on beams and panel zones

As previously mentioned, the distribution of plastic demands between beams and panel zones strongly relies on the design approach adopted for the panel zones. Figure 4.29 show, for each joint, the ratio between the maximum beam ductility and the panel zone ductility demands. A ratio close to one means that both components have a similar contribution to the joint deformation,

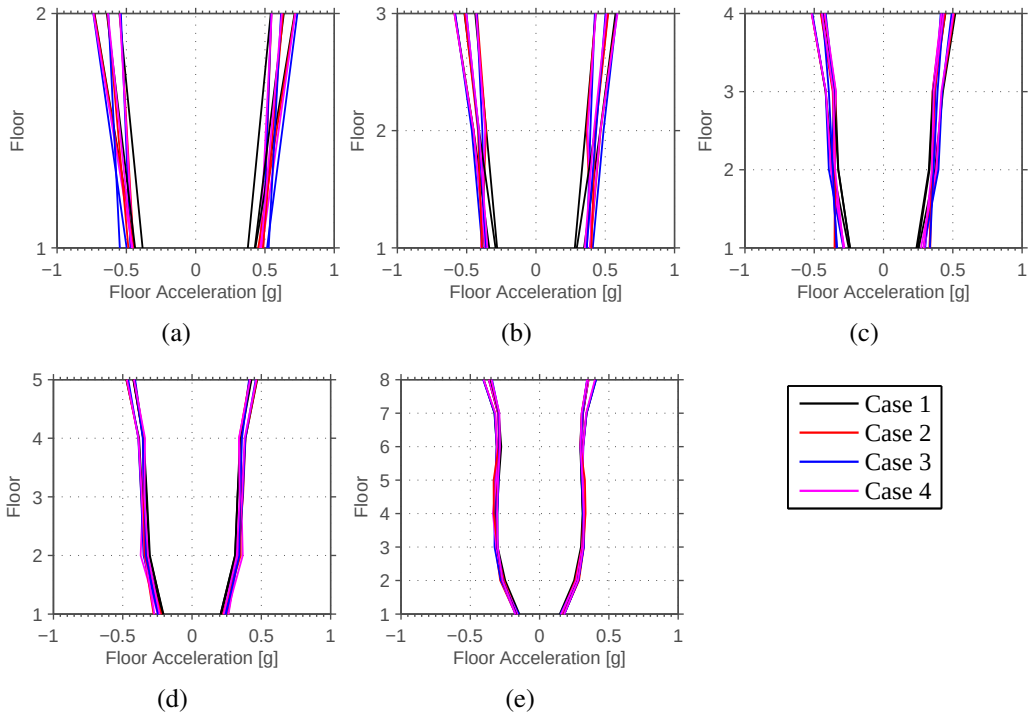

Figure 4.28: Maximum peak floor acceleration at ULS for buildings: a) 2 storeys, b) 3 storeys, c) 4 storeys, d) 5 storeys and e) 8 storeys.

a ratio higher than one reveals a greater participation of the beams and a ratio lower than one corresponds to a higher participation of the panel zone. Analysis of the results shown in the figures reveals that buildings designed with strong panel zones (Case 1) concentrate the deformation on the beams. Conversely, in buildings with panel zones designed according to Case 3 and 4, most of the deformation occurs in the panel zones. Furthermore, buildings designed with balanced panel zones (Case 2) show a uniform distribution of the plasticity between the beams and panel zones. Thus, the use of balanced panel zones allows for the reduction in the beam deformation demands. Despite the noticeable performance exhibited by the buildings designed with balanced panel zones, with an effective participation in the plastic deformation, it is necessary to ensure that the level of plastic deformation occurring in the panel zones are within certain limits. ASCE-41-13 (ASCE/SEI, 2013) defines, for both ULS and CLS, a limit of plastic deformation in the panel zone of $12 \times \gamma_y$, where γ_y is the yield shear rotation of the panel zone. In this research study, a limit of $4 \times \gamma_y$, corresponding to the formation of plastic hinges in the column flanges was considered for ULS, in order to avoid excessive deformation of the panel zones, which may cause problems in the welded connections.

Figure 4.30 show the panel zone ductility demands at ULS and CLS. As expected, the panel zones designed according to Case 3 exhibited the higher ductility demands, exceeding, in several joints, the limit defined for the ULS. Consequently, the use of this approach for design is not recommended, since undesirable effects on the welded connections could occur (El-Tawil et al., 1999). Conversely, panel zones designed according to Case 1 exhibited ductility demands below 1

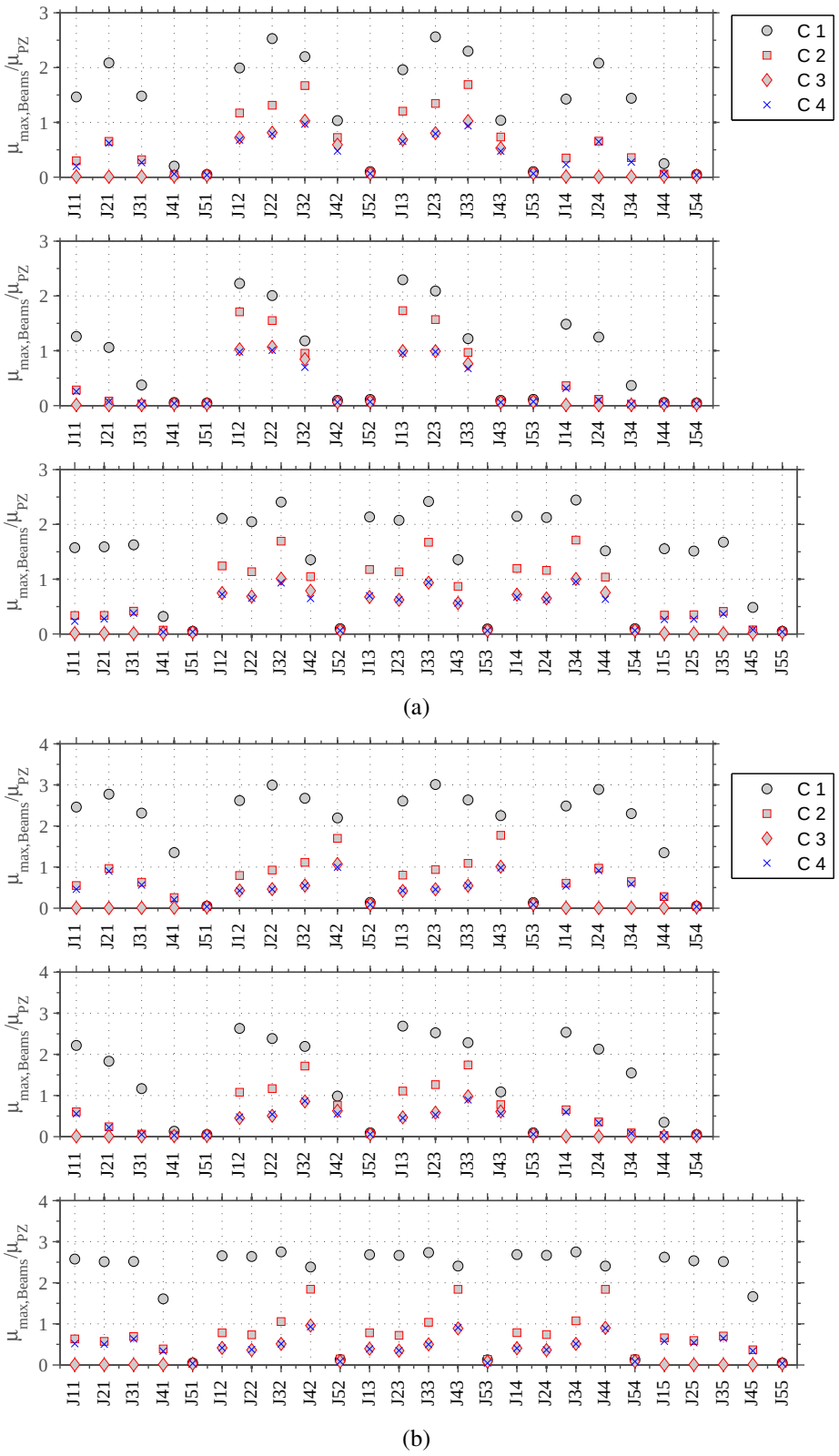

(a)

(b)

Figure 4.29: Beams and panel zone ductility demands ratio for the 5-storey buildings at: a) ULS and b) CLS.

for both ULS and CLS, implying that they remain elastic. Moreover, Case 2 and Case 4 exhibited more adequate values of panel zone ductility demands, complying with the established limits. It is, however, important to note that panel zones designed according to Case 2 ensure a more balanced distribution of plastic deformations between the beams and panel zones, which may be a major aspect to avoid excessive deformations of the panel zone and consequent problems in the welded connections. Another aspect that highlights the advantages of using panel zones designed according Case 2 is the use of the generalized and discretionary 80% factor in Case 3 and Case 4. In fact, examination of the non-linear static and response-history analysis results allows concluding that the effect of considering this factor results in the concentration of plasticity in the panel zone and in one of the connecting beams. For this reason, the advantages of using the approach of Case 2 was confirmed, with which there was an effective, but at the same time controlled, inelastic participation of the panel zone.

4.5.4 Probabilistic seismic assessment

The seismic performance assessment of buildings is conducted through incremental dynamical analysis (IDA) (Vamvatsikos and Cornell, 2002). The first mode spectral acceleration was considered as the seismic intensity measure, IM, and three engineering demand parameters, EDP, were considered: maximum inter-storey drift ratio (ISDR), maximum panel zone distortion (PZD) and maximum residual inter-storey drift (RISDR). For each EDP, the fragility curve was obtained by fitting a lognormal cumulative distribution function to the EDP limit state $S_a(T_1)$ values of each building. The curves were computed using the maximum likelihood method proposed by Baker (2015). In each analysis, the sideway collapse was defined as the instant in which dynamic instability occurs, that is, the point where a significant increase of displacements is verified without an increase of lateral force (Karavasilis et al., 2015; Ramirez and Miranda, 2012; Hwang and Lignos, 2017). In order to accurately evaluate the maximum RISDR, each dynamic analysis is significantly extended and the maximum RISDR is evaluated for each storey by averaging the RISDR obtained in the last 5 seconds of the response-history analysis. In the evaluation of the collapse fragility curve of each building, aleatory or record-to-record uncertainty, β_{RTR}, and epistemic or modelling uncertainty, β_{MDL}, were taken into account. The total uncertainty, β_{TOT}, was computed as shown in Equation 4.36, assuming that both uncertainties are lognormally distributed and independent (Liel et al., 2009; Tzimas et al., 2016).

$$\beta_{TOT} = \sqrt{\beta_{RTR}^2 + \beta_{MDL}^2} \tag{4.36}$$

Following the recommendations of FEMA P695 (FEMA, 2009), record-to-record and modelling uncertainties were taken as 0.40 and 0.35, respectively, resulting in a value of total system uncertainty equal to 0.53. The median collapse capacity was adjusted in order to account for the spectral shape effect accordingly to Method 2 proposed by Haselton et al. (2009). Figure 4.31 shows the IDA curves and the corresponding collapse fragility curves before spectral shape adjustment.

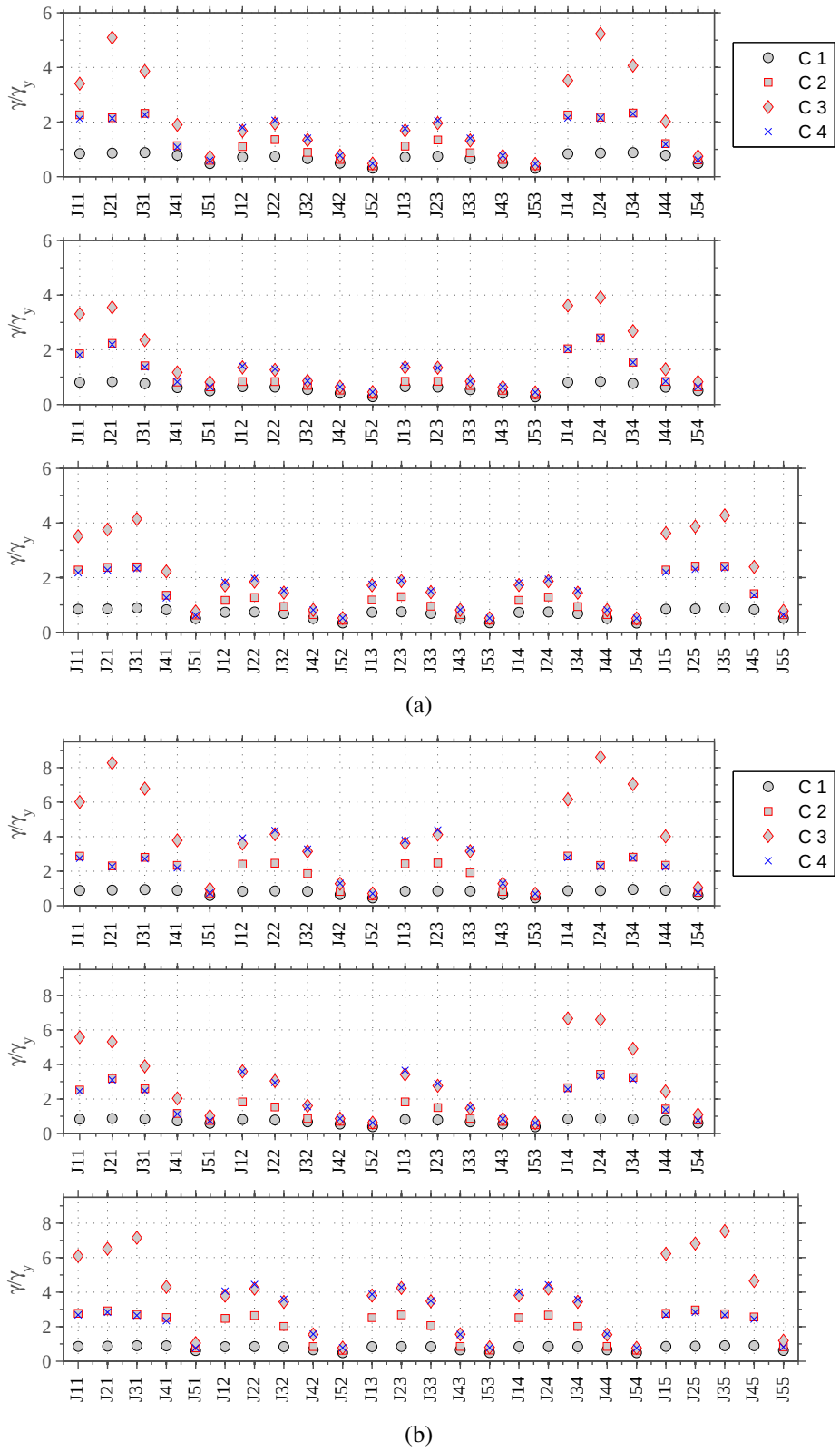

(a)

(b)

Figure 4.30: Panel zone ductility demands for the 5storey buildings at: a) ULS and b) CLS.

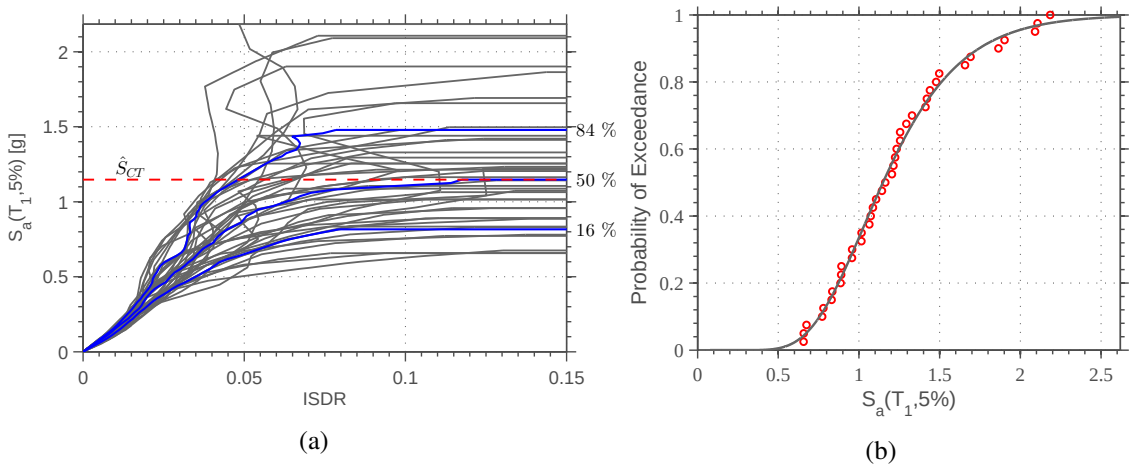

(a) (b)

Figure 4.31: IDA curves and collapse fragility curves for configuration 1 (5-storey building designed with strong panel zones).

Figure 4.32 and Figure 4.33 shows the collapse fragility curves of all the buildings. The seismic intensity measure, $S_a(T_1)$, was normalized by the elastic spectral acceleration at the fundamental period of the building in order to simplify the identification of the collapse probability. The dashed red line depict the design level intensity.

Inspection of the results shown in Figure 4.32 and Figure 4.33 reveals that, for the seismic design intensity level (ULS), all buildings exhibit a probability of collapse lower than 0.25%. Moreover, the differences between the obtained collapse fragility curves for the four design cases were minor, with buildings with panel zones designed according to cases 3 and 4 exhibiting slightly higher capacity. Consequently, it may be concluded that, independently of the assumed panel zone behaviour, all buildings met the no-collapse performance requirement. Furthermore, for the 2% in 50 years intensity level, the maximum probability of collapse obtained from the fragility analysis was 8%, a value below the limit of 10% of probability of "collapse" defined in several guidelines, namely in FEMA 695 (FEMA, 2009).

The performance of the buildings was also evaluated based on the deformations of the panel zone. The derivation of the panel zone distortion fragility curves followed the approach previously described. A panel zone distortion, γ, equal to $4 \times \gamma_y$, which is the value corresponding to the formation of plastic hinges in the column flanges, was defined as the limit state. Two sources of uncertainty were considered in the computation of panel zone distortion fragility curves, namely record-to-record uncertainty, β_{RTR}, obtained from analysis results, and modelling uncertainty, β_{APZD}, set equal to 0.20 (FEMA, 2012a,b). The total uncertainty in residual drift, β_{PZD}, was evaluated according to Equation 4.37.

$$\beta_{PZD} = \sqrt{\beta_{RTR}^2 + \beta_{APZD}^2} \tag{4.37}$$

Figure 4.34 and Figure 4.35 show the fragility curves that specify the probability of exceedance of the $4 \times \gamma_y$ limit state. The seismic intensity measure, $S_a(T_1)$, was again normalized by the

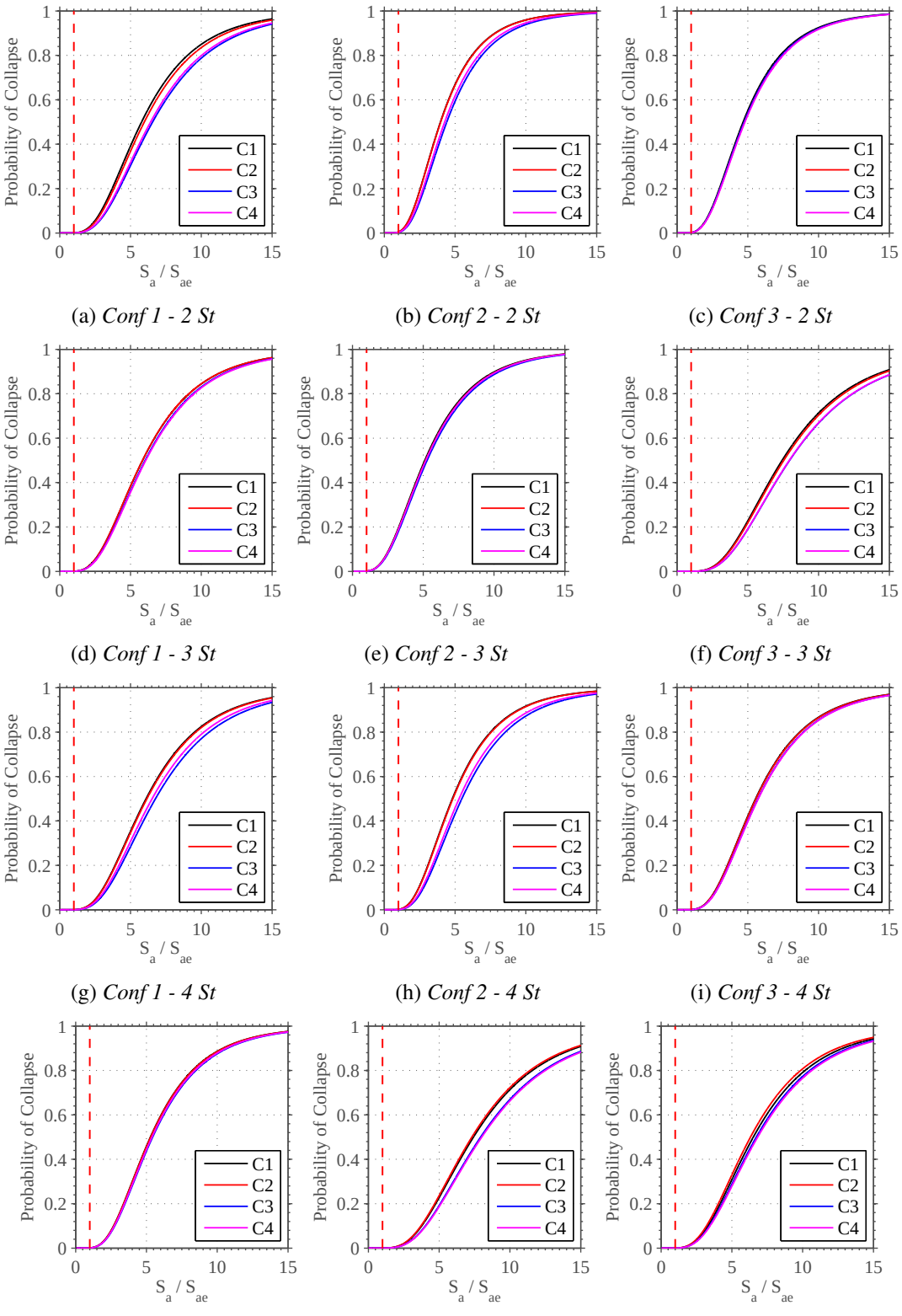

(a) *Conf 1 - 2 St* (b) *Conf 2 - 2 St* (c) *Conf 3 - 2 St*

(d) *Conf 1 - 3 St* (e) *Conf 2 - 3 St* (f) *Conf 3 - 3 St*

(g) *Conf 1 - 4 St* (h) *Conf 2 - 4 St* (i) *Conf 3 - 4 St*

(j) *Conf 1 - 5 St* (k) *Conf 2 - 5 St* (l) *Conf 3 - 5 St*

Figure 4.32: Collapse fragility functions for the 2-, 3-, 4- and 5-storey buildings.

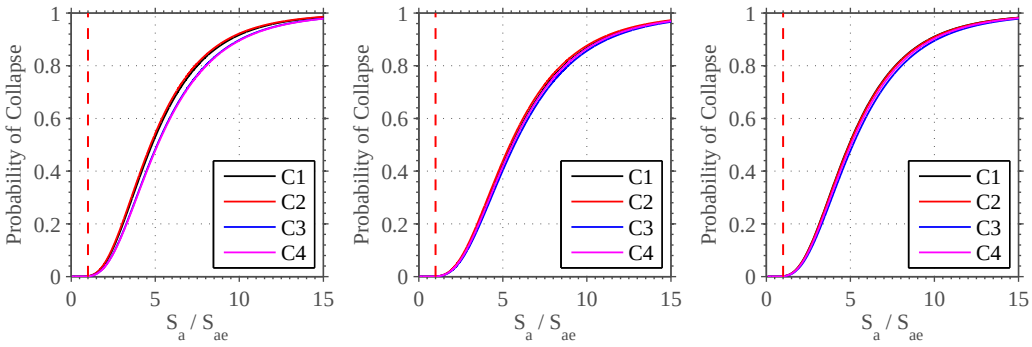

(a) *Conf 1 - 8 St* (b) *Conf 2 - 8 St* (c) *Conf 3 - 8 St*

Figure 4.33: Collapse fragility functions for the 8-storey buildings.

design spectral acceleration at the fundamental period of the building, in order to simplify the identification of the probability of exceeding the panel zone distortion limit state for the design intensity level. The dashed red line and the dashed black line define the design intensity level and the collapse intensity level, respectively. Through an analysis of Figure 4.34 and Figure 4.35, one can realise that buildings with panel zones designed according to Case 3 exhibit high probabilities of exceedance the adopted distortion limit. Conversely, and as expected, strong panel zones (Case 1) showed the highest capacity, with zero probability for the collapse intensity level. Furthermore, panel zones designed according to Case 2 and Case 4 exhibited an intermediate behaviour, with the latter having higher probabilities of exceedance at the design intensity level (15% in the worst case vs. 2% for Case 2). Further analysis of the figure indicates that, with the exception of buildings with Configuration 2, the probabilities of exceedance at the collapse level intensity were always less than 20%. Although this can be pointed out as a lower participation of the panel zone, it is the opinion of the author that a controlled inelastic behaviour of the panel zone avoiding excessive damage and the use of not exceptionally thick additional plates is preferred.

The residual drift has been increasingly considered as an important engineering demand parameter for the seismic performance assessment of building structures (Ramirez and Miranda, 2009, 2012; Tzimas et al., 2016; Bojórquez and Ruiz-García, 2013; Hwang et al., 2015; FEMA, 2012a). It is therefore crucial to evaluate the influence of the design criteria of the panel zone on the level of residual drifts. Tzimas et al. (2016) and McCormick et al. (2008) recommended a value of 0.5% for the acceptable residual drift, arguing that for a higher value it becomes financially unreasonable to repair the buildings. Moreover, FEMA (2012a) defines four residual drift limit states ranging from the onset of damage to non-structural components to near-collapse of the structure. The suggested values of residual drift for each limit state are 0.2, 0.5, 1 and 2% (Kitayama and Constantinou, 2016). In the evaluation of residual drift fragility curve of each building, both the record-to-record uncertainty, β_{RTR}, and modelling uncertainty, β_{ARD}, were considered once again. The total uncertainty in residual drift, β_{RD}, was computed according to Equation 4.38 assuming that both uncertainties are lognormally distributed and independent (FEMA, 2012a). In accordance with FEMA (2012a), the record-to-record uncertainty was considered in the analysis

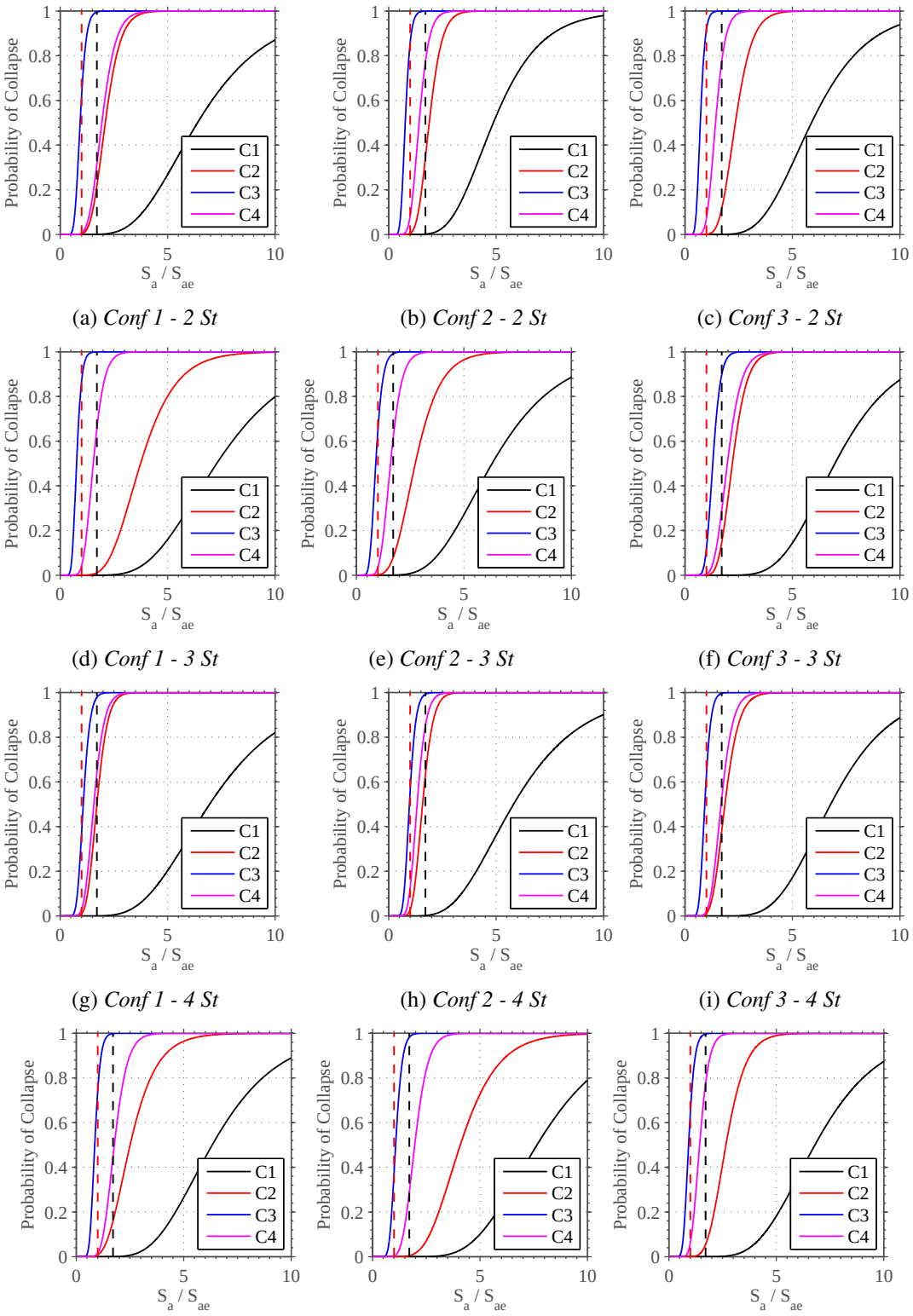

(a) *Conf 1 - 2 St* (b) *Conf 2 - 2 St* (c) *Conf 3 - 2 St*

(d) *Conf 1 - 3 St* (e) *Conf 2 - 3 St* (f) *Conf 3 - 3 St*

(g) *Conf 1 - 4 St* (h) *Conf 2 - 4 St* (i) *Conf 3 - 4 St*

(j) *Conf 1 - 5 St* (k) *Conf 2 - 5 St* (l) *Conf 3 - 5 St*

Figure 4.34: Panel zone distortion fragility functions for the 2-, 3-, 4- and 5-storey buildings.

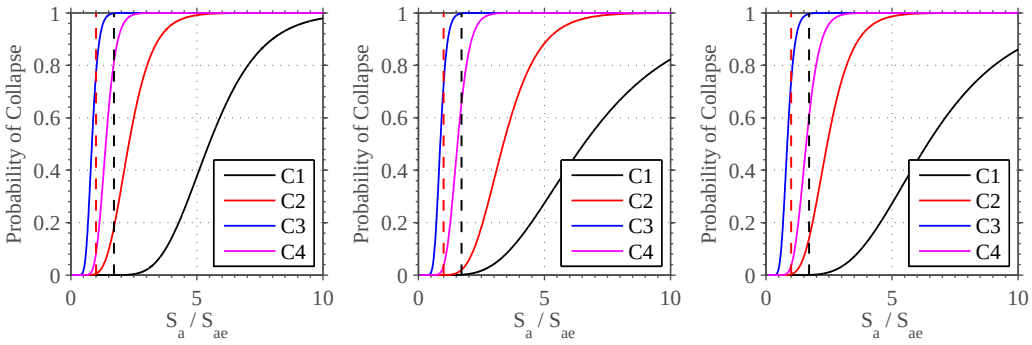

(a) *Conf 1 - 8 St* (b) *Conf 2 - 8 St* (c) *Conf 3 - 8 St*

Figure 4.35: Panel zone distortion fragility functions for the 8-storey buildings.

process and the modelling uncertainty was set equal to 0.20.

$$\beta_{RD} = \sqrt{\beta_{RTR}^2 + \beta_{ARD}^2} \tag{4.38}$$

Figure 4.36 and Figure 4.37 illustrate the residual drift fragility curves for a residual drift of 0.5% ($P[RISDR \geq 0.5\% | S_a(T_1) = x]$). Again, the seismic intensity measure, $S_a(T_1)$, was normalized by the design spectral acceleration at the fundamental period of vibration of the building. A careful inspection of the figure indicates that buildings designed with different panel zone design criteria exhibit similar probabilities of exceedance of the residual drift limit. Moreover, probabilities of exceedance below 4% were obtained for the design intensity level. In line with the results obtained for the collapse probabilities, buildings with panel zones designed according to Cases 3 and 4 exhibited, in most of the cases, slightly higher capacities. However, the differences are not significant.

Finally, the probability of exceedance of the distortion limit and the residual drift limit over the buildings lifetime (typically 50 years) was computed. Based on the Poisson assumption, the probability of exceedance over the building lifetime can be computed as shown in Equation 4.39, where λ_x is the mean annual frequency of exceeding a specific limit state.

$$P(Collapsein50years) = 1 - e^{-\lambda_x \times 50} \tag{4.39}$$

Computation of the mean annual frequency of exceeding a specific limit state was performed by integrating the corresponding fragility curve of the structure over the seismic hazard curve at the site, as shown in Equation 4.40 (Eads et al., 2013; Kitayama and Constantinou, 2016), where $P(x|IM)$ is the probability that the structure will exceed a specific limit given that the ground motion intensity is $IM = im$, $\lambda(IM)$ is the mean annual frequency of the ground motion intensity and $|d\lambda(IM)/d(IM)|$ is the derivative of the seismic hazard curve.

$$\lambda_x = \int_0^\infty P(x|IM) d\lambda(IM) = \int_0^\infty P(x|IM) \left| \frac{d\lambda(IM)}{dIM} \right| dIM \tag{4.40}$$

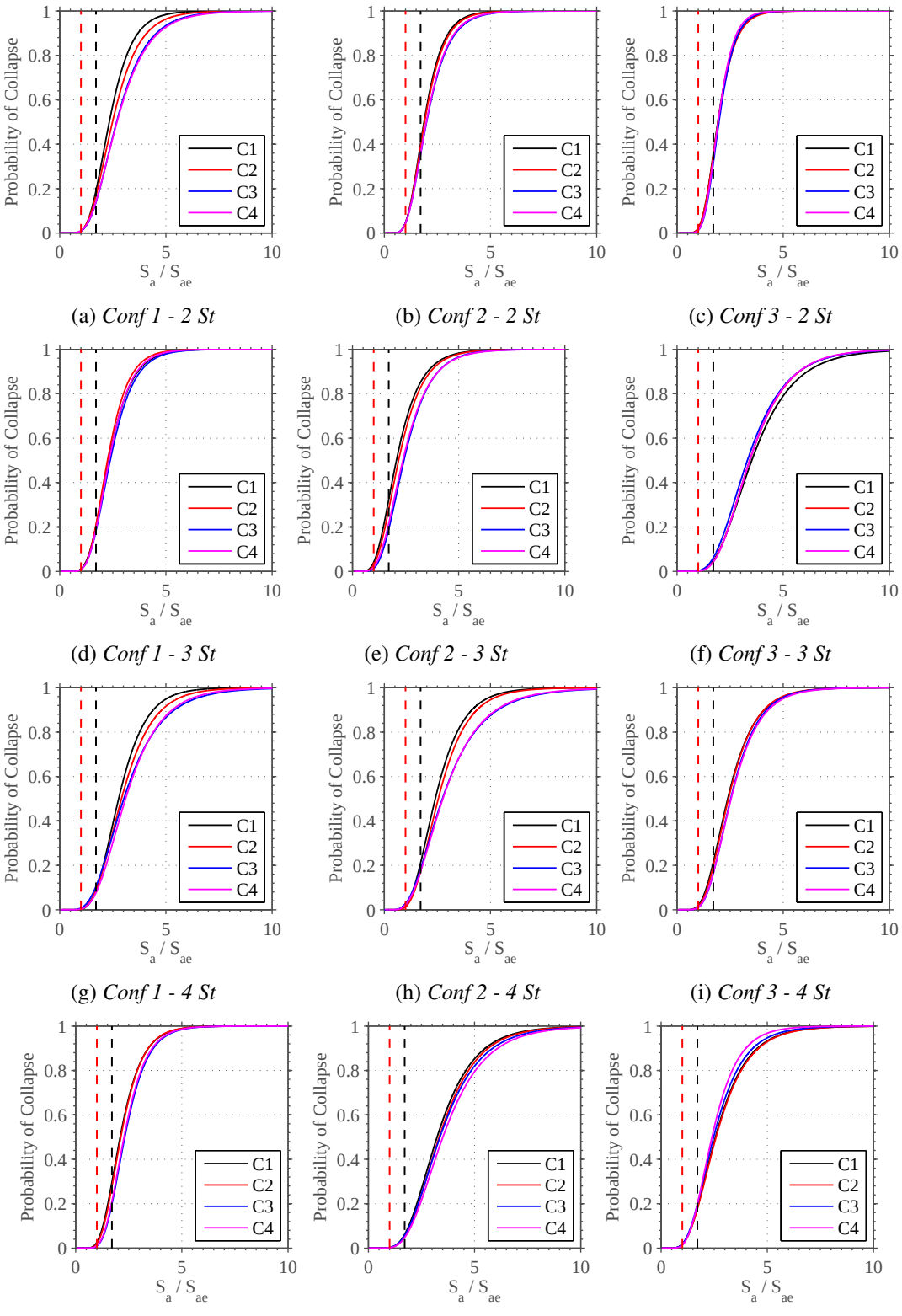

(a) *Conf 1 - 2 St* (b) *Conf 2 - 2 St* (c) *Conf 3 - 2 St*

(d) *Conf 1 - 3 St* (e) *Conf 2 - 3 St* (f) *Conf 3 - 3 St*

(g) *Conf 1 - 4 St* (h) *Conf 2 - 4 St* (i) *Conf 3 - 4 St*

(j) *Conf 1 - 5 St* (k) *Conf 2 - 5 St* (l) *Conf 3 - 5 St*

Figure 4.36: Residual drift fragility functions for the 2-, 3-, 4- and 5-storey buildings.

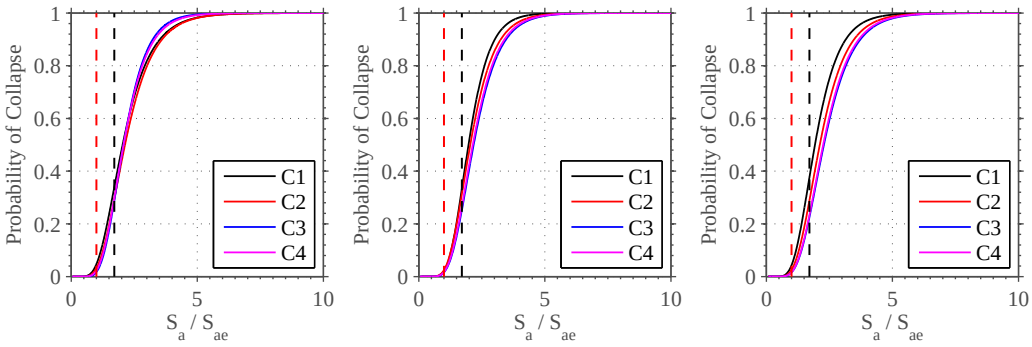

(a) *Conf 1 - 8 St* (b) *Conf 2 - 8 St* (c) *Conf 3 - 8 St*

Figure 4.37: Residual drift fragility functions for the 8-storey buildings.

The seismic hazard curves used in this research study were obtained from Chapter 2 . Table 4.4 shows the probabilities of exceedance of the residual inter-storey drift and panel zone distortion in 50 years for each building. As expected, buildings with panel zones designed according to Case

Table 4.4: Probability of exceedance of residual inter-storey drift and panel zone distortion in 50 years.

Conf.	ID	Storeys	$P[RISD \geq 0.5\%$ *in* 50 *years*$]$ [%]				$P[\gamma \geq 4\times\gamma_y$ *in* 50 *years*$]$ [%]			
			Case 1	Case 2	Case 3	Case 4	Case 1	Case 2	Case 3	Case 4
1	St93	2	0.81	0.77	0.69	0.69	0.10	0.92	3.78	1.06
	St96	3	0.98	0.89	0.85	0.85	0.15	0.78	3.82	1.35
	St99	4	0.76	0.77	0.73	0.76	0.08	0.50	4.17	1.28
	St102	5	0.55	0.58	0.46	0.56	0.05	0.21	3.22	1.11
	St105	8	0.62	0.60	0.44	0.53	0.05	0.34	2.48	0.95
2	St123	2	0.43	0.38	0.42	0.38	0.06	0.77	2.10	0.98
	St126	3	0.60	0.50	0.52	0.47	0.09	1.15	2.68	1.39
	St129	4	0.63	0.58	0.60	0.57	0.11	1.15	2.78	1.61
	St132	5	0.68	0.54	0.51	0.51	0.07	0.77	2.67	0.93
	St135	8	0.55	0.54	0.46	0.48	0.05	0.40	2.61	0.70
3	St138	2	0.48	0.45	0.41	0.38	0.06	0.27	2.77	0.96
	St141	3	0.64	0.64	0.69	0.70	0.07	0.49	3.28	1.53
	St144	4	0.84	0.77	0.64	0.78	0.10	0.61	2.96	1.45
	St147	5	0.75	0.63	0.58	0.59	0.08	0.22	2.72	0.96
	St150	8	0.67	0.60	0.55	0.55	0.05	0.42	3.01	0.94

1 and Case 2 exhibit the lower probability of exceedance of the panel zone distortion limit state

in 50 years. However, the differences are not significant for Case 4. Regarding the residual inter-storey drifts, although the highest probabilities are associated with the buildings with panel zones designed according to Case 1 and Case 2, the exceedance probabilities in 50 years never exceed the code target of 1%.

4.6 Conclusions

The main objective of the research presented in this chapter was to propose a consistent and reliable design procedure for the design of the panel zone in steel moment-resisting frames. A critical overview of the European design requirements was conducted, identifying the most important difficulties regarding its application. The simulation of several monotonic and cyclic experimental tests validated the numerical models developed, and a design procedure based on European and American standards and guidelines was proposed. This procedure seeks to distribute the plasticity between the beams and the panel zone, whilst avoiding excessive deformation in the panel zone and the development of shear buckling. The influence of the design criterion adopted for the design of the panel zone on both the local and global behaviour of steel moment frames was then assessed through non-linear static and response-history analyses. From within the scope of the results obtained in this research study, the following conclusions can be withdrawn:

- The European seismic design code (EC8-1, (CEN, 2005c)) refers to Part 1-1 of Eurocode 3 for the evaluation of the shear capacity. However, some inconsistencies can be identified. In the evaluation of the shear area, EC8 clearly states that no reduction should be performed to take into account the effect of axial force and bending moment on the plastic resistance in shear. However, Part 1-1 of EC3 proposes an expression for the evaluation of the shear area considering a reduction factor of 0.9 to account for the reduction in the shear strength due to axial loads. Part 1-1 of EC3 establishes that the panel zone can only be reinforced with one supplementary web plate, with a maximum thickness equal to that of the column's web. However, for seismic design situations, this criterion is extremely restrictive, resulting in many cases in the need of increasing the column size;

- EC8 does not explicitly define if the panel zone should be considered a dissipative or non-dissipative component, without any reference for which capacity design procedure should be adopted. However, the recommended calculation approach for the shear strength of the code is indicative that the dissipative behaviour of the panel zone may be considered. Moreover, in the beam-to-column joint plastic rotation, EC8 allows for the contribution of the panel zone to be as high as 30%;

- Non-linear static and response-history analyses showed that, for all the adopted panel zone design criteria, the global lateral behaviour of the structures is not sensitive to the approach adopted. However, it should be mentioned that the non-design of the panel zone significantly affects the lateral capacity of the building. Furthermore, it was demonstrated that the

dynamic properties can be evaluated without explicit consideration of the panel zone in the numerical models;

- Adoption of balanced panel zones, in accordance to the proposed procedure, allows for a reduction of the inelastic demands of the beams, without excessive deformation of the panel zone. Moreover, the panel zone distortion was found to comply with the distortion limit of 4γ, considered for non-collapse-related checks (ULS). This value corresponds to the formation of plastic hinges in the column flanges, and was defined as the distortion limit to avoid excessive deformation of the panel zones which may cause problems in the welded connections.

From the probabilistic seismic assessment three important observations could be inferred:

- The collapse fragilities were not significantly affected by the panel zone design criteria;
- If designed according to Case 1 or Case 2, the panel zone distortion fragility functions shows very low probability of exceedance of the 4γ distortion limit, for the design level seismic intensity. Moreover, for the collapse seismic intensity level, the probabilities of exceedance were always lower than 20%;
- The residual inter-storey drift is not affected by the panel zone design criteria.

Chapter 5

SelEQ: An advanced ground motion record selection and scaling framework

5.1 Introduction

The increasing tendency to follow performance-based guidelines in design and assessment techniques, whilst allowing for more realistic and economically feasible structures, also requires the ability to conduct advanced structural analysis. Among the possible analysis techniques, the nonlinear response-history analysis (NRHA) methodology is becoming a common procedure when designing or assessing earthquake-resistant buildings. In addition to all the issues related with the numerical modelling and design assumptions, the definition of the seismic input, typically in the form of acceleration time-history records, is also an important requirement. These can either be obtained from real earthquake events or be artificially generated (Amiri et al., 2012). However, as noted by several authors (Padgett and DesRoches, 2007; Katsanos et al., 2010; Katsanos and Sextos, 2013; Araújo et al., 2016), the estimation of seismic response strongly relies on the selection of an appropriate suite of ground motion records. Additionally, an accurate selection not only reduces the bias in the obtained structural response, but it also allows contributes to improve the reliability of the results provided by the structural analysis (Katsanos and Sextos, 2013; Shome et al., 1998; Iervolino and Cornell, 2005).

Over the past years, several ground motion record selection techniques have been proposed. The simplest record selection methodology, namely the scenario-based record selection (Shome et al., 1998; Ghafory-Ashtiany et al., 2012), consists of obtaining a suite of ground motion records based on magnitude, distance and site conditions, which adequately represent the seismic hazard scenario. Subsequently, the ground motion records are scaled in order to ensure a compatibility between the average intensity measure (IM) of the ground motion group and the targeted level of earthquake hazard. However, whilst Shome et al. (1998) claimed that scaling the ground motion records by the median of the suite results in minor dispersion in the estimated structural response, the authors also highlighted that, for structures that exhibit highly nonlinear behaviour, the dispersion observed can be substantial (Ay and Akkar, 2014). Furthermore, several authors recognized

the lack of sufficient evidence to support the argument that magnitude and distance should be adopted as a criteria for ground motion record selection (Iervolino and Cornell, 2005; Stewart et al., 2002; Bommer and Acevedo, 2004).

It is important to note that, most of the methods developed so far, rely on spectral compatibility between the average of the suite of ground motions and a target spectrum. Typically, the latter can either be obtained from a seismic design code or derived from a probabilistic seismic hazard assessment analysis. Current seismic design and assessment codes (e.g. Eurocode 8 Part 1 (CEN, 2005c), Eurocode 8 Part 2 (CEN, 2005d), ASCE 41-13 (ASCE/SEI, 2013), NZS 1170.5:2004 (Standard, 2004) define the criteria for the record selection process, namely in terms of the number of ground motions to consider in the analysis and the degree of compatibility between the average ground motion spectrum and the code spectrum. Usually, for structures of low to medium complexity, site-specific seismological studies are not available and the designer is therefore limited by code guidance (Iervolino et al., 2010). However, the target spectra typically defined in seismic codes is a uniform hazard spectrum (UHS), which can be derived from a probabilistic seismic hazard analysis (PSHA) for a given range of periods and a given probability of exceedance. This methodology leads to an envelope of maximum spectral accelerations that is unlikely to be observed from a single ground motion, as concluded by different authors (Naeim and Lew, 1995; Bommer et al., 2010; Baker, 2010; Haselton et al., 2012). In order to overcome this limitation, Baker and Cornell (2005, 2006b) proposed an alternative target spectrum, designated by Conditional Mean Spectrum (CMS), which is the mean response spectrum conditioned on the occurrence of a target spectral acceleration at the period of interest. The concept behind CMS relies on two major factors, namely ε, which is an accurate indicator of the spectral shape Baker and Cornell (2005, 2006b), and the correlation between response spectrum values (Jayaram et al., 2011). This methodology requires the results of seismic hazard disaggregation for the site and period of interest, and has been gaining popularity in recent years due to the significant advances in the definition of the target spectrum. Nevertheless, the accuracy of the available tools to compute the CMS for the European territory are still scarce and difficult to use.

Although a significant number of research studies concerning the new and more accurate methodologies for the selection and scaling of ground motion records have been developed, its practical application can prove difficult to attain, since these are highly constrained problems. However, it is important to highlight the increasing availability of strong-motion databases containing a large number of real ground motion records (e.g. ESD (Ambraseys et al., 2004), ITACA (Luzi et al., 2008; Pacor et al., 2011), RESORCE (Akkar et al., 2014), PEER NGA (Chiou et al., 2008) and PEER NGA-WEST2 (Ancheta et al., 2013, 2014)), which make more proficient the use of real ground motion records. On the other hand, even when a preliminary selection based on seismological parameters is conducted, the number of eligible ground motion records can be significant, and the possible number of permutations considerably large. The total number of possible suites that can be assembled is given by (Sextos, 2014), as follows:

$$N_{sol} = C_r^n = \frac{n!}{r!(n-r)!} \tag{5.1}$$

where n is the total number of ground motion records in the preliminary selection and r is the number of records per suite. As an example, a preliminary database with a total number of 170 records has 7.184×10^{11} possible suites. Furthermore, when using additional selection criteria (e.g. spectral shape indicators), the preliminary selection can be relaxed (total number of ground motion records in the preliminary selection increases), and resulting therefore in a considerably larger number of possible groups.

An efficient record selection process usually requires the use of time-consuming iterative procedures, which might not necessarily lead to the most optimized ground motion sets. However, an optimization-based approach can be implemented in order to determine the best possible ground motion group. This methodology makes use of mathematical algorithms, targeted at the optimization of a given problem with a given set of constraints. A number of meta-heuristic (higher-level partial search algorithm) optimization methods have been applied to engineering problems (Azad and Hasançebi, 2013; Hejazi et al., 2013; Hasançebi and Carbas, 2014; Hasançebi et al., 2009; Alberdi and Khandelwal, 2015; Aydoğdu et al., 2016; Hare et al., 2013; Doğan and Saka, 2012), in most of the cases due to their computational efficiency in determining a mathematical solution for complex and high constrained problems. However, the implementation of these optimization algorithms for record selection procedures has been limited (Jayaram et al., 2011; Naeim et al., 2004; Kottke and Rathje, 2008; Kayhan et al., 2011). Kayhan et al. (2011) proposed the use of the Harmony Search algorithm for the selection and scaling of real ground motion records, concluding that the proposed methodology provides an efficient way to develop ground motion datasets that are consistent with code-based design spectra. Additionally, Macedo et al. (2013) conducted a parametric study on the influence of different optimization algorithms on record selection procedures, and concluded that the Adaptive Harmony Search algorithm (Hasançebi et al., 2009) combines the best features for ground motion record selection and scaling.

Despite the availability of several databases of ground motion records, and various selection and scaling techniques, the amount of record selection tools is still very limited. Additionally, most of the existing tools only allow record selection based on spectral compatibility between the mean response spectrum of a record suite and a target response spectrum. One of the reference tools developed in Europe, REXEL (Iervolino et al., 2010), implements a code-based record selection methodology providing suites of 7, 14 or 21 records compatible with the response spectra prescribed in Eurocode 8 (CEN, 2005c,d) and the Italian seismic design code (dei Lavori Pubblici , CS. LL. PP.) or with a user-defined response spectrum. More recently, Katsanos and Sextos (2013) developed the ISSARS tool, which allows record selection according to European and American seismic design codes, and enables the user to retrieve suites of ground motions that ensure a target level of dispersion of structural response quantities. PEER updated the web-based application for ground motion record selection based on the compatibility to a target response spectrum (Chiou et al., 2008). Jayaram et al. (2011) proposed a tool for record selection based on the compatibility to a target CMS mean and variance, making use of the Greedy algorithm to select the appropriate suites of earthquake records.

This Chapter describes both the development and application of a fully integrated framework,

which not only allows the optimized selection and scaling of suites of real ground motion records according to several procedures, but also the possibility of obtaining the UHS, disaggregation and CMS spectra for any location in the European territory. The framework makes uses of the open source software OpenQuake (OQ) (Pagani et al., 2014) and the seismic hazard model developed within the SHARE project (Woessner et al., 2015) to conduct probabilistic seismic hazard assessment. Since the Conditional Mean Spectrum is not directly obtained from the OQ software, the methodology proposed by Lin, Harmsen, Baker and Luco (2013); Lin, Haselton and Baker (2013a,b) to compute the exact CMS was implemented and tested for several locations.

5.2 Ground motion record selection

5.2.1 Code-based record selection

Currently, most of seismic design codes establish provisions for ground motion record selection and scaling. Whilst Part 1 of Eurocode 8 (EC8-1) (CEN, 2005c) establishes that either artificial, simulated or recorded ground motion records can be used to perform response-history analysis, Part 2 of Eurocode 8 (EC8-2) (CEN, 2005d), ASCE41-13 (ASCE/SEI, 2013) and NZS 1170.5:2004 (Standard, 2004) only allow the use of artificial or simulated ground motion records when real earthquake records are either unavailable or considered to be inadequate for the site location. Generally, a preliminary selection criteria based on seismological parameters (magnitude, source-to-site distance, rupture mechanism and soil profile) that are consistent with the seismic hazard scenario, shall be performed, followed by spectral matching to a target spectrum. In the following sections, the provisions of Eurocode 8 (Parts 1 and 2), ASCE41-13 and NZS 1170.5:2004 regarding the requirements for ground motion record selection are described in detail.

5.2.1.1 Eurocode 8 – Part 1 (CEN, 2005c)

Part 1 of Eurocode 8 (EC8-1) establishes a number of criteria for the selection and scaling of ground motion records for the seismic analysis of buildings. Firstly, the code states that a minimum of three ground motion records should be used for a given group. In such case, the structural response estimates should be taken based on the most unfavourable value observed for all the ground motions considered. However, if the suite of earthquake records is composed by at least seven records, the structural response estimates can be considered to be equal to the average of the structural response quantities. Additionally, the European code prescribes that the mean of the zero period spectral response acceleration values calculated from the individual time histories should not be smaller than the value of $a_g S$ for the site under study, a_g being the design ground acceleration on rock and S the soil parameter. Furthermore, in the range of periods between $0.2T_1$ and $2.0T_1$, where T_1 is the fundamental period of the structure in the direction in which the record will be applied, no value of the mean 5% damping elastic spectrum (calculated from the average between the response spectra of the considered ground motions), should be less than 90% of the corresponding value of the targeted 5% damping elastic response spectrum. Finally, EC8-1

establishes that, for 3D structural analysis, the seismic motion shall consist of three simultaneously acting ground motion records (two horizontal and one vertical earthquake directions). Moreover, the same ground motion record cannot be used simultaneously along both horizontal directions. It is important to note that, for these cases, there is no explicit guidance in the code regarding spectral compatibility requirements. In the absence of such recommendations, Beyer and Bommer (2007) proposed the use of the geometric mean of the spectral ordinate of the two horizontal components.

5.2.1.2 Eurocode 8 – Part 2 (CEN, 2005d)

To what concerns the response-history analysis of bridges, Part 2 of Eurocode 8 (EC8-2) establishes various criteria for the selection and scaling of ground motion records, by generally adopting or modifying the requirements of EC8-1. The code states that at least three pairs (two directions) of horizontal ground motion time-history components shall be used, although more than seven pairs are preferable (if attained, the average of the individual responses may be used as the design value of the action effects, and if not, the most unfavourable value of the structural response needs to be considered). For each earthquake, consisting of a pair of horizontal motions, the SRSS spectrum shall be established by taking the square root of the sum of the squares of the 5%-damped spectra of each component. The spectrum of the ensemble of earthquakes shall be formed by taking the average value of the SRSS spectra. It is important to note that the ensemble spectrum shall be scaled so that it is not lower than 1.3 times the 5% damping elastic response spectrum of the design seismic action, in the range of periods between $0.2T_1$ and $1.5T_1$. The scaling factor shall be applied to all individual seismic motion components. Both EC8-1 and EC8-2 have specific provisions to consider near source effects by setting the need of site-specific spectra.

5.2.1.3 ASCE41-13 (ASCE/SEI, 2013)

To what concerns the American standard for the seismic evaluation and retrofit of existing buildings, ASCE41-13 establishes that the selection of ground motion records for response-history analysis should follow a minimum of three pairs of ground motion records (from no fewer than three recorded events). Depending on the type of action and performance objectives, the code requires a minimum of seven independent pairs of horizontal ground motions to compute the mean structural responses. Otherwise, the most unfavourable structural response shall be considered. For each earthquake consisting of a pair of horizontal motions, the SRSS spectrum shall be established by taking the square root of the sum of squares of the 5%-damped spectra of each component. The average of the SRSS spectra from the suite of ground motions should not fall below the corresponding ordinate of the target response spectrum, for periods between $0.2T_1$ and $1.5T_1$. For sites within 5km of an active fault that controls the hazard, each pair of horizontal ground motion records shall be rotated to the fault-normal and fault-parallel directions. The components shall be scaled so that the average of the fault-normal components is not lower than the target spectrum in the period range of interest.

5.2.1.4 NZS 1170.5:2004 Standard (2004)

According to the New Zealand standard NZS 1170.5:2004, that defines the procedures and criteria for establishing the earthquake actions, the selection and scaling of ground motion records shall consider a minimum of three ground motion records per group. As opposed to the European and American methodologies, the code defines that, regardless of the number of ground motion records used, the least favourable structural response shall be used. Additionally, the ground motion records shall be scaled by a record scaling factor k_1 and a family scaling factor k_2, both applied in the time domain, i.e. the record ordinates shall be multiplied by the product $k_1 \times k_2$. The record scaling factor, k_1, is defined as the scalar value that minimizes, in a least square sense, the function $log(k_1 S_{ac}/S_{at})$, where S_{ac} refers to the spectrum associated to each record component and S_{at} to the code target spectrum for the given site, over the period range of interest, between $0.4T_1$ and $1.3T_1$. It is recommended in the code that $0.33 < k_1 < 3.0$ and that the record selected should exhibit a reasonable fit to the target spectrum. The latter condition may be met by ensuring that $D_1 < log(1.5)$, where:

$$D_1 = \sqrt{\frac{1}{n}\sum_{i=1}^{n}\left(log\left(S_{ac}\right) - log\left(S_{at}\right)\right)^2} \tag{5.2}$$

The family scaling factor, k_2, is defined as the maximum value of the ratio $S_{at}/max\left(S_{ac}\right) > 1.0$ over the period range of interest for the direction under consideration, where $max\left(S_{ac}\right)$ is the maximum component of each record within a family at each period considered. It shall be verified that $1.0 < k_2 < 1.3$.

5.2.2 CMS-based record selection

As mentioned previously in this Chapter, the target spectra used in code-based selection is typically a uniform hazard spectrum (UHS). This spectrum is commonly obtained through PSHA for a given probability of exceedance and includes all possible earthquake scenarios that have the potential of generating ground motions at a given site. Therefore, the UHS is unlikely to be observed in a single ground motion and hence is considered to be an excessively conservative earthquake ground motion scenario. Recognizing the aforementioned limitations, Baker and Cornell (2005, 2006a,b) proposed the so-called Conditional Mean Spectrum (CMS) as an alternative target spectrum. PSHA is used to develop the CMS, in order to find the value of spectral acceleration for a given fundamental period of vibration, $S_a(T_1)$, for the target probability of exceedance, denoted as $S_a(T_1)^*$. Additionally, from the disaggregation results, it is possible to obtain the mean values $\left(\overline{M}, \overline{R}, \overline{\varepsilon}\right)$ of parameters M, R and ε (magnitude, distance and epsilon, respectively) that lead to $S_a(T_1)^*$. Moreover, with the use of $\overline{M}$ and $\overline{R}$, the means and standard deviations of the response spectra for all periods can be determined. Furthermore, using the disaggregation results ($\overline{\varepsilon}(T_1)$ and the correlations of ε) the conditional mean and standard deviation of the target response spectrum

can be predicted using the following equations:

$$\mu_{lnS_a(T_i)|lnS_a(T_1)} = lnS_a(T_i)^* = \mu_{lnS_a}\left(\overline{M},\overline{R},T_i\right) + \sigma_{lnS_a}\left(\overline{M},\overline{R},T_i\right) \times \rho\left(T_i|T_1\right) \times \overline{\varepsilon}\left(T_1\right) \quad (5.3)$$

$$\sigma_{lnS_a(T_i)|lnS_a(T_1)} = \sigma_{lnS_a}\left(\overline{M},\overline{R},T_i\right) \times \sqrt{1-\rho^2\left(T_i|T_1\right)} \quad (5.4)$$

where $\overline{M},\overline{R},\overline{\varepsilon}(T_1)$ are obtained from disaggregation given that $S_a(T_1) = S_a(T_1)^*$. and are the mean and standard deviation of at obtained from the ground motion prediction model, respectively. Finally, $\rho(T_i|T_1)$ is the correlation between lnS_a at the two periods of vibration.

Recently, Lin, Harmsen, Baker and Luco (2013); Lin, Haselton and Baker (2013a,b) presented several alternatives for computing the CMS. Among them, the most complex approach allows the calculation of the exact CMS considering multiple causal earthquakes and multiple ground motion prediction equations (GMPE) that are often included in the PSHA computation. According to the proposal, the conditional mean and standard deviation target response spectrum are given by:

$$\mu_{lnS_a,j,k(T_i)|lnS_a(T_1)} = \mu_{lnS_a,k}\left(M_j,R_j,T_i\right) + \sigma_{lnS_a,k}\left(M_j,R_j,T_i\right) \times \rho\left(T_i|T_1\right) \times \overline{\varepsilon}\left(T_1\right) \quad (5.5)$$

$$\sigma_{lnS_a,j,k(T_i)|lnS_a(T_1)} = \sigma_{lnS_a}\left(M_j,R_j,T_i\right) \times \sqrt{1-\rho^2\left(T_i|T_1\right)} \quad (5.6)$$

$$\mu_{lnS_a(T_i)|lnS_a(T_1)} = \sum_k \sum_j p^d_{j,k} \mu_{lnS_a,j,k(T_i)|lnS_a(T_1)} \quad (5.7)$$

$$\sigma_{lnS_a,j,k(T_i)|lnS_a(T_1)} = \sqrt{\sum_k \sum_j p^d_{j,k}\left(\sigma^2_{lnS_a,j,k(T_i)|lnS_a(T_1)} + \left(\mu_{lnS_a,j,k(T_i)|lnS_a(T_1)} - \mu_{lnS_a(T_i)|lnS_a(T_1)}\right)^2\right)} \quad (5.8)$$

where $p^d_{j,k}$ indicates the contribution of each M_j/R_j pair and $GMPE_k$ to the exceedance of the S_a of interest. In contrast to the simplified CMS, the exact CMS considers all contributions of individual M_j/R_j pairs instead of using mean values of $\overline{M}$ and $\overline{R}$.

According to Bradley (2010), the reasoning behind the CMS is based on the observation that spectral accelerations have a multivariate lognormal distribution (Jayaram and Baker, 2008). It is important to note that the calculation of the exact CMS for a given site requires the use of PSHA tools and consistent hazard models. However, current PSHA tools do not automatically generate the exact CMS and hence additional implementations are required. The computation of the exact CMS involves a number of steps, as described next. Firstly, the sources contributing to the hazard must be identified (area sources, fault sources and point sources). For each source the disaggregation results are obtained and the individual mean and standard deviation are calculated. Additionally the corresponding contribution, $p^d_{j,k}$, needs also to be computed. Finally, the results are aggregated according to Equation 5.7 and 5.8. In the current version of SelEQ all PSHA

calculations are performed using the recently proposed SHARE seismic hazard model (Woessner et al., 2015).

After an appropriate definition of the means and standard deviations of the target spectrum, the ground motion record selection should ensure that the suits of ground motion records match the target mean spectrum and variance.

Nevertheless, Bradley (2010) argued, that when the CMS is used, only characteristics of the ground motion represented in terms of spectral accelerations are considered and hence ground motion attributes such as duration and energy are neglected. Therefore, to overcome this limitation, Bradley (2010) proposed the General Conditional Intensity Measure (GCIM), where multiple ground motion intensity measures are considered to obtain the conditional mean spectrum and corresponding standard deviation.

Currently, SelEQ performs the calculation of the exact CMS as proposed by Lin, Harmsen, Baker and Luco (2013); Lin, Haselton and Baker (2013a,b) for a given probability of exceedance or, if requested by the user, for a given probability of occurrence (Bradley, 2010). However, due to the modular architecture of the framework, the implementation of the GCIM or other future proposals for conditional spectra, is a relatively simple task to perform.

5.3 Harmony search algorithm

5.3.1 General aspects

The meta-heuristic algorithms belong to the family of optimization algorithms that are inspired by natural phenomena and seek to solve generic optimization problems (e.g. Harmony Search algorithm, Genetic algorithm, Simulated Annealing algorithm, Ant Colony algorithm). The general formulation of a population based meta-heuristic optimization algorithm can be described by the pseudocode shown in Algorithm 1.

Algorithm 1 Population based heuristic algorithm

```
1: Parameters definition
2: Evaluate fitness of generated population
3: while stop criteria not met do
4:     Performs selection procedure
5:     Applies the intensification and diversification procedures
6:     Evaluate fitness of new candidates
7: end while
8: end
```

To what concerns the meta-heuristic Harmony Search (HS) optimization algorithm (Geem et al., 2001), its formulation is based on the jazz music improvisation, wherein a set of music players are looking for combinations that are more aesthetically pleasing, through an extemporaneously process of memorization. In this process, improvisational musicians always look to

produce a piece of music in perfect harmony. Algorithm 2 shows the pseudocode of the Harmony Search algorithm, which mainly involves the following steps:

I. Initialize the problem and the HS algorithm parameters. In this step, the optimization problem is defined, the objective function (Equation 5.9) is set and the decision variable intervals are introduced. Additionally, the intrinsic parameters of the HS need to be specified, namely the harmony memory size (HMS), the harmony memory consideration rate ($HMCR$), the pitch adjusting rate (PAR), the distance bandwidth (BW) and the number of improvisations/iterations (NI);

$$Minimize\ f(x) \quad x_i \in \left[x_i^L \quad x_i^U\right] \quad i = 1,\ 2,\ 3, \ldots,\ N \tag{5.9}$$

II. Initialize the harmony memory. At this stage, the harmony memory is filled with randomly chosen solutions. Calculate and store the objective function value of each solution vector, in accordance with Equation 5.10;

$$[HM] = \left[\begin{array}{ccccc|c} x_1^1 & x_2^1 & \cdots & x_{N-1}^1 & x_N^1 & f\left(x^1\right) \\ x_1^2 & x_2^2 & \cdots & x_{N-1}^2 & x_N^2 & f\left(x^2\right) \\ \vdots & \vdots & \vdots & \vdots & \vdots & \vdots \\ x_1^{HMS-1} & x_2^{HMS-1} & \cdots & x_{N-1}^{HMS-1} & x_N^{HMS-1} & f\left(x^{HMS-1}\right) \\ x_1^{HMS} & x_2^{HMS} & \cdots & x_{N-1}^{HMS} & x_N^{HMS} & f\left(x^{HMS}\right) \end{array}\right] \tag{5.10}$$

III. Improvise a new harmony, $x^* = [x_1^*\ x_2^*\ \cdots\ x_{N-1}^*\ x_N^*]$. A new potential solution is generated applying one of the three rules: a) memory consideration, the values of decision variables, x_i^*, are chosen from any specified value in the specified HM, $x_i^* \in [x_i^1\ x_i^{HMS}]$, with a probability of $HMCR$; b) random selection, the values of decision variables, x_i^*, are chosen from possible range of the variable, $x_i^* \in [x_i^{min}\ x_i^{max}]$, with a probability of $(1-HMCR)$ in accordance with Equation 5.11; c) pitch adjustment, when values of decision variables are obtained from the HM an additional search for good solutions is achieved tuning the decision variables, with a probability of PAR, in accordance with Equation 5.12 (BW is the distance bandwidth used to improve the performance of HS and is a random number between 0 and 1). The combination of $HMCR$ and PAR parameters establishes the balance between global and local search on the range of possible solutions, respectively.

$$x_i^* = \begin{cases} x_i^* \in \left[x_i^1\ x_i^{HMS}\right], & \text{with probability } HMCR \\ x_i^* \in \left[x_i^{min}\ x_i^{max}\right], & \text{with probability } (1-HMCR) \end{cases} \quad i = 1,\ 2,\ \cdots,\ N \tag{5.11}$$

$$x_i^* = \begin{cases} x_i^* \pm Rand(0,1) \times BW, & \text{with probability } PAR \\ x_i^*, & \text{with probability } (1-PAR) \end{cases} \quad i = 1,\ 2,\ \cdots,\ N \tag{5.12}$$

IV. Update the harmony memory. If the new solution is better than any of the solutions present in the harmony memory, the worst solution is replaced by the new solution.

V. Check the stopping criterion. The algorithm is terminated if the maximum number of improvisations is reached.

Algorithm 2 Harmony Search algorithm

Parameters: HMS, HMCR, PAR, NI, BW
Start
Objective Function: $f(x), \quad x = [x_1, x_2, \cdots, x_N]$
Initialize Harmony Memory (HM): $x^i, \quad i = 1, 2, \cdots, HMS$
Evaluate each Harmony in HM: $f(x^i)$
$iter \leftarrow 1$
while $iter < NI$ **do**
  for $j \leftarrow 1$ *till* N **do**
    if $rand \leq HMCR$ **then**
      Rate of Memory Consideration:
      $x_j^* \leftarrow x_j^i, \quad i \in [1, HMS]$ *chosen randomly*
      if $rand \leq PAR$ **then**
        Pitch Adjusting Rate:
        $x_j^* \leftarrow x_j^* \pm r \times BW \quad$ *with r random*
      end if
    else
      Random Selection:
      Generate x_j^* randomly
    end if
  end for
  Evaluate new Harmony generated: $f(x^*)$
  if $f(x^*)$ is better than worst harmony in Harmony Memory **then**
    Update Harmony Memory
  end if
  $iter \leftarrow iter + 1$
end while
end

Since its inception, the HS algorithm has been applied to an extensive range of engineering optimization problems, from structural design to water network design and analysis or dam scheduling. Concerning ground motion selection and scaling, Kayhan et al. (2011) demonstrated

that the HS algorithm is efficient to select and scale ground motion sets compliant with the code requirements. Despite the efficiency of the HS algorithm, the parameters of the method are problem dependent. This means that the method can lose accuracy depending on the number of records per suited targeted by the user or on the number of available records resulting from the preliminary selection. Macedo et al. (2013) conducted a parametric study comparing various optimization algorithms and concluded that the Adaptive Harmony Search (AHS) algorithm is more suitable for selection and scaling of ground motion records. In the AHS algorithm, the parameters are adaptively tuned during the optimization process based on the parameters observed on each iteration in the harmony memory matrix. Just after a new solution vector is generated in cycle i, a new set of values are assigned for the parameters $(HMCR)^i$ and $(PAR)^i$, through a probabilistic process of selection around the average values of these parameters in the current harmony memory matrix, as given by:

$$(HMCR)^i = \left(1 + \frac{1-(HMCR)^*}{(HMCR)^*} \times e^{-\gamma \cdot N(0,1)}\right)^{-1} \tag{5.13}$$

$$(PAR)^i = \left(1 + \frac{1-(PAR)^*}{(PAR)^*} \times e^{-\gamma \cdot N(0,1)}\right)^{-1} \tag{5.14}$$

$$(HMCR)^* = \frac{\sum_{i=1}^{HMS}(HMCR)^i}{HMS} \tag{5.15}$$

$$(PAR)^* = \frac{\sum_{i=1}^{HMS}(PAR)^i}{HMS} \tag{5.16}$$

where $(HMCR)^i$ and $(PAR)^i$ are the values of the control parameters for a new harmony vector. $N(0,1)$ is a normally distributed random number having the expected value equal to 0 and a standard deviation of 1. $(HMCR)^*$ and $(PAR)^*$ are the mean of the control parameters within the harmony memory matrix and parameter γ is the learning rate of control parameters, recommended to be within the range of $[0.25, 0.50]$. The Adaptive Harmony Search algorithm has been selected for implementation in SelEQ. A flowchart of the algorithm is illustrated in Figure 5.1. It is worth noting that the modular structure of the framework facilitates the implementation of other optimization algorithms.

5.3.2 Objective functions

As mentioned before, the selection and scaling of groups of ground motion records according to code requirements can be considered an engineering optimization problem. According to the majority of seismic design and assessment codes, the aim should be to control the mean (or median) spectrum of the suite of scaled records in relation to the code response spectrum, for the range of

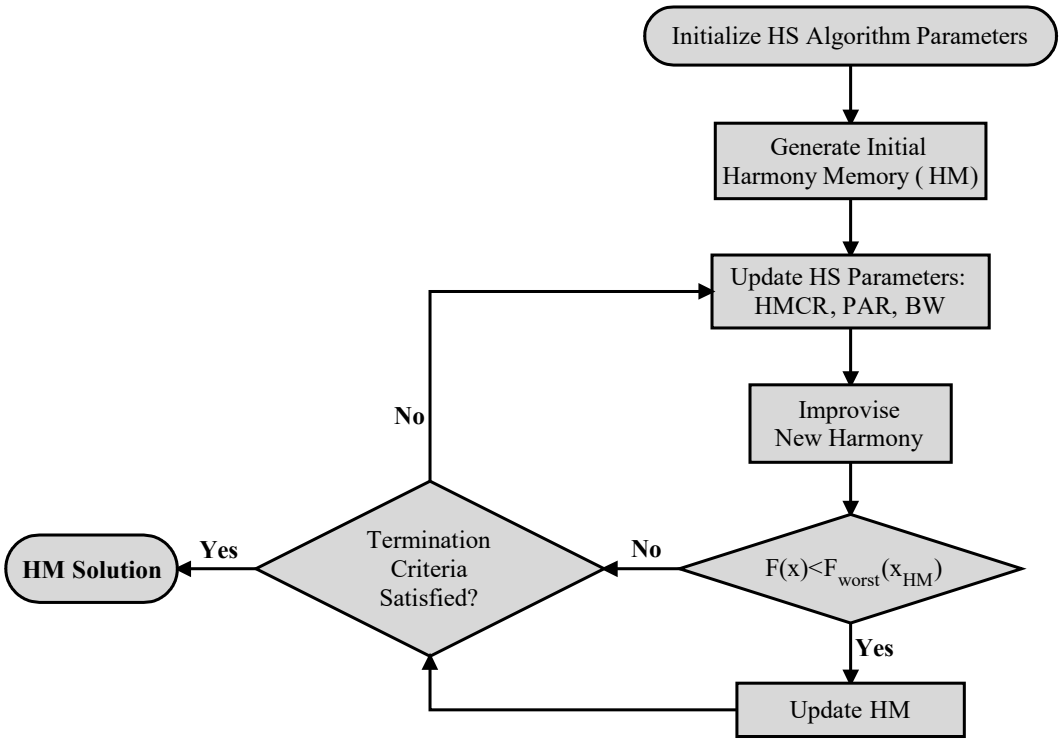

Figure 5.1: Flowchart of the Adaptive Harmony Search algorithm implemented in SelEQ.

periods of interest, considering a number of additional constraints (e.g. EC8 imposes that, for the period range of interest, the mean spectrum of the suite should be above 90% of the code elastic response spectrum). Recently, Araújo et al. (2016) demonstrated that an improvement in the estimation of the mean seismic demands is attained when record selection based on minimization of the differences between the mean (or median) spectrum of the suite of scaled records and the code response spectrum is conducted and if additional control of mismatch between the spectra of the individual records and the code response spectrum is imposed. Figure 5.2 shows an example of the intended spectral shape compatibility. The mean spectrum of a suite composed by n earthquake records can be obtained by the average of the spectral values of the records as follows:

$$S_a^{mean} = \frac{\sum_{i=1}^{n} sf_i \times S_{a_i}(T)}{n} \tag{5.17}$$

where sf_i and $S_{a_i}(T)$ are the scaling factor and the elastic response spectrum of each record, respectively.

In order to attain a solution for the optimization problem, an objective function, $f(x)$, needs to be defined. To what concerns a code-based record selection, the objective function is aimed at minimizing the difference between the mean spectrum of the ground motion suite and the target code spectrum. Several measures of spectral compatibility have been proposed in the literature (Iervolino et al., 2010; Beyer and Bommer, 2007; Buratti et al., 2010), among which is the square root of the sum of the squared errors (DRMS). However, Beyer and Bommer (2007) pointed out

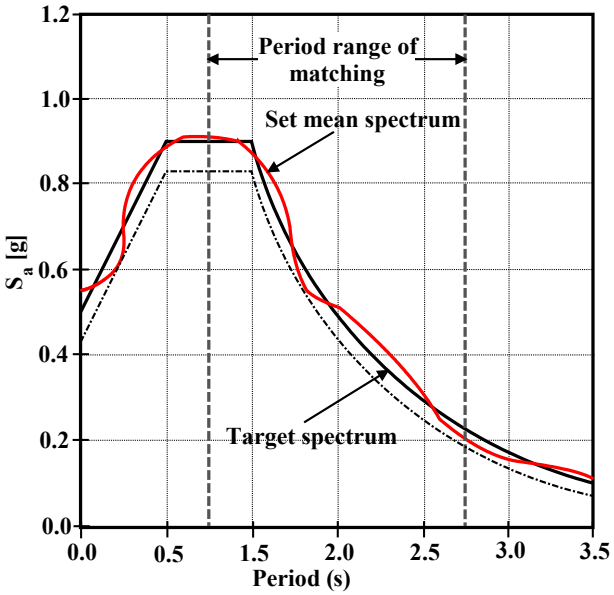

Figure 5.2: Code response spectrum compatibility example.

that the median is of greater engineering significance, since the mean gives excessive weight to singular events. By applying this observation to the optimization problem, two different objective functions can be defined to determine the mean (Equation 5.18) and median (Equation 5.19) spectrum of the ground motion suite with the highest compatibility to the target code spectrum.

$$f(x) = \sqrt{\frac{1}{n_T}\sum_{i=1}^{n_T}\left(S_a^{mean}(T_i) - S_a^{ref}(T_i)\right)^2} \tag{5.18}$$

$$f(x) = \sqrt{\frac{1}{n_T}\sum_{i=1}^{n_T}\left(lnS_a^{mean}(T_i) - lnS_a^{ref}(T_i)\right)^2} \tag{5.19}$$

where n_T is the total number of vibration periods under consideration.

To what concerns the conditional mean spectrum, the optimization algorithm must ensure that the record selection attains a compatibility between the mean and variance of the target response spectrum, as shown in Figure 5.3.

The methodology proposed by Jayaram et al. (2011) sets an objective function that seeks a minimization of the mismatch of both the mean and the variance, as shown in Equation 5.20.

$$f(x) = \sum_{i=1}^{n_T}\left[\left(\hat{m}_{lnS_a(T_i)} - \mu^t_{lnS_a(T_i)}\right)^2 + w \times \left(\hat{s}_{lnS_a(T_i)} - \sigma^t_{lnS_a(T_i)}\right)^2\right] \tag{5.20}$$

where, $\hat{m}_{lnS_a(T_i)}$ is the mean ln_{S_a} of the set at period T_i, $\mu^t_{lnS_a(T_i)}$ is the target mean ln_{S_a} at period T_i, $\hat{s}_{lnS_a(T_i)}$ is the standard deviation of the ln_{S_a} of the set at period T_i, $\sigma^t_{lnS_a(T_i)}$ is the target standard deviation of the ln_{S_a} at period T_i. w is a weigh parameter that establishes the balance between

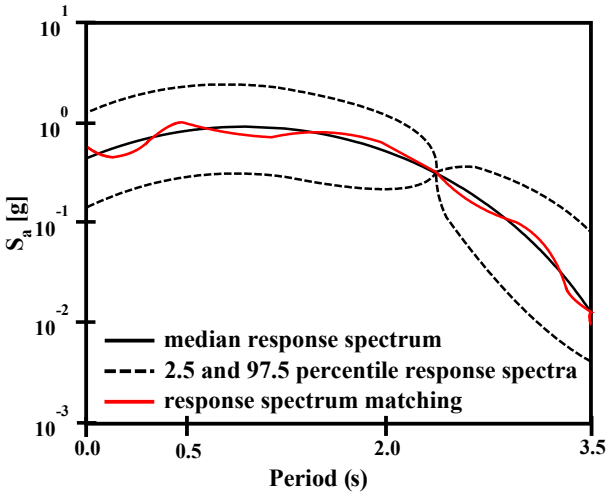

Figure 5.3: Conditional mean spectrum compatibility example.

importance of the errors in the standard deviation and the mean, and n_T is the total number of periods of vibration considered.

5.3.3 Problems constraints

In addition to the minimization of the objective function, the ground motion record selection involves the consideration of further optimization constraints (e.g. no ground motion record should be used more than once in the suite of records). These constraints can be implemented in optimization algorithms by converting the constrained optimization problem in an unconstrained problem. One of the techniques that is commonly adopted consists of using penalty functions to impose additional conditions. The objective function can thus be re-written as:

$$F(x) = f(x) + \sum w_i \times g_i(x) \tag{5.21}$$

where $g_i(x)$ are the penalty functions and w_i the constraint weights associated to each penalty function.

The performance of the optimization problem is highly dependent on the penalty functions and corresponding weights. An alternative technique proposed by Dong et al. (2005), defined as the Fitness Priority-Based Ranking Method, defines two different objective functions, the optimal objective function $F_{obj}(x)$ and the constraint objective function $F_{con}(x)$, in accordance to Equation 5.22 and 5.23, respectively.

$$F_{obj}(x) = f(x) \tag{5.22}$$

$$F_{con}(x) = \sum_{i=1}^{n} w_i \times F_i(x), \qquad \sum_{i=1}^{n} w_i = 1, \quad 0 < w_i < 1 \tag{5.23}$$

where:

$$F_i(x) = \begin{cases} 1, & g_i(x) \leq 0 \\ 1 - \frac{g_i(x)}{g_{max}(x)}, & g_i(x) > 0 \end{cases} \qquad g_{max}(x) = max(g_i(x)) \tag{5.24}$$

The weight associated to each restriction may be randomly generated (to ensure sufficient diversity) or can be obtained by Equation 5.25 as follows:

$$w_i = \frac{g_i(x)}{\sum_{i=1}^{n} g_i(x)} \tag{5.25}$$

The constraint objective function, $F_{con}(x)$, defines the relation between the new solution vector and the domain of possible solutions. If $F_{con}(x)$ is equal to 1, the new solution vector belongs to the domain of possible solutions. On the other hand, if the value of the constraint objective function is between $0 < F_{con}(x) < 1$, the smaller it is the lowest is the probability that the solution vector is part of the domain of possible solutions.

Ye et al. (2012) applied the aforementioned technique to ground motion selection methodologies and defined a two-stage ranking procedure. Firstly, the HM matrix is ranked based on the value of the constraint objective function, $F_{con}(x)$. After that, the functions with the same value of the constraint objective function are ranked by the optimal objective function, $F_{obj}(x)$.

It is important to note that code-based record selection suggests a compatibility between the mean spectrum of the suite of earthquake records and the code design spectrum. However, whilst a lower bound limit is defined for the mean spectrum (90%), no upper bound is prescribed in seismic codes. A lower, (low), and upper, $(upper)$, bound constraint functions can be defined as follows:

$$g_1(x) = \begin{cases} low - min\left[S_a^{mean}(T)/S_a^{target}(T)\right], & \text{if } min\left[S_a^{mean}(T)/S_a^{target}(T)\right] < low \\ 0, & \text{if } min\left[S_a^{mean}(T)/S_a^{target}(T)\right] \geq low \end{cases} \tag{5.26}$$

$$g_2(x) = \begin{cases} max\left[S_a^{mean}(T)/S_a^{target}(T)\right] - upper, & \text{if } max\left[S_a^{mean}(T)/S_a^{target}(T)\right] > upper \\ 0, & \text{if } min\left[S_a^{mean}(T)/S_a^{target}(T)\right] \leq upper \end{cases} \tag{5.27}$$

Additionally, EC8-1 defines that mean of the zero period spectral response acceleration values calculated from the individual time histories should not be smaller than the zero period spectral acceleration of the target response spectrum. Thus, the constraint function is given by:

$$g_3(x) = \begin{cases} 0, & S_a^{mean}(0) \geq S_a^{target}(0) \\ 1, & S_a^{mean}(0) < S_a^{target}(0) \end{cases} \tag{5.28}$$

In both code-based and conditional mean spectrum based record selection no ground motion record should be used more than once in the suite of records. Moreover, the suites of records should contain the largest possible number of ground-motions from different earthquake events. This can

be mathematically formulated as follows:

$$g_4(x) = \begin{cases} 1, & \text{same ground motion used more than once in the set} \\ 0, & \text{otherwise} \end{cases} \tag{5.29}$$

$$g_5(x) = \begin{cases} 1, & \text{same event used more than once in the set} \\ 0, & \text{otherwise} \end{cases} \tag{5.30}$$

Moreover, an additional constraint can be implemented regarding the ability to allow the user to specify the maximum individual mismatch of the ground motion records in relation to the target spectrum. Even though codes lack any specification concerning the control of the individual mismatch, this plays an important role in the estimation of the structural response, since large variability at the record level combined with a small number of ground motion records can greatly influence the accuracy of the structural response estimates (Araújo et al., 2016; Iervolino et al., 2010; Buratti et al., 2010; Cornell, 2004).The individual mismatch constraint functions can be defined as follows:

$$g_6(x) = \begin{cases} low - min\left[S_a^{record}(T)/S_a^{target}(T)\right], & \text{if } min\left[S_a^{record}(T)/S_a^{target}(T)\right] < low \\ 0, & \text{if } min\left[S_a^{record}(T)/S_a^{target}(T)\right] \geq low \end{cases} \tag{5.31}$$

$$g_7(x) = \begin{cases} max\left[S_a^{record}(T)/S_a^{target}(T)\right] - upper, & \text{if } max\left[S_a^{record}(T)/S_a^{target}(T)\right] > upper \\ 0, & \text{if } min\left[S_a^{record}(T)/S_a^{target}(T)\right] \leq upper \end{cases} \tag{5.32}$$

where (low) and $(upper)$ are the limits set for the spectral mismatch of each individual record in relation to the target spectrum.

5.4 Ground motion record selection and scaling framework

A preliminary and very simple prototype version of the current framework was developed several years ago at the University of Porto (Dias et al., 2010). It was made available as a web-based application and only allowed for the selection of individual records based on compatibility with a target response spectrum. Recently, an advanced record selection and scaling framework (SelEQ) was developed based on the record selection techniques and optimization procedures detailed in the previous sections. The version of SelEQ described hereafter follows a modular and extensible development approach, allowing for easy implementation of new features in the future. In its current state, SelEQ includes three different modules, namely: i) a seismological module; ii) a preliminary selection module which is currently powered by the NGA-WEST2 ground motion

database (Ancheta et al., 2013, 2014) and iii) a record-selection module. All the models are integrated within a user-friendly graphical user interface. The algorithms and the graphical user interface were developed using the Python programming. The architecture of the SelEQ framework is presented in the following sections, along with a detailed description of the calculation modules.

5.4.1 Architecture of SelEQ

As shown in Figure 5.4, the SelEQ framework consists of three integrated modules already mentioned before. The seismological module, which is powered by the OpenQuake framework, provides, for any site of the European territory, the hazard curves, disaggregation matrices, uniform hazard spectra and conditional mean spectrum. These results can be then used as preliminary search criteria in the pre-selection module. The pre-selection module connects to the NGA-WEST2 ground motion database to perform the preliminary selection of ground motion records. A temporary database is created with the information of the eligible records (M, R, response spectra, etc.). Having determined a set of eligible ground motions, the user can then utilize the record selection module to conduct the final code-based or CMS-based record selection. It is important to note that if the user intends to perform a CMS-based ground motion selection, than it becomes necessary to obtain the conditional spectrum in the seismological module.

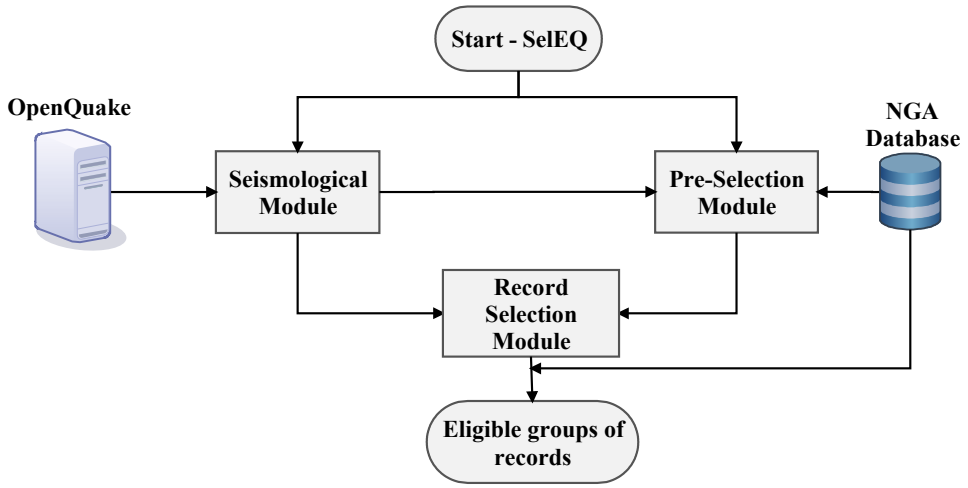

Figure 5.4: Architecture of the SelEQ framework.

It should be noted that the seismological module can also be employed to derive information that can be used as preliminary criteria for the pre-selection of a code-based record selection. It allows for example to obtain, for a given site under investigation, the range of magnitudes and distances with the highest contribution to the hazard. One of the major advantages of this methodology is that a more accurate pre-selection of eligible ground motions can be carried out, and therefore a more realistic suite of ground motion records is achieved. On the other hand,

if CMS-based record selection is sought, the seismological module not only allows for a refined preliminary selection, but it is also used for the calculation of the CMS spectrum.

5.4.2 Description of the modules

The usability of the SelEQ framework was also an important factor in its development. Thus, a user friendly graphical user interface (GUI) was developed using the Python binding PyQt. The GUI consists of three different user dialog windows corresponding to each of the modules identified in Figure 5.4. In the following paragraphs each module, corresponding to each step performed in SelEQ regarding the selection and scaling process, is detailed.

Concerning the first module (Seismological), and as shown in Figure 5.5, the user is asked to introduce the coordinates of the site under study, the soil classification, the fundamental period of vibration of the structure, and the occurrence probability (see box 1). Currently, all the hazard calculations are based on the recently proposed SHARE model (Woessner et al., 2015) and hence the site must be located in the European territory. Nevertheless, SelEQ has been developed in a modular way and hence the implementation of additional hazard models is a relatively simple task. In addition to the data referred above, the user should also specify the type of analysis to be performed (classical probabilistic seismic hazard assessment to obtain site specific hazard curves, disaggregation matrices, uniform hazard spectra or conditional spectra), as shown in box 2 of Figure 5.5. The results obtained using the OpenQuake analysis are then plotted on the right side of the windows (box 3).

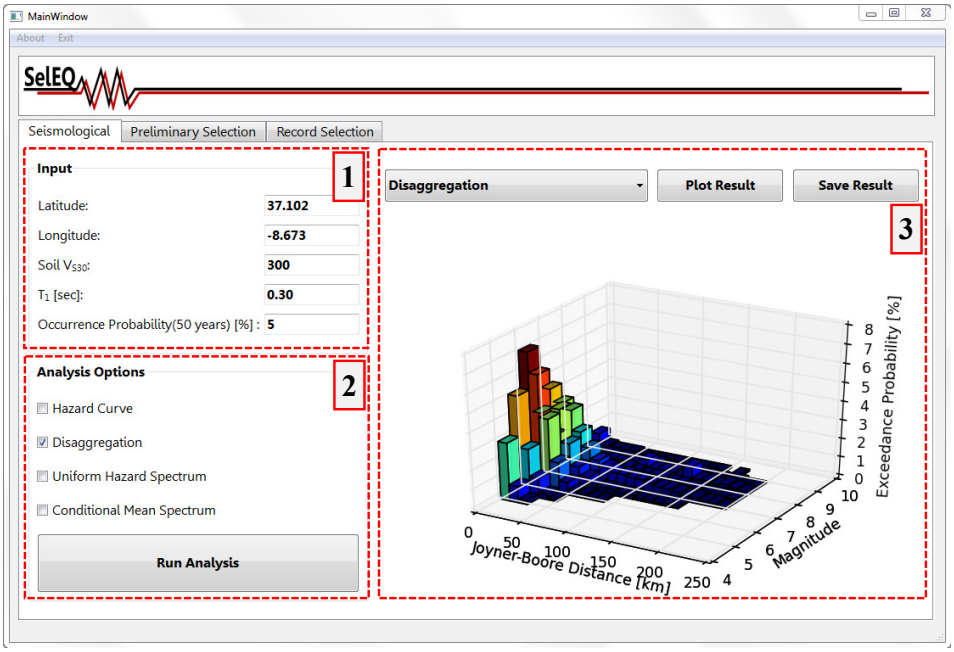

Figure 5.5: Seismological module input, analysis options and results visualization.

Within this module, the SelEQ framework internally generates an OpenQuake analysis file and runs a probabilistic seismic hazard analysis (PSHA). As already mentioned before in this Chapter, OpenQuake does not generate the Conditional Mean Spectrum (CMS). Therefore, the methodology proposed by Lin, Harmsen, Baker and Luco (2013); Lin, Haselton and Baker (2013a,b) was implemented in the record selection tool. It is important to note that the computation of the exact version of the CMS as defined by Lin, Harmsen, Baker and Luco (2013); Lin, Haselton and Baker (2013a,b) can take several hours, depending on the site location and the number of sources contributing to the hazard, since individual PSHA of each source is required to build the CMS. After the calculations are performed by SelEQ, the user is able to both visualize and save the results obtained (box 3 of Figure 5.5). The results can be used later in the selection module, particularly when a CMS-based ground motion record selection is to be performed.

Regarding the second module (Preliminary Selection), the user is able to conduct a preliminary selection of ground motion records, based on seismological and strong-motion parameters. Several criteria have been recognized as appropriate for performing an initial selection (Katsanos et al., 2010). Among these criteria are the magnitude, epicentral distance, average soil shear-wave velocity of the top 30m (V_{s30}), peak ground acceleration (PGA), peak ground velocity (PGV) and lowest usable frequency (LUF) are commonly used parameters. As shown in Figure 5.6, filters associated with these parameters were implemented in the SelEQ framework (box 1), allowing the user to perform a preliminary refinement of the ground motion database that will be then used in the record selection module.

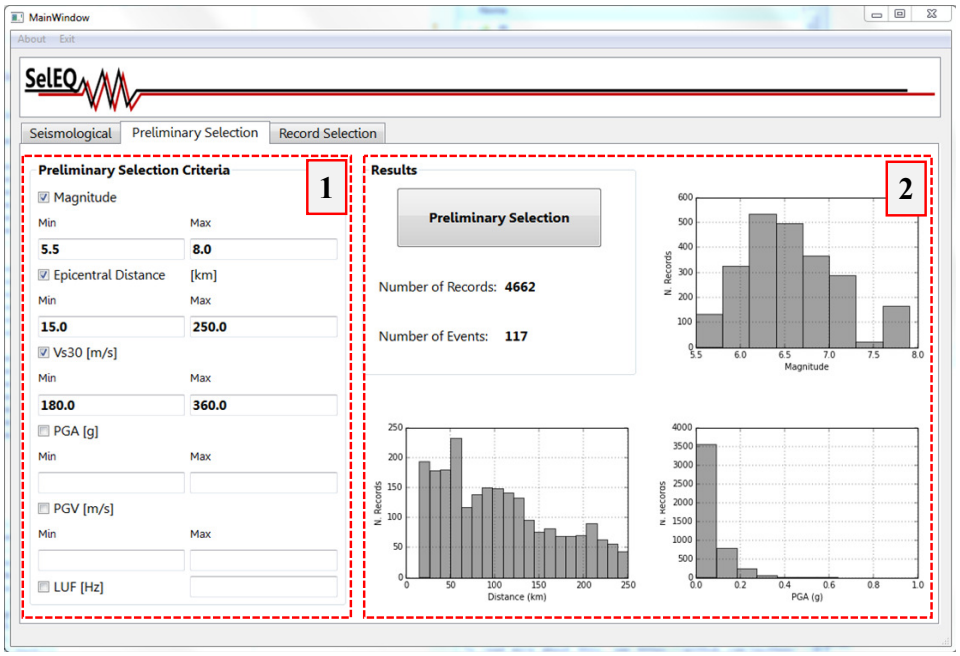

Figure 5.6: Preliminary selection module input and results visualization.

Currently, SelEQ enables the search of ground motions available in the NGA-WEST2 record

database. Among the various ground motion databases, NGA-WEST2 (Figure 5.7) is one of most recent and more updated, with more than 21000 three-component records originated from around 600 earthquake events. Nonetheless, the modular nature of SelEQ facilitates the incorporation of additional ground motion databases in the future.

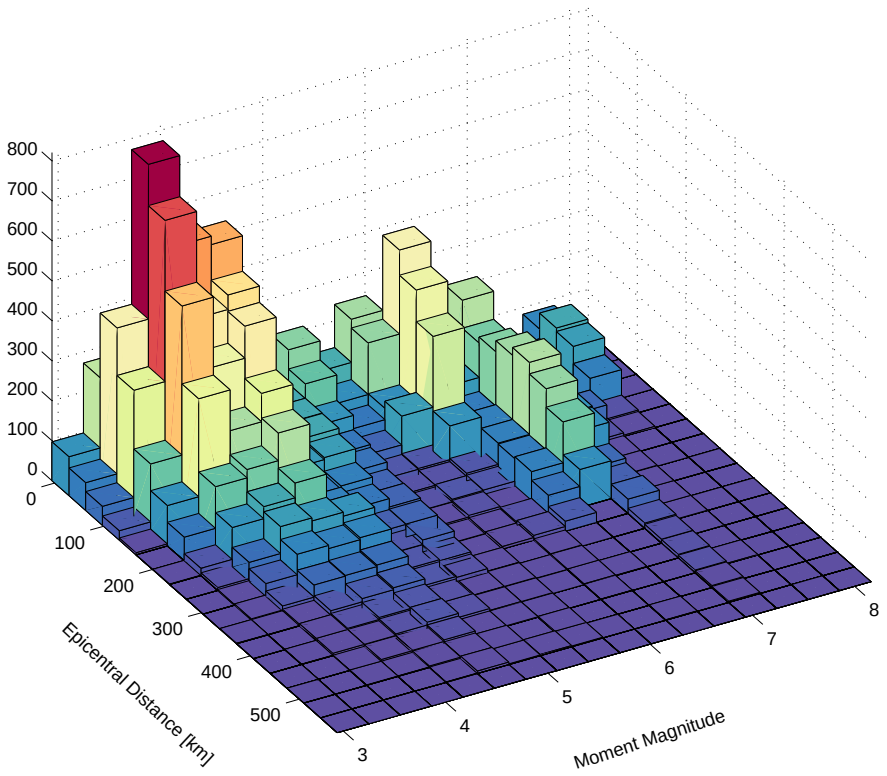

Figure 5.7: Preliminary selection module input and results visualization.

Upon conducting the preliminary record selection using the filters shown in box 1 of Figure 5.6, the number of available records and corresponding magnitude, distance and PGA distributions are presented to the user in box 2 of the same figure. In this way, the user can decide to refine or expand the preliminary selection criteria.

After the definition of the preliminary ground motion database, SelEQ is able to perform the record selection and scaling operations. To this end, the third module (Record Selection), the GUI of which is depicted in Figure 5.8, allows for the definition of the type of target spectrum (code-based or CMS) as well as the number of scaled records that will compose the record set. To what concerns a code-based record selection, the user must define the seismic design code according to which the record selection will be performed (box 1 of Figure 5.8). Additionally, SelEQ allows the user to define additional selection criteria (box 2 of Figure 5.8), namely the range of periods of vibration for which spectral compatibility is required, the mismatch (in percentage)

between the target response spectrum and the average response spectrum, the individual mismatch (in percentage) between the response spectrum of each individual record and the target response spectrum, and the range of acceptable scaling factors. It is important to note that these additional criteria pose major advantages concerning the possibility of conducting parametric studies and evaluating the influence of the record selection process on the structural response.

It is worth noting that SelEQ enables ground motion record selection for 3D analysis, by ensuring compatibility between the mean of the geometrical mean of horizontal components and the target spectrum. In its present version, SelEQ does not allow the simultaneous selection of horizontal and vertical components.

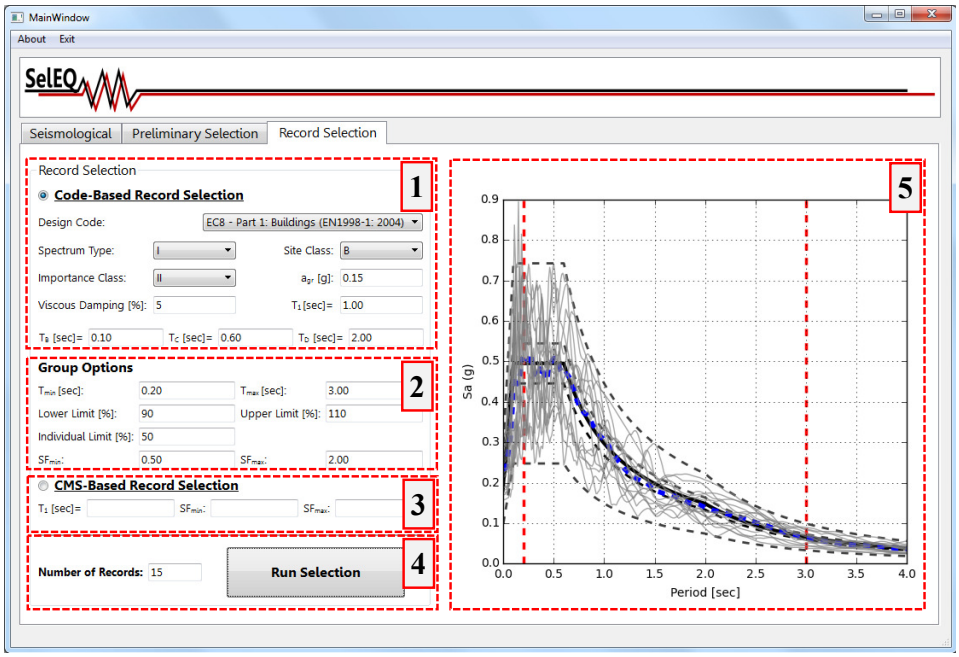

Figure 5.8: Record selection module input and results visualization.

For a CMS-based record selection (box 3 of Figure 5.8), the user must specify the fundamental period of the structure under investigation, as well as the range of acceptable scaling factors. The tool automatically sets the last obtained CMS calculated in the seismological module as the target spectrum. Finally, the number of records of the ground motion set must be defined in box 4 (Figure 5.8) and the optimization algorithm launched by pressing the "Run Selection" button. The obtained results will be represented graphically in box 5 (Figure 5.8) and a text file identifying the records and the corresponding scaling factors is generated and saved to an output directory.

5.5 Application examples of SelEQ

The application of the SelEQ framework to various ground motion record selection and scaling problems is now presented. In the following sections, some illustrative applications of the developed tool for code-based and CMS-based record selection are shown, and the flexibility and

robustness of the proposed framework is demonstrated.

5.5.1 Code-based record selection

This first application of SelEQ is performed within the context of a comparative study of different code-based record selection methods (Araújo et al., 2016). The main objectives of the research were to investigate the influence of the number of selected ground motion records on the estimation of the mean structural response and also the importance and efficiency of considering additional selection criteria such as the control of spectral mismatch of each individual record with respect to the target spectrum. This section will only report on the ground motion record selection process. A detailed discussion on the results of the study are available in (Araújo et al., 2016). The study comprised the seismic performance assessment of four steel buildings located in Portugal, in the city of Lisbon. The structures consist of 5-storey 3-bay steel buildings, composed by moment-resisting frames (MRF), with a regular configuration in plan and elevation. Each building was designed according to different criteria. The first building, denoted as GB, was designed to withstand gravity loads. The remaining three buildings were seismically designed according to Part 1 of Eurocode 8 (EC8-1) assuming medium ductility class (DCM), with a behaviour factor q of 4.0, and to comply with different limits for the inter-storey drift sensitivity coefficient, θ, which is defined in the code to address the treatment of second-order effects. The fundamental periods of vibration of the four buildings range between 0.9 and 1.6 seconds. A detailed description of the buildings is available in (Araújo and Castro, 2017; Araújo et al., 2017). The seismological preliminary criteria were defined according to the Portuguese Type 1 and Zone 3 seismic action as defined in the Portuguese National Annex of EC8-1 (CEN, 2010). Accordingly, magnitudes and epicentral distances higher than 5.5 and 20 km, respectively were considered in the preliminary selection. Additionally, an interval of values of the average shear wave velocity, V_{s30}, between 360 m/s and 800 m/s was adopted, in agreement with soil type B defined in EC8-1. A total of 2504 records were obtained from the preliminary selection. The record selection was carried out by imposing spectral compatibility between the mean spectrum of the group and the target (code) response spectrum in the period intervals defined in each seismic code considered. In the optimization process, the scaling factors were limited to the interval [0.5; 2.0] and the constraints described in section 5.3.3 were adopted. These include the control of the mismatch between the mean spectrum of the suite of ground motion records and the target spectrum within an interval of $\pm 10\%$ (Equation 5.26 and 5.27), the enforcement that the mean PGA value is greater than the PGA of the target response spectrum (Equation 5.28). Additional constraints were considered, namely the limitation of a maximum of one ground motion record from a given earthquake event (Equation 5.30) and the restriction that a given ground motion record cannot be repeated in a given group (Equation 5.29). Furthermore, some additional selections were performed by considering improved selection criteria that consisted on imposing spectral mismatch limits relative to the target spectrum of $\pm 50\%$ for each individual record (Equation 5.31 and 5.32). Figure 5.9 shows the obtained suites of seven ground motion records, which were selected and scaled in accordance to

the European (EC8-1), American (ASCE41-13) and New Zealand (NZS 1170.5:2004) recommendations. The designations "EC8-IM" and "ASCE41-13-IM" refer to groups in which control of the spectral mismatch between the individual record and the target spectrum was imposed in the selection process.

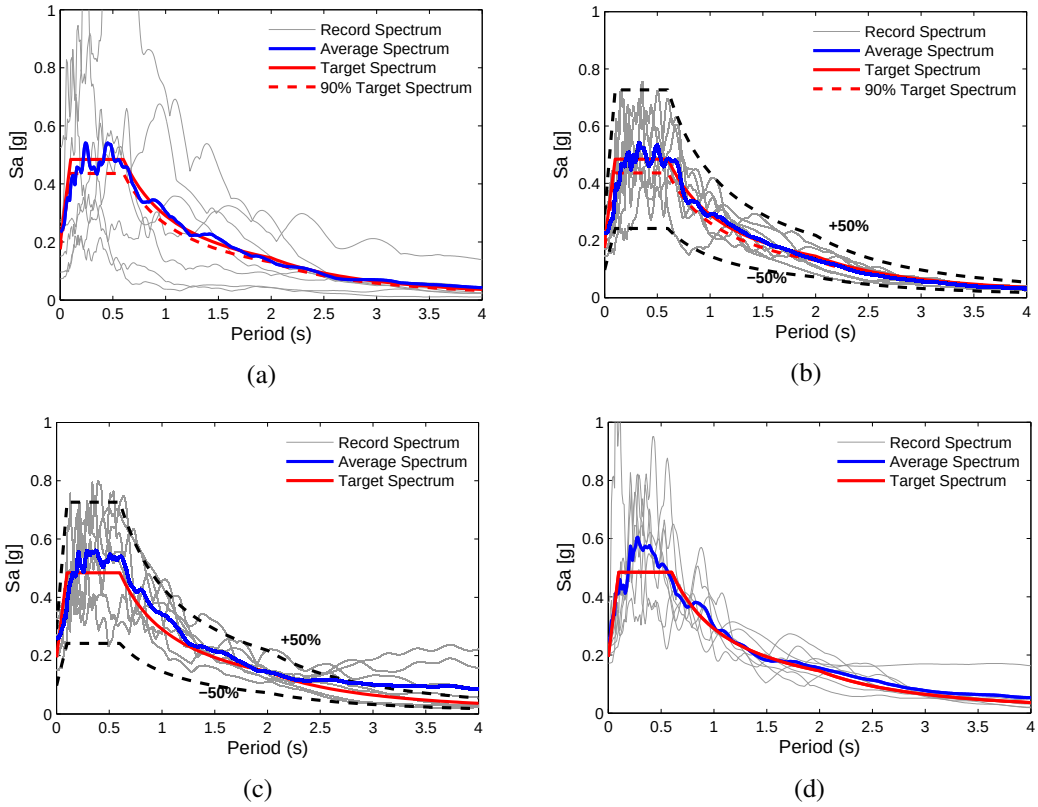

Figure 5.9: Application of SelEQ to a code-based record selection case: (a) EC8, (b) EC8-IM, (c) ASCE41-13-IM and (d) NZS1170.5:2004.

It is worth noting that the application of SelEQ in this study allowed demonstrating that an improvement on the estimation of the average structural response is accomplished when the additional criteria of controlling the mismatch of each individual record in relation to the target spectrum is considered in the record selection process. Furthermore, the study also demonstrated that the use of a minimum of seven records, proposed by most codes, to calculate the mean seismic demands is only accurate when the additional selection criteria referred above is adopted. A detailed discussion of the results of the above-mentioned study is provided in Araújo et al. (2016).

The SelEQ framework performed both accurately and efficiently, allowing to obtain the intended record sets, each one in less than 300 seconds when running on a 8GB RAM 2.80GHz Intel i7 CPU. A total of 200000 iterations were required to obtain each record set. Despite the large number of available records in the NGA-WEST2 database, the use of SelEQ for this type of record selection can be impaired when highly restrictive preliminary selection criteria is defined by the user. This results from the fact that, due to the reduced number of ground motion records,

the framework may not be able to find a group that is fully compliant with all the constraint conditions set by the user. In such a situation, SelEQ returns the group that minimized the objective function even though violating one or more constraints. However, in most cases these situations do not occur and hence SelEQ is able to perform both quickly and efficiently the record selection and scaling specified by the user.

5.5.2 CMS-based record selection

Concerning the CMS-based record selection, the first application example concerns the use of the SelEQ framework for the calculation of the CMS for Istanbul, considering several occurrence probabilities and suites of forty scaled ground motion records. Two structures, namely a 4-storey RC building (Haselton et al., 2010) and a 5-storey steel building (Araújo and Castro, 2017; Araújo et al., 2017) were considered. The lateral resistance in both structures is provided by moment-resisting frames. The fundamental periods of vibration are equal to 1.1s and 1.63s for the RC and steel buildings, respectively.

CMS for the two fundamental periods of vibration have been developed considering four probabilities of exceedance in 50 years, namely 1%, 2%, 5% and 10% and assuming a site characterised by an average shear wave velocity equal to 600 m/s. Figure 5.10 shows the CMS computed which were then employed in the record selection.

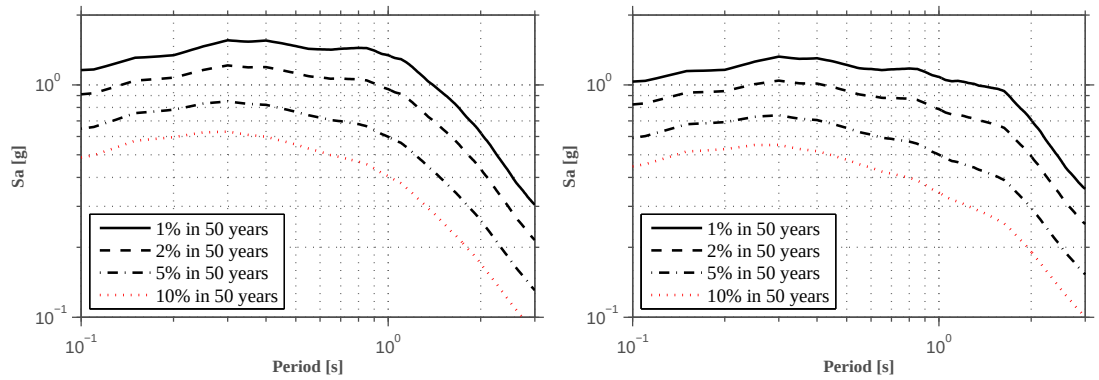

Figure 5.10: CMS for Istanbul for different probabilities of exceedance in 50 years: a) T1=1.1s, b) T1=1.63s.

Concerning the seismological preliminary criteria, magnitudes between 5.5 and 8.0, epicentral distances between 10 to 600 km and average shear wave velocity, V_{s30}, between 180 m/s and 800 m/s were adopted.

Depending on the target CMS, the preliminary selection returned a total number of ground motion records between 1000 and 3400, depending on the probability of exceedance under consideration. It is worth noting that the maximum scaling factor was limited to 10. The output of the preliminary selection, particularly for cases of low probability of exceedance in zones of high seismicity, is highly dependent on the limit defined for this parameter.

The record selection process consisted of minimizing the mismatch of both the mean and the variance in relation to the target mean and standard deviation of the CMS (Equation 5.20). Additionally, two constraints described in section 5.3.3 were adopted, namely the limitation of a maximum of one ground motion record from a given earthquake event (Equation 5.30) and the restriction that a given ground motion record cannot be repeated in a given group (Equation 5.29). Figure 5.11 shows the suites of forty records selected and scaled according to the aforementioned criteria.

The figures clearly show the efficiency of the record selection, particularly in terms of the good match between mean and variance response spectrum of the suite of ground motions and the CMS target spectrum.

The second application example concerns the CMS-based record selection for two sites located in Portugal, namely the city of Porto and Lagos, for a probability of occurrence of 5% in 50 years. This was carried out within the context of a research study which aimed at evaluating the seismic risk of cold-formed steel shear wall systems located in regions of low and moderate seismicity. Six structures with 2, 4 and 5 storeys were considered. The fundamental periods of vibration were equal to 0.25s and 0.35s for the 2-storey structures, 0.37s and 0.93s for the 4-storey structures and 0.42s and 1.14s for the 5-storey structures. Full details about the gravity and seismic design of the buildings is available in Kechidi et al. (2017).

CMS for the six fundamental periods of vibration have been developed considering a probability of exceedance of 5% in 50 years and assuming a site characterised by an average shear wave velocity equal to 360 m/s. It should be noted that, for this particular study involving the Portuguese territory, the SHARE hazard model was complemented with additional hazard sources (Vilanova and Fonseca, 2007) and the ground motion prediction equations proposed by Atkinson and Boore (2006) and Akkar and Bommer (2010) with a weight of 70 and 30%, respectively. This approach is in line with that recently adopted by Silva et al. (2015). Figure 5.12 shows the CMS computed which were then employed in the record selection.

Concerning the seismological preliminary criteria, magnitudes between 5.5 and 7.5, epicentral distances between 10 to 600 km and average shear wave velocity, V_{s30}, between 180 m/s and 800 m/s were adopted. Depending on the target CMS, the preliminary selection returned a total number of ground motion records between 4500 and 5700.

The record selection process followed the procedure described in the previous application example and the same constraints were adopted. Figure 5.13 shows the suites of records selected and scaled according the aforementioned criteria.

In this application example SelEQ was also able to perform both accurately and efficiently the CMS-based record selection. However, the methodology is entirely dependent on the OpenQuake (OQ) simulations. Thus, the higher the number of sources present in the hazard model, the longer the analysis time. As an example, for a site with approximately 4000 sources, a large number of simulations are required, and the calculation time of the CMS performed on a 8GB RAM 2.80GHz Intel i7 CPU ranges from 10 to 12 hours. However, the remaining part of the methodology, namely the selection and scaling of the records based on the targeted CMS, is performed in a matter of

minutes, similar to a code-based selection. As already mentioned, over restrictive preliminary selection criteria can make impossible for SelEQ to successfully provide a set of ground motion records that is fully compliant with all the constraints specified by the user. Therefore, the definition of the preliminary selection criteria is a fundamental step in the record selection and scaling process and it strongly influence the efficiency of the optimization procedure. Additionally, it should be mentioned that the high performance of SelEQ enables its use to derive multiple suites of ground motions for a given record selection problem, allowing in this way the user to select the suite that better complies with the pre-defined criteria.

5.6 Conclusions

In this Chapter, SelEQ, an advanced ground motion selection and scaling framework, was described followed by its application to code-based and probabilistic-based record selection cases. SelEQ follows a modular and extensible development approach, allowing for easy implementation of new features in the future. Currently, three modules have been implemented which allow for a seismological characterization, preliminary selection and selection and scaling of suites of ground motion records. One of the major advances of the tool is the possibility to compute the Conditional Mean Spectrum (CMS) for the European territory. To this end, SelEQ makes use of the open source platform OpenQuake and the recently proposed SHARE seismic hazard model. The current version of SelEQ enables the search of ground motions available in the NGA-WEST2 record database. However, due to modular architecture of the framework, the inclusion of additional strong-motion databases can be easily integrated. Another important feature of SelEQ is the ability to perform code-based record selection incorporating advanced criteria, namely the control of spectral mismatch between each individual record and the target response spectrum, which provides significant improvements in terms of estimating structural mean response.

In order to significantly reduce the computational cost and analysis time associated with the selection and scaling of suites of ground motion records, the Adaptive Harmony Search metaheuristic optimization algorithm was implemented. As expected, the performance of the tool is sensitive to overly stringent preliminary selections. However, common preliminary selection criteria enable the successful selection and scaling of suites of ground motion records.

The efficiency and robustness of the tool was demonstrated with two application examples, namely a code- based and a CMS-based ground motion record selection cases. The record suites obtained confirm the effectiveness of SelEQ for the selection and scaling of suites of ground motions in accordance to current seismic guidelines and state-of-the-art record selection techniques.

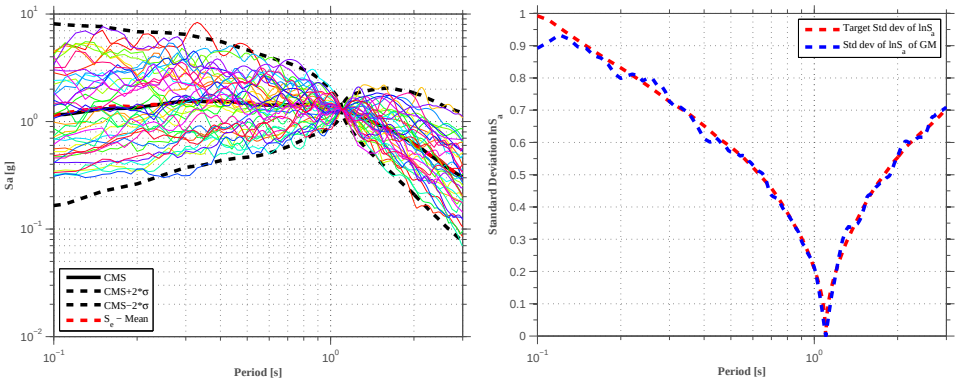

(a) 1% in 50 years - Mean

(b) 1% in 50 years - Variance

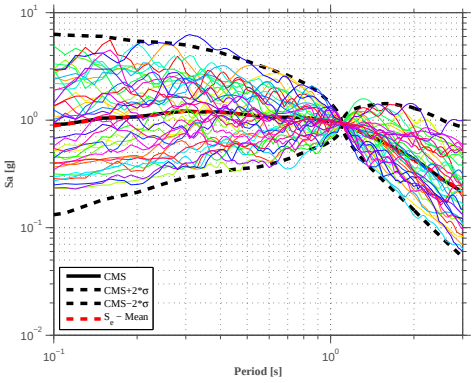

(c) 2% in 50 years - Mean

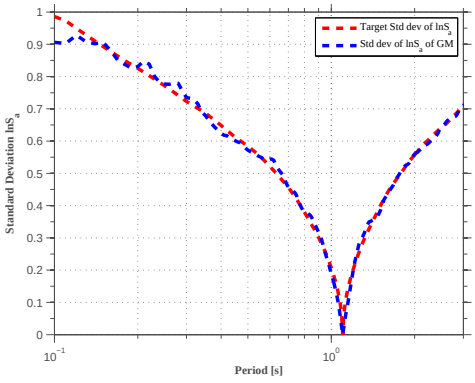

(d) 2% in 50 years - Variance

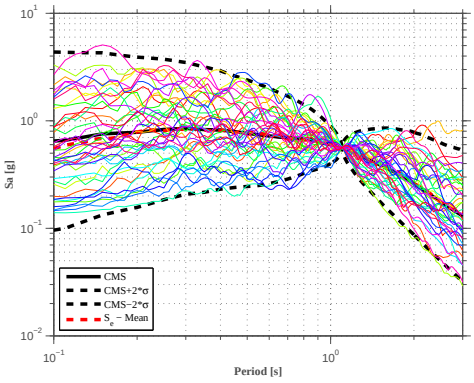

(e) 5% in 50 years - Mean

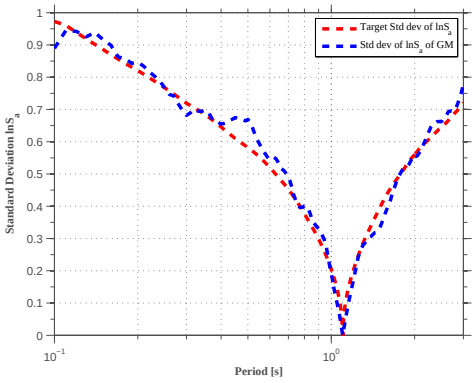

(f) 5% in 50 years - Variance

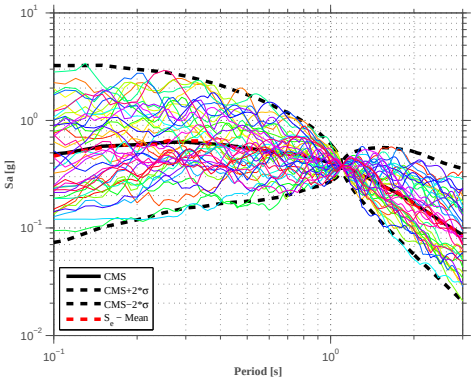

(g) 10% in 50 years - Mean

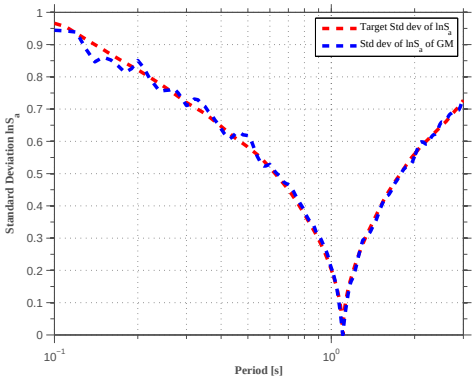

(h) 10% in 50 years - Variance

Figure 5.11: Application of SelEQ to a CMS-based record selection case (Istanbul, T1=1.1s).

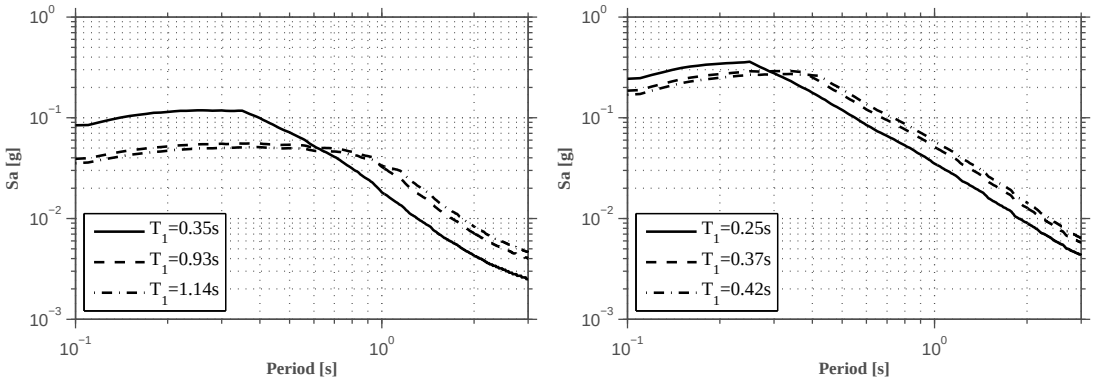

(a) (b)

Figure 5.12: CMS for a probability of exceedance of 5% in 50 years for different periods of vibration: a) Porto, b) Lagos.

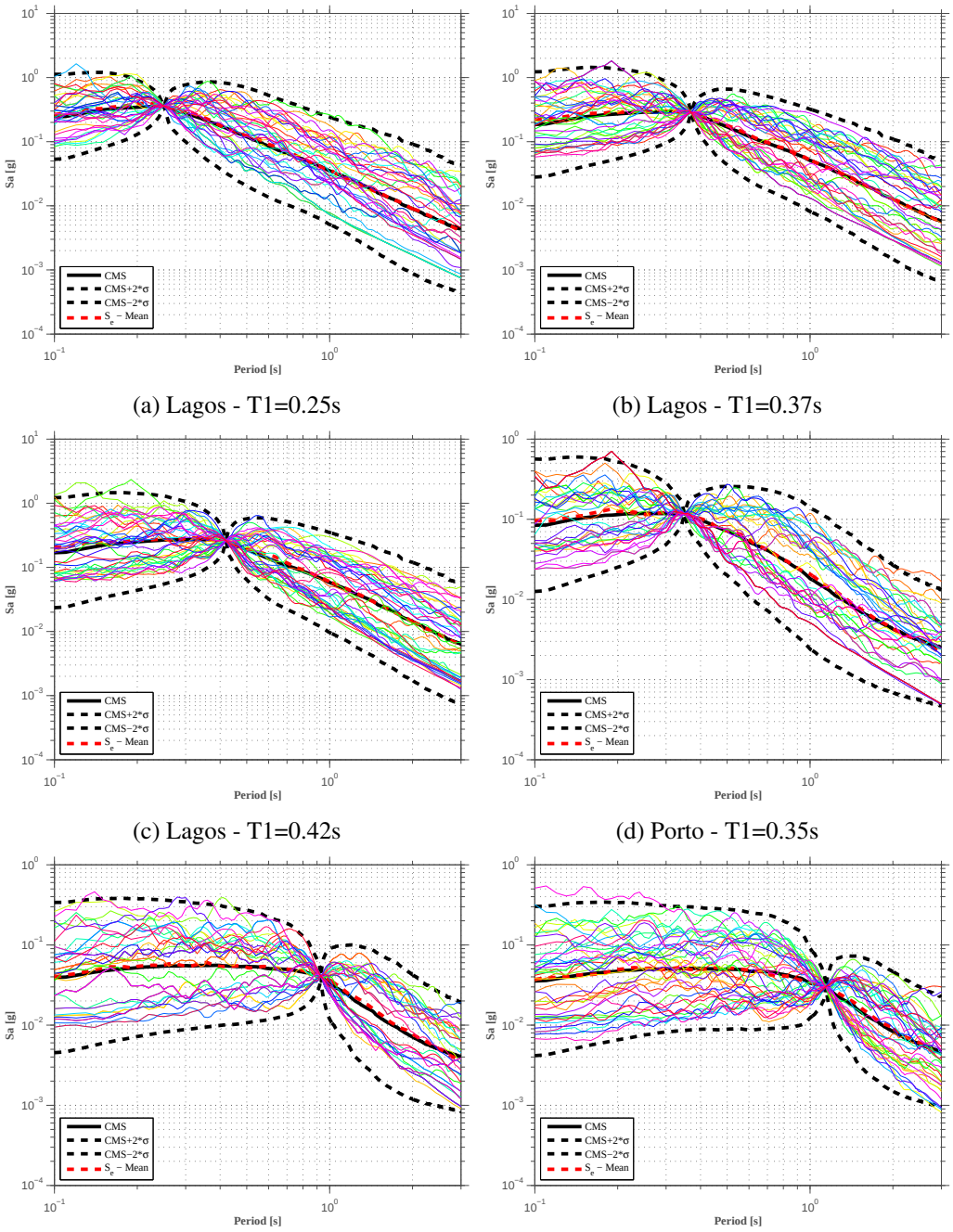

(a) Lagos - T1=0.25s

(b) Lagos - T1=0.37s

(c) Lagos - T1=0.42s

(d) Porto - T1=0.35s

(e) Porto - T1=0.93s

(f) Porto - T1=1.14s

Figure 5.13: CMS-based SelEQ application example (CMS for 5% in 50 years).

Chapter 6

Collapse performance assessment of steel moment-resisting frames designed according to Eurocode 8

6.1 Introduction

Current practices in seismic design of structures are closely linked to their ductility and energy dissipation capacity. According to modern seismic design codes (e.g. Eurocode 8 – Part 1 (EC8) (CEN, 2005c); ASCE/SEI 7-10 (ASCE/SEI, 2010); AISC 341-16 (ANSI, 2016)) seismic design targeting elastic response under the design earthquake should be confined to structures located in low seismicity areas or structures of special importance (Elghazouli, 2005). For ordinary structures, it would not be economically and architecturally feasible to perform seismic design considering elastic response in mind. Thus, current design guidelines allow for controlled levels of damage for pre-defined levels of seismic intensity. Among the typical seismic-resistant structural systems, steel moment-resisting frames (MRFs) are considered to be ductile structures with proper energy dissipation capacity. In this sense, their use in seismic areas is seen as very advantageous and attractive.

To what concerns the European code, EC8 specifies performance requirements for seismic design of new buildings. The code prescribes a no-collapse requirement, aiming to prevent local or global collapse under the design earthquake, and a damage limitation requirement which intends to limit structural and non-structural damage under more frequent earthquake events. Different probabilities of occurrence of the seismic action are therefore defined in the code for each performance requirement (Elghazouli, 2009). With regard to the no-collapse requirement, the code code tries to to ensure the development of stable plastic mechanisms under seismic loading, through the application of capacity design procedures. Strategic locations for the dissipative regions are defined during the design in order to achieve the desired failure mechanisms. For steel MRFs with rigid connections, the inelastic behaviour should occur at the end regions of the beams and

at the base of the first-floor columns. The remaining structural members must then be designed to remain elastic throughout the earthquake.

Similarly to other seismic codes, EC8 adopts a force-based design approach in which a behaviour factor is considered to reduce the lateral strength requirement of a structure and, in this way, indirectly consider energy dissipation which will occur through inelastic response of the structural components. The behaviour factor defined in EC8, q, is directly linked to the parameters that define the energy dissipation capacity of the structure, namely the type of structural system, redundancy as well as member ductility and overstrength (Ferraioli et al., 2014) (Chapter 2). Figure 6.1 shows the typical lateral behaviour curve of steel MRFs, in which the physical meaning of the behaviour factor is illustrated.

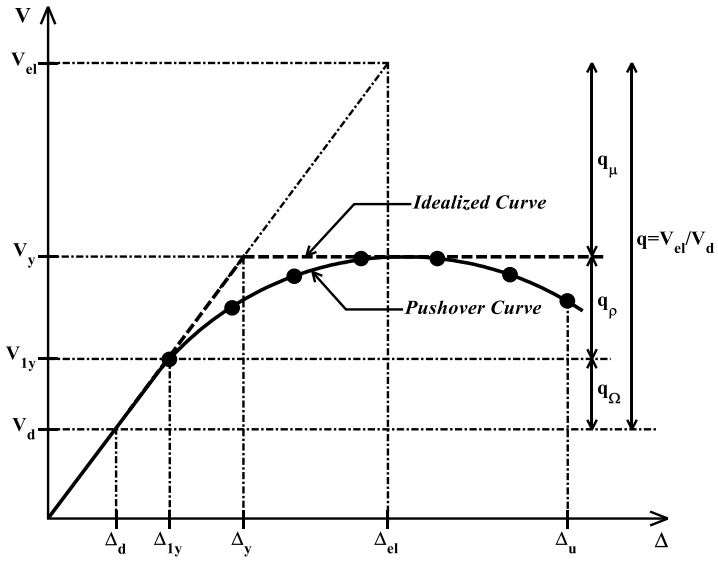

Figure 6.1: Typical lateral behaviour curve of steel MRFs.

EC8 prescribes upper limits for q in accordance to the structural system and ductility class. To what concerns steel MRFs, EC8 prescribes different limits to the medium (DCM) and high (DCH) ductility classes, in accordance with Table 6.1.

Table 6.1: Cross-sectional requirements for local ductility of steel elements

Structural ductility class	**Range of the reference values of q**	**Required cross-sectional class**
DCM (medium)	1.5 <q <2.0	Class 1, 2 or 3
	2.0 <q <4.0	Class 1 or 2
DCH (high)	q >4.0	Class 1

In order to provide an improvement to the force-based design procedure of EC8, Villani et al. (2009) proposed a methodology for the rational selection of the value of the behaviour factor,

instead of the use of code-prescribed upper-bound reference values. This Improved Force-Based Design (IFBD) methodology consists of a simple reordering of the design steps and is in full compliance with the design requirements of EC8. Whilst aiming to achieve structural design solutions that perform more consistently with the requirements prescribed in performance-based guidelines, IFBD allows for the adoption of a behaviour factor based on the actual properties of the structure and seismic hazard. In simple terms, the authors proposed that the selection of the behaviour factor value should be established by ensuring that the design base shear, V_d, is equal to the base shear that would lead to the formation of the first plastic hinge in the structure, V_{1y}. Thus, q is defined as:

$$q = \frac{V_{el}}{V_{1y}} \tag{6.1}$$

According to Chapter 2, the adoption of a behaviour factor based on the actual properties of each structure and the level of seismic action, can result in a considerable reduction of the cost, yet maintaining the structure within adequate safety levels.

A methodology has been proposed by the Applied Technology Council (ATC) (FEMA P695 (FEMA, 2009)) that allows for the assessment of the seismic performance factors that are used for structural design when linear methods of analysis are used. In brief terms, this methodology evaluates the safety margin against collapse of an earthquake load resisting system designed with a specific behaviour factor, and then compares it with acceptable safety criteria. The latter depends on an admissible probability of collapse and the uncertainty of such probability (Zareian et al., 2010). This methodology has been applied to a wide range of structural systems, ranging from masonry shear wall structures to buckling-restrained steel braced frames. Zareian et al. (2010) applied the FEMA P695 methodology to assess the seismic collapse performance of special MRFs designed in accordance with ASCE 7-10 (ASCE/SEI, 2005) and AISC 341-05 (ANSI, 2005). However, that research study considered a reduced number of structural configurations and adopted the seismic performance factors suggested by the American provisions which are different from those proposed in the European seismic code. Table 6.2 shows a comparison between the European (EC8) and American (ASCE 7-10 and AISC 341-05) seismic performance factors for steel MRFs (Ordinary moment resisting frames (OMF, low ductility), Intermediate moment frames (IMF, medium ductility) and special moment frames (SMF, high ductility).

The main objective of this chapter is to evaluate if the behaviour factors (or seismic performance factors) proposed by EC8 for steel MRFs are adequate and provide sufficient margin against collapse under maximum considered earthquake (MCE) ground motions. Furthermore, it is investigated if the behaviour factors considered with the IFBD methodology lead to adequate seismic performance within acceptable safety levels. To this end, the aforementioned methodology proposed in FEMA P695 is used.

Table 6.2: Comparison of European and American seismic performance factors.

Seismic Force-Resisting System	Ductility Class	EC8	ASCE-7-10	
		$q = q_d$	R	C_d
Steel Moment-Resisting Frame Systems	DCL	1.5	3.5	3
	DCM	4.0	4.5	4
	DCH	$5 \times (\alpha_1/\alpha_u)$	8	5.5

6.2 Definition and design of archetype frames

The application of FEMA P695 requires the definition of a set of structures (designated as archetypes), that are representative of the current building stock. Furthermore, the document specifies that the archetypes should reflect the expected range of geometrical and structural parameters of the investigated earthquake load resisting systems, since the evaluation of the performance of an entire class of buildings is to be performed. Therefore, six building configurations with different bay numbers and widths were defined. For all configurations, buildings with 2, 3, 4, 5 and 8 storeys, corresponding to low to medium rise buildings, were considered. Figure 6.2 shows the elevation and plan views of one of the building configurations, whilst also identifying the analysed frame. It should be mentioned that in all the defined configurations the resistance to seismic loads is provided by the MRFs in the longitudinal direction (x direction) and by a bracing system in the transversal direction (y direction). In this research study, only the longitudinal internal longitudinal frames were subject of investigation. Table 6.3 shows a detailed definition of each of the building configurations.

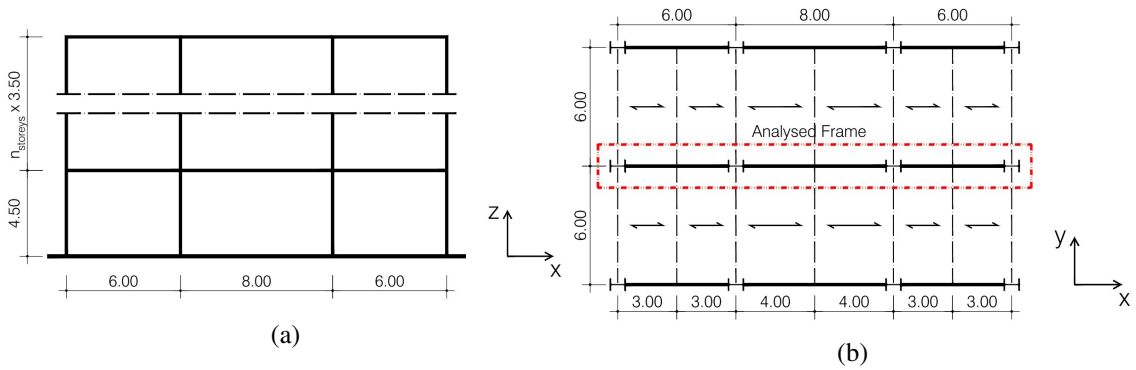

Figure 6.2: Building configuration 2: a) Elevation view, b) Plan view.

Three different geographic locations in Portugal, corresponding to different seismic intensities, were considered for the archetypes: Porto (low seismicity), Lisbon (moderate seismicity) and Lagos (moderate-to-high seismicity). Furthermore, for the Lagos location two soil types were considered (Type B and Type C). According to FEMA 695, after the definition of the archetype

Table 6.3: Building configurations and geometrical properties

Config.	x-z plane		y-z plane		h_1 [m]	h_{others} [m]
	N. of frames	Bays [m]	N. of frames	Bays [m]		
1	3	6+6+6	4	6+6	4.5	3.5
2	3	6+8+6	4	6+6		
3	3	8+8+8	4	8+8		
4	4	6+6+6+6	5	6+6+6		
5	3	8+6+8	4	6+6		
6	5	8+8+8+8+8	6	8+8+8+8		

buildings, they should be assembled into performance groups that exhibit the expected differences in the archetype design space. Parameters like basic configuration, seismicity level and behaviour factor used in the design stage, have been considered in the definition of the performance groups. Moreover, FEMA 695 defines that structures with short periods of vibration (in constant acceleration region of design spectrum) and long periods of vibration (in constant velocity region of design spectrum) should be analysed separately since the inelastic response tends to be different. However, because steel MRFs are typically characterised as flexible structures, it was not possible to define archetypes in the short period domain. A summary of the performance groups considered in this research study is shown in Table 6.4.

Regarding the structural design of the archetypes, the frames were firstly designed for gravity loads in accordance with the provisions of Eurocode 3 – Part 1-1 (EC3-1) (CEN, 2005a) for sectional resistance, stability checks and deflection limits. European steel HE profiles were adopted for the columns whereas steel IPE profiles were adopted for the beams. The seismic design was performed in accordance with the provisions of EC8, considering the two behaviour factors recommended by the standard, namely q=6.5 and q=4 corresponding to medium and high ductility classes, respectively, and the value obtained with the IFBD methodology. The serviceability inter-storey drift ratios (IDR) were limited to 1% and the inter-storey drift sensitivity coefficient (or stability coefficient), θ, as defined in EC8, was limited to 0.2. The capacity design of the non-dissipative members was conducted according to the EC8 criteria with the modifications proposed by Elghazouli (2009). The EC8 capacity design beam-column joint requirement, $\sum M_{Rc} \geq 1.3 \sum M_{Rb}$, was also taken into account in the design of all frames. A total of 360 structural archetypes have been designed, Member sizes have been dictated either by strength or stiffness (drift and P-Delta checks) criteria.

During the design process, the archetypes designed with the EC8 recommended behaviour factors for medium and high ductility class were usually controlled by P-Delta considerations, even though some two and three storey archetypes designed for medium ductility class were governed

Table 6.4: Performance group summary

Performance group			**Grouping criteria**			**No. of archetypes**
q**=6.5**	q**=4**	q**=IFBD**	**Basic configuration**	**Seismicity level**	**Soil type**	
PG-1	PG-25	PG-49	1	Low	B	5
PG-2	PG-26	PG-50		Moderate		5
PG-3	PG-27	PG-51		Moderate-High		5
PG-4	PG-28	PG-52		Moderate-High	C	5
PG-5	PG-29	PG-53	2	Low	B	5
PG-6	PG-30	PG-54		Moderate		5
PG-7	PG-31	PG-55		Moderate-High		5
PG-8	PG-32	PG-56		Moderate-High	C	5
PG-9	PG-33	PG-57	3	Low	B	5
PG-10	PG-34	PG-58		Moderate		5
PG-11	PG-35	PG-59		Moderate-High		5
PG-12	PG-36	PG-60		Moderate-High	C	5
PG-13	PG-37	PG-61	4	Low	B	5
PG-14	PG-38	PG-62		Moderate		5
PG-15	PG-39	PG-63		Moderate-High		5
PG-16	PG-40	PG-64		Moderate-High	C	5
PG-17	PG-41	PG-65	5	Low	B	5
PG-18	PG-42	PG-66		Moderate		5
PG-19	PG-43	PG-67		Moderate-High		5
PG-20	PG-44	PG-68		Moderate-High	C	5
PG-21	PG-45	PG-69	6	Low	B	5
PG-22	PG-46	PG-70		Moderate		5
PG-23	PG-47	PG-71		Moderate-High		5
PG-24	PG-48	PG-72		Moderate-High	C	5
					Total	3 x 120

by strength criteria. On the other hand, archetypes designed with the IFBD procedure were typically governed by strength criteria. Moreover, it is important to note that most of the archetypes controlled by the P-Delta criterion (designed with q=6.5 and q=4) resulted in the same structural solution independently of the seismic intensity level. As discussed in Chapter 2, the treatment of P-Delta effects currently implemented in EC8 can be interpreted as a lateral stiffness requirement. As shown in Equation 6.2, a minimum lateral stiffness condition is imposed by the code, which is proportional to the value of behaviour factor adopted. In the equation, P_{tot} is the total gravity load at and above the storey under consideration, d_r is the design inter-storey drift of the storey, V_{tot} is the total seismic storey shear and h is the height of the storey).

$$\theta = \frac{P_{tot} \times d_r}{V_{tot} \times h} \leq 0.2 \Leftrightarrow \frac{P_{tot} \times \frac{d_{el}}{q} \times q_d}{\frac{V_{tot,el}}{q} \times h} \leq 0.2 \Leftrightarrow \frac{P_{tot} \times d_{el}}{V_{tot,el} \times h} \times q \leq 0.2 \Leftrightarrow K_e \geq \frac{P_{tot} \times q}{0.2 \times h} \quad (6.2)$$

Although it may seem excessive to conclude about the adequacy of the behaviour factor when the seismic design of archetypes are controlled by stiffness criteria (since they are not directly related), it is important to note that, according to EC8, the P-Delta check makes use of the behaviour factor to obtain the inelastic displacement, which makes it a decisive factor in the obtained design solution (Chapter 2).

Finally, it should be emphasized, as highlighted by Zareian et al. (2010), that the structural solution is eminently dependent on the adopted design decisions, namely the relative size of column versus beam, constructive aspects, among others. Table 6.5 shows the design properties of some of the archetypes considered in this research study, where $S_e(T_1)$ is the design spectral acceleration at the fundamental period of the structure, $S_{MT}(T_1)$ is the maximum considered earthquake, MCE, spectral demand level at the fundamental period of vibration and R stands for residential gravity loads. The MCE intensity level represents a ground motion acceleration with 2% exceedance probability in 50 years (return period of 2475 years). A detailed discussion on the definition of the value of spectral acceleration corresponding to MCE intensity level is provided later in this Chapter.

6.3 Nonlinear structural analysis

6.3.1 Numerical modelling

The assessment of the structures is carried out through nonlinear static and response-history analysis conducted with the nonlinear finite element analysis program OpenSEES (McKenna, 2011). The material nonlinear behaviour is considered through a concentrated plasticity approach considering strength, stiffness, and deterioration effects (Lignos and Krawinkler, 2010; Araújo and Castro, 2016). Figure 6.3 illustrates the backbone curve and the stiffness and deterioration parameters for a European steel open cross-section HEB300 according to the aforementioned proposals. The effect of the axial load on the flexural capacity of the columns is taken into account in an approximate manner: 1) a preliminary pushover analysis is firstly conducted to evaluate the expected

Table 6.5: Archetype design properties

Archetype ID	No. Stories	Loads	Design parameters				
			Seismic design parameters				$S_{MT}(T_1)$
			q	T_1 [sec]	$S_e(T_1)$ [g]	M [ton]	
PG-1/PG-25/PG-49							
St1/St2/St3	2	R	6.5/4/1.5	0.65/0.8/0.8	0.11/0.09/0.09	82.78	0.19/0.15/0.15
St4/St5/St6	3		6.5/4/1.5	0.76/0.96/1.16	0.1/0.08/0.06	130.28	0.16/0.13/0.11
St7/St8/St9	4		6.5/4/1.5	0.83/1.05/1.42	0.09/0.07/0.05	176.89	0.15/0.12/0.09
St10/St11/St12	5		6.5/4/1.5	0.93/1.16/1.77	0.08/0.06/0.04	223.5	0.13/0.11/0.07
St13/St14/St15	8		6.5/4/1.5	1.11/1.42/2.55	0.07/0.05/0.02	363.33	0.11/0.09/0.04
PG-6/PG-30/PG54							
St106/St107/St108	2	R	6.5/4/1.57	0.68/0.77/0.77	0.44/0.38/0.38	297.49	0.74/0.66/0.66
St109/St110/St111	3		6.5/4/1.58	0.77/0.95/1.01	0.38/0.31/0.29	463.2	0.66/0.53/0.5
St112/St113/St114	4		6.5/4/2.11	0.83/1.07/1.3	0.36/0.28/0.23	628.91	0.61/0.47/0.39
St115/St116/St117	5		6.5/4/2.10	0.91/1.2/1.53	0.33/0.25/0.19	794.62	0.56/0.42/0.33
St118/St119/St120	8		6.5/4/1.89	1.12/1.43/2.03	0.26/0.21/0.14	1291.74	0.45/0.35/0.25
PG-11/PG-35/PG-59							
St211/St212/St213	2	R	6.5/4/1.68	0.57/0.57/0.57	0.75/0.75/0.75	102.26	1.28/1.28/1.28
St214/St215/St216	3		6.5/4/2.10	0.75/0.81/0.81	0.6/0.55/0.55	159.23	1.02/0.95/0.95
St217/St218/St219	4		6.5/4/2.40	0.83/1.04/1.06	0.54/0.43/0.42	216.19	0.93/0.74/0.72
St220/St221/St222	5		6.5/4/2.82	0.89/1.11/1.24	0.5/0.4/0.36	273.15	0.86/0.69/0.62
St223/St224/St225	8		6.5/4/2.90	1.11/1.43/1.73	0.4/0.31/0.26	444.04	0.69/0.54/0.44
PG-24/PG-48/PG-72							
St346/St347/St348	2	R	6.5/4/2.28	0.64/0.64/0.64	0.78/0.78/0.78	297.49	1.33/1.33/1.33
St349/St350/St351	3		6.5/4/2.73	0.81/0.86/0.86	0.61/0.58/0.58	463.2	1.05/0.99/0.99
St352/St353/St354	4		6.5/4/2.97	0.84/1.15/1.16	0.59/0.43/0.43	628.91	1.01/0.74/0.73
St355/St356/St357	5		6.5/4/3.88	0.93/1.21/1.37	0.53/0.41/0.36	794.62	0.91/0.7/0.62
St358/St359/St360	8		6.5/4/3.61	1.2/1.52/1.7	0.41/0.33/0.29	1291.74	0.71/0.56/0.5

average axial force under the combined actions of gravity and lateral loading ($P_{grav} + 0.5 \times P_E^{max}$, where P_{grav} and P_E^{max} are the axial load due to gravity loads and the maximum axial force due to lateral loading, respectively) (Zareian et al., 2010); 2) the backbone curve is modified by reducing the bending moment strength according to the interaction equations proposed in EC3-1-1, whilst no modification of the stiffness and deterioration parameters is performed.

The panel zones were represented with a beam-column joint element, “JOINT2D”, that is

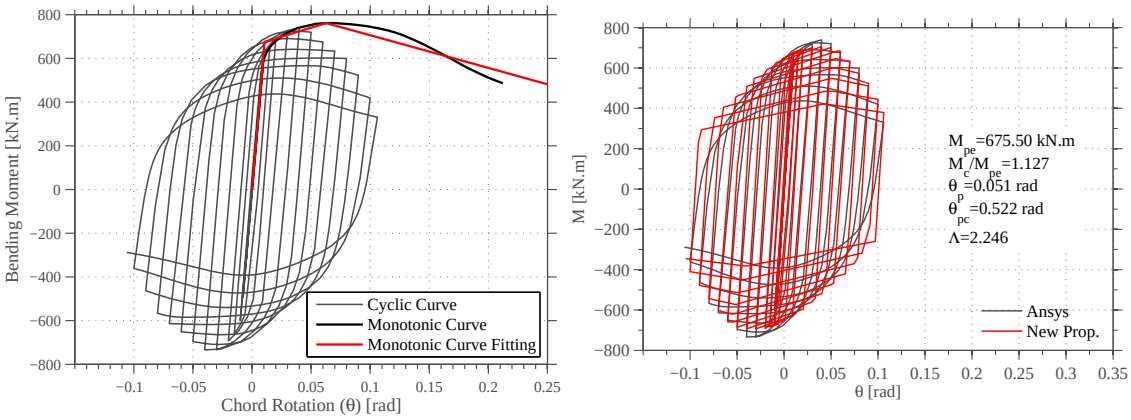

(a) (b)

Figure 6.3: Example of the calibration procedure of a HEB300 steel profile: a) Calculation of the strength and stiffness degradation parameters; b) Cyclic flexural behaviour of the member with the calibrated degradation parameters.

available in OpenSEES. For the panel zone, a tri-linear moment-distortion relation was adopted (Krawinkler, 1978). It is worth noting that the panel zones were designed with a "balanced" design methodology, and no strength degradation was considered. Figure 6.4 illustrates the adopted modelling strategy for the modelling of the panel zones.

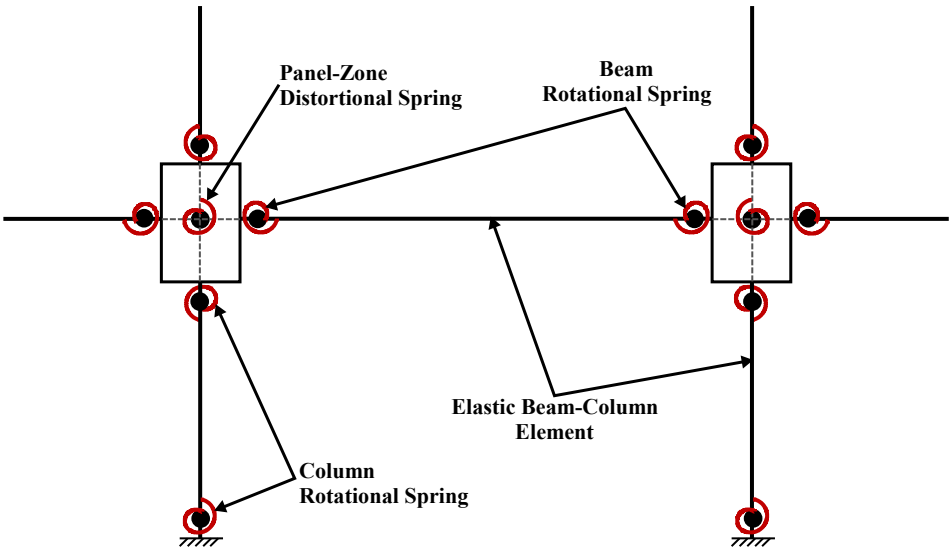

Figure 6.4: Modelling of the structural elements and panel zones.

6.3.2 Nonlinear static analysis

Nonlinear static analyses have been performed on each structure by assuming a first mode proportional lateral load pattern. A displacement-controlled analysis has been adopted, whilst the load

pattern followed the formulation provided in Equation 6.3, where F_i is the horizontal force acting on floor i, λ is the load factor; m_i is the mass at floor i, $\phi_{(1,i)}$ is the ordinate of the fundamental mode at floor i, and N is the number of storeys.

$$F_i = \lambda \frac{m_i \phi_{1,i}}{\sum_1^N m_i \phi_{1,i}} \tag{6.3}$$

Following the recommendations of FEMA P695, the nonlinear static analyses have been conducted until a reduction of at least 20% in strength after the peak lateral force was attained, V_{80}. This allows for the quantification of the peak base shear ,V_{max}, as well as the roof displacement at V_{80}, δ_u. Whilst the former allows for the calculation of the overstrength, Ω, the latter is used to compute the period-based ductility, μ_T. The overstrength factor is defined as the ratio of the maximum base shear, V_{max}, to the design base shear, V_d, according to Equation 6.4. The period-based ductility is defined as the ratio of ultimate roof drift displacement, δ_u, to the effective yield roof drift displacement $\delta_{y,eff}$, as shown in Equation 6.5.

$$\Omega = \frac{V_{max}}{V_d} \tag{6.4}$$

$$\mu_T = \frac{\delta_u}{\delta_{y,eff}} \tag{6.5}$$

An example of the nonlinear static pushover analysis results is shown in Figure 6.5, where the lateral behaviour along with the period-based ductility and overstrength factor are depicted.

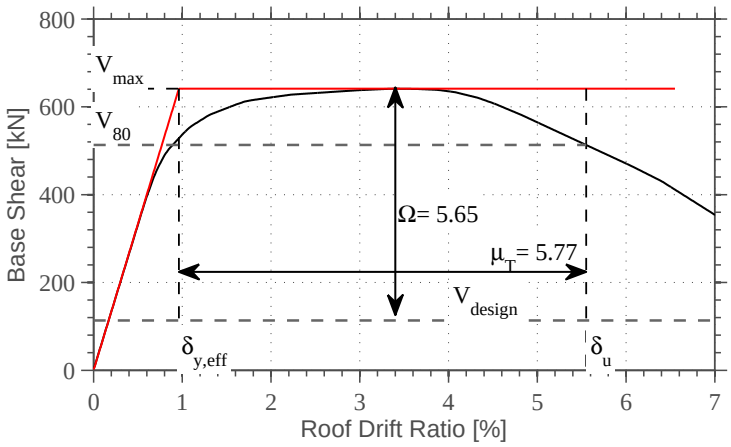

Figure 6.5: Results of nonlinear static analysis for Archetype St113.

Figure 6.6 depicts the nonlinear static analysis results for all the archetype structures. Regarding the period-based ductility (μ_T) it may be observed that all archetypes exhibit similar ductility, independently of the assumed ductility class considered at the design stage. However, it should be noted that several archetypes designed for a low seismicity level (Porto) and for a lower value of

q, which is usually the case when the IFBD procedure is adopted, exhibit lower ductility (values close to 3). It is worth noting that these archetypes have been designed with a value of q of 1.5. The value of q equal to 1.5 is defined in EC8 as the minimum value of behaviour factor that should be used in order to account for overstrengths.

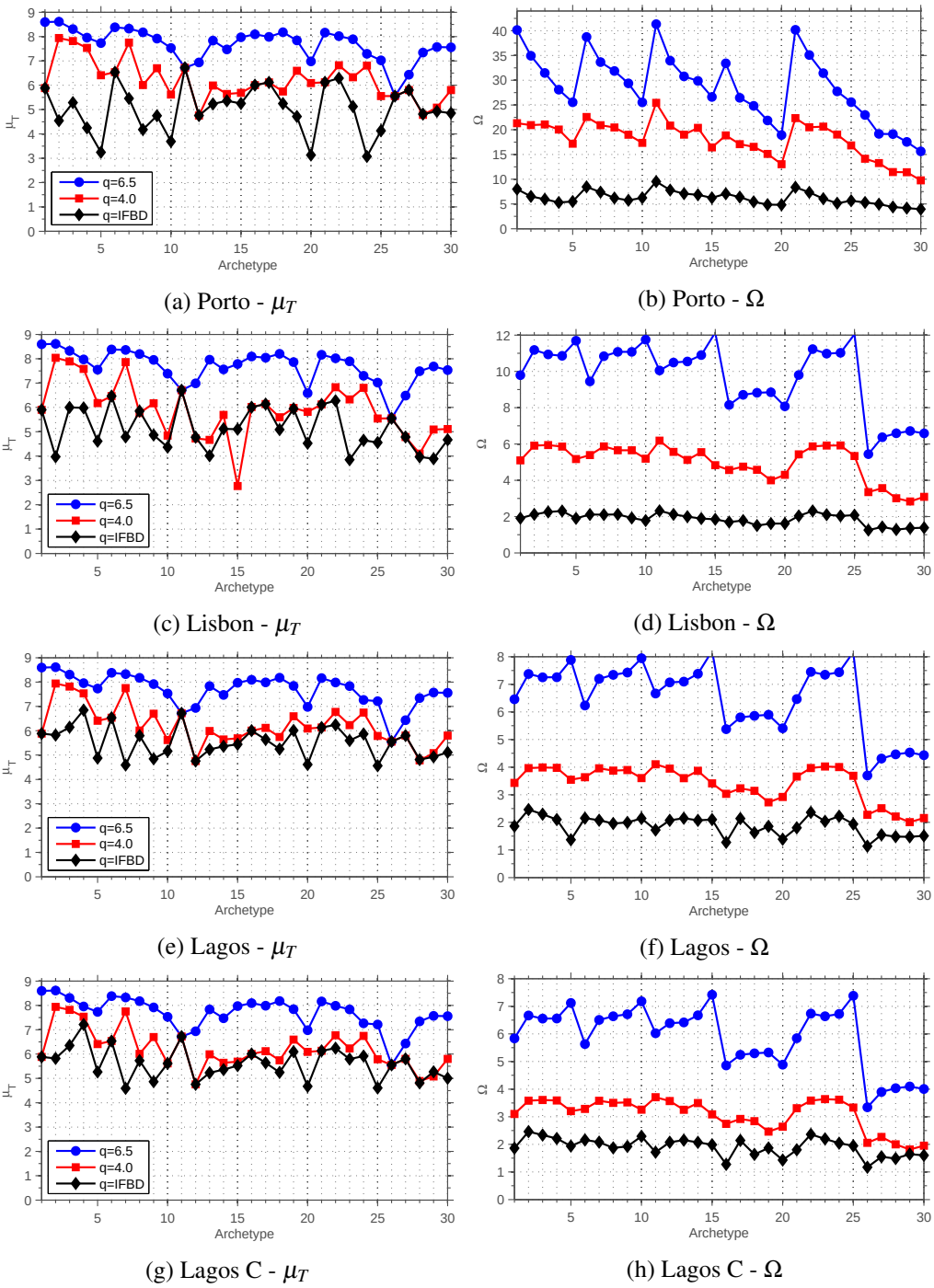

(a) Porto - μ_T (b) Porto - Ω

(c) Lisbon - μ_T (d) Lisbon - Ω

(e) Lagos - μ_T (f) Lagos - Ω

(g) Lagos C - μ_T (h) Lagos C - Ω

Figure 6.6: Period-based ductility (μ_T) and system overstrength (Ω)

In what concerns to system overstrength (Ω), there is a clear trend of higher system overstrength being associated with the higher ductility class designs. These results may seem unexpected. However, the underlying reason is the fact that the design of the archetypes was controlled, in some cases, by stiffness requirements related with the control of P-Delta effects. As previously mentioned, in the current EC8 formulation, the inter-storey drift sensitivity coefficient (θ) is directly proportional to the behaviour factor. Therefore, the higher is the behaviour factor the higher is the lateral stiffness required for the structure to comply with a given limit θ. On the other hand, the archetypes designed with behaviour factors selected according to the IFBD procedure exhibit a more stable behaviour with system overstrength close to 2. Finally, the high system overstrength observed in the archetypes designed for Porto are directly related with the fact that gravity loads controlled the structural design.

6.3.3 Nonlinear response-history analysis

Following the procedure proposed in FEMA P695, the median collapse capacity of the archetypes was assessed through incremental dynamical analysis (IDA) (Vamvatsikos and Cornell, 2002). The 5% damped first mode spectral acceleration was considered as the seismic intensity measure (IM) and the maximum inter-storey drift as the engineering demand parameter (EDP). The set of 22 far-field ground motion records provided in FEMA P695 was used and scaled to increasing intensities until median collapse was achieved. It should be noted that this record scaling process involved two steps: 1) each record was normalized with respect to its peak ground velocity, PGV, in order to remove unwarranted variability between records due to differences in event magnitude, distance to source, source type and site conditions FEMA (2009); 2) the normalised records were sequentially scaled such that the geometric mean of the 5% damped spectral acceleration at the fundamental period of the ground motion record suite matched the considered intensity. Whilst the first step is embedded in the ground motion suite definition, the second is performed during the IDA procedure.

Figure 6.7 shows the median spectrum of the FEMA P695 Far-Field ground motion record suite anchored to the EC8 elastic response spectra at a period of 1 second for the locations under study. It is important to note that, although the ground motion record suite has been selected in consistency with ASCE/SEI 7-05 (ASCE/SEI, 2005), the acceleration response spectra showed a good compliance with the EC8 spectral shape for the Portuguese territory.

Figure 6.8 shows full IDA curves and corresponding fractile IDA curves for two archetypes. Each line in the figures represents one ground motion record and the points along the line the increasing intensity level. The definition of collapse is essential for the application of FEMA P695 procedure. Therefore, in this research, collapse was characterised by the flattening of the IDA curves, which was considered to occur when the slope of the IDA curve drops to 10% of the initial value. The results from the IDA were then used to compute the median collapse intensity, $\hat{S}_{CT}$, for each archetype, which is defined as the intensity for which half of the ground motion records lead to the collapse of the archetype. The collapse margin ratio, CMR, was also evaluated, being the ratio between $\hat{S}_{CT}$ and the maximum considered earthquake, MCE, spectral demand level, S_{MT}

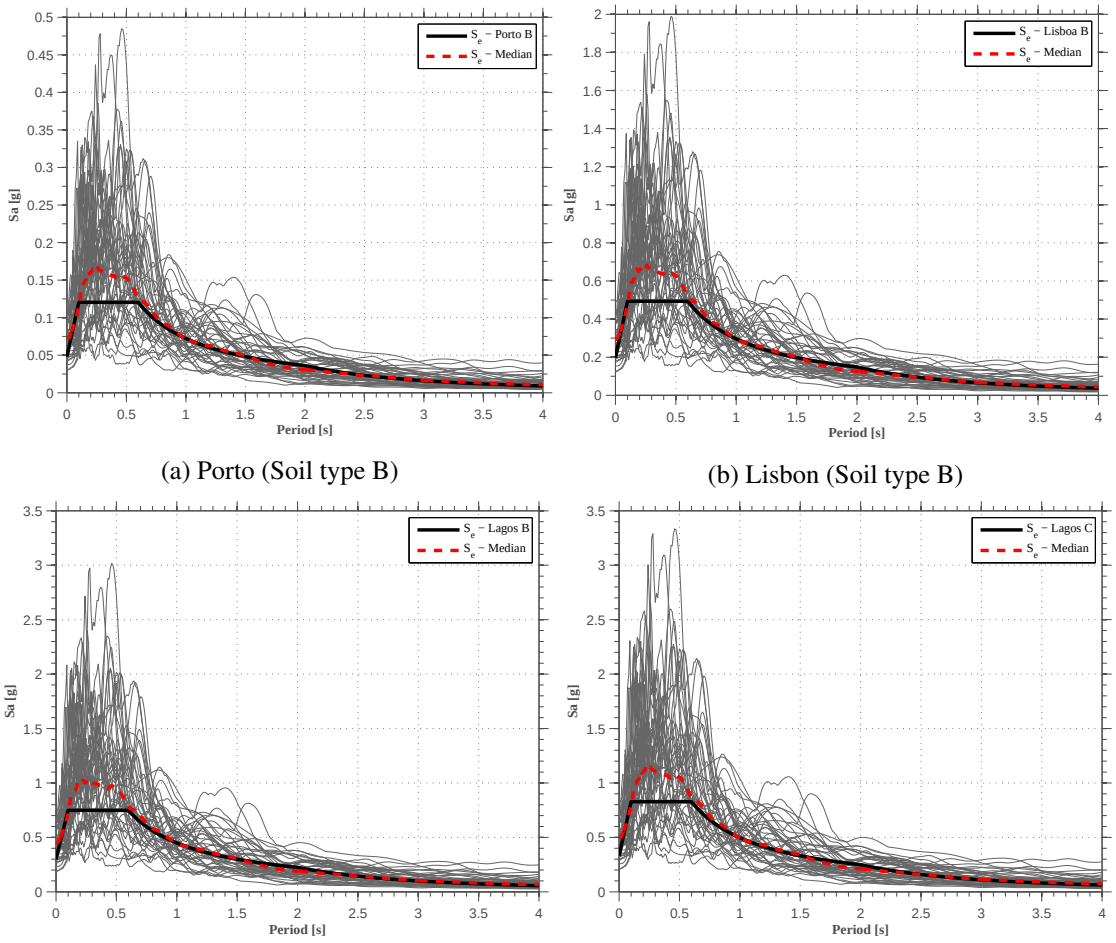

(a) Porto (Soil type B)

(b) Lisbon (Soil type B)

(c) Lagos (Soil type B)

(d) Lagos (Soil type C)

Figure 6.7: Median spectra of the far-field record set anchored to the elastic response spectra at the 1 sec period.

(Equation 6.6).

$$CMR = \frac{\hat{S}_{CT}}{S_{MT}} \tag{6.6}$$

The MCE intensity level represents a ground motion acceleration with 2% exceedance probability in 50 years (return period of 2475 years). Conversely to ASCE 7-10 (ASCE/SEI, 2010), that defines MCE intensity level as the reference seismic action, EC8 defines the reference seismic action for ordinary buildings as a peak ground acceleration with 10% exceedance probability in 50 years (return period of 475 years). Consequently, the application of the FEMA P695 procedure in this research study involved the transformation of the seismic intensity considered in the design of the archetypes to the intensity associated to a return period of 2475 years. Therefore, and in line with EC8 recommendations, an importance factor of 1.71 $\left(\gamma_I = (0.02/0.10)^{-1/3} = 1.71\right)$ was used to obtain the spectral demand for a 2475 years return period.

As shown in the figures, the obtained IDA curves exhibited the typical behaviour of steel

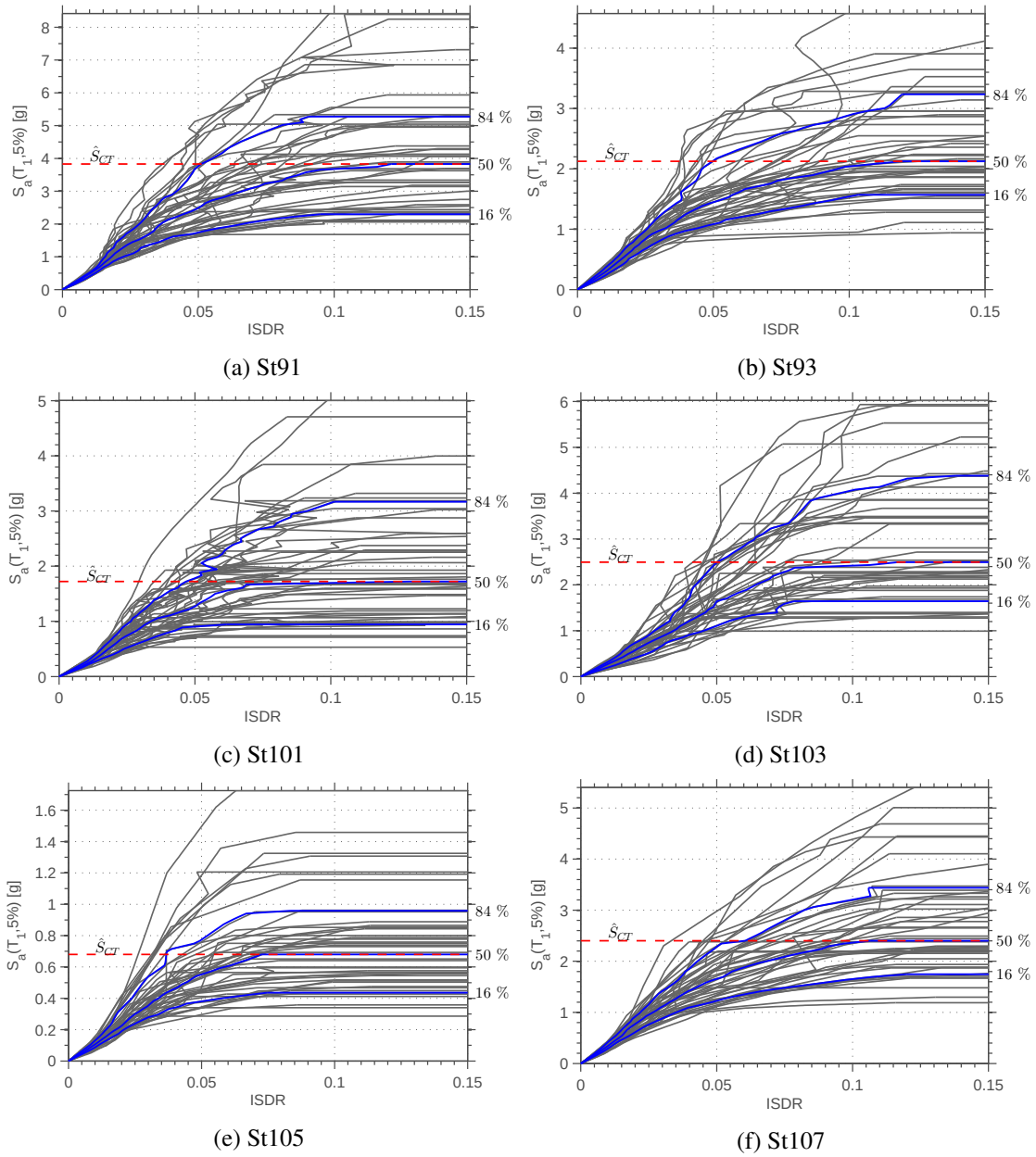

(a) St91 (b) St93

(c) St101 (d) St103

(e) St105 (f) St107

Figure 6.8: Results of Incremental Dynamical Analysis.

moment-resisting frames, with an initial slope followed by an increasing reduction for higher intensities up to the flattening of the curves. At this point, collapse was considered to occur for a specific ground motion. As expected, even for low intensities, some dispersion can be observed between the IDA curves. This is due to the scaling process adopted in the IDA procedure, in which the geometric mean of the 5% damped spectral acceleration at the fundamental period of the ground motion record suite matches the considered intensity. A summary of the key analysis results of response-history analysis is shown in Table 6.7 and 6.8.

6.4 Behaviour factor, q

The evaluation of the performance of each archetype is carried out by comparing the adjusted collapse margin ration, $ACMR$, with reference acceptable values that are dependent on total system collapse uncertainty, β_{TOT}. For a given performance group, the behaviour factor adopted in the design of the archetype buildings is considered to be acceptable if the probability of collapse for the MCE ground motions is 20% or less for each archetype, and 10% or less on average for each performance group (FEMA, 2009; Denavit et al., 2016). The two basic collapse prevention objectives can thus be represented by Equation 6.7 and 6.8:

$$ACMR_i \geq ACMR_{20\%} \tag{6.7}$$

$$\overline{ACMR_i} \geq ACMR_{10\%} \tag{6.8}$$

where $AMCR_i$ is the adjusted collapse margin ratio of archetype i, $\overline{ACMR_i}$ is the average value of adjusted collapse margin ratio for each performance group, $ACMR_{20\%}$ is the acceptable value of the adjusted collapse margin ratio for a 20% collapse probability and $ACMR_{10\%}$ is the acceptable value of the adjusted collapse margin ratio for a probability of collapse of 10%. The reason for the consideration of an higher limit for the probability of collapse of the individual archetypes is associated with the perception of the existence of potential "outliers" within a performance group (Sato and Uang, 2013).

The adjusted collapse margin ratio is the product of the collapse margin ratio by a spectral shape factor, as shown in Equation 6.9.

$$ACMR_i \geq SSF_i \times CMR_i \tag{6.9}$$

Recognising that the evaluation of the collapse capacity of a structure can be highly affected by the spectral shape of the ground motion record suite (Baker and Cornell, 2006a,b), FEMA P695 proposes an adjustment of the CMR using a spectral shape factor, SSF, which depends on the fundamental period and on the period-based ductility. A more rigorous approach to account for spectral shape would be to select a suite of ground motions records that adequately takes into account the spectral shape for each site, hazard level, and structural period of interest (FEMA, 2009). Baker and Cornell (2006a,b) proposed the so-called Conditional Mean Spectrum (CMS) as an alternative target spectrum that accounts for the spectral shape. However, the computation of a CMS for such a large number of structures located in different geographical regions is impractical due to computational requirements. Equally important is the fact that the SSF was deducted based on data provided by the United States Geological Survey (USGS) for US locations, which may call into question its application to other geographical locations. The application of the SSF as it is defined always results in an increase of the collapse margin ratio. The extension of the current research study to define the SSF for Portugal is therefore advisable.

As previously mentioned, the definition of the acceptable values for the adjusted collapse margin ratio requires the characterisation of the total system collapse uncertainty which depends on the following sources of uncertainty: 1) record-to-record variability (β_{RTR}); 2) quality of the design requirements (β_{DR}); 3) availability and quality of test data (β_{TD}); 4) quality/accuracy of the nonlinear modelling (β_{MDL}). Moreover, for archetypes with period-based ductility greater than 3 ($\mu_T \geq 3$) FEMA P695 (FEMA, 2009) defines a fixed value of the uncertainty due to record-to-record variability equal to $\beta_{RTR} = 0.4$. Otherwise, for archetypes with period-based ductility lower than 3, the record-to-record uncertainty can be calculated as follows:

$$\beta_{RTR} = 0.1 + 0.1\mu_T \leq 0.4 \tag{6.10}$$

where β_{RTR} must be greater than or equal to 0.20.

In this study, the uncertainty associated with the quality of design requirements was rated as "Good" since despite the EC8 design provisions have been subject of study for several years, the practice in steel construction in Portugal is still less developed than that of reinforced concrete structures. Test data was rated as "Good" considering the large amount of tests conducted on steel members under cyclic bending that are available in the literature in contrast with the reduced number of test data on the inelastic behaviour of columns subjected to high axial load and cyclic bending moments (Zareian et al., 2010). Finally, the quality of the model was rated as "Good". Whilst the developed numerical nonlinear models can accurately simulate most of the collapse modes, there is still room for improvement in the modelling of plastic hinging in columns (Zareian et al., 2010) namely in what concerns the axial force bending moment interaction. Table 6.6 shows the assigned quality ratings and corresponding lognormal standard deviation of each source of uncertainty. Since all sources of uncertainty are assumed to be independent and to follow a

Table 6.6: Characterization of uncertainty

System	Quality of design requirements	Quality of test data	Quality of nonlinear modelling
Steel - MRF	B (Good)	B (Good)	B (Good)
	$\beta_{DR} = 0.2$	$\beta_{TD} = 0.2$	$\beta_{MDL} = 0.2$

lognormal distribution with a median equal to 1 and lognormal standard deviation parameters ($\beta_{RTR}, \beta_{DR}, \beta_{TD}, \beta_{MDL}$), the lognormal standard deviation describing the total collapse uncertainty (β_{TOT}), is given by Equation 6.11:

$$\beta_{TOT} = \sqrt{\beta_{RTR}^2 + \beta_{DR}^2 + \beta_{TD}^2 + \beta_{MDL}^2} \tag{6.11}$$

The total system collapse uncertainty, β_{TOT}, considering the quality ratings defined above is equal to 0.53. According to Table 7-3 of FEMA P695, the values of $ACMR_{10\%}$ and $ACMR_{20\%}$ are 1.96 and 1.56, respectively.

Table 6.7 and 6.8 show the calculated *ACMR* values for each archetype building (due to space limitations, only results for some performance groups are presented) and the corresponding performance evaluation.

Table 6.7: Collapse performance evaluation of a set of archetype buildings

Design Conf.		Pushover and IDA Results								Acceptance Check	
ID	No. of Stories	T_1 [sec]	*Static* Ω	S_{MT} [g]	$\hat{S}_{CT}$ [g]	*CMR*	μ_T	*SSF*	*ACMR*	Accept. *ACMR*	Pass/Fail
Performance Group No. PG-1 (Conf. 1 ; Porto ; q=6.5)											
St1	2	0.65	40.15	0.19	3.23	17	8.71	1.16	19.72	1.56	P
St4	3	0.76	38.97	0.16	3.24	19.93	8.7	1.2	23.92	1.56	P
St7	4	0.83	38.33	0.15	3.06	20.55	8.38	1.2	24.66	1.56	P
St10	5	0.93	38.34	0.13	2.72	20.49	8.01	1.22	25	1.56	P
St13	8	1.11	41.64	0.11	2.67	23.99	7.78	1.27	30.47	1.56	P
		Mean of Performance Group:							24.75	1.96	P
Performance Group No. PG-30 (Conf. 2 ; Lisbon ; q=4.0)											
St107	2	0.77	5.39	0.66	2.54	3.84	6.57	1.17	4.51	1.56	P
St110	3	0.95	4.99	0.53	1.99	3.72	7.96	1.22	4.54	1.56	P
St113	4	1.07	4.81	0.47	1.6	3.39	5.83	1.23	4.17	1.56	P
St116	5	1.2	4.81	0.42	1.54	3.64	6.22	1.25	4.55	1.56	P
St119	8	1.43	5.19	0.35	1.33	3.76	4.88	1.23	4.63	1.56	P
		Mean of Performance Group:							4.48	1.96	P
Performance Group No. PG-59 (Conf. 3 ; Lagos ; q=IFBD)											
St213	2	0.57	1.72	1.28	3.58	2.8	6.89	1.13	3.16	1.56	P
St216	3	0.81	1.76	0.95	2.06	2.17	4.83	1.14	2.47	1.56	P
St219	4	1.06	1.83	0.72	1.22	1.69	5.3	1.23	2.08	1.56	P
St222	5	1.24	2.07	0.62	1.22	1.97	5.43	1.25	2.47	1.56	P
St225	8	1.73	2.1	0.44	0.85	1.92	5.51	1.35	2.53	1.56	P
		Mean of Performance Group:							2.54	1.96	P

Based on the results presented in Table 6.7 and 6.8, it can be concluded that all archetype buildings pass the performance evaluation by a significant margin. Therefore, it is clear the exceptional

Table 6.8: Collapse performance evaluation of some of the archetype buildings

Design Conf.				Pushover and IDA Results						Acceptance Check	
ID	No. of Stories	T_1 [sec]	*Static* Ω	S_{MT} [g]	$\hat{S}_{CT}$ [g]	*CMR*	μ_T	*SSF*	*ACMR*	Accept. *ACMR*	Pass/Fail
Performance Group No. PG-16 (Conf. 4 ; Lagos C ; q=6.5)											
St316	2	0.66	4.86	1.29	3.22	2.5	7.71	1.18	2.95	1.56	P
St319	3	0.79	4.46	1.08	2.98	2.77	7.63	1.2	3.33	1.56	P
St322	4	0.85	4.5	1	2.94	2.94	7.88	1.22	3.58	1.56	P
St325	5	0.97	4.53	0.88	2.5	2.86	7.6	1.25	3.57	1.56	P
St328	8	1.21	4.89	0.7	1.97	2.81	6.81	1.25	3.51	1.56	P
Mean of Performance Group:									3.39	1.96	P
Performance Group No. PG-42 (Conf. 5 ; Lisbon ; q=4.0)											
St152	2	0.75	5.43	0.68	2.59	3.83	6.25	1.15	4.41	1.56	P
St155	3	0.98	4.99	0.52	1.78	3.44	6.91	1.21	4.16	1.56	P
St158	4	1.06	5.03	0.48	1.78	3.73	6.41	1.23	4.59	1.56	P
St161	5	1.18	5.03	0.43	1.78	4.14	6.88	1.25	5.18	1.56	P
St164	8	1.44	5.34	0.35	1.44	4.09	5.59	1.3	5.32	1.56	P
Mean of Performance Group:									4.73	1.96	P
Performance Group No. PG-72 (Conf. 6 ; Lagos C; q=IFBD)											
St348	2	0.64	1.17	1.33	2.98	2.25	5.26	1.13	2.54	1.56	P
St351	3	0.86	1.32	0.99	2.07	2.1	5.44	1.19	2.5	1.56	P
St354	4	1.16	1.26	0.73	1.12	1.56	4.47	1.2	1.87	1.56	P
St357	5	1.37	1.65	0.62	1.18	1.9	4.83	1.23	2.33	1.56	P
St360	8	1.7	1.6	0.5	0.73	1.47	4.64	1.25	1.83	1.56	P
Mean of Performance Group:									2.21	1.96	P

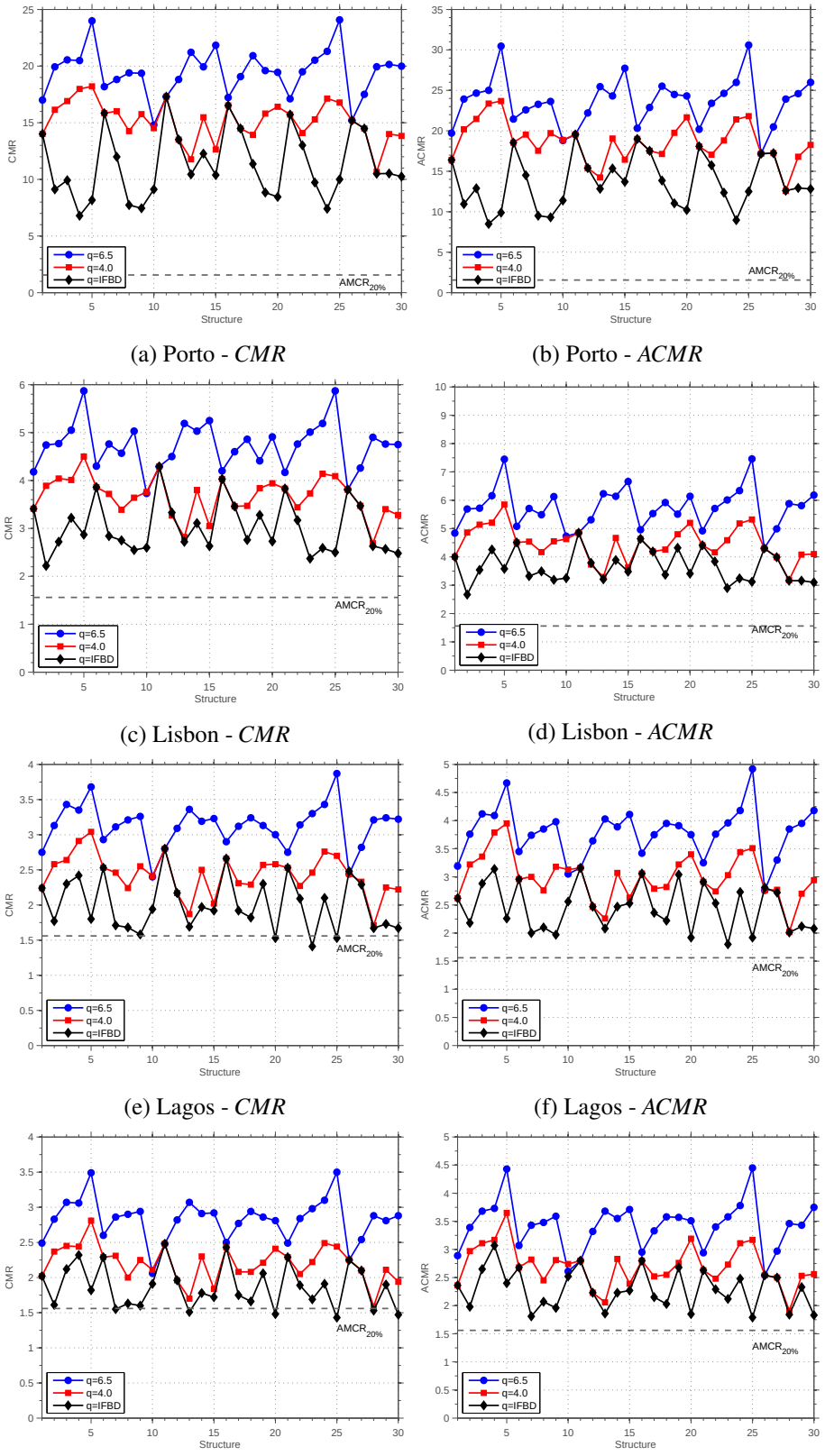

(a) Porto - *CMR* (b) Porto - *ACMR*

(c) Lisbon - *CMR* (d) Lisbon - *ACMR*

(e) Lagos - *CMR* (f) Lagos - *ACMR*

(g) Lagos C - *CMR* (h) Lagos C - *ACMR*

Figure 6.9: CMR and ACMR.

seismic performance of steel MRF's designed according to EC8. Recently, a similar research study conducted on a limited number of archetype buildings designed according to American standards, also concluded about the excellent performance of steel MRF's (Zareian et al., 2010). Individually speaking, all the archetypes comply with the FEMA P695 (FEMA, 2009) acceptability check as illustrated in Figure 6.9. An important trend that can be identified in the results is the significant reduction of the *ACMR* values with the increase of the seismic intensity level for the archetypes designed with the behaviour factors recommended in EC8. This effect is less noticeable in the archetypes designed with the behaviour factor selected according to the IFBD procedure. The primary reason for this observation is related with the governing design criteria. Archetypes designed with the behaviour factors recommended in the European code are primarily controlled by lateral stiffness requirements related with the treatment of P-Delta effects. As previously discussed, in the current EC8 prescriptions the inter-storey drift sensitivity coefficient is directly proportional to the behaviour factor. Therefore, the adoption of high values of the behaviour factor is reflected in high lateral stiffness requirements. Moreover, the required lateral stiffness is independent of the design seismic intensity level, as it can be concluded from the interpretation of Equation 6.2. The reduction in the *ACMR* values is generally caused by the increase in the maximum considered earthquake spectral demand level (S_{MT}) and not by the reduction of the median collapse intensity ($\hat{S}_{CT}$), since several archetypes structural solutions are the same, independently of the design location considered. Regarding the archetypes designed using the behaviour factors defined according to IFBD procedure it could be noted that all the archetypes pass the acceptance criteria on collapse probability and exhibit a more predictable behaviour. Therefore it could be concluded that buildings designed using IFBD behaviour factors comply with the code no-collapse requirement. To summarise, it is important to note the excellent performance of all the buildings considered in this study with special focus to the buildings designed using behaviour factors defined according to IFBD procedure that are associated with significant material savings, whilst exhibiting acceptable collapse probability.

6.5 Influence of using pre-defined spectral shape factors

As previously mentioned, a more rigorous approach to account for the spectral shape should involve the selection of a suite of ground motions records that adequately considers the spectral shape for each site, hazard level, and structural period of interest. To assess the influence of adotping the *SSF* proposed in FEMA P695 in the performance evaluation of buildings designed according to EC8, a simple sensitivity study is now conducted. By resorting to SelEQ, an advanced ground motion record selection and scaling framework (Macedo and Castro, 2017), the CMS was computed for two locations and three fundamental periods of vibration. Figure 6.10 shows the suites of 40 records selected and scaled for Porto and Lagos.

The performance evaluation was conducted for six structures (namely: St6, St23, St85, St203, St216 and St251) designed with the above mentioned criteria. The selection of these structures was based on the number of storeys and structural configurations, ensuring that they have been

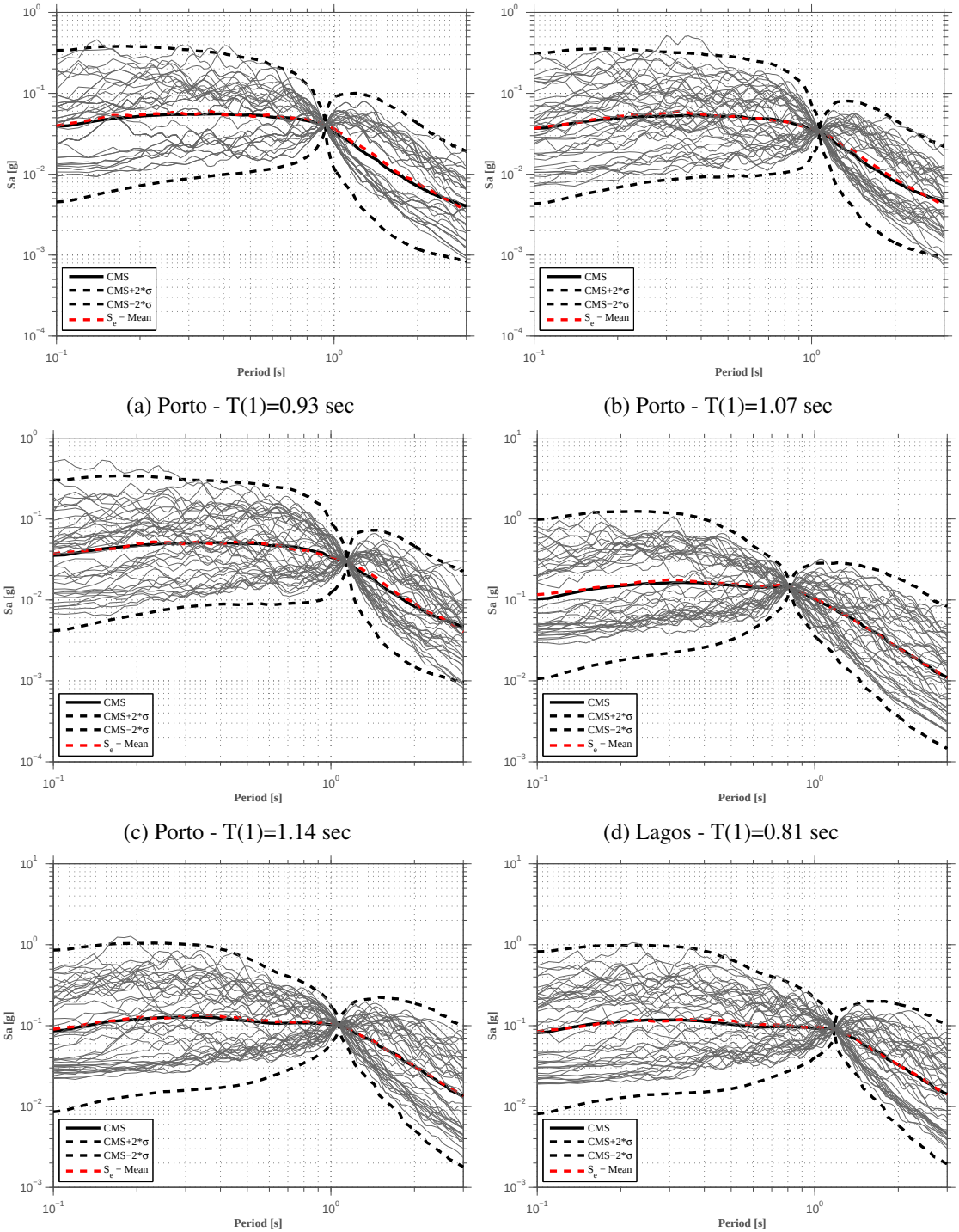

(a) Porto - T(1)=0.93 sec

(b) Porto - T(1)=1.07 sec

(c) Porto - T(1)=1.14 sec

(d) Lagos - T(1)=0.81 sec

(e) Lagos - T(1)=1.07 sec

(f) Lagos - T(1)=1.18 sec

Figure 6.10: CMS and ground motion record selection for Porto and Lagos.

designed with different ductility criteria. The performance results obtained are shown in Table 6.9.

A detailed analysis of Table 6.9 allows concluding that the median collapse intensity obtained

Table 6.9: Median collapse intensity

ID	No. of Stories	Location	T_1	$\hat{S}_{CT}(T_1)-FEMA$	SSF	$A\hat{S}_{CT}(T_1)$	$\hat{S}_{CT}(T_1)-CMS$
			[sec]	[g]		[g]	[g]
St6	3	Porto	1.16	0.97	1.20	1.16	1.08
St23	4		1.07	1.65	1.23	2.03	1.73
St85	5		0.93	2.18	1.22	2.65	2.30
St203	4	Lagos	1.07	1.61	1.23	1.98	1.87
St216	3		0.81	2.06	1.14	2.35	2.13
St251	5		1.19	1.78	1.25	2.23	1.87

with the new suite of ground motion records is usually higher than the one obtained with the FEMA P695 set. Comparing the adjusted median collapse intensity, which takes into account the SSF, the values of the two sets are similar. This justifies the use of the SSF proposed in FEMA P695 in this research study. However, the number of examined archetypes was limited and possible generalisations require further investigation.

6.6 Conclusions

In this Chapter, a research study was conducted to evaluate the collapse performance of steel moment-resisting frames designed according to Eurocode 8. For this purpose, the methodology proposed in FEMA P695 was applied. A set of 360 archetype buildings with 2, 3, 4, 5 and 8 storeys that are representative of the current building stock were designed according to EC8 using different behaviour factors. For high and medium structural ductility class the upper-limit behaviour factors proposed by EC8 were used (q=6.5 and q=4.0, respectively). Furthermore, behaviour factors defined according to the IFBD methodology were also adopted in the design. The application of the IFBD procedure allows the designer to achieve significant material savings, whilst the structural solutions obtained are in full compliance with the requirements of the European seismic design code. Nonlinear static and response-history analyses were performed to evaluate the performance of the frames, which allowed for the evaluation of the seismic performance factors.

All archetype buildings, independently of the ductility class, passed the performance evaluation as defined in FEMA P695 by a considerable margin, enhancing the exceptional seismic performance in terms of collapse of steel MRF's. The archetypes designed using the EC8 recommended behaviour factors exhibited remarkably high values of adjusted collapse margin ratios ($ACMR$), mainly because the seismic design was largely governed by lateral stiffness requirements related with the treatment of P-Delta effects.

Moreover, all the archetypes designed with behaviour factors selected according to the IFBD methodology pass the acceptance criteria on collapse probability and exhibited more stable and predictable behaviour, demonstrating the advantage of adopting behaviour factors based on the actual properties of the structure and seismicity level. Furthermore, it could important to note that despite the significant material savings the archetypes exhibit appropriate collapse probability complying with the EC8 no-collapse requirement.

Finally, a sensitivity study conducted to assess the influence of using spectral shape factors (SSF) revealed that, for the analysed structures, it is appropriate to use the SSF values proposed in FEMA P695. However, the number of examined archetypes was limited and possible generalisations for this and other building typologies in the European territory requires additional research.

Chapter 7

Earthquake loss assessment of steel moment-resisting frames designed according to Eurocode 8

7.1 Introduction

Current seismic design guidelines allow for the inelastic behaviour of the structure to be explored during the design earthquake intensity level and, therefore, some degree of damage is therefore expected to occur under the design earthquake intensity level. Although this is acceptable from an engineering point of view, given the ductile nature of structures designed according to modern provisions, stakeholders and building owners generally perceive that seismic design ensures both the safety and the development of minor damage levels for any seismic intensity level. It is therefore crucial to provide information to support the decision making process of these agents in order to help stakeholders and building owners to take an informed selection of design opinions.

Seismic design according to current practices and standards aims, primarily, at the protection of life-safety, with a heavy focus on strength control, incorporating comparatively minor provisions for deformation and damage control (Ramirez and Miranda, 2012; Castro et al., 2008). However, even though code design procedures seek to ensure that buildings meet certain levels of seismic performance, the actual performance is not normally assessed throughout the design process (FEMA, 2006). This concept (performance-based design) was firstly introduced in Vision 2000 (Vision, 1995) after the 1994 Northridge and 1995 Kobe earthquakes. In these earthquakes, even though most structures exhibited acceptable non-collapse performances, there were high financial losses due to downtime, damage on non-structural components and losses/damage in building contents. These findings triggered the need for a more effective control of the buildings' performance at different seismic intensity levels, leading to the concept of performance-based earthquake engineering. The first generation of performance-based design procedures defined a set of discrete performance levels (e.g.: collapse prevention, life safety, immediate occupancy, and fully operational), associated with different seismic intensity levels, which were directly linked

to deformation and damage in the structural components. This design philosophy was later implemented in the most recent existing seismic assessment standards/guidelines (e.g. ASCE 41-13 (ASCE/SEI, 2013); Part 3 of Eurocode 8 (EC8-3) (CEN, 2005e)). In the case of the European code, EC8-3 defines three performance levels for which existing buildings must be assessed, as well as the associated seismic hazard levels (defined either in terms of the probability of exceedance in 50 years or in terms of return period), as shown in Table 7.1.

Table 7.1: EC8-3 building performance levels.

Hazard level	**Performance level**
2% in 50 years ($T_R = 2475$ years)	Near collapse (NC): building heavily damaged, very low residual strength and stiffness, large permanent drifts but still standing.
10% in 50 years ($T_R = 475$ years)	Significant damage (SD): building significantly damaged, some residual strength and stiffness, non-structural components damaged, uneconomic to repair.
20% in 50 years ($T_R = 225$ years)	Limited damage (LD): building only lightly damaged, damage to non-structural components economically repairable.

Moreover, for steel moment-resisting frames (MRFs), EC8-3 defines acceptance criteria for the buildings' performance at different earthquake intensity levels by specifying that local deformation demands should be lower than pre-defined local deformation capacities (Araújo and Castro, 2016). According to the performance criteria specified by the European code for seismic assessment, the damage on non-structural components is controlled in an indirect manner through the verification of local deformation demands imposed on structural components. Despite being proposed for existing buildings, these provisions are also used in performance-assessment of new buildings. Notwithstanding the significant progress associated to the first generation of performance-based design procedures, it is undeniable that they provide a relatively vague measure of the buildings' performance, which, in most cases, is neither meaningful nor useful for stakeholders and decision-makers. Consequently, several research studies (Ramirez and Miranda, 2012; Hwang et al., 2015; Hwang and Lignos, 2017; Tzimas et al., 2016; Karavasilis et al., 2015) proposed more explicit and improved seismic-performance metrics (e.g. casualties, economic losses associated with repair/replacement, downtime) which can help stakeholders and building owners in their decision making process (Krawinkler et al., 2006; Ramirez and Miranda, 2009). The Pacific Earthquake Engineering Research (PEER) Center proposed the so-called Performance-Based Earthquake Engineering (PBEE) that is a fully probabilistic framework that can be used to evaluate damage and economic losses resulting from an earthquake (Cornell and Krawinkler, 2000; Porter, 2003; Ramirez and Miranda, 2012). Moreover, the next generation of PBEE procedures (FEMA, 2012a,b) have been recently proposed, providing a series of guidelines and companion tools that aim to promote its use among the community (Ramirez and Miranda, 2009; Hwang et al., 2015; Hwang and Lignos, 2017).

The main objective of this Chapter is to evaluate the expected direct economic losses, resulting from an earthquake, of steel moment-resisting frame structures designed according to Eurocode 8.

A set of 360 buildings, that are representative of the current steel building stock in Europe, were designed according to Part 1 of Eurocode 8 (EC8) adopting three different values for the behaviour factor, q. Code-prescribed upper bound limits of q for medium and high ductility classes (DCM and DCH, respectively), and the behaviour factor obtained from the Improved Force-Based Design (IFBD) (Villani et al., 2009; Peres et al., 2016) procedure were used. To this end, the PEER-PBEE methodology, with the improvements proposed by Ramirez and Miranda (2012), was implemented and used. The expected economic losses and their disaggregation are evaluated for the seismic intensity levels specified in Part 3 of Eurocode 8 (EC8-3). Additionally, the expected annual losses (EAL) are presented and discussed.

7.2 Seismic loss assessment of building structures

As previously mentioned, there is an increasing tendency to adopt analysis procedures that can provide stakeholders and building owners with meaningful structural performance indicators that can help in their decision process. Among the possible methodologies, the PBEE methodology developed by the Pacific Earthquake Engineering Research (PEER) Center (Cornell and Krawinkler, 2000; Porter, 2003; Ramirez and Miranda, 2012) is the reference procedure to evaluate damage and economic losses resulting from an earthquake. Figure 7.1 illustrates the fully probabilistic framework of the PEER-PBEE methodology, which is composed of four main steps: hazard analysis, demand or structural analysis, fragility or damage analysis and loss analysis.

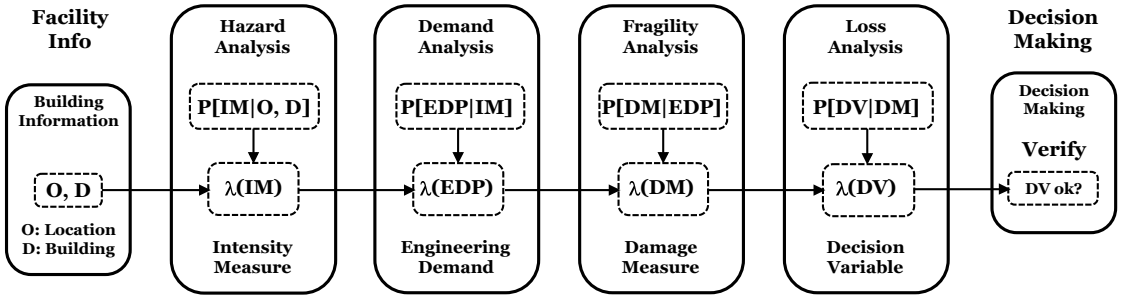

Figure 7.1: PEER-PBEE methodology (Porter, 2003).

The first step of the methodology consists on the application of probabilistic seismic hazard analysis (PSHA) to obtain the seismic hazard curve for the site under consideration, which describes the annual frequency of exceedance (or the probability of exceedance within a certain time frame, or the return period) of a given ground motion intensity measure or IM (e.g. PGA, PGV, $S_a(T_1)$. This stage may also include the selection of hazard consistent ground motion records to use in the second step of the methodology, namely the analysis of the response of the structure (Porter, 2003). In the second step, response-history analysis is performed for several intensity levels of the same IM, in order to compute the desired engineering demand parameters or $EDPs$ (e.g. inter-storey drift ratio, residual interstorey drift ratio, peak floor accelerations). The third step (fragility

analysis) correlates the *EDPs* to the probability of equalling or exceeding particular levels of damage, producing damage measures (*DMs*). Finally, in the fourth step, the probabilistic estimation of the structural performance conditioned on damage is performed. The structural performance is quantified via decision variables (*DVs*) that can be, for example, the repair cost, downtime, loss of life or other metrics that allow stakeholders and building owners to take informed decisions. In mathematical terms, the PEER-PBEE methodology is expressed by Equation 7.1, in terms of the mean annual occurrence rate of the decision variable, $\lambda(DV)$ (Cornell and Krawinkler, 2000; Porter, 2003).

$$\lambda(DV) = \int\int\int G(DV \mid DM)\, dG(DM \mid EDP)\, dG(EDP \mid IM)\, \mid d\lambda(IM) \mid \tag{7.1}$$

In this research study, the first mode spectral acceleration, $S_a(T_1)$, is used as the *IM*, the *EDPs* considered are the interstorey and maximum residual interstorey drifts, and the peak floor accelerations. Additionally, the damage functions, *DM*, have been derived from the HAZUS (FEMA, 1999) consequence and fragility models and the considered *DVs* are the ones related with the economic losses associated to repair costs.

The numerical integration of Equation 7.1 can be used to estimate the expected annual losses in the building. Following the improvements proposed by Ramirez and Miranda (2012), the expected total economic losses in the building can be due to three mutually exclusive events: i) the building does not collapse and can be repaired; ii) the building does not collapse but needs to be demolished and rebuilt; iii) the building collapses and needs to be rebuilt. Therefore, the expected value of total economic losses in a building can be computed as:

$$L_T = L_{NC\cap R} + L_{NC\cap D} + L_C \tag{7.2}$$

where L_T is the expected value of total loss in the building, $L_{NC\cap R}$ is the expected value of loss in the building given that collapse does not occur and the structure is repaired, $L_{NC\cap R}$ is the expected value of loss in the building when there is no collapse but the building is demolished and L_C is the expected loss in the building when collapse occurs.

According to Ramirez and Miranda (2012) and Hwang and Lignos (2017), the expected value of economic losses for a given ground motion intensity, *IM*, can be estimated as:

$$\begin{aligned} E[L_T \mid IM] = {} & E[L_T \mid NC\cap R, IM]\cdot P(NC\cap R \mid IM) + \\ & E[L_T \mid NC\cap D]\cdot P(NC\cap D \mid IM) + \\ & E[L_T \mid C]\cdot P(C \mid IM) \end{aligned} \tag{7.3}$$

where, $E[L_T \mid NC\cap R, IM]$, $E[L_T \mid NC\cap D]$ and $E[L_T \mid C]$ are the expected value of losses for $IM = im$ given that collapse does not occur and the building is repaired, the expected value of losses for $IM = im$ when there is no collapse but the building is demolished and the expected value of losses for $IM = im$ when collapse occurs, respectively. Furthermore, $P(NC\cap R \mid IM)$, $P(NC\cap D \mid IM)$ and $P(C \mid IM)$ are, respectively, the probability that the building will not collapse

but that it will be repaired, the probability that the building will not collapse but it will be demolished due to large residual deformations and the probability that the building will collapse given that the ground motion intensity is $IM = im$.

Given that all events are mutually exclusive, Equation 7.3 can be re-written (Ramirez and Miranda, 2012; Hwang and Lignos, 2017):

$$\begin{aligned} E[L_T \mid IM] = {} & E[L_T \mid NC \cap R, IM] \cdot \{1 - P(D \mid NC, IM)\} \cdot \{1 - P(C \mid IM)\} + \\ & E[L_T \mid NC \cap D] \cdot P(D \mid NC, IM) \cdot \{1 - P(C \mid IM)\} + \\ & E[L_T \mid C] P(C \mid IM) \end{aligned} \tag{7.4}$$

In this research study, the probability that the building will collapse given that the ground motion intensity is $IM = i$m, $P(C \mid IM)$, is determined based on Incremental Dynamical Analysis (IDA) (Vamvatsikos and Cornell, 2002). For each IDA curve, the building is assumed to have collapsed if the slope of the IDA curve reduces to 10% of the initial value, or if the interstorey drift ratio of any storey exceeds 20%.

The probability that the building will not collapse but will be demolished due to large residual deformations, given that the ground motion intensity is $IM = im$, can be computed as:

$$P(D \mid NC, IM) = \int_0^\infty P(D \mid RIDR)\, dP(RIDR \mid NC, IM) \tag{7.5}$$

where, $P(D \mid NC, IM)$ is the probability of having to demolish the structure conditioned on the maximum residual interstorey drift ratio ($RIDR$) from all stories in the building and $P(RIDR \mid NC, IM)$ is the probability of experiencing a certain level of $RIDR$ in the building given that it has not collapsed and that it has been subjected to an earthquake with a given ground motion intensity $IM = im$.

According to Ramirez and Miranda (2012), $P(D \mid RIDR)$ should follow a lognormal distribution with a median of 0.015 and a logarithmic standard deviation of 0.3 for concrete structures. Jayaram et al. (2012) proposed to increase the median by 25% for steel structures. In this research study, a median of 0.0185 and a logarithmic standard deviation of 0.3 were assumed. Figure 7.2 shows the resulting cumulative probability distribution.

The expected value of losses given that collapse does not occur and the building is repaired for a ground motion intensity $IM = im$, $(E[L_T \mid NC \cap R, IM])$, is obtained from the sum of the repair costs of each individual structural and non-structural component. Therefore, a preliminary inventory of all the components of the building should be conducted with the objective of deriving the fragility functions and consequence models for each type of component. This procedure may prove to be highly complex and difficult to implement. An alternative is to use simplified storey-based building-specific loss estimation methods (Ramirez and Miranda, 2009; Zareian and Krawinkler, 2006). These methods provide an estimate of the total losses based on the sum of the repair costs at each storey of the building. Moreover, at each storey the components can be grouped into three categories: i) drift-sensitive structural components $(L_S \mid IDR)$; ii) drift-sensitive

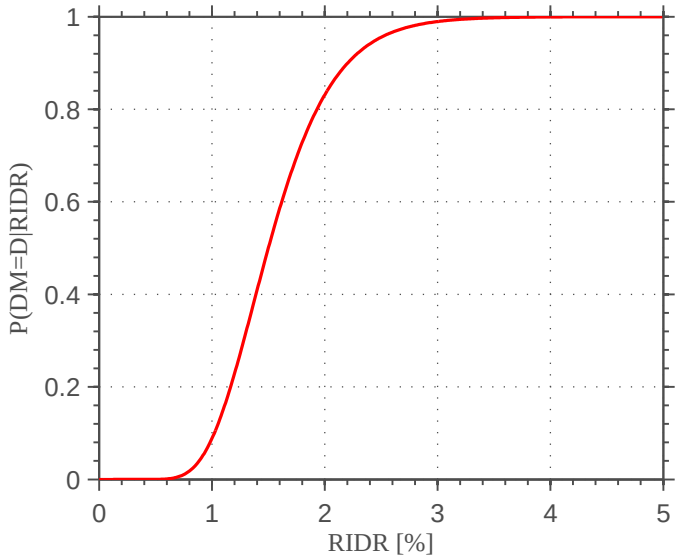

Figure 7.2: Probability of having to demolish the structure conditioned on the maximum residual interstorey drift ratio.

non-structural components $(L_{NS} \mid IDR)$; iii) acceleration-sensitive components $(L_{NS} \mid PFA)$. At each storey, these categories are weighted to translate the value of each component category that exists in a given storey. Figure 7.3 shows the components weight adopted by HAZUS for three different occupancies.

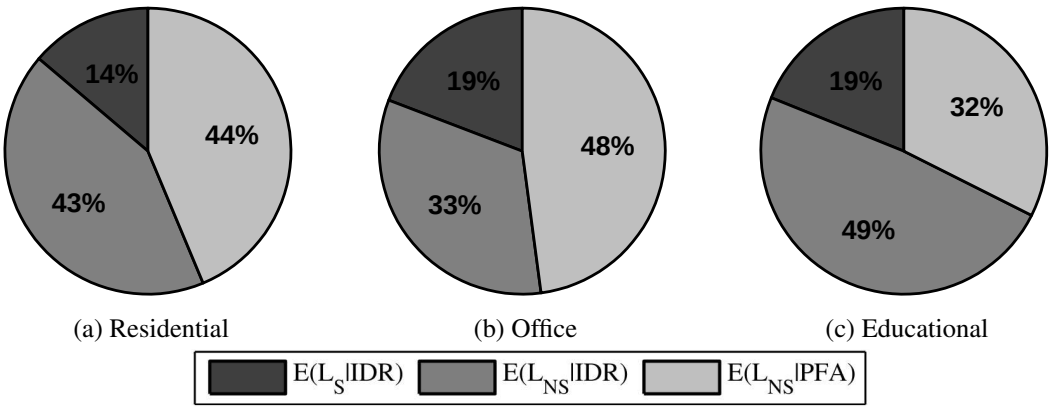

Figure 7.3: Losses distribution for three different occupancies according to HAZUS generic data.

The weights adopted in this study for residential buildings in Portugal are shown in Table 7.2. These weights were based on information collected from several design offices and reflect typical cost ratios in the Portuguese construction sector.

The total losses, which are evaluated based on the sum of the repair costs at each storey of the building considering the three component categories, can be computed using Equations 7.6 and

Table 7.2: Storey component weight.

Storey component category	Weigth
Drift-sensitive, structural components	25 %
Drift-sensitive, non-structural components	55 %
Acceleration-sensitive, non-structural components	20 %

7.7.

$$E\left[L_T \mid R, IM\right] = \sum_{i=1}^{NS} \sum_{k=1}^{n=3} E\left[L_{i,k} \mid NC \cap R, IM\right] \tag{7.6}$$

$$E\left[L_{i,k} \mid NC \cap R, IM\right] = \int_0^{\infty} E\left[L_{i,k} \mid NC \cap R, EDP_k\right] \mid dP\left(EDP_k > edp_k \mid NC \cap R, IM\right) \mid \tag{7.7}$$

where $E\left[L_{i,k} \mid NC \cap R, IM\right]$ is the expected loss at the ith storey and the kth component category (e.g. drift sensitive, structural components) given that collapse does not occur and the building is repaired for a ground motion intensity level, $IM = im$, $E\left[L_{i,k} \mid NC \cap R, EDP_k\right]$ is the expected loss at the ith storey and the kth component category given that collapse does not occur and the building is repaired for a EDP associated with the kth component category, and $P\left(EDP_k > edp_k \mid NC \cap R, IM\right)$ is the probability of EDP_k exceeding the value of edp_k given that collapse does not occur and the building is repaired for a ground motion intensity level, $IM = im$. Typically, the values of $E\left[L_{i,k} \mid NC \cap R, EDP_k\right]$ are obtained from damage functions and the values of $P\left(EDP_k > edp_k \mid NC \cap R, IM\right)$ are extracted from IDA results (Ramirez and Miranda, 2012).

Adopting the procedure proposed by Ramirez and Miranda (2012), the storey fragility and consequence models have been derived from HAZUS (FEMA, 1999) generic data which, for residential multi-family dwelling, corresponds to the following damage-to-loss model:

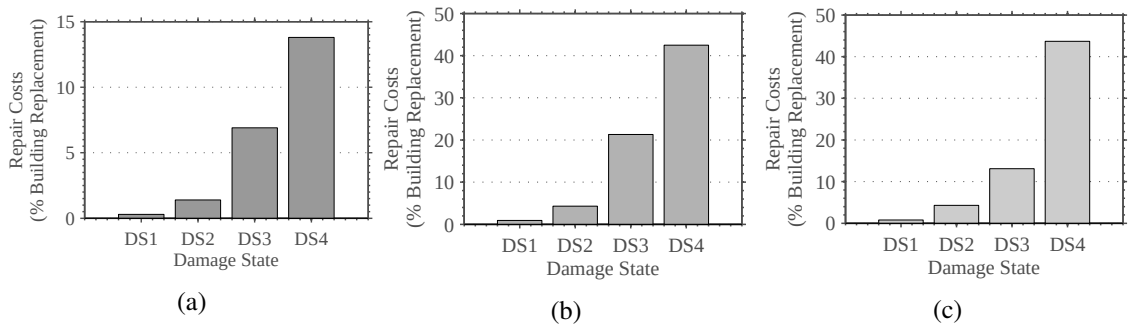

Figure 7.4: HAZUS damage-to-loss model: (a) Structural components (drift-sensitive); (b) Non-structural components (drift-sensitive) and (c) Non-structural components (acceleration-sensitive).

For each component category, the adopted storey fragility functions were based on the HAZUS (FEMA, 1999) fragility functions for steel moment-resisting frame buildings (S1L, S1M and S1H) designed to a "highcode" level. The parameters of each component fragility functions are shown in Table 7.3 and Table 7.4.

Table 7.3: HAZUS (FEMA, 1999) structural fragility functions adopted.

Damage state	Structural			
	S1L	S1M	S1H	β
	Median (ISDR)	Median (ISDR)	Median (ISDR)	
DS1	0.60%	0.40%	0.30%	0.5
DS2	1.20%	0.80%	0.60%	
DS3	3.00%	2.00%	1.50%	
DS4	8.00%	5.33%	4.00%	

Table 7.4: HAZUS (FEMA, 1999) non-structural fragility functions adopted.

Damage state	Non-structural			
	Drift-sensitive		Acceleration-sensitive	
	Median (ISDR)	β	Median (% g)	β
DS1	0.40%	0.5	3.10%	0.6
DS2	0.80%		6.10%	
DS3	2.50%		12.00%	
DS4	5.00%		24.00%	

By combining the consequence models with the corresponding fragility functions, the storey-based damage functions can be obtained. Moreover, the storey damage functions should be re-scaled with the component category weights presented in Table 7.2. Figure 7.5 shows the storey damage functions used in this research study.

The expected annual loss (EAL) can be computed as:

$$EAL = \int_0^\infty E(L_T \mid IM)\, d\lambda(IM) = \int_0^\infty E(L_T \mid IM) \left| \frac{d\lambda(IM)}{dIM} \right| dIM \tag{7.8}$$

where, $\lambda(IM)$ is the mean annual frequency of the ground motion intensity and $|\, d\lambda(IM)/dIM \,|$ is the derivative of the seismic hazard curve.

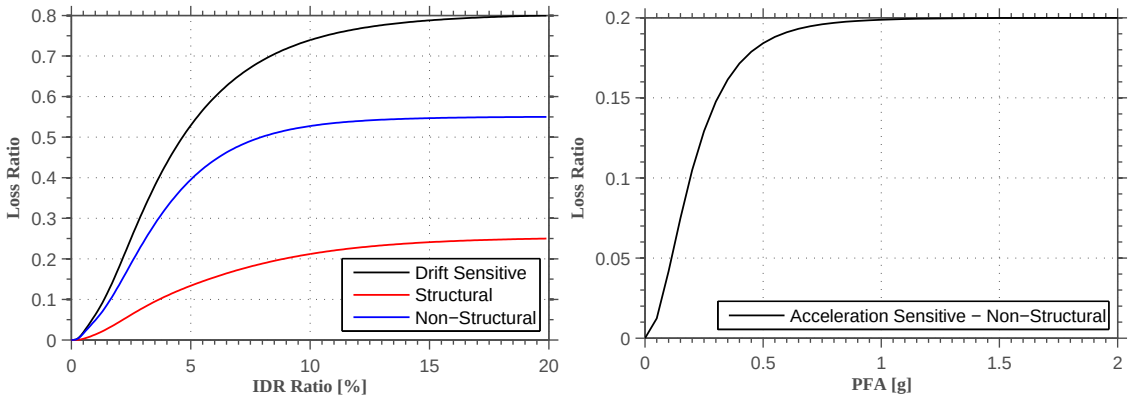

(a) (b)

Figure 7.5: Storey-based damage functions: a) Drift-sensitive and b) Acceleration-sensitive.

Finally, the expected present value (PV) of life-cycle losses are given by (Beck et al., 2004):

$$PV = EAL \times \left(\frac{1 - e^{r \cdot t}}{r} \right) \tag{7.9}$$

where, r is the discount rate and t is the expected lifetime. In the current research study, a 5% discount rate and 50 years lifetime span were assumed.

7.3 Description of the steel buildings

This study aims to quantify the seismic losses in moment-resisting steel frame buildings designed according to EC8 considering different ductility classes. The buildings considered in this study have already been extensively analysed to assess the collapse performance (Chapter 6) and the performance assessment according to the EC8 requirements (Chapter 2). The selected steel buildings are representative of the current steel building stock in Europe and consist of six building configurations with different number of bays and span length. Buildings with 2, 3, 4, 5 and 8 storeys, corresponding to low to medium rise buildings, were considered, making a total of 360 buildings. Three different site locations in Portugal, corresponding to different seismic intensities, were considered, namely i) Porto (low seismic load level), ii) Lisbon (moderate seismic load level) and ii) Lagos (moderate seismic load level). For Lagos, two soil types were considered (Type B and Type C) according to the EC8 classification. Figure 7.6 shows the elevation and plan views of one of the building configurations. The analysed frame is also identified in the figure. Seismic resistance was considered to be provided by the MRFs in the longitudinal (x) direction and by a bracing system in the transversal (y) direction. In this research study, only the internal longitudinal frames were subject of investigation. Table 7.5 shows a detailed description of all the building configurations considered in this study.

The steel buildings were initially designed for gravity loads in accordance with the provisions of Part 1-1 of Eurocode 3 (EC3-1-1) (CEN, 2005a) for cross-sectional resistance, stability checks

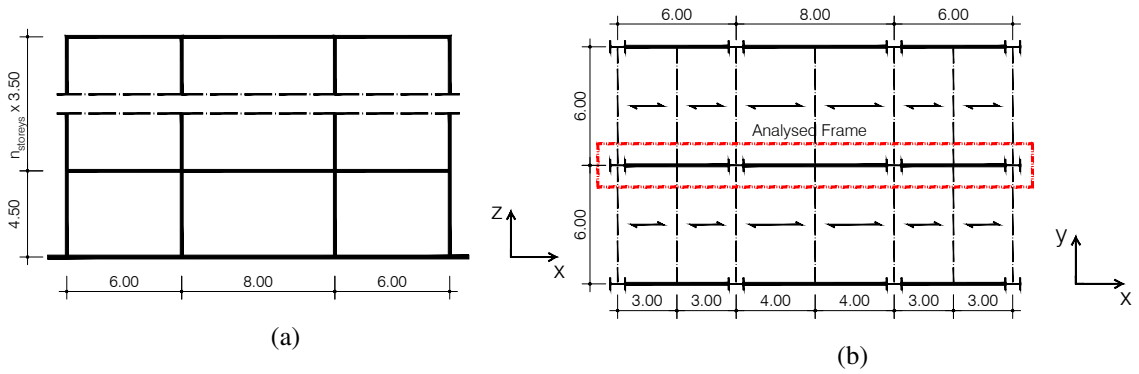

Figure 7.6: Building configuration 2: (a) Elevation view, (b) Plan view.

Table 7.5: Building configurations and geometrical properties

Config.	x-z plane		y-z plane		h_1 [m]	h_{others} [m]
	N. of frames	Bays [m]	N. of frames	Bays [m]		
1	3	6+6+6	4	6+6	4.5	3.5
2	3	6+8+6	4	6+6		
3	3	8+8+8	4	8+8		
4	4	6+6+6+6	5	6+6+6		
5	3	8+6+8	4	6+6		
6	5	8+8+8+8+8	6	8+8+8+8		

and deflection limits. Seismic design was performed in accordance with the provisions of Part 1 of Eurocode 8 (EC8) (CEN, 2005c), considering medium and high ductility class levels (DCM and DCH), corresponding to two different reference values of behaviour factor recommended by the standard (q = 4.0 for DCM and q = 6.5 for DCH). Additionally, a new scenario was considered in which the behaviour factor was selected based on the Improved Force-Based Design (IFBD) procedure (Villani et al., 2009). In this procedure, the behaviour factor is selected based on the properties of the structure as well as on the level of seismic intensity. The serviceability inter-storey drift ratio (IDR) was limited to 1% and the stability coefficient, θ, as defined in EC8, was limited to 0.2. Capacity design of the non-dissipative members was conducted according to the requirements of EC8, with the modifications proposed by Elghazouli (2010). The EC8 capacity design requirement at beam-column joints, $\sum M_{Rc} \geq 1.3 \sum M_{Rb}$, was also taken into account in the design of all frames. A total of 360 steel buildings were designed and member sizes were dictated by strength or stiffness (drift and P-Delta checks) design criteria. Steel buildings designed using EC8 recommended behaviour factors for medium and high ductility class were mostly controlled by stiffness requirements related with the control of P-Delta effects. On the other hand, steel

buildings designed with the IFBD procedure were typically governed by strength design criteria. Moreover, for a large number of design cases, the steel buildings in which the design has been controlled by the P-Delta criterion (q = 6.5 and q = 4) resulted in the same structural solution independently of the site location (seismic intensity). In Figure 7.7, the steel weight of the lateral load resisting system of each design solution is shown, for the location of Porto. In the figure, bar plots summarizing the design solution's weights are shown for the six building configurations, five frame heights (2, 3, 4, 5 and 8 storeys) and three behaviour factors considered (q=IFBD, q=4 and q=6.5). Furthermore, it should be mentioned that, contrarily to what would be expected, the frames

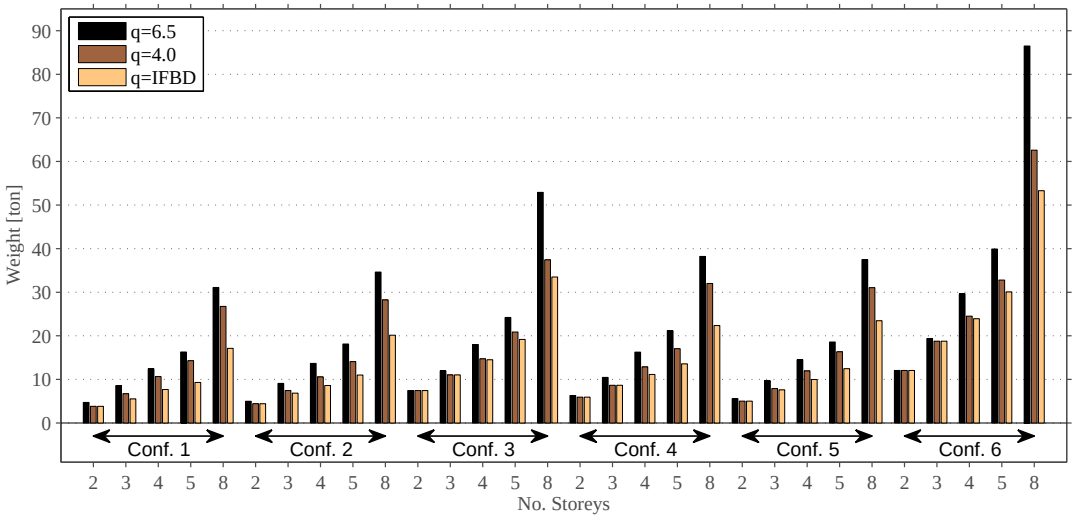

Figure 7.7: Steel weight comparison of the various building configurations, for Porto.

designed with higher behaviour factors were associated with higher quantities of steel due to the need to comply with stiffness requirements imposed by the control of P-Delta effects. Further details about the adopted design criteria and an extensive discussion on the obtained solutions can be found in Chapter 2. The next sections of this paper will focus on a detailed characterisation of the seismic performance of the archetypes.

7.4 Site hazard and ground motion record selection

7.4.1 Site hazard characterization

As mentioned before, three different site locations in Portugal, corresponding to different seismic hazards, were considered for the buildings, namely Porto, Lisbon and Lagos. For Lagos, two different soil conditions were considered (soil type B and C according to EC8). Probabilistic seismic hazard analysis (PSHA) was performed for the three sites under study, using the open source software OpenQuake (OQ) (Pagani et al., 2014) and the seismic hazard models proposed in the recently finished SHARE project (Woessner et al., 2015). It should be noted that, for the Portuguese territory, the seismic hazard models developed in the SHARE project were implemented, but with

the inclusion of additional hazard sources (Vilanova and Fonseca, 2007) and using the ground motion prediction equations from Atkinson and Boore (2006) and Akkar and Bommer (2010), with a weight of 70% and 30%, respectively (Silva et al., 2015). The site hazard curves for all buildings were obtained from a PSHA analysis. An example for Lisbon and Lagos is shown in Figure 7.8, where site-specific hazard curves for different periods of vibration are shown in terms of $S_a(T_1)$. Figure 7.9 shows the mean uniform hazard spectra (UHS) for five different hazard levels and the corresponding EC8 Type 1 and 2 response spectra for a probability of exceedance of 10% in 50 years. Despite the differences that can be observed when the UHS (obtained with the considered hazard model) and the EC8 response spectra are compared, the considered seismic hazard model is the most recent model available for the Portuguese territory, being therefore considered the most appropriate for the hazard characterization.

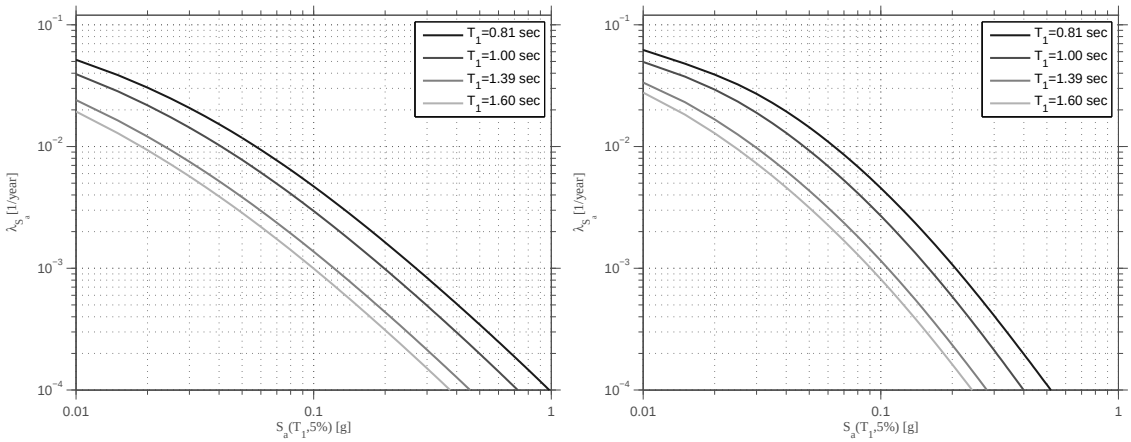

(a) Lisbon (b) Lagos

Figure 7.8: Seismic hazard curves.

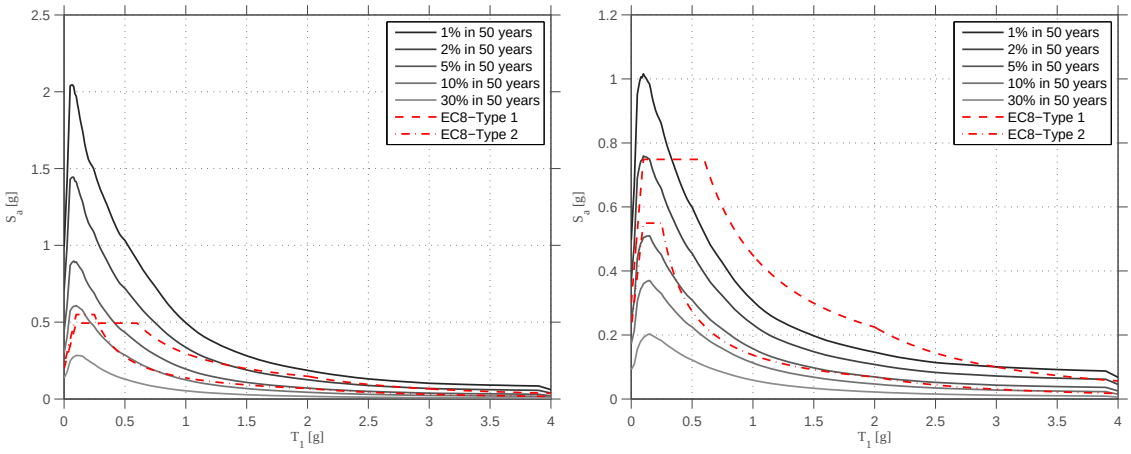

(a) Lisbon (b) Lagos

Figure 7.9: Uniform hazard spectra (UHS) and EC8 spectra.

Additionally, disaggregation of the seismic hazard (Bazzurro and Cornell, 1999) on magnitude, distance and ε was performed in order to identify the hazard scenario that contributes most to the seismic hazard. Figure 7.11 shows the disaggregation for six hazard levels, for Lisbon. The hazard levels have been defined using the corresponding UHS spectral acceleration at $T_1 = 1.0s$. Figure 7.11 allows concluding that, for high hazard levels, the major contributions come from hazard sources generating 6 to 7 magnitude earthquakes at close distances. On the other hand, as the seismic hazard level decreases, the number of scenarios contributing increases, with several magnitude-distance bins showing similar contributions (Goulet et al., 2007; Haselton et al., 2009).

7.4.2 Ground motion record selection

Over the past years, several ground motion record selection techniques have been proposed. The different alternatives range from simple techniques that consist on selection of ground motion records based on magnitude, distance and site conditions to advanced techniques that adequately take into account the spectral shape for each site, hazard level, and structural vibration period of interest. Several research studies (Baker and Cornell, 2006a,b; Goulet et al., 2007; Haselton et al., 2009; Eads et al., 2013) have demonstrated that the consideration of the spectral shape can contribute to a significant increase of the collapse capacity of a structure in comparison with that obtained from a ground motion record suite that does not consider the spectral shape. Baker and Cornell (2005) have shown that the ε parameter is an adequate predictor of spectral shape, concluding that ground motion record selection should also be based on ε obtained from disaggregation for each hazard level and fundamental period of vibration of interest (Goulet et al., 2007). More recently, Baker and Cornell (2006a,b, 2005) proposed the so-called Conditional Mean Spectrum (CMS) as an alternative target spectrum that directly accounts for the spectral shape. However, the selection of ground motion records based on ε or the computation of the CMS for such a large number of structures located in different geographic regions is impractical due to computational requirements and large number of ground motion record suites to select. Haselton et al. (2009) proposed an alternative method where a general ground motion record suite is selected without taking into account the ε values, with the results being post-processed to account for the expected ε at a specific site and hazard level.

In the current research study, the ground motion record selection was performed based on disaggregation results and average shear wave velocity for the first 30 meters of soil, $v_{s,30}$, in agreement with the requirements of EC8. For each site location, a suite of 40 ground motion records were selected and scaled in order to obtain an appropriate matching between the median spectra of the suite and the EC8 elastic response spectra, for the range of periods of interest. A similar technique was applied in FEMA 695 project (FEMA, 2009). The ground motion record selection was conducted using the SelEQ framework (Chapter 5), an advanced ground motion record selection and scaling framework, that allows the user to obtain not only the ground motion selection but incorporates the possibility to conduct PSHA for the European territory, making use of the open source platform OpenQuake. Figure 7.10 shows the response spectra of the selected ground motion records for the site locations under study and the corresponding mean and median

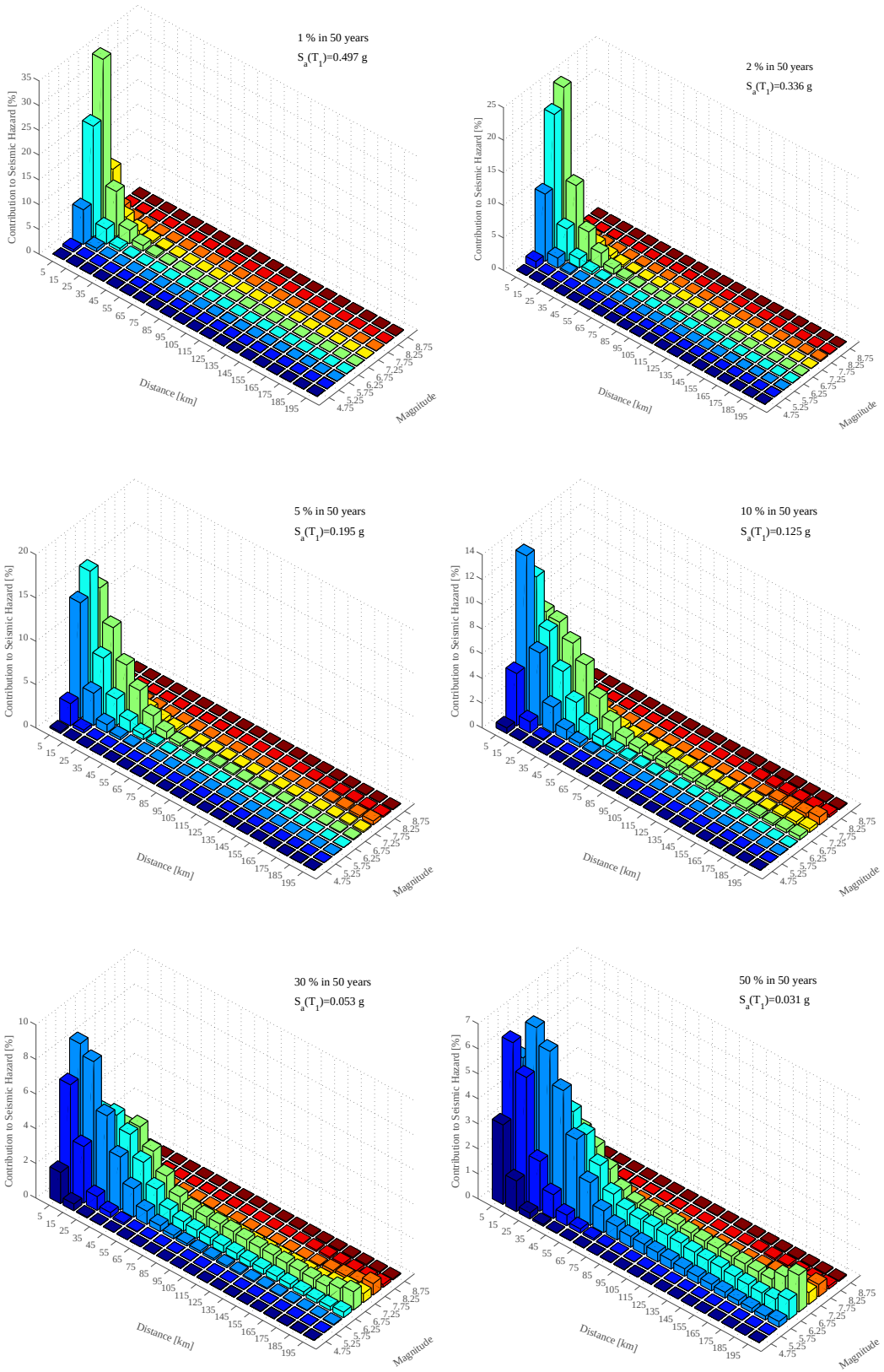

Figure 7.11: Seismic hazard disaggregation for six hazard levels for Lisbon (T_1=1.0 s).

spectral ordinates. The EC8 elastic response spectra for a probability of exceedance of 10% in 50 years hazard level are also plotted in the figure.

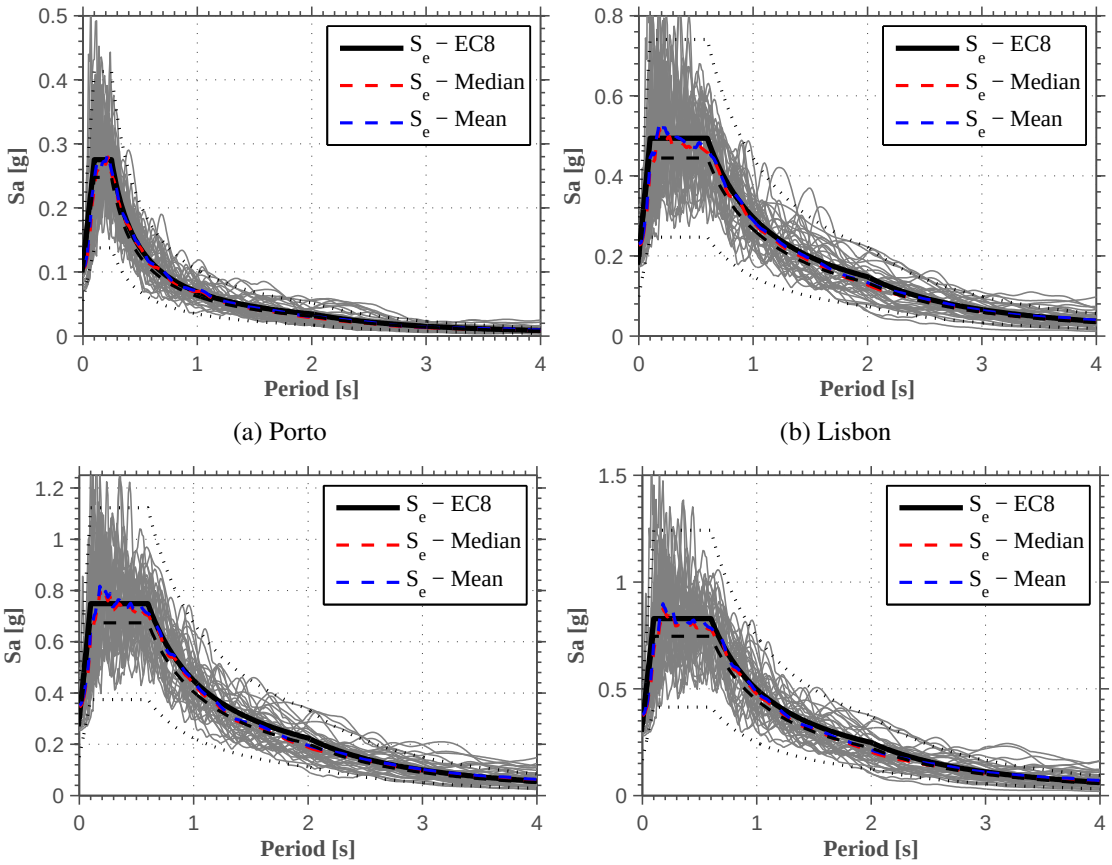

(a) Porto (b) Lisbon

(c) Lagos (d) Lagos C

Figure 7.10: Response spectra of selected ground motion records and EC8 elastic response spectra.

As shown in Figure 7.10, there is a good correlation between the mean and median spectra of the selected ground motions and the code target spectra.

7.5 Numerical modelling and nonlinear structural analysis

7.5.1 Numerical modelling

The assessment of the structures was carried out based on response-history analyses conducted with the nonlinear finite element analysis program OpenSEES (McKenna, 2011). The material nonlinear behaviour was considered through a concentrated plasticity approach considering strength, stiffness, and deterioration effects (Lignos and Krawinkler, 2010; Araújo and Castro, 2016). Figure 7.12 illustrates the backbone curve and the stiffness and deterioration parameters for a European steel open cross-section HEB300 according to the aforementioned proposals. The effect of the axial load on the flexural capacity of the columns was taken into account in an approximate manner: 1) a preliminary pushover analysis was conducted to evaluate the expected

average axial force under the combined actions of gravity and lateral loading (($P_{grav} + 0.5 \times P_E^{max}$, where P_{grav} and P_E^{max} are the axial load due to gravity loads and the maximum axial force due to lateral loading, respectively) (Zareian et al., 2010); 2) the backbone curve is modified by reducing the bending moment capacity according to the interaction equations proposed in EC3-1-1, whilst no modification of the stiffness and deterioration parameters is done.

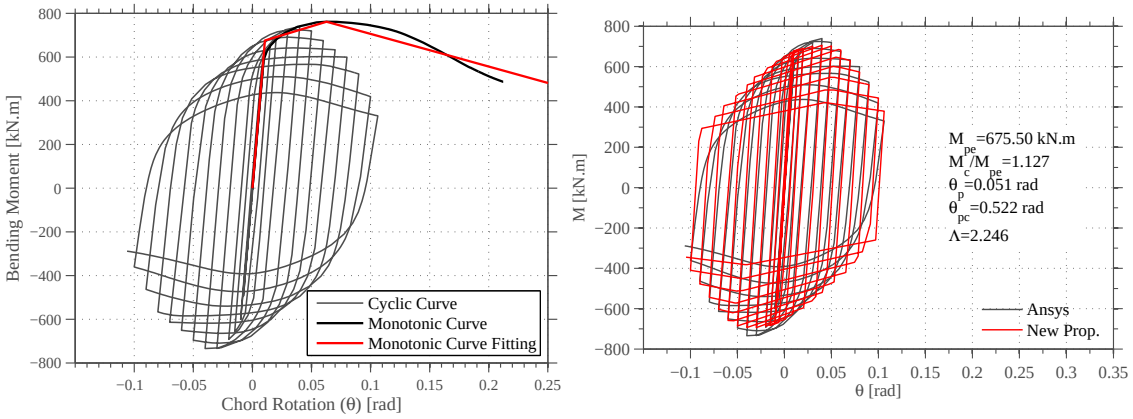

(a) (b)

Figure 7.12: Example of calibration/modelling procedure of a HEB300 steel profile: a) calculation of strength and stiffness degradation parameters; b) Cyclic flexural behaviour of the member with the calibrated degradation parameters.

The panel zones were represented with a beam-column joint element, "JOINT2D", that is available in the software. For the panel zone, the Krawinkler (1978) tri-linear moment-distortion relation was adopted. Furthermore, the panel zones were designed with a "balanced" design methodology (Castro et al., 2008), and no strength degradation was considered (Chapter 4). Figure 7.13 illustrates the strategy adopted for the modelling of the panel zones.

Inherent damping was included using the Rayleigh damping approach, considering a damping ratio of 2.0% assigned to the first two fundamental periods of vibration. Following the recommendation and coefficient modifications proposed by Zareian and Medina (2010), initial stiffness proportional damping was assigned to elements that remain elastic, and mass proportional damping to nodes where the mass is lumped. Regarding the maximum time step used in the analysis, a sensitivity analysis was conducted for multiple engineering demand parameters, and a maximum value of 0.005s was defined. Additionally, in case of non-convergence during the analysis, a procedure was implemented that reduces the time step down to a value of 0.0002s. Similar conclusions were drawn by Barbosa et al. (2017), in which the authors pointed out that a time step of 0.002s produces negligible errors in the evaluation of the roof acceleration time-history response.

7.5.2 Nonlinear response-history analysis

The seismic performance of the buildings was assessed through incremental dynamical analysis (IDA) (Vamvatsikos and Cornell, 2002). The 5% damped first mode spectral acceleration was considered as the seismic intensity measure, *IM*, and three engineering demand parameter, *EDP*, con-

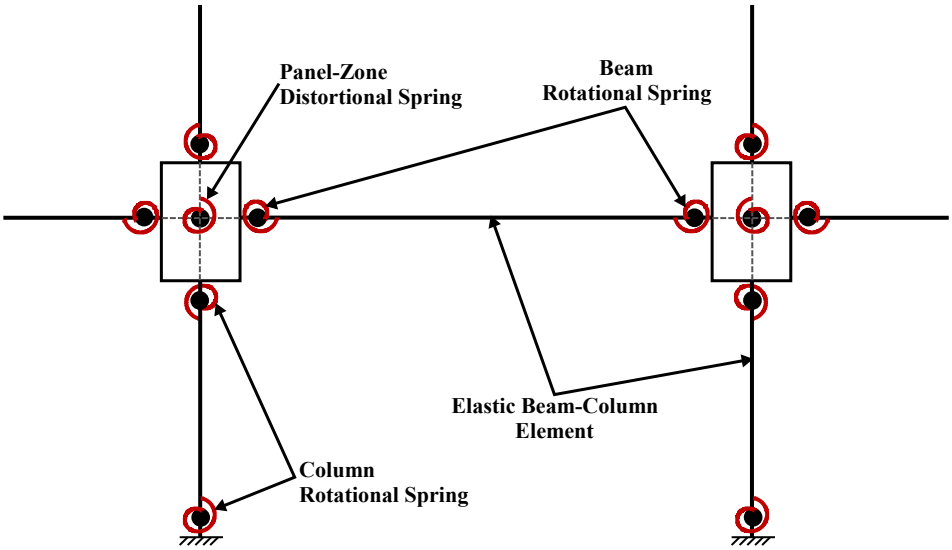

Figure 7.13: Numerical modelling illustration of the structural elements and panel zones.

sidered were selected, namely maximum inter-storey drift (*ISDR*), peak floor acceleration (*PFA*) and maximum residual inter-storey drift (*RISDR*). Figure 7.14 shows an example of maximum values of the *EDPs* along the building height for several hazard levels.

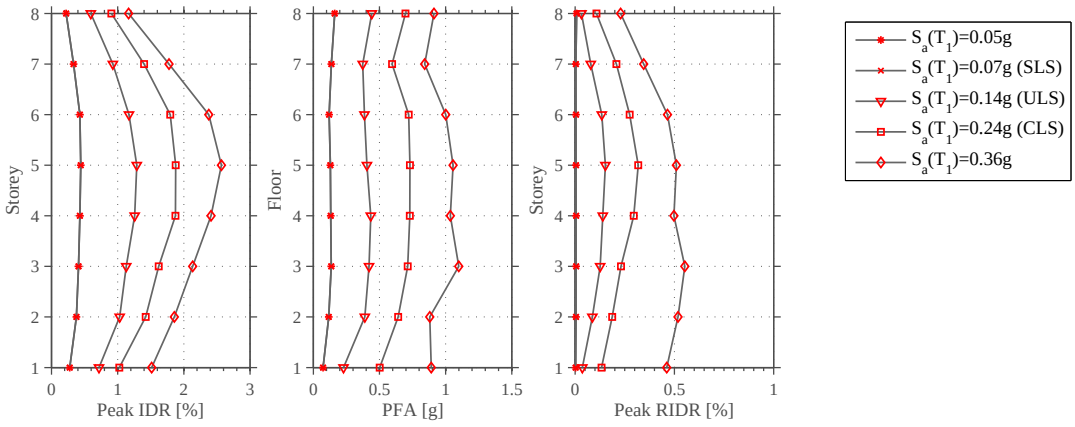

Figure 7.14: Maximum ISDR, PFA and RISDR along building height for building St105.

In each analysis, the sidesway collapse was defined as the instant in which dynamic instability occurs, that is, the point where a significant increase of displacements is observed withou a relevant increase of lateral inertia forces (Karavasilis et al., 2015; Ramirez and Miranda, 2012; Hwang and Lignos, 2017). In order to accurately evaluate the maximum *RISDR*, each dynamic analysis is significantly extended and the maximum *RISDR* is evaluated for each storey by averaging the *RISDR* obtained in the last 5 seconds of the response-history analysis.

In the evaluation of the collapse fragility curve of each building, aleatory (record-to-record) uncertainty, β_{RTR}, and epistemic (modelling) uncertainty, β_{MDL}, were taken into account. The

total uncertainty, β_{TOT}, is computed with Equation 7.10, assuming that both uncertainties are lognormally distributed and independent (Liel et al., 2009; Tzimas et al., 2016).

$$\beta_{TOT} = \sqrt{\beta_{RTR}^2 + \beta_{MDL}^2} \tag{7.10}$$

In line with what was assumed in Chapter 6, the value of total system uncertainty was taken as 0.53. The median collapse capacity was adjusted in order to account for the spectral shape effect, in accordance with Method 2 proposed by Haselton et al. (2009). Figure 7.15 shows some of the IDA curves and the corresponding collapse fragility curves, before spectral shape adjustment, obtained in this study.

7.6 Economic Seismic Losses

There are several useful metrics for the characterization of economic seismic losses in buildings (Ramirez and Miranda, 2012; Hwang and Lignos, 2017; Tzimas et al., 2016; Goulet et al., 2007; Welch et al., 2014). Among them, the most used are: i) the expected losses conditioned on the seismic intensity; ii) the expected annual losses (EAL) and iii) the expected present value (PV) of life-cycle costs. Each of these metrics can provide relevant information to stakeholders and building owners. For example, the expected annual losses can be compared to annual insurance premiums and the expected present value of life-cycle costs shows the potential financial expenses during the lifetime of the building. At the design stage, building owners and stakeholders can adopt measures to mitigate these potential expenses. In the following sections, the aforementioned metrics are quantified for all the buildings considered in this study and the results obtained are compared.

7.6.1 Expected losses conditioned on seismic intensity

Computing the loss vulnerability curves (Ramirez and Miranda, 2012) for a building allows obtaining, for each seismic intensity level, the expected losses. Therefore, it is possible, for pre-specified intensities of interest, to quantify the corresponding losses. Additionally, and if the vulnerability curves are disaggregated, the major contributors to the total losses can be identified. Figure 7.16 shows the vulnerability curves for three buildings with 2, 5 and 8 storeys and the corresponding losses for four different intensities. The seismic intensity levels considered are those defined in EC8-3 for checking three performance levels (as shown in Table 7.1: SLS-3 – limited damage, ULS – Significant damage or design intensity, CLS – Near collapse) and that prescribed in EC8 to check the damage limitation limit state (SLS-1).

A trend that can be identified in Figure 7.16 is that, in the total loss vulnerability curves, there is a linear increase for lower intensities where most of the damage occurs in non-structural elements. The linear relationship between seismic intensity and damage in non-structural elements reflects the direct correlation between intensity and lateral deformations and floor accelerations when the structure is responding in the elastic range. It is also interesting to note the important

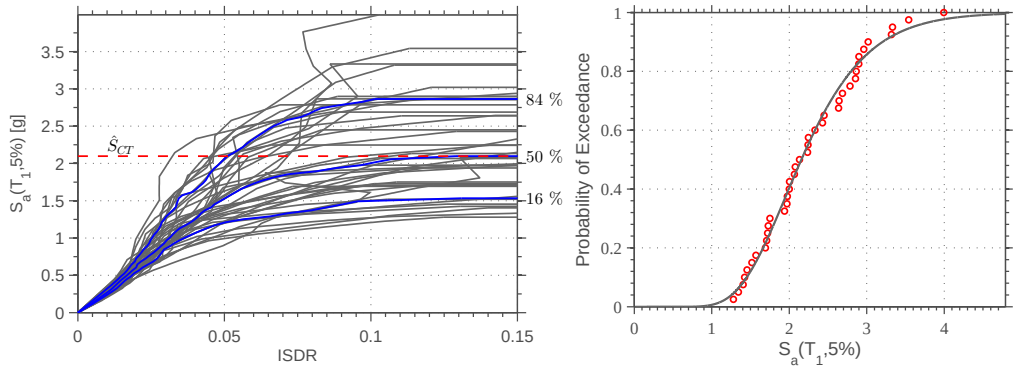

(a) St93 - 2 Storey (b) St93 - 2 Storey

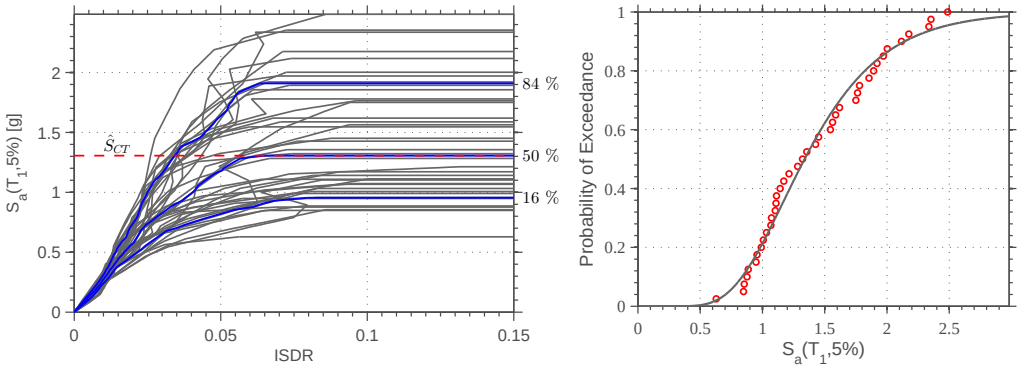

(c) St129 - 4 Storey (d) St129 - 4 Storey

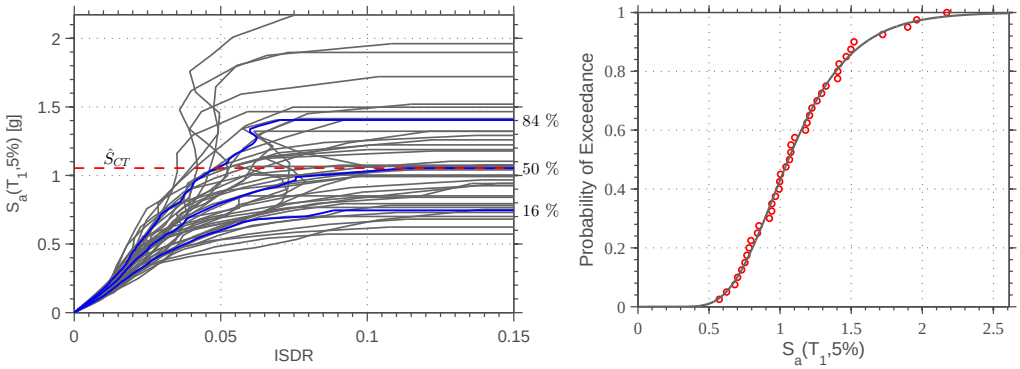

(e) St147 - 5 Storey (f) St147 - 5 Storey

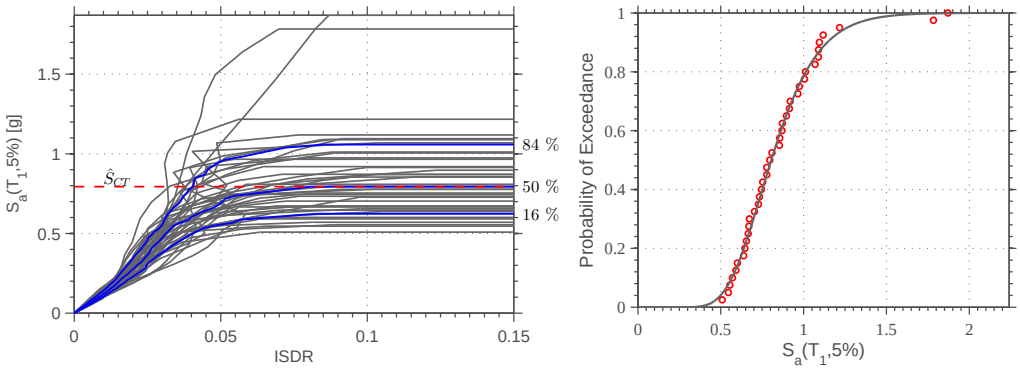

(g) St165 - 8 Storey (h) St165 - 8 Storey

Figure 7.15: IDA curves and collapse fragility curves for buildings located in Lisbon.

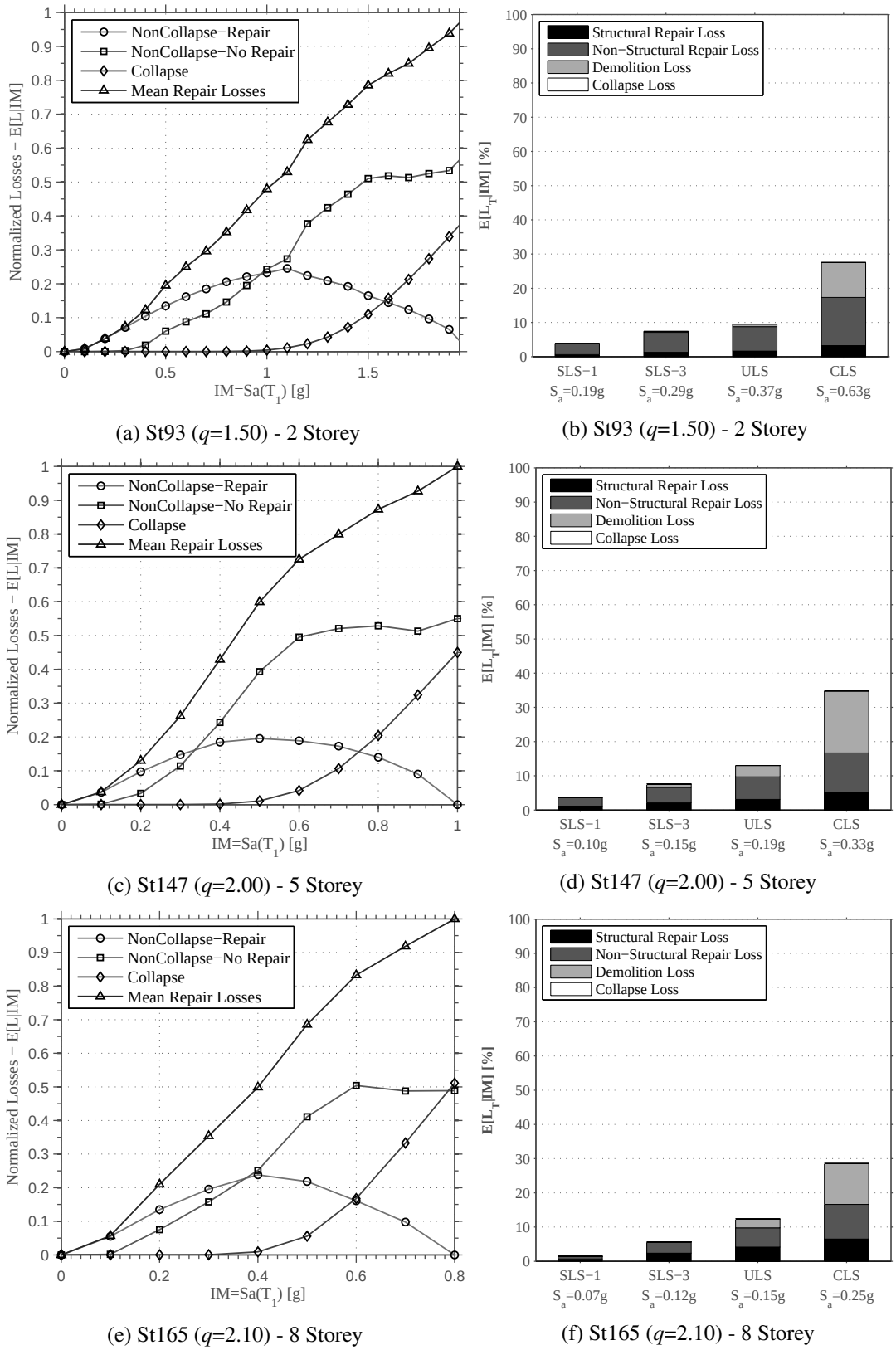

(a) St93 (q=1.50) - 2 Storey

(b) St93 (q=1.50) - 2 Storey

(c) St147 (q=2.00) - 5 Storey

(d) St147 (q=2.00) - 5 Storey

(e) St165 (q=2.10) - 8 Storey

(f) St165 (q=2.10) - 8 Storey

Figure 7.16: Vulnerability curves and corresponding normalized expected losses at design level intensity for buildings.

contribution of demolition losses, which occur, in several cases, for much lower intensities than the collapse intensity. Analysing the losses at the above mentioned intensities, it is possible to conclude that, for the damage limit states (SLS-1 and SLS-3), most of the losses are associated to the repair of non-structural components, with a slight contribution from structural repair losses. It is worth mentioning that a similar behaviour is found for the ULS design intensity level with losses controlled by damage developing on non-structural elements. However, for this intensity level, demolition losses are already present. Finally, for the near collapse seismic intensity level (CLS), there is an increase in the demolition losses, but the most interesting aspect is the absence of losses due to collapse of the buildings. Recent research work conducted by Hwang and Lignos (2017) on steel special moment-resisting frames designed according to American provisions resulted in similar observations for the SLS-1 and ULS intensity levels. However, for the near collapse intensity level, the authors reported an important contribution from collapse losses that are not noticeable in the frames designed according to EC8.

Figure 7.17 shows the normalized expected losses at the design intensity level (ULS) for all the buildings and locations under study. Except for the buildings located in Porto, the buildings designed with the upper-bound behaviour factor proposed by the European seismic design code typically exhibit lower values of expected losses in comparison with the buildings designed according to the IFBD procedure.

A careful inspection of Figure 7.17 and Tables 7.6 and 7.7 allows concluding that, for the design intensity level, the expected losses due to collapse in buildings designed according to EC8 is minimal. However, the expected losses could be considerable, ranging from 0.00% to 32.19%, depending on the building location. By analysing the distribution of losses by building location, it is possible to conclude that, for buildings located in Porto (low seismicity region), the expected losses at the design intensity level are between 0.00% and 3.21% of the replacement cost of the building. On the other hand, buildings located in Lisbon and Lagos (moderate to high seismicity regions) are expected to exhibit losses ranging from 5.40% to 18.08% and 10.07% to 27.21%, respectively. Regarding the effect of considering different soil conditions, the results show an increase of up to 5% in the expected losses when soil type C is considered in comparison to soil type B.

It is also worth analysing the disaggregated normalized expected losses at a given seismic intensity level. Tables 7.6 and 7.7 summarize the average of the disaggregated normalized expected losses at the design intensity level for each behaviour factor and number of storeys. In the table, $E[L_S]]$ refers to structural repair losses, $E[L_{NS}]]$ to non-structural repair losses, $E[L_D]]$ to demolition losses, $E[L_C]]$ to collapse losses and $E[L_T]]$ to total losses. The remaining columns, EAL and PV, will be focus of discussion later in this chapter.

From the inspection of the disaggregation of expected losses showed in Table 7.6 and Table 7.7, it can be concluded that for Porto (low seismicity), regardless of the adopted behaviour factor, more than 60% of the repair costs are due to damage in non-structural elements, the remainder being from structural damage. For the other locations (Lisbon and Lagos), the contribution of non-structural repair costs decreases with the increase of the seismicity of the site, with significant

Table 7.6: Mean disaggregated normalized expected losses for the design level intensity, EAL and PV, for Porto and Lisbon.

Site	q	N. Stories	$E[L_S]$	$E[L_{NS}]$	$E[L_D]$	$E[L_C]$	$E[L_T]$	*EAL*	*PV*
			[%]	[%]	[%]	[%]	[%]	[%]	[%]
Porto	6.5	2	0.02	0.36	0	0	0.38	0.003	0.059
		3	0.03	0.47	0	0	0.50	0.003	0.052
		4	0.13	0.53	0	0	0.65	0.003	0.051
		5	0.14	0.54	0	0	0.68	0.003	0.049
		8	0.07	0.12	0	0	0.19	0.002	0.045
	4	2	0.05	0.53	0	0	0.58	0.004	0.066
		3	0.08	0.70	0	0	0.77	0.004	0.065
		4	0.05	0.15	0	0	0.20	0.003	0.055
		5	0.07	0.21	0	0	0.28	0.003	0.056
		8	0.24	0.35	0	0	0.59	0.003	0.055
	IFBD	2	0.05	0.53	0	0	0.58	0.004	0.066
		3	0.03	0.38	0	0	0.42	0.004	0.067
		4	0.17	0.43	0	0	0.60	0.004	0.072
		5	0.33	0.81	0	0	1.14	0.004	0.072
		8	0.42	0.64	0.02	0	1.05	0.004	0.064
Lisbon	6.5	2	1.24	6.83	0.27	0	8.34	0.028	0.508
		3	1.07	5.78	0.11	0	6.96	0.023	0.415
		4	1.87	5.10	0.01	0	6.97	0.021	0.391
		5	1.66	4.44	0.06	0	6.17	0.019	0.340
		8	2.25	3.64	0	0	5.90	0.018	0.326
	4	2	1.35	6.76	0.2	0	8.32	0.029	0.536
		3	1.25	5.92	1.56	0	8.74	0.027	0.494
		4	2.5	5.78	0.68	0	8.96	0.025	0.467
		5	2.31	5.34	1.21	0	8.86	0.023	0.423
		8	3.24	4.67	0.36	0	8.27	0.022	0.403
	IFBD	2	1.35	6.77	0.2	0	8.32	0.029	0.536
		3	1.37	6.19	2.22	0	9.77	0.029	0.527
		4	2.96	6.39	1.14	0	10.48	0.030	0.549
		5	2.85	6.20	1.51	0	10.56	0.028	0.516
		8	4.14	5.65	2.77	0	12.57	0.025	0.465

Table 7.7: Mean disaggregated expected losses for the design level intensity, *EAL* and *PV*, for Lagos and Lagos (soil type C).

Site	q	N. Stories	$E[L_S]$	$E[L_{NS}]$	$E[L_D]$	$E[L_C]$	$E[L_T]$	*EAL*	*PV*
			[%]	[%]	[%]	[%]	[%]	[%]	[%]
Lagos	6.5	2	2.10	10.84	1.98	0	14.92	0.016	0.291
		3	1.84	9.68	1.59	0	13.10	0.013	0.248
		4	3.29	8.90	0.94	0	13.13	0.012	0.221
		5	3.00	7.98	1.08	0	12.06	0.012	0.216
		8	4.10	6.80	1.21	0.03	12.14	0.012	0.218
	4	2	2.30	11.33	2.72	0	16.34	0.018	0.332
		3	2.04	9.40	4.66	0	16.10	0.017	0.312
		4	3.75	8.91	6.13	0	18.79	0.018	0.330
		5	3.76	8.87	4.99	0	17.63	0.016	0.299
		8	5.24	8.12	3.51	0	16.87	0.020	0.376
	IFBD	2	2.30	11.33	2.72	0	16.34	0.018	0.332
		3	2.25	9.80	8.78	0	20.83	0.020	0.036
		4	4.28	9.86	7.18	0.02	21.34	0.023	0.431
		5	4.32	9.79	4.15	0.01	18.28	0.025	0.452
		8	6.19	9.15	4.96	0	20.31	0.023	0.417
Lagos C	6.5	2	2.42	12.42	2.73	0	17.57	0.046	0.840
		3	2.00	10.56	2.65	0	15.21	0.037	0.675
		4	3.67	9.98	1.97	0	15.62	0.035	0.649
		5	3.26	8.55	2.12	0.01	13.94	0.032	0.583
		8	4.67	7.87	1.47	0.08	14.09	0.032	0.590
	4	2	2.51	12.43	3.68	0	18.63	0.049	0.906
		3	2.32	10.57	5.45	0	18.34	0.045	0.825
		4	4.15	9.93	7.83	0	21.92	0.050	0.925
		5	4.14	9.81	6.42	0	20.38	0.044	0.808
		8	5.78	9.09	3.58	0.01	18.46	0.047	0.859
	IFBD	2	2.51	12.43	3.68	0	18.63	0.049	0.906
		3	2.52	11.04	11.53	0.02	25.12	0.055	1.002
		4	4.80	11.33	8.19	0	24.32	0.057	1.053
		5	4.45	10.39	7.70	0.02	22.57	0.056	1.035
		8	6.39	9.82	10.57	0.05	26.83	0.055	1.017

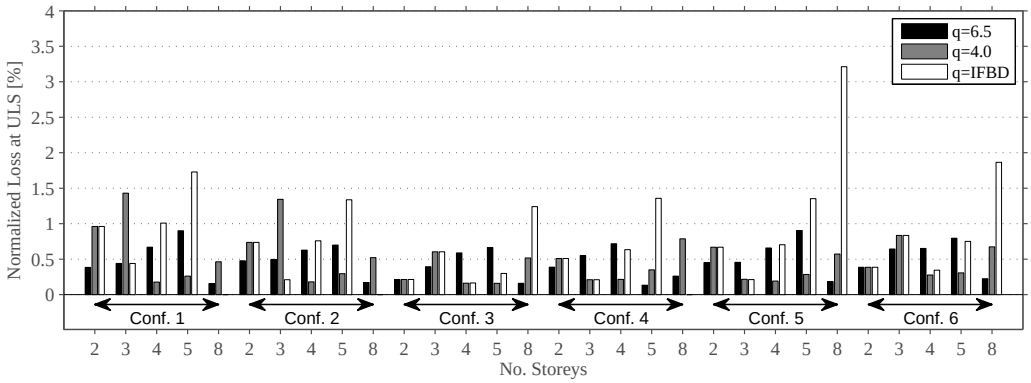

(a) Porto

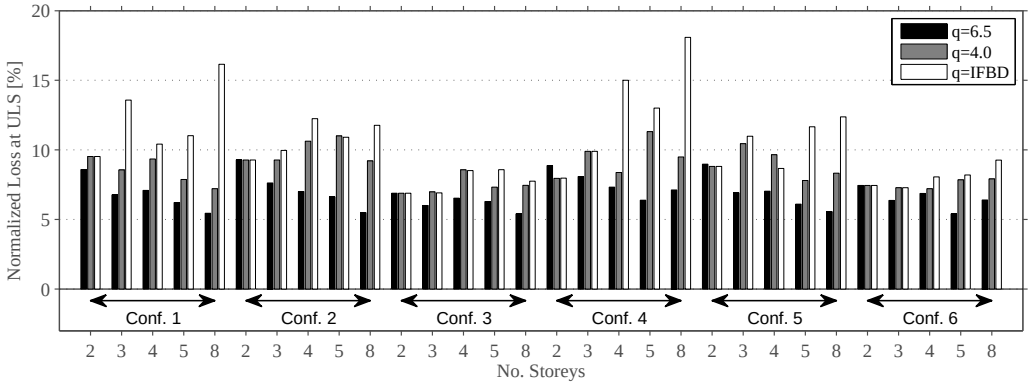

(b) Lisbon

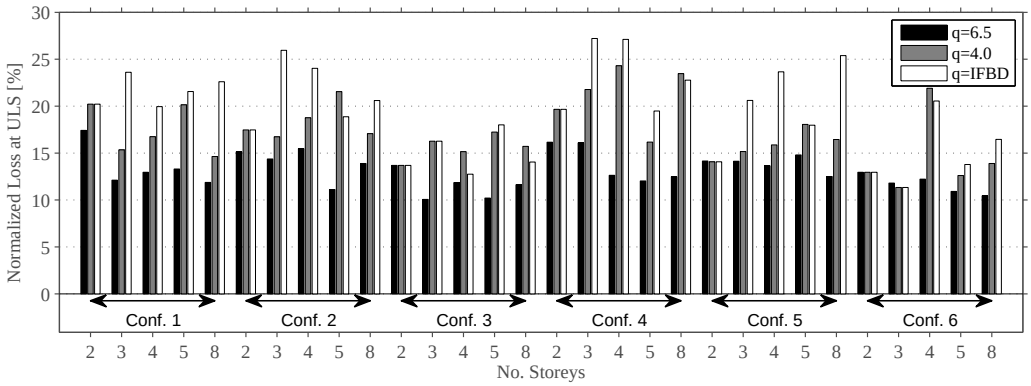

(c) Lagos

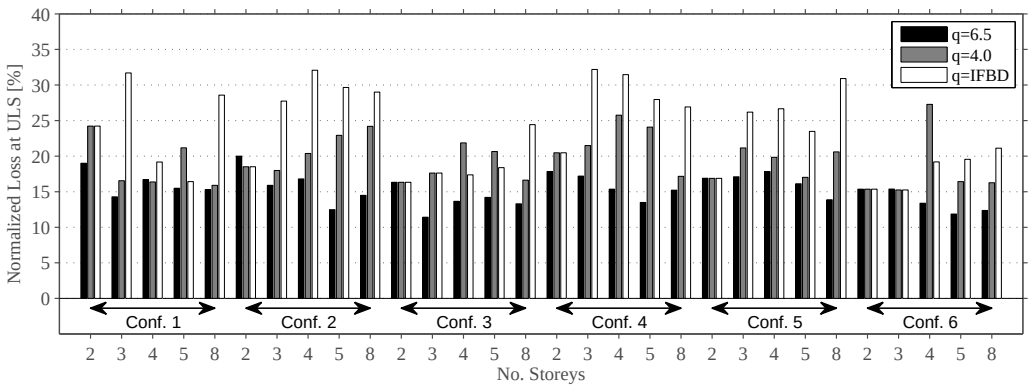

(d) Lagos (soil type C)

Figure 7.17: Normalized expected losses at the design intensity level (ULS).

contributions emerging from demolition losses. Moreover, the losses due to demolition were more noticeable when the behaviour factor adopted in the design was defined according to the IFBD procedure. For example, for three storey MRFs located in Lagos and designed using the IFBD, the contribution for the total expected repair losses at the design level intensity are: 14% from structural components, 74% from non-structural and 12% from demolition losses. Buildings designed using the behaviour factors recommended in EC8 for medium and high ductility class were mostly controlled by P-Delta stiffness requirements, resulting in much more robust/stiff structural solutions then the buildings designed using IFBD procedure. This is the underlining justification for the higher demolition losses observed. These results indicate that, even though steel MRFs designed in accordance with the requirements of EC8 are expected to have low probabilities of collapse for the design intensity leve, the level of induced damage could imply repair costs up to 33% of the building replacement value. Even for serviceability limit state (SLS) intensity level, which the code specified for controlling the level of damage for lower seismic intensities, the extent of damage can lead to repair costs of around 12% of the building replacement value.

Figure 7.18 shows the expected non-collapse losses due to repair disaggregated by storey at the design intensity level for buildings located in Lisbon.

The results shown in Figure 7.18 allow concluding about the uniform distribution of losses over the building height. Since it was assumed that the total building cost was uniformly distributed by all storeys, the results obtained point to relatively uniform lateral deformation patterns along the height. This, in turn, reveals that there is no concentration of deformation in a single or group of storeys, which often leads to the development of unstable collapse mechanisms (e.g. soft-storeys). This observation, regardless of the loss level, points to the adequacy of the capacity design procedure prescribed in EC8. Although not shown here due to space limitations, the same behaviour was observed for higher seismic intensity levels, namely for the near-collapse intensity level, and for the various site locations considered. Furthermore, no relevant influence of the behaviour factor was found in this described behaviour.

7.6.2 Expected annual losses and present value of life-cycle costs

The normalized expected annual losses, *EAL*, and corresponding present value, *PV*, of life-cycle costs are shown in Figure 7.19. Additionally, Table 7.6 and Table 7.7 summarize the average *EAL* and *PV* of life-cycle costs for each behaviour factor and number of storeys.

As one may infer from the results, the *EAL* values range between 0.0023%-0.0048%, 0.016%-0.036% and 0.01%-0.028% for Porto, Lisbon and Lagos, respectively. The consideration of a more flexible soil foundation in Lagos significantly increased the *EAL* values, with these varying between 0.028% and 0.070%. Additionally, the *EAL* values typically decrease with the increase of building height. This can be explained by the reduction of the seismic hazard with the increase of the fundamental period of vibration. Ramirez and Miranda (2012) and Haselton et al. (2010) have reported similar trends. With regard to the present value of life-cycle costs of seismic damage, the average value varies between 0.042%-0.09%, 0.30%-0.66%, 0.19%-0.52% and 0.52%-1.29% of the total replacement value for Porto, Lisbon, Lagos and Lagos soil type C, respectively. This

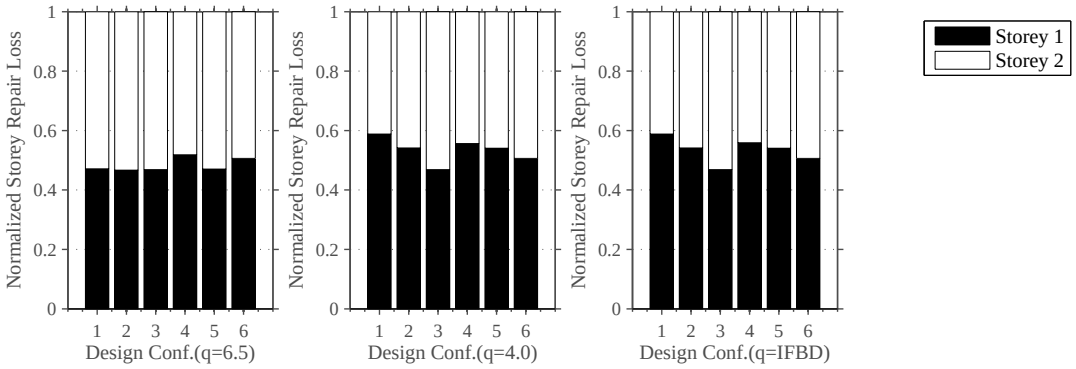

(a) 2 Storeys

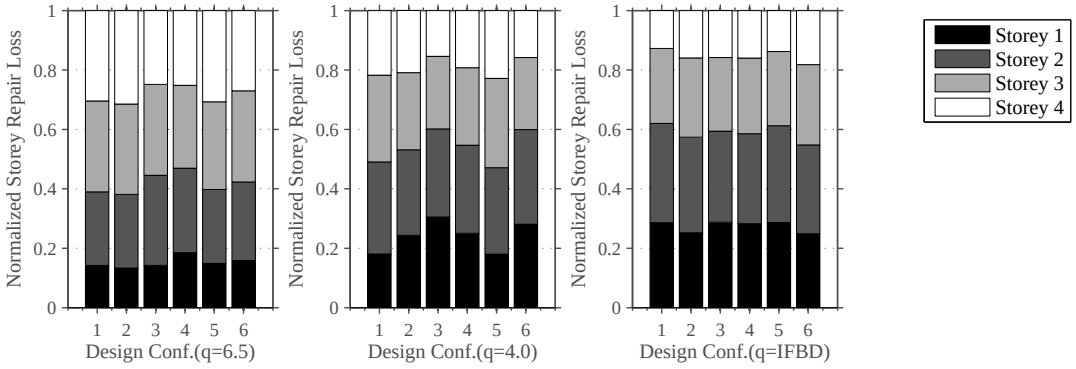

(b) 4 Storeys

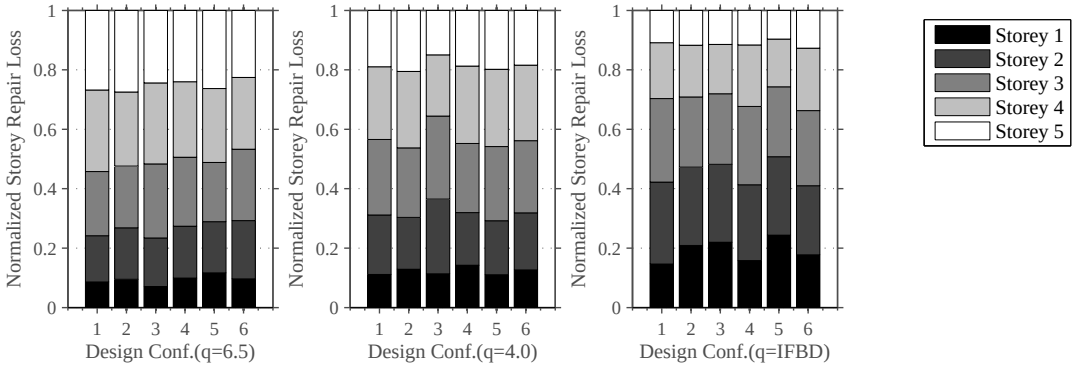

(c) 5 Storeys

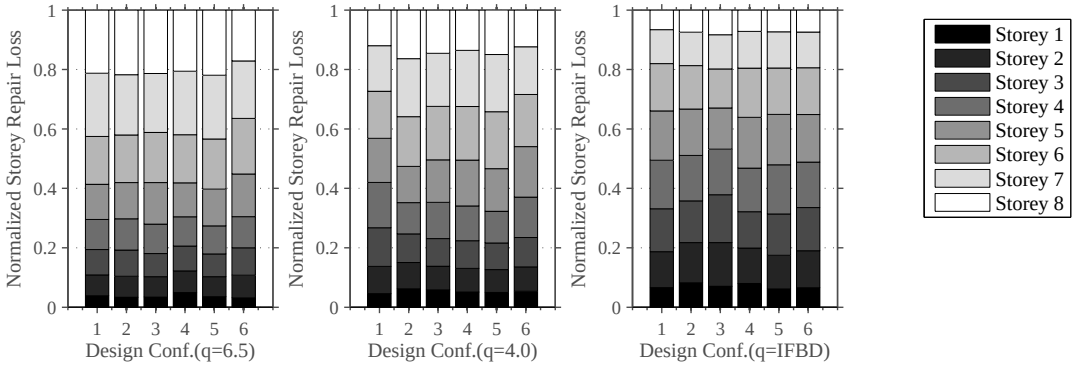

(d) 8 Storeys

Figure 7.18: Normalized storey repair losses for buildings located in Lisbon.

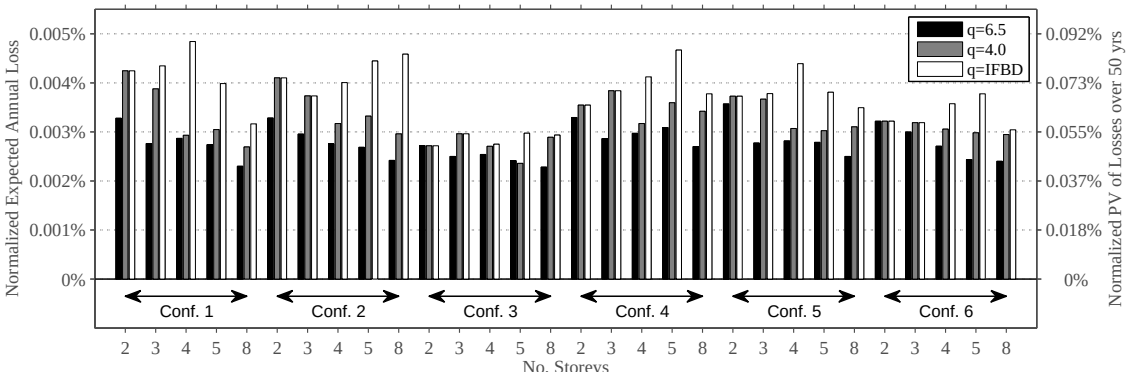

(a) Porto

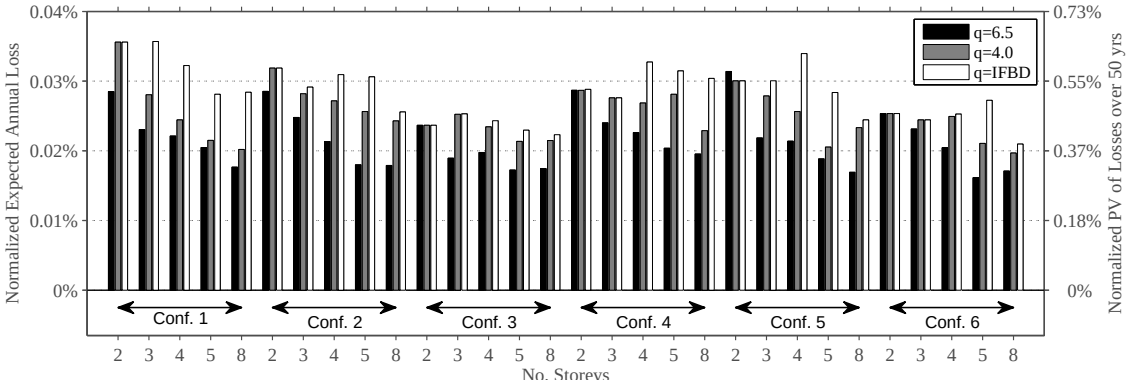

(b) Lisbon

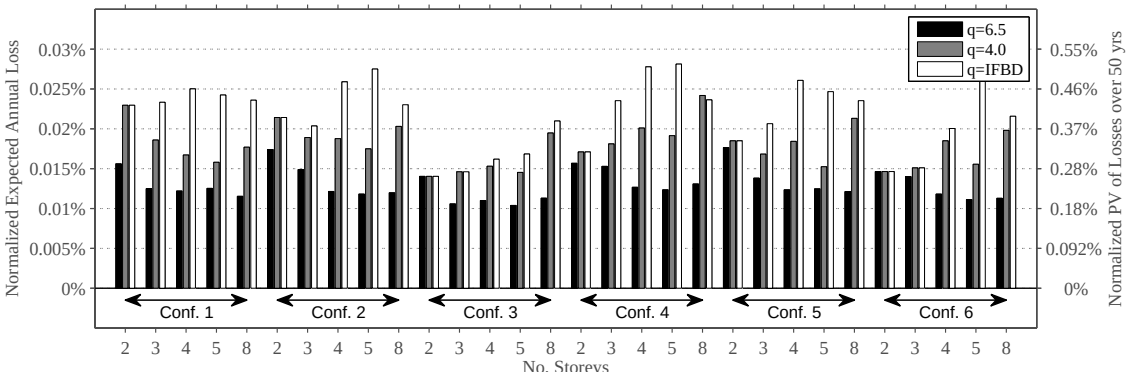

(c) Lagos

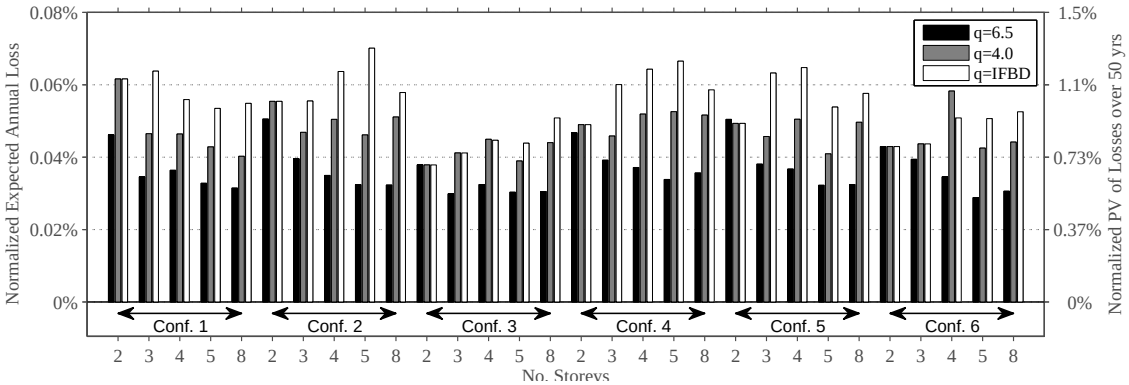

(d) Lagos (soil type C).

Figure 7.19: Normalized expected annual loss.

means that stakeholders and building owners should expect to spend between 0.042% and 0.66% of the initial construction cost in repair costs due to earthquake damage occurring during the building's service life, depending on the site location. This type of results are useful, at the design stage, for building owners and stakeholders to adopt measures aiming at the improvement of seismic performance. However, a value of 1.30% for present-value of life- cycles costs seems reasonable when compared with values obtained for code designed reinforced concrete buildings, with values ranging between 12% and 34%, as concluded by Ramirez and Miranda (2012).

Importantly, the results shown in Figure 7.17 and Figure 7.19 clearly show the advantage of adopting the *EAL* as a seismic-performance metric, in comparison with the expected loss conditioned on seismic intensity. Conversely to *EAL*, which considers all possible levels of seismic intensity weighted by the corresponding probabilities of occurrence, the expected loss conditioned on seismic intensity only considers a single intensity level (Ramirez and Miranda, 2012; Hwang and Lignos, 2017). These differences may have a considerable effect on the perception of losses in the building. For example, in Figure 7.17, the buildings located in Lisbon exhibited lower values of expected losses for the design intensity level in comparison with the buildings located in Lagos. However, when the *EAL* of the buildings is considered, the results point to the opposite conclusion, with buildings located in Lagos exhibiting the lower values of *EAL*. This demonstrates the importance of taking into account the effect of the hazard at the site location for a more appropriate quantification of the expected losses.

Finally, it should be emphasized that the obtained results of *EAL* are conditioned on the seismic hazard considered, and therefore the use of a different hazard model could lead to different results. However, the hazard model used in this research study is the most recent and available hazard model for European countries, meaning that the most up-to-date information was considered.

7.7 Conclusions

In this Chapter, a research study concerning the evaluation of earthquake losses of steel moment-resisting frames (MRFs) designed in accordance with the requirements of Part 1 of Eurocode 8 (EC8), for different ductility classes, is reported. The steel buildings were designed using the reference values of behaviour factor proposed in the European seismic code for moderate and high ductility class structures. Additionally, the Improved Force-Based Design (IFBD) procedure for the definition of the behaviour factor was also adopted. The PEER-PBEE methodology procedure with the improvements proposed by Ramirez and Miranda (2012) was implemented and used to evaluate a set of 360 steel MRF archetypes, that are representative of the Portuguese building stock. Due to the large number of buildings and corresponding difficulty to generate a realistic inventory of architectural components, the seismic losses were evaluated using a storey-based building-specific loss estimation methodology, adjusting the storey fragility and consequence models from the proposed HAZUS generic data (Ramirez and Miranda, 2012). Probabilistic seismic hazard analysis (PSHA) was conducted for the three site locations considered, with the aim of computing

the hazard curves and performing the collapse adjustment due to the spectral shape effect (Haselton et al., 2010). The hazard model used in the PSHA was obtained from the SHARE project (Woessner et al., 2015), updated with information described in recent studies (Silva et al., 2015). This is the most recent and available hazard model for European countries. The expected economic losses were based on three loss metrics: the expected losses conditioned on the seismic intensity (evaluated at EC8-3 intensity levels), the expected annual losses and the expected present value of life-cycle costs. Within the scope of the results obtained in this study, the following conclusions can be withdrawn:

- The steel MRF archetypes designed in accordance with the requirements of EC8 comply with the non-collapse criteria defined in the code for the design intensity level. However, the level of damage could imply repair costs repair costs up to 33% of the building replacement value. For the serviceability limit state (SLS) seismic intensity level, most of repair losses came from the non-structural components. The obtained values of repair costs ranged from 0% to 23% for the intensity level specified in EC8-3 and from 0% to 12% for the intensity level defined in EC8. Hwang and Lignos (2017) conducted a similar study on special steel moment-resisting frames designed according to the American design code and obtained similar results for the SLS limit state. However, for ULS intensity level, the authors reported an important contribution from the collapse losses that was not observed in the frames designed to EC8;
- The buildings designed with the IFBD procedure exhibited, in most cases, higher values of losses for all the code defined intensity levels. Moreover, an increase in the demolition losses was identified when this procedure was used;
- The influence of different soil conditions on the design caused an increase of up to 5% in the expected losses, namely when using soil type C in comparison to soil type B for buildings located in Lagos (Portugal);
- A uniform distribution of losses over the building's height was observed, revealing that there was no concentration of deformation in a single or a group of storeys, which is usually associated with the development of unstable collapse mechanisms;
- The advantages of using the Expected Annual Loss, EAL, as a performance metric or the Present-Value of life cycle costs, PV, was demonstrated. The value of EAL ranges from 0.0023% to 0.070% of the building replacement value, depending on the building location. The corresponding present-value of annualized losses over an assumed lifespan of 50 years ranges from 0.042% to 1.29%. Conversely, recent studies conducted on code-designed reinforced concrete buildings resulted in values of present-value of life cycle costs ranging from 12% to 34%.;
- Conversely to the conclusions obtained when assessing the expected losses for the design intensity level, the buildings located in Lagos exhibited lower values of EAL and PV of life cycle costs relatively to buildings located in Lisbon.

Finally, it should be mentioned that, despite the good performance of the buildings for the ULS as defined in EC8, the associated value of repair costs for that seismic intensity level is significant. Moreover, repair costs up to 22% for the SLS limit state seem fairly excessive. As previously mentioned, most of the repair costs for the lower intensities are associated to non-structural components. It is therefore critical that the next generation of seismic codes incorporate more detailed specifications that take into consideration the relevant influence of these components on the performance of buildings.

Chapter 8

Conclusions and Future Developments

8.1 Conclusions

In this thesis, the seismic performance of steel moment-resisting framed (MRF) buildings designed to Eurocode 8 was investigated. Several subjects were addressed in order to better understand the response and performance of current code-designed steel MRF buildings when subjected to earthquake excitations. Throughout the document, the main findings and conclusions were provided in a detailed manner. In the following paragraphs, the main conclusions and observations are summarised.

In Chapter 2, the current European seismic design framework for steel MRF buildings, as delineated in Part 1 of Eurocode 8 (EC8-1, (CEN, 2005c)), was thoroughly detailed. A comprehensive set of archetype buildings was designed, considering several parameters that encompass the archetypical workspace considered (e.g. building configuration, number of storeys and seismic location). These buildings were designed using both code-recommended upper-bound reference levels of the behaviour factor (as per two different ductility classes of the code), as well as with the Improved Force-Based Design (IFBD) procedure proposed by Villani et al. (2009). In total, 360 archetypes were considered. Generally speaking, it was found that buildings designed with code-specified behaviour factors were typically controlled by stiffness requirements associated with the control of second-order effects. This was related with the current formulation of the inter-storey drift sensitivity coefficient (θ), which was shown to be directly proportional to the adopted value of the behaviour factor. As a consequence of the design-governing criterion being unrelated to demand-to-capacity checks, such archetypes were typically associated with significant overstrength levels. Nonlinear analyses demonstrated a general discrepancy between the design assumptions and the actual structural response, with buildings designed for a high ductility class remaining elastic for the seismic design intensity level. This inconsistency, which is a consequence of the aforementioned high overstrength levels, all but defeats the purpose of employing a behaviour factor in the design process to begin with. Furthermore, and in line with the main findings of Peres and Castro (2010), the values of θ associated with the design estimates and the response-history analyses differed considerably. To what concerns the application of the IFBD

for the selection of the behaviour factor, this procedure was found to provide the designer with a more realistic and accurate prediction of the actual structural response, and, consequently, of the expected inelastic demands. Structural overstrength levels were generally minimised, meaning that the design base shear matches well the design estimates of lateral strength of the MRF. In basic terms, the IFBD-based archetypes were found to take better advantage of the available structural ductility under the design earthquake demands, precisely due to the fact that the level of overstrength (strictly in terms of demand-to-capacity relation in a seismic context) is minimised. Furthermore, significant material savings were generally achieved with this approach since the aforementioned limitations of the currently-prescribed formulation of (θ) are addressed. It is important to note that these benefits came not at the detriment of seismic performance. Compliance with damage limitation and non-collapse limit states was generally observed across all archetypes, including those designed with IFBD-based behaviour factors. Additionally, no evidence was found of the formation of undesirable soft-storey mechanisms in any of the buildings considered in this study, under the design seismic intensity level. Finally, comparisons of mean annual frequency of collapse, or seismic risk, showed that, despite the higher values exhibited by IFBD-based archetypes, all buildings complied with the limit proposed by Pinto and Franchin (2014).

In Chapter 3, a research study was conducted with the aim of evaluating the appropriate strength and stiffness deterioration parameters of the Ibarra et al. (2005) hysteretic model for laterally-restrained steel elements made with standard European open-section profiles. It was demonstrated that the recent Lignos and Krawinkler (2012) proposal for these parameters, which was obtained from calibration of an extensive database with more than 350 experimental tests carried out on typical American steel profiles, does not seem to lead to reliable cyclic flexural response predictions of typical European profiles. This is because both construction industries (i.e. European, American) make use of different standardised web and flange slenderness levels, aspects of vital importance to the strength and stiffness deterioration parameters. As such, an efficient calibration procedure was proposed and implemented. Through a detailed FE model developed in ANSYS (ANSYS, 2013), accurate simulations of the monotonic and cyclic flexural response of steel members were accomplished. This was attained by validation against experimental data available in the literature (D'Aniello et al., 2012). A calibration procedure was then implemented to obtain the optimum combination of strength and deterioration parameters of the Ibarra et al. (2005) hysteretic model in OpenSees McKenna (2011), that entail the most appropriate match between the "exact" response (i.e. that obtained with ANSYS) and the simplified model (i.e., the one obtained with OpenSees). This procedure makes use of the Harmony Search meta-heuristic optimization algorithm (Geem et al., 2001). With the framework adopted, trial-and-error approaches to determine the optimum set of degradation parameters are avoided, which may be both extremely demanding in terms of computational effort and entail excessive ambiguity in the definition of the optimum solution. Through the simulation of an existing full-scale experimental test of a steel moment-resisting frame under lateral loads Ryu et al. (2011), this calibration procedure was validated. Finally, the framework was applied to a comprehensive set of stan-

dard European steel open-section profiles, allowing for the proposal of nonlinear-regression-based prediction equations for the Ibarra et al. (2005) degradation parameters in the European context. These equations are of singular interest and convenience for application in simplified numerical modelling of European steel members through a concentrated plasticity approach.

In Chapter 4, the seismic design of the so-called panel zone region (i.e. beam-column intersection region) in steel moment-resisting frame buildings was addressed. A critical overview of the European design requirements was conducted in which the most important difficulties and inconsistencies were identified. In order to address both aspects, a design procedure based on the combination of European and American guidelines was proposed. In basic terms, this procedure seeks to distribute the plasticity between the beams and the panel zone, whilst avoiding excessive deformation in the panel zone and the development of shear buckling. Several archetypes were utilised to demonstrate the influence of the panel zone design approach on the local and global responses of steel MRFs. By resorting to nonlinear static and response-history analyses, the global response of the structures was shown to be insensitive to the panel zone design approach adopted. However, it is worth mentioning that the design of the panel zone can have a direct influence on the lateral capacity of the building. Furthermore, it was demonstrated that the dynamic properties of a MRF can be evaluated without explicit consideration of the panel zone in the numerical models. Adoption of balanced panel zones, in accordance to the proposed procedure, allows for a reduction of the inelastic demands imposed to the beams, without excessive deformation of the panel zones. Moreover, the panel zone distortion was found to comply with the imposed distortion limit of 4γ, associated with non-collapse-related design checks (ULS). This value corresponds to the formation of plastic hinges in the column flanges and was defined as the distortion limit to avoid excessive deformation of the panel zones, which may be problematic in welded connections. From probabilistic seismic performance assessment, it was inferred that collapse fragility was generally unaffected by the panel zone design criteria. Such lack of sensitivity was also observed to what concerns the levels of residual lateral deformations. Furthermore, panel zone distortion fragility functions showed very low probability of exceedance of the 4γ distortion limit, for the seismic design intensity level.

In Chapter 5, the development of SelEQ, an advanced ground motion selection and scaling framework, was detailed. This tool allows for a reliable code-based and probabilistic-based record selection to be conducted, an aspect of particular relevance within the Earthquake Engineering community. In particular, one should emphasise one of the major advances of the tool, namely the possibility to compute the Conditional Mean Spectrum (CMS) Baker (2010) for the European territory. To this end, SelEQ makes use of the open source platform OpenQuake Pagani et al. (2014), coupled with the recently proposed SHARE seismic hazard model Woessner et al. (2015). Additionally, SelEQ is able to perform code-based record selection incorporating advanced criteria, namely the control of spectral mismatch between the spectrum of each individual record and the target response spectrum, which provides significant improvements in terms of mean structural response estimates. SelEQ makes use of the Adaptive Harmony Search (Hasançebi et al., 2009) meta-heuristic optimization algorithm. Both the efficiency and robustness of the tool was shown

via two application examples, namely a code-based and a CMS-based ground motion record selections.

In Chapter 6, the methodology proposed in the FEMA P695 (FEMA, 2009) guideline, aimed at the evaluation of the performance factors and collapse performance of new structural systems, was applied to the archetype suite previously outlined in Chapter 2. These buildings, whose main characteristics reflect the existing building stock in Portugal, were designed according to EC8 using different behaviour factors (i.e. code-based, according to two different ductility classes, and IFBD-based). From the results obtained, all archetype buildings, regardless of the behaviour factor adopted at the design stage, were found to comply with the the performance evaluation criteria by a considerable margin. This was found to highlight the exceptional seismic performance of steel MRFs, designed in a European context, when subjected to earthquake ground motions. Furthermore, frames designed using the EC8-proposed behaviour factors showed remarkably high values of acceptance collapse margin ratios (ACMR). This was mainly due to the fact that, in those cases, seismic design was mainly controlled by stiffness requirements related with the control of second-order effects, which entailed significant lateral demand-to-capacity (i.e. overstrength) levels. Moreover, the frames designed with IFBD-based behaviour factors exhibited more predictable behaviour, demonstrating the advantage of adopting behaviour factors based on the actual properties of the structure and on the seismic hazard level. As concluded in Chapter 2, the use of IFBD was also shown herein to not be detrimental to the collapse performance. Full compliance with the EC8 no-collapse requirement was observed for all archetypes. Moreover, a sensitivity analysis to gauge the influence of the Spectral Shape Factor (SSF) on the performance evaluation was conducted, indicating that the use of the FEMA P695-specified SSF seems appropriate.

Finally, in Chapter 7, earthquake-induced economic losses were evaluated for all the archetype buildings considered in the previous chapters. The PEER Performance-Based Earthquake Engineering methodology (Porter, 2003), with the improvements proposed by Ramirez and Miranda (2012), was implemented and used. The expected economic losses, computed trough a simplified storey-based loss assessment approach (Ramirez and Miranda, 2009), were based on three loss metrics: i) expected losses conditioned on the seismic intensity level of interest (evaluated for the EC8-1 and EC8-3 intensity levels defined for ordinary buildings); ii) the expected annual losses, EAL; and iii) expected present value of life-cycle costs, PV. Regarding the latter two loss metrics, one should emphasise their increased significance in relation to the first one, since they reflect the expected economic loss levels across different hazard levels when convoluted with the corresponding probabilities of occurrence. From the obtained results, it was possible to conclude that steel MRF archetypes designed in accordance with EC8-1 comply with the non-collapse performance requirement defined in the European code for the design level intensity. However, the levels of damage incurred could entail reparation costs up to 33% of the building's replacement value. For a serviceability limit state (SLS) intensity level, it was found that most of the repair losses result from damage to non-structural contents. The obtained values of repair costs range from from 0% to 23% for the intensity level specified in EC8-3 and from 0% to 12% for the intensity level defined in EC8-1. Hwang and Lignos (2017) conducted a similar study on special steel moment-

resisting frames designed according to the American design code and obtained similar results for the SLS limit state. However, for the ULS intensity level, the authors reported an important contribution from the collapse losses that was not observed in the frames designed to EC8-1. This, once again, denotes the general notion of previous chapters: EC8-designed MRFs seem to exhibit exceptional performance against collapse. Moreover, the buildings designed with IFBD-based behaviour factors exhibited higher levels of total economic losses for all the code-defined intensity levels. Moreover, an increase in the demolition losses when this procedure is adopted was also observed. Also interesting, comparison of the results for the different soil conditions considered in the design process, indicated an increase of up to 5% in the expected loss level, namely when using type C comparatively to type B soil. To what pertains more comprehensive loss metrics, *EAL* levels ranged between 0.0023% to 0.070% of the building's replacement value, depending on the location. The corresponding present-value of annual losses over an assumed lifespan of 50 years ranged from 0.042% to 1.29%, significantly lower than that obtained in recent studies for code designed reinforced concrete buildings (12% to 34%, as denoted by Ramirez and Miranda (2012)). Finally, it is also relevant to highlight that, despite the good performance of the buildings for the ULS as defined in EC8-1, the observed repair costs were significant. Moreover, repair costs up to 22% for the SLS limit state seem fairly excessive. As previously mentioned, most of the repair costs for the lower intensities are associated to damage to non-structural contents. It is therefore critical that the next generation of seismic codes incorporate more detailed specifications that take into consideration the relevant influence of these components on the performance of buildings.

8.2 Future Developments

The research work presented in this thesis dealt with the seismic performance of steel moment-resisting framed (MRF) buildings designed to Eurocode 8. Several topics have been addressed, namely: code-based design procedures, numerical modelling of the behaviour of steel elements including stiffness and strength deterioration effects, ground motion record selection and scaling, collapse assessment and loss assessment. Throughout the thesis, several topics were identified as requiring additional research:

- Chapter 3 addressed the calibration of strength and stiffness deterioration parameters for European steel open-sections. One of the limitations previously identified in Chapter 3 is related with the fact that the obtained strength and stiffness deterioration parameters were based in only one steel material and all the parameters have been derived for the same element length. Extension of the current work should consider variation of the material properties, element length and uncertainties related with the cross-section dimensions. Moreover, the effect of axial loads should also be considered;
- Regarding Chapter 4, experimental work on the characterization of the cyclic behaviour of beam-to-column joints is required in order to have a better understanding of the influence of adopting "balanced" panel zones on the behaviour of steel moment-resisting frames;

- As previously mentioned in Chapter 5, SelEQ follows a modular architecture. Currently SelEQ enables ground motion record selection and scaling only based on one intensity measure ($S_a(T_1)$). A significant improvement could be the implementation of the generalised conditional intensity measure (GCIM) approach proposed by Bradley (2010) that considers multiple intensity measures (e.g. PGA, SA, PGV, Duration);
- In Chapter 6 a sensitivity study was conducted to assess the influence of using the FEMA P695 (FEMA, 2009) spectral shape factors (SSF) to European regions. However, the number of examined archetypes was limited and possible generalisations for this and other building typologies in the European territory requires additional research.
- With respect to the loss assessment framework adopted in Chapter 7 a possible improvement could be achieved by applying a more robust loss estimation framework based on the realistic inventory of structural and architectural components (FEMA, 2012a,b).

Appendix A

Calibration of strength and stiffness deterioration parameters for European steel profiles

In the following figures a summary of the calibration of the Ibarra et al. (2005) model parameters for European steel profiles is shown.

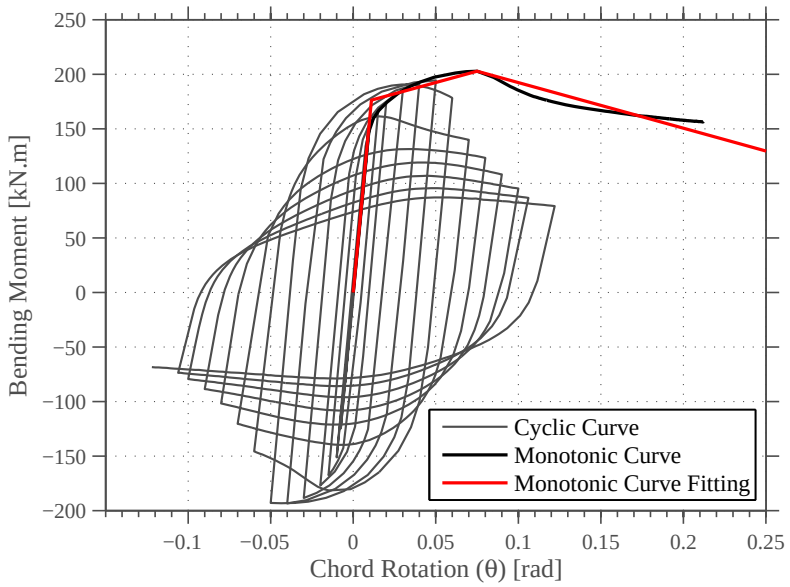

(a) Monotonic backbone calibration: IPE270.

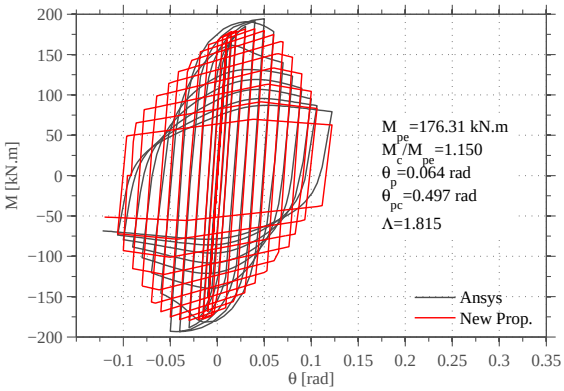

(b) Proposal

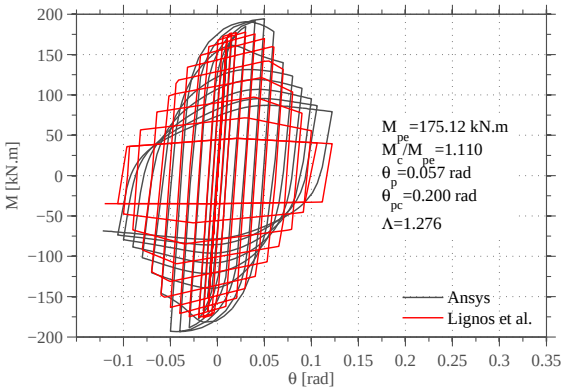

(c) Lignos and Krawinkler (2012)

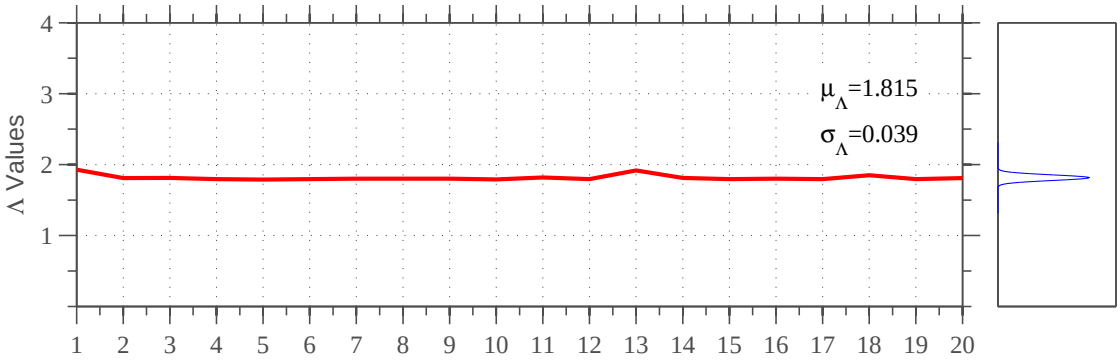

(d) Calibration Stability.

Figure A.1: Ibarra et al. (2005) calibration: IPE270.

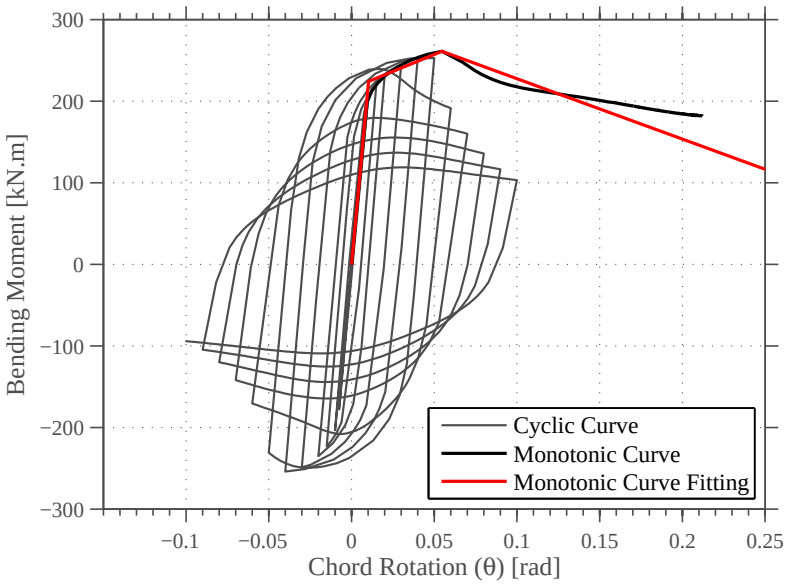

(a) Monotonic backbone calibration: IPE300.

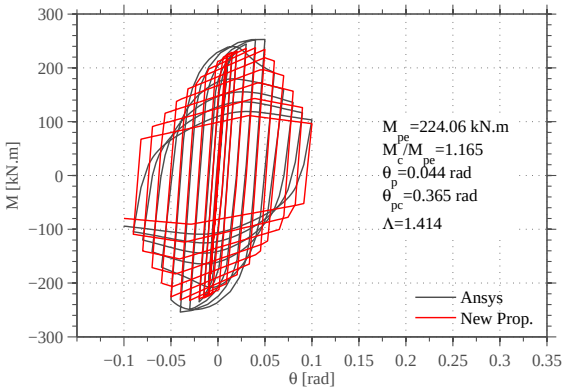

(b) Proposal

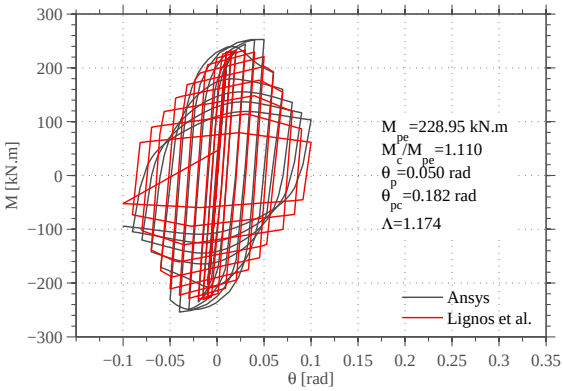

(c) Lignos and Krawinkler (2012)

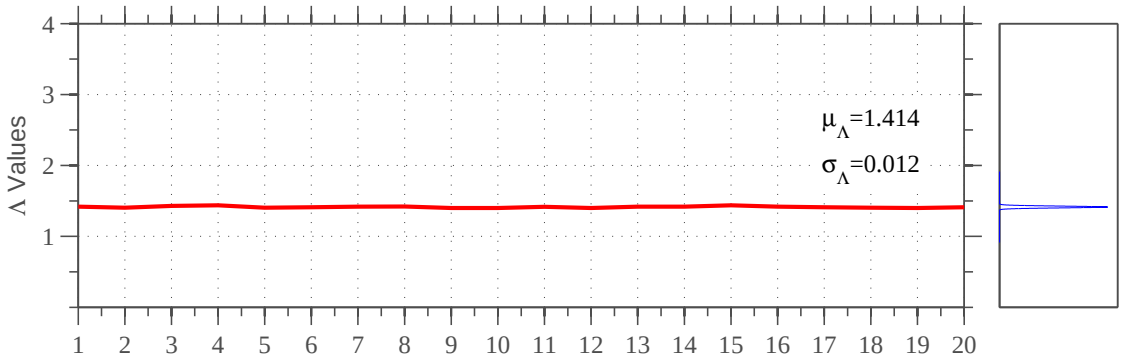

(d) Calibration Stability.

Figure A.2: Ibarra et al. (2005) calibration: IPE300.

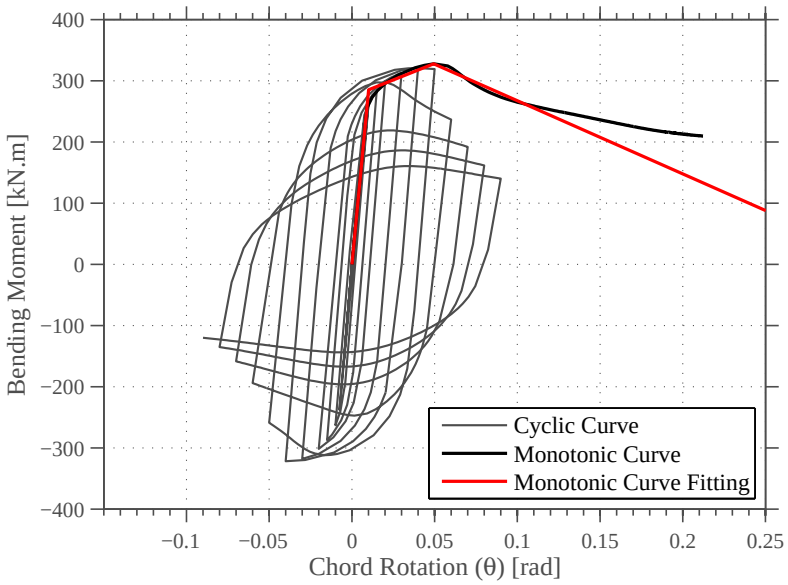

(a) Monotonic backbone calibration: IPE330.

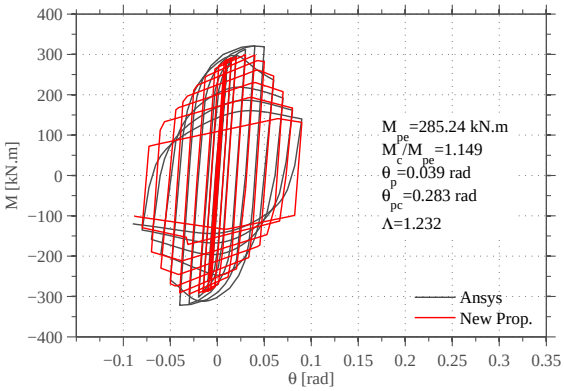

(b) Proposal

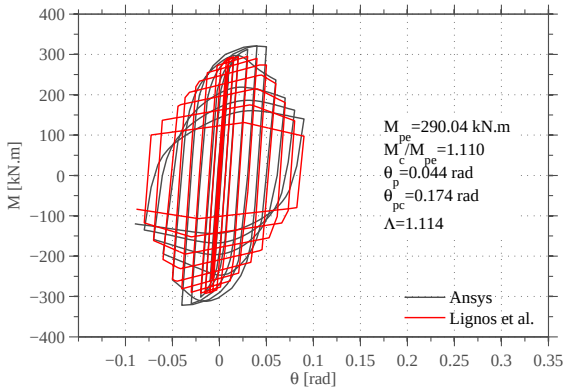

(c) Lignos and Krawinkler (2012)

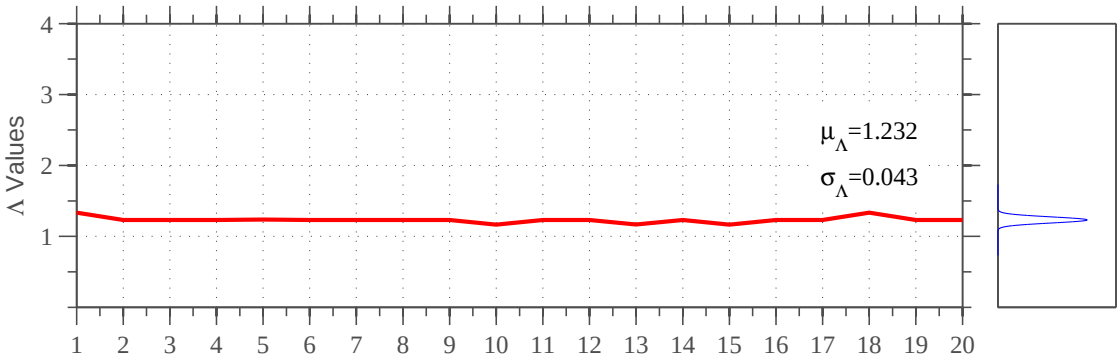

(d) Calibration Stability.

Figure A.3: Ibarra et al. (2005) calibration: IPE330.

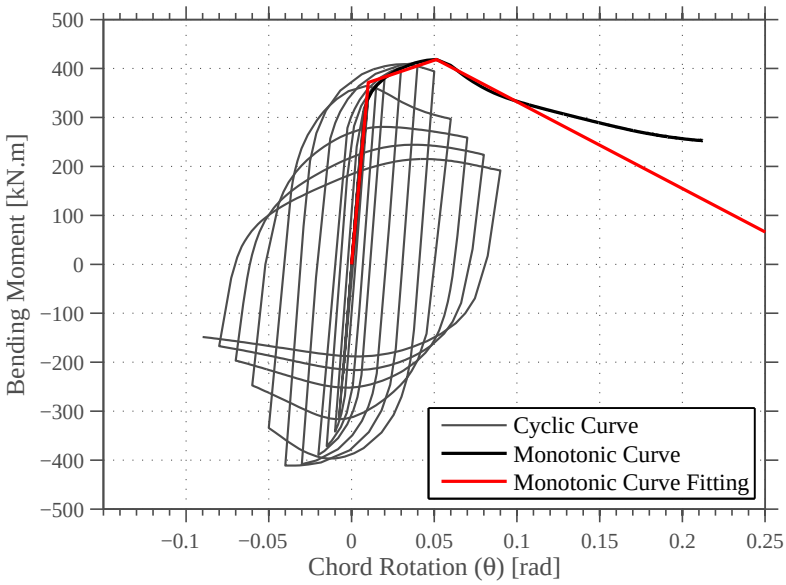

(a) Monotonic backbone calibration: IPE360.

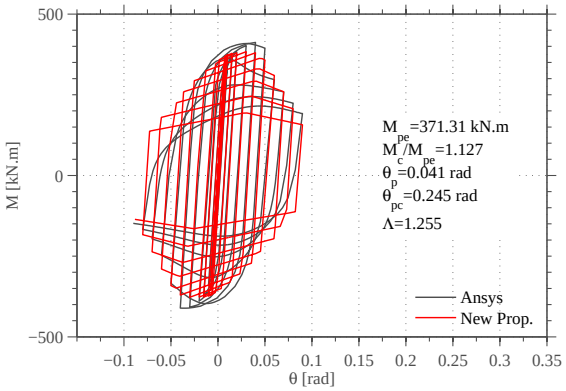

(b) Proposal

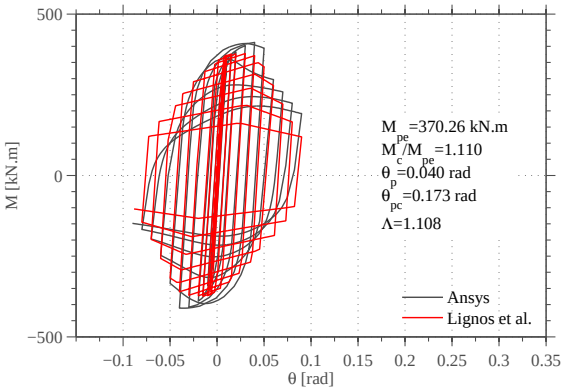

(c) Lignos and Krawinkler (2012)

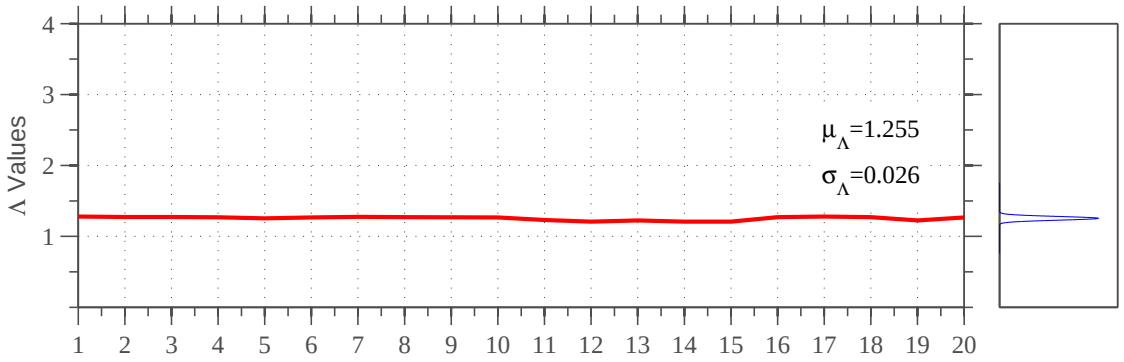

(d) Calibration Stability.

Figure A.4: Ibarra et al. (2005) calibration: IPE360.

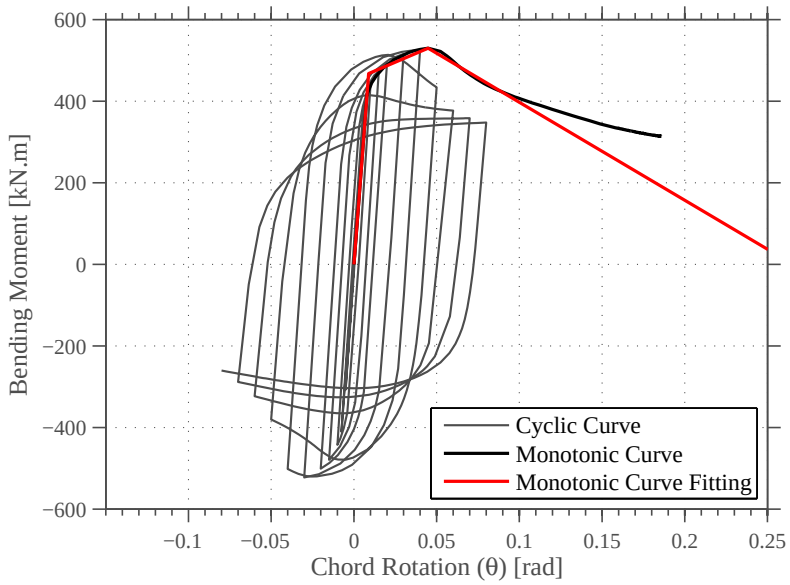

(a) Monotonic backbone calibration: IPE400.

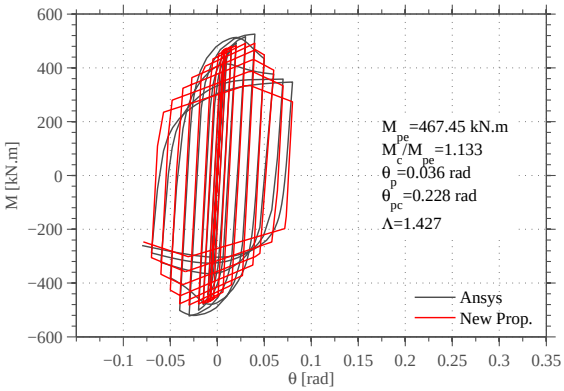

(b) Proposal

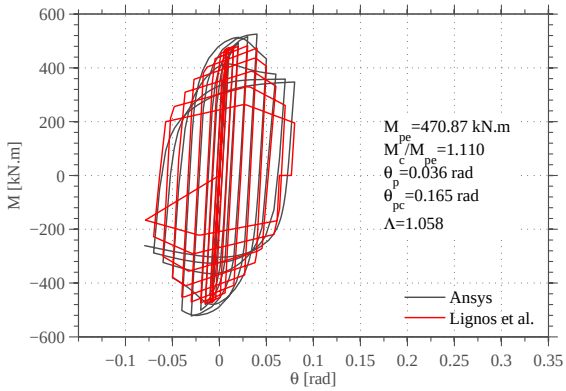

(c) Lignos and Krawinkler (2012)

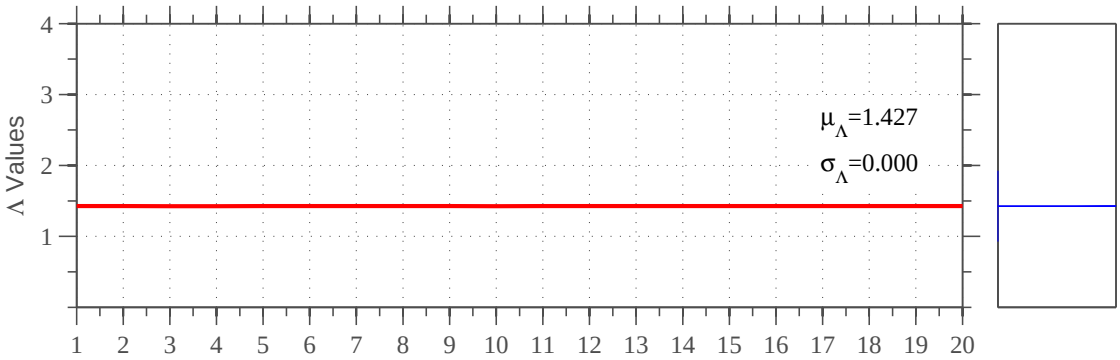

(d) Calibration Stability.

Figure A.5: Ibarra et al. (2005) calibration: IPE400.

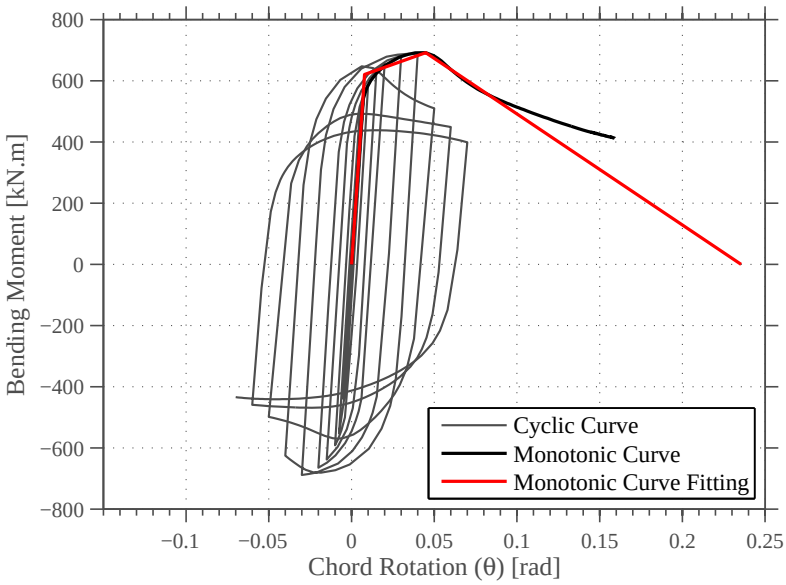

(a) Monotonic backbone calibration: IPE450.

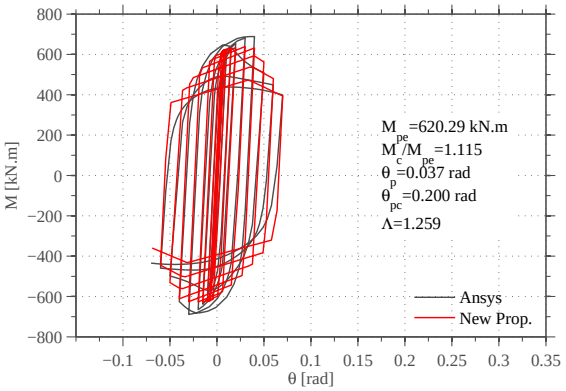

(b) Proposal

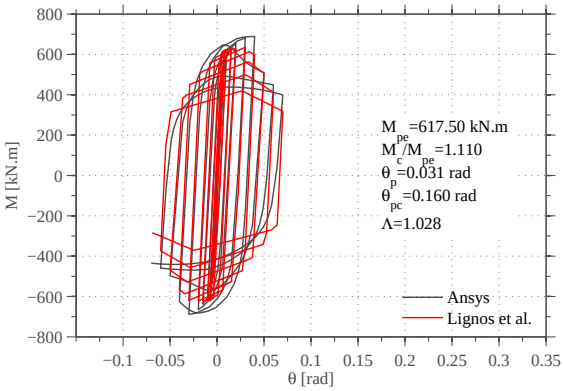

(c) Lignos and Krawinkler (2012)

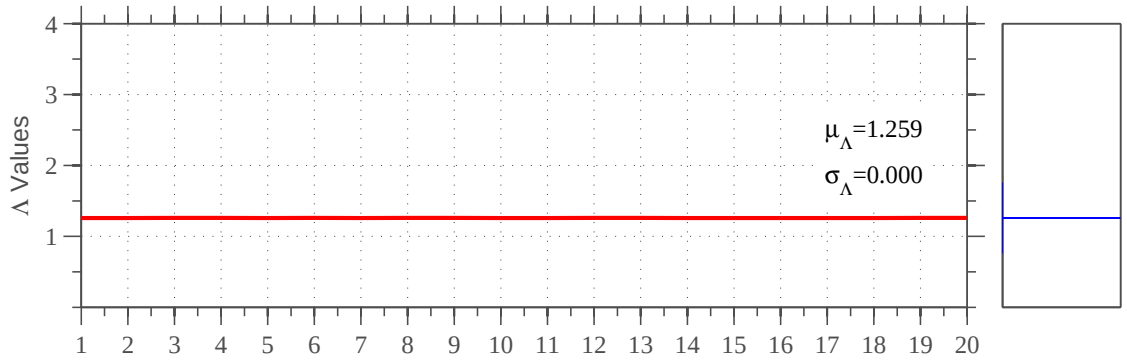

(d) Calibration Stability.

Figure A.6: Ibarra et al. (2005) calibration: IPE450.

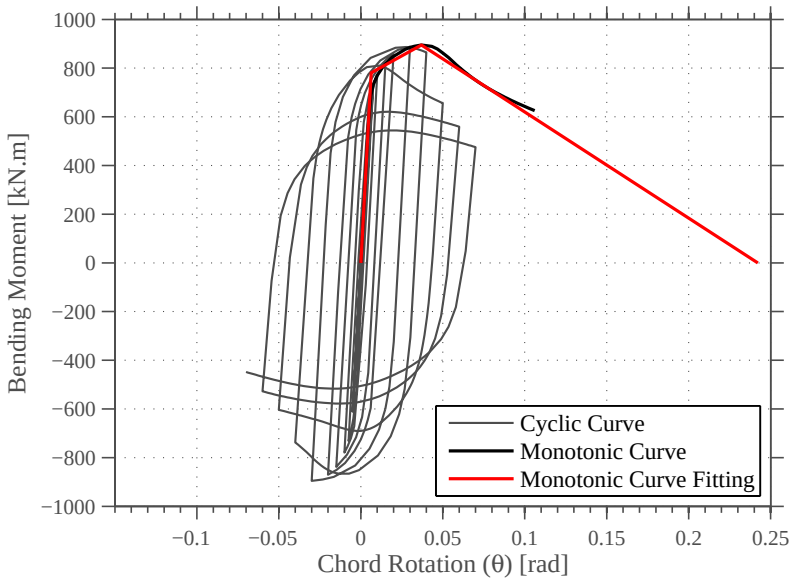

(a) Monotonic backbone calibration: IPE500.

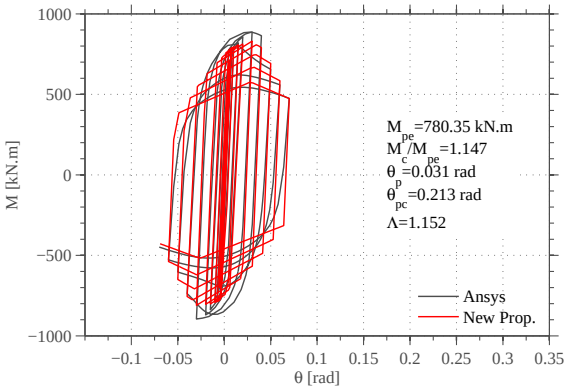

(b) Proposal

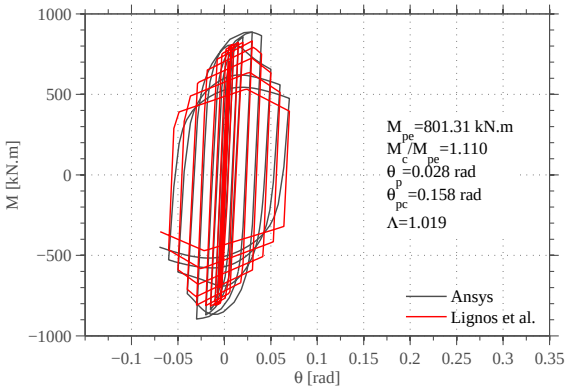

(c) Lignos and Krawinkler (2012)

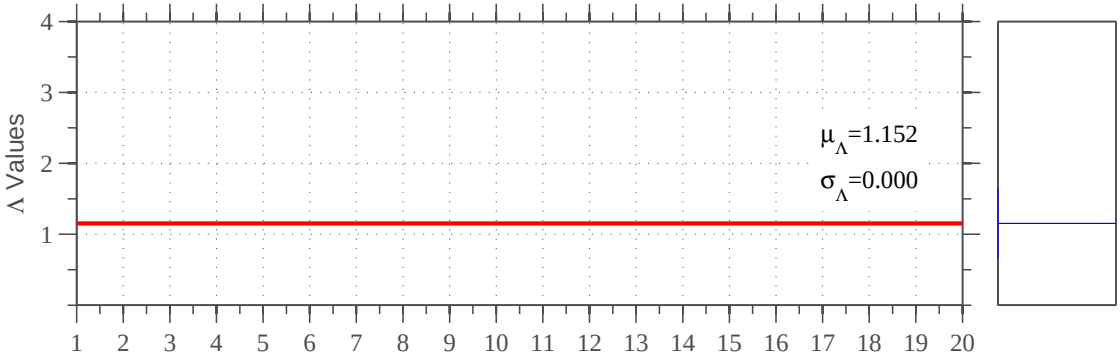

(d) Calibration Stability.

Figure A.7: Ibarra et al. (2005) calibration: IPE500.

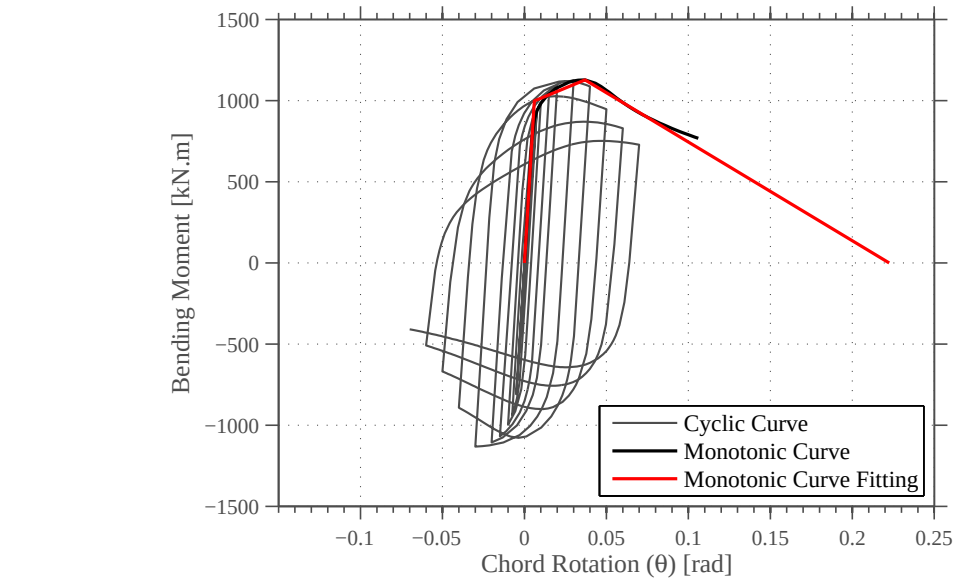

(a) Monotonic backbone calibration: IPE550.

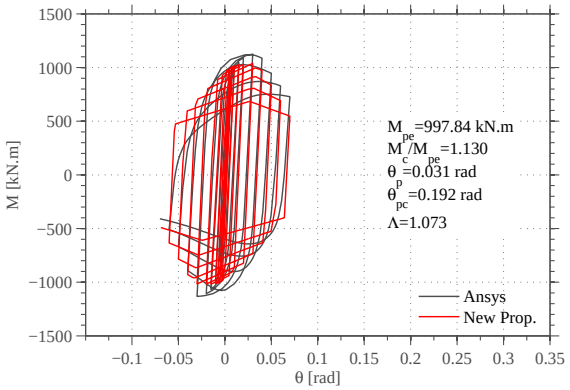

(b) Proposal

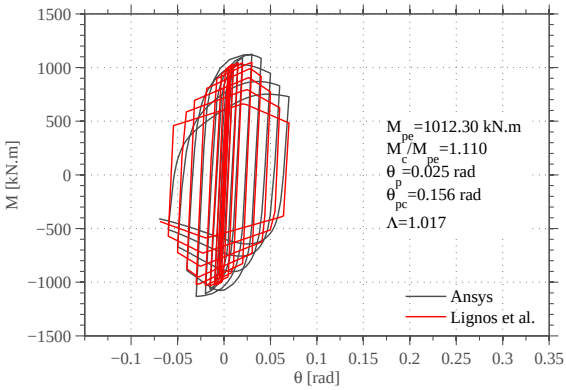

(c) Lignos and Krawinkler (2012)

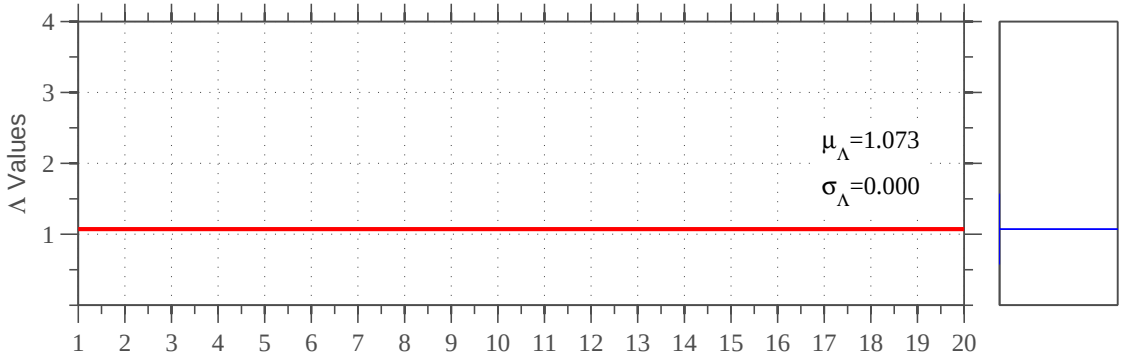

(d) Calibration Stability.

Figure A.8: Ibarra et al. (2005) calibration: IPE550.

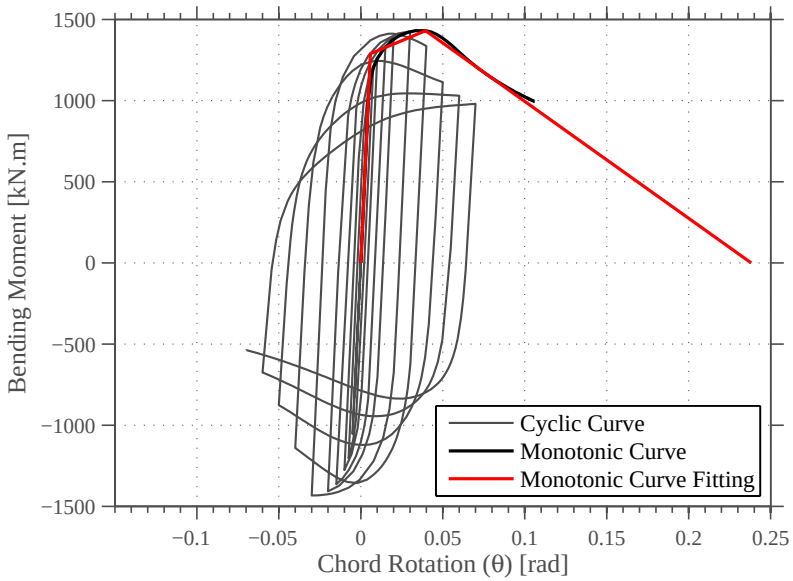

(a) Monotonic backbone calibration: IPE600.

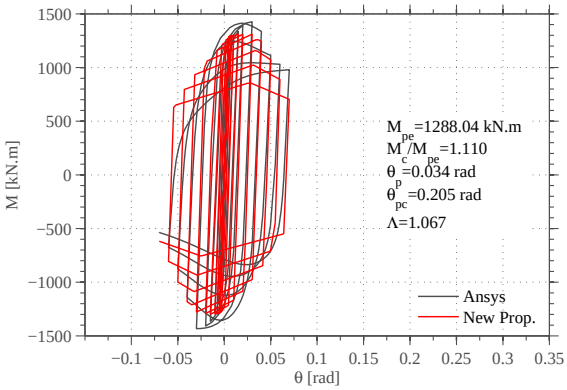

(b) Proposal

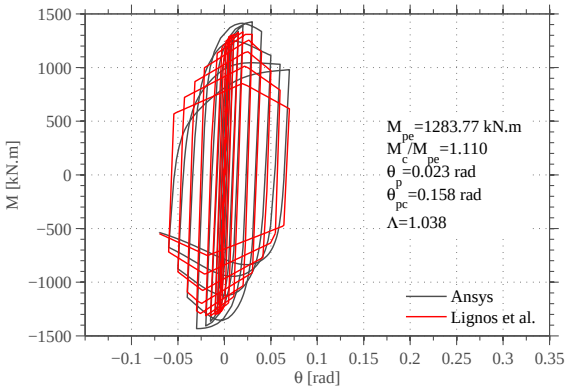

(c) Lignos and Krawinkler (2012)

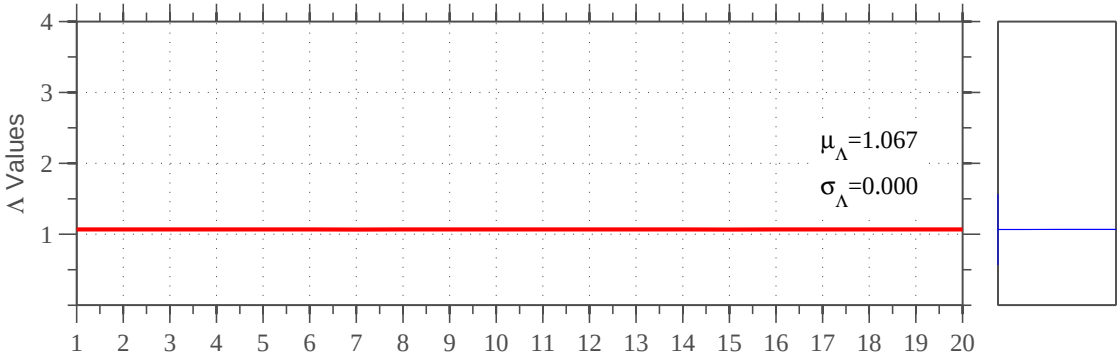

(d) Calibration Stability.

Figure A.9: Ibarra et al. (2005) calibration: IPE600.

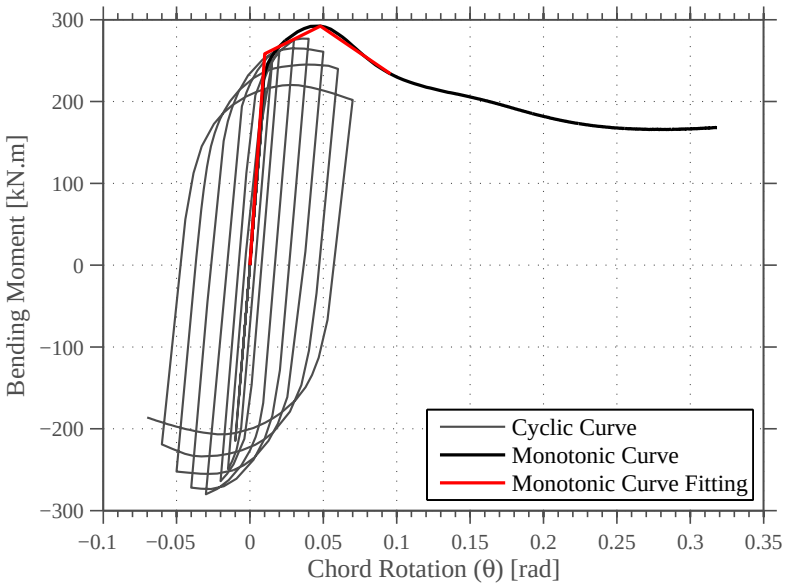

(a) Monotonic backbone calibration: HEA240.

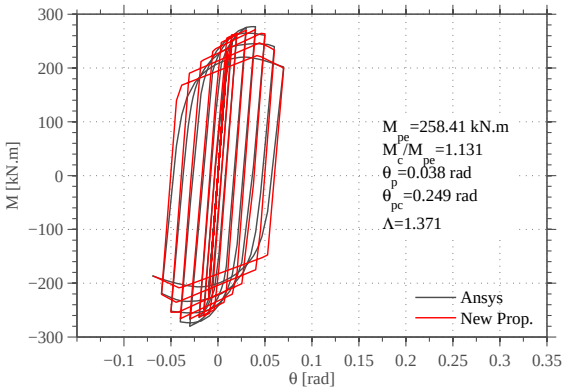

(b) Proposal

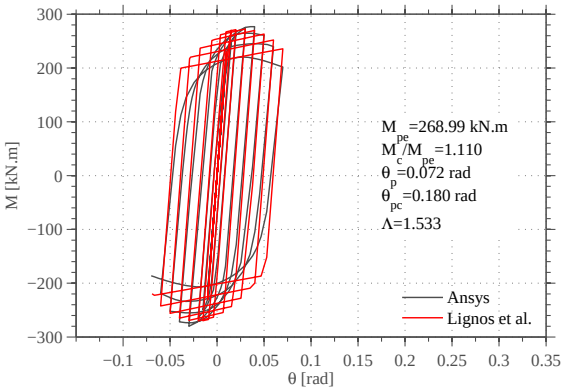

(c) Lignos and Krawinkler (2012)

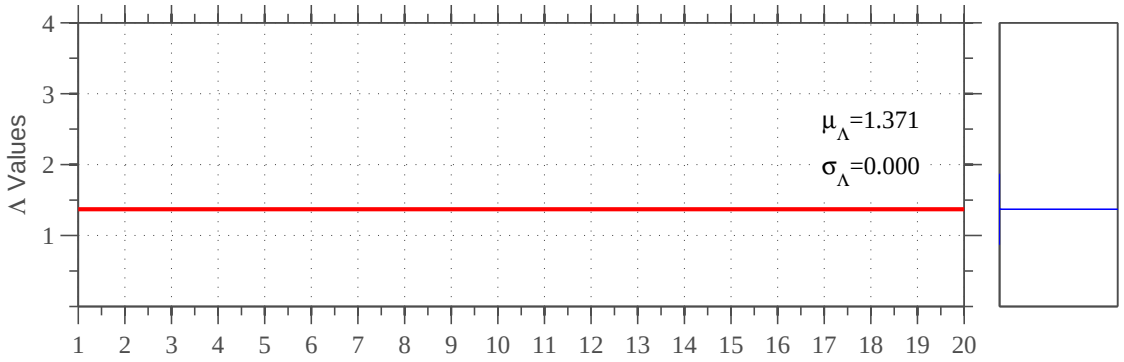

(d) Calibration Stability.

Figure A.10: Ibarra et al. (2005) calibration: HEA240.

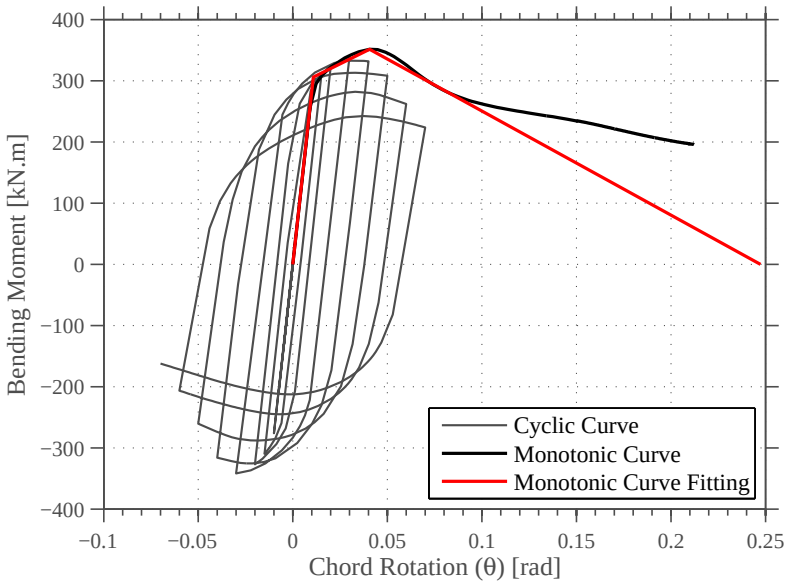

(a) Monotonic backbone calibration: HEA260.

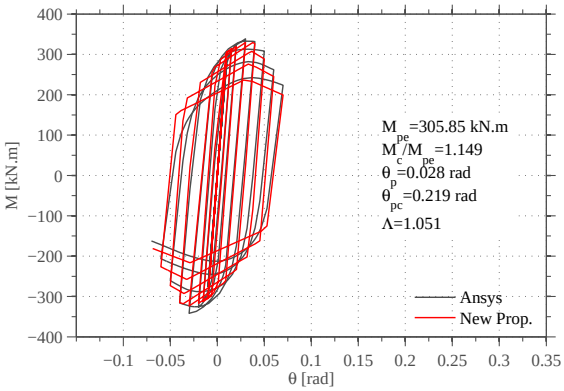

(b) Proposal

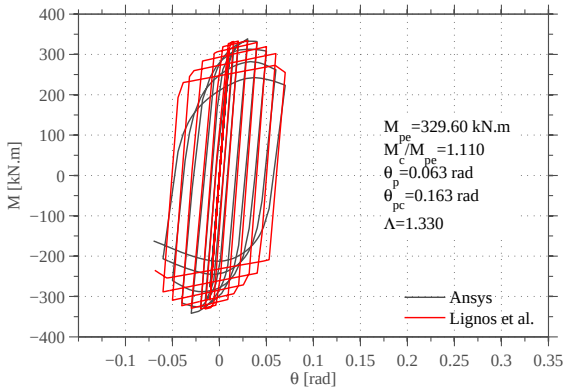

(c) Lignos and Krawinkler (2012)

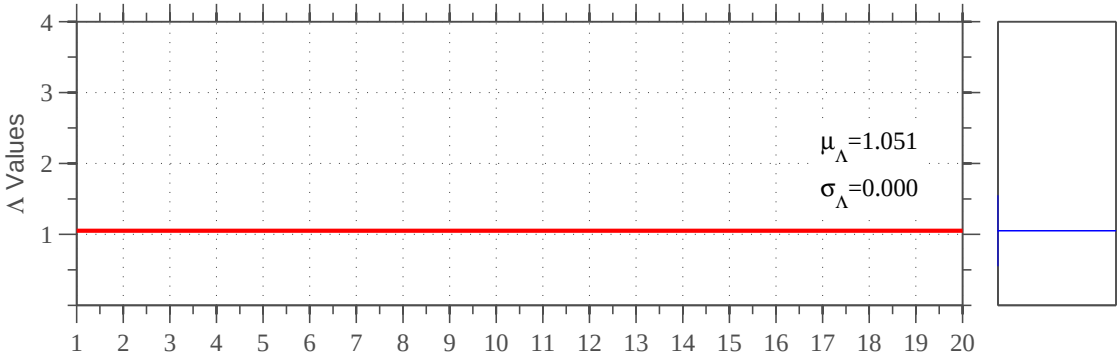

(d) Calibration Stability.

Figure A.11: Ibarra et al. (2005) calibration: HEA260.

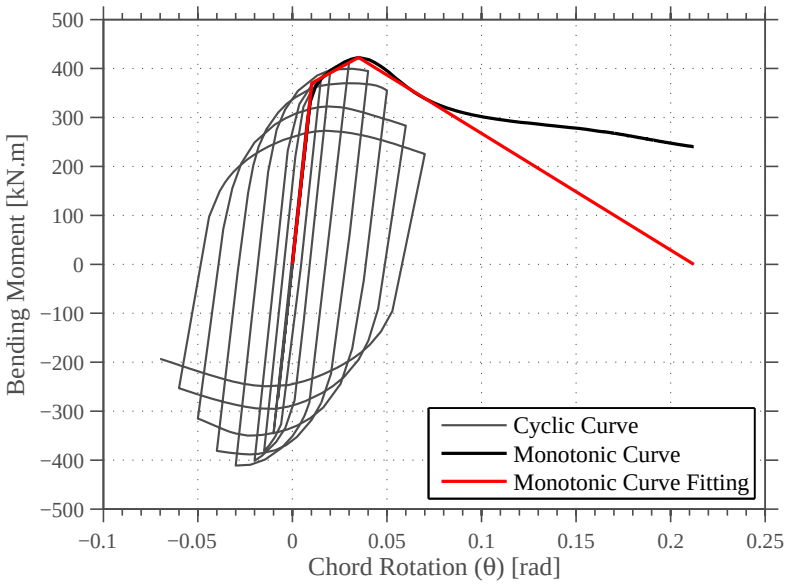

(a) Monotonic backbone calibration: HEA280.

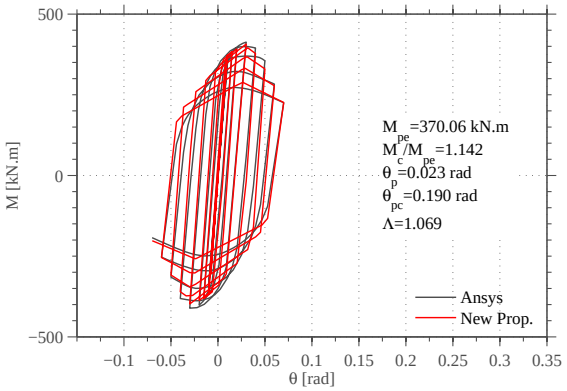

(b) Proposal

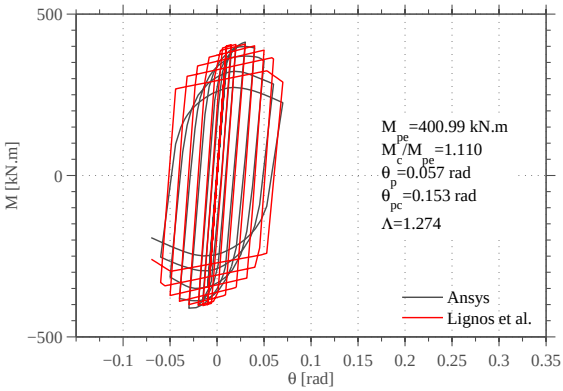

(c) Lignos and Krawinkler (2012)

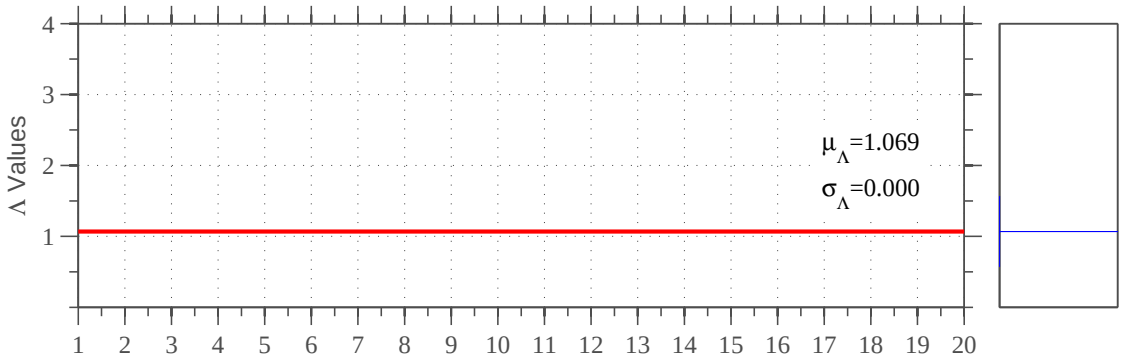

(d) Calibration Stability.

Figure A.12: Ibarra et al. (2005) calibration: HEA280.

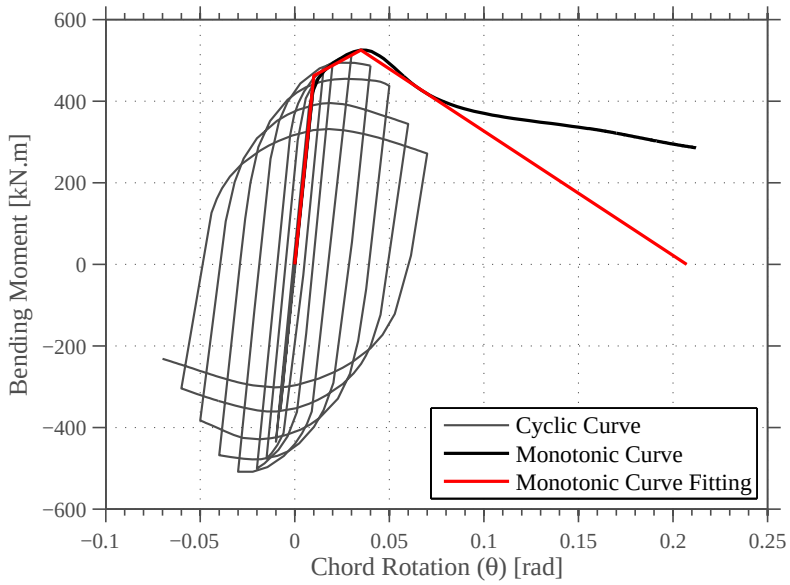

(a) Monotonic backbone calibration: HEA300.

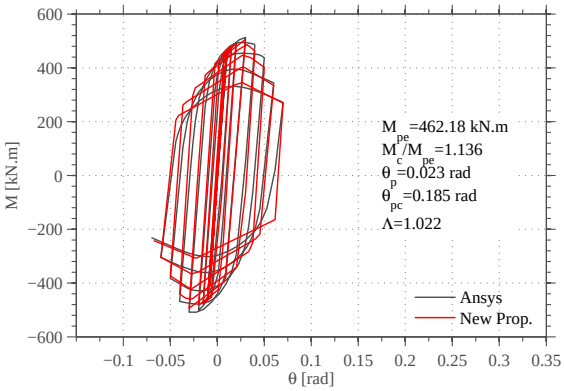

(b) Proposal

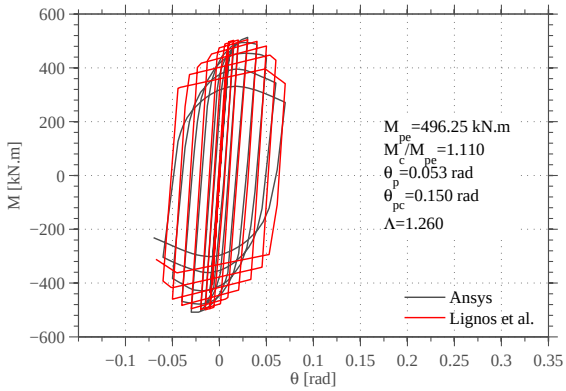

(c) Lignos and Krawinkler (2012)

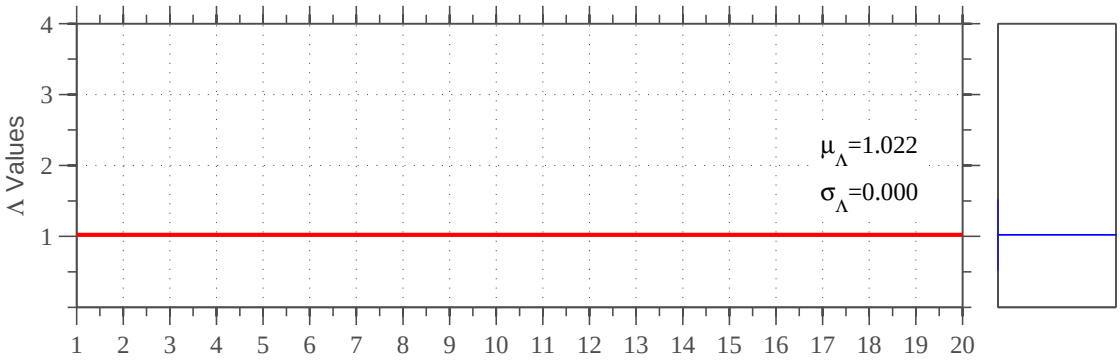

(d) Calibration Stability.

Figure A.13: Ibarra et al. (2005) calibration: HEA300.

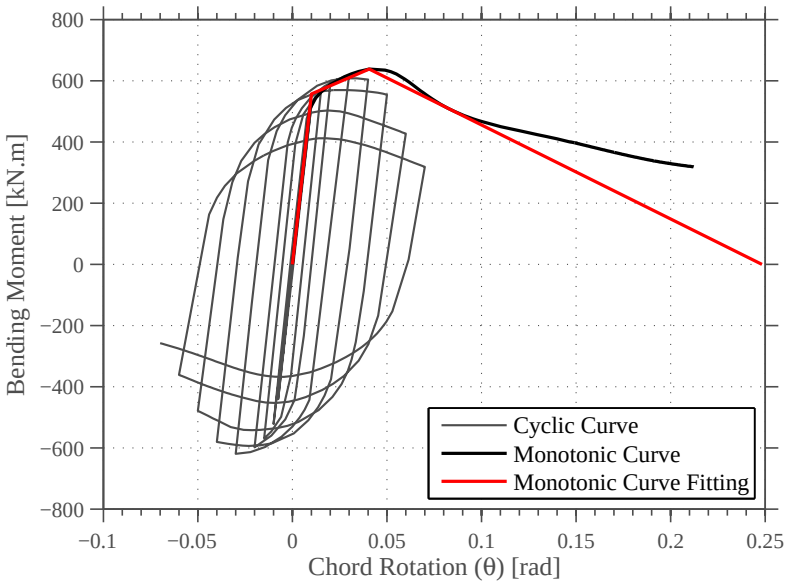

(a) Monotonic backbone calibration: HEA320.

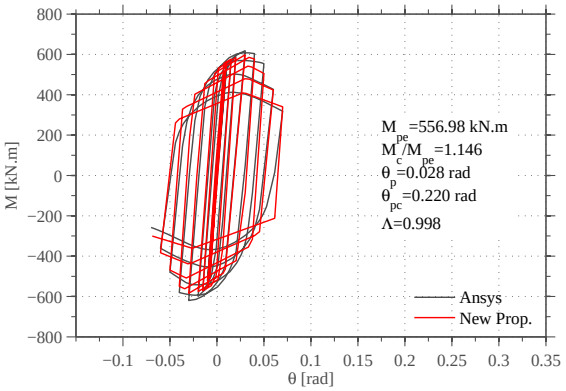

(b) Proposal

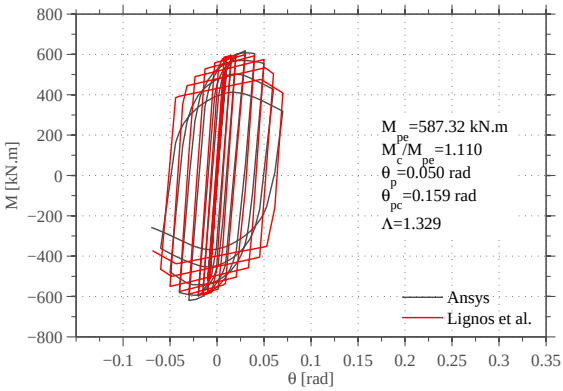

(c) Lignos and Krawinkler (2012)

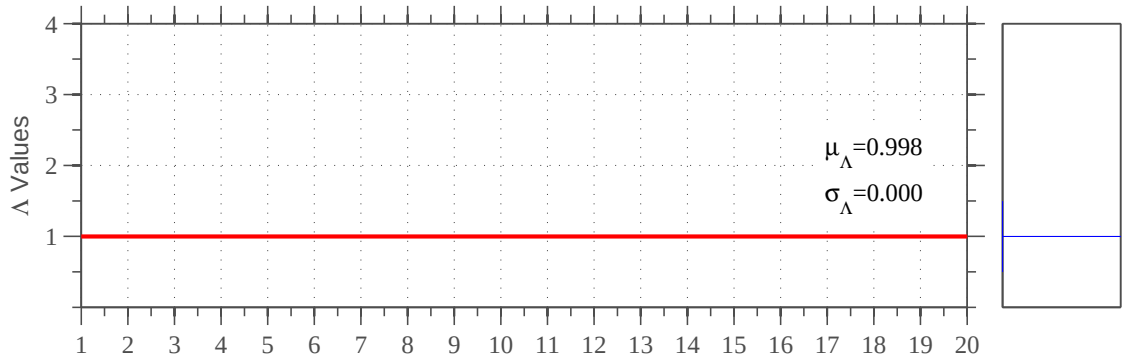

(d) Calibration Stability.

Figure A.14: Ibarra et al. (2005) calibration: HEA320.

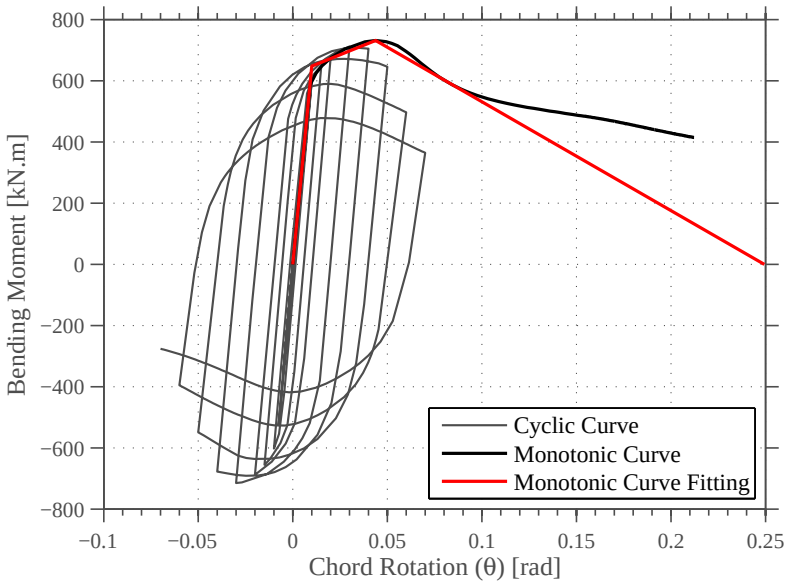

(a) Monotonic backbone calibration: HEA340.

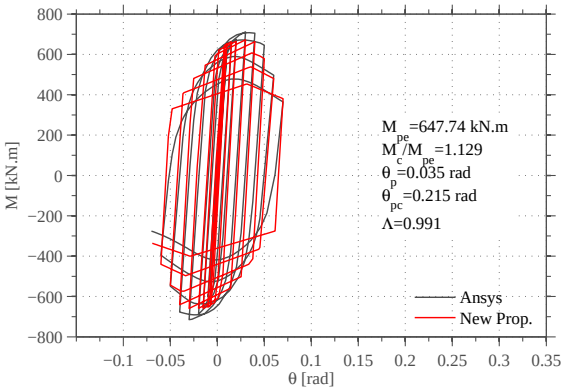

(b) Proposal

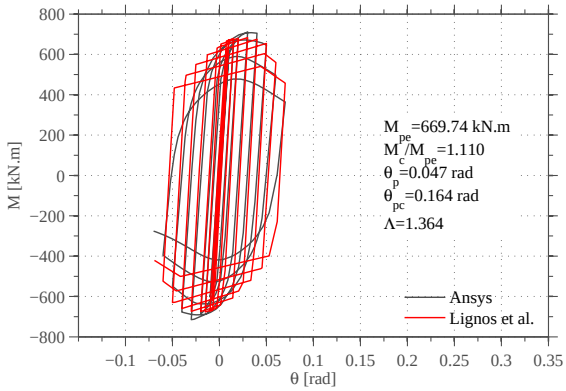

(c) Lignos and Krawinkler (2012)

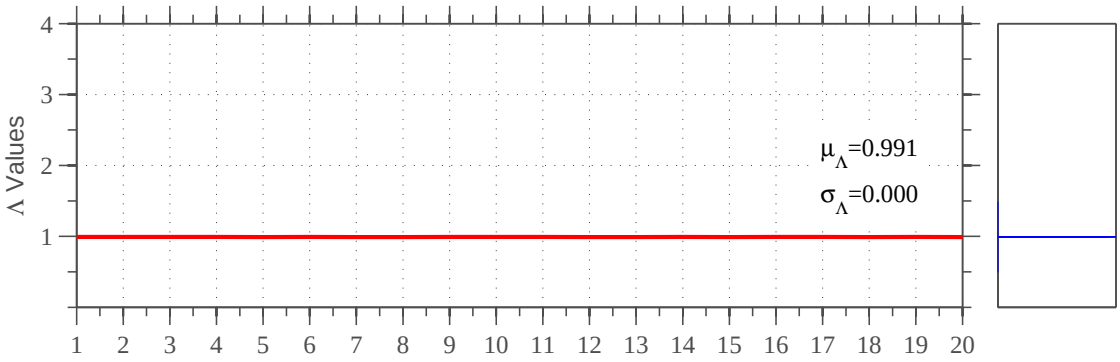

(d) Calibration Stability.

Figure A.15: Ibarra et al. (2005) calibration: HEA340.

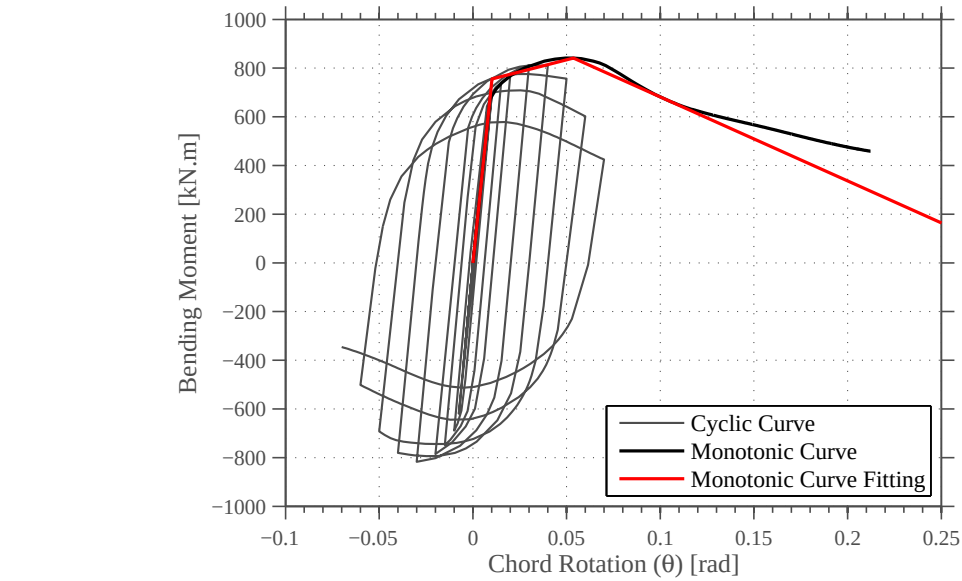

(a) Monotonic backbone calibration: HEA360.

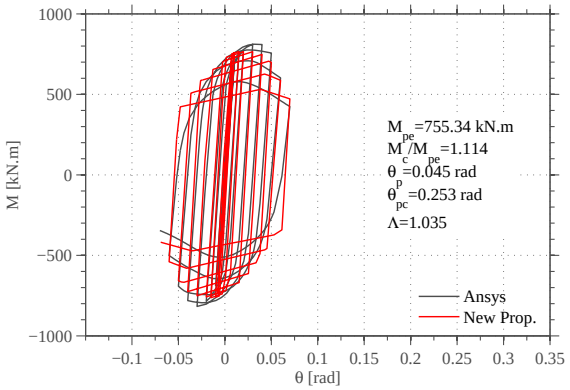

(b) Proposal

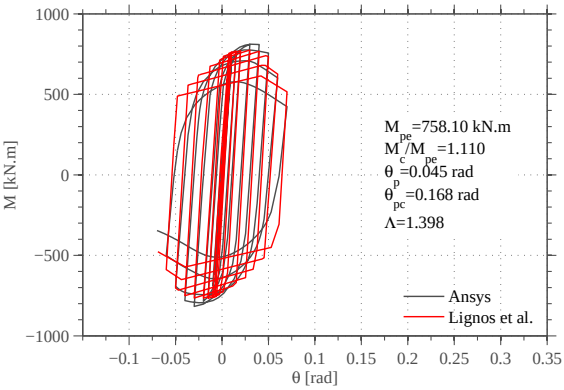

(c) Lignos and Krawinkler (2012)

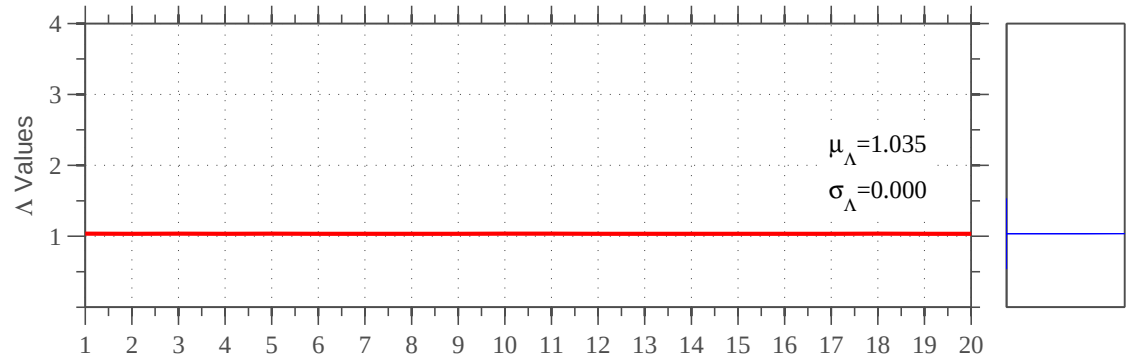

(d) Calibration Stability.

Figure A.16: Ibarra et al. (2005) calibration: HEA360.

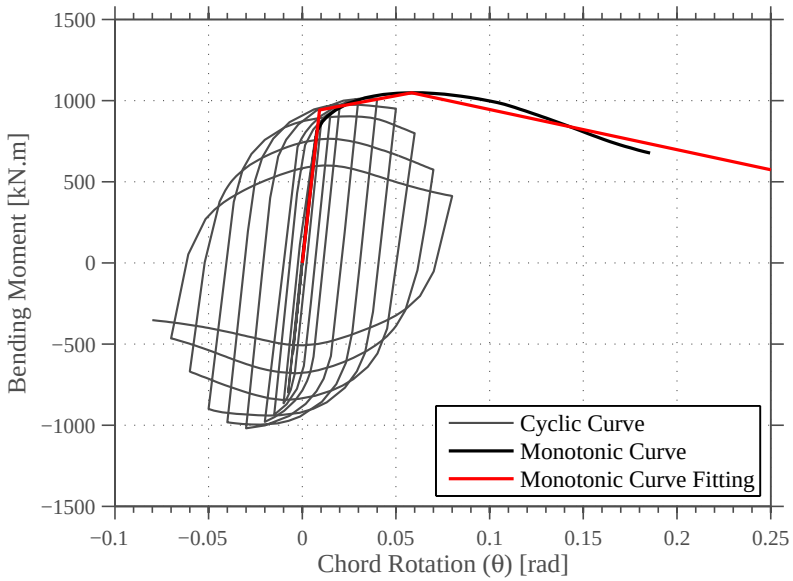

(a) Monotonic backbone calibration: HEA400.

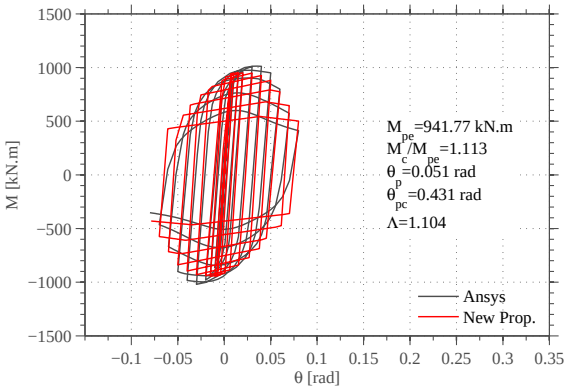

(b) Proposal

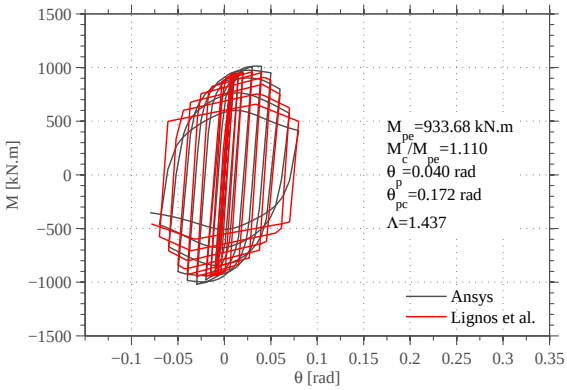

(c) Lignos and Krawinkler (2012)

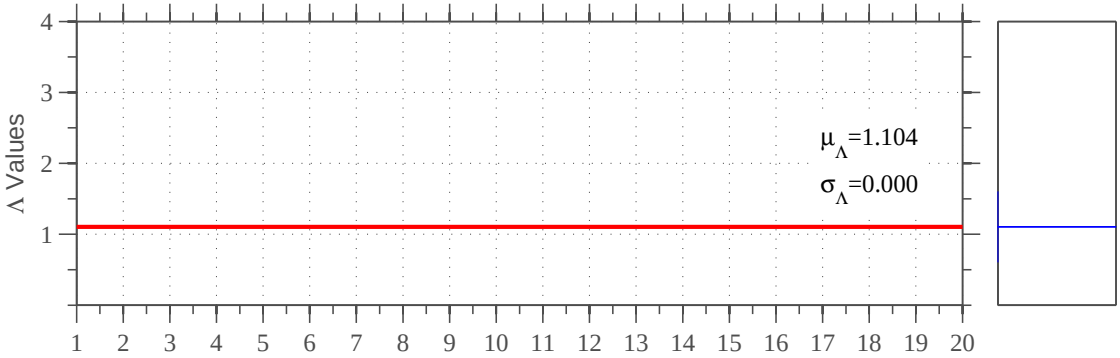

(d) Calibration Stability.

Figure A.17: Ibarra et al. (2005) calibration: HEA400.

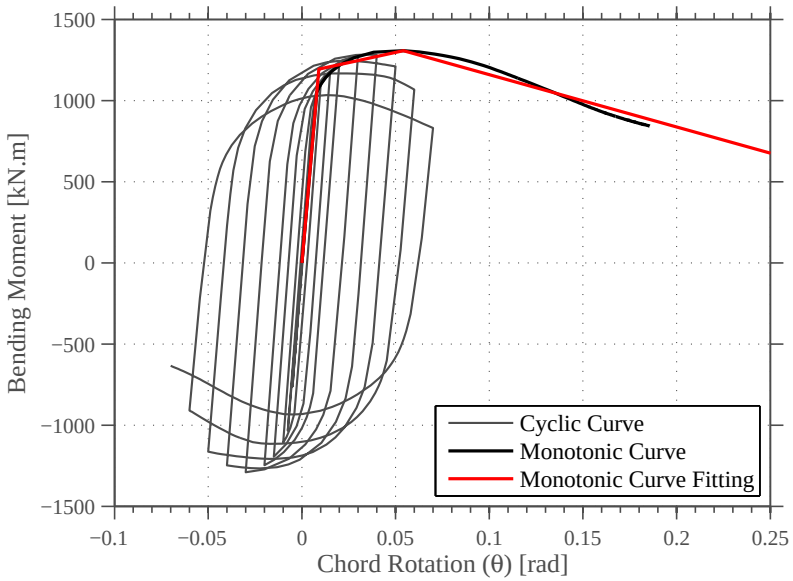

(a) Monotonic backbone calibration: HEA450.

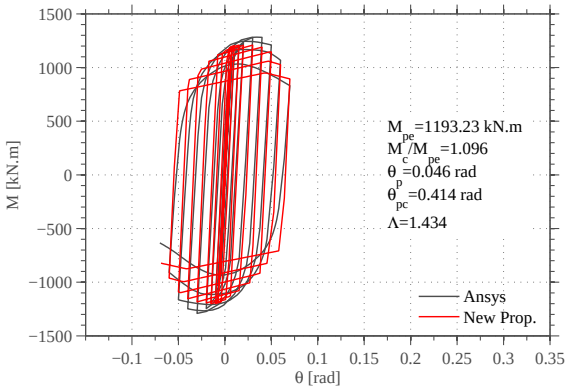

(b) Proposal

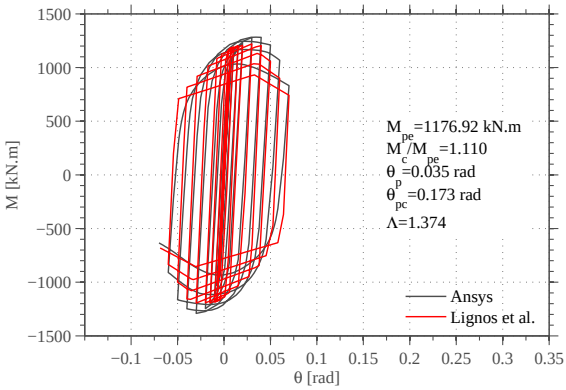

(c) Lignos and Krawinkler (2012)

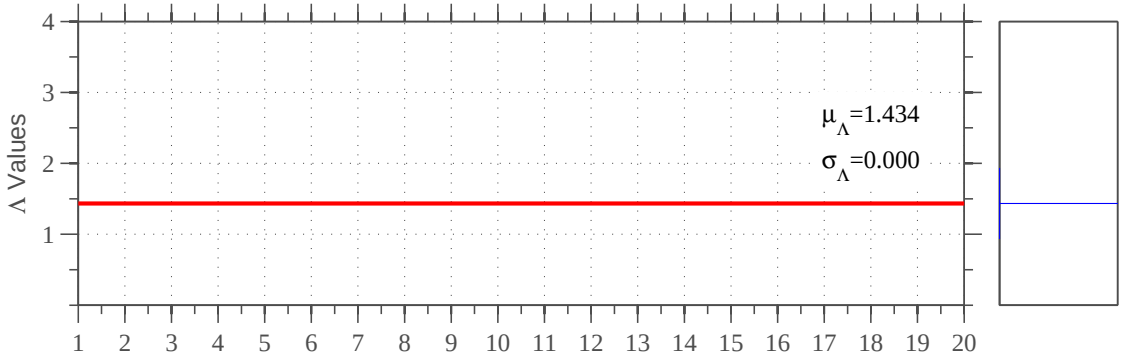

(d) Calibration Stability.

Figure A.18: Ibarra et al. (2005) calibration: HEA450.

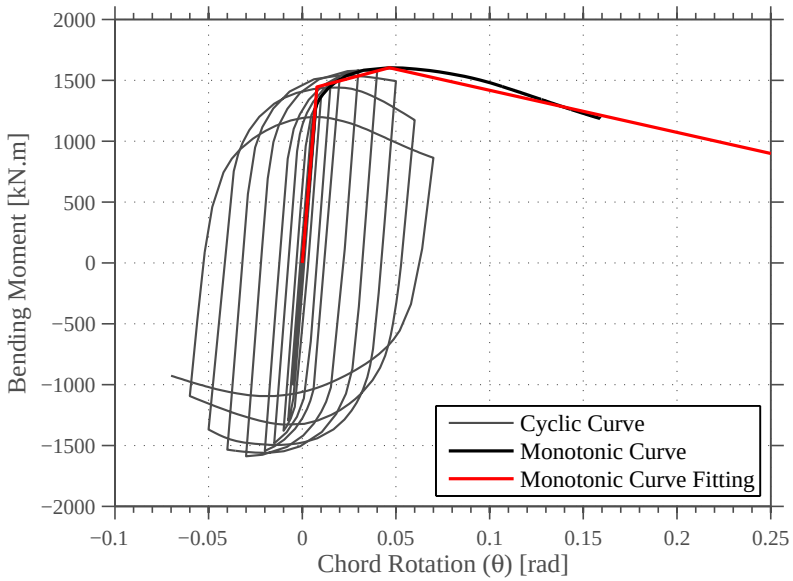

(a) Monotonic backbone calibration: HEA500.

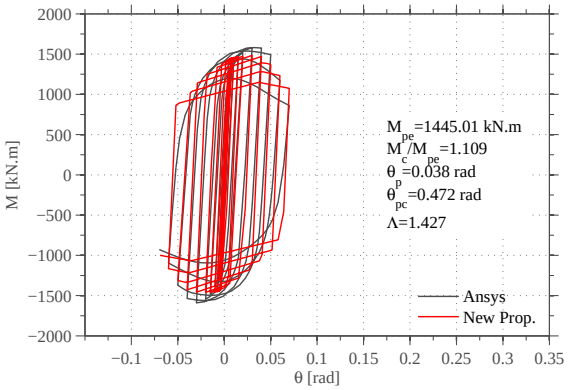

(b) Proposal

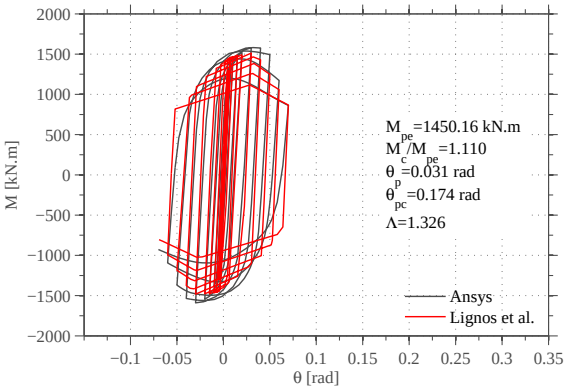

(c) Lignos and Krawinkler (2012)

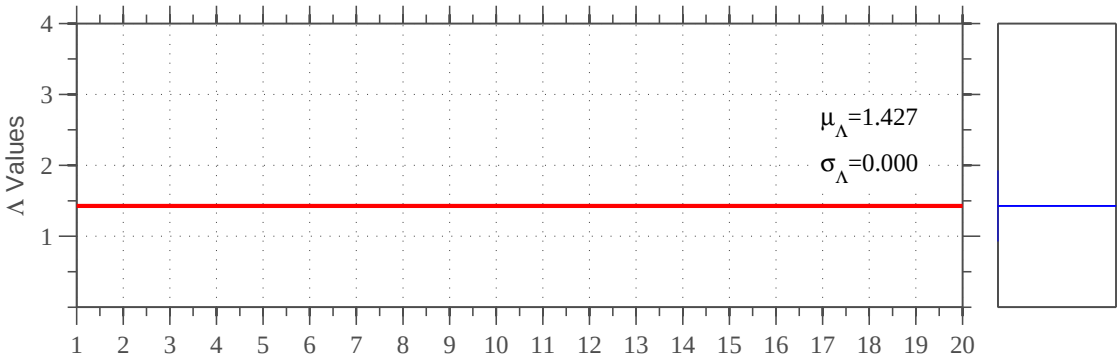

(d) Calibration Stability.

Figure A.19: Ibarra et al. (2005) calibration: HEA500.

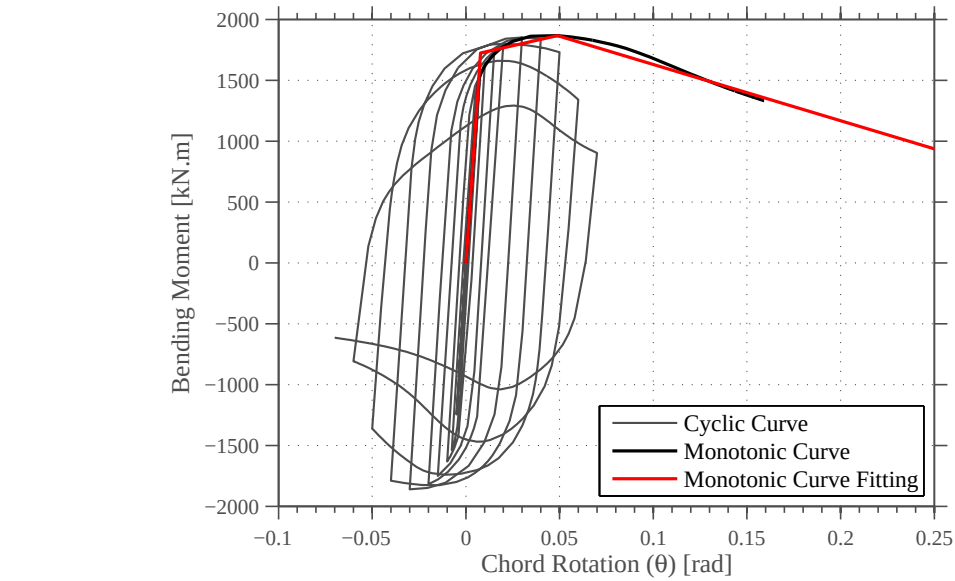

(a) Monotonic backbone calibration: HEA550.

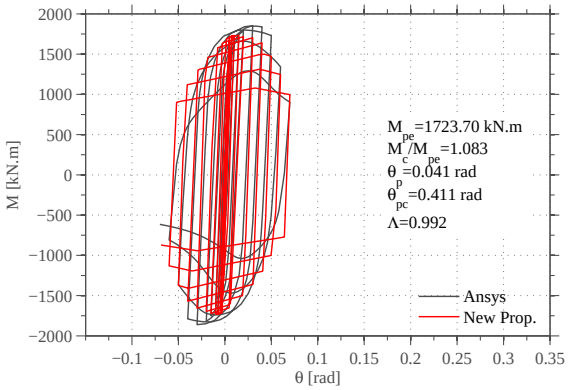

(b) Proposal

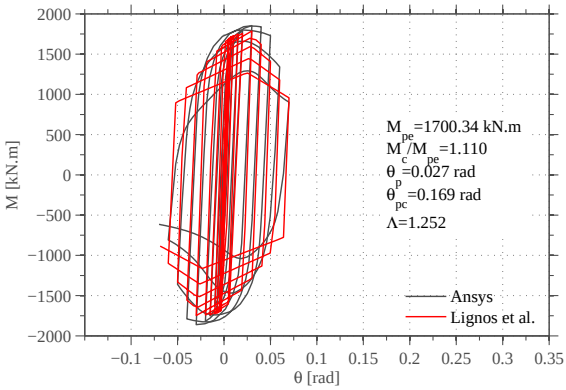

(c) Lignos and Krawinkler (2012)

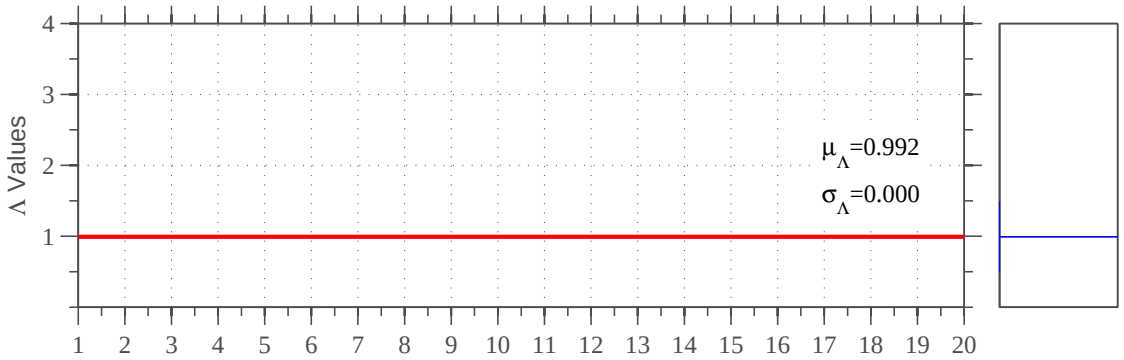

(d) Calibration Stability.

Figure A.20: Ibarra et al. (2005) calibration: HEA550.

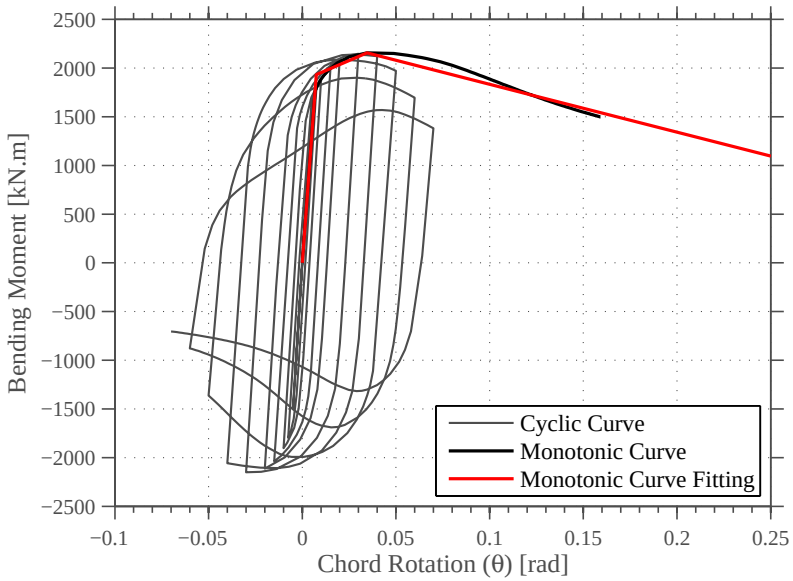

(a) Monotonic backbone calibration: HEA600.

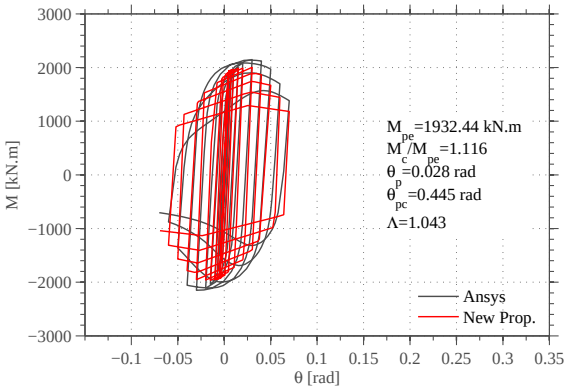

(b) Proposal

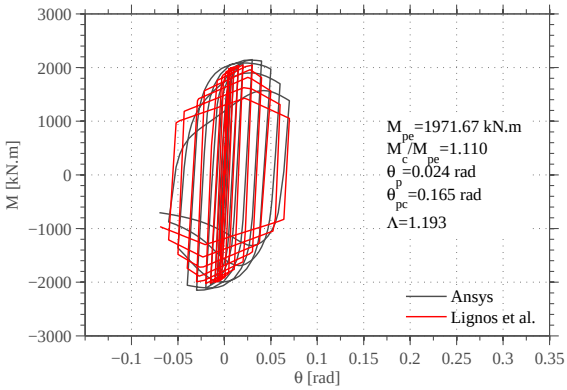

(c) Lignos and Krawinkler (2012)

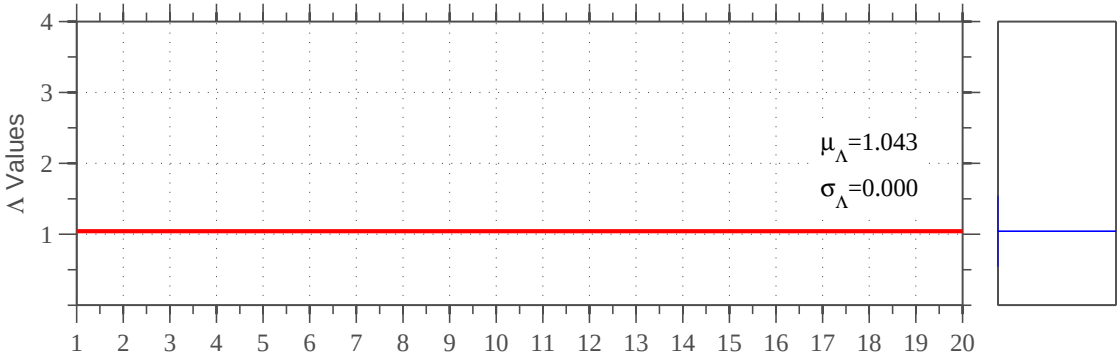

(d) Calibration Stability.

Figure A.21: Ibarra et al. (2005) calibration: HEA600.

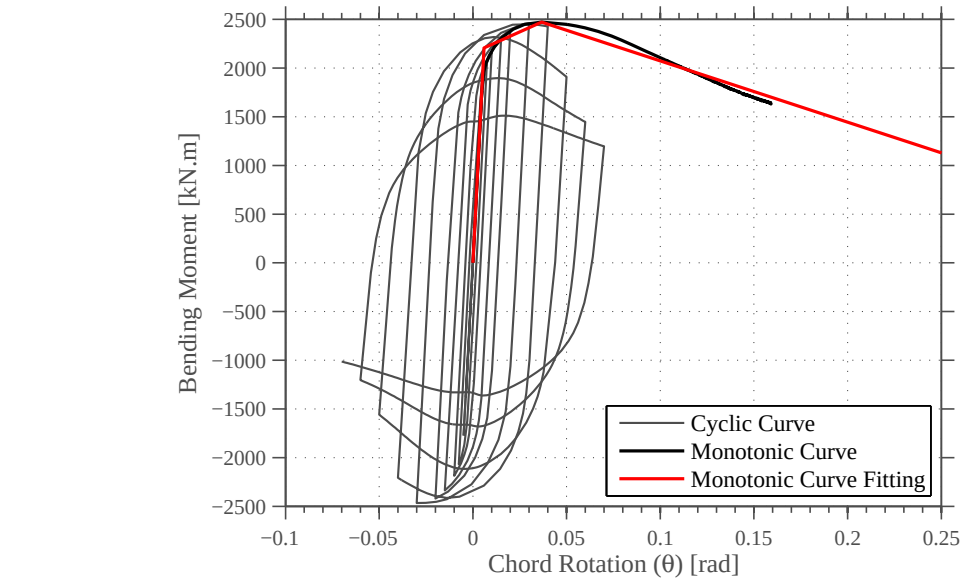

(a) Monotonic backbone calibration: HEA650.

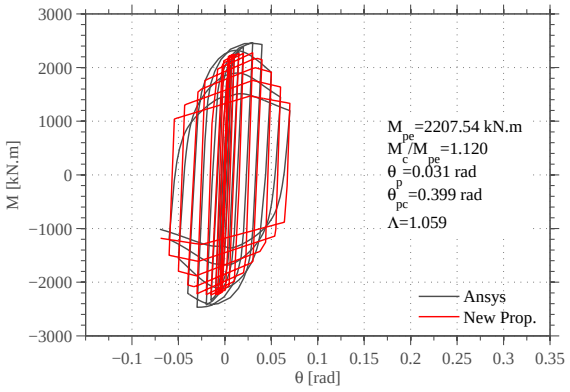

(b) Proposal

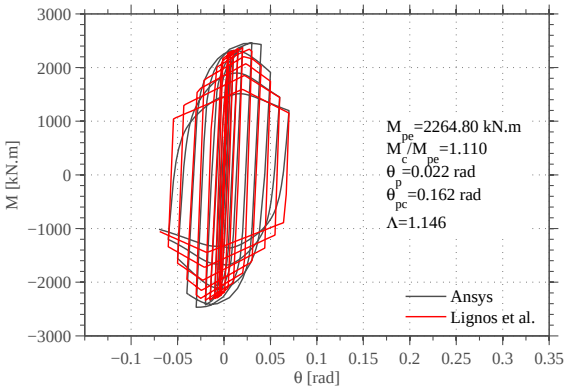

(c) Lignos and Krawinkler (2012)

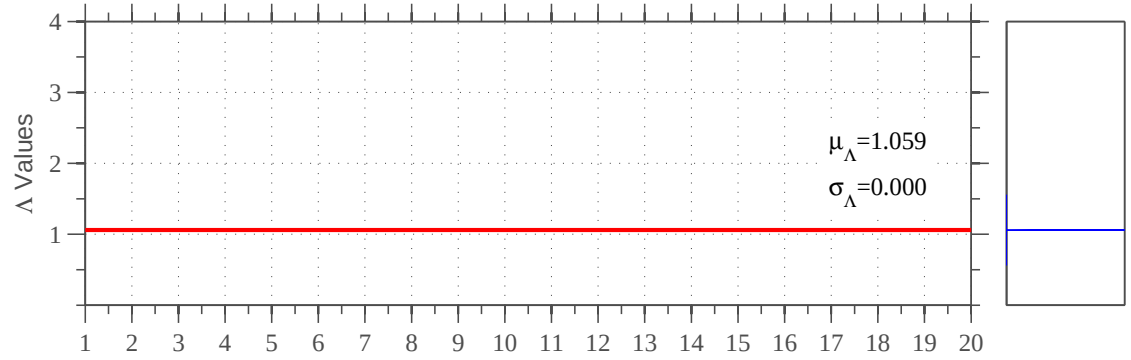

(d) Calibration Stability.

Figure A.22: Ibarra et al. (2005) calibration: HEA650.

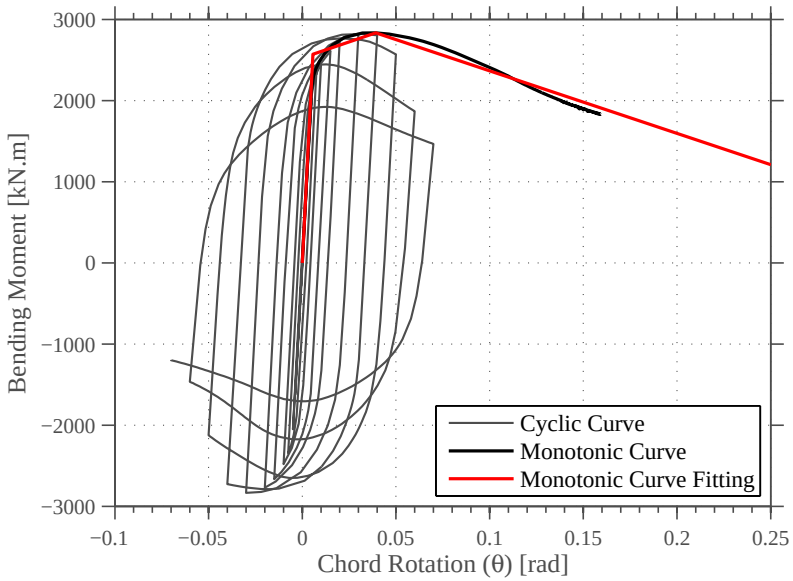

(a) Monotonic backbone calibration: HEA700.

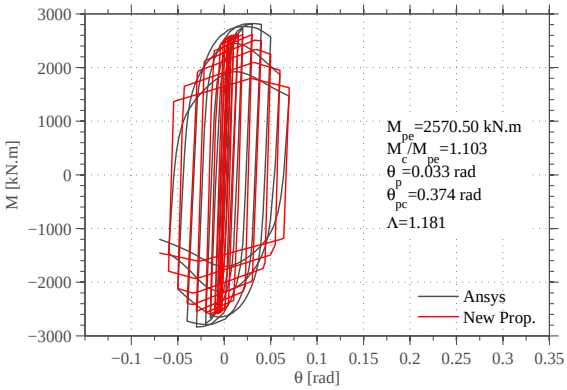

(b) Proposal

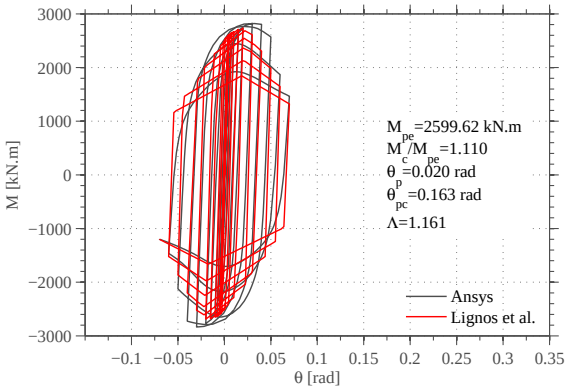

(c) Lignos and Krawinkler (2012)

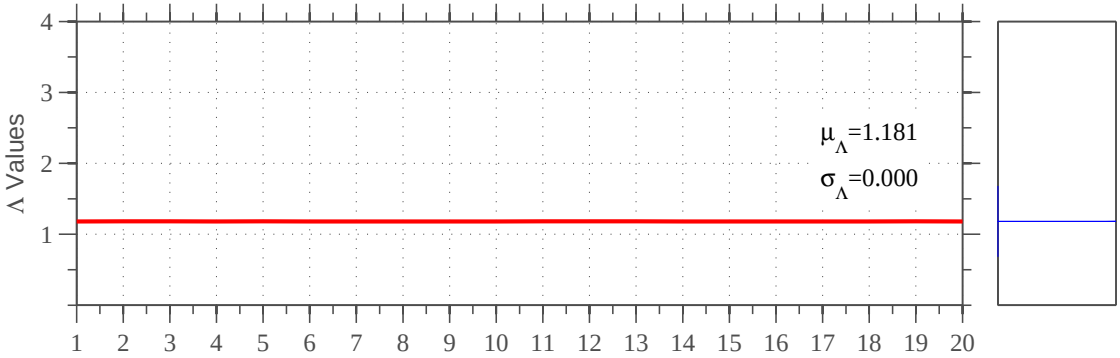

(d) Calibration Stability.

Figure A.23: Ibarra et al. (2005) calibration: HEA700.

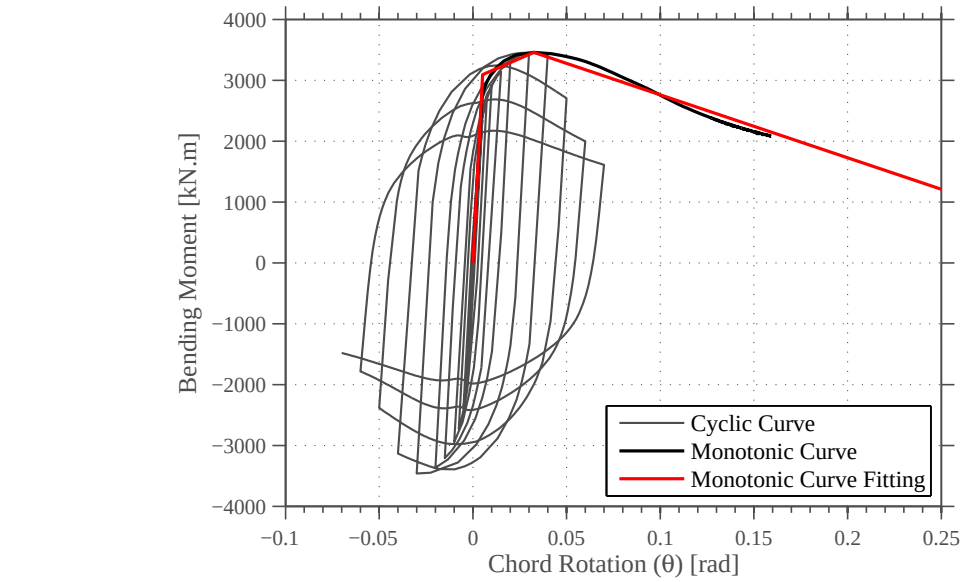

(a) Monotonic backbone calibration: HEA800.

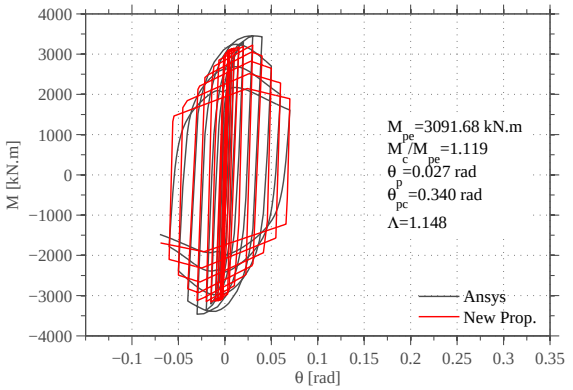

(b) Proposal

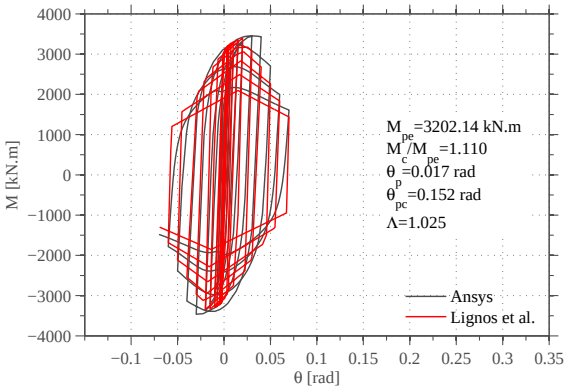

(c) Lignos and Krawinkler (2012)

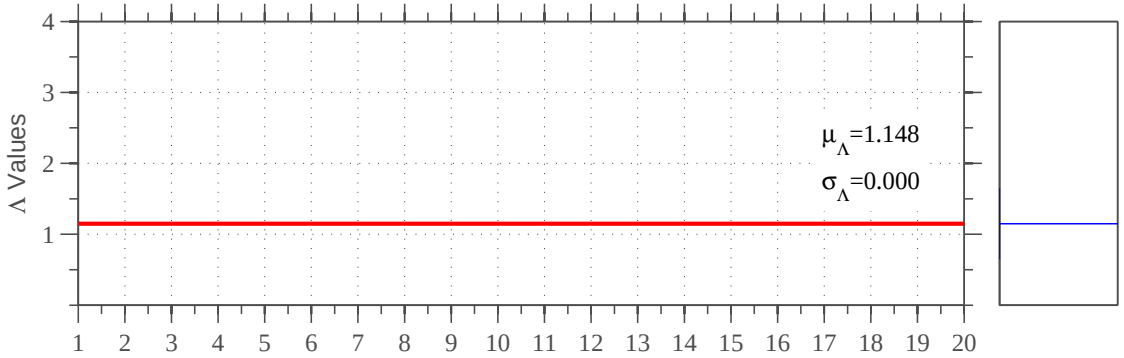

(d) Calibration Stability.

Figure A.24: Ibarra et al. (2005) calibration: HEA800.

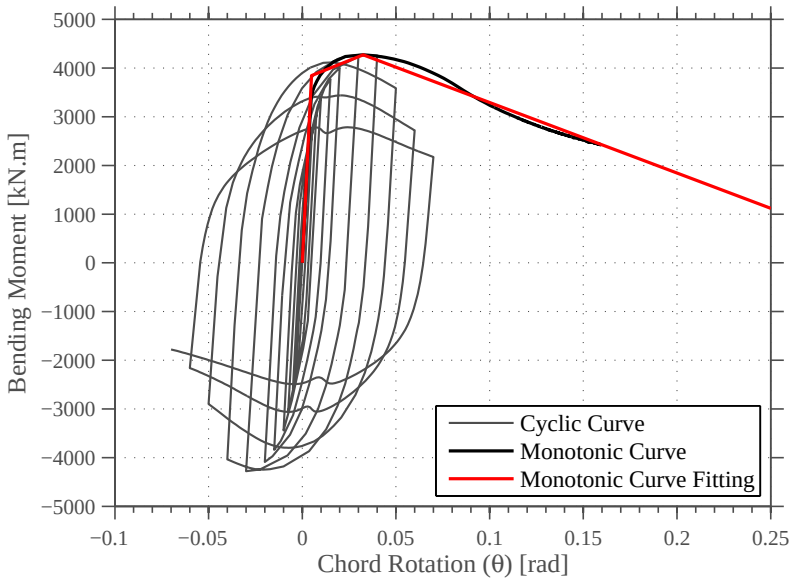

(a) Monotonic backbone calibration: HEA900.

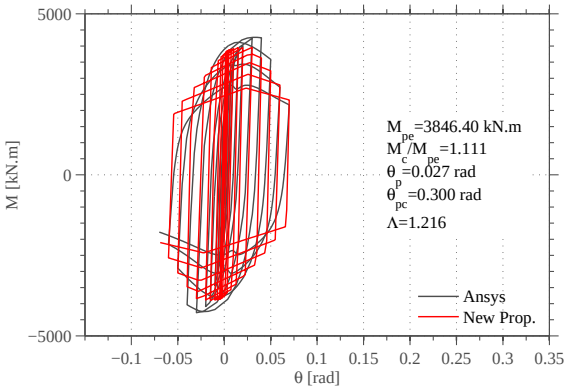

(b) Proposal

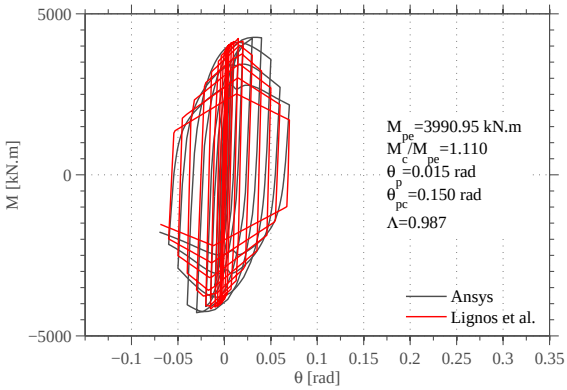

(c) Lignos and Krawinkler (2012)

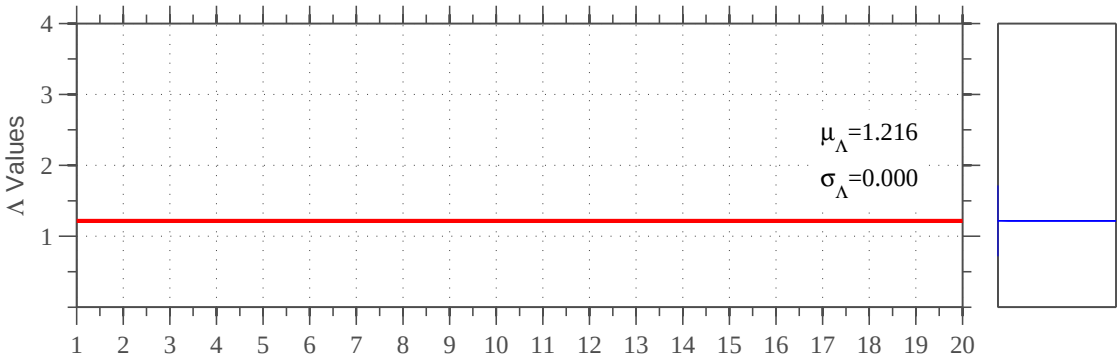

(d) Calibration Stability.

Figure A.25: Ibarra et al. (2005) calibration: HEA900.

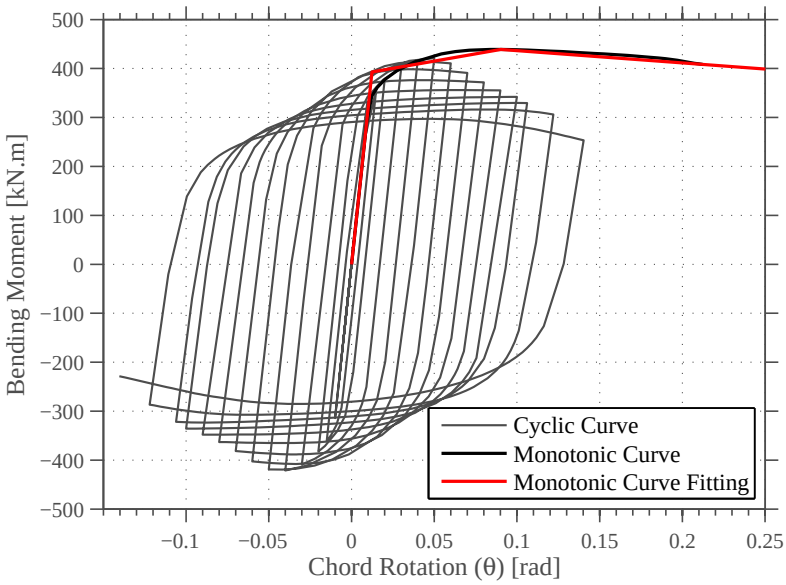

(a) Monotonic backbone calibration: HEB240.

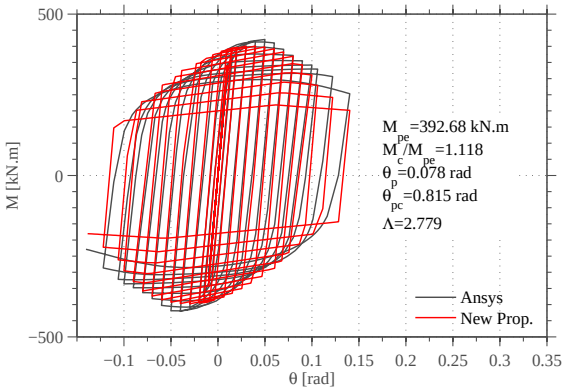

(b) Proposal

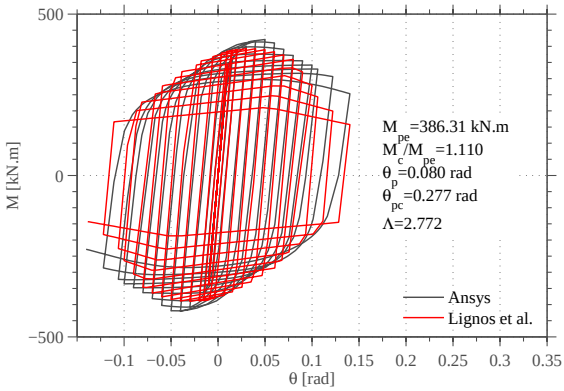

(c) Lignos and Krawinkler (2012)

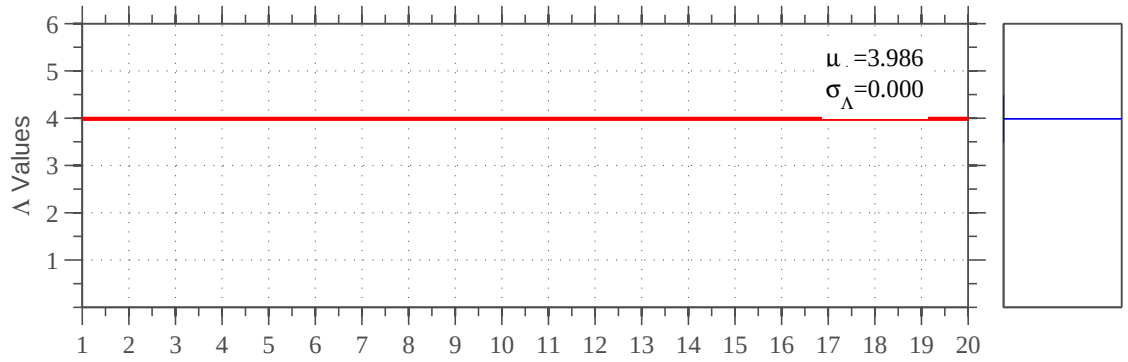

(d) Calibration Stability.

Figure A.26: Ibarra et al. (2005) calibration: HEB240.

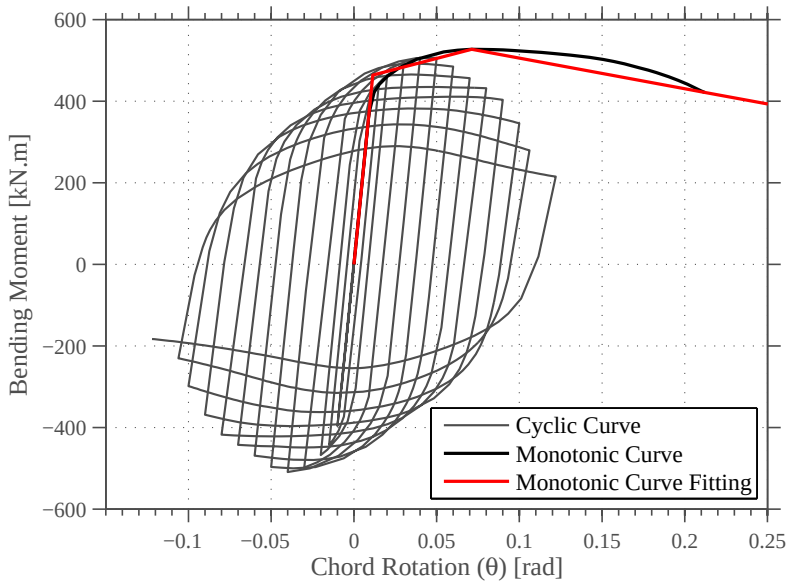

(a) Monotonic backbone calibration: HEB260.

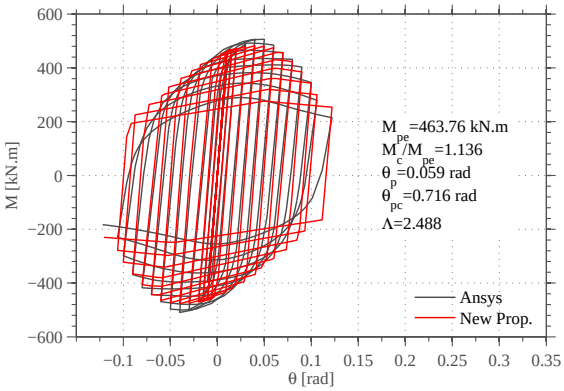

(b) Proposal

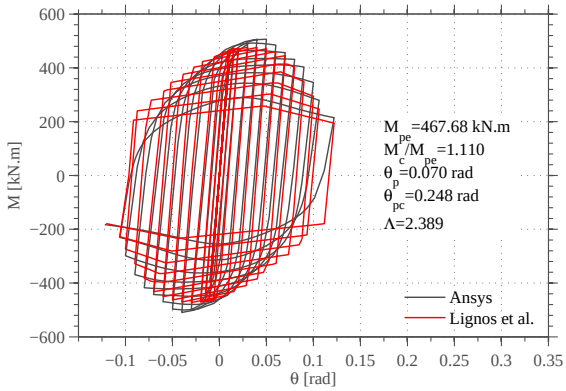

(c) Lignos and Krawinkler (2012)

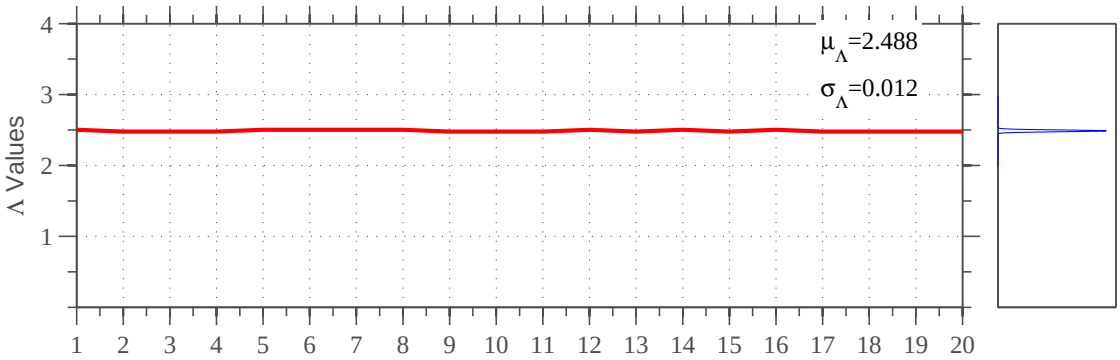

(d) Calibration Stability.

Figure A.27: Ibarra et al. (2005) calibration: HEB260.

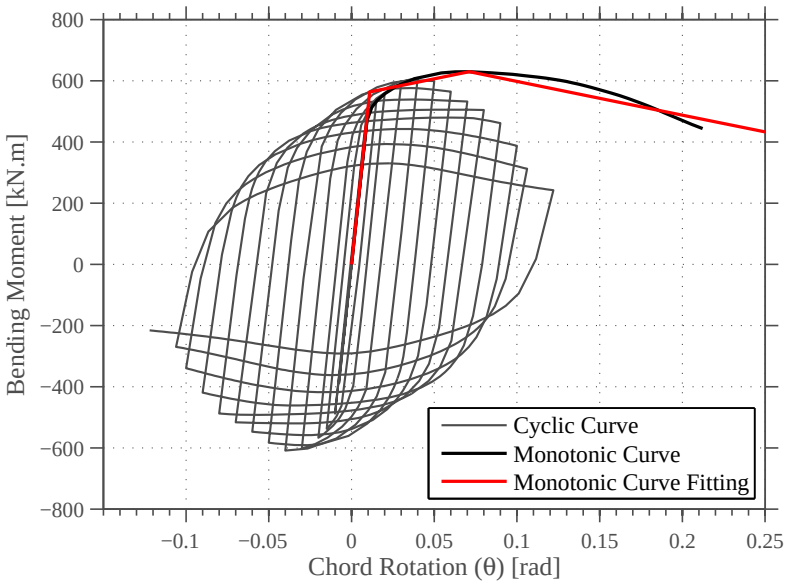

(a) Monotonic backbone calibration: HEB280.

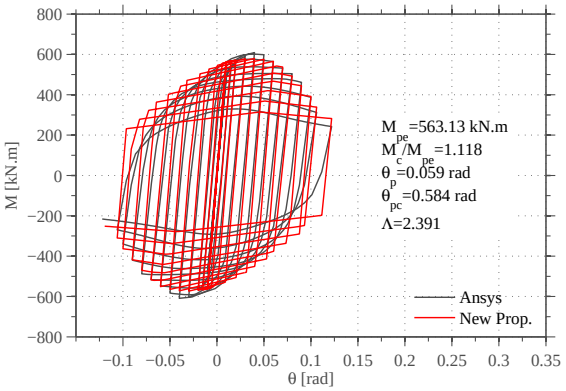

(b) Proposal

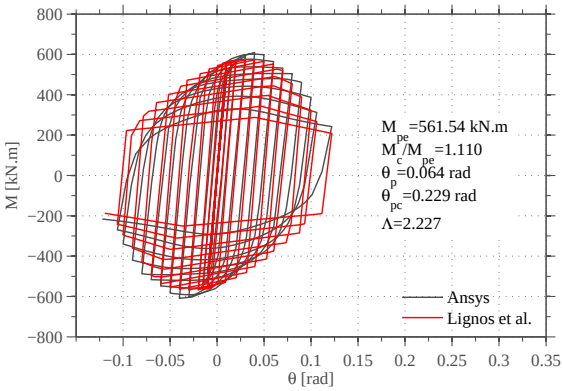

(c) Lignos and Krawinkler (2012)

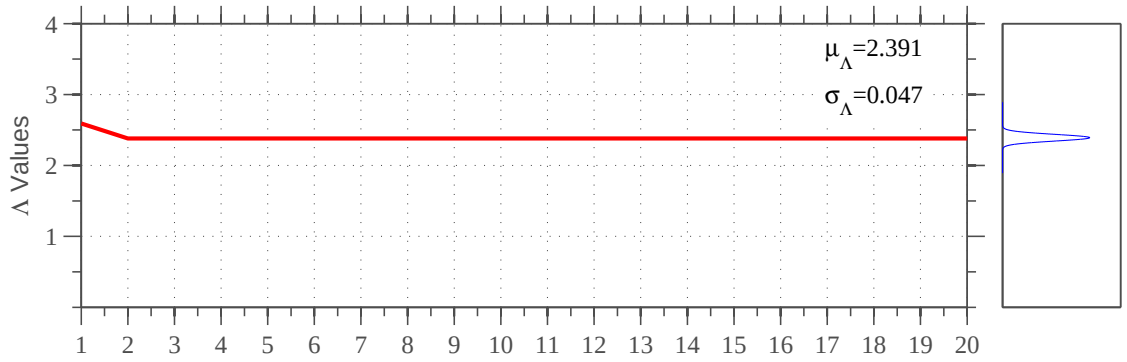

(d) Calibration Stability.

Figure A.28: Ibarra et al. (2005) calibration: HEB280.

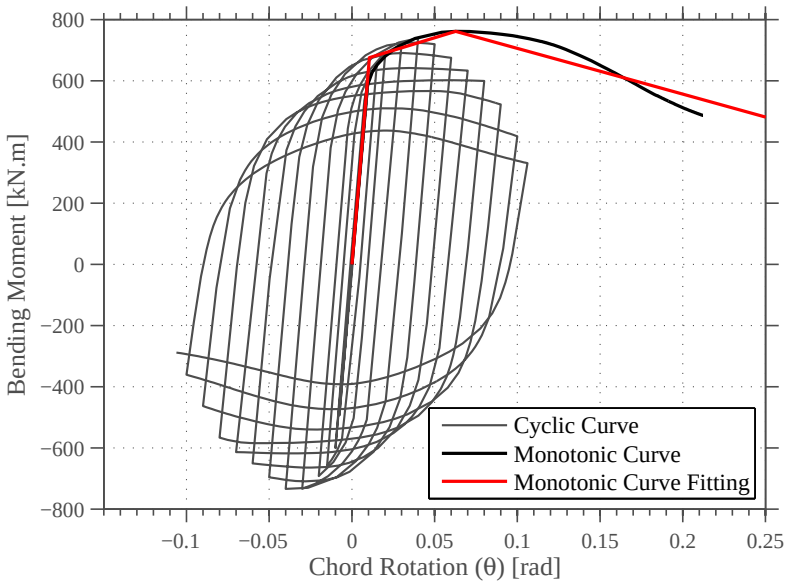

(a) Monotonic backbone calibration: HEB300.

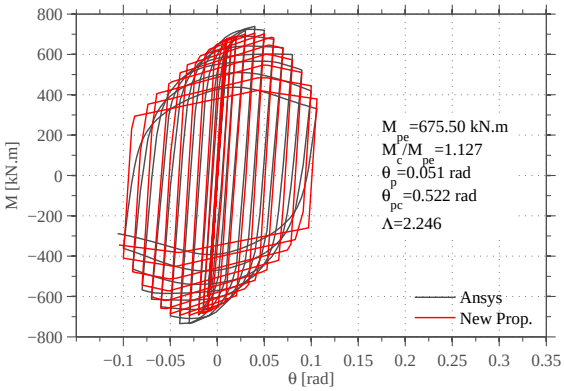

(b) Proposal

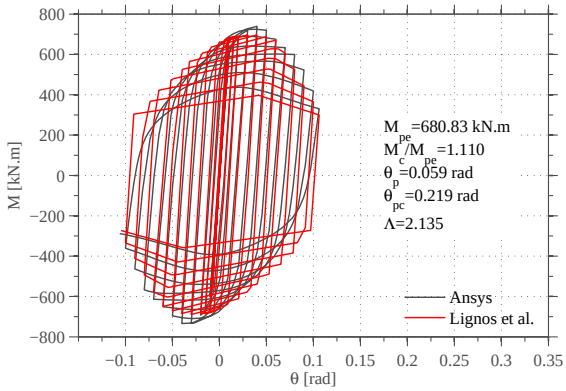

(c) Lignos and Krawinkler (2012)

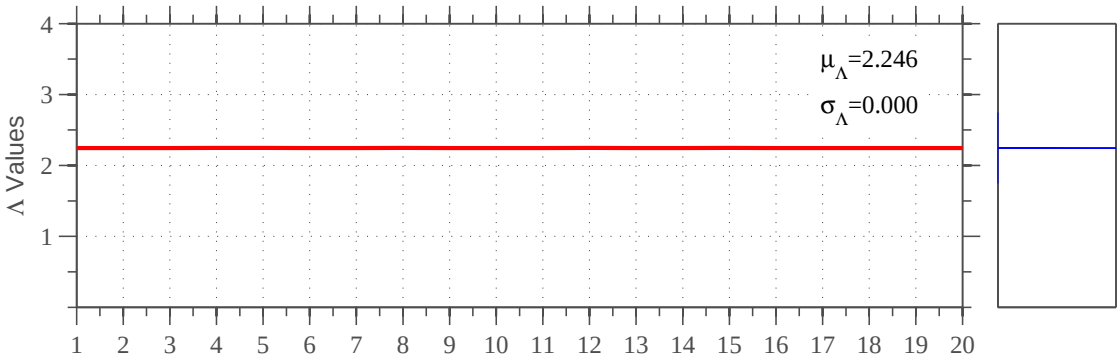

(d) Calibration Stability.

Figure A.29: Ibarra et al. (2005) calibration: HEB300.

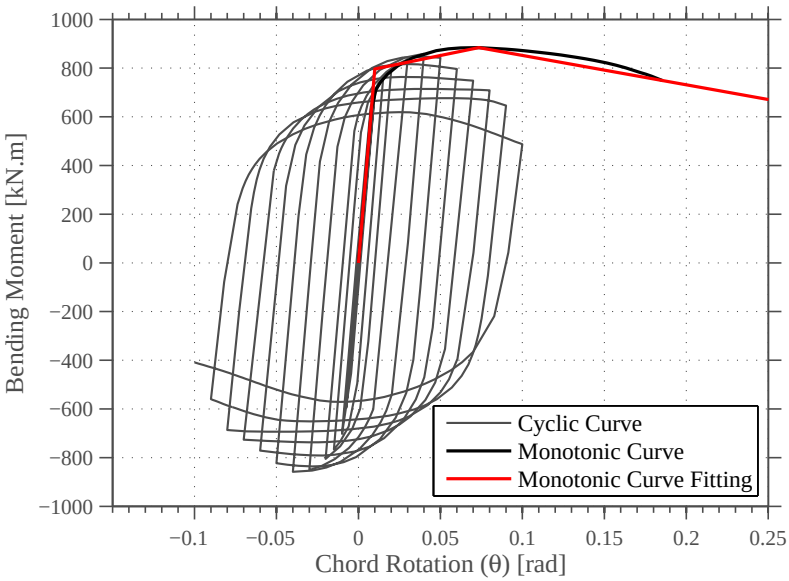

(a) Monotonic backbone calibration: HEB320.

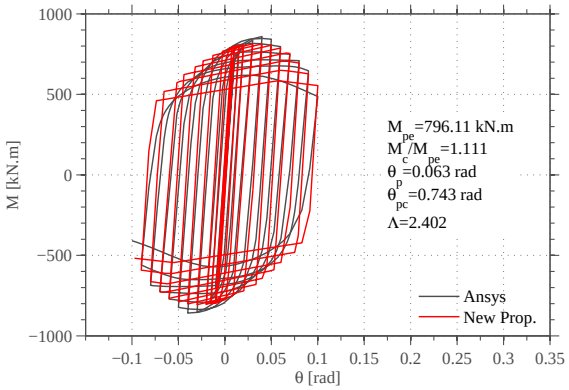

(b) Proposal

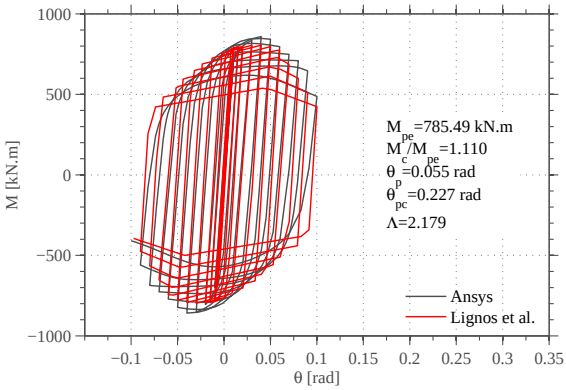

(c) Lignos and Krawinkler (2012)

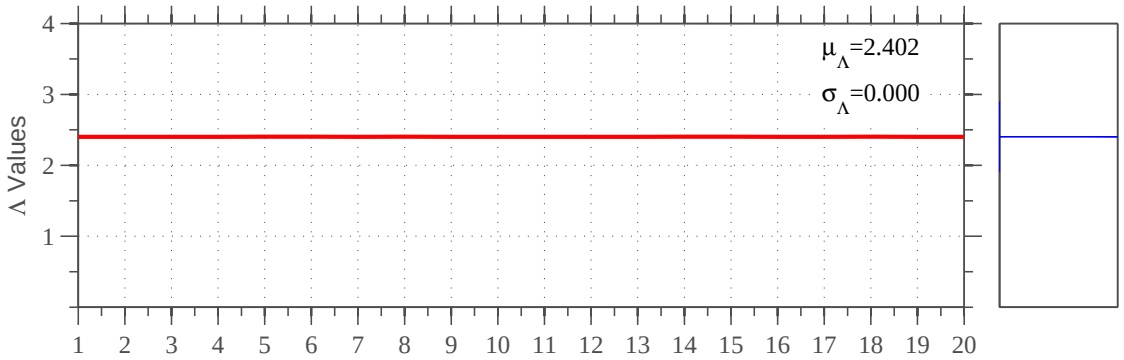

(d) Calibration Stability.

Figure A.30: Ibarra et al. (2005) calibration: HEB320.

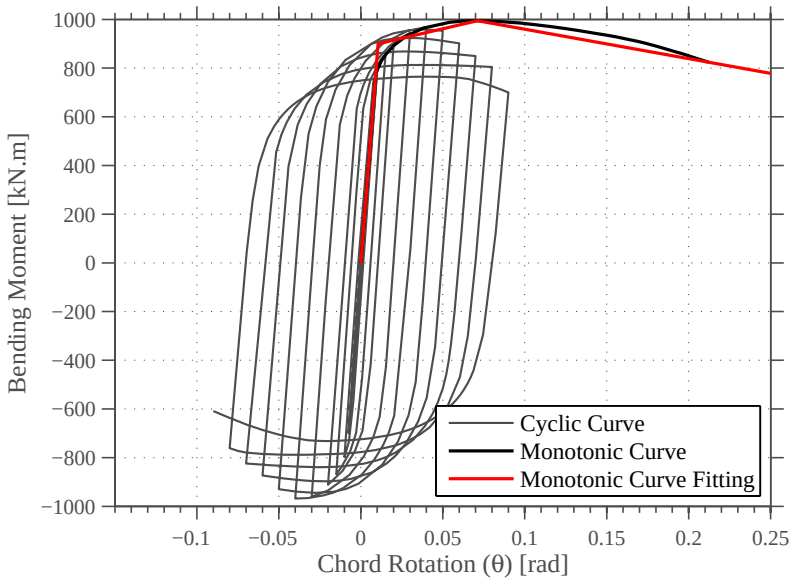

(a) Monotonic backbone calibration: HEB340.

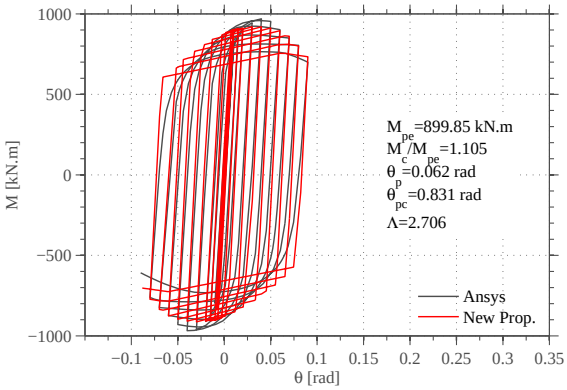

(b) Proposal

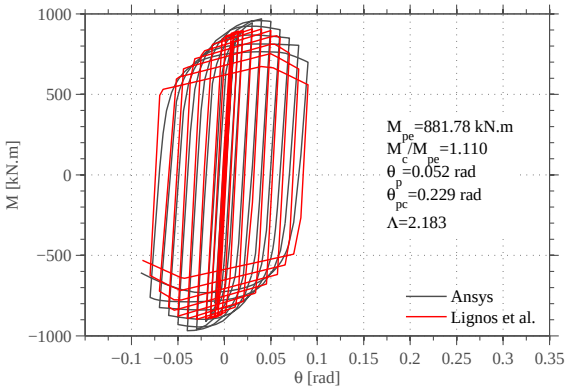

(c) Lignos and Krawinkler (2012)

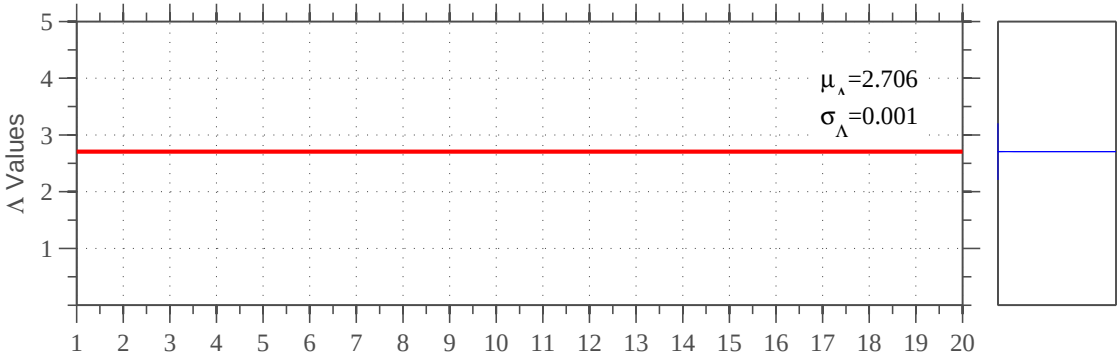

(d) Calibration Stability.

Figure A.31: Ibarra et al. (2005) calibration: HEB340.

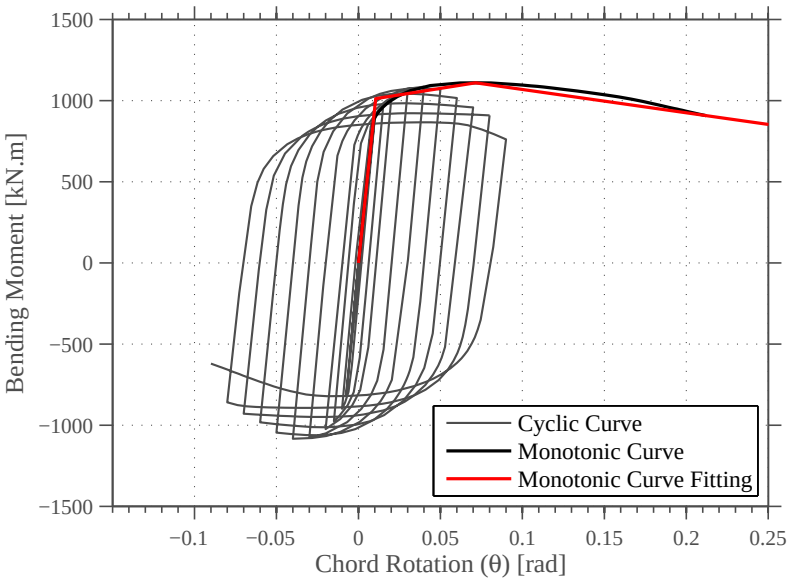

(a) Monotonic backbone calibration: HEB360.

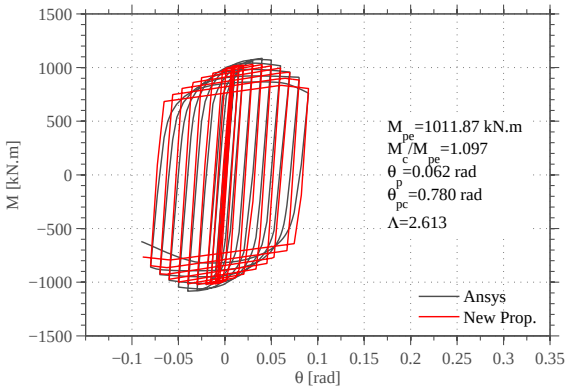

(b) Proposal

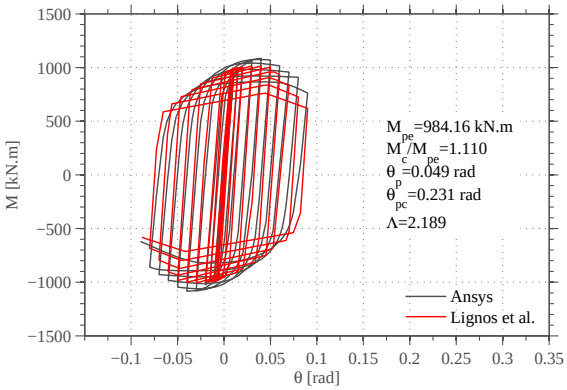

(c) Lignos and Krawinkler (2012)

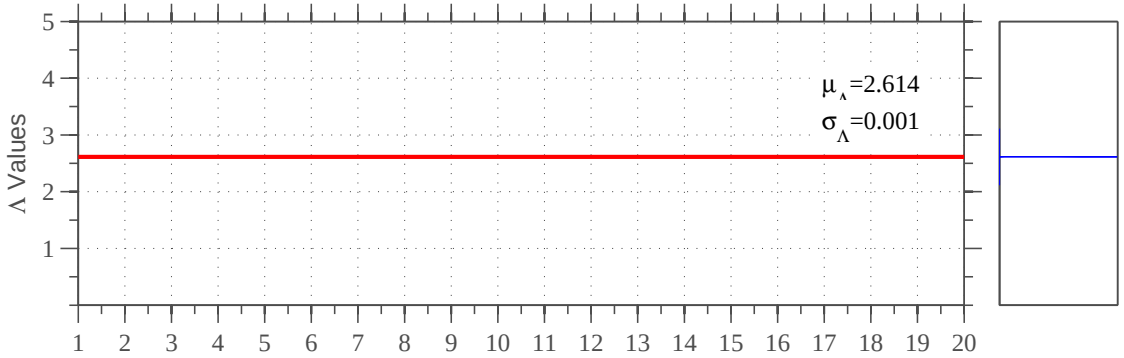

(d) Calibration Stability.

Figure A.32: Ibarra et al. (2005) calibration: HEB360.

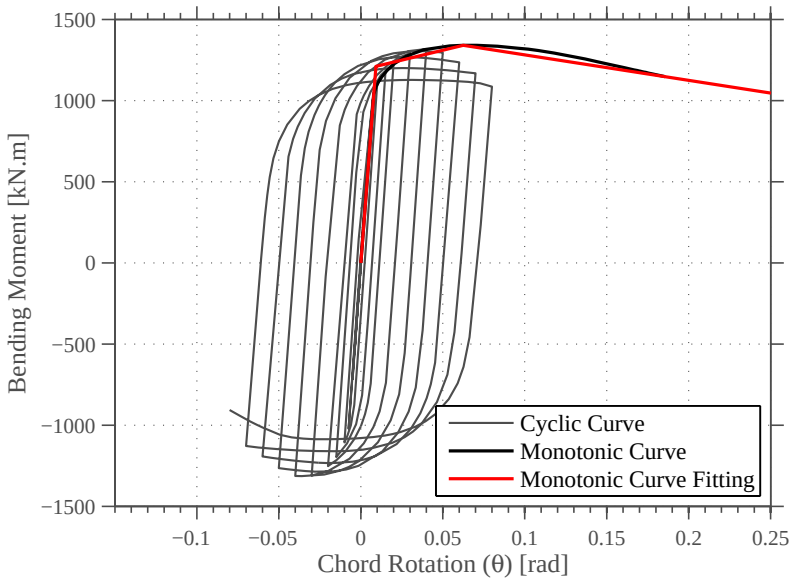

(a) Monotonic backbone calibration: HEB400.

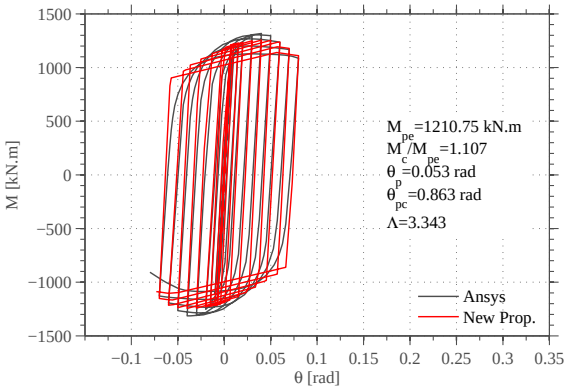

(b) Proposal

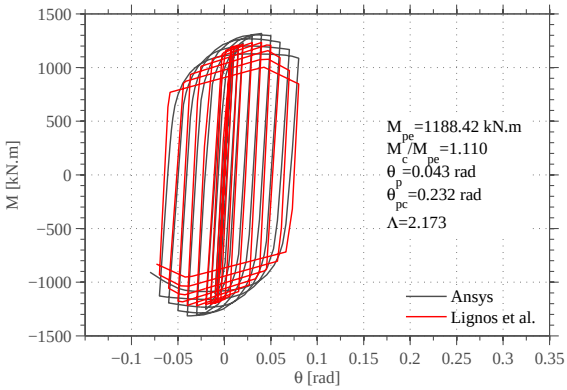

(c) Lignos and Krawinkler (2012)

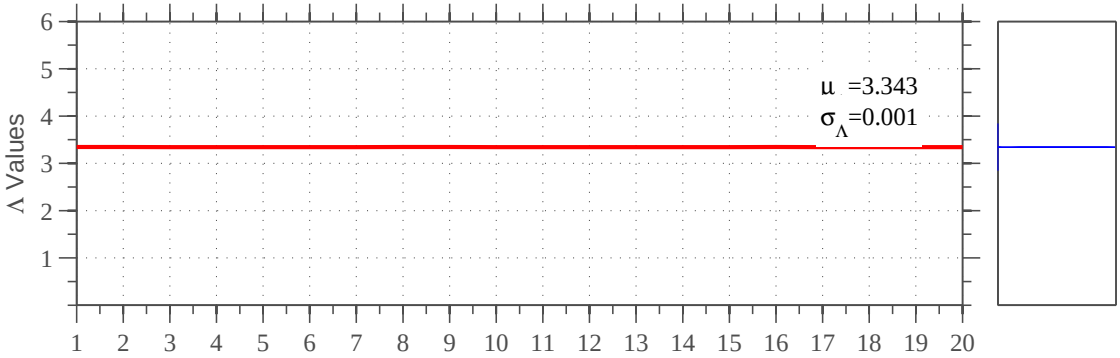

(d) Calibration Stability.

Figure A.33: Ibarra et al. (2005) calibration: HEB400.

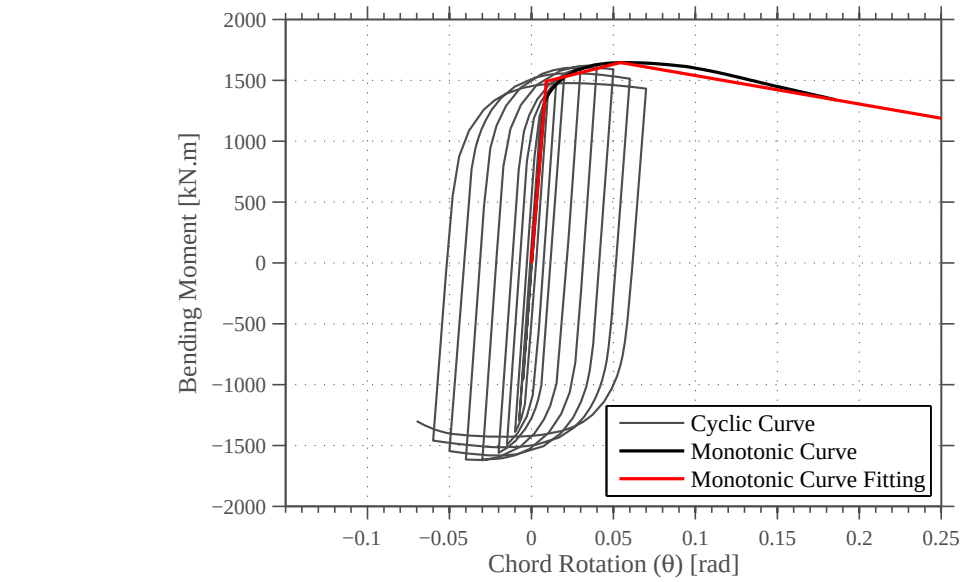

(a) Monotonic backbone calibration: HEB450.

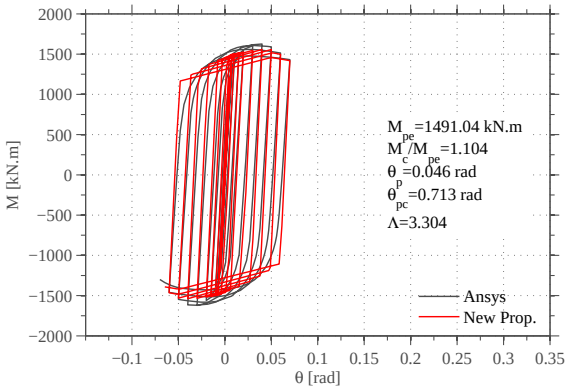

(b) Proposal

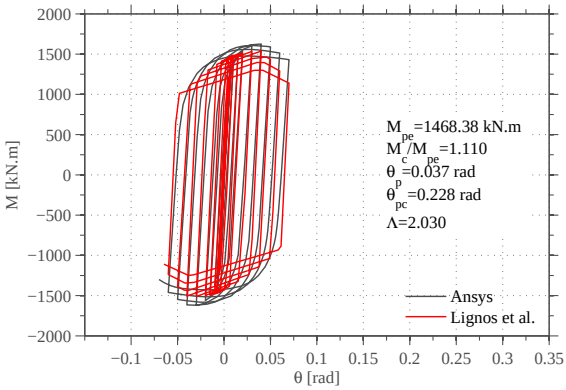

(c) Lignos and Krawinkler (2012)

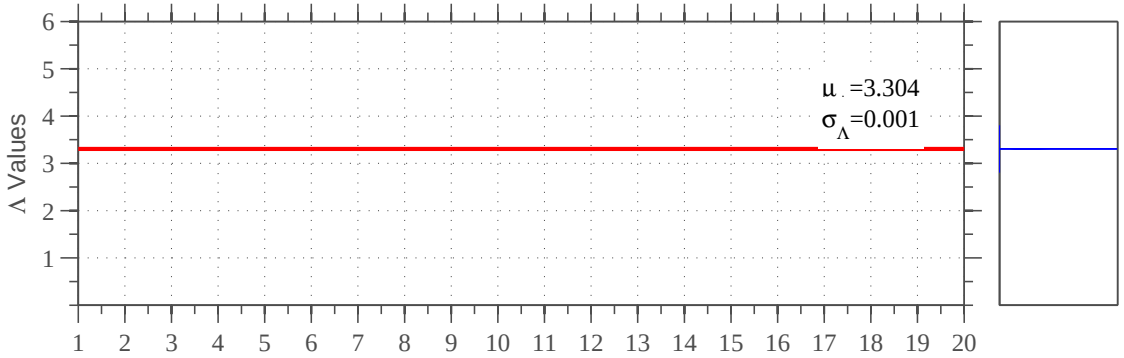

(d) Calibration Stability.

Figure A.34: Ibarra et al. (2005) calibration: HEB450.

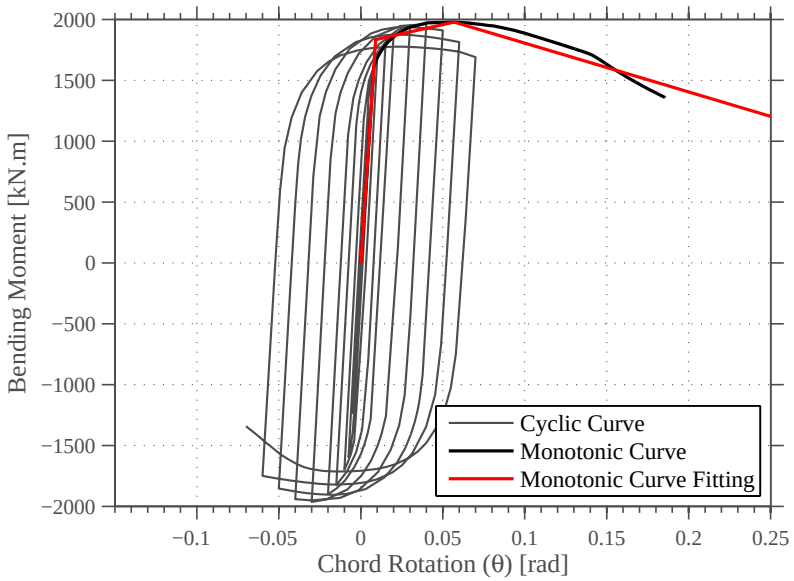

(a) Monotonic backbone calibration: HEB500.

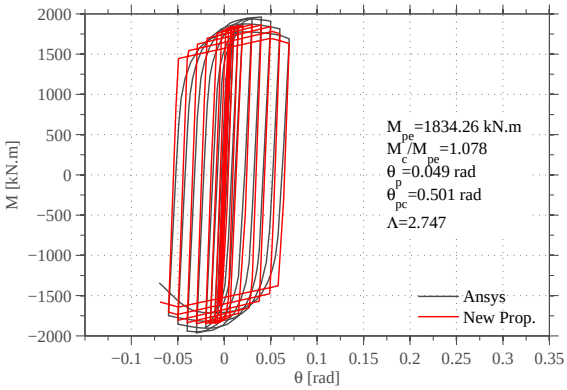

(b) Proposal

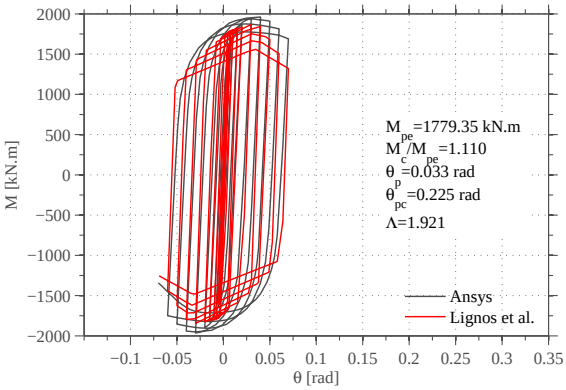

(c) Lignos and Krawinkler (2012)

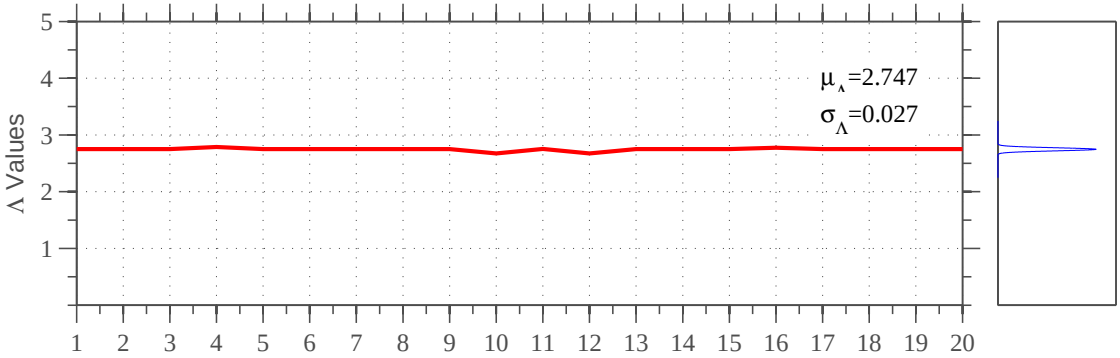

(d) Calibration Stability.

Figure A.35: Ibarra et al. (2005) calibration: HEB500.

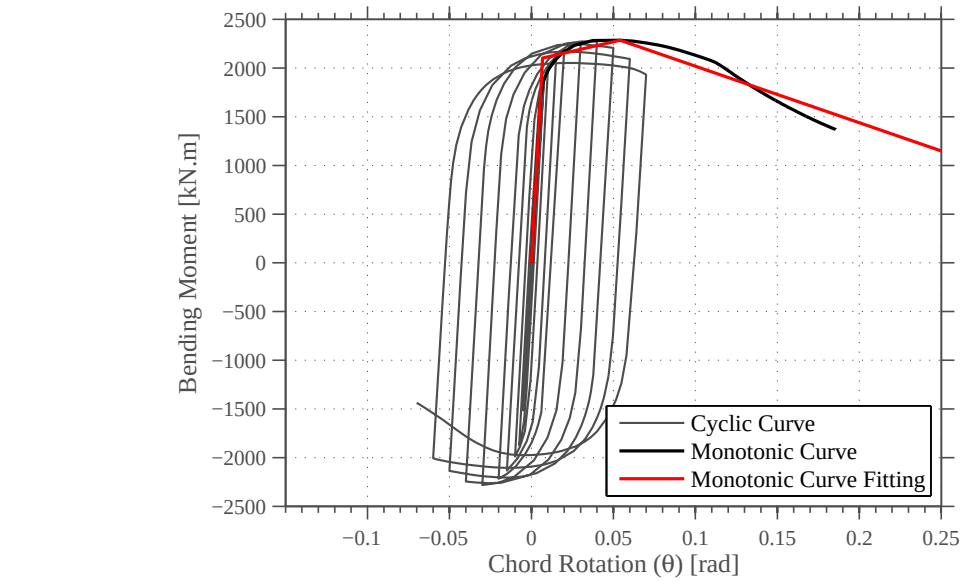

(a) Monotonic backbone calibration: HEB550.

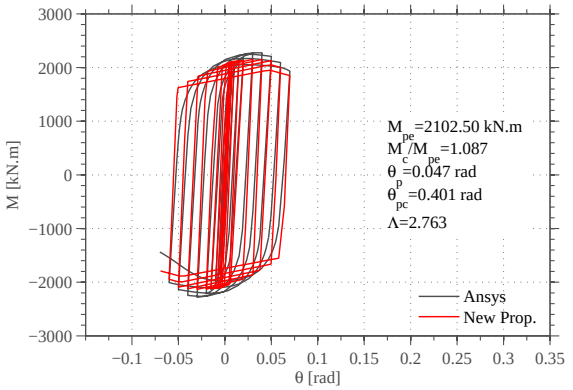

(b) Proposal

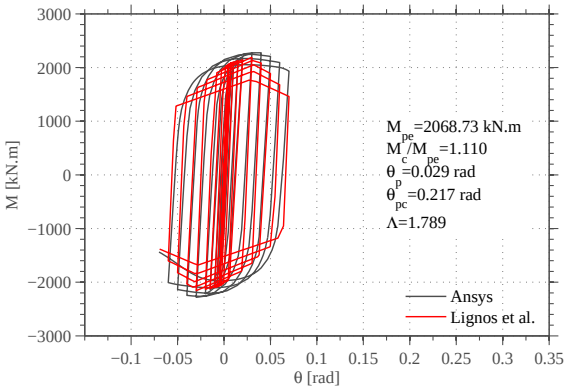

(c) Lignos and Krawinkler (2012)

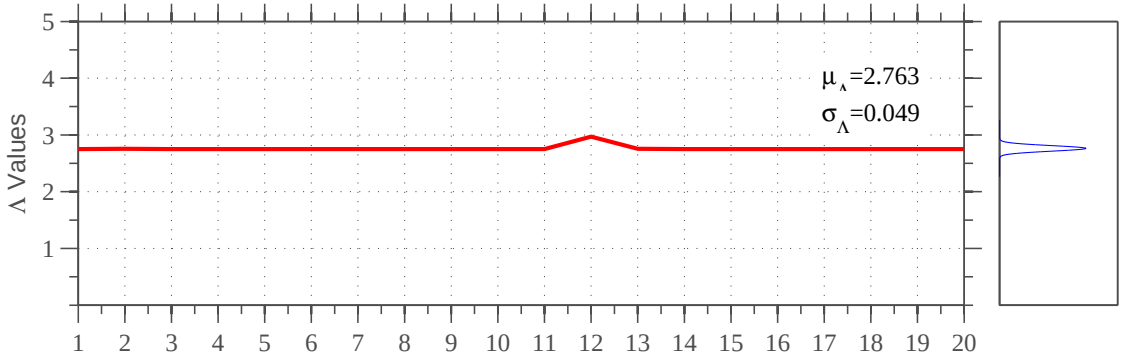

(d) Calibration Stability.

Figure A.36: Ibarra et al. (2005) calibration: HEB550.

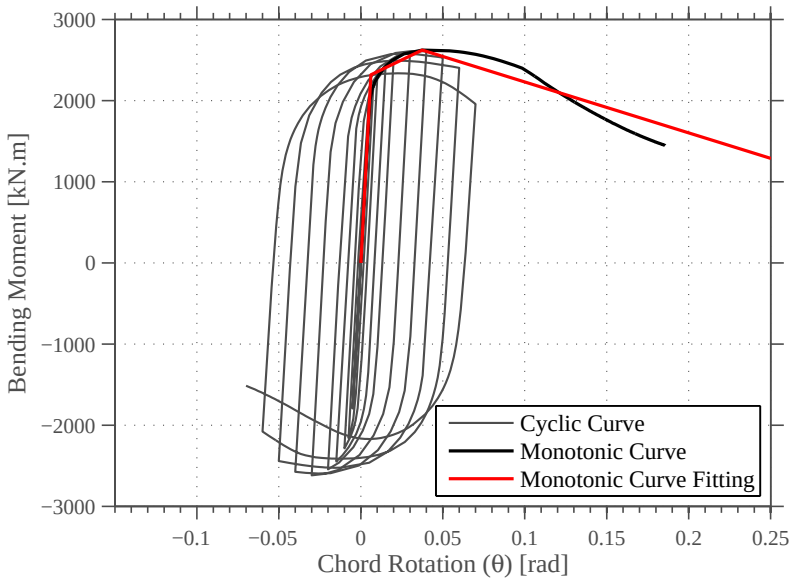

(a) Monotonic backbone calibration: HEB600.

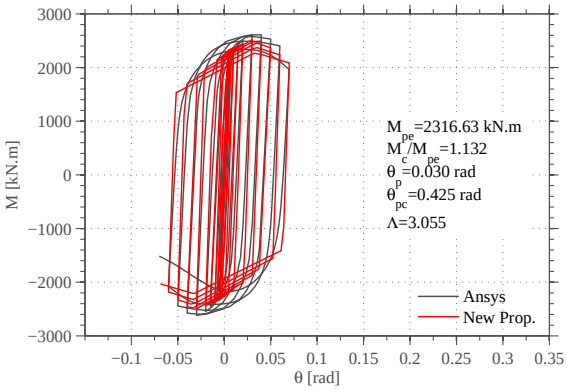

(b) Proposal

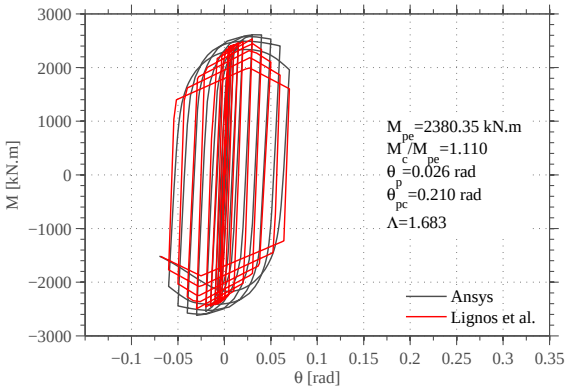

(c) Lignos and Krawinkler (2012)

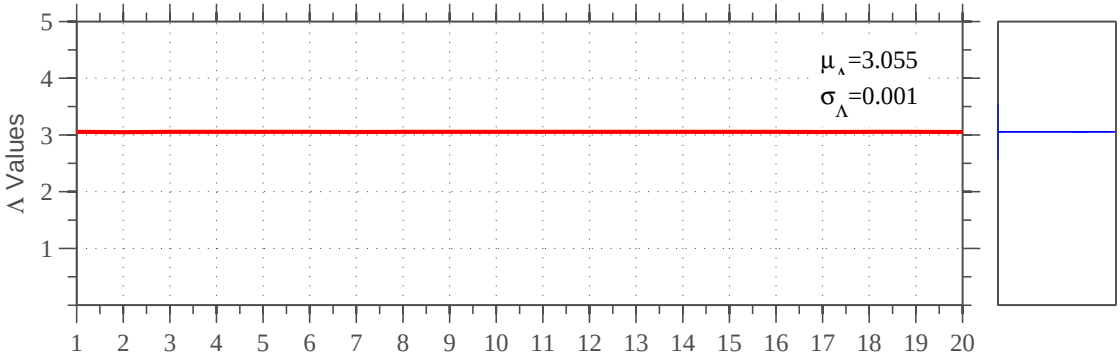

(d) Calibration Stability.

Figure A.37: Ibarra et al. (2005) calibration: HEB600.

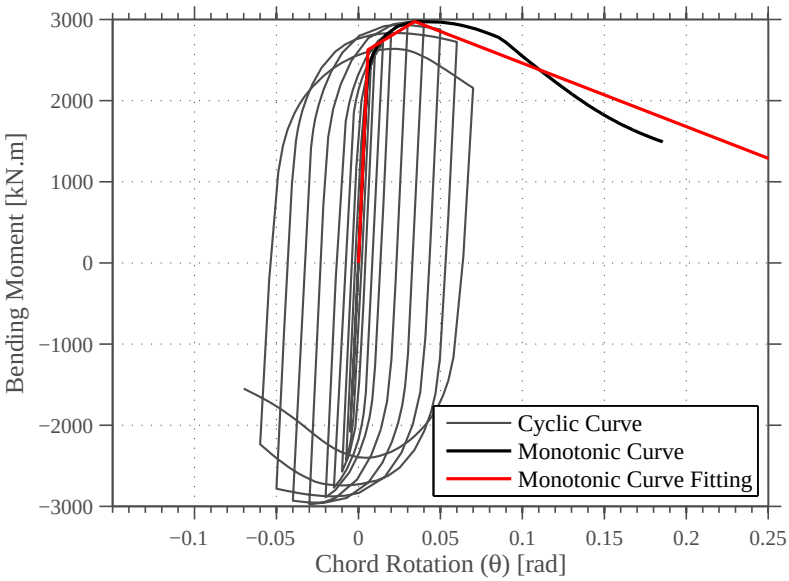

(a) Monotonic backbone calibration: HEB650.

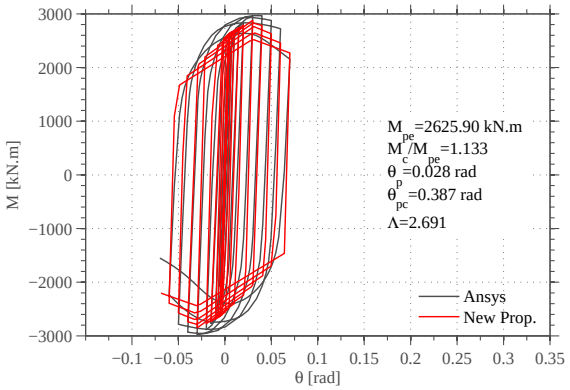

(b) Proposal

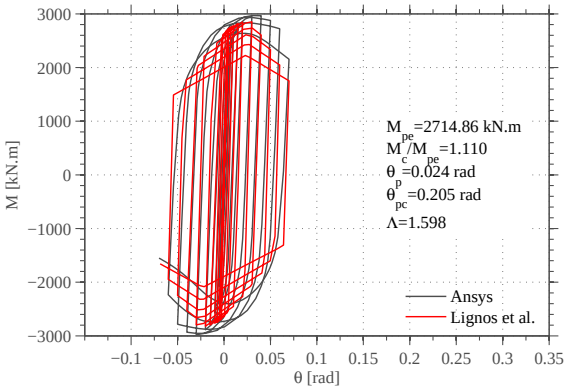

(c) Lignos and Krawinkler (2012)

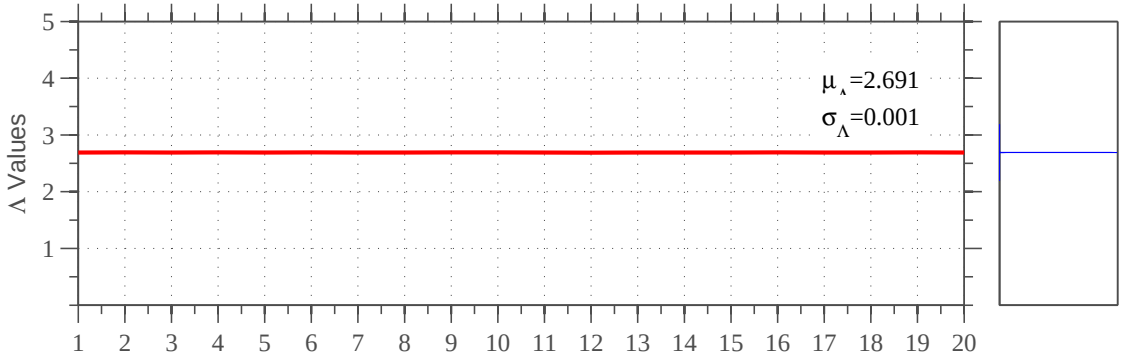

(d) Calibration Stability.

Figure A.38: Ibarra et al. (2005) calibration: HEB650.

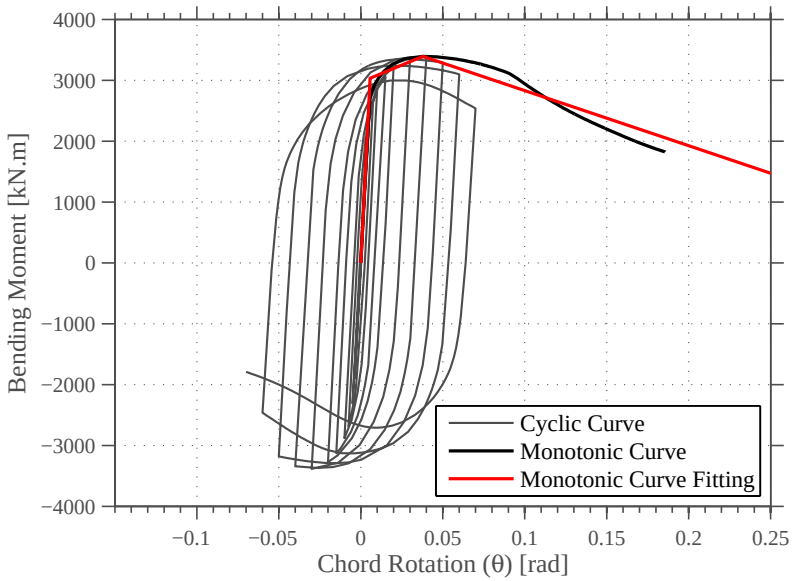

(a) Monotonic backbone calibration: HEB700.

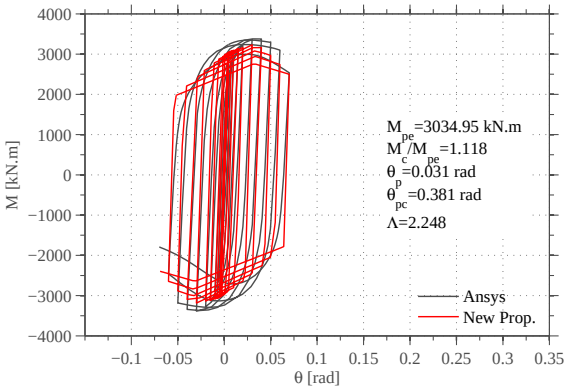

(b) Proposal

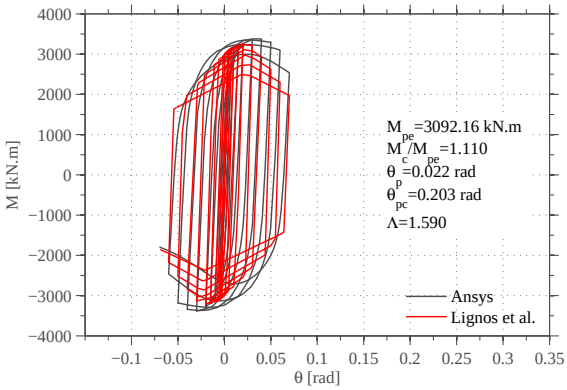

(c) Lignos and Krawinkler (2012)

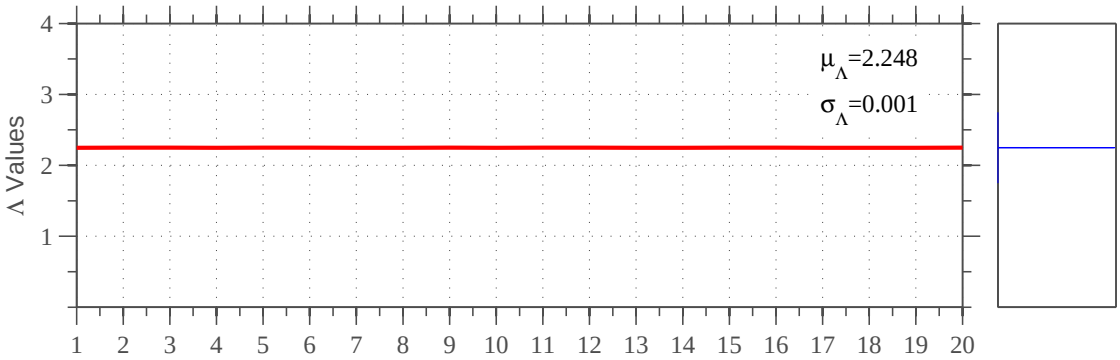

(d) Calibration Stability.

Figure A.39: Ibarra et al. (2005) calibration: HEB700.

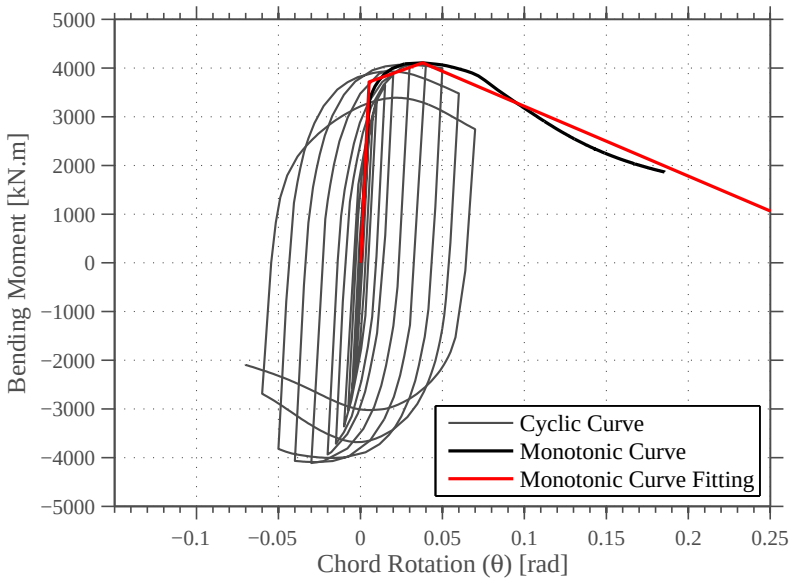

(a) Monotonic backbone calibration: HEB800.

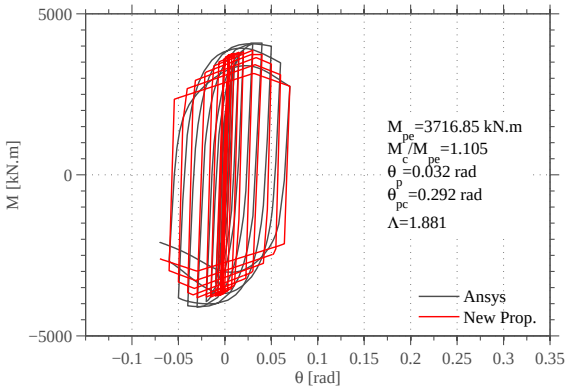

(b) Proposal

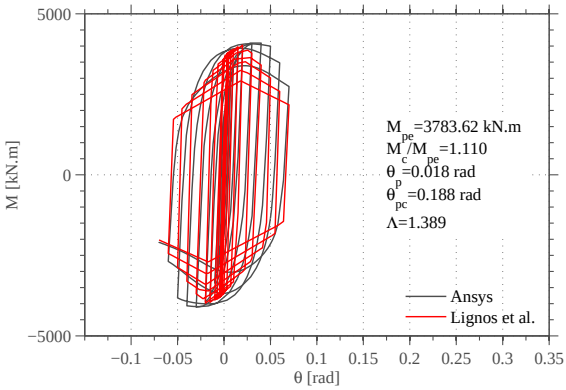

(c) Lignos and Krawinkler (2012)

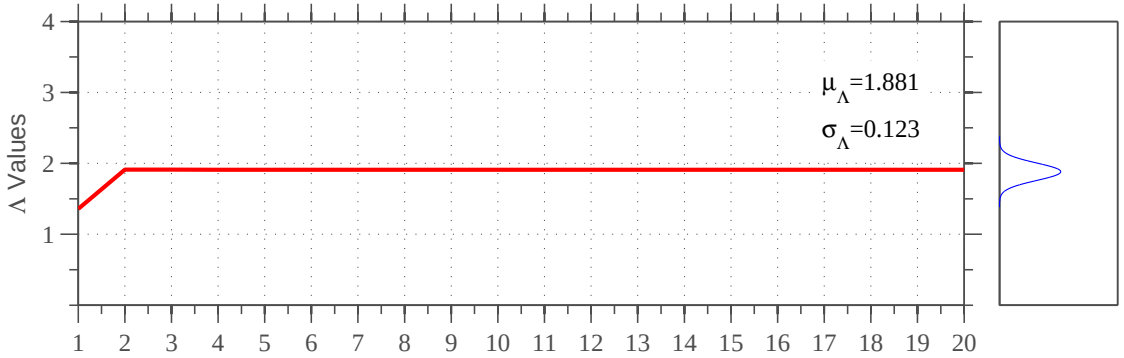

(d) Calibration Stability.

Figure A.40: Ibarra et al. (2005) calibration: HEB800.

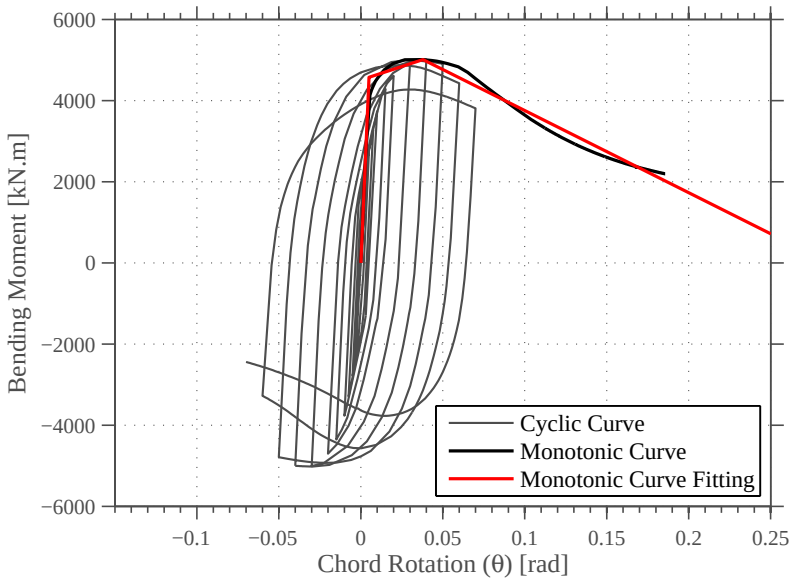

(a) Monotonic backbone calibration: HEB900.

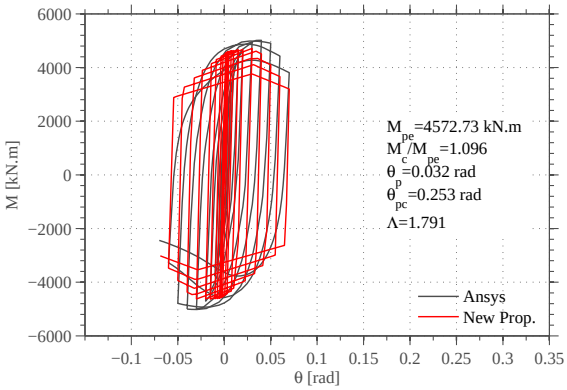

(b) Proposal

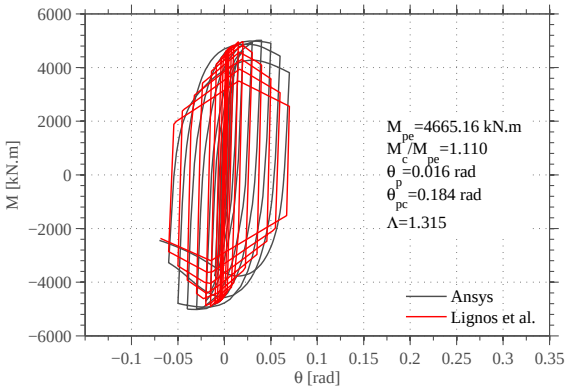

(c) Lignos and Krawinkler (2012)

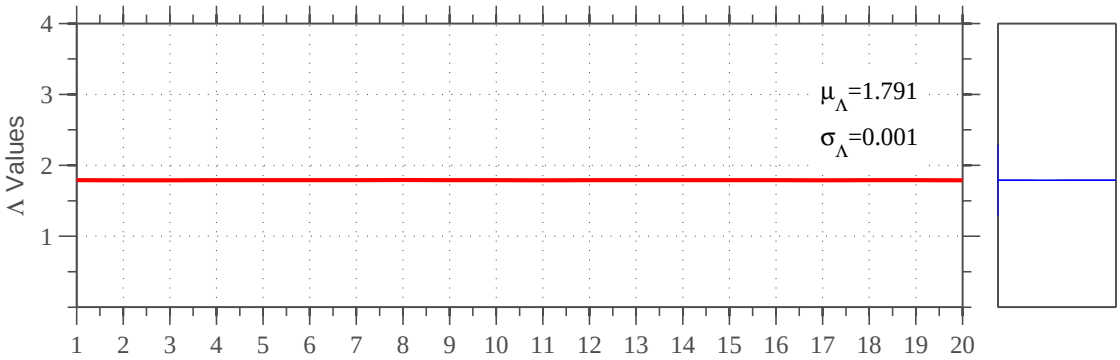

(d) Calibration Stability.

Figure A.41: Ibarra et al. (2005) calibration: HEB900.

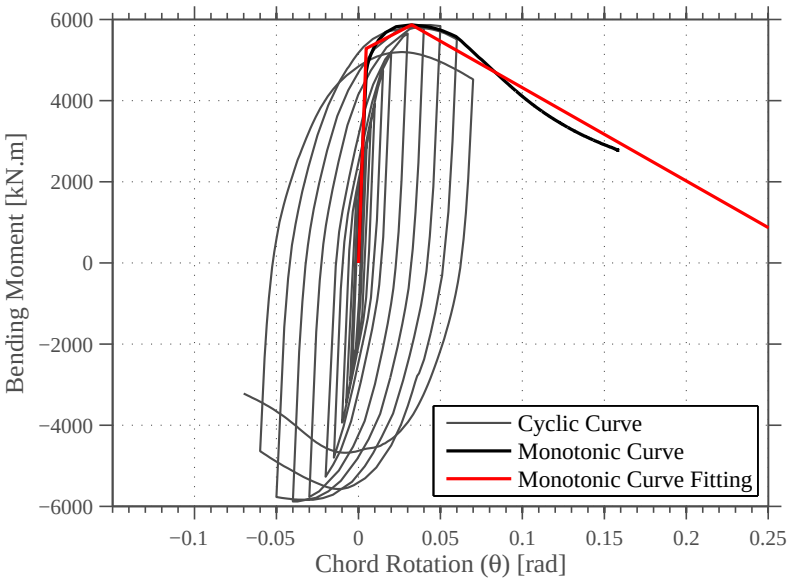

(a) Monotonic backbone calibration: HEB1000.

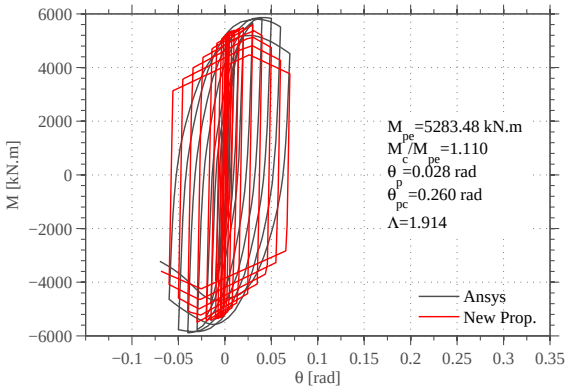

(b) Proposal

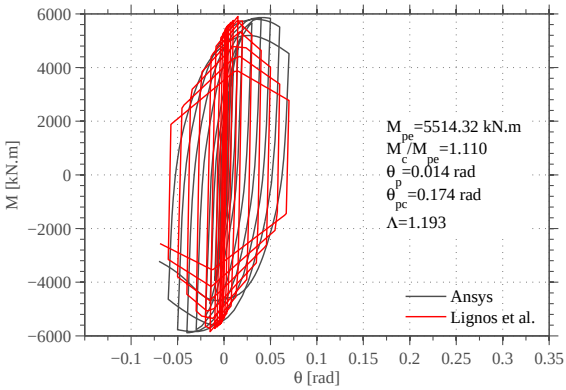

(c) Lignos and Krawinkler (2012)

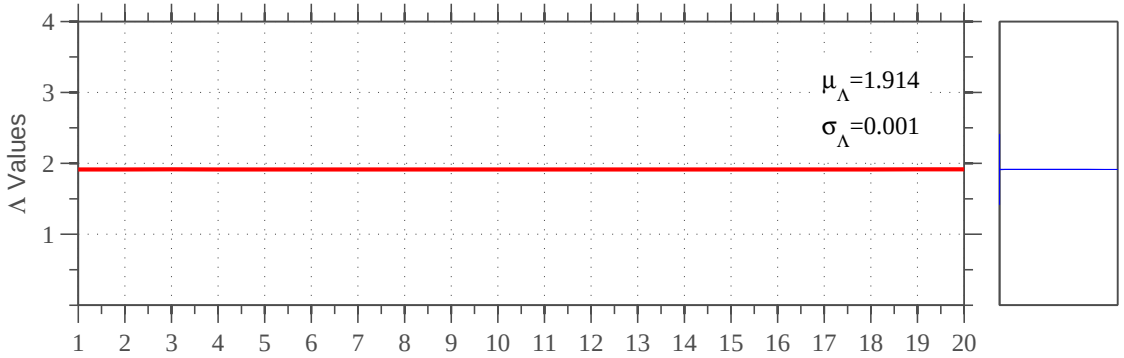

(d) Calibration Stability.

Figure A.42: Ibarra et al. (2005) calibration: HEB1000.

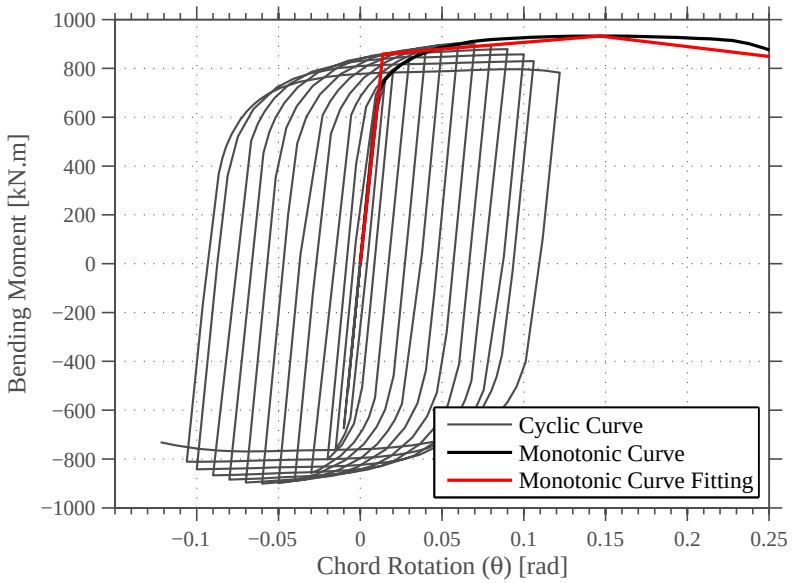

(a) Monotonic backbone calibration: HEM240.

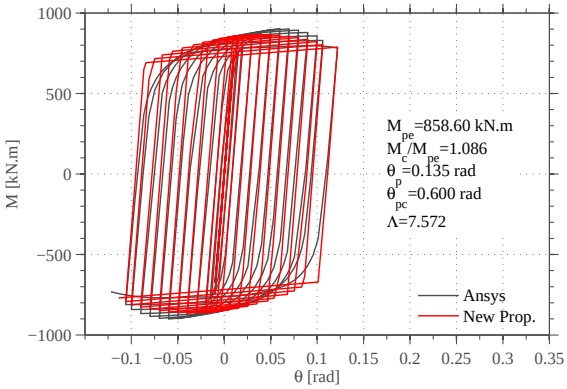

(b) Proposal

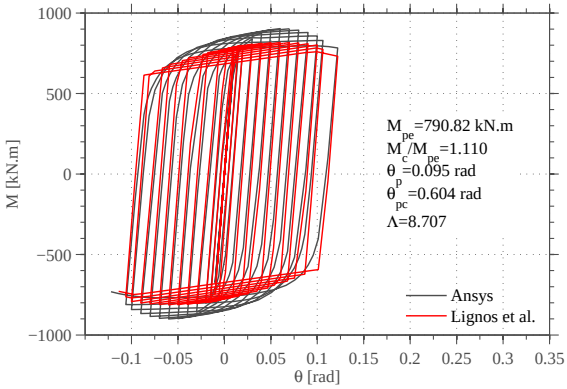

(c) Lignos and Krawinkler (2012)

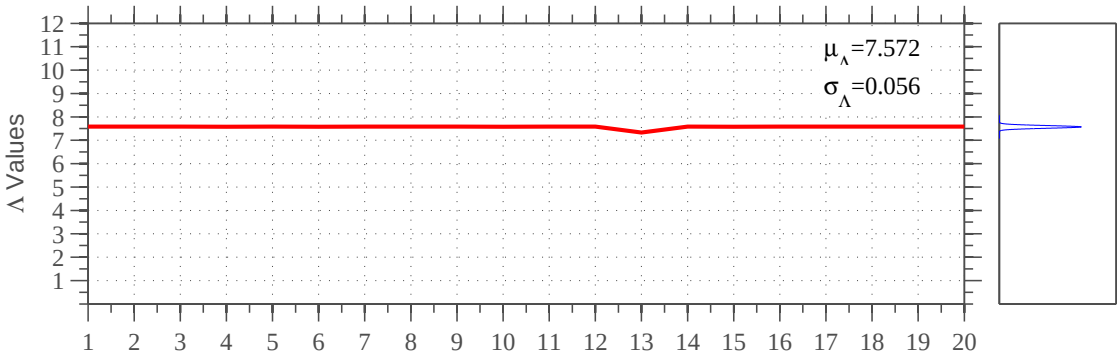

(d) Calibration Stability.

Figure A.43: Ibarra et al. (2005) calibration: HEM240.

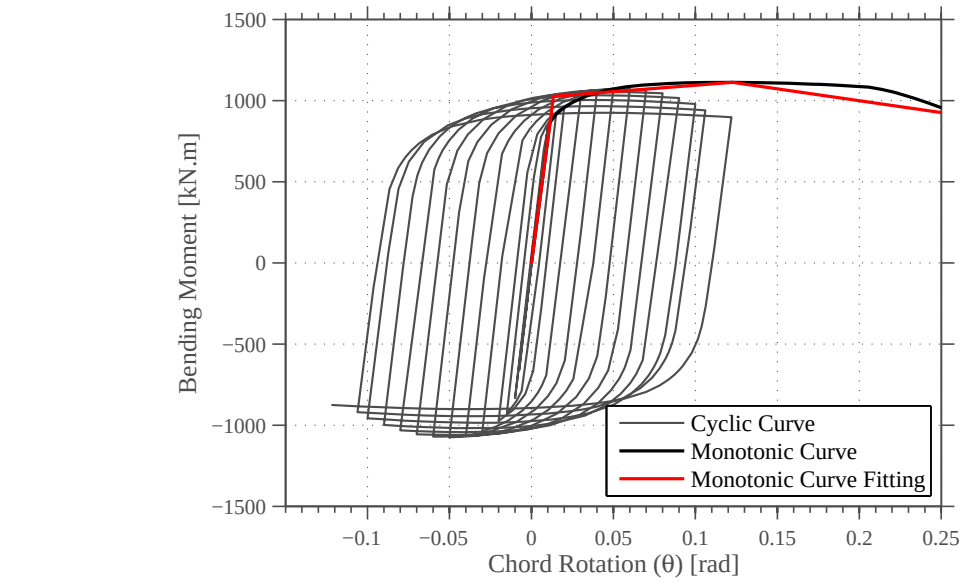

(a) Monotonic backbone calibration: HEM260.

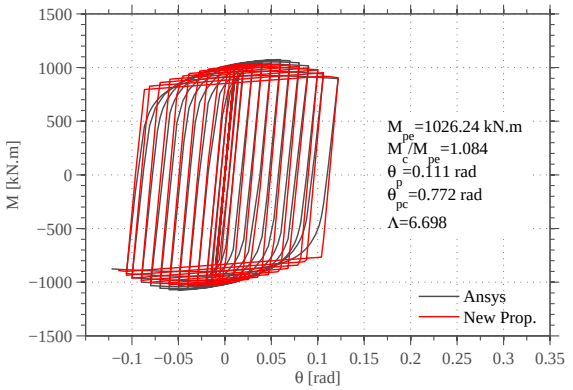

(b) Proposal

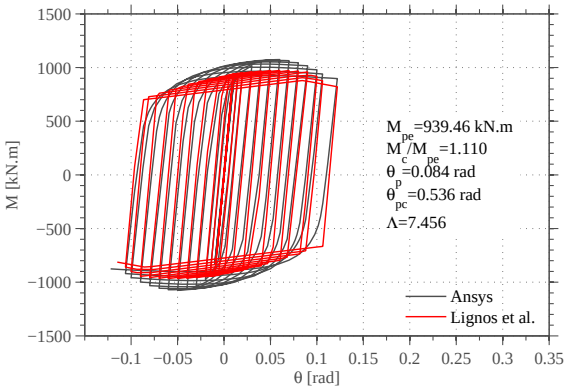

(c) Lignos and Krawinkler (2012)

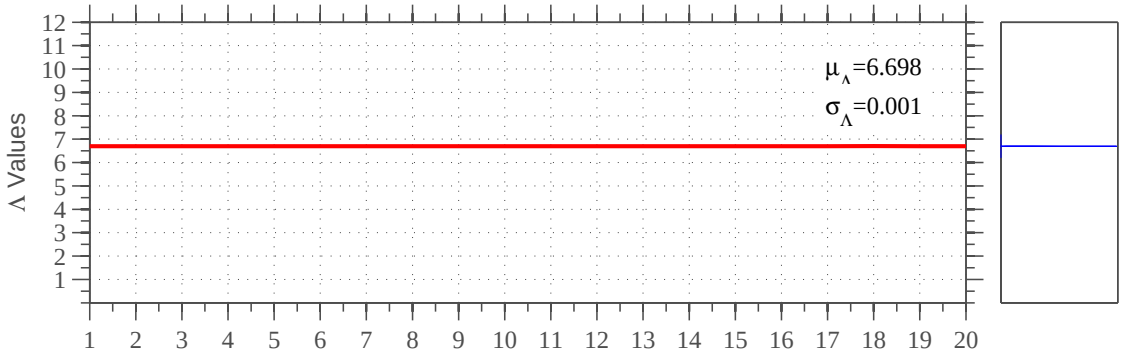

(d) Calibration Stability.

Figure A.44: Ibarra et al. (2005) calibration: HEM260.

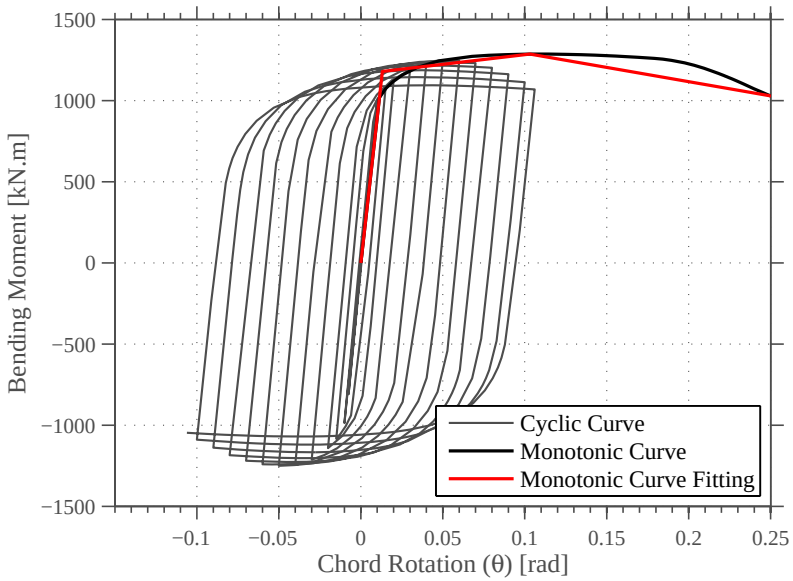

(a) Monotonic backbone calibration: HEM280.

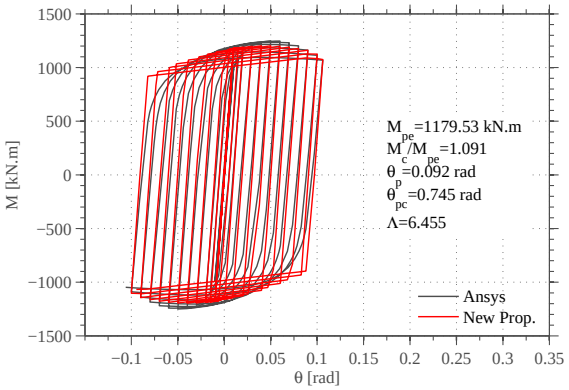

(b) Proposal

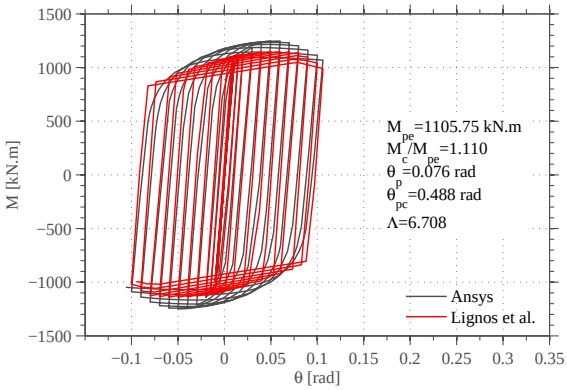

(c) Lignos and Krawinkler (2012)

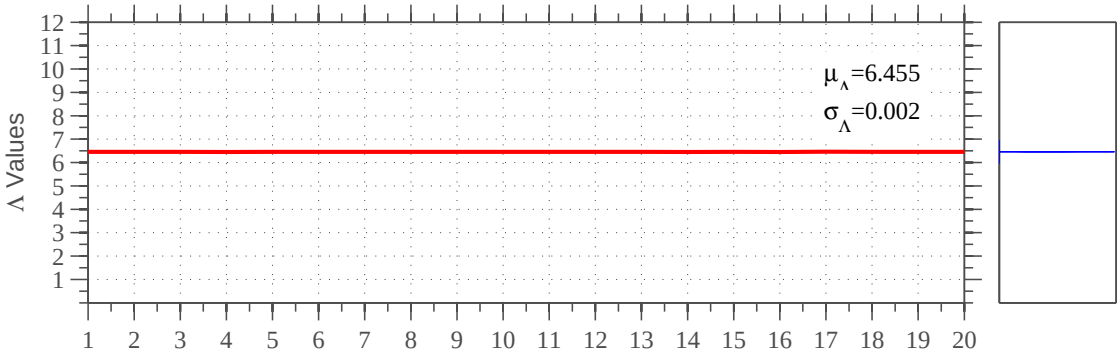

(d) Calibration Stability.

Figure A.45: Ibarra et al. (2005) calibration: HEM280.

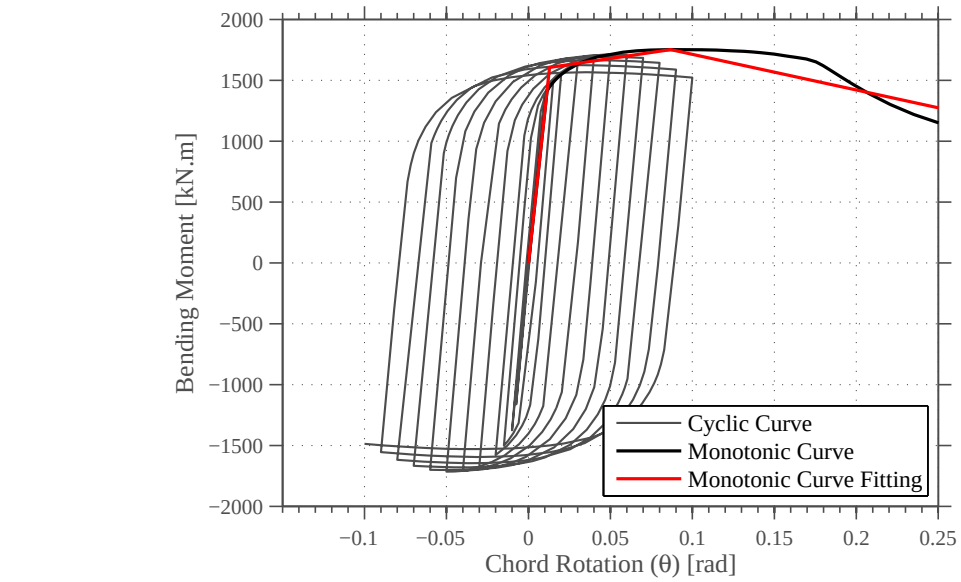

(a) Monotonic backbone calibration: HEM300.

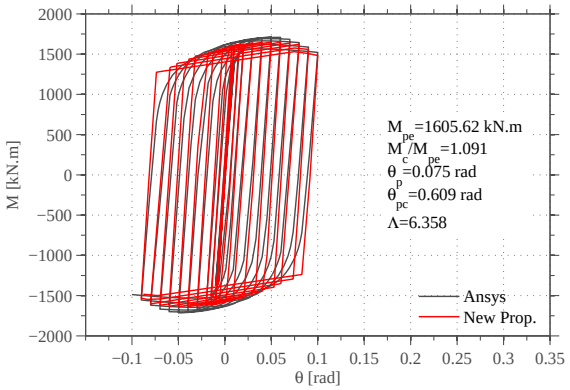

(b) Proposal

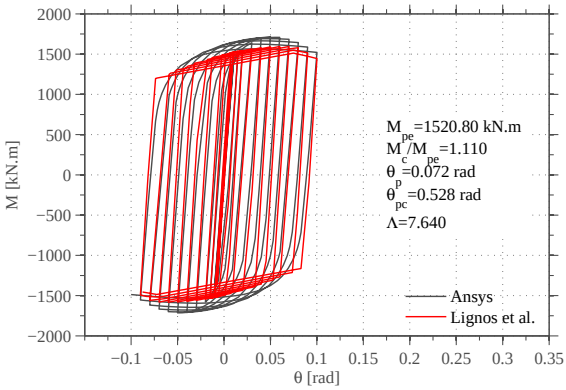

(c) Lignos and Krawinkler (2012)

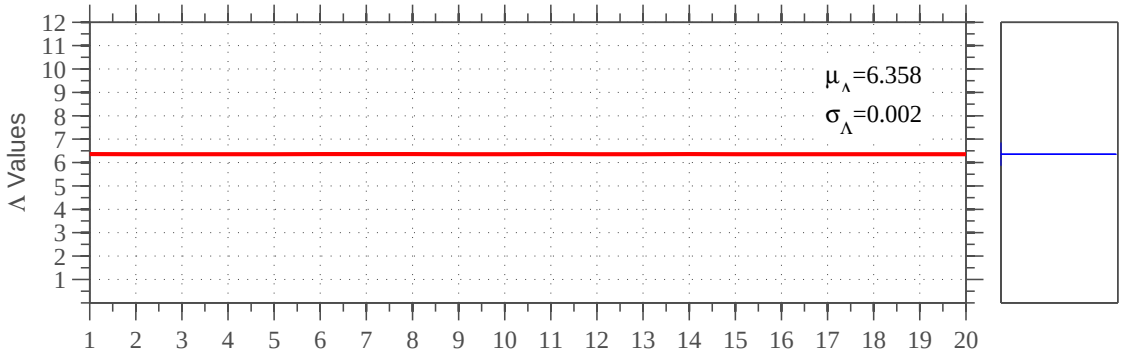

(d) Calibration Stability.

Figure A.46: Ibarra et al. (2005) calibration: HEM300.

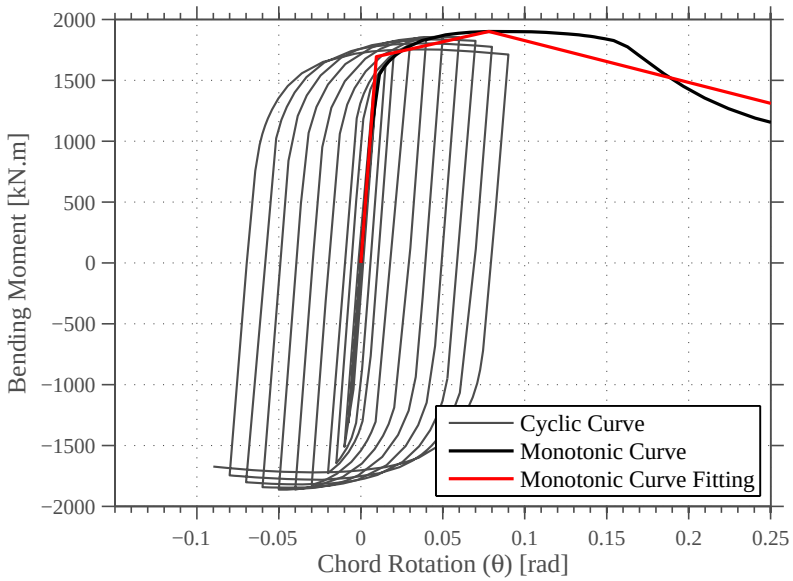

(a) Monotonic backbone calibration: HEM320.

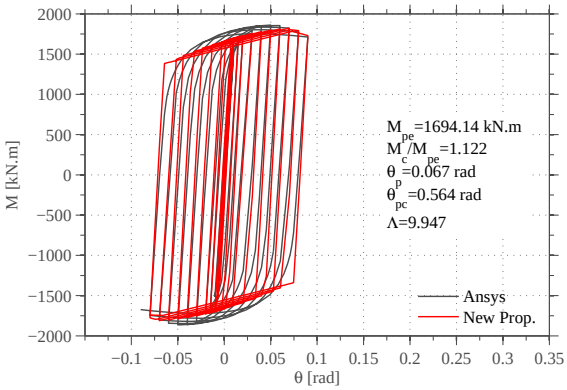

(b) Proposal

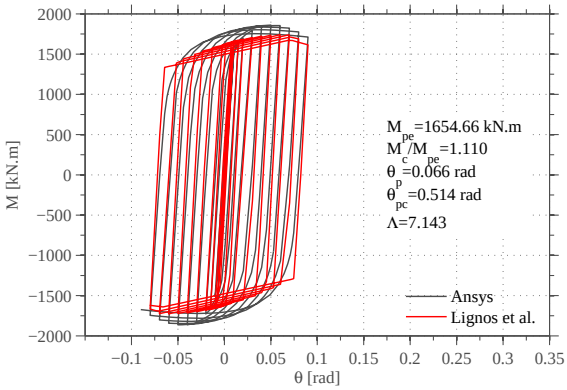

(c) Lignos and Krawinkler (2012)

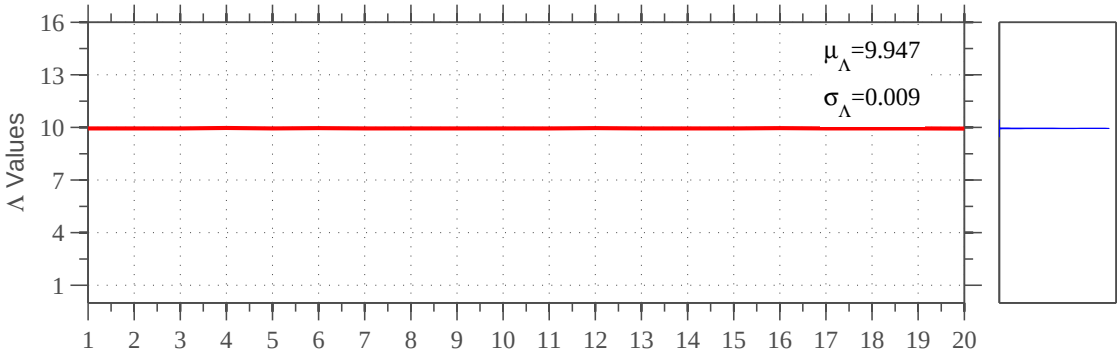

(d) Calibration Stability.

Figure A.47: Ibarra et al. (2005) calibration: HEM320.

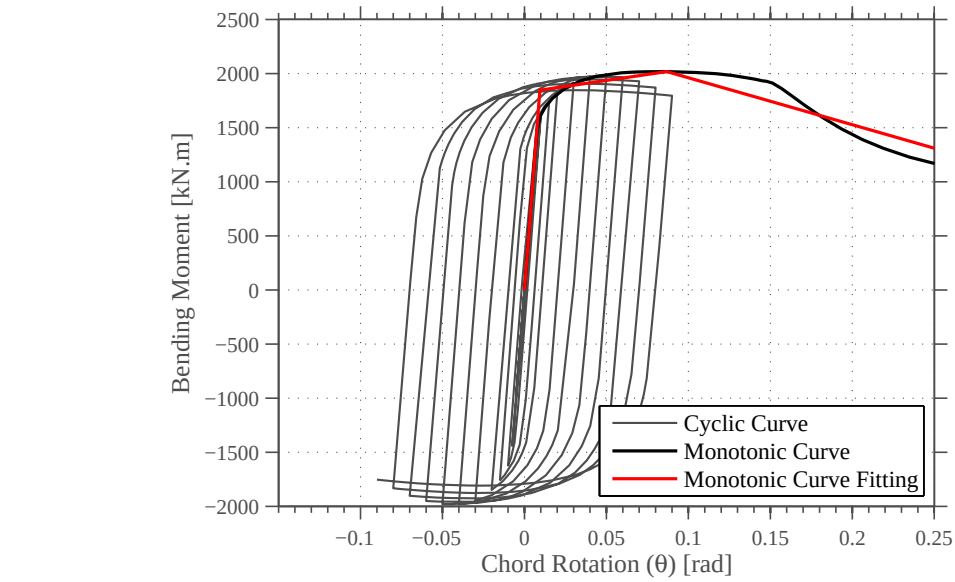

(a) Monotonic backbone calibration: HEM340.

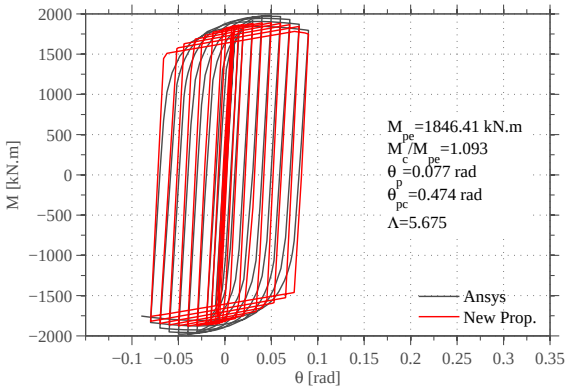

(b) Proposal

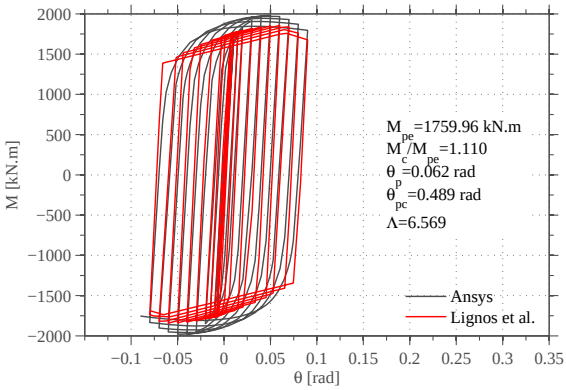

(c) Lignos and Krawinkler (2012)

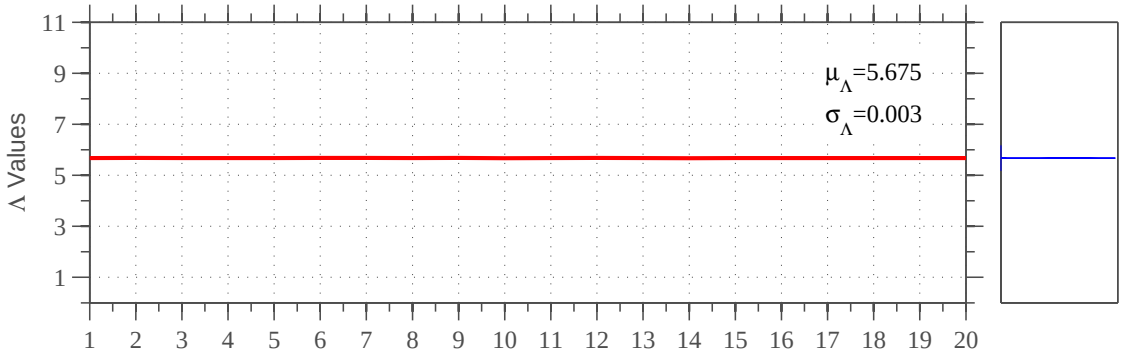

(d) Calibration Stability.

Figure A.48: Ibarra et al. (2005) calibration: HEM340.

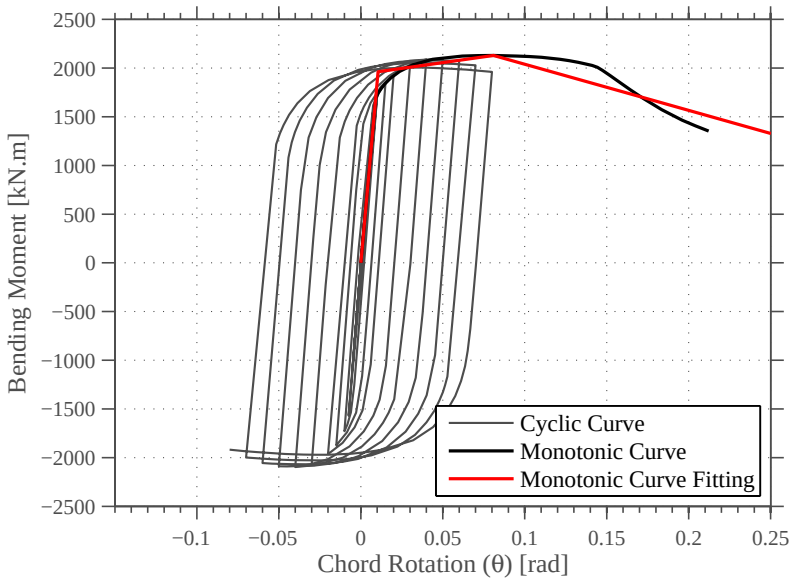

(a) Monotonic backbone calibration: HEM360.

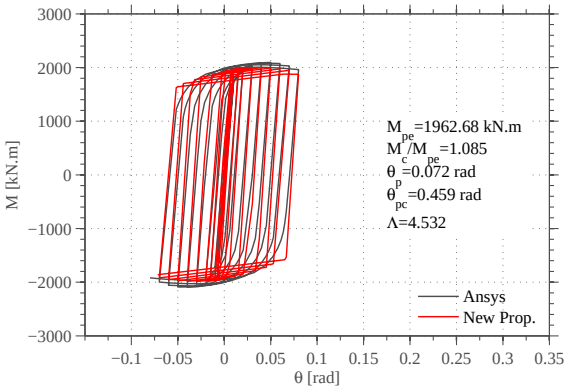

(b) Proposal

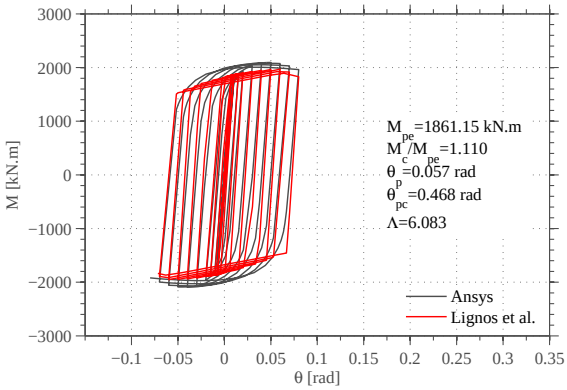

(c) Lignos and Krawinkler (2012)

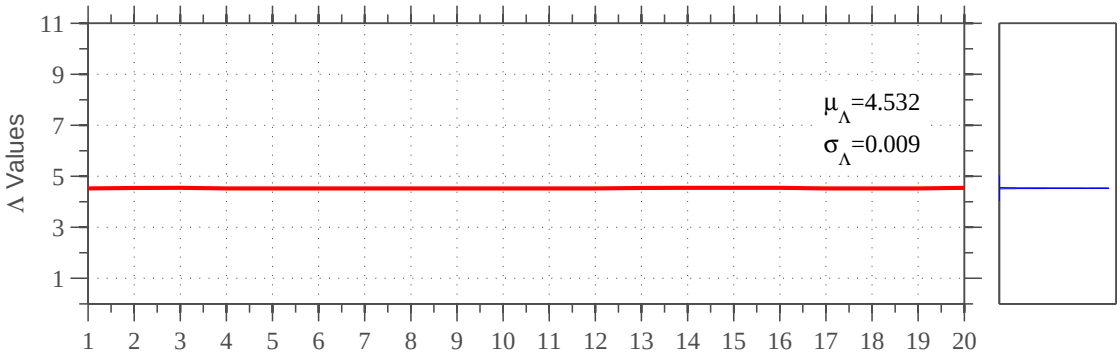

(d) Calibration Stability.

Figure A.49: Ibarra et al. (2005) calibration: HEM360.

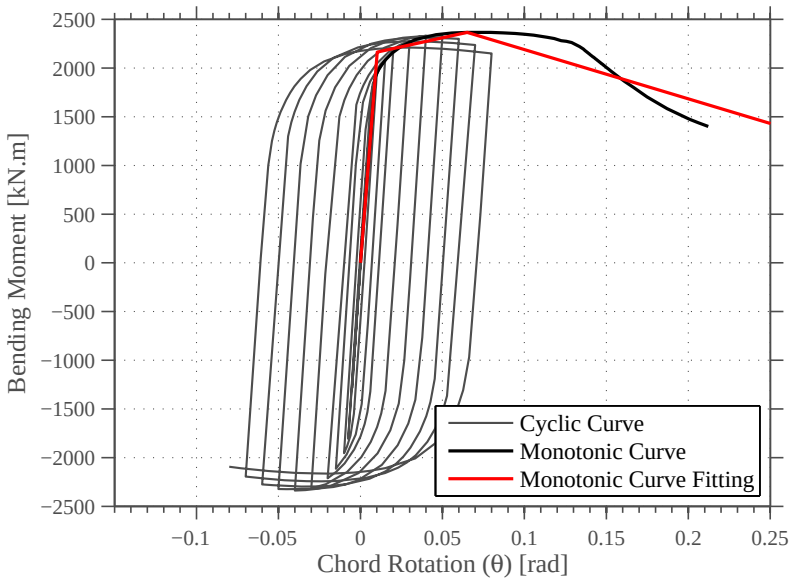

(a) Monotonic backbone calibration: HEM400.

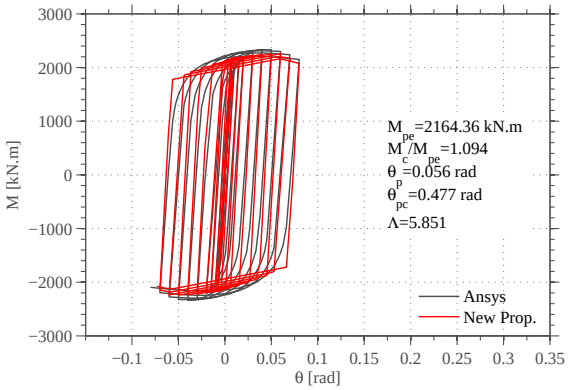

(b) Proposal

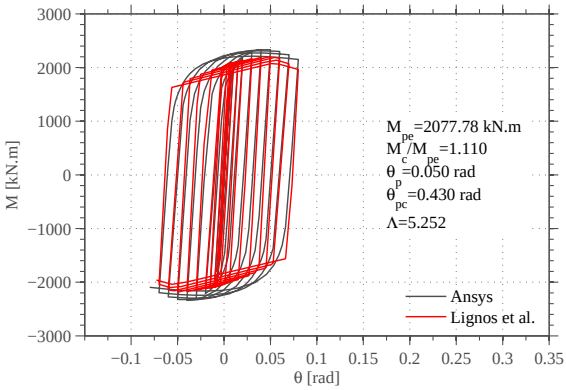

(c) Lignos and Krawinkler (2012)

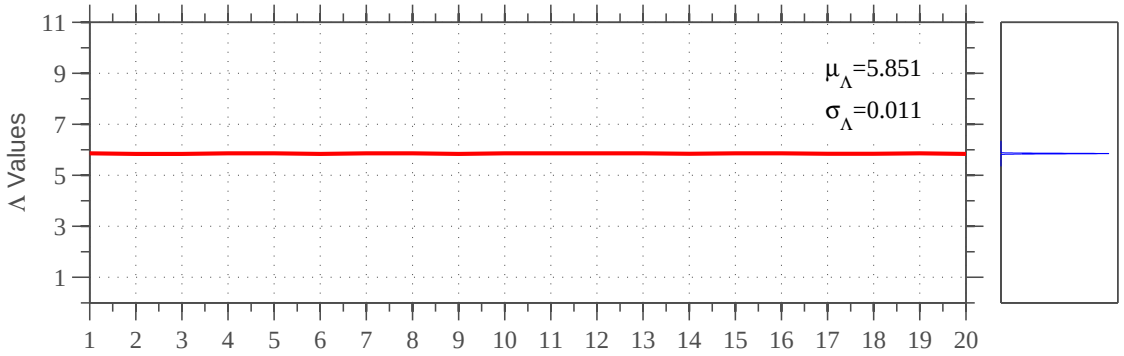

(d) Calibration Stability.

Figure A.50: Ibarra et al. (2005) calibration: HEM400.

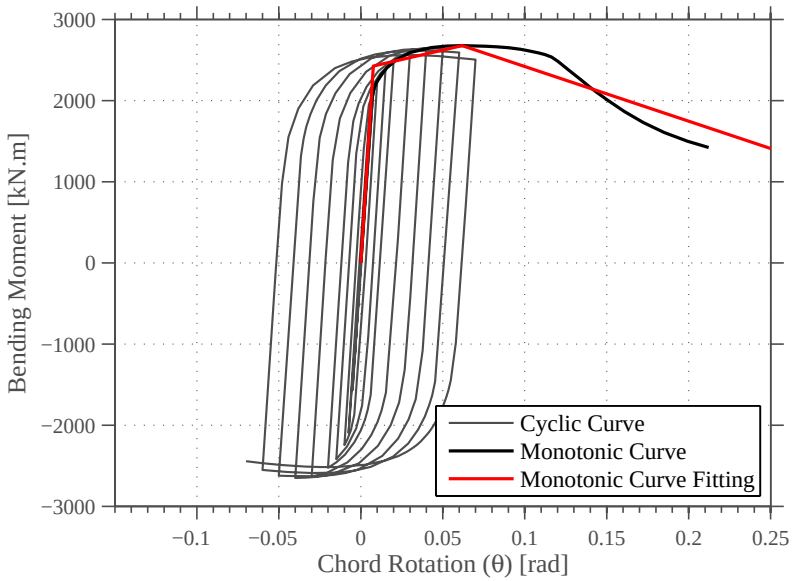

(a) Monotonic backbone calibration: HEM450.

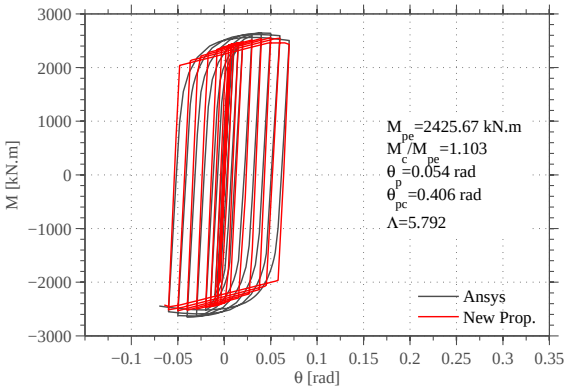

(b) Proposal

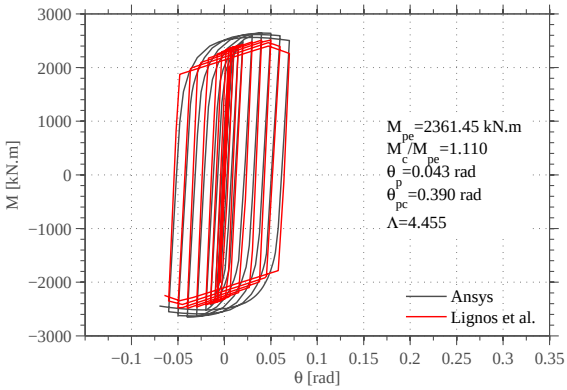

(c) Lignos and Krawinkler (2012)

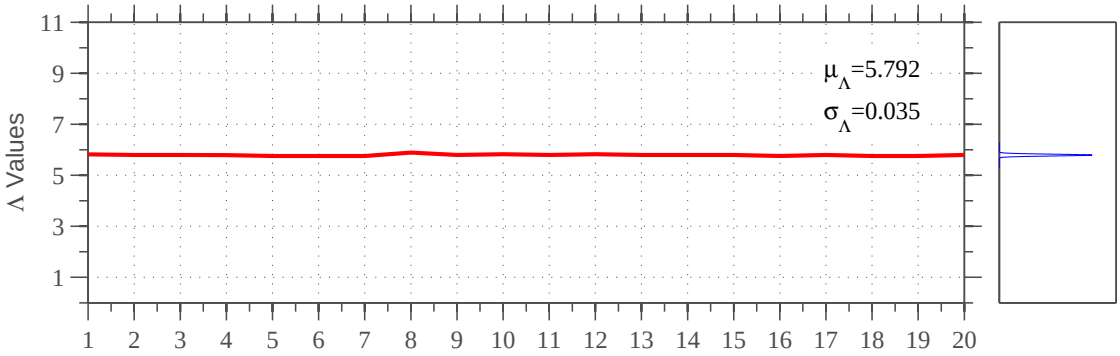

(d) Calibration Stability.

Figure A.51: Ibarra et al. (2005) calibration: HEM450.

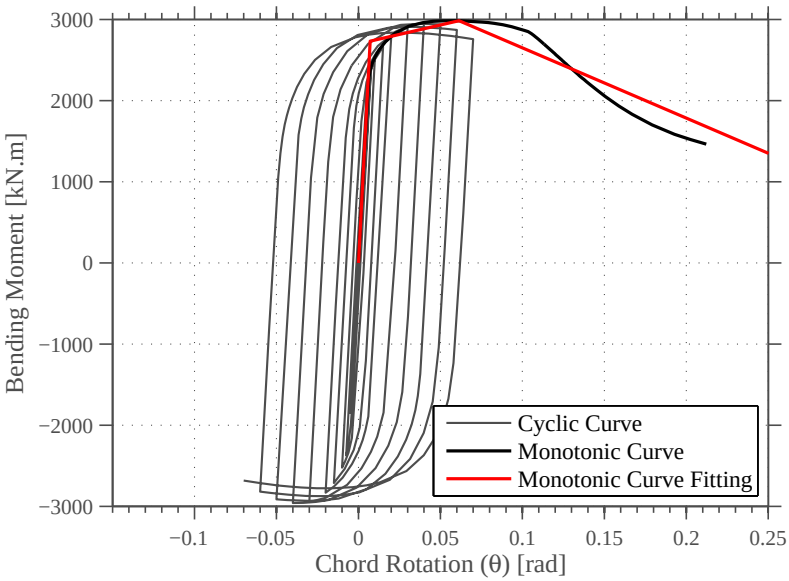

(a) Monotonic backbone calibration: HEM500.

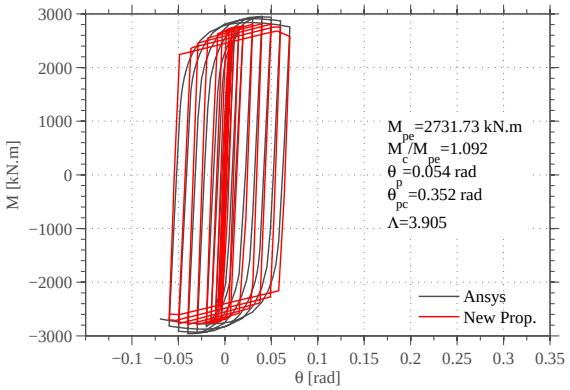

(b) Proposal

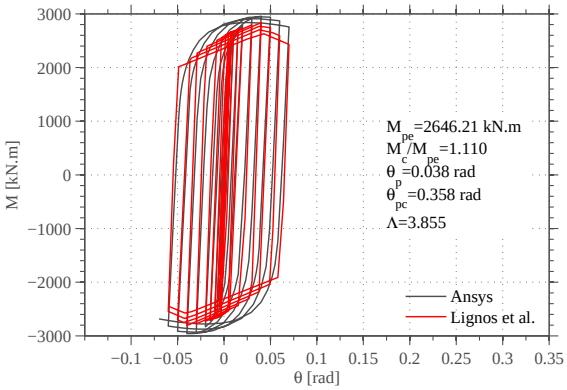

(c) Lignos and Krawinkler (2012)

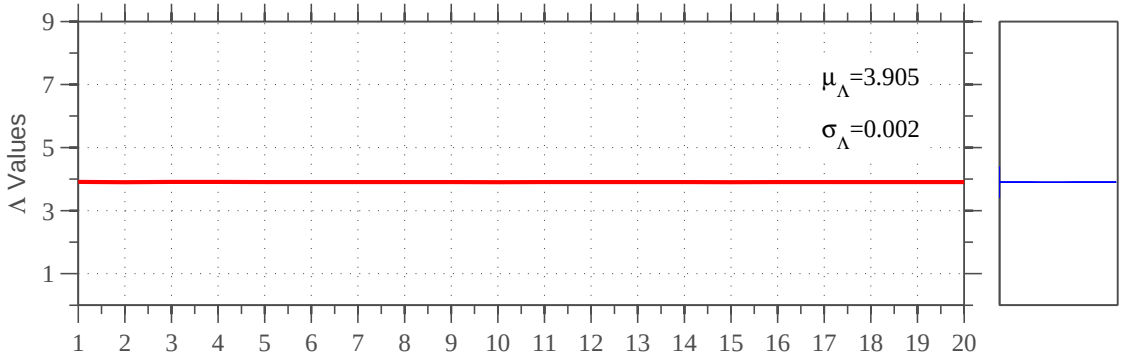

(d) Calibration Stability.

Figure A.52: Ibarra et al. (2005) calibration: HEM500.

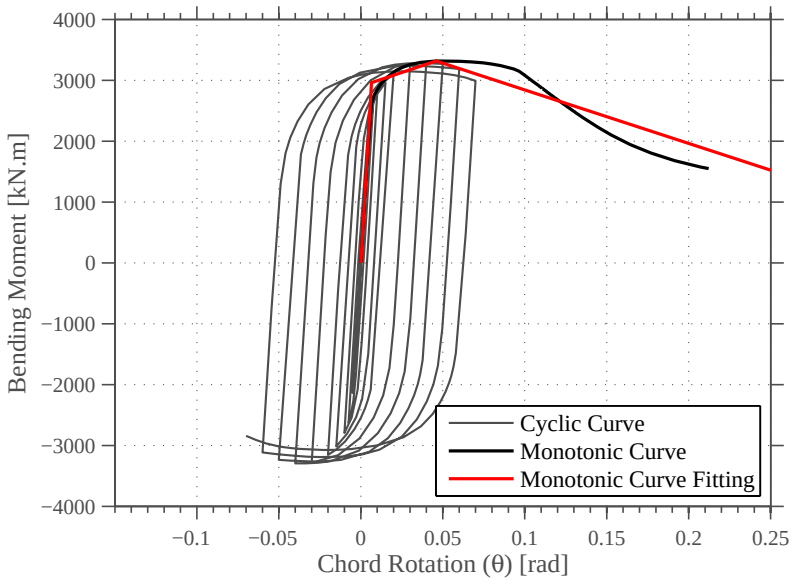

(a) Monotonic backbone calibration: HEM550.

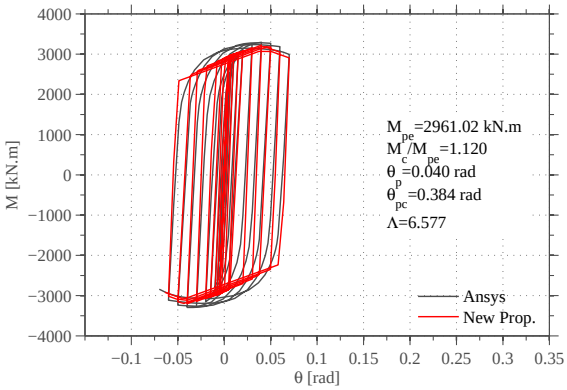

(b) Proposal

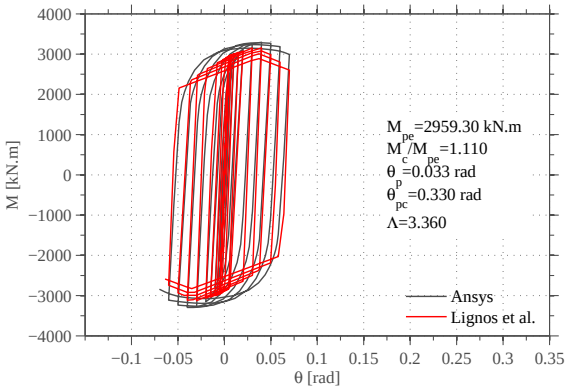

(c) Lignos and Krawinkler (2012)

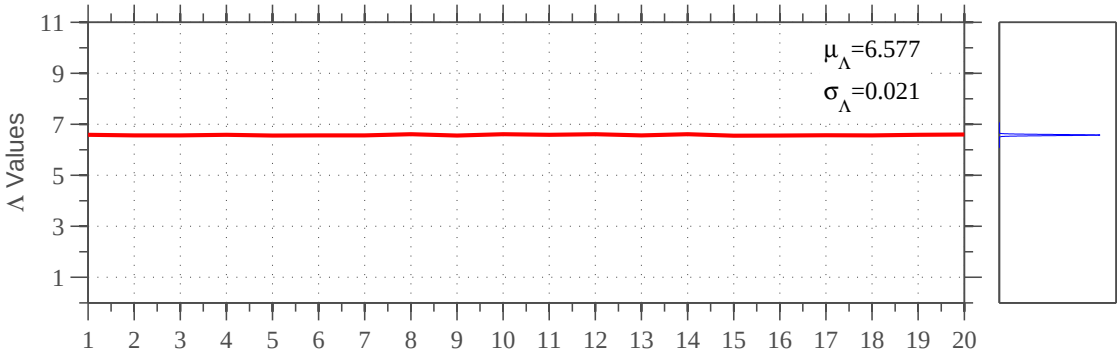

(d) Calibration Stability.

Figure A.53: Ibarra et al. (2005) calibration: HEM550.

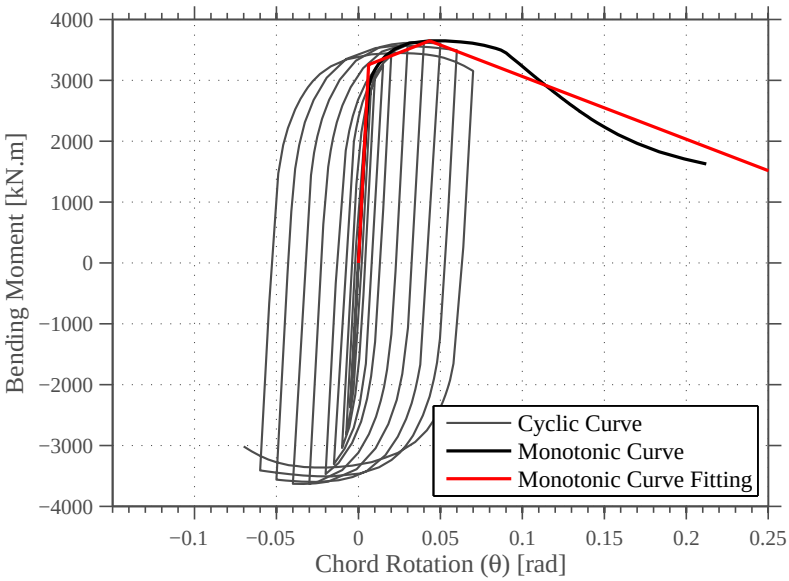

(a) Monotonic backbone calibration: HEM600.

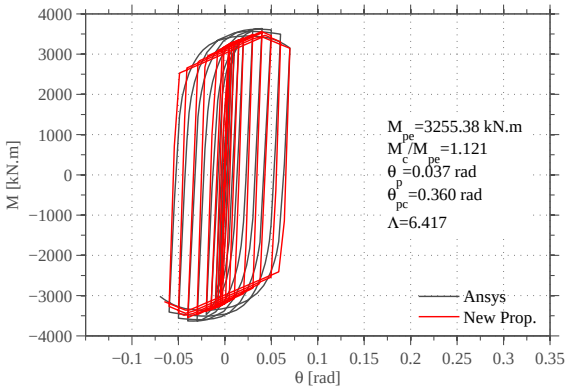

(b) Proposal

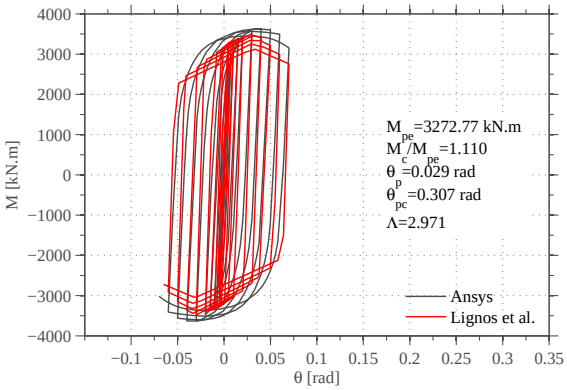

(c) Lignos and Krawinkler (2012)

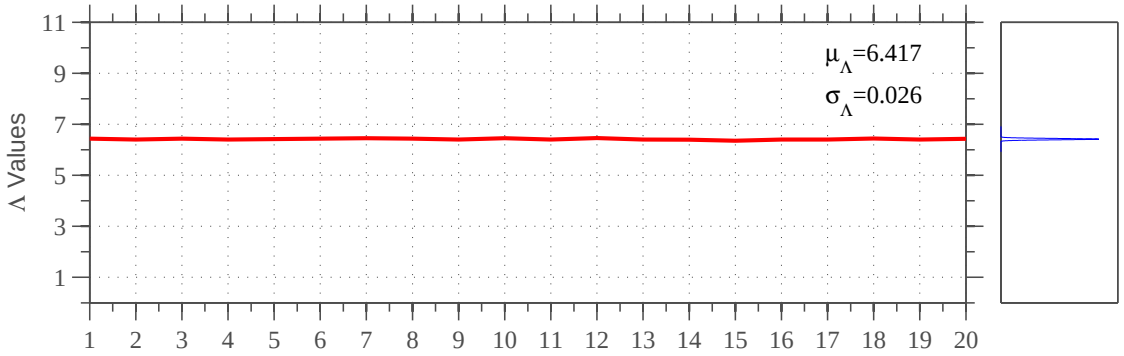

(d) Calibration Stability.

Figure A.54: Ibarra et al. (2005) calibration: HEM600.

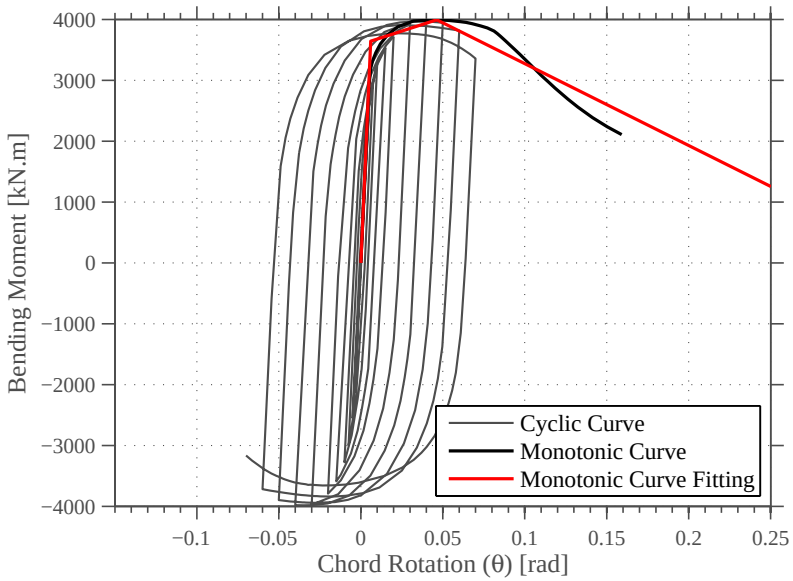

(a) Monotonic backbone calibration: HEM650.

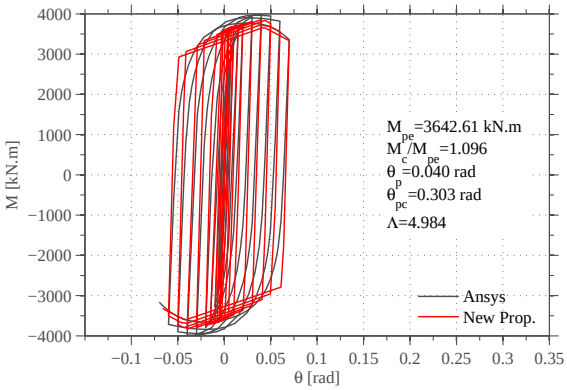

(b) Proposal

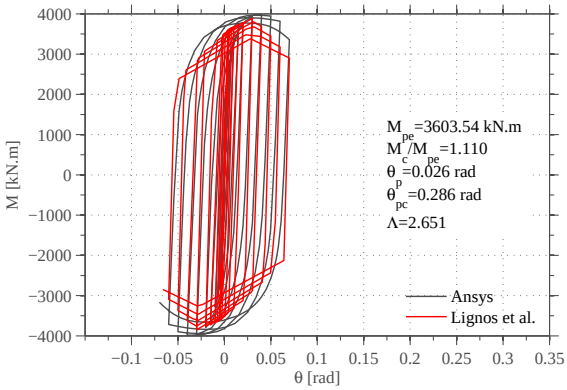

(c) Lignos and Krawinkler (2012)

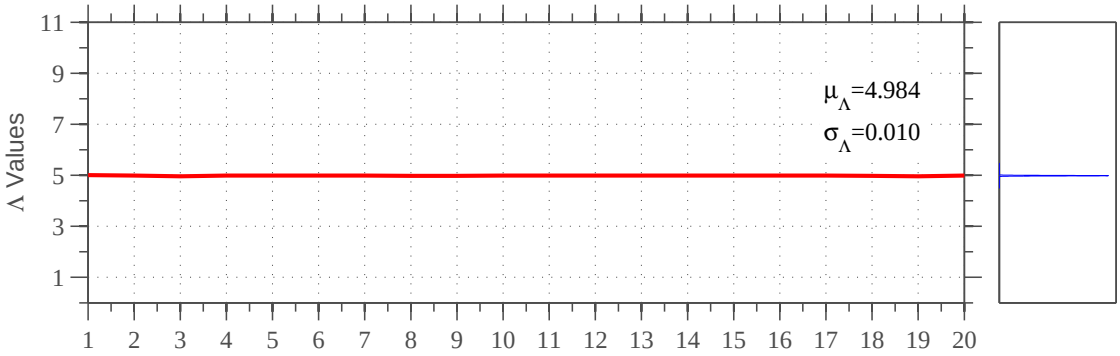

(d) Calibration Stability.

Figure A.55: Ibarra et al. (2005) calibration: HEM650.

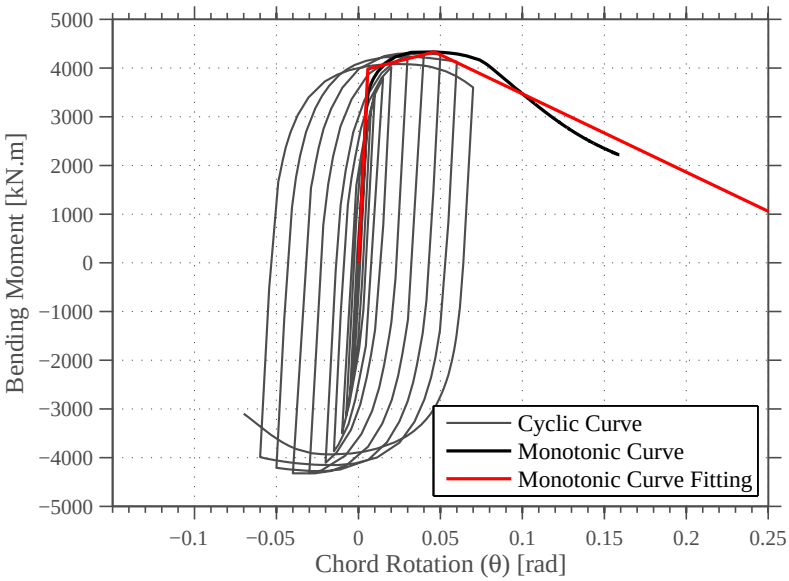

(a) Monotonic backbone calibration: HEM700.

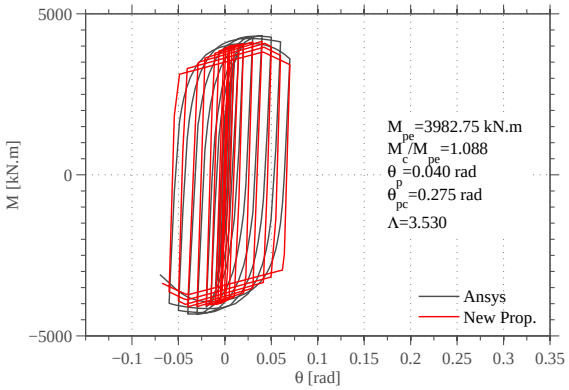

(b) Proposal

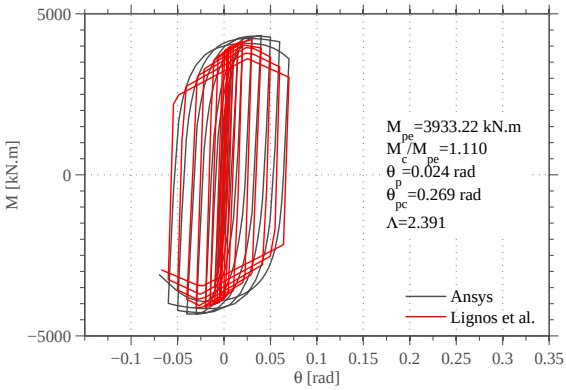

(c) Lignos and Krawinkler (2012)

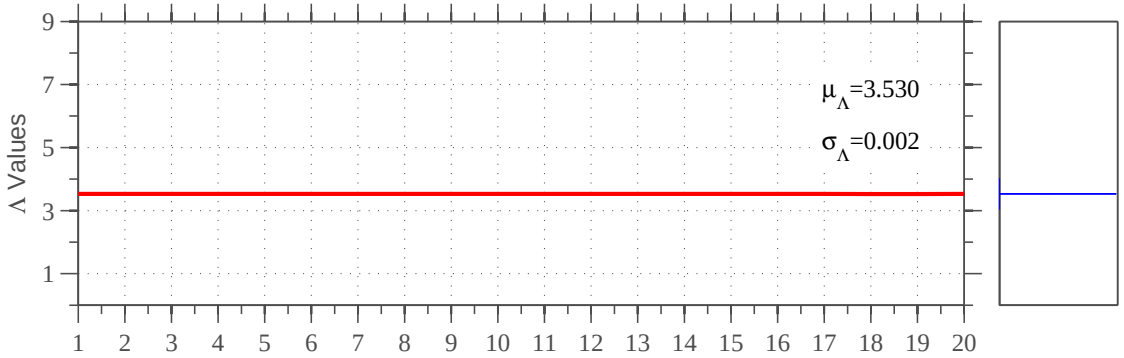

(d) Calibration Stability.

Figure A.56: Ibarra et al. (2005) calibration: HEM700.

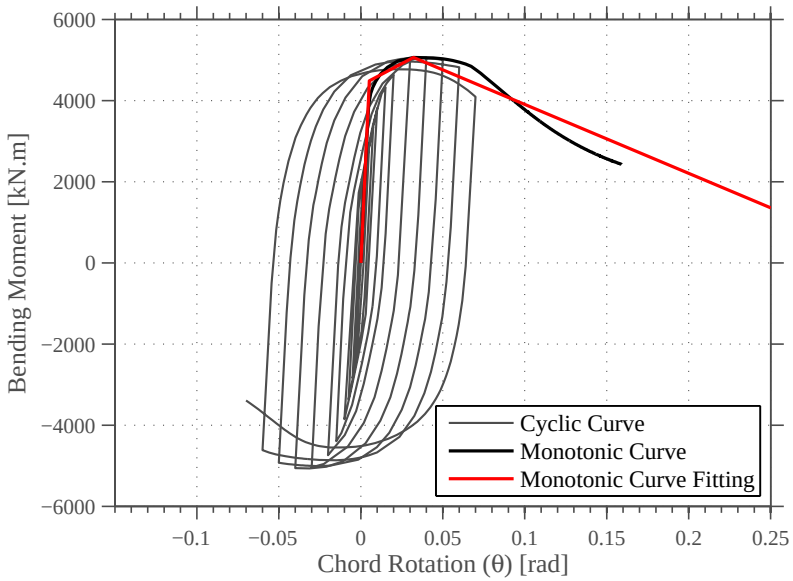

(a) Monotonic backbone calibration: HEM800.

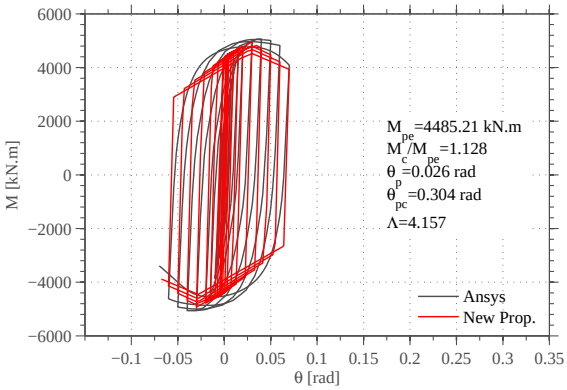

(b) Proposal

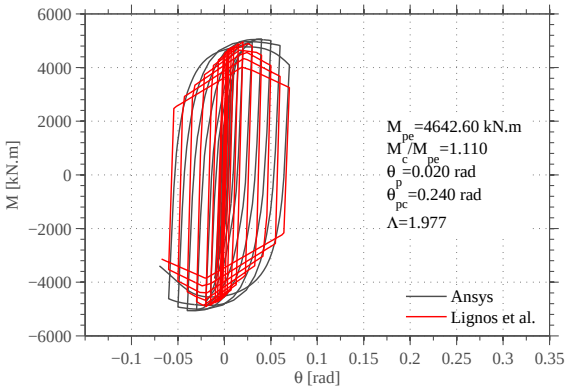

(c) Lignos and Krawinkler (2012)

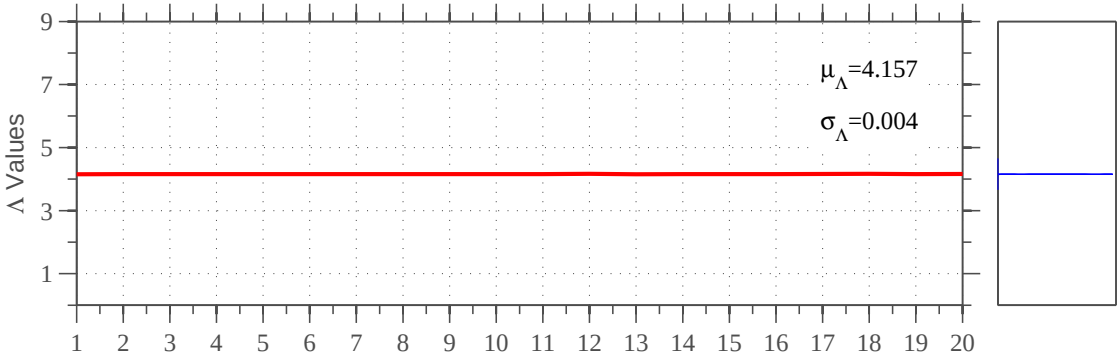

(d) Calibration Stability.

Figure A.57: Ibarra et al. (2005) calibration: HEM800.

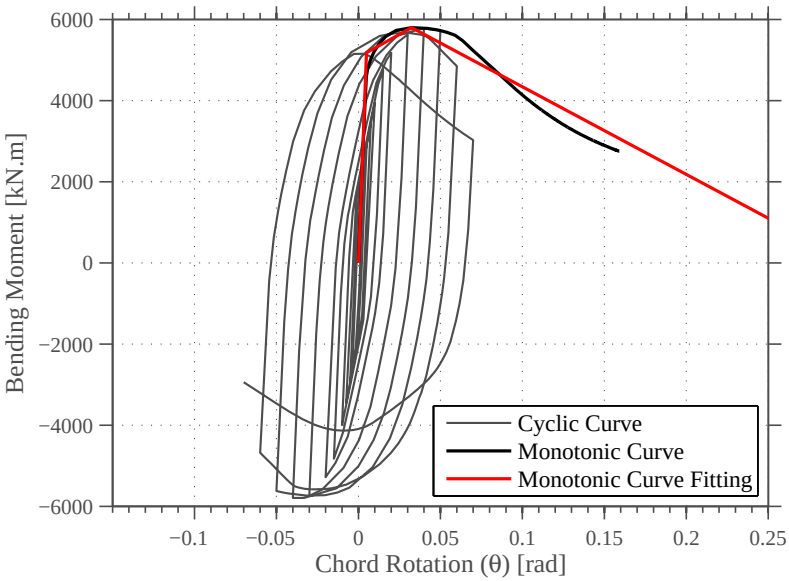

(a) Monotonic backbone calibration: HEM900.

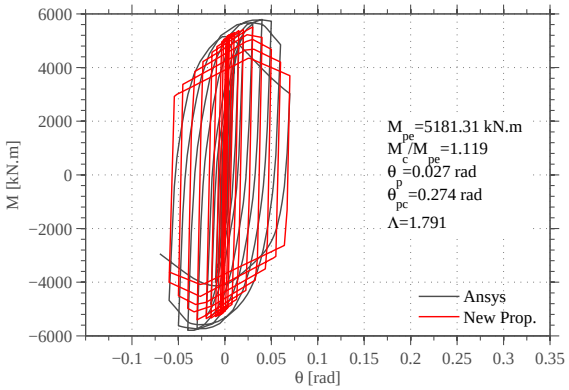

(b) Proposal

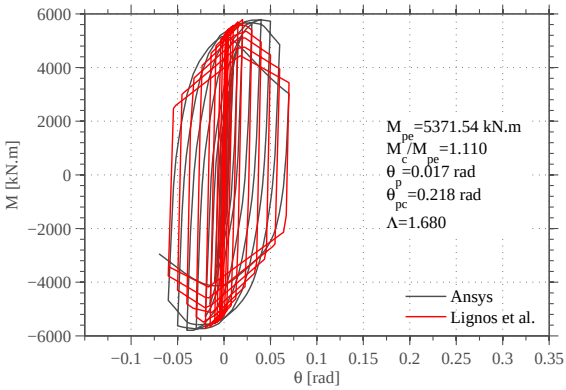

(c) Lignos and Krawinkler (2012)

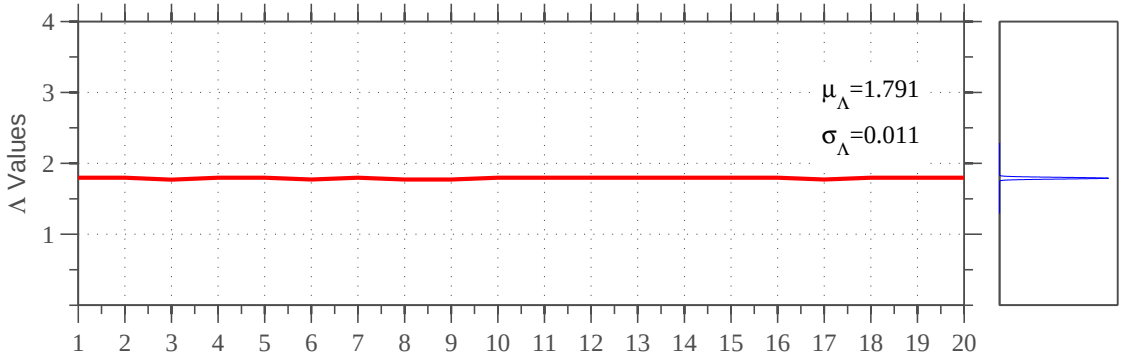

(d) Calibration Stability.

Figure A.58: Ibarra et al. (2005) calibration: HEM900.

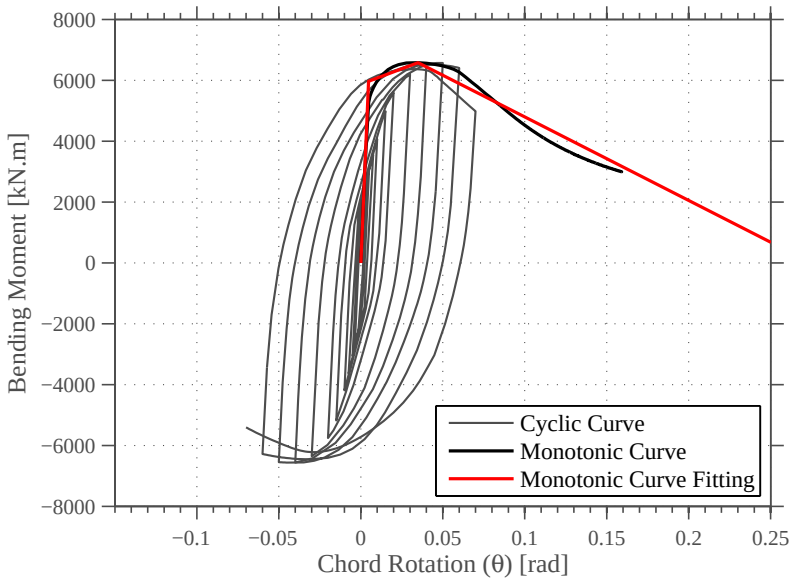

(a) Monotonic backbone calibration: HEM1000.

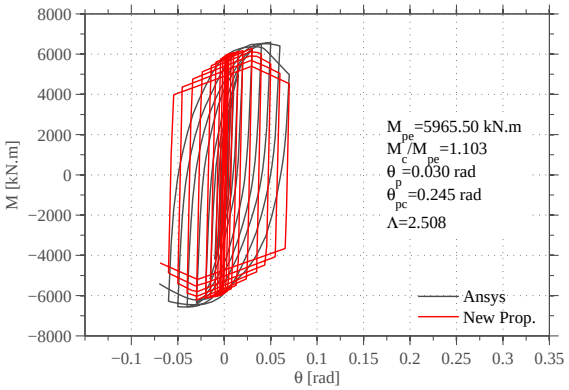

(b) Proposal

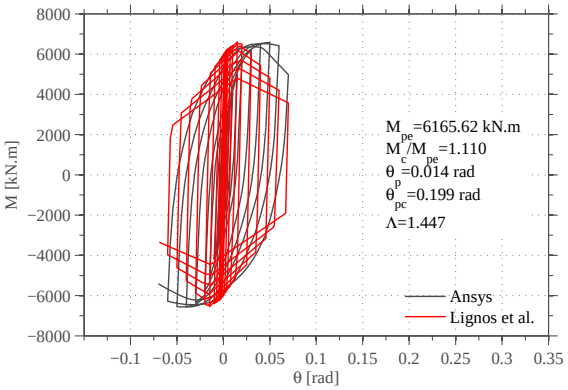

(c) Lignos and Krawinkler (2012)

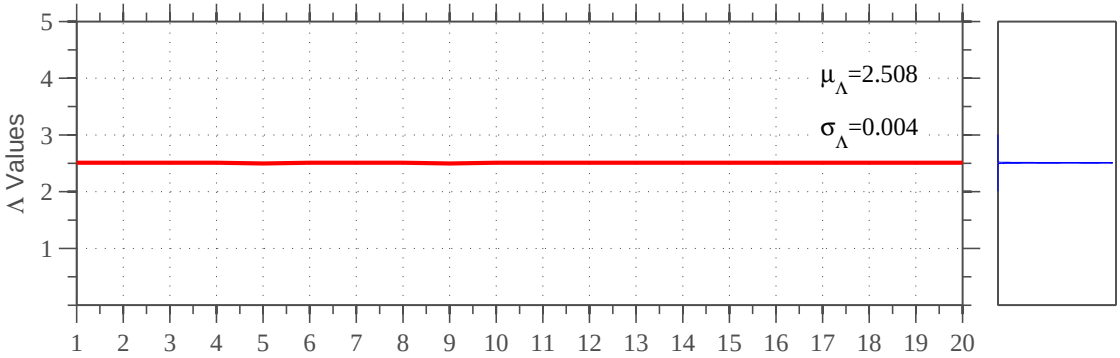

(d) Calibration Stability.

Figure A.59: Ibarra et al. (2005) calibration: HEM1000.

Appendix B

Assessment of harmony search based optimization algorithms for earthquake record selection

B.1 Introduction

Nonlinear response history analysis is becoming a common procedure when designing or assessing earthquake-resistant buildings. In addition to all the issues related with numerical modelling, an important requirement is the definition of the seismic input, typically under acceleration time-history records. These can either be obtained from real earthquake events or be artificially generated. Moreover, seismic design and assessment codes, such as the European code Eurocode 8 (CEN, 2005c), the American code ASCE 41-13 (ASCE/SEI, 2013) and the New Zealand code NZS 1170.5:2004 (Standard, 2004), define criteria related with the ground motion selection process (e.g. number of seismic records to adopt in the analysis, degree of compatibility between the average response spectrum of the ground motion group and the targeted code response spectrum).

Despite the availability of extensive ground motion record databases, an efficient record selection process usually requires the use of time-consuming iterative procedures, which might not necessarily lead to the most optimized ground motion groups. However, an optimization-based approach can be implemented in order to determine the best possible ground motion group. This methodology makes use of mathematical algorithms, targeted at the optimization of a given problem with a given set of constraints. A number of meta-heuristic optimization methods have been used for engineering problems (Saka et al., 2016; Lagaros and Karlaftis, 2011; Azad and Hasançebi, 2013; Hasançebi and Carbas, 2014; Hasançebi et al., 2009; Alberdi and Khandelwal, 2015), in the most part due to their efficiency and the attained reductions in determining a mathematical solution. Moreover, the implementation of such optimization algorithms to record selection procedures has had few research contributions (Naeim et al., 2004; Kottke and Rathje, 2008; Kayhan et al., 2011; Jayaram et al., 2011).

This Chapter describes a sensitivity study on different variants of the Harmony Search optimization algorithm, and their influence on a ground motion record selection and scaling applicability. The software framework SelEQ (Chapter 5) was used to evaluate the performance of each algorithm variant and to assess specific definition parameters.

B.2 Optimization algorithms for record selection

The selection and scaling of groups of real earthquake ground motion records compliant with predefined constraints is an engineering optimization problem. Several research studies have been carried out using meta-heuristic optimization methods for the selection and scaling of earthquake records. Both Naeim et al. (2004) and Kottke and Rathje (2008) proposed the use of the Genetic Algorithm for record selection methodologies. Whilst the first only considered the compatibility, for a range of considered periods of vibration, of the average group response spectrum and the targeted code spectrum, the latter also established some level of control on the standard deviation of the selected ground motions. On a similar note, Kayhan et al. (2011) and Jayaram et al. (2011) implemented the Harmony Search and Greedy optimization techniques for selection and scaling of real ground motion records. The results obtained by Kayhan et al. (2011) demonstrated that the use of the Harmony Search algorithm is an efficient methodology to develop suits of ground motion records that are compatible with code-based spectra. Despite this efficiency, the parameters of the method are problem dependent, meaning that if one wants to search for groups of records based of different sized record databases, some level of accuracy might be compromised.

B.2.1 Harmony search

To what concerns the meta-heuristic Harmony Search (HS) optimization algorithm (Geem, 2000; Geem et al., 2001), its formulation is based on the jazz music improvisation, wherein a set of music players are looking for combinations that are more aesthetically pleasing, through an extemporaneously process of memorization. In this process, improvisational musicians always look to produce a piece of music in perfect harmony. Algorithm 3 shows the pseudocode of the Harmony search algorithm, which mainly consists of the following steps:

I. Initialize the problem and the HS algorithm parameters. In this step, the optimization problem is defined, the objective function (equation B.1) is set and the decision variable intervals are introduced. Additionally, the intrinsic parameters of the HS need to be specified, namely the harmony memory size (HMS), the harmony memory consideration rate ($HMCR$), the pitch adjusting rate (PAR), the distance bandwidth (BW) and the number of improvisations/iterations (NI);

$$Minimize\ f(x) \quad x_i \in \left[x_i^L \quad x_i^U\right] \quad i = 1,\ 2,\ 3, \ldots,\ N \tag{B.1}$$

II. Initialize the harmony memory. At this stage, the harmony memory is filled with randomly chosen solutions. Calculate and store the objective function value of each solution vector, in accordance with equation B.2;

$$[HM] = \left[\begin{array}{ccccc|c} x_1^1 & x_2^1 & \cdots & x_{N-1}^1 & x_N^1 & f\left(x^1\right) \\ x_1^2 & x_2^2 & \cdots & x_{N-1}^2 & x_N^2 & f\left(x^2\right) \\ \vdots & \vdots & \vdots & \vdots & \vdots & \vdots \\ x_1^{HMS-1} & x_2^{HMS-1} & \cdots & x_{N-1}^{HMS-1} & x_N^{HMS-1} & f\left(x^{HMS-1}\right) \\ x_1^{HMS} & x_2^{HMS} & \cdots & x_{N-1}^{HMS} & x_N^{HMS} & f\left(x^{HMS}\right) \end{array}\right] \tag{B.2}$$

III. Improvise a new harmony, $x^* = [x_1^* \; x_2^* \; \cdots \; x_{N-1}^* \; x_N^*]$. A new potential solution is generated applying one of the three rules: a) memory consideration, the values of decision variables, x_i^*, are chosen from any specified value in the specified HM, $x_i^* \in [x_i^1 \; x_i^{HMS}]$, with a probability of *HMCR*; b) random selection, the values of decision variables, x_i^*, are chosen from possible range of the variable, $x_i^* \in [x_i^{min} \; x_i^{max}]$, with a probability of $(1-HMCR)$ in accordance with equation B.3; c) pitch adjustment, when values of decision variables are obtained from the HM an additional search for good solutions is achieved tuning the decision variables, with a probability of *PAR*, in accordance with equation B.4 (*BW* is the distance bandwidth used to improve the performance of HS and is a random number between 0 and 1). The combination of *HMCR* and *PAR* parameters establishes the balance between global and local search on the range of possible solutions, respectively.

$$x_i^* = \begin{cases} x_i^* \in \left[x_i^1 \; x_i^{HMS}\right], & \text{with probability } HMCR \\ x_i^* \in \left[x_i^{min} \; x_i^{max}\right], & \text{with probability } (1-HMCR) \end{cases} \quad i = 1, 2, \cdots, N \tag{B.3}$$

$$x_i^* = \begin{cases} x_i^* \pm Rand(0,1) \times BW, & \text{with probability } PAR \\ x_i^*, & \text{with probability } (1-PAR) \end{cases} \quad i = 1, 2, \cdots, N \tag{B.4}$$

IV. Update the harmony memory. If the new solution is better than any of the solutions present in the harmony memory, the worst solution is replaced by the new solution.

V. Check the stopping criterion. The algorithm is terminated if the maximum number of improvisations is reached.

B.2.2 Variants to the harmony search algorithm

As already mentioned, various modified HS optimization algorithms have been proposed in recent years. These variants aim to overcome the difficulty related with the definition of the mathematical parameters of the procedure, how the constraints are handled and the premature (or false) convergence. One of the first amendments, named as Improved Harmony Search (IHS), proposed

Algorithm 3 Harmony Search algorithm

Parameters: HMS, HMCR, PAR, NI, BW
Start
Objective Function: $f(x), \quad x = [x_1, x_2, \cdots, x_N]$
Initialize Harmony Memory (HM): $x^i, \quad i = 1, 2, \cdots, HMS$
Evaluate each Harmony in HM: $f(x^i)$
$iter \leftarrow 1$
while $iter < NI$ **do**
  for $j \leftarrow 1$ *till* N **do**
    if $rand \leq HMCR$ **then**
      Rate of Memory Consideration:
      $x_j^* \leftarrow x_j^i, \quad i \in [1, HMS]$ *chosen randomly*
      if $rand \leq PAR$ **then**
        Pitch Adjusting Rate:
        $x_j^* \leftarrow x_j^* \pm r \times BW \quad$ *with r random*
      end if
    else
      Random Selection:
      Generate x_j^* randomly
    end if
  end for
  Evaluate new Harmony generated: $f(x^*)$
  if $f(x^*)$ is better than worst harmony in Harmony Memory **then**
    Update Harmony Memory
  end if
  $iter \leftarrow iter + 1$
end while
end

by Mahdavi et al. (2007), allows for the dynamic updating of the *PAR* and *BW* parameters at the generation of a new solution. In this algorithm, *PAR* and *BW* are defined as follows:

$$PAR(i) = PAR_{min} + \frac{(PAR_{max} - PAR_{min})}{NI} \times i \tag{B.5}$$

where *PAR(i)* is the pitch adjusting rate for each generation, and PAR_{min} and PAR_{max} are the minimum and maximum pitch adjusting rate, respectively. *NI* is total number of generations and i

the generation number.

$$BW(i) = BW_{max} \times e^{c \times i} \tag{B.6}$$

$$c = \frac{ln\left(\frac{BW_{min}}{BW_{max}}\right)}{NI} \tag{B.7}$$

where *BW(gn)* is the bandwidth for each generation, and BW_{min} and BW_{max} are the minimum and maximum bandwidth, respectively.

According to Omran and Mahdavi (2008), the major difficulty in the use of the IHS algorithm concerns the definition of the BW_{min} and BW_{max} parameters, as they are problem dependent. Based on the concept of Particle Swarm Optimization methodology, the authors proposed a new variant of the HS algorithm, the Global-Best Harmony Search (GHS). In this algorithm, the pitch adjustment step is modified with the elimination of the bandwidth adjustment. Thus, the main improvement of the GHS is the fact that it takes advantage of the best harmony vector to generate a new vector. Algorithm 4 shows the pseudocode with the necessary modifications to implement the GHS algorithm.

Algorithm 4 Global-Best Harmony Search algorithm (modification)

for $j \leftarrow 1$ *till* N **do**
  if $rand \leq HMCR$ **then**
    {Rate of Memory Consideration}:
    $x_j^* \leftarrow x_j^i, \quad i \in [1, HMS]$ {*chosen randomly*}
    if $rand \leq PAR$ **then**
      {Pitch Adjusting Rate}:
      $x_j^* \leftarrow x_j^{best}$ {where best is the index of the best harmony in the HM and $k \sim U(1,N)$.}
    end if
  else
    {Random Selection}:
    Generate x_j^* randomly
  end if
end for

Inspired by the GHS algorithm, Pan et al. (2010) proposed the Self-Adaptive Global-Best Harmony Search (SGHS). This variant of the HS algorithm applies a new improvisation methodology and an adaptive parameter definition. *PAR* and *HMCR* are self-adaptive during the optimization process and *BW* dynamically changes based on the follow conditions:

$$BW(i) = \begin{cases} BW_{max} - \frac{(BW_{max} - BW_{min})}{NI} \times 2 \times i, & \text{for } i < Ni/2 \\ BW_{min}, & \text{for } i \geq Ni/2 \end{cases} \tag{B.8}$$

The values of HMCR and PAR are assumed to be normally distributed in the range of [0.9,1.0] and [0.0, 1.0] with mean $HMCR_m$, PAR_m and standard deviation of 0.01 and 0.05, respectively. The mean values of *HMCR* and *PAR* are initially defined equal to 0.98 and 0.90 and after a pre-defined number of iterations, *Plimit*, $HMCR_m$ and PAR_m are recalculated by averaging the values of *HMCR* and *PAR* obtained during the *Plimit* iterations. According to the authors, the main advantage of the SGHS algorithm lies in the fact that the user does not need to define the parameters with great precision since they are self-adapted by either a learning mechanism or dynamically change during the optimization process. Algorithm 5 shows SGHS algorithm pseudocode.

With the same objective of the SGHS, Hasançebi et al. (2009) proposed the Adaptive Harmony Search (AHS) optimization algorithm. This variant of the HS algorithm also has the capability of dynamically adjusting the parameters of the algorithm. The parameters are adaptively tuned during the optimization process based on the parameters observed at each iteration in the harmony memory matrix. For each new solution vector improvisation the control parameters *HMCR* and *PAR* are computed according to equation B.9 and equation B.10.

$$HMCR_i = \left(1 + \frac{1 - HMCR_m}{HMCR_m} \times e^{-\gamma \times N(0,1)}\right)^{-1} \tag{B.9}$$

$$PAR_i = \left(1 + \frac{1 - PAR_m}{PAR_m} \times e^{-\gamma \times N(0,1)}\right)^{-1} \tag{B.10}$$

where $HMCR_i$ and PAR_i are the sampled values of the control parameters for a new harmony vector. $N(0,1)$ is a normally distributed random number with mean 0 and standard deviation 1. $HMCR_m$ and PAR_m are the average values of control parameters within the harmony memory matrix. γ is the learning rate of control parameters. According to Saka and Hasancebi (2009) and Ye et al. (2012) the value of the learning rate should be selected within a range of [0.25,0.50]. In this study the learning rate is set to 0.35. Additionally, according Mukhopadhyay et al. (2008) and Ye et al. (2012) the population-variance of harmony solution vectors vary exponentially when the distance bandwidth is equal to the standard deviation of the current population. Therefore the HS algorithm becomes much stronger in the explorative power. In the current study, the distance bandwidth, *BW*, for the AHS algorithm have been set to change dynamically according to the variance of the best harmony solution vector in the current harmony memory matrix (equation B.11). Algorithm 6 shows the AHS algorithm pseudocode.

$$BW_i = \sqrt{var(x)} \tag{B.11}$$

Algorithm 5 Self-Adaptive Global-Best Harmony Search

Parameters: HMS, P_{limit}, BW_{min}, BW_{max}
Start
Objective Function: $f(x), \quad x = [x_1, x_2, \cdots, x_N]$
Initialize Harmony Memory (HM): $x^i, \quad i = 1, 2, \cdots, HMS$
Evaluate each Harmony in HM: $f(x^i)$
Generate HMCR and PAR according to $HMCR_m$ and PAR_m
$iter \leftarrow 1$ and $lp \leftarrow 1$
while $iter < NI$ **do**
  for $j \leftarrow 1$ *till* N **do**
    if $rand \leq HMCR$ **then**
      Rate of Memory Consideration:
      $x_j^* \leftarrow x_j^* \pm r \times BW \quad with\ r\ random$
      if $rand \leq PAR$ **then**
        Pitch Adjusting Rate:
        $x_j^* \leftarrow x_j^{best}$ {where best is the index of the best harmony in the HM and $k \sim U(1,N)$.}
      end if
    else
      Random Selection:
      Generate x_j^* randomly
    end if
  end for
  Evaluate new Harmony generated: $f(x^*)$
  if $f(x^*)$ is better than worst harmony in Harmony Memory **then**
    Update Harmony Memory
  end if
  if $lp = P_{limit}$ **then**
    Recalculate $HMCR_m$ and PAR_m, $\quad lp \leftarrow 1$
  else
    $lp \leftarrow lp + 1$
  end if
  $iter \leftarrow iter + 1$
end while
end

Algorithm 6 Adaptive Harmony Search algorithm

Parameters: HMS, HMCR, PAR, NI
Start
Objective Function: $f(x), \quad x = [x_1, x_2, \cdots, x_N]$
Initialize Harmony Memory (HM): $x^i, \quad i = 1, 2, \cdots, HMS$
Evaluate each Harmony in HM: $f(x^i)$
$iter \leftarrow 1$
while $iter < NI$ **do**
  Generate $HMCR_i$, PAR_i and BW_i
  for $j \leftarrow 1$ *till* N **do**
    if $rand \leq HMCR$ **then**
      Rate of Memory Consideration:
      $x_j^* \leftarrow x_j^i, \quad i \in [1, HMS]$ *chosen randomly*
      if $rand \leq PAR$ **then**
        Pitch Adjusting Rate:
        $x_j^* \leftarrow x_j^* \pm r \times BW \quad$ *with r random*
      end if
    else
      Random Selection:
      Generate x_j^* randomly
    end if
  end for
  Evaluate new Harmony generated: $f(x^*)$
  if $f(x^*)$ is better than worst harmony in Harmony Memory **then**
    Update Harmony Memory and values of HMCR and PAR
  end if
  $iter \leftarrow iter + 1$
end while
end

B.3 Ground motion record selection and scaling

This research study aims to evaluate the performance of the various HS algorithms in a ground motion record selection and scaling framework, and to evaluate the parameter dependence in each

algorithm. The ultimate objective is to propose the best combination of algorithm and corresponding parameters to adopt in earthquake record selection problems. After the implementation of the various HS algorithms in the SelEQ framework (Chapter 5), a number of selection scenarios were taken into account, namely the size of preliminary-search database and the number of ground motion records in each ground motion record suite. According to most seismic design codes (e.g. EC8 (CEN, 2005c)), the minimum number of records that should be used in a nonlinear dynamic analysis is three. In such case the most unfavourable seismic response measure observed should be considered. However, if at least seven records are used in the analyses, the average response of the record group can be considered. It is important to note that for more advanced applications, such as probabilistic seismic risk assessment, the number of records recommended is usually higher. In order to cover the wide range of applications of the SelEQ framework, ground motion groups of 3, 7, 15 and 20 records were considered. In the current study a structure with a fundamental period of 1.0 seconds have been considered.

B.3.1 Preliminary selection databases

When performing code-based ground motion record selection or ground motion record selection for probabilistic-based assessment and risk analysis, it is recommended that a preliminary record search is carried out considering the expected magnitude range, source-to-site distance, rupture mechanism and soil characteristics consistent with the location of the structure under study (Bommer and Acevedo, 2004). For example, EC8 (CEN, 2005c) considers two levels of earthquake magnitude scenarios: low to moderate seismicity, in which the earthquakes have magnitudes not greater than 5.5 (Spectrum type 2) and high seismicity associate with the magnitudes greater than 5.5 (Spectrum type 1). Based on these magnitude scenarios and the values of *Vs30* (the average shear-wave velocity in the first 30m of subsoil) compatible with the soil types defined in the European seismic code, the PEER-NGA database (Chiou et al., 2008) was used for the creation of five preliminary selection databases (or database subsets). Table B.1 summarises the criteria adopted to obtain each pre-selection database.

Table B.1: Pre-selection databases

Database	Magnitude	Vs30	Number of Ground Motions	Number of Records
1	≤ 5.5	360-800	133	266
2	≤ 5.5	180-360	220	440
3	> 5.5	360-800	907	1814
4	> 5.5	180-360	964	1928

B.3.2 Objective function and problem constraints

As indicated earlier, the selection and scaling of groups of ground motion records according to code requirements can be considered an engineering optimization problem. According to the majority of seismic design and assessment codes, the aim should be to control the mean (or median) spectrum of the suite of scaled records in relation to the code response spectrum, for the range of periods of interest, considering a number of additional constraints (e.g. EC8 imposes that, for the period range of interest, the mean spectrum of the suite should be above 90% of the code elastic response spectrum). Figure B.1 shows the spectral compatibility concept.

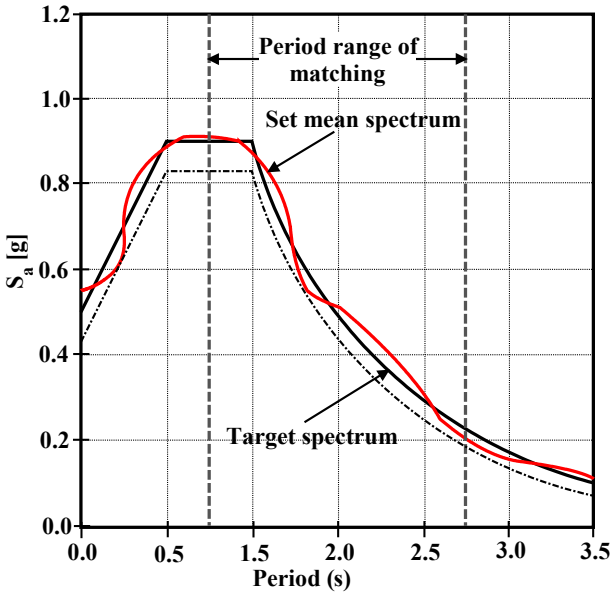

Figure B.1: Code response spectrum compatibility example.

The mean spectrum of a ground motion records suite composed by n earthquake records can be obtained by the average of the spectral values of the records as follows:

$$S_a^{mean} = \frac{\sum_{i=1}^{n} sf_i \times S_{a_i}(T)}{n} \tag{B.12}$$

where sf_i and $Sa_i(T)$ are the scaling factor and the elastic response spectrum of each ground motion record, respectively.

The objective function considered in this parametric study aims to minimize the differences between the (target) code spectrum and the average spectral ordinates of the chosen ground motion records suite. Additionally, the following criteria prescribed in EC8 (CEN, 2005c) regarding ground motion record selection if history response analysis were adopted:

- The mean of the zero period spectral response acceleration values calculated from the individual time histories should not be smaller than the value of $a_g S$ for the site under study, a_g being the design ground acceleration on rock and S the soil parameter;

- In the range of periods between $0.2T_1$ and $2.0T_1$, where T_1 is the fundamental period of the structure in the direction in which the records will be applied, no value of the mean 5% damping elastic spectrum (calculated from the average between the response spectra of the considered ground motions), should be less than 90% of the corresponding value of the targeted 5% damping elastic response spectrum.

Furthermore an additional constraint was introduced imposing that no value of the mean 5% damping elastic spectrum (calculated from the average between the response spectra of the considered ground motions suite), should be higher than 110% of the corresponding value of the targeted 5% damping elastic response spectrum. Further details of the formulation and implementation of the problem constrains could be found in Chapter 5.

The objective function for the optimization problem can be formulated as follows:

$$f(x) = \sqrt{\frac{1}{n_T}\sum_{i=1}^{n_T}\left(S_a^{mean}(T_i) - S_a^{ref}(T_i)\right)^2} \tag{B.13}$$

where n_T is the total number of vibration periods under consideration, S_a^{mean} and S_a^{ref} are the ground motion records suite mean spectrum and code spectrum, respectively.

B.4 Sensitivity analysis

B.4.1 Algorithms parameter selection

As already mentioned in this Chapter, all the algorithms detailed in Section B.2 have been implemented in SelEQ framework (Chapter 5). In order to analyse the dependence of each algorithm in solution parameters it is initially performed a sensitivity study to evaluate the importance of each parameter and define the best set/range of parameter values. Traditionally the definition of the parameters for a specific problem is based on a one-at-a-time (OTA) sensitivity analysis. However, even leading to good results in most of problems, these sensitivity techniques ignore the interaction between parameters which can assume an essential role in the optimization process (Saltelli et al., 2010; Kayhan, 2016). In order to compare and if necessary overcome this problem three different sensitivity analysis methods are use: One-at-a-time (OTA), Morris method (or Elementary Effects method) and Sobol global sensitivity analysis.

B.4.2 One-at-a-time (OAT) sensitivity analysis

OAT sensitivity analysis consists in evaluating consecutively our model changing the value of one parameter while keeping the others constant. Some of the advantages of using OTA sensitivity analysis is the reduced number of simulations that are necessary and the inherent concept of baseline around which the sensitivity analysis is conducted (Saltelli et al., 2010). On the contrary, for high dimensional space problems, OAT sensitivity analysis is naturally non-explorative and cannot identify interactions among the parameters. Even recognizing the limitations of OAT sensitivity

analysis it is important to confirm its performance for the parameter tuning problem (Saltelli et al., 2010).

The parameter sets used in the OAT sensitivity analysis are presented in Table B.2 and Table B.3. Moreover, each time one parameter is changed the others are kept with original algorithm recommendation. A total of thirty simulations are performed for each set of parameters allowing to conclude about the stability of the algorithm with the defined parameters. The parameters dependence on the preliminary selection database size and number of ground motion records per suite are also evaluated. Results for each parameter set are defined as mean and standard deviation over the thirty independent runs. Robust statistics have been used for the calculation of mean and standard deviation since they avoid the potential bias introduced by the outliers (Romão et al., 2012a,b).

Table B.2: HS, IHS, GHS and AHS parameter sets.

			HS		IHS				GHS			AHS	
	HMS	$HMCR$	PAR	BW	PAR_{min}	PAR_{max}	BW_{min}	BW_{max}	$HMCR_m$	PAR_{min}	PAR_{max}	$HMCR_0$	PAR_0
PS1	10	0.8	0.4	10^{-2}	0.25	0.99	10^{-5}	10^{-2}	0.8	0.25	0.99	0.8	0.2
PS2	25												
PS3	50												
PS4	75												
PS5	100												
PS6	75	0.5	0.4	10^{-2}	0.25	0.99	10^{-5}	10^{-2}	0.5	0.25	0.99	0.5	0.2
PS7		0.6							0.6			0.6	
PS8		0.7							0.7			0.7	
PS9		0.9							0.9			0.9	
PS10		0.95							0.95			0.95	
PS11	75	0.8	0.1	10^{-2}	0.1	0.99	10^{-5}	10^{-2}	0.8	0.01	0.99	0.8	0.1
PS12			0.2		0.2					0.2			0.15
PS13			0.3		0.3					0.3			0.3
PS14			0.5		0.4					0.5			0.4
PS15			0.6		0.5								0.5
PS16			0.8		0.7								
PS17			0.9		0.9								
PS18	75	0.8	0.4	10^{-4}	0.25	0.99	10^{-6}	10^{-4}					
PS19				10^{-3}			10^{-5}	10^{-3}					
PS20				10^{-1}			10^{-4}	10^{-1}					

Table B.3: SGHS parameter sets.

	SGHS					
	HMS	$HMCR_m$	PAR_m	BW_{min}	BW_{max}	P_{limit}
PS1	10	0.95	0.9	10^{-5}	10^{-2}	50
PS2	25					
PS3	50					
PS4	75					
PS5	100					
PS6	75	0.5	0.9	10^{-5}	10^{-2}	50
PS7		0.7				
PS8		0.8				
PS9		0.9				
PS10		0.98				
PS11	75	0.95	0.3	10^{-5}	10^{-2}	50
PS12			0.4			
PS13			0.5			
PS14			0.6			
PS15			0.7			
PS16			0.8			
PS17			0.95			
PS18	75	0.95	0.9	10^{-6}	10^{-4}	50
PS19				10^{-5}	10^{-3}	
PS20				10^{-4}	10^{-1}	
PS21	75	0.95	0.9	10^{-5}	10^{-2}	20
PS22						30
PS23						70
PS24						100

Figure B.2 to Figure B.6 show the OAT sensitivity analysis results for all the algorithms. It became evident from the figures that all the algorithm are sensitive to the definition of the HMCR

probability value (PS6, PS7, PS8). This parameter is responsible for using parts of current best solution in the new solution. Choosing a lower value of HMCR means lower probability of using the HMC rule. It has been demonstrated by several authors that using a higher value of HMCR reduces the premature convergence and increases the convergence speed of the algorithm. Nevertheless, an appropriate value of the PAR and BW should be defined when defining a higher value of HMCR probability. It is interesting to note that HS algorithm exhibit higher sensitivity to the definition of these parameters since all other algorithms dynamically update the parameters over the generations. Figure B.2 clearly shows that for higher values of PAR (PS15, PS16 and PS17) and higher values of BW (PS19 and PS20) the HS algorithm exhibit worst performance. Even though the other algorithms dynamically update PAR and BW over the new solution generation particular attention to the definition of the variation interval should be given. Additionally, conversely to other algorithms AHS revealed lower sensitivity to parameter definition when preliminary selection databases 1 and 2 are used (Figure B.6) maintaining sensitivity trends to HMCR for the other preliminary selection databases. Based on the results provided before for different parameter values (considering the different record databases, HS variants and parameter value ranges), the performance of each algorithm was assessed with the most appropriate set of parameters. This analysis will allow to compare all algorithms. Figure B.7 shows the mean and standard deviation value of the objective function for each algorithm variant (HS, IHS, GHS, SGHS, AHS), preliminary selection database (1 through 4) and number of ground motion records in the suite (3, 7, 15 and 20).

The first conclusion to be drawn from analysis of Figure B.7, is that regardless of number of ground motion records of the group or preliminary selection database, the AHS algorithm exhibited consistently the best results (i.e. the lowest objective function value and lower value of standard deviation). A more detailed analysis of the results depicted in Figure B.7 allow concluding that in some cases other algorithms exhibit similar performance (e.g. AHS, HS, IHS and GHS for the selection of suits of 3 ground motion records from preliminary selection Database 2, 3 and 4) records, however for other selection cases the algorithms the algorithm exhibit relevant differences (e.g. HS for the selection of suits of 20 ground motion records from preliminary selection Database 1). From the results obtained so far, with the parameters defined according to the OTA sensitivity analysis, it is possible to conclude that the AHS algorithm showed the best overall performance, regardless of the size of the preliminary selection database and number of ground motion records considered. Nevertheless, as previously mentioned, OAT sensitivity analysis and parameter definition cannot identify interactions among the parameters. A possible improvement on the parameters definition could be attained using sensitivity methods that consider the interaction between algorithm parameters. In the following section Morris method is applied to identify the more relevant parameters and evaluate the higher order effects, i.e., the interaction with other parameters.

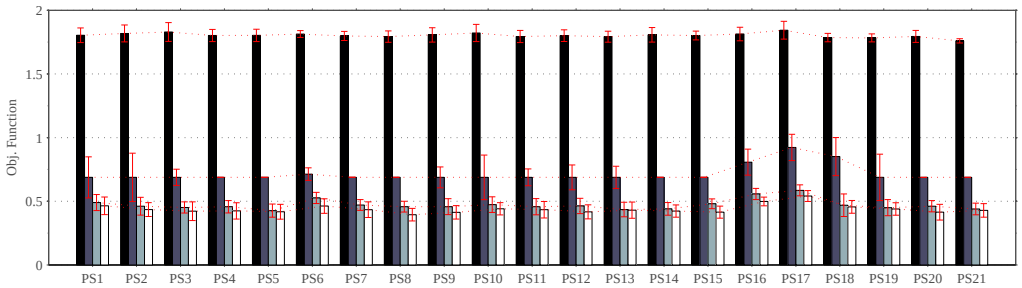

(a) 3 Records

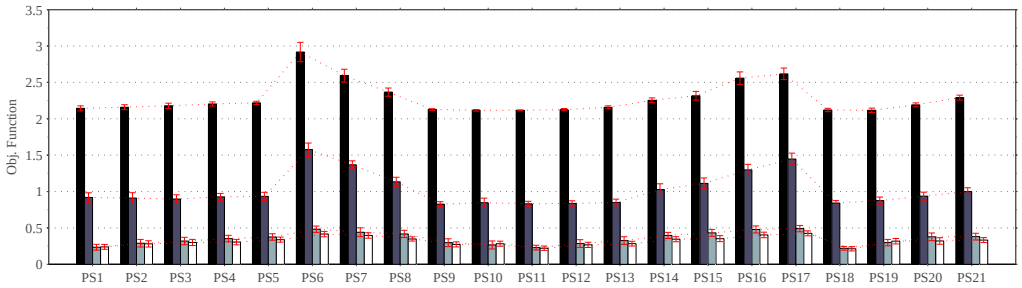

(b) 7 Records

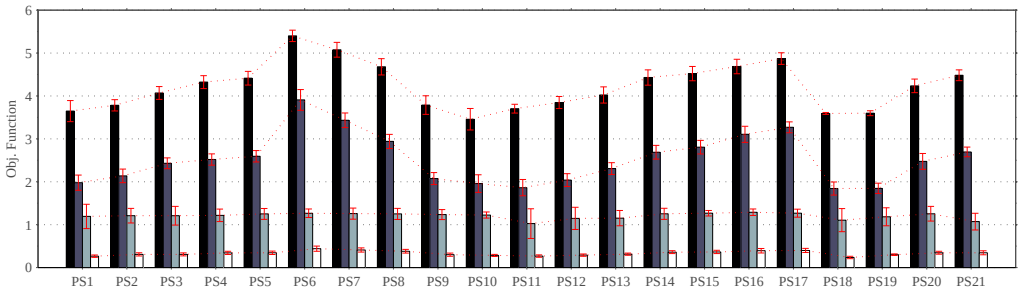

(c) 15 Records

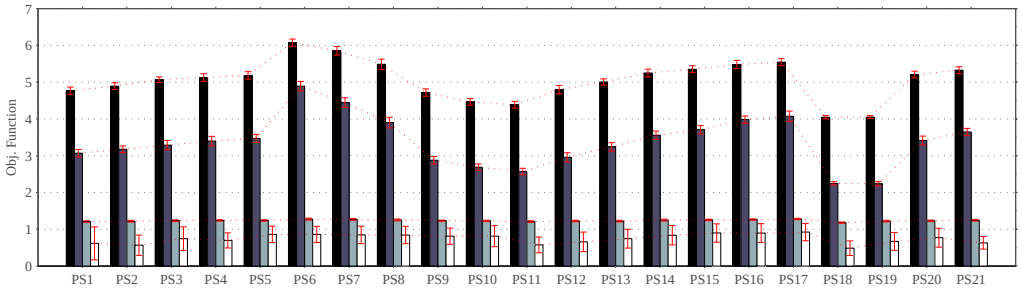

(d) 20 Records

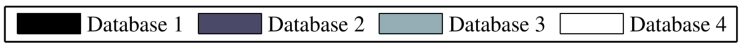

Figure B.2: Harmony Search.

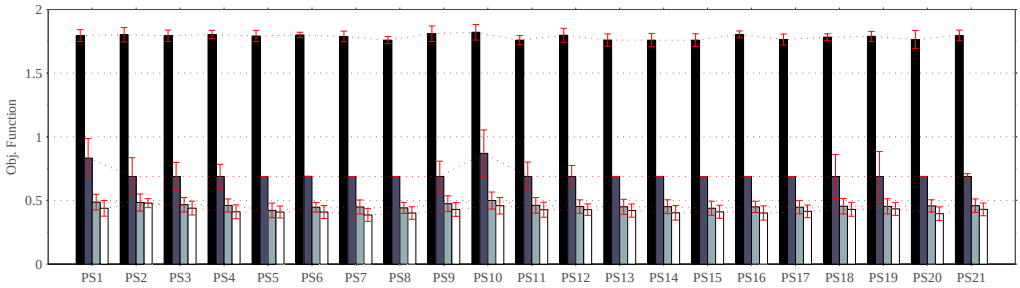

(a) 3 Records

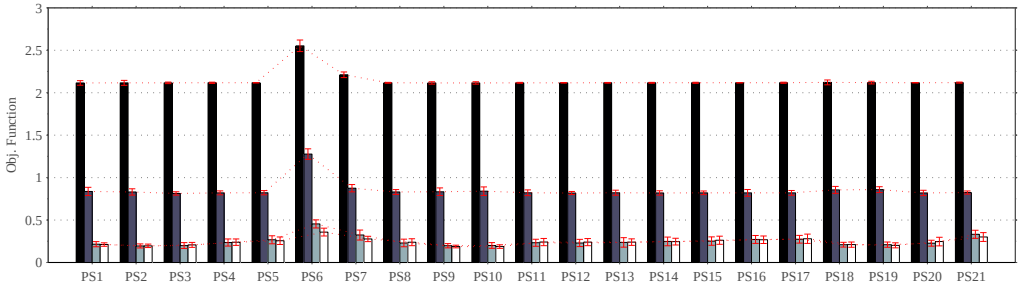

(b) 7 Records

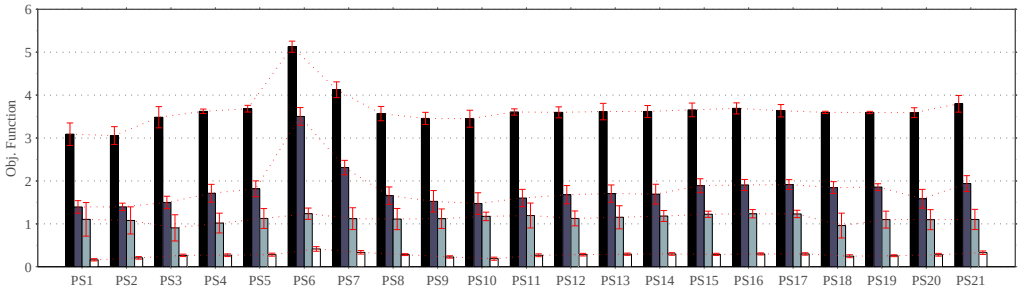

(c) 15 Records

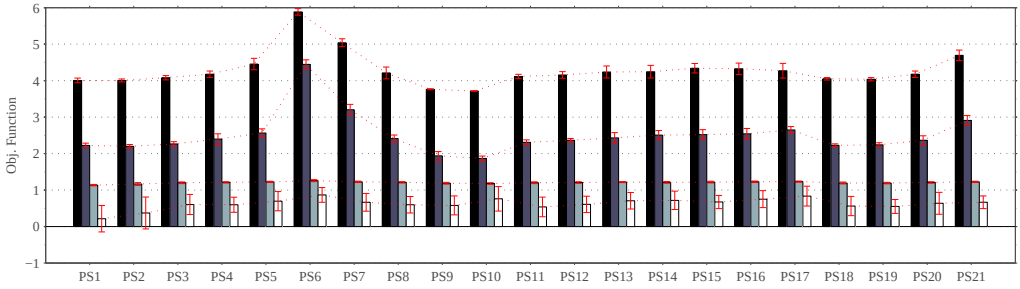

(d) 20 Records

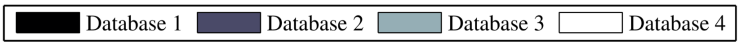

Figure B.3: Improved Harmony Search.

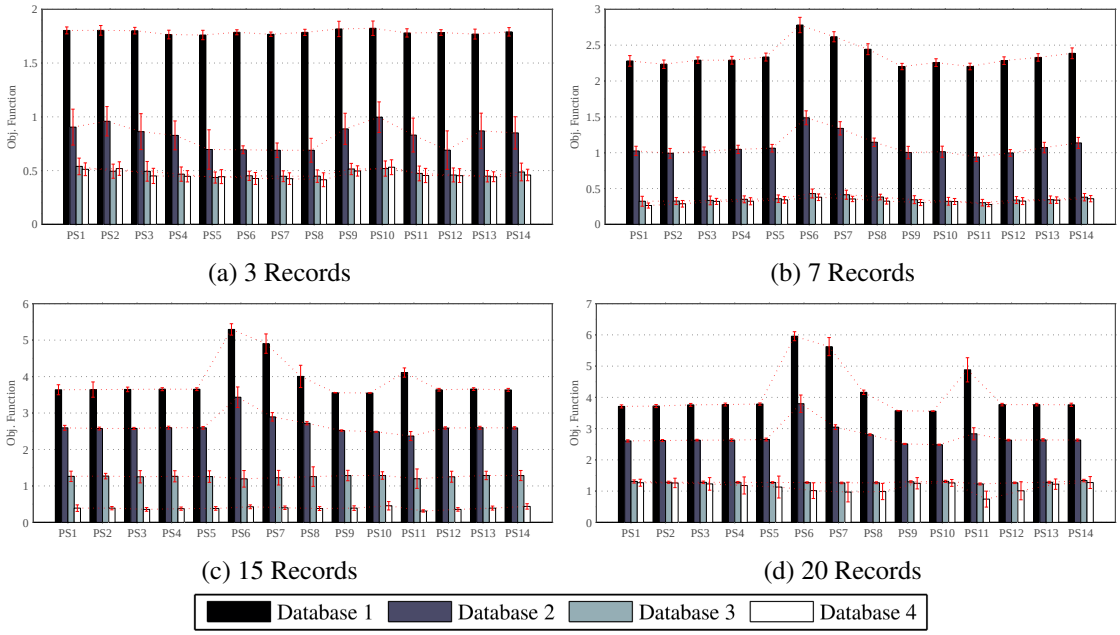

Figure B.4: Global-Best Harmony Search.

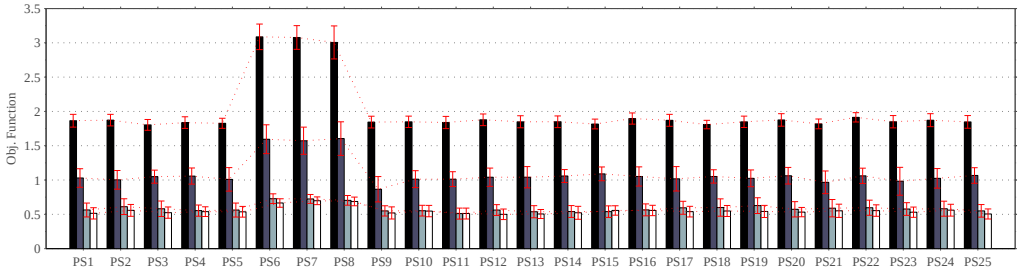

(a) 3 Records

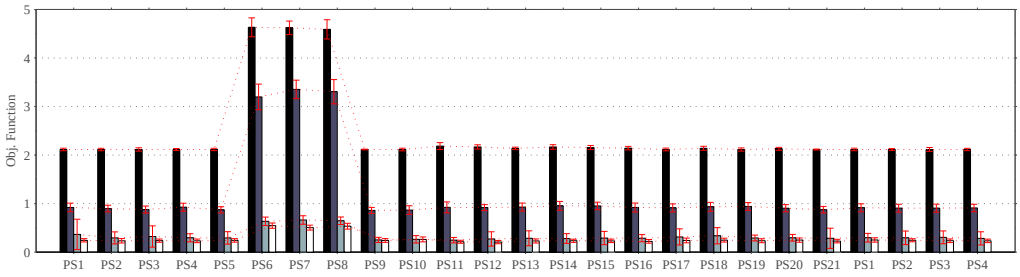

(b) 7 Records

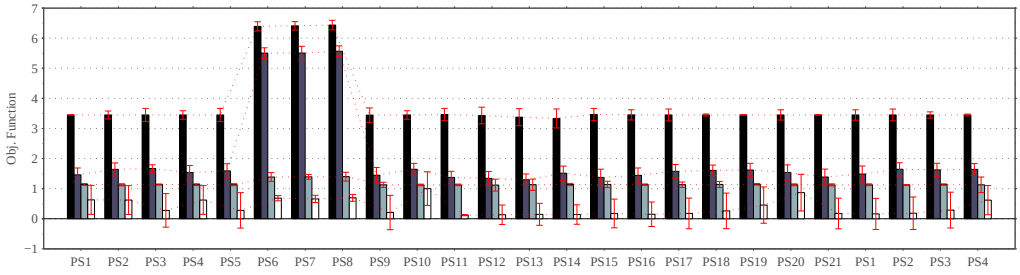

(c) 15 Records

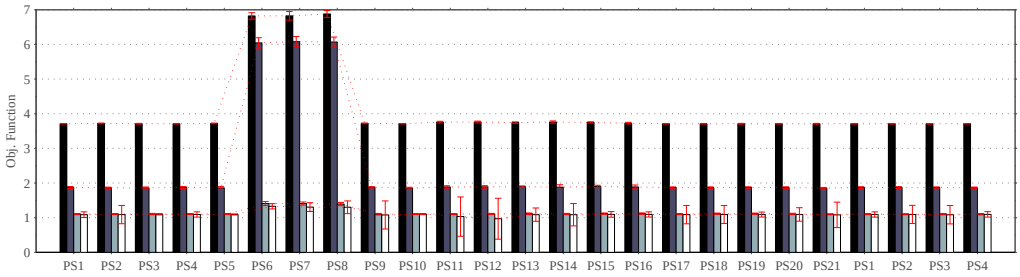

(d) 20 Records

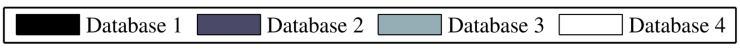

Figure B.5: Self-Adaptive Global-Best Harmony Search.

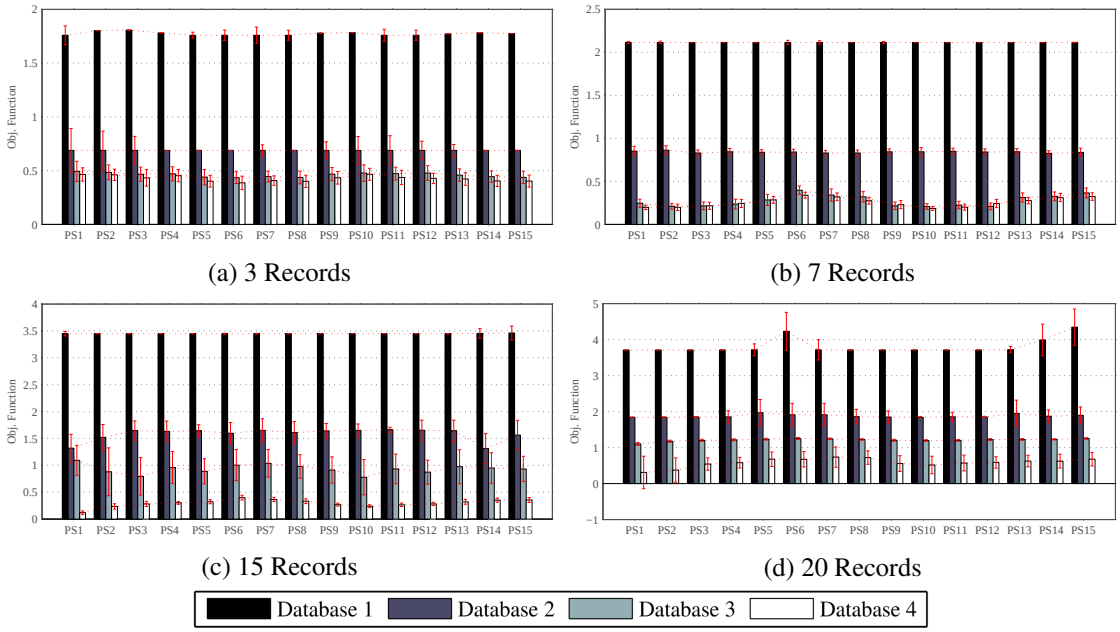

Figure B.6: Adaptive Harmony Search.

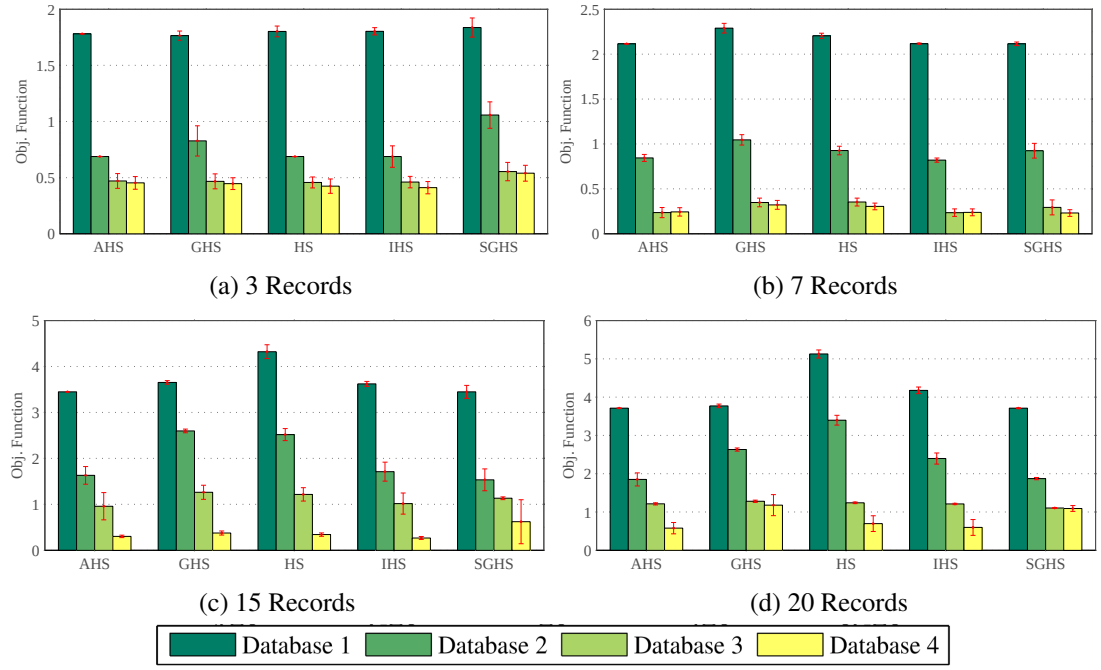

Figure B.7: Algorithms comparison.

B.4.3 Sobol global sensitivity analysis

A global sensitivity analysis allows to evaluate how the variation in the output of a model is dependent on the variation of the model parameters, namely, how uncertainty in the output can be apportioned to different sources of uncertainty in model input (Saltelli et al., 2004). Variance based methods have been widely used in sensitivity analysis. Among the variance based methods the Sobol's method (Sobol, 1993) is one of the most prominent and used when conducting global sensitivity analysis (Saltelli et al., 2010). The method is a global and model independent sensitivity analysis method based on the decomposition of variance (Nossent et al., 2011). If the mathematical model is described by a function, Equation B.14:

$$Y = f(X) = f(X_1, \ldots, X_n) \tag{B.14}$$

where X is the model parameter set and Y is the model objective function. According to Sobol's the function f can be decomposed into summands of increasing dimensionality, namely,

$$f(X_1, \ldots, X_n) = f_0 + \sum_{i=1}^{n} f_i(X_i) + \sum_{i=1}^{n-1} \sum_{j=i+1}^{n} f_{ij}(X_i, X_j) + \cdots + f_{1,\ldots,n}(X_1, \ldots, X_n) \tag{B.15}$$

If each term in the above expansion has zero mean and is square integrable then all terms of the decomposition are mutually orthogonal, f_0 is to the expectation value of the output and the decomposition is unique (Sobol, 1993; Saltelli et al., 2004, 2010; Cannavó, 2012).

The variances of the terms in decomposition, Equation B.15, can be computed using equation Equation B.16:

$$V_{i_1 \ldots i_s} = \int_0^1 \cdots \int_0^1 f^2_{i_1 \ldots i_s}(X_{i_1}, \ldots, X_{i_s}) \tag{B.16}$$

where $1 \leq i_1 \leq \cdots \leq i_s \leq n$ and $s = 1, \cdots, n$. The value of variances of the terms in decomposition are in reality a measure of the importance of parameters.

The total unconditional variance is defined as (Equation B.17):

$$V(Y) = \int_0^1 f^2(X)\, dX - f_0^2 \tag{B.17}$$

Based on assumption that parameters are orthogonal in pairs the variance decomposition can be defined according to Equation B.18.

$$V(Y) = \sum_{i=1}^{n} V_i + \sum_{i=1}^{n-1} \sum_{j=i+1}^{n} V_{ij} + \cdots + V_{1,\ldots,n} \tag{B.18}$$

The Sobol' first order sensitivity indexes can then be computed dividing the partial variance

by total unconditional variance (Equation B.19).

$$S_i = \frac{V_i}{V(Y)} \tag{B.19}$$

The interaction effects or higher order sensitivity indexes can be computed similarly.

$$S_{ij} = \frac{V_{ij}}{V(Y)} \tag{B.20}$$

Another sensitivity index that is commonly used is the total effect index (Homma and Saltelli, 1996; Saltelli et al., 2004). The total sensitivity index is defined as (Equation B.20):

$$S_{T_i} = S_i + \sum_{j \neq i} S_{ij} + \sum_{k \neq j \neq i} S_{ijk} + \cdots = 1 - \frac{V_{\sim i}}{V(Y)} \tag{B.21}$$

The total effect index gives a measure of the total contribution to the output of the variation of parameter X_i and its interactions.

One of the disadvantages of variance based methods, as Sobol's method, is the high computational cost associated with more complex models. In the current study the Sobol's first order and total sensitivity indexes have been calculated for each algorithm considering the parameters and distributions shown in Table B.4. Sobol's quasi-random sequences have been used for sampling the parameters. Each sample have been discretized with 10000 points. The model function have been defined as the mean of thirty realisations for each Sobol's simulation. Moreover, the solution are obtained after 250000 iterations. The number of iterations has not been considered as a parameter in this research study, however for the number of iterations have been defined as a balance between efficiency and computational time. It should be noted that only ground motion suites satisfying all the code required constraints have been considered.

Figure B.8 to Figure B.12 summarizes the Sobol' first-order and total effect indexes for all the algorithms parameters considering 2 preliminary selection databases (Database 2 and Database 4) and ground motion record suites of 3 and 7 ground motion records.

Figure B.8 to Figure B.12 summarizes the Sobol' first-order and total effect indexes for all the algorithms parameters considering 2 preliminary selection databases (Database 2 and Database 4) and ground motion record suites of 3 and 7 ground motion records.

Regarding HS algorithm, analysis of Figure B.8 allow conclude that PAR has a participation higher than 50% for groups with higher number of records, regardless of the Database size. Moreover, for groups with lower number of records (3), HS algorithm is not sensitive to each parameter individually but depends in the interactions between the parameters. Similar results were obtained for GHS algorithm (Figure B.10). Figure B.9 shows the Sobol' sensitivity indexes for the IHS algorithm. For IHS algorithm the HMCR parameter is the one with greater influence for groups with higher number of records. Furthermore, it can be observed from Figure B.11 that for SGHS algorithm no single parameter has a relevant influence with values for higher order indexes greater than 86% for all the scenarios. Finally, for the AHS algorithm (Figure B.12) it was observed a

Table B.4: Global sensitivity parameters.

Parameter	Distribution	Values	Algorithm				
			HS	IHS	GHS	SGHS	AHS
NI			200000				
HMS	Uniform	Lo.	10				
		Rec.	75				
		Up.	100				
$HMCR$	Uniform	Lo.	0.5			0.9	0.5
		Rec.	0.8			0.95	0.8
		Up.	0.95			0.98	0.95
PAR	Uniform	Lo.	0.1	[0.01 , 0.99]		0.3	0.1
		Rec.	0.4	[0.25 , 0.99]		0.9	0.2
		Up.	0.9	[0.90 , 0.99]		0.95	0.5
$BW\,(Value \times (UB - LB))$	Uniform	Lo.	10^{-5}	$[10^{-6}, 10^{-3}]$	-	$[10^{-6}, 10^{-3}]$	-
		Rec.	10^{-3}	$[10^{-5}, 10^{-2}]$		$[10^{-5}, 10^{-2}]$	
		Up.	10^{-1}	$[10^{-4}, 10^{-1}]$		$[10^{-4}, 10^{-1}]$	
P_{limit}	Uniform	Lo.	-			20	-
		Rec.				50	
		Up.				100	

greater sensitivity to HMS and HMCR when selecting groups with higher number of records from a Database with larger size. A common aspect observed in almost all algorithms is the importance of the interactions between the parameters.

Furthermore, despite the low values of the first order indexes the high values of the total effect indexes indicate that all the parameters are relevant for the problem under study. The results point out high interaction dependence between the parameters in all the algorithms.

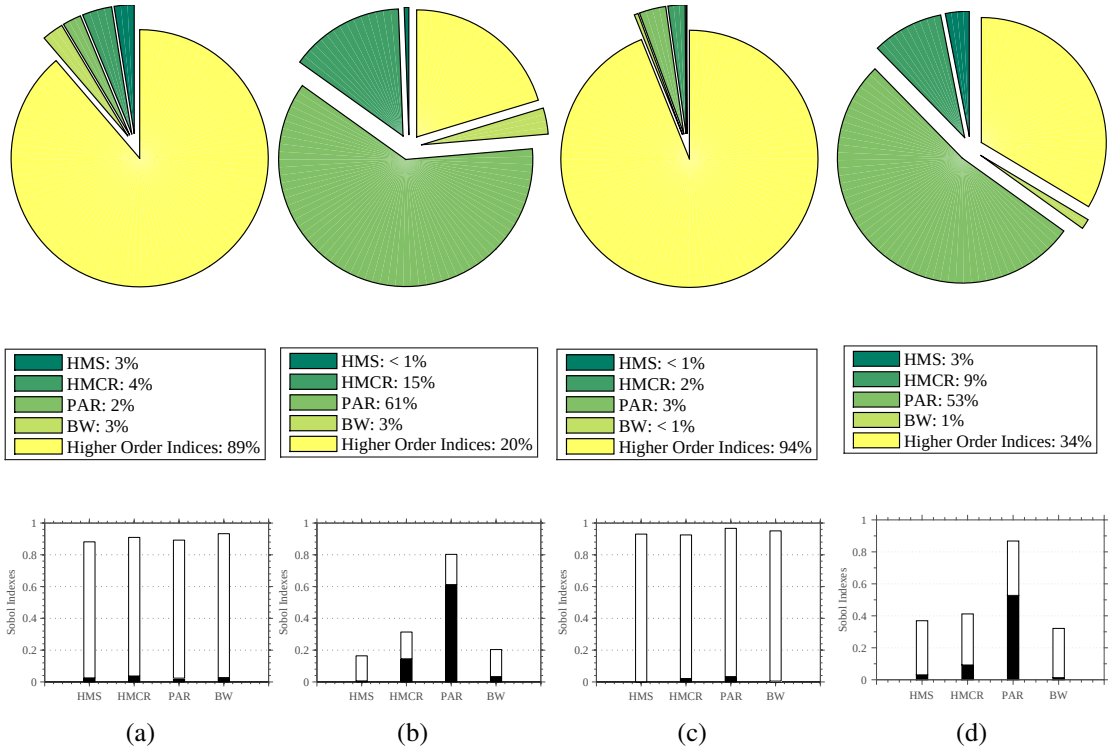

Figure B.8: Sobol Sensitivity Indexes – HS algorithm : a) 3 records Database 2; b) 7 records Database 2; c) 3 records Database 4; d) 7 records Database 4.

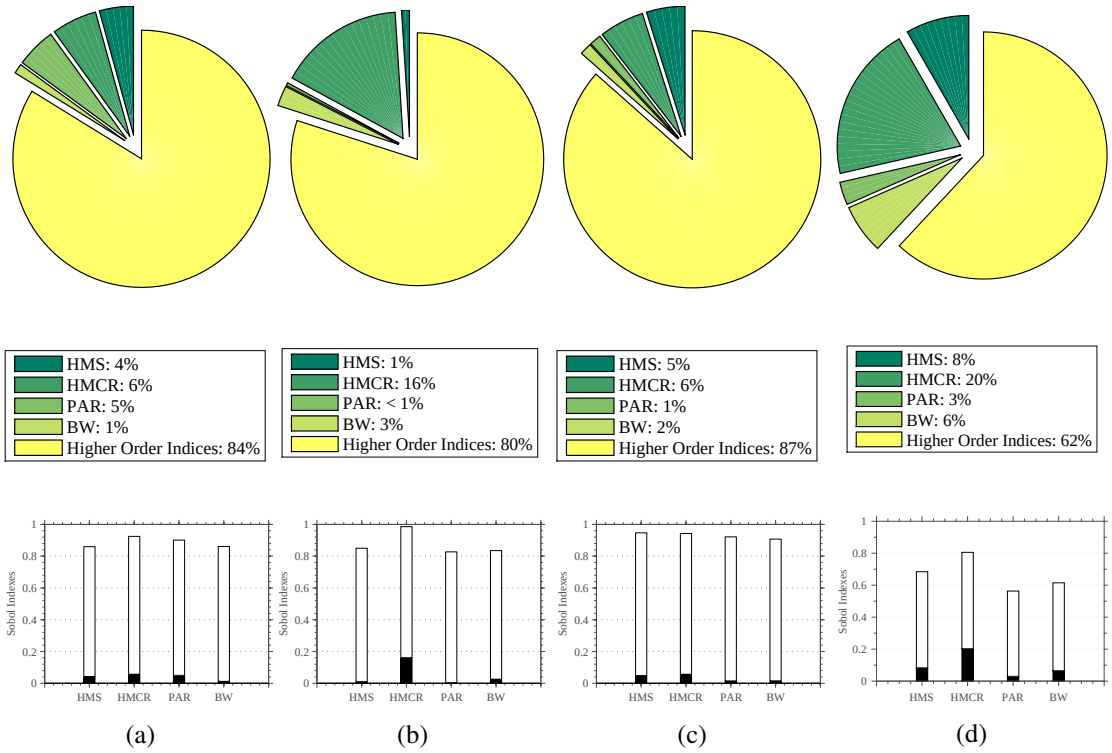

Figure B.9: Sobol Sensitivity Indexes – IHS algorithm : a) 3 records Database 2; b) 7 records Database 2; c) 3 records Database 4; d) 7 records Database 4.

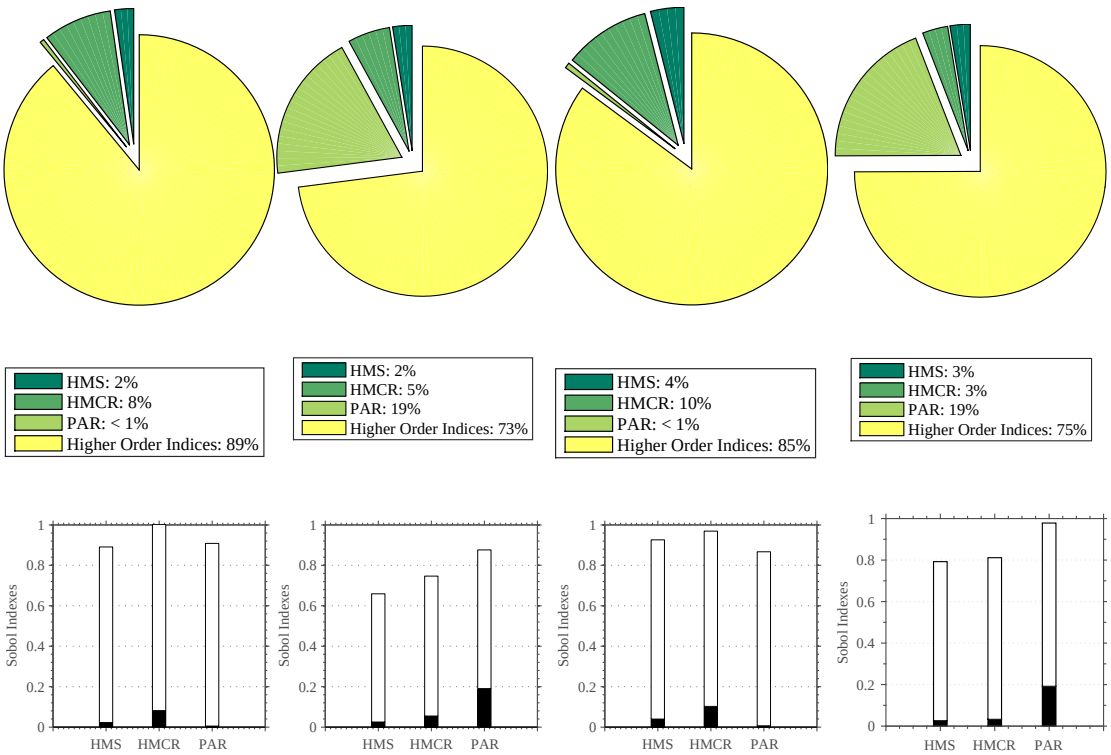

Figure B.10: Sobol Sensitivity Indexes – GHS algorithm : a) 3 records Database 2; b) 7 records Database 2; c) 3 records Database 4; d) 7 records Database 4.

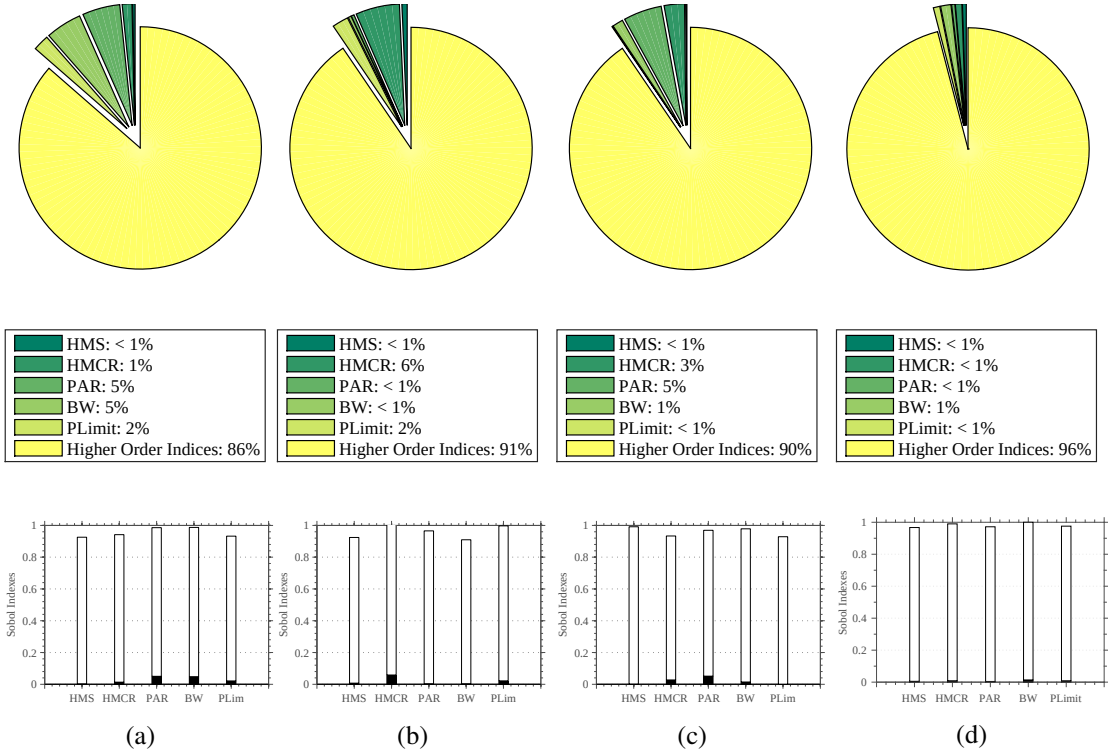

Figure B.11: Sobol Sensitivity Indexes – SGHS algorithm : a) 3 records Database 2; b) 7 records Database 2; c) 3 records Database 4; d) 7 records Database 4.

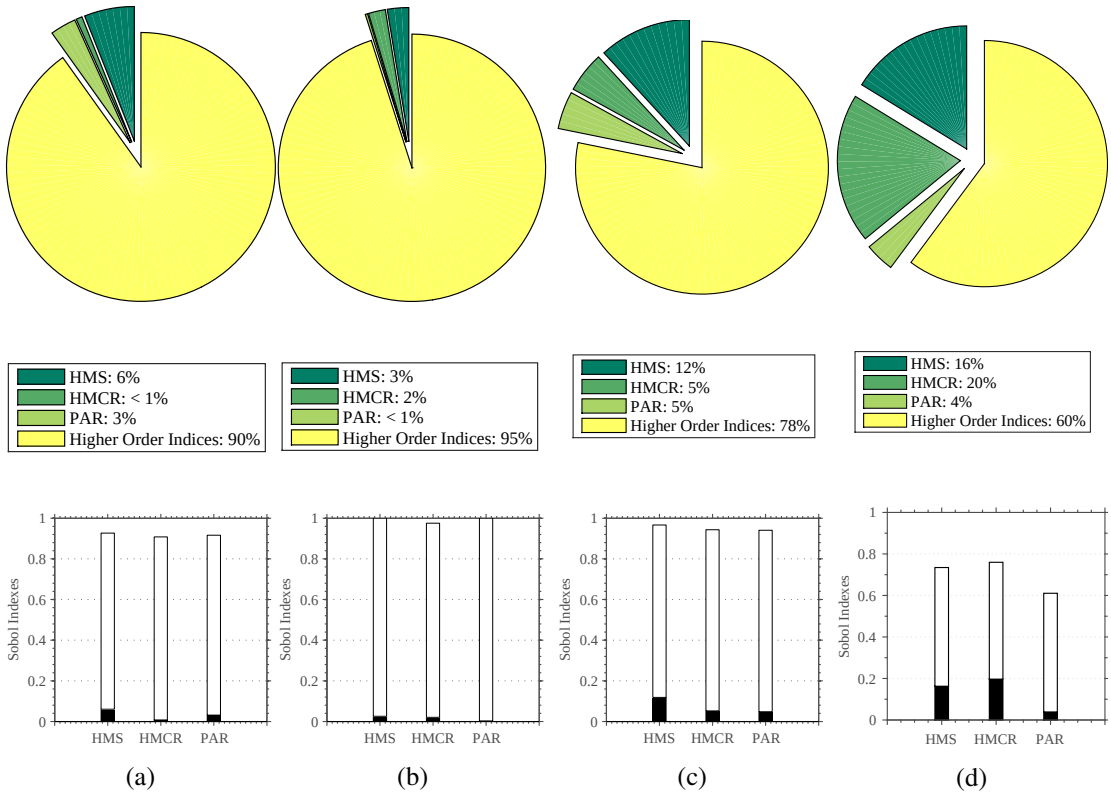

Figure B.12: Sobol Sensitivity Indexes – AHS algorithm : a) 3 records Database 2; b) 7 records Database 2; c) 3 records Database 4; d) 7 records Database 4.

B.4.4 Parallel coordinates plot

The results obtained with Sobol's method exposed the high dependence of the interactions between the parameters in the solution obtained by the algorithms. Analysis and visualisation of the relations between the parameters could be complex and time consuming. One of the technique that could be used for data analysis in multivariate problems, that allows comparing the effect of each parameter and the relationships between them is the parallel coordinates plots (Inselberg and Dimsdale, 1991). In parallel coordinates plots, each parameter is given a axis and all the axis are placed in parallel to each other. Moreover, each axis can have a different scale that corresponds to the possible range of the parameter. The sensitivity of the solution to the parameters is derived by analyzing the distribution of the points on the vertical axes. To evaluate the relation between the parameters, a sample of 100 realizations of each input random variable was adopted, which has been seen to provide stable estimates. Latin Hypercube Sampling method proposed by Owen (1994), which enables the reduction of spurious correlation in the sampling process was used.

Figure B.13 to Figure B.32 shows the parallel coordinates for all the algorithms parameters considering all preliminary selection databases and ground motion record suites of 3, 7 15 and 20 ground motion records. The five sets of parameters with better value of the objective function are highlighted in blue.

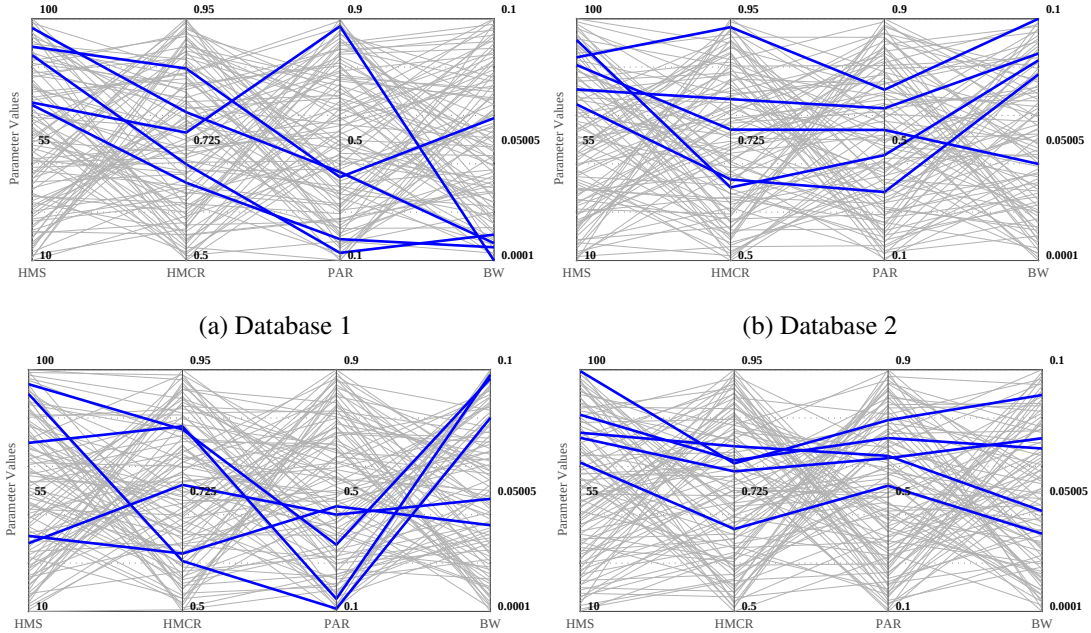

(a) Database 1

(b) Database 2

(c) Database 3

(d) Database 4

Figure B.13: HS algorithm: 3 records.

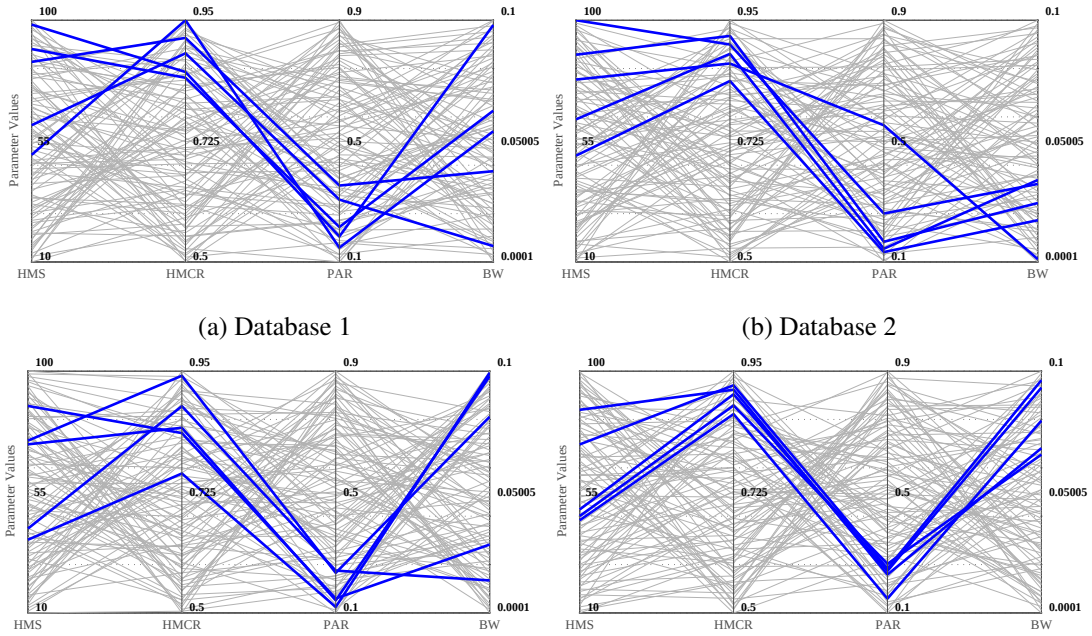

(a) Database 1

(b) Database 2

(c) Database 3

(d) Database 4

Figure B.14: HS algorithm: 7 records.

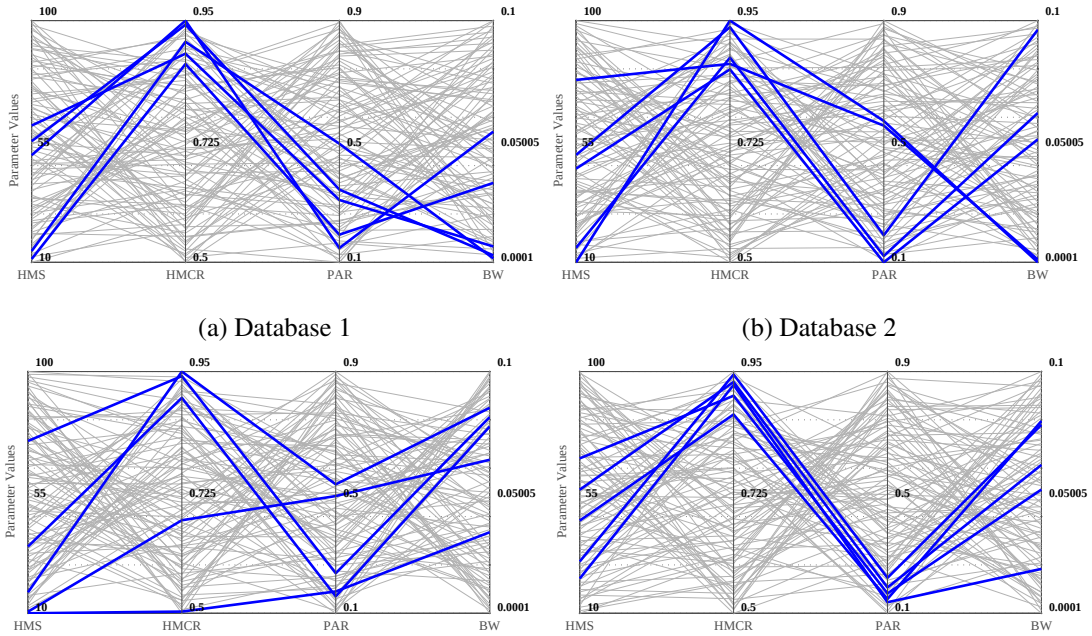

(a) Database 1

(b) Database 2

(c) Database 3

(d) Database 4

Figure B.15: HS algorithm: 15 records.

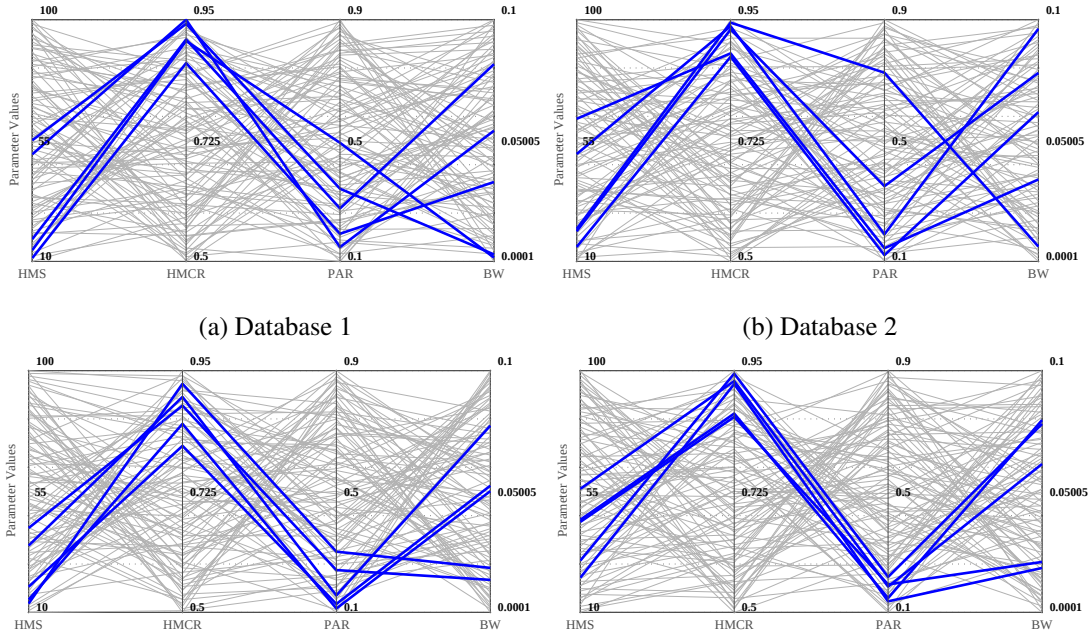

(a) Database 1

(b) Database 2

(c) Database 3

(d) Database 4

Figure B.16: HS algorithm: 20 records.

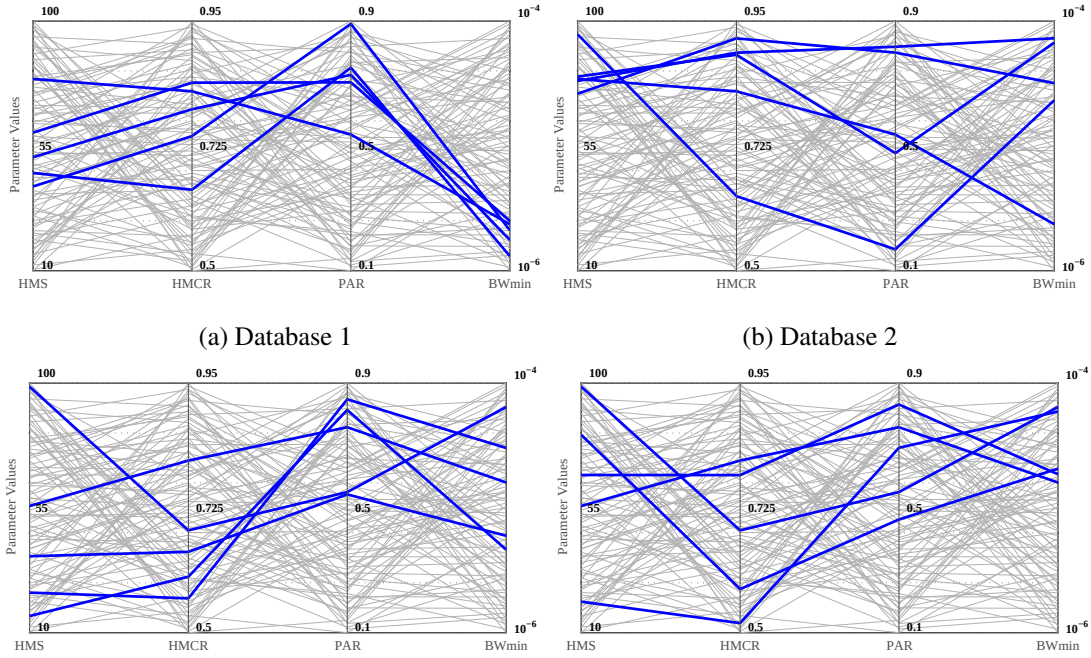

(a) Database 1

(b) Database 2

(c) Database 3

(d) Database 4

Figure B.17: IHS algorithm: 3 records.

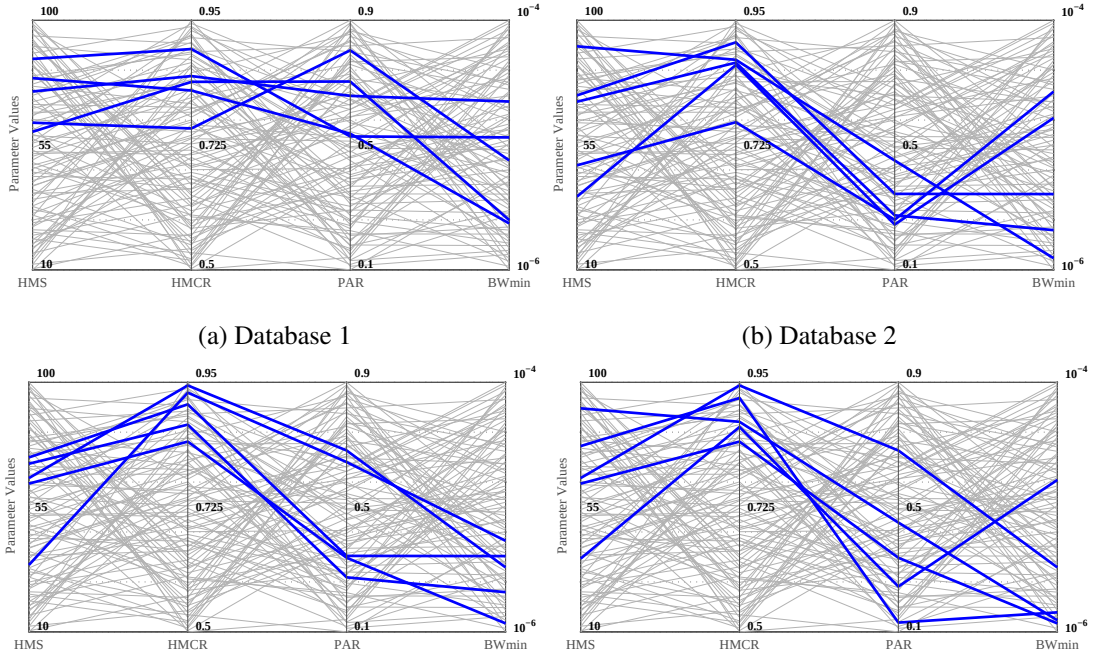

(a) Database 1

(b) Database 2

(c) Database 3

(d) Database 4

Figure B.18: IHS algorithm: 7 records.

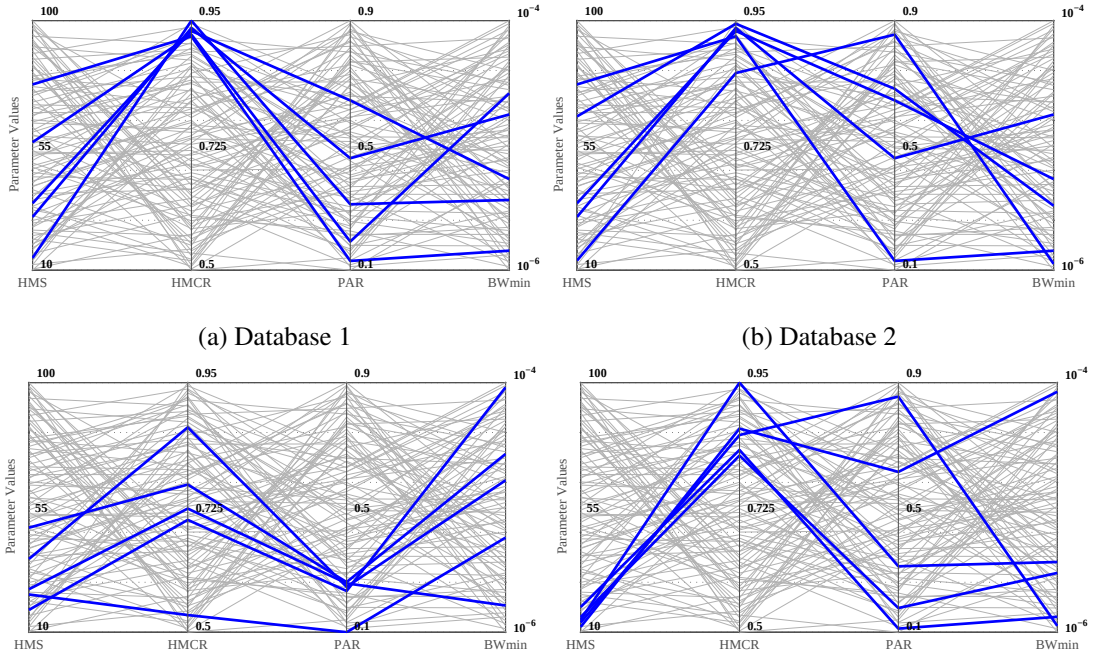

(a) Database 1

(b) Database 2

(c) Database 3

(d) Database 4

Figure B.19: IHS algorithm: 15 records.

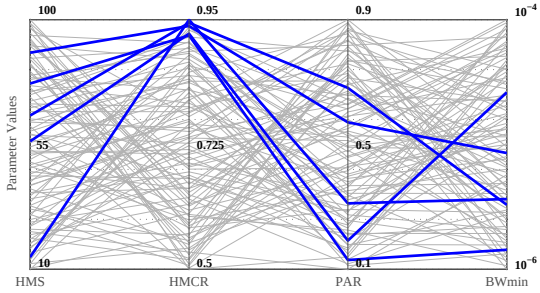

(a) Database 1

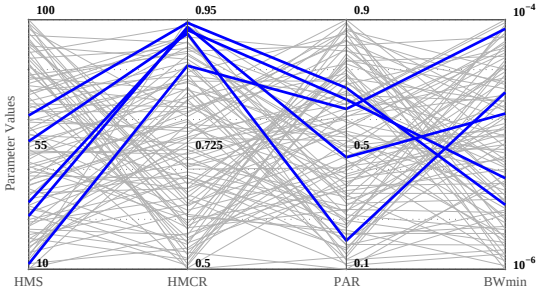

(b) Database 2

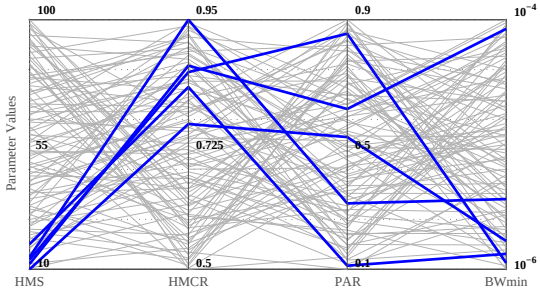

(c) Database 3

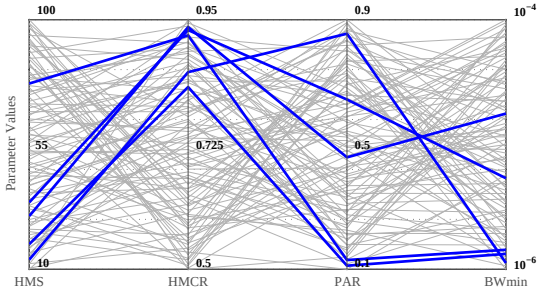

(d) Database 4

Figure B.20: IHS algorithm: 20 records.

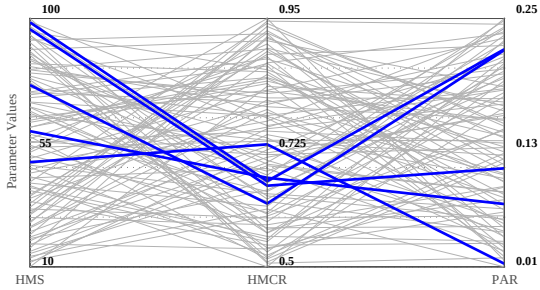

(a) Database 1

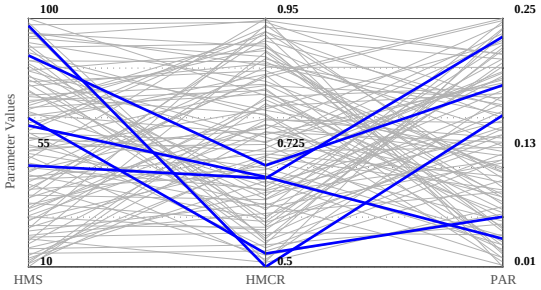

(b) Database 2

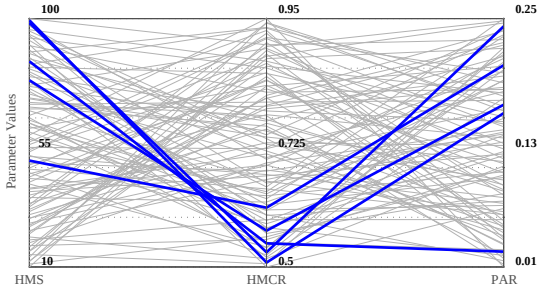

(c) Database 3

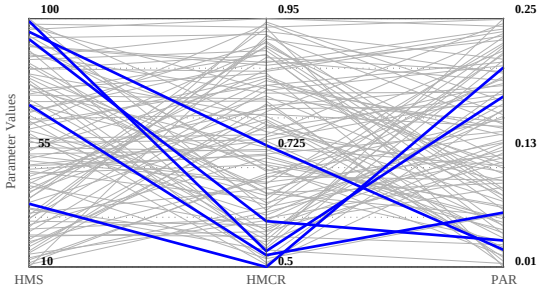

(d) Database 4

Figure B.21: GHS algorithm: 3 records.

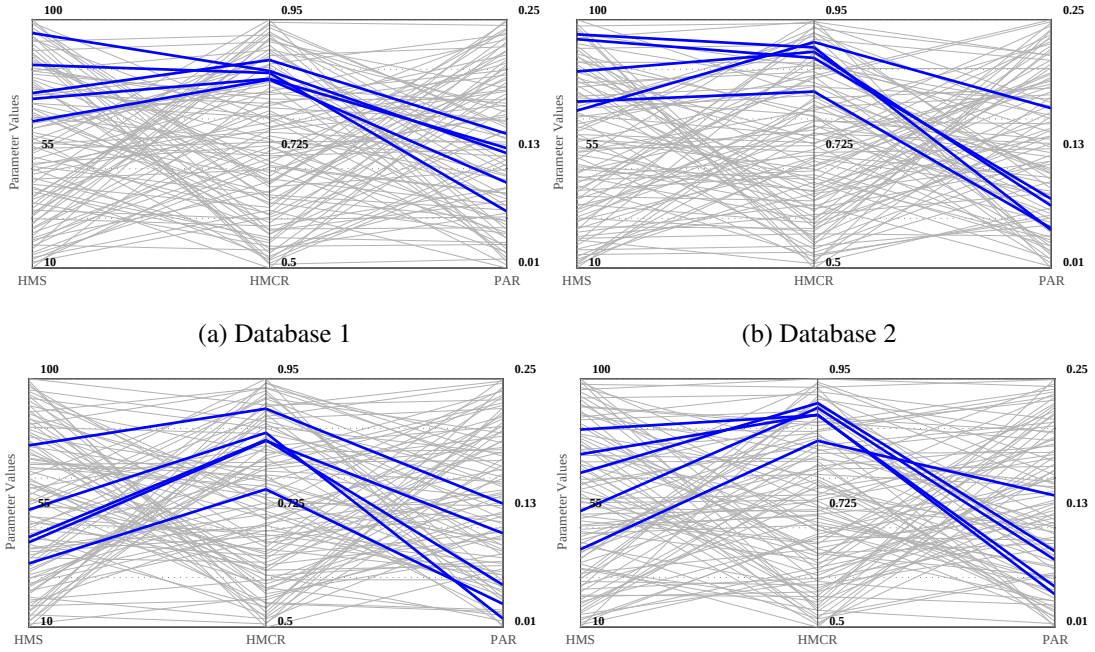

(a) Database 1

(b) Database 2

(c) Database 3

(d) Database 4

Figure B.22: GHS algorithm: 7 records.

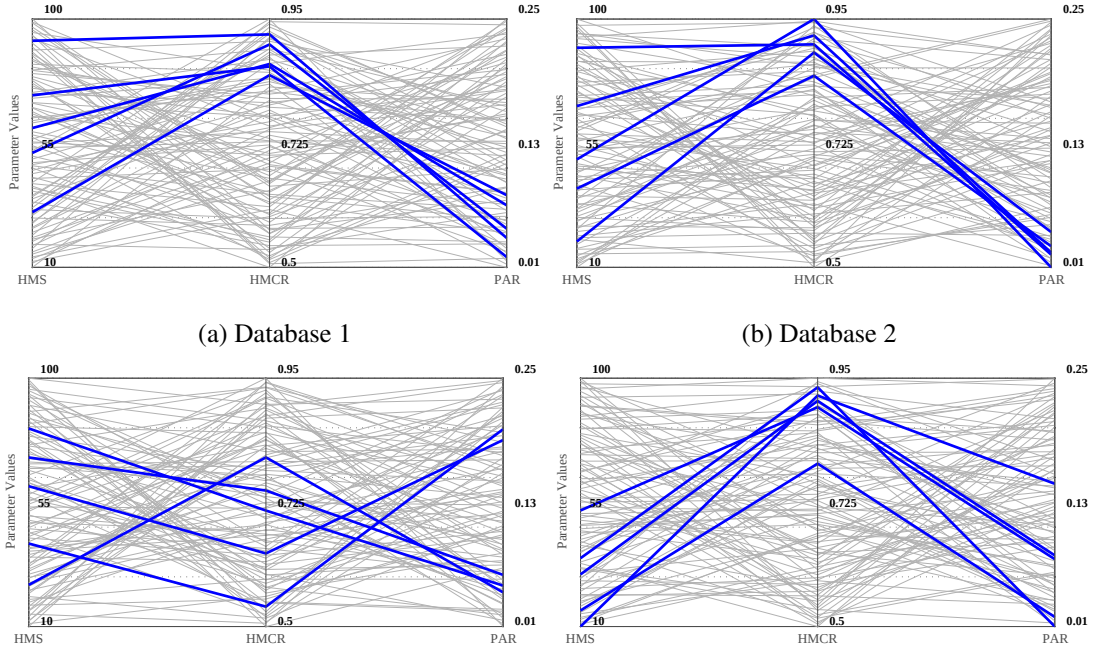

(a) Database 1

(b) Database 2

(c) Database 3

(d) Database 4

Figure B.23: GHS algorithm: 15 records.

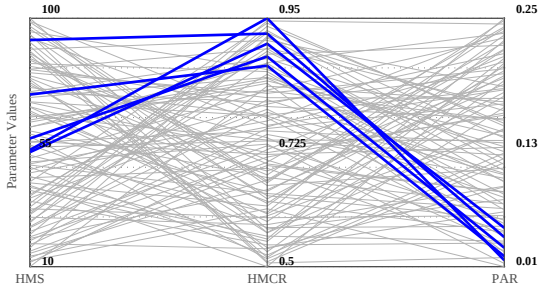

(a) Database 1

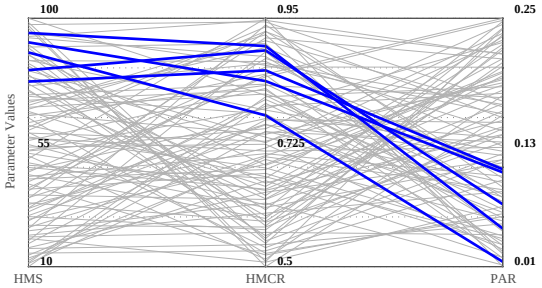

(b) Database 2

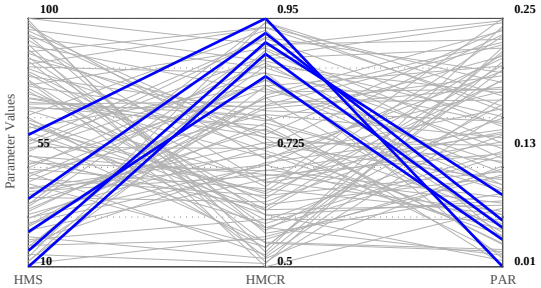

(c) Database 3

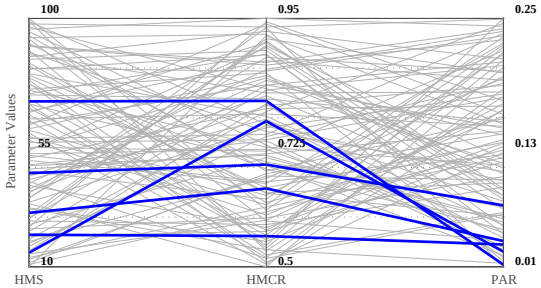

(d) Database 4

Figure B.24: GHS algorithm: 20 records.

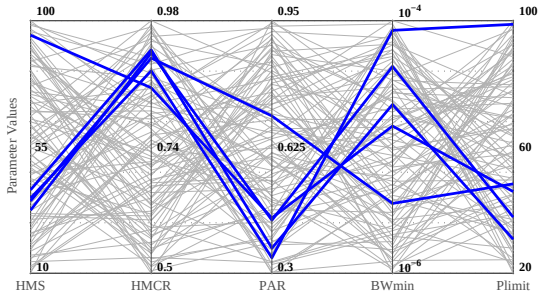

(a) Database 1

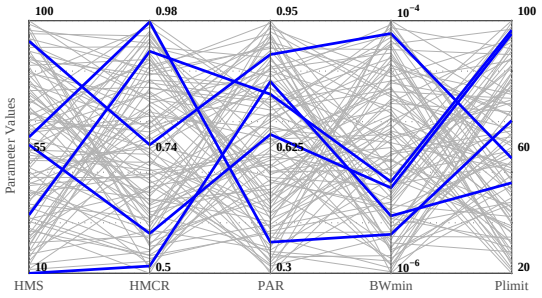

(b) Database 2

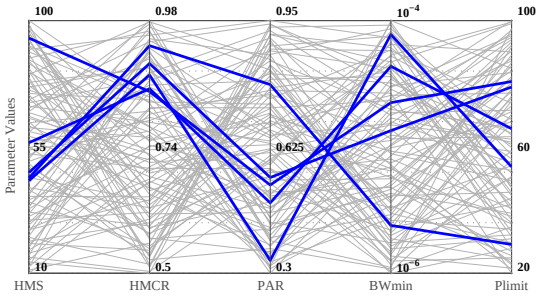

(c) Database 3

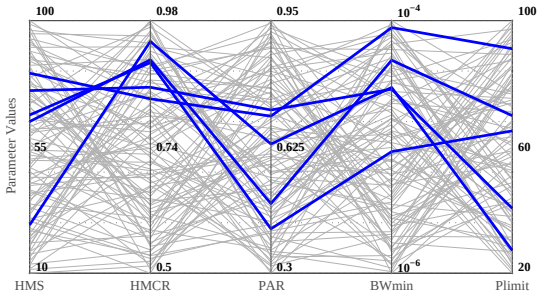

(d) Database 4

Figure B.25: SGHS algorithm: 3 records.

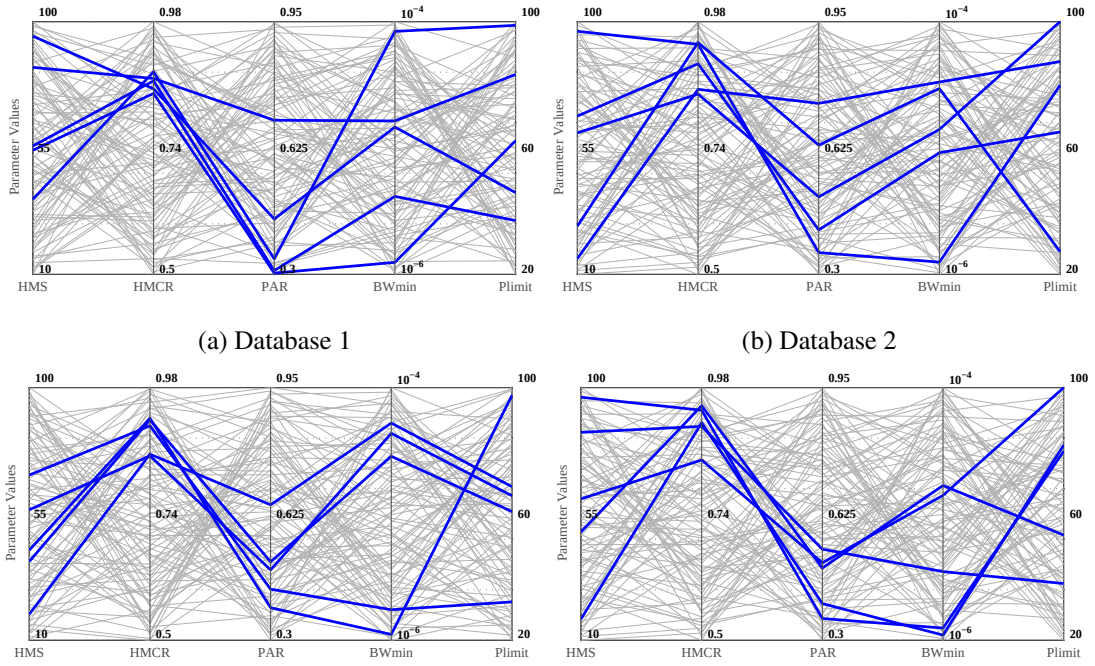

(a) Database 1

(b) Database 2

(c) Database 3

(d) Database 4

Figure B.26: SGHS algorithm: 7 records.

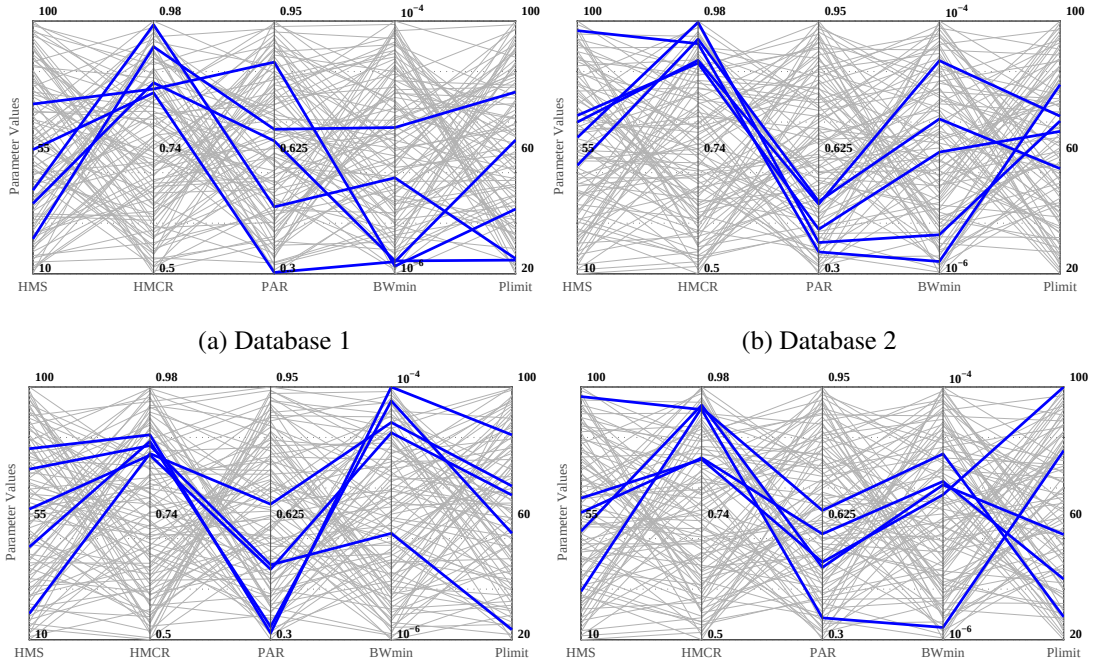

(a) Database 1

(b) Database 2

(c) Database 3

(d) Database 4

Figure B.27: SGHS algorithm: 15 records.

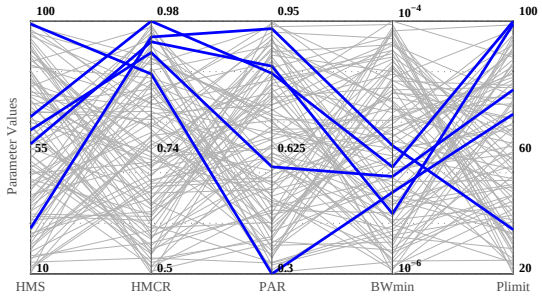

(a) Database 1

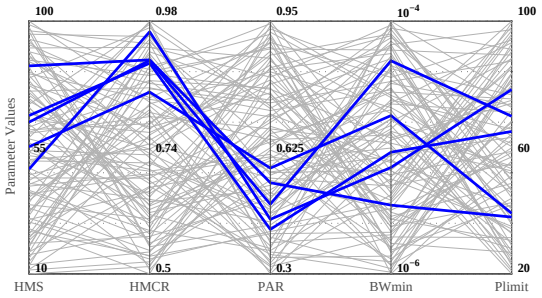

(b) Database 2

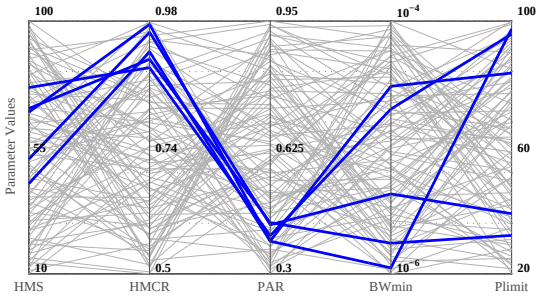

(c) Database 3

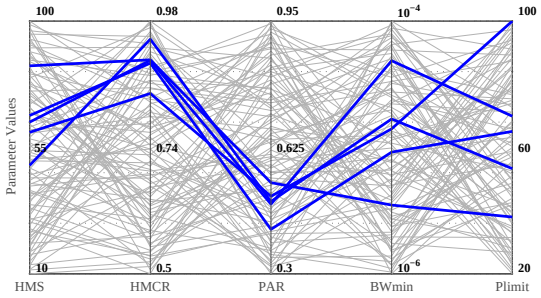

(d) Database 4

Figure B.28: SGHS algorithm: 20 records.

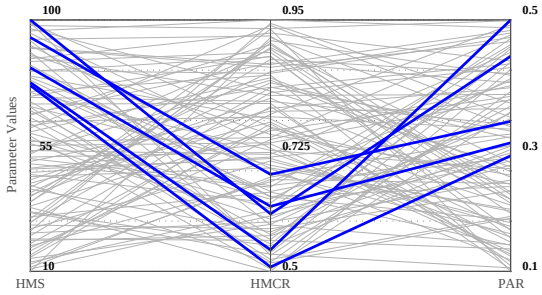

(a) Database 1

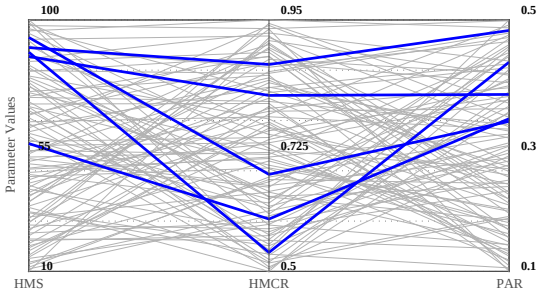

(b) Database 2

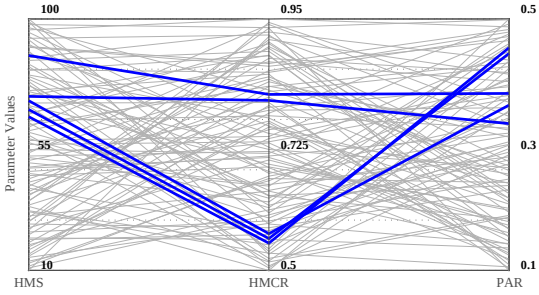

(c) Database 3

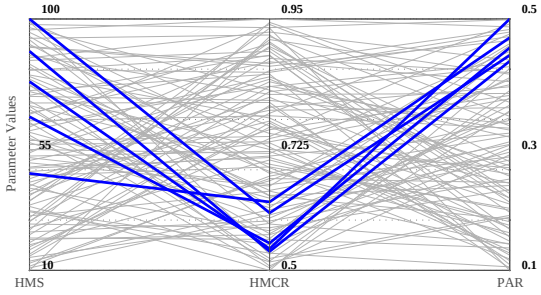

(d) Database 4

Figure B.29: AHS algorithm: 3 records.

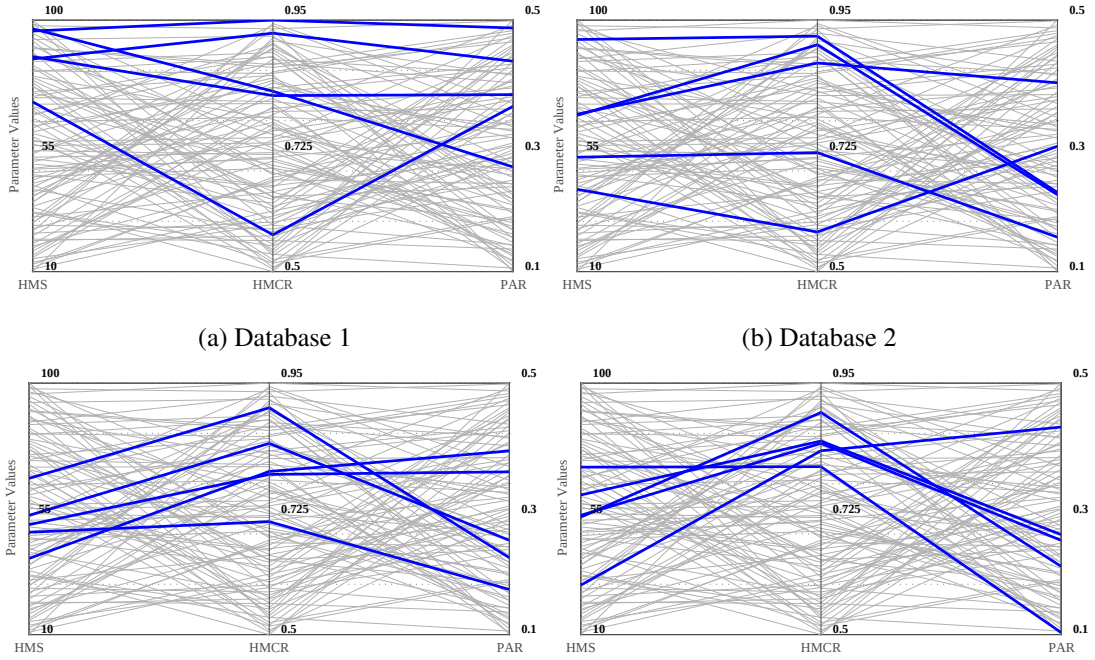

(a) Database 1

(b) Database 2

(c) Database 3

(d) Database 4

Figure B.30: AHS algorithm: 7 records.

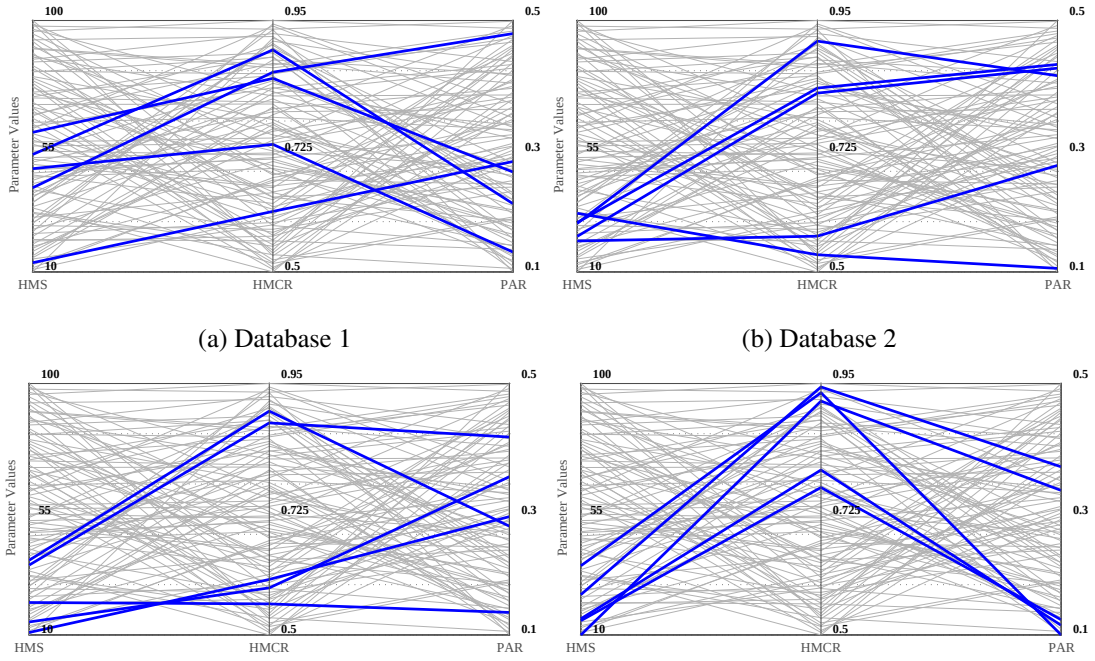

(a) Database 1

(b) Database 2

(c) Database 3

(d) Database 4

Figure B.31: AHS algorithm: 15 records.

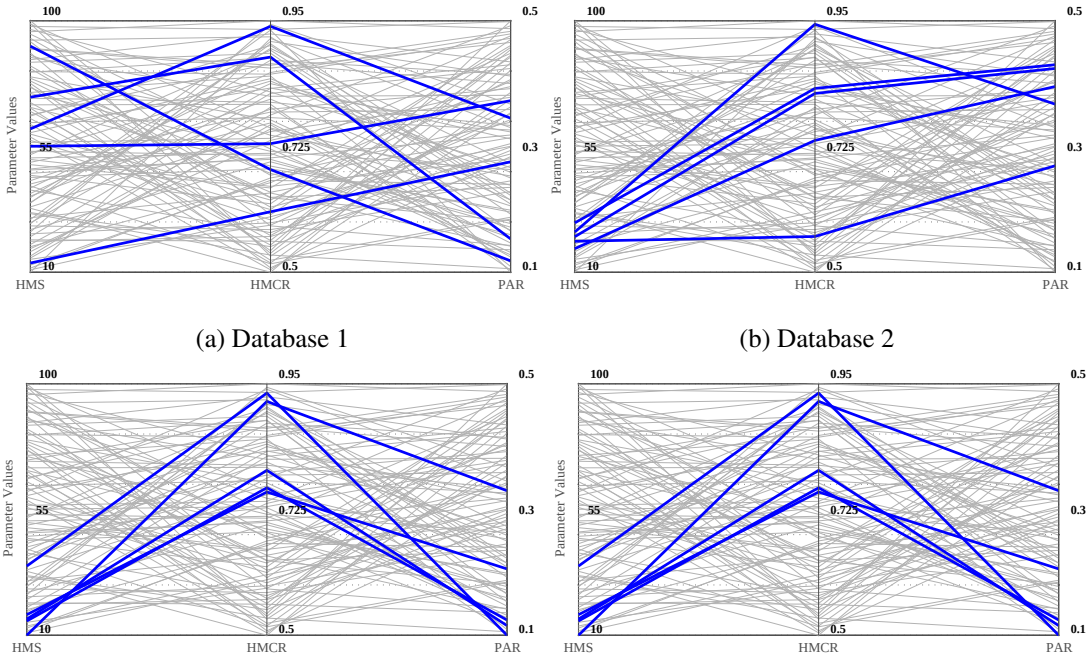

(a) Database 1

(b) Database 2

(c) Database 3

(d) Database 4

Figure B.32: AHS algorithm: 20 records.

Regarding HS algorithm, analysis of Figure B.13 to Figure B.16 allow conclude that for suites of 3 and 7 ground motion records the parameters HMS and HMCR should be defined in the intervals of $[50;90]$ and $[0.80;0.95]$, respective. Moreover, PAR parameter should have a value of $[0.40;0.55]$ for suites with 3 ground motion records and $[0.15;0.20]$ for the other cases. IFB algorithm the HMCR parameter should take values between $[0.75;0.90]$ for groups with more then 3 ground motion records and $[0.60;0.90]$ otherwise. Additionally, the value of of HMCR should take a value between $[60;80]$ for groups with 3 and 7 ground motion records and $[10;20]$ for the other cases. Regarding the GHS algorithm, for selection and scaling of groups with 3 ground motion records, the values of HMS and HMCR should be defined in with values bettween $[50;100]$ and $[0.5;0.7]$, respectively. Otherwise, for groups with 7, 15 and 20 ground motion records the HMS, HMCR and PAR should assume values of $[10;60]$, $[0.75;0.90]$ and $[0.01,0.13]$, respectively. In regard to the SGHS algorithm the values of $[40;75]$, $[0.80;0.98]$ and $[0.30;0.50]$ for HMS, HMCR and PAR should be defined. Finally for the AHS algorithm the parameters HMS, HMCR and PAR should take values of $[55;100]$, $[0.5;0.75]$ and $[0.3;0.5]$, respectively, for groups with 3 ground motion records. For groups with 7 ground motion records HMS, HMCR and PAR should take values of $[55;100]$, $[0.70;0.80]$ and $[0.1;0.3]$, respectively. Furthermore, for groups with 15 and 20 records the values of HMS, HMCR and PAR should take values of $[10;30]$, $[0.75;0.90]$ and $[0.1;0.3]$, respectively.

B.5 Objective function sensitivity analysis

Although a given optimization algorithm might show the best performance indicators concerning to the objective function (e.g. mean), it is possible to question if these indicators are statistically different from the averages presented by other algorithms. Therefore, an analysis of variance (ANOVA) allows for a comparison of the groups means by analysis of sample variances. The null hypothesis of ANOVA analysis assumes that all population means are equal, whilst the rejection of the null hypothesis assumes a p-value less than a test of significance level (typically set to 5%). This rejection signifies that at least one of the population means is different from the others. In the case of rejection of the null hypothesis, a method of multiple comparisons of means is applied in order to identify which algorithms have statistically different means. For the current research study, the ANOVA methodology was carried-out with the Tukey-Kramer (Tukey, 1949) test of multiple comparisons. Figure B.33 to Figure B.36 show the ANOVA methodology results and the obtained p-value. It is important to note that the null hypothesis was rejected for all cases, and thus the Tukey-Kramer (Tukey, 1949) methodology was followed. The recommended values obtained in the last Section are used in the algorithms. In the figures, the AHS algorithm is marked with a blue coloured symbol, whilst algorithms with statistically identical (grey coloured symbols) and different (red coloured symbols) means are marked accordingly.

Analysis of the results shown in the previous figures allow concluding that the mean of the objective function (of thirty analysis) for each algorithm, using the last section recommended values for the definition parameters, can be considered to be statistically different. It is important

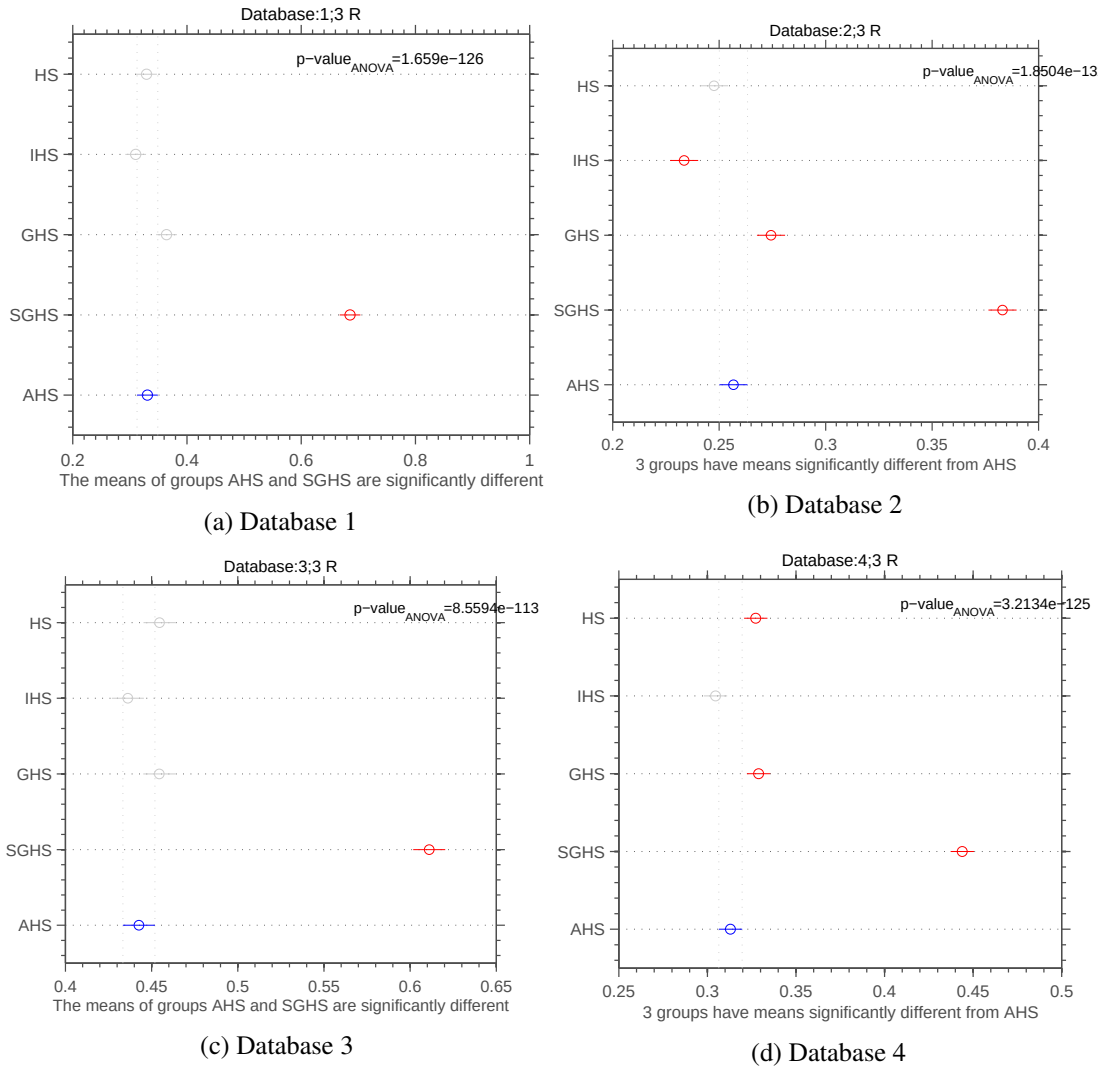

(a) Database 1

(b) Database 2

(c) Database 3

(d) Database 4

Figure B.33: ANOVA: 3 records.

to note that in several cases, the AHS algorithm showed the best mean of the objective function, whilst being statistically different from the mean of all remaining algorithms. The HS, IHS and GHS algorithms exhibited mean objective function values statistically similar to the AHS algorithm in some cases, such as for selected groups of three ground motion records selected from the pre-selection Database 1 or Database 3..

On the basis of the results shown, it was well established that the AHS was the HS optimization algorithm variant with the best overall performance. Moreover, the results obtained for the ANOVA methodology allow concluding that the remaining variants can be moderately to highly (statistically) different from the AHS results, to what concerns the objective function values. This highlights the importance of the use of the calibrated optimization algorithm in a record selection and scaling application, as different methodologies may lead to considerably different results.

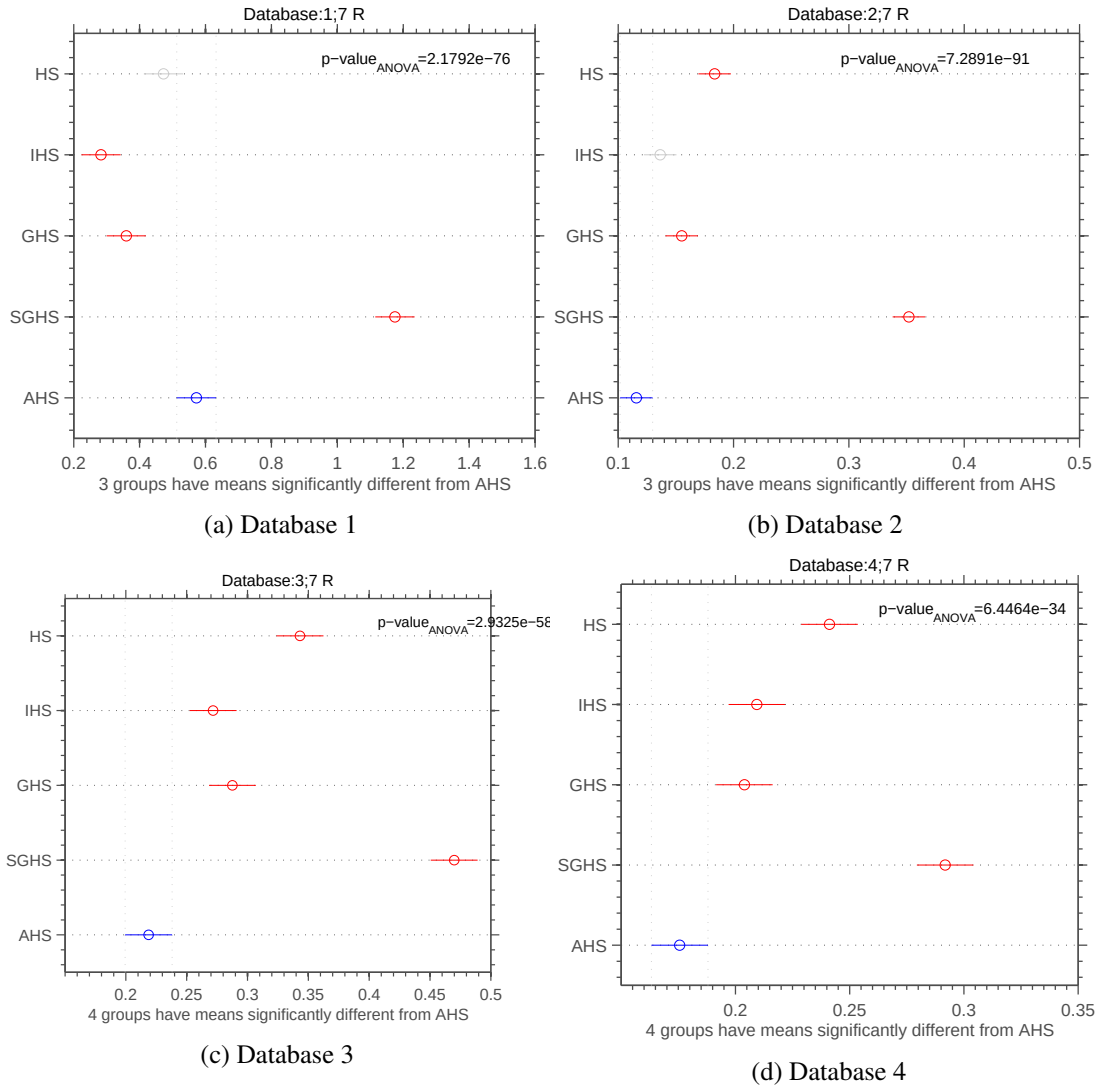

(a) Database 1

(b) Database 2

(c) Database 3

(d) Database 4

Figure B.34: ANOVA: 7 records.

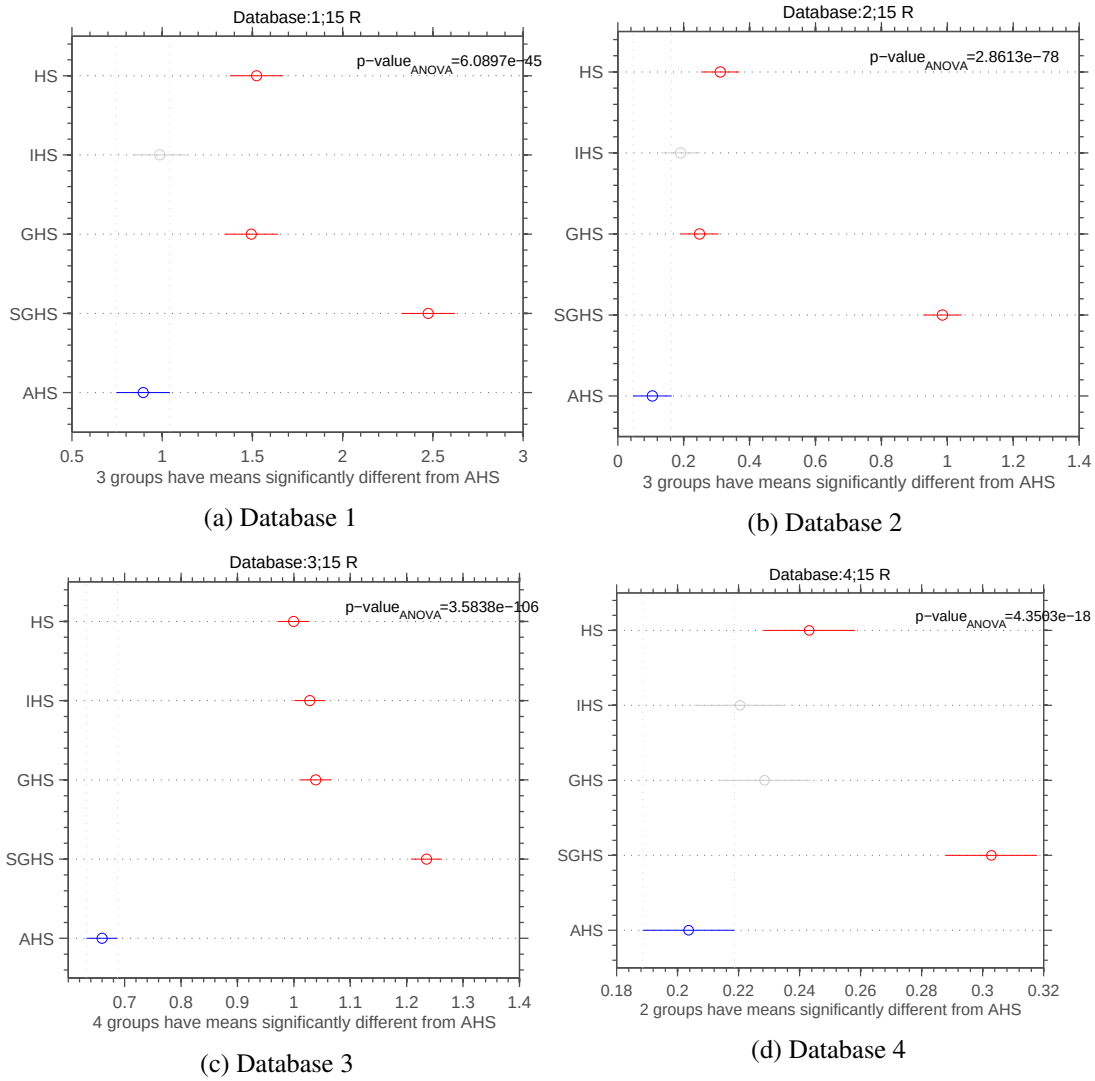

(a) Database 1

(b) Database 2

(c) Database 3

(d) Database 4

Figure B.35: ANOVA: 15 records.

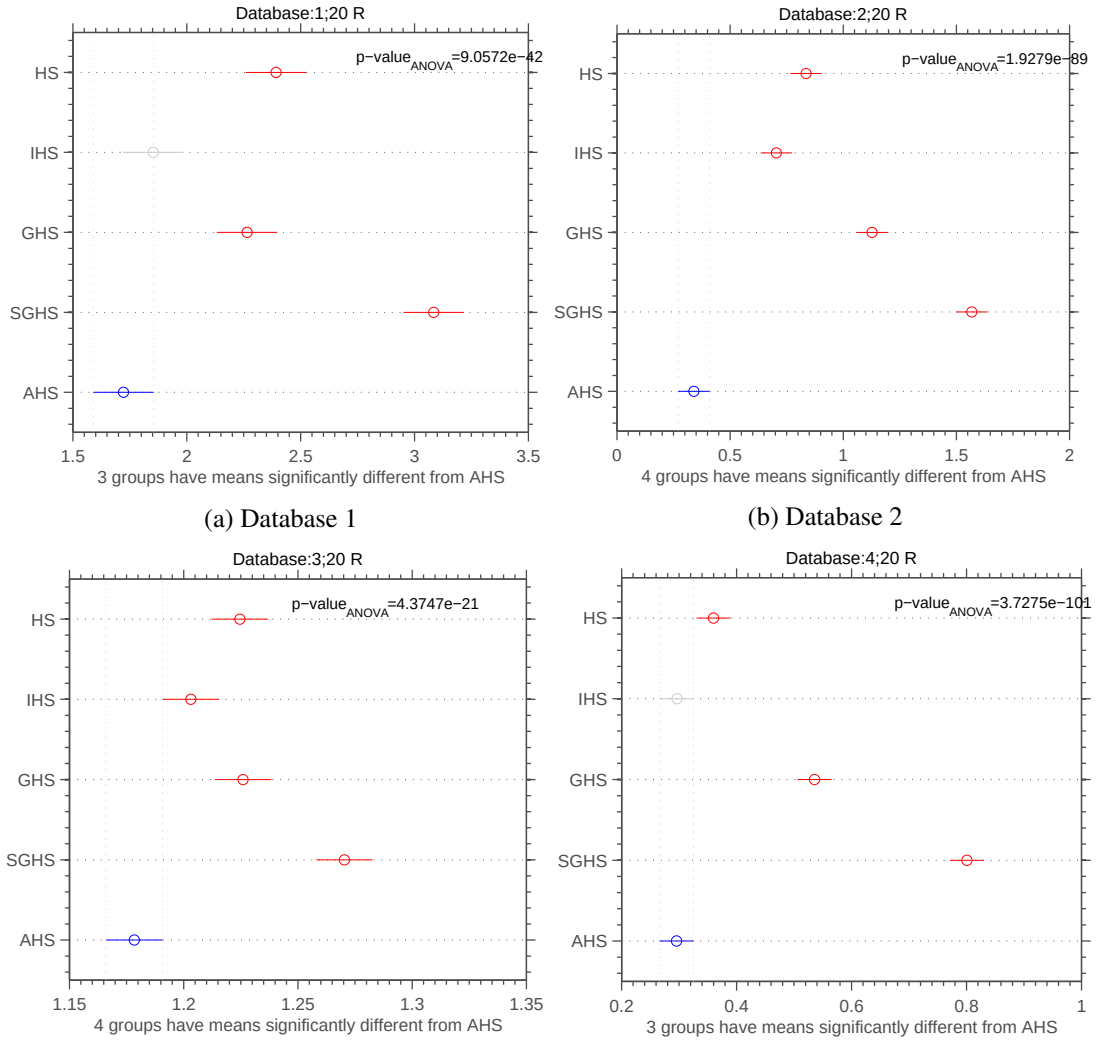

(a) Database 1

(b) Database 2

(c) Database 3

(d) Database 4

Figure B.36: ANOVA: 20 records.

B.6 Conclusions

In this Appendix a parametric study was conducted with the aim of investigating the performance of the Harmony Search algorithm for earthquake ground motion record selection. Several variants of the HS algorithm available in the literature have been tested and their performance compared. The results allow concluding that the performance of each algorithm is dependent on the number of ground motion ground motion records per group and the size of the pre-selection database considered. Overall the AHS algorithm exhibited better performance independently of number of records per set and pre-selection databases.

A sensitivity analysis of the parameters of each method was also conducted. It was possible to conclude that even for the methods that dynamically adjust the parameters of the algorithm during the optimization process, the algorithm is still sensitive to some parameters and their interaction. The results obtained with Sobol's method exposed the high dependence of the interactions between the parameters in the solution obtained by the algorithms. Moreover, despite the low values of the Sobol's first order indexes the high values of the total effect indexes indicate that all the parameters are relevant for the algorithm solution. In addition the parallel coordinates plots allow defining the appropriate range of values for all parameters.

In conclusion, AHS algorithm exhibited the better performance to efficiently obtain stable and consistent solutions.

Appendix C

Structural Design Database

This appendix includes documentation and details of the structural designs used in this research thesis. This documentation is organized as a structural steel moment-resisting frame (MRF) database and provides relevant information that can be used by other researchers.

As mentioned before, an extensive parametric study was defined in the context of this research study, intended to quantify the influence of different behaviour factors on the seismic design of steel MRFs to EC8. A number of defining parameters were considered, namely the building configuration (number and width of the bays), the number of storeys, the seismic location and the behaviour factor.

Six building configurations were defined by varying both the number (3, 4 or 5) and the width of the bays (equal and different between bays) in the main frame direction, as well as the number of the bays in the orthogonal direction (2, 3 or 4). The geometrical properties of the building configurations are shown in Table C.1.

Table C.1: Building configurations and geometrical properties.

Config.	x-z plane		y-z plane		h_1 [m]	h_{others} [m]
	N. of frames	Bays [m]	N. of frames	Bays [m]		
1	3	6+6+6	4	6+6	4.5	3.5
2	3	6+8+6	4	6+6		
3	3	8+8+8	4	8+8		
4	4	6+6+6+6	5	6+6+6		
5	3	8+6+8	4	6+6		
6	5	8+8+8+8+8	6	8+8+8+8		

Figure C.1 shows the elevation and plan views of one of the building configurations. The analysed frame is also identified in the figure. Seismic resistance was considered to be provided by

the MRFs in the longitudinal (x) direction and by a bracing system in the transversal (y) direction. In this research study, only the internal longitudinal frames were subject of investigation.

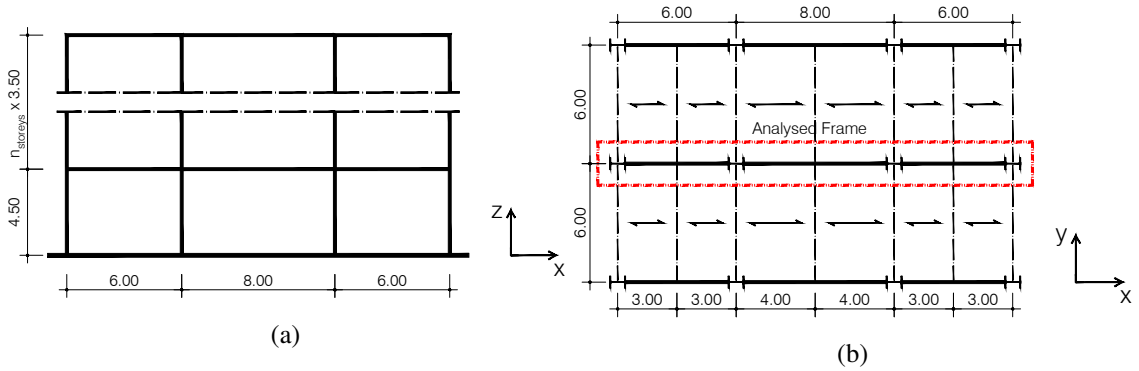

Figure C.1: Building configuration 2: (a) Elevation view, (b) Plan view.

C.1 Design information

Table C.2: Frames - Porto Configuration 1

ID	Floor	B1	B2	B3	C1	C2	C3	C4	St.	T_1	q	ISD	Mass	θ_{EC8}	Ω
St1	1	IPE300	IPE300	IPE300	HEB240	HEB300	HEB300	HEB240	2	0.65	6.50	0.111	46.61	0.189	16.181
	2	IPE300	IPE300	IPE300	HEB240	HEB300	HEB300	HEB240				0.12	37.06	0.157	
St2	1	IPE300	IPE300	IPE300	HEB200	HEB240	HEB240	HEB200	2	0.80	4.00	0.151	46.61	0.193	10.222
	2	IPE300	IPE300	IPE300	HEB200	HEB240	HEB240	HEB200				0.12	37.06	0.119	
St3	1	IPE300	IPE300	IPE300	HEB200	HEB240	HEB240	HEB200	2	0.80	1.50	0.151	46.61	0.068	2.555
	2	IPE300	IPE300	IPE300	HEB200	HEB240	HEB240	HEB200				0.12	37.06	0.04	
St4	1	IPE330	IPE330	IPE330	HEB320	HEB360	HEB360	HEB320	3	0.76	6.50	0.109	46.61	0.183	15.784
	2	IPE330	IPE330	IPE330	HEB320	HEB360	HEB360	HEB320				0.147	46.61	0.197	
	3	IPE300	IPE300	IPE300	HEB300	HEB340	HEB340	HEB300				0.118	37.06	0.134	
St5	1	IPE300	IPE300	IPE300	HEB240	HEB300	HEB300	HEB240	3	0.96	4.00	0.13	46.61	0.193	8.057
	2	IPE300	IPE300	IPE300	HEB240	HEB300	HEB300	HEB240				0.157	46.61	0.186	
	3	IPE300	IPE300	IPE300	HEB220	HEB280	HEB280	HEB220				0.103	37.06	0.108	
St6	1	IPE300	IPE300	IPE300	HEB200	HEB240	HEB240	HEB200	3	1.16	1.50	0.18	46.61	0.11	3.019
	2	IPE300	IPE300	IPE300	HEB200	HEB240	HEB240	HEB200				0.17	46.61	0.084	
	3	IPE300	IPE300	IPE300	HEB200	HEB220	HEB220	HEB200				0.112	37.06	0.048	
St7	1	IPE400	IPE400	IPE400	HEB360	HEB400	HEB400	HEB360	4	0.83	6.50	0.098	46.61	0.168	13.966
	2	IPE400	IPE400	IPE400	HEB360	HEB400	HEB400	HEB360				0.139	46.61	0.196	
	3	IPE300	IPE300	IPE300	HEB320	HEB360	HEB360	HEB320				0.148	46.61	0.174	
	4	IPE300	IPE300	IPE300	HEB320	HEB360	HEB360	HEB320				0.137	37.06	0.142	
St8	1	IPE330	IPE330	IPE330	HEB300	HEB360	HEB360	HEB300	4	1.05	4.00	0.104	46.61	0.167	10.299
	2	IPE330	IPE330	IPE330	HEB300	HEB360	HEB360	HEB300				0.153	46.61	0.199	
	3	IPE300	IPE300	IPE300	HEB280	HEB320	HEB320	HEB280				0.135	46.61	0.154	
	4	IPE300	IPE300	IPE300	HEB280	HEB320	HEB320	HEB280				0.102	37.06	0.101	
St9	1	IPE300	IPE300	IPE300	HEB220	HEB260	HEB260	HEB220	4	1.42	1.50	0.174	46.61	0.125	2.576
	2	IPE300	IPE300	IPE300	HEB220	HEB260	HEB260	HEB220				0.201	46.61	0.119	
	3	IPE300	IPE300	IPE300	HEB200	HEB240	HEB240	HEB200				0.155	46.61	0.086	
	4	IPE300	IPE300	IPE300	HEB200	HEB240	HEB240	HEB200				0.089	37.06	0.042	

Table C.2: Frames - Porto Configuration 1

ID	Floor	B1	B2	B3	C1	C2	C3	C4	St.	T_1	q	ISD	Mass	θ_{EC8}	Ω
St10	1	IPE450	IPE450	IPE450	HEB360	HEB450	HEB450	HEB360	5	0.93	6.50	0.096	46.61	0.166	11.929
	2	IPE450	IPE450	IPE450	HEB360	HEB450	HEB450	HEB360				0.135	46.61	0.198	
	3	IPE360	IPE360	IPE360	HEB340	HEB400	HEB400	HEB340				0.159	46.61	0.197	
	4	IPE300	IPE300	IPE300	HEB340	HEB400	HEB400	HEB340				0.175	46.61	0.188	
	5	IPE300	IPE300	IPE300	HEB320	HEB360	HEB360	HEB320				0.154	37.06	0.151	
St11	1	IPE400	IPE400	IPE400	HEB320	HEB360	HEB360	HEB320	5	1.16	4.00	0.1	46.61	0.161	10.172
	2	IPE360	IPE360	IPE360	HEB320	HEB360	HEB360	HEB320				0.146	46.61	0.197	
	3	IPE330	IPE330	IPE330	HEB320	HEB340	HEB340	HEB320				0.154	46.61	0.183	
	4	IPE300	IPE300	IPE300	HEB320	HEB340	HEB340	HEB320				0.14	46.61	0.148	
	5	IPE300	IPE300	IPE300	HEB300	HEB320	HEB320	HEB300				0.109	37.06	0.103	
St12	1	IPE300	IPE300	IPE300	HEB220	HEB260	HEB260	HEB220	5	1.77	1.50	0.186	46.61	0.161	2.429
	2	IPE300	IPE300	IPE300	HEB220	HEB260	HEB260	HEB220				0.226	46.61	0.164	
	3	IPE300	IPE300	IPE300	HEB200	HEB240	HEB240	HEB200				0.198	46.61	0.134	
	4	IPE300	IPE300	IPE300	HEB200	HEB240	HEB240	HEB200				0.139	46.61	0.088	
	5	IPE300	IPE300	IPE300	HEB200	HEB200	HEB200	HEB200				0.089	37.06	0.05	
St13	1	IPE550	IPE550	IPE550	HEB450	HEB550	HEB550	HEB450	8	1.11	6.50	0.086	46.61	0.151	10.627
	2	IPE550	IPE550	IPE550	HEB450	HEB550	HEB550	HEB450				0.119	46.61	0.189	
	3	IPE500	IPE500	IPE500	HEB450	HEB550	HEB550	HEB450				0.129	46.61	0.182	
	4	IPE500	IPE500	IPE500	HEB400	HEB500	HEB500	HEB400				0.142	46.61	0.179	
	5	IPE450	IPE450	IPE450	HEB400	HEB500	HEB500	HEB400				0.15	46.61	0.172	
	6	IPE360	IPE360	IPE360	HEB400	HEB500	HEB500	HEB400				0.174	46.61	0.181	
	7	IPE300	IPE300	IPE300	HEB360	HEB450	HEB450	HEB360				0.191	46.61	0.178	
	8	IPE300	IPE300	IPE300	HEB360	HEB450	HEB450	HEB360				0.173	37.06	0.155	

Table C.2: Frames - Porto Configuration 1

ID	Floor	B1	B2	B3	C1	C2	C3	C4	St.	T_1	q	ISD	Mass	θ_{EC8}	Ω
St14	1	IPE500	IPE500	IPE500	HEB400	HEB450	HEB450	HEB400	8	1.42	4.00	0.086	46.61	0.138	9.504
	2	IPE450	IPE450	IPE450	HEB400	HEB450	HEB450	HEB400				0.13	46.61	0.186	
	3	IPE400	IPE400	IPE400	HEB400	HEB450	HEB450	HEB400				0.154	46.61	0.199	
	4	IPE400	IPE400	IPE400	HEB360	HEB400	HEB400	HEB360				0.168	46.61	0.198	
	5	IPE400	IPE400	IPE400	HEB360	HEB400	HEB400	HEB360				0.157	46.61	0.17	
	6	IPE330	IPE330	IPE330	HEB360	HEB400	HEB400	HEB360				0.153	46.61	0.154	
	7	IPE330	IPE330	IPE330	HEB340	HEB360	HEB360	HEB340				0.136	46.61	0.129	
	8	IPE300	IPE300	IPE300	HEB340	HEB360	HEB360	HEB340				0.107	37.06	0.094	
St15	1	IPE300	IPE300	IPE300	HEB260	HEB300	HEB300	HEB260	8	2.55	1.50	0.161	46.61	0.194	2.563
	2	IPE300	IPE300	IPE300	HEB260	HEB300	HEB300	HEB260				0.238	46.61	0.253	
	3	IPE300	IPE300	IPE300	HEB260	HEB300	HEB300	HEB260				0.228	46.61	0.229	
	4	IPE300	IPE300	IPE300	HEB240	HEB280	HEB280	HEB240				0.213	46.61	0.202	
	5	IPE300	IPE300	IPE300	HEB240	HEB280	HEB280	HEB240				0.178	46.61	0.161	
	6	IPE300	IPE300	IPE300	HEB240	HEB280	HEB280	HEB240				0.14	46.61	0.121	
	7	IPE300	IPE300	IPE300	HEB220	HEB260	HEB260	HEB220				0.097	46.61	0.085	
	8	IPE300	IPE300	IPE300	HEB220	HEB260	HEB260	HEB220				0.061	37.06	0.044	

Table C.3: Frames - Porto Configuration 2

ID	Floor	B1	B2	B3	C1	C2	C3	C4	St.	T_1	q	ISD	Mass	θ_{EC8}	Ω
St16	1	IPE300	IPE360	IPE300	HEB240	HEB300	HEB300	HEB240	2	0.68	6.50	0.119	51.784	0.19	14.545
	2	IPE270	IPE330	IPE270	HEB240	HEB300	HEB300	HEB240				0.139	41.182	0.144	
St17	1	IPE300	IPE360	IPE300	HEB220	HEB260	HEB260	HEB220	2	0.77	4.00	0.137	51.784	0.157	9.345
	2	IPE270	IPE330	IPE270	HEB220	HEB260	HEB260	HEB220				0.132	41.182	0.103	
St18	1	IPE300	IPE360	IPE300	HEB220	HEB260	HEB260	HEB220	2	0.77	1.50	0.137	51.784	0.059	2.337
	2	IPE270	IPE330	IPE270	HEB220	HEB260	HEB260	HEB220				0.132	41.182	0.039	
St19	1	IPE360	IPE400	IPE360	HEB300	HEB360	HEB360	HEB300	3	0.77	6.50	0.111	51.784	0.175	17.432
	2	IPE330	IPE400	IPE300	HEB300	HEB360	HEB360	HEB300				0.144	51.784	0.175	
	3	IPE270	IPE330	IPE270	HEB300	HEB360	HEB360	HEB300				0.128	41.182	0.122	
St20	1	IPE330	IPE360	IPE330	HEB240	HEB300	HEB300	HEB240	3	0.95	4.00	0.13	51.784	0.178	9.807
	2	IPE300	IPE360	IPE300	HEB240	HEB300	HEB300	HEB240				0.149	51.784	0.161	
	3	IPE270	IPE330	IPE270	HEB240	HEB300	HEB300	HEB240				0.114	41.182	0.099	
St21	1	IPE330	IPE360	IPE330	HEB220	HEB280	HEB280	HEB220	3	1.01	1.50	0.154	51.784	0.085	3.645
	2	IPE300	IPE360	IPE300	HEB220	HEB280	HEB280	HEB220				0.155	51.784	0.07	
	3	IPE270	IPE330	IPE270	HEB220	HEB280	HEB280	HEB220				0.109	41.182	0.04	
St22	1	IPE400	IPE450	IPE400	HEB360	HEB450	HEB450	HEB360	4	0.83	6.50	0.096	51.784	0.15	15.106
	2	IPE400	IPE450	IPE400	HEB360	HEB450	HEB450	HEB360				0.141	51.784	0.174	
	3	IPE330	IPE360	IPE330	HEB320	HEB400	HEB400	HEB320				0.138	51.784	0.152	
	4	IPE270	IPE330	IPE270	HEB320	HEB400	HEB400	HEB320				0.14	41.182	0.12	
St23	1	IPE360	IPE400	IPE360	HEB240	HEB340	HEB340	HEB240	4	1.07	4.00	0.124	51.784	0.184	11.240
	2	IPE360	IPE400	IPE360	HEB240	HEB340	HEB340	HEB240				0.15	51.784	0.179	
	3	IPE330	IPE360	IPE330	HEB220	HEB320	HEB320	HEB220				0.125	51.784	0.139	
	4	IPE270	IPE330	IPE270	HEB220	HEB320	HEB320	HEB220				0.102	41.182	0.091	
St24	1	IPE330	IPE360	IPE330	HEB200	HEB280	HEB280	HEB200	4	1.37	1.50	0.169	51.784	0.119	2.999
	2	IPE300	IPE360	IPE300	HEB200	HEB280	HEB280	HEB200				0.19	51.784	0.011	
	3	IPE300	IPE360	IPE300	HEB200	HEB260	HEB260	HEB200				0.15	51.784	0.081	
	4	IPE270	IPE330	IPE270	HEB200	HEB260	HEB260	HEB200				0.098	41.182	0.044	

Table C.3: Frames - Porto Configuration 2

ID	Floor	B1	B2	B3	C1	C2	C3	C4	St.	T_1	q	ISD	Mass	θ_{EC8}	Ω
St25	1	IPE450	IPE500	IPE450	HEB360	HEB500	HEB500	HEB360	5	0.91	6.50	0.094	51.784	0.147	14.000
	2	IPE450	IPE500	IPE450	HEB360	HEB500	HEB500	HEB360				0.136	51.784	0.174	
	3	IPE400	IPE450	IPE400	HEB340	HEB450	HEB450	HEB340				0.143	51.784	0.164	
	4	IPE330	IPE360	IPE330	HEB340	HEB450	HEB450	HEB340				0.149	51.784	0.15	
	5	IPE270	IPE330	IPE270	HEB320	HEB400	HEB400	HEB320				0.15	41.182	0.124	
St26	1	IPE400	IPE450	IPE400	HEB280	HEB360	HEB360	HEB280	5	1.20	4.00	0.118	51.784	0.174	8.780
	2	IPE400	IPE450	IPE400	HEB280	HEB360	HEB360	HEB280				0.148	51.784	0.181	
	3	IPE330	IPE360	IPE330	HEB260	HEB340	HEB340	HEB260				0.158	51.784	0.176	
	4	IPE300	IPE360	IPE300	HEB260	HEB340	HEB340	HEB260				0.154	51.784	0.152	
	5	IPE270	IPE330	IPE270	HEB220	HEB300	HEB300	HEB220				0.124	41.182	0.105	
St27	1	IPE330	IPE360	IPE330	HEB200	HEB300	HEB300	HEB200	5	1.64	1.50	0.165	51.784	0.134	2.546
	2	IPE300	IPE360	IPE300	HEB200	HEB300	HEB300	HEB200				0.209	51.784	0.143	
	3	IPE300	IPE360	IPE300	HEB200	HEB280	HEB280	HEB200				0.188	51.784	0.119	
	4	IPE300	IPE360	IPE300	HEB200	HEB280	HEB280	HEB200				0.134	51.784	0.079	
	5	IPE270	IPE330	IPE270	HEB200	HEB260	HEB260	HEB200				0.09	41.182	0.045	
St28	1	IPE550	IPE600	IPE550	HEB500	HEB600	HEB600	HEB500	8	1.12	6.50	0.082	51.784	0.129	11.000
	2	IPE550	IPE600	IPE550	HEB500	HEB600	HEB600	HEB500				0.124	51.784	0.167	
	3	IPE500	IPE550	IPE500	HEB500	HEB600	HEB600	HEB500				0.135	51.784	0.167	
	4	IPE500	IPE550	IPE500	HEB450	HEB550	HEB550	HEB450				0.148	51.784	0.167	
	5	IPE450	IPE500	IPE450	HEB450	HEB550	HEB550	HEB450				0.158	51.784	0.161	
	6	IPE360	IPE400	IPE360	HEB450	HEB550	HEB550	HEB450				0.18	51.784	0.168	
	7	IPE330	IPE360	IPE330	HEB400	HEB450	HEB450	HEB400				0.19	51.784	0.165	
	8	IPE270	IPE330	IPE270	HEB400	HEB450	HEB450	HEB400				0.182	41.182	0.134	

Table C.3: Frames - Porto Configuration 2

ID	Floor	B1	B2	B3	C1	C2	C3	C4	St.	T_1	q	ISD	Mass	θ_{EC8}	Ω
St29	1	IPE500	IPE500	IPE500	HEB360	HEB450	HEB450	HEB360	8	1.43	4.00	0.101	51.784	0.15	7.767
	2	IPE500	IPE500	IPE500	HEB360	HEB450	HEB450	HEB360				0.134	51.784	0.173	
	3	IPE450	IPE500	IPE450	HEB360	HEB450	HEB450	HEB360				0.138	51.784	0.164	
	4	IPE450	IPE500	IPE450	HEB340	HEB400	HEB400	HEB340				0.146	51.784	0.161	
	5	IPE400	IPE450	IPE400	HEB340	HEB400	HEB400	HEB340				0.15	51.784	0.151	
	6	IPE330	IPE360	IPE330	HEB340	HEB400	HEB400	HEB340				0.166	51.784	0.155	
	7	IPE300	IPE360	IPE300	HEB320	HEB360	HEB360	HEB320				0.161	51.784	0.143	
	8	IPE270	IPE330	IPE270	HEB320	HEB360	HEB360	HEB320				0.139	41.182	0.103	
St30	1	IPE300	IPE360	IPE300	HEB260	HEB360	HEB360	HEB260	8	2.43	1.50	0.136	51.784	0.166	2.671
	2	IPE300	IPE360	IPE300	HEB260	HEB360	HEB360	HEB260				0.216	51.784	0.229	
	3	IPE300	IPE360	IPE300	HEB260	HEB360	HEB360	HEB260				0.21	51.784	0.21	
	4	IPE300	IPE360	IPE300	HEB240	HEB320	HEB320	HEB240				0.197	51.784	0.187	
	5	IPE300	IPE360	IPE300	HEB240	HEB320	HEB320	HEB240				0.166	51.784	0.149	
	6	IPE300	IPE360	IPE300	HEB240	HEB320	HEB320	HEB240				0.13	51.784	0.112	
	7	IPE300	IPE360	IPE300	HEB220	HEB320	HEB320	HEB220				0.088	51.784	0.076	
	8	IPE270	IPE330	IPE270	HEB220	HEB320	HEB320	HEB220				0.066	41.182	0.045	

Table C.4: Frames - Porto Configuration 3

ID	Floor	B1	B2	B3	C1	C2	C3	C4	St.	T_1	q	ISD	Mass	θ_{EC8}	Ω
St31	1	IPE450	IPE450	IPE450	HEB260	HEB400	HEB400	HEB260	2	0.57	6.50	0.098	82.854	0.142	20.797
	2	IPE400	IPE400	IPE400	HEB260	HEB400	HEB400	HEB260				0.109	65.892	0.099	
St32	1	IPE450	IPE450	IPE450	HEB260	HEB400	HEB400	HEB260	2	0.57	4.00	0.098	82.854	0.087	12.798
	2	IPE400	IPE400	IPE400	HEB260	HEB400	HEB400	HEB260				0.109	65.892	0.061	
St33	1	IPE450	IPE450	IPE450	HEB260	HEB400	HEB400	HEB260	2	0.57	1.50	0.098	82.854	0.033	4.800
	2	IPE400	IPE400	IPE400	HEB260	HEB400	HEB400	HEB260				0.109	65.892	0.023	
St34	1	IPE450	IPE450	IPE450	HEB300	HEB450	HEB450	HEB300	3	0.75	6.50	0.114	82.854	0.181	14.857
	2	IPE450	IPE450	IPE450	HEB300	HEB450	HEB450	HEB300				0.14	82.854	0.169	
	3	IPE400	IPE400	IPE400	HEB300	HEB450	HEB450	HEB300				0.107	65.892	0.102	
St35	1	IPE450	IPE450	IPE450	HEB260	HEB400	HEB400	HEB260	3	0.81	4.00	0.115	82.854	0.14	10.542
	2	IPE450	IPE450	IPE450	HEB260	HEB400	HEB400	HEB260				0.126	82.854	0.119	
	3	IPE400	IPE400	IPE400	HEB260	HEB400	HEB400	HEB260				0.089	65.892	0.067	
St36	1	IPE450	IPE450	IPE450	HEB260	HEB400	HEB400	HEB260	3	0.81	1.50	0.115	82.854	0.053	3.953
	2	IPE450	IPE450	IPE450	HEB260	HEB400	HEB400	HEB260				0.126	82.854	0.045	
	3	IPE400	IPE400	IPE400	HEB260	HEB400	HEB400	HEB260				0.089	65.892	0.025	
St37	1	IPE500	IPE500	IPE500	HEB450	HEB550	HEB550	HEB450	4	0.83	6.50	0.095	82.854	0.151	13.526
	2	IPE450	IPE450	IPE450	HEB450	HEB550	HEB550	HEB450				0.158	82.854	0.193	
	3	IPE450	IPE450	IPE450	HEB400	HEB450	HEB450	HEB400				0.146	82.854	0.161	
	4	IPE400	IPE400	IPE400	HEB400	HEB450	HEB450	HEB400				0.121	65.892	0.102	
St38	1	IPE450	IPE450	IPE450	HEB300	HEB400	HEB400	HEB300	4	1.04	4.00	0.118	82.854	0.178	9.683
	2	IPE450	IPE450	IPE450	HEB300	HEB400	HEB400	HEB300				0.153	82.854	0.178	
	3	IPE450	IPE450	IPE450	HEB260	HEB340	HEB340	HEB260				0.12	82.854	0.136	
	4	IPE400	IPE400	IPE400	HEB260	HEB340	HEB340	HEB260				0.084	65.892	0.073	
St39	1	IPE450	IPE450	IPE450	HEB280	HEB400	HEB400	HEB280	4	1.06	1.50	0.121	82.854	0.07	3.632
	2	IPE450	IPE450	IPE450	HEB280	HEB400	HEB400	HEB280				0.151	82.854	0.069	
	3	IPE450	IPE450	IPE450	HEB260	HEB340	HEB340	HEB260				0.117	82.854	0.051	
	4	IPE400	IPE400	IPE400	HEB260	HEB340	HEB340	HEB260				0.081	65.892	0.027	

Table C.4: Frames - Porto Configuration 3

ID	Floor	B1	B2	B3	C1	C2	C3	C4	St.	T_1	q	ISD	Mass	θ_{EC8}	Ω
St40	1	IPE600	IPE600	IPE600	HEB500	HEB600	HEB600	HEB500	5	0.89	6.50	0.081	82.854	0.128	12.719
	2	IPE550	IPE550	IPE550	HEB500	HEB600	HEB600	HEB500				0.132	82.854	0.167	
	3	IPE450	IPE450	IPE450	HEB450	HEB500	HEB500	HEB450				0.161	82.854	0.181	
	4	IPE450	IPE450	IPE450	HEB450	HEB500	HEB500	HEB450				0.159	82.854	0.155	
	5	IPE400	IPE400	IPE400	HEB340	HEB400	HEB400	HEB340				0.134	65.892	0.108	
St41	1	IPE500	IPE500	IPE500	HEB400	HEB500	HEB500	HEB400	5	1.11	4.00	0.091	82.854	0.138	9.308
	2	IPE450	IPE450	IPE450	HEB400	HEB500	HEB500	HEB400				0.148	82.854	0.178	
	3	IPE450	IPE450	IPE450	HEB360	HEB400	HEB400	HEB360				0.144	82.854	0.16	
	4	IPE450	IPE450	IPE450	HEB360	HEB400	HEB400	HEB360				0.112	82.854	0.113	
	5	IPE400	IPE400	IPE400	HEB320	HEB360	HEB360	HEB320				0.09	65.892	0.072	
St42	1	IPE450	IPE450	IPE450	HEB300	HEB450	HEB450	HEB300	5	1.24	1.50	0.113	82.854	0.075	3.311
	2	IPE450	IPE450	IPE450	HEB300	HEB450	HEB450	HEB300				0.159	82.854	0.085	
	3	IPE450	IPE450	IPE450	HEB300	HEB400	HEB400	HEB300				0.137	82.854	0.069	
	4	IPE450	IPE450	IPE450	HEB300	HEB400	HEB400	HEB300				0.099	82.854	0.046	
	5	IPE400	IPE400	IPE400	HEB280	HEB360	HEB360	HEB280				0.074	65.892	0.027	
St43	1	HEA600	HEA600	HEA600	HEM500	HEM650	HEM650	HEM500	8	1.11	6.50	0.082	82.854	0.129	9.614
	2	HEA600	HEA600	HEA600	HEM500	HEM650	HEM650	HEM500				0.122	82.854	0.165	
	3	HEA600	HEA600	HEA600	HEM500	HEM650	HEM650	HEM500				0.125	82.854	0.154	
	4	IPE600	IPE600	IPE600	HEM450	HEM600	HEM600	HEM450				0.143	82.854	0.161	
	5	IPE500	IPE500	IPE500	HEM450	HEM600	HEM600	HEM450				0.173	82.854	0.177	
	6	IPE500	IPE500	IPE500	HEM450	HEM600	HEM600	HEM450				0.186	82.854	0.172	
	7	IPE400	IPE400	IPE400	HEB450	HEB600	HEB600	HEB450				0.182	82.854	0.159	
	8	IPE360	IPE360	IPE360	HEB450	HEB600	HEB600	HEB450				0.182	65.892	0.129	

Table C.4: Frames - Porto Configuration 3

ID	Floor	B1	B2	B3	C1	C2	C3	C4	St.	T_1	q	ISD	Mass	θ_{EC8}	Ω
St44	1	IPE600	IPE600	IPE600	HEB400	HEB600	HEB600	HEB400	8	1.43	4.00	0.094	82.854	0.14	6.252
	2	IPE600	IPE600	IPE600	HEB400	HEB600	HEB600	HEB400				0.133	82.854	0.17	
	3	IPE550	IPE550	IPE550	HEB400	HEB600	HEB600	HEB400				0.144	82.854	0.17	
	4	IPE500	IPE500	IPE500	HEB360	HEB550	HEB550	HEB360				0.167	82.854	0.182	
	5	IPE500	IPE500	IPE500	HEB360	HEB550	HEB550	HEB360				0.171	82.854	0.171	
	6	IPE400	IPE400	IPE400	HEB360	HEB550	HEB550	HEB360				0.174	82.854	0.161	
	7	IPE400	IPE400	IPE400	HEB340	HEB500	HEB500	HEB340				0.158	82.854	0.139	
	8	IPE360	IPE360	IPE360	HEB340	HEB500	HEB500	HEB340				0.136	65.892	0.097	
St45	1	IPE450	IPE450	IPE450	HEB400	HEB550	HEB550	HEB400	8	1.84	1.50	0.097	82.854	0.09	3.040
	2	IPE450	IPE450	IPE450	HEB400	HEB550	HEB550	HEB400				0.168	82.854	0.131	
	3	IPE450	IPE450	IPE450	HEB400	HEB550	HEB550	HEB400				0.166	82.854	0.123	
	4	IPE450	IPE450	IPE450	HEB400	HEB500	HEB500	HEB400				0.156	82.854	0.107	
	5	IPE450	IPE450	IPE450	HEB400	HEB500	HEB500	HEB400				0.137	82.854	0.089	
	6	IPE400	IPE400	IPE400	HEB400	HEB500	HEB500	HEB400				0.122	82.854	0.074	
	7	IPE400	IPE400	IPE400	HEB340	HEB450	HEB450	HEB340				0.095	82.854	0.059	
	8	IPE360	IPE360	IPE360	HEB340	HEB450	HEB450	HEB340				0.086	65.892	0.038	

Table C.5: Frames - Porto Configuration 4

ID	Floor	B1	B2	B3	B4	C1	C2	C3	C4	C5	St.	T_1	q	ISD	Mass	θ_{EC8}	Ω
St46	1	IPE330	IPE330	IPE330	IPE330	HEB260	HEB280	HEB280	HEB280	HEB260	2	0.66	6.50	0.12	69.91	0.17	20.503
	2	IPE330	IPE330	IPE330	IPE330	HEB260	HEB280	HEB280	HEB280	HEB260				0.112	55.59	0.109	
St47	1	IPE330	IPE330	IPE330	IPE330	HEB240	HEB260	HEB260	HEB260	HEB240	2	0.71	4.00	0.131	69.91	0.125	13.218
	2	IPE330	IPE330	IPE330	IPE330	HEB240	HEB260	HEB260	HEB260	HEB240				0.109	55.59	0.073	
St48	1	IPE330	IPE330	IPE330	IPE330	HEB240	HEB260	HEB260	HEB260	HEB240	2	0.71	1.50	0.131	69.91	0.047	4.957
	2	IPE330	IPE330	IPE330	IPE330	HEB240	HEB260	HEB260	HEB260	HEB240				0.109	55.59	0.027	
St49	1	IPE360	IPE360	IPE360	IPE360	HEB300	HEB320	HEB320	HEB320	HEB300	3	0.79	6.50	0.13	69.91	0.183	17.023
	2	IPE360	IPE360	IPE360	IPE360	HEB300	HEB320	HEB320	HEB320	HEB300				0.149	69.91	0.164	
	3	IPE300	IPE300	IPE300	IPE300	HEB280	HEB280	HEB280	HEB280	HEB280				0.122	55.59	0.109	
St50	1	IPE330	IPE330	IPE330	IPE330	HEB240	HEB280	HEB280	HEB280	HEB240	3	0.98	4.00	0.142	69.91	0.18	2.844
	2	IPE330	IPE330	IPE330	IPE330	HEB240	HEB280	HEB280	HEB280	HEB240				0.145	69.91	0.148	
	3	IPE300	IPE300	IPE300	IPE300	HEB220	HEB260	HEB260	HEB260	HEB220				0.097	55.59	0.081	
St51	1	IPE330	IPE330	IPE330	IPE330	HEB240	HEB280	HEB280	HEB280	HEB240	3	0.98	1.50	0.19	69.91	0.11	2.687
	2	IPE330	IPE330	IPE330	IPE330	HEB240	HEB280	HEB280	HEB280	HEB240				0.179	69.91	0.084	
	3	IPE300	IPE300	IPE300	IPE300	HEB220	HEB260	HEB260	HEB260	HEB220				0.102	55.59	0.041	
St52	1	IPE400	IPE400	IPE400	IPE400	HEB360	HEB400	HEB400	HEB400	HEB360	4	0.85	6.50	0.111	69.91	0.156	17.492
	2	IPE400	IPE400	IPE400	IPE400	HEB360	HEB400	HEB400	HEB400	HEB360				0.151	69.91	0.17	
	3	IPE360	IPE360	IPE360	IPE360	HEB340	HEB340	HEB340	HEB340	HEB340				0.138	69.91	0.139	
	4	IPE300	IPE300	IPE300	IPE300	HEB340	HEB340	HEB340	HEB340	HEB340				0.121	55.59	0.098	
St53	1	IPE360	IPE360	IPE360	IPE360	HEB280	HEB300	HEB300	HEB300	HEB280	4	1.11	4.00	0.133	69.91	0.179	11.236
	2	IPE360	IPE360	IPE360	IPE360	HEB280	HEB300	HEB300	HEB300	HEB280				0.157	69.91	0.171	
	3	IPE330	IPE330	IPE330	IPE330	HEB260	HEB280	HEB280	HEB280	HEB260				0.131	69.91	0.131	
	4	IPE300	IPE300	IPE300	IPE300	HEB260	HEB280	HEB280	HEB280	HEB260				0.098	55.59	0.079	
St54	1	IPE330	IPE330	IPE330	IPE330	HEB240	HEB280	HEB280	HEB280	HEB240	4	1.30	1.50	0.161	69.91	0.099	3.339
	2	IPE330	IPE330	IPE330	IPE330	HEB240	HEB280	HEB280	HEB280	HEB240				0.177	69.91	0.09	
	3	IPE300	IPE300	IPE300	IPE300	HEB220	HEB260	HEB260	HEB260	HEB220				0.133	69.91	0.063	
	4	IPE300	IPE300	IPE300	IPE300	HEB220	HEB260	HEB260	HEB260	HEB220				0.084	55.59	0.033	

Table C.5: Frames - Porto Configuration 4

ID	Floor	B1	B2	B3	B4	C1	C2	C3	C4	C5	St.	T_1	q	ISD	Mass	θ_{EC8}	Ω
St55	1	IPE450	IPE450	IPE450	IPE450	HEB360	HEB450	HEB450	HEB450	HEB360	5	0.97	6.50	0.107	69.91	0.15	13.728
	2	IPE450	IPE450	IPE450	IPE450	HEB360	HEB450	HEB450	HEB450	HEB360				0.15	69.91	0.173	
	3	IPE360	IPE360	IPE360	IPE360	HEB340	HEB400	HEB400	HEB400	HEB340				0.173	69.91	0.176	
	4	IPE330	IPE330	IPE330	IPE330	HEB340	HEB400	HEB400	HEB400	HEB340				0.177	69.91	0.159	
	5	IPE300	IPE300	IPE300	IPE300	HEB320	HEB360	HEB360	HEB360	HEB320				0.152	55.59	0.115	
St56	1	IPE400	IPE400	IPE400	IPE400	HEB280	HEB340	HEB340	HEB340	HEB280	5	1.24	4.00	0.127	69.91	0.17	9.322
	2	IPE400	IPE400	IPE400	IPE400	HEB280	HEB340	HEB340	HEB340	HEB280				0.155	69.91	0.172	
	3	IPE330	IPE330	IPE330	IPE330	HEB260	HEB320	HEB320	HEB320	HEB260				0.166	69.91	0.167	
	4	IPE300	IPE300	IPE300	IPE300	HEB260	HEB320	HEB320	HEB320	HEB260				0.162	69.91	0.145	
	5	IPE300	IPE300	IPE300	IPE300	HEB240	HEB300	HEB300	HEB300	HEB240				0.121	55.59	0.093	
St57	1	IPE330	IPE330	IPE330	IPE330	HEB240	HEB280	HEB280	HEB280	HEB240	5	1.64	1.50	0.0161	69.91	0.12	3.245
	2	IPE330	IPE330	IPE330	IPE330	HEB240	HEB280	HEB280	HEB280	HEB240				0.195	69.91	0.122	
	3	IPE300	IPE300	IPE300	IPE300	HEB240	HEB260	HEB260	HEB260	HEB240				0.183	69.91	0.105	
	4	IPE300	IPE300	IPE300	IPE300	HEB240	HEB260	HEB260	HEB260	HEB240				0.145	69.91	0.077	
	5	IPE300	IPE300	IPE300	IPE300	HEB220	HEB220	HEB220	HEB220	HEB220				0.095	55.59	0.043	
St58	1	IPE550	IPE550	IPE550	IPE550	HEB400	HEB500	HEB500	HEB500	HEB400	8	1.21	6.50	0.112	69.91	0.156	9.359
	2	IPE550	IPE550	IPE550	IPE550	HEB400	HEB500	HEB500	HEB500	HEB400				0.143	69.91	0.175	
	3	IPE500	IPE500	IPE500	IPE500	HEB400	HEB500	HEB500	HEB500	HEB400				0.151	69.91	0.169	
	4	IPE500	IPE500	IPE500	IPE500	HEB360	HEB450	HEB450	HEB450	HEB360				0.167	69.91	0.17	
	5	IPE450	IPE450	IPE450	IPE450	HEB360	HEB450	HEB450	HEB450	HEB360				0.174	69.91	0.162	
	6	IPE360	IPE360	IPE360	IPE360	HEB360	HEB450	HEB450	HEB450	HEB360				0.203	69.91	0.172	
	7	IPE300	IPE300	IPE300	IPE300	HEB340	HEB400	HEB400	HEB400	HEB340				0.223	69.91	0.176	
	8	IPE300	IPE300	IPE300	IPE300	HEB340	HEB400	HEB400	HEB400	HEB340				0.194	55.59	0.132	

Table C.5: Frames - Porto Configuration 4

ID	Floor	B1	B2	B3	B4	C1	C2	C3	C4	C5	St.	T_1	q	ISD	Mass	θ_{EC8}	Ω
St59	1	IPE500	IPE500	IPE500	IPE500	HEB300	HEB450	HEB450	HEB450	HEB300	8	1.54	4.00	0.109	69.91	0.144	7.268
	2	IPE450	IPE450	IPE450	IPE450	HEB300	HEB450	HEB450	HEB450	HEB300				0.148	69.91	0.173	
	3	IPE450	IPE450	IPE450	IPE450	HEB300	HEB450	HEB450	HEB450	HEB300				0.159	69.91	0.17	
	4	IPE400	IPE400	IPE400	IPE400	HEB280	HEB400	HEB400	HEB400	HEB280				0.182	69.91	0.178	
	5	IPE360	IPE360	IPE360	IPE360	HEB280	HEB400	HEB400	HEB400	HEB280				0.201	69.91	0.18	
	6	IPE330	IPE330	IPE330	IPE330	HEB280	HEB400	HEB400	HEB400	HEB280				0.206	69.91	0.17	
	7	IPE300	IPE300	IPE300	IPE300	HEB260	HEB360	HEB360	HEB360	HEB260				0.186	69.91	0.145	
	8	IPE300	IPE300	IPE300	IPE300	HEB260	HEB360	HEB360	HEB360	HEB260				0.139	55.59	0.095	
St60	1	IPE330	IPE330	IPE330	IPE330	HEB260	HEB300	HEB300	HEB300	HEB260	8	2.57	1.50	0.151	69.91	0.169	2.601
	2	IPE330	IPE330	IPE330	IPE330	HEB260	HEB300	HEB300	HEB300	HEB260				0.21	69.91	0.2	
	3	IPE300	IPE300	IPE300	IPE300	HEB260	HEB300	HEB300	HEB300	HEB260				0.218	69.91	0.2	
	4	IPE300	IPE300	IPE300	IPE300	HEB240	HEB280	HEB280	HEB280	HEB240				0.226	69.91	0.196	
	5	IPE300	IPE300	IPE300	IPE300	HEB240	HEB280	HEB280	HEB280	HEB240				0.195	69.91	0.16	
	6	IPE300	IPE300	IPE300	IPE300	HEB240	HEB280	HEB280	HEB280	HEB240				0.156	69.91	0.121	
	7	IPE300	IPE300	IPE300	IPE300	HEB220	HEB240	HEB240	HEB240	HEB220				0.114	69.91	0.089	
	8	IPE300	IPE300	IPE300	IPE300	HEB220	HEB240	HEB240	HEB240	HEB220				0.071	55.59	0.045	

Table C.6: Frames - Porto Configuration 5

ID	Floor	B1	B2	B3	C1	C2	C3	C4	St.	T_1	q	ISD	Mass	θ_{EC8}	Ω
St61	1	IPE360	IPE300	IPE360	HEB260	HEB300	HEB300	HEB260	2	0.67	6.50	0.116	56.96	0.187	16.605
	2	IPE330	IPE300	IPE330	HEB260	HEB300	HEB300	HEB260				0.134	45.3	0.137	
St62	1	IPE360	IPE300	IPE360	HEB240	HEB260	HEB260	HEB240	2	0.75	4.00	0.134	56.96	0.151	11.256
	2	IPE330	IPE300	IPE330	HEB240	HEB260	HEB260	HEB240				0.131	45.3	0.097	
St63	1	IPE360	IPE300	IPE360	HEB240	HEB260	HEB260	HEB240	2	0.75	1.50	0.134	56.96	0.057	4.220
	2	IPE330	IPE300	IPE330	HEB240	HEB260	HEB260	HEB240				0.131	45.3	0.036	
St64	1	IPE400	IPE360	IPE400	HEB320	HEB360	HEB360	HEB320	3	0.76	6.50	0.114	56.96	0.179	17.628
	2	IPE400	IPE360	IPE400	HEB320	HEB360	HEB360	HEB320				0.144	56.96	0.173	
	3	IPE330	IPE300	IPE330	HEB280	HEB300	HEB300	HEB280				0.126	45.3	0.12	
St65	1	IPE360	IPE300	IPE360	HEB260	HEB300	HEB300	HEB260	3	0.98	4.00	0.132	56.96	0.188	8.693
	2	IPE360	IPE300	IPE360	HEB260	HEB300	HEB300	HEB260				0.158	56.96	0.172	
	3	IPE330	IPE300	IPE330	HEB220	HEB260	HEB260	HEB220				0.123	45.3	0.112	
St66	1	IPE360	IPE300	IPE360	HEB260	HEB280	HEB280	HEB260	3	1.01	1.50	0.142	56.96	0.078	3.358
	2	IPE360	IPE300	IPE360	HEB260	HEB280	HEB280	HEB260				0.161	56.96	0.068	
	3	IPE330	IPE300	IPE330	HEB220	HEB240	HEB240	HEB220				0.118	45.3	0.042	
St67	1	IPE450	IPE450	IPE450	HEB340	HEB450	HEB450	HEB340	4	0.83	6.50	0.101	56.96	0.158	14.667
	2	IPE450	IPE450	IPE450	HEB340	HEB450	HEB450	HEB340				0.141	56.96	0.175	
	3	IPE360	IPE330	IPE360	HEB320	HEB400	HEB400	HEB320				0.143	56.96	0.158	
	4	IPE330	IPE300	IPE330	HEB320	HEB400	HEB400	HEB320				0.141	45.3	0.12	
St68	1	IPE400	IPE360	IPE400	HEB320	HEB340	HEB340	HEB320	4	1.06	4.00	0.109	56.96	0.164	11.832
	2	IPE400	IPE360	IPE400	HEB320	HEB340	HEB340	HEB320				0.152	56.96	0.176	
	3	IPE360	IPE300	IPE360	HEB260	HEB280	HEB280	HEB260				0.142	56.96	0.156	
	4	IPE330	IPE300	IPE330	HEB260	HEB280	HEB280	HEB260				0.115	45.3	0.096	
St69	1	IPE360	IPE300	IPE360	HEB260	HEB280	HEB280	HEB260	4	1.34	1.50	0.156	56.96	0.109	1.000
	2	IPE360	IPE300	IPE360	HEB260	HEB280	HEB280	HEB260				0.195	56.96	0.107	
	3	IPE360	IPE300	IPE360	HEB220	HEB260	HEB260	HEB220				0.149	56.96	0.079	
	4	IPE330	IPE300	IPE330	HEB220	HEB260	HEB260	HEB220				0.098	45.3	0.041	

Table C.6: Frames - Porto Configuration 5

ID	Floor	B1	B2	B3	C1	C2	C3	C4	St.	T_1	q	ISD	Mass	θ_{EC8}	Ω
St70	1	IPE500	IPE500	IPE500	HEB340	HEB450	HEB450	HEB340	5	0.94	6.50	0.111	56.96	0.174	13.790
	2	IPE500	IPE500	IPE500	HEB340	HEB450	HEB450	HEB340				0.144	56.96	0.184	
	3	IPE450	IPE450	IPE450	HEB320	HEB400	HEB400	HEB320				0.148	56.96	0.171	
	4	IPE360	IPE330	IPE360	HEB320	HEB400	HEB400	HEB320				0.154	56.96	0.158	
	5	IPE330	IPE300	IPE330	HEB300	HEB360	HEB360	HEB300				0.149	45.3	0.125	
St71	1	IPE450	IPE400	IPE450	HEB320	HEB400	HEB400	HEB320	5	1.19	4.00	0.104	56.96	0.156	7.695
	2	IPE450	IPE360	IPE450	HEB320	HEB400	HEB400	HEB320				0.151	56.96	0.183	
	3	IPE360	IPE300	IPE360	HEB300	HEB360	HEB360	HEB300				0.168	56.96	0.184	
	4	IPE360	IPE300	IPE360	HEB300	HEB360	HEB360	HEB300				0.157	56.96	0.154	
	5	IPE330	IPE300	IPE330	HEB280	HEB320	HEB320	HEB280				0.122	45.3	0.099	
St72	1	IPE360	IPE300	IPE360	HEB260	HEB280	HEB280	HEB260	5	1.66	1.50	0.168	56.96	0.139	2.680
	2	IPE360	IPE300	IPE360	HEB260	HEB280	HEB280	HEB260				0.216	56.96	0.148	
	3	IPE360	IPE300	IPE360	HEB240	HEB260	HEB260	HEB240				0.185	56.96	0.119	
	4	IPE360	IPE300	IPE360	HEB240	HEB260	HEB260	HEB240				0.132	56.96	0.079	
	5	IPE330	IPE300	IPE330	HEB220	HEB260	HEB260	HEB220				0.088	45.3	0.045	
St73	1	IPE600	IPE600	IPE600	HEB500	HEB600	HEB600	HEB500	8	1.12	6.50	0.085	56.96	0.133	10.223
	2	IPE600	IPE600	IPE600	HEB500	HEB600	HEB600	HEB500				0.123	56.96	0.165	
	3	IPE600	IPE550	IPE600	HEB500	HEB600	HEB600	HEB500				0.126	56.96	0.155	
	4	IPE550	IPE500	IPE550	HEB450	HEB550	HEB550	HEB450				0.143	56.96	0.162	
	5	IPE500	IPE450	IPE500	HEB450	HEB550	HEB550	HEB450				0.165	56.96	0.168	
	6	IPE400	IPE360	IPE400	HEB450	HEB550	HEB550	HEB450				0.192	56.96	0.178	
	7	IPE360	IPE300	IPE360	HEB400	HEB500	HEB500	HEB400				0.202	56.96	0.173	
	8	IPE330	IPE300	IPE330	HEB400	HEB500	HEB500	HEB400				0.19	45.3	0.137	

Table C.6: Frames - Porto Configuration 5

ID	Floor	B1	B2	B3	C1	C2	C3	C4	St.	T_1	q	ISD	Mass	θ_{EC8}	Ω
St74	1	IPE550	IPE500	IPE550	HEB360	HEB500	HEB500	HEB360	8	1.44	4.00	0.095	56.96	0.14	7.079
	2	IPE550	IPE500	IPE550	HEB360	HEB500	HEB500	HEB360				0.129	56.96	0.166	
	3	IPE500	IPE450	IPE500	HEB360	HEB500	HEB500	HEB360				0.138	56.96	0.163	
	4	IPE500	IPE450	IPE500	HEB340	HEB450	HEB450	HEB340				0.153	56.96	0.166	
	5	IPE400	IPE360	IPE400	HEB340	HEB450	HEB450	HEB340				0.174	56.96	0.173	
	6	IPE360	IPE330	IPE360	HEB340	HEB450	HEB450	HEB340				0.194	56.96	0.176	
	7	IPE360	IPE300	IPE360	HEB320	HEB400	HEB400	HEB320				0.171	56.96	0.148	
	8	IPE330	IPE300	IPE330	HEB320	HEB400	HEB400	HEB320				0.138	45.3	0.1	
St75	1	IPE400	IPE330	IPE400	HEB300	HEB360	HEB360	HEB300	8	2.29	1.50	0.116	56.96	0.139	2.738
	2	IPE360	IPE330	IPE360	HEB300	HEB360	HEB360	HEB300				0.187	56.96	0.192	
	3	IPE360	IPE300	IPE360	HEB300	HEB360	HEB360	HEB300				0.196	56.96	0.19	
	4	IPE360	IPE300	IPE360	HEB280	HEB340	HEB340	HEB280				0.188	56.96	0.173	
	5	IPE360	IPE300	IPE360	HEB280	HEB340	HEB340	HEB280				0.161	56.96	0.14	
	6	IPE360	IPE300	IPE360	HEB280	HEB340	HEB340	HEB280				0.128	56.96	0.105	
	7	IPE360	IPE300	IPE360	HEB260	HEB320	HEB320	HEB260				0.087	56.96	0.073	
	8	IPE330	IPE300	IPE330	HEB260	HEB320	HEB320	HEB260				0.066	45.3	0.042	

Table C.7: Frames - Porto Configuration 6

ID	Floor	B1	B2	B3	B4	B5	C1=C6	C2=C5	C3=C4	St.	T_1	q	ISD	Mass	θ_{EC8}	Ω
St76	1	IPE450	IPE450	IPE450	IPE450	IPE450	HEB300	HEB360	HEB340	2	0.64	6.50	0.117	165.708	0.162	18.229
	2	IPE400	IPE400	IPE400	IPE400	IPE400	HEB300	HEB360	HEB340				0.134	131.784	0.108	
St77	1	IPE450	IPE450	IPE450	IPE450	IPE450	HEB300	HEB360	HEB340	2	0.64	4.00	0.116	165.708	0.1	11.331
	2	IPE400	IPE400	IPE400	IPE400	IPE400	HEB300	HEB360	HEB340				0.133	131.784	0.067	
St78	1	IPE450	IPE450	IPE450	IPE450	IPE450	HEB300	HEB360	HEB340	2	0.64	1.50	0.116	165.708	0.037	4.249
	2	IPE400	IPE400	IPE400	IPE400	IPE400	HEB300	HEB360	HEB340				0.133	131.784	0.025	
St79	1	IPE450	IPE450	IPE450	IPE450	IPE450	HEB360	HEB450	HEB400	3	0.81	6.50	0.134	165.708	0.183	12.055
	2	IPE450	IPE450	IPE450	IPE450	IPE450	HEB360	HEB450	HEB400				0.173	165.708	0.175	
	3	IPE400	IPE400	IPE400	IPE400	IPE400	HEB340	HEB400	HEB360				0.139	131.784	0.108	
St80	1	IPE450	IPE450	IPE450	IPE450	IPE450	HEB340	HEB400	HEB360	3	0.86	4.00	0.118	165.708	0.132	9.434
	2	IPE450	IPE450	IPE450	IPE450	IPE450	HEB340	HEB400	HEB360				0.141	165.708	0.117	
	3	IPE400	IPE400	IPE400	IPE400	IPE400	HEB340	HEB400	HEB360				0.111	131.784	0.068	
St81	1	IPE450	IPE450	IPE450	IPE450	IPE450	HEB340	HEB400	HEB360	3	0.86	1.50	0.118	165.708	0.05	3.538
	2	IPE450	IPE450	IPE450	IPE450	IPE450	HEB340	HEB400	HEB360				0.141	165.708	0.044	
	3	IPE400	IPE400	IPE400	IPE400	IPE400	HEB340	HEB400	HEB360				0.111	131.784	0.026	
St82	1	IPE550	IPE550	IPE550	IPE550	IPE550	HEB400	HEB600	HEB500	4	0.84	6.50	0.103	165.708	0.139	14.547
	2	IPE500	IPE500	IPE500	IPE500	IPE500	HEB400	HEB600	HEB500				0.158	165.708	0.165	
	3	IPE450	IPE450	IPE450	IPE450	IPE450	HEB360	HEB550	HEB450				0.155	165.708	0.144	
	4	IPE400	IPE400	IPE400	IPE400	IPE400	HEB360	HEB550	HEB450				0.141	131.784	0.098	
St83	1	IPE450	IPE450	IPE450	IPE450	IPE450	HEB340	HEB400	HEB360	4	1.13	4.00	0.14	165.708	0.182	7.768
	2	IPE450	IPE450	IPE450	IPE450	IPE450	HEB340	HEB400	HEB360				0.184	165.708	0.185	
	3	IPE450	IPE450	IPE450	IPE450	IPE450	HEB320	HEB360	HEB340				0.151	165.708	0.142	
	4	IPE400	IPE400	IPE400	IPE400	IPE400	HEB320	HEB360	HEB340				0.118	131.784	0.082	
St84	1	IPE450	IPE450	IPE450	IPE450	IPE450	HEB320	HEB400	HEB360	4	1.16	1.50	0.128	165.708	0.07	3.256
	2	IPE450	IPE450	IPE450	IPE450	IPE450	HEB320	HEB400	HEB360				0.166	165.708	0.07	
	3	IPE400	IPE400	IPE400	IPE400	IPE400	HEB320	HEB360	HEB340				0.135	165.708	0.053	
	4	IPE400	IPE400	IPE400	IPE400	IPE400	HEB320	HEB360	HEB340				0.107	131.784	0.031	

Table C.7: Frames - Porto Configuration 6

ID	Floor	B1	B2	B3	B4	B5	C1=C6	C2=C5	C3=C4	St.	T_1	q	ISD	Mass	θ_{EC8}	Ω
St85	1	IPE550	IPE550	IPE550	IPE550	IPE550	HEB450	HEB700	HEB650	5	0.93	6.50	0.098	165.708	0.133	13.453
	2	IPE550	IPE550	IPE550	IPE550	IPE550	HEB450	HEB700	HEB650				0.161	165.708	0.172	
	3	IPE500	IPE500	IPE500	IPE500	IPE500	HEB400	HEB650	HEB550				0.169	165.708	0.163	
	4	IPE450	IPE450	IPE450	IPE450	IPE450	HEB400	HEB650	HEB550				0.162	165.708	0.137	
	5	IPE400	IPE400	IPE400	IPE400	IPE400	HEB360	HEB600	HEB500				0.147	131.784	0.099	
St86	1	IPE500	IPE500	IPE500	IPE500	IPE500	HEB400	HEB500	HEB450	5	1.21	4.00	0.11	165.708	0.144	8.557
	2	IPE500	IPE500	IPE500	IPE500	IPE500	HEB400	HEB500	HEB450				0.165	165.708	0.168	
	3	IPE450	IPE450	IPE450	IPE450	IPE450	HEB340	HEB400	HEB360				0.174	165.708	0.165	
	4	IPE400	IPE400	IPE400	IPE400	IPE400	HEB340	HEB400	HEB360				0.158	165.708	0.133	
	5	IPE400	IPE400	IPE400	IPE400	IPE400	HEB340	HEB360	HEB340				0.128	131.784	0.082	
St87	1	IPE450	IPE450	IPE450	IPE450	IPE450	HEB360	HEB400	HEB400	5	1.43	1.50	0.122	165.708	0.08	2.822
	2	IPE450	IPE450	IPE450	IPE450	IPE450	HEB360	HEB400	HEB400				0.178	165.708	0.091	
	3	IPE400	IPE400	IPE400	IPE400	IPE400	HEB340	HEB360	HEB360				0.169	165.708	0.082	
	4	IPE400	IPE400	IPE400	IPE400	IPE400	HEB340	HEB360	HEB360				0.137	165.708	0.06	
	5	IPE400	IPE400	IPE400	IPE400	IPE400	HEB320	HEB360	HEB340				0.101	131.784	0.033	
St88	1	HEA600	HEA600	HEA600	HEA600	HEA600	HEM600	HEM700	HEM700	8	1.20	6.50	0.09	165.708	0.12	8.763
	2	HEA550	HEA550	HEA550	HEA550	HEA550	HEM600	HEM700	HEM700				0.151	165.708	0.173	
	3	HEA550	HEA550	HEA550	HEA550	HEA550	HEM600	HEM700	HEM700				0.163	165.708	0.17	
	4	HEA550	HEA550	HEA550	HEA550	HEA550	HEM550	HEM600	HEM600				0.173	165.708	0.164	
	5	IPE500	IPE500	IPE500	IPE500	IPE500	HEM550	HEM600	HEM600				0.203	165.708	0.176	
	6	IPE450	IPE450	IPE450	IPE450	IPE450	HEM550	HEM600	HEM600				0.228	165.708	0.18	
	7	IPE450	IPE450	IPE450	IPE450	IPE450	HEB550	HEB600	HEB600				0.209	165.708	0.152	
	8	IPE400	IPE400	IPE400	IPE400	IPE400	HEB550	HEB600	HEB600				0.183	131.784	0.11	

Table C.7: Frames - Porto Configuration 6

ID	Floor	B1	B2	B3	B4	B5	C1=C6	C2=C5	C3=C4	St.	T_1	q	ISD	Mass	θ_{EC8}	Ω
St89	1	IPE600	IPE600	IPE600	IPE600	IPE600	HEB500	HEB600	HEB600	8	1.52	4.00	0.098	165.708	0.127	6.132
	2	IPE600	IPE600	IPE600	IPE600	IPE600	HEB500	HEB600	HEB600				0.15	165.708	0.163	
	3	IPE550	IPE550	IPE550	IPE550	IPE550	HEB500	HEB600	HEB600				0.165	165.708	0.165	
	4	IPE500	IPE500	IPE500	IPE500	IPE500	HEB450	HEB550	HEB550				0.194	165.708	0.179	
	5	IPE450	IPE450	IPE450	IPE450	IPE450	HEB450	HEB550	HEB550				0.211	165.708	0.179	
	6	IPE450	IPE450	IPE450	IPE450	IPE450	HEB450	HEB550	HEB550				0.2	165.708	0.156	
	7	IPE400	IPE400	IPE400	IPE400	IPE400	HEB400	HEB500	HEB500				0.167	165.708	0.125	
	8	IPE400	IPE400	IPE400	IPE400	IPE400	HEB400	HEB500	HEB500				0.14	131.784	0.081	
St90	1	IPE450	IPE450	IPE450	IPE450	IPE450	HEB400	HEB550	HEB550	8	2.03	1.50	0.097	165.708	0.09	2.754
	2	IPE450	IPE450	IPE450	IPE450	IPE450	HEB400	HEB550	HEB550				0.172	165.708	0.131	
	3	IPE450	IPE450	IPE450	IPE450	IPE450	HEB400	HEB550	HEB550				0.173	165.708	0.123	
	4	IPE450	IPE450	IPE450	IPE450	IPE450	HEB360	HEB500	HEB500				0.165	165.708	0.112	
	5	IPE400	IPE400	IPE400	IPE400	IPE400	HEB360	HEB500	HEB500				0.157	165.708	0.099	
	6	IPE400	IPE400	IPE400	IPE400	IPE400	HEB360	HEB500	HEB500				0.14	165.708	0.084	
	7	IPE400	IPE400	IPE400	IPE400	IPE400	HEB340	HEB450	HEB450				0.103	165.708	0.06	
	8	IPE400	IPE400	IPE400	IPE400	IPE400	HEB340	HEB450	HEB450				0.085	131.784	0.034	

Table C.8: Frames - Lisbon Configuration 1

ID	Floor	B1	B2	B3	C1	C2	C3	C4	St.	T_1	q	ISD	Mass	θ_{EC8}	Ω
St91	1	IPE300	IPE300	IPE300	HEB240	HEB300	HEB300	HEB240	2	0.65	6.50	0.283	46.61	0.189	4.441
	2	IPE300	IPE300	IPE300	HEB240	HEB300	HEB300	HEB240				0.287	37.06	0.157	
St92	1	IPE300	IPE300	IPE300	HEB200	HEB240	HEB240	HEB200	2	0.80	4.00	0.38	46.61	0.193	2.793
	2	IPE300	IPE300	IPE300	HEB200	HEB240	HEB240	HEB200				0.285	37.06	0.119	
St93	1	IPE300	IPE300	IPE300	HEB200	HEB240	HEB240	HEB200	2	0.80	1.50	0.38	46.61	0.068	1.000
	2	IPE300	IPE300	IPE300	HEB200	HEB240	HEB240	HEB200				0.285	37.06	0.04	
St94	1	IPE330	IPE330	IPE330	HEB320	HEB360	HEB360	HEB320	3	0.76	6.50	0.236	46.61	0.183	5.089
	2	IPE330	IPE330	IPE330	HEB320	HEB360	HEB360	HEB320				0.315	46.61	0.197	
	3	IPE300	IPE300	IPE300	HEB300	HEB340	HEB340	HEB300				0.247	37.06	0.134	
St95	1	IPE300	IPE300	IPE300	HEB240	HEB300	HEB300	HEB240	3	0.96	4.00	0.325	46.61	0.193	2.201
	2	IPE300	IPE300	IPE300	HEB240	HEB300	HEB300	HEB240				0.385	46.61	0.186	
	3	IPE300	IPE300	IPE300	HEB220	HEB280	HEB280	HEB220				0.257	37.06	0.108	
St96	1	IPE300	IPE300	IPE300	HEB200	HEB240	HEB240	HEB200	3	1.16	1.83	0.441	46.61	0.139	1.000
	2	IPE300	IPE300	IPE300	HEB200	HEB240	HEB240	HEB200				0.41	46.61	0.107	
	3	IPE300	IPE300	IPE300	HEB200	HEB220	HEB220	HEB200				0.244	37.06	0.057	
St97	1	IPE400	IPE400	IPE400	HEB360	HEB400	HEB400	HEB360	4	0.83	6.50	0.202	46.61	0.168	5.001
	2	IPE400	IPE400	IPE400	HEB360	HEB400	HEB400	HEB360				0.281	46.61	0.196	
	3	IPE300	IPE300	IPE300	HEB320	HEB360	HEB360	HEB320				0.306	46.61	0.174	
	4	IPE300	IPE300	IPE300	HEB320	HEB360	HEB360	HEB320				0.273	37.06	0.142	
St98	1	IPE330	IPE330	IPE330	HEB300	HEB360	HEB360	HEB300	4	1.05	4.00	0.256	46.61	0.167	2.845
	2	IPE330	IPE330	IPE330	HEB300	HEB360	HEB360	HEB300				0.367	46.61	0.199	
	3	IPE300	IPE300	IPE300	HEB280	HEB320	HEB320	HEB280				0.334	46.61	0.154	
	4	IPE300	IPE300	IPE300	HEB280	HEB320	HEB320	HEB280				0.24	37.06	0.101	
St99	1	IPE300	IPE300	IPE300	HEB220	HEB280	HEB280	HEB220	4	1.37	2.41	0.451	46.61	0.191	1.000
	2	IPE300	IPE300	IPE300	HEB220	HEB280	HEB280	HEB220				0.543	46.61	0.193	
	3	IPE300	IPE300	IPE300	HEB200	HEB240	HEB240	HEB200				0.459	46.61	0.144	
	4	IPE300	IPE300	IPE300	HEB200	HEB240	HEB240	HEB200				0.252	37.06	0.073	

Table C.8: Frames - Lisbon Configuration 1

ID	Floor	B1	B2	B3	C1	C2	C3	C4	St.	T_1	q	ISD	Mass	θ_{EC8}	Ω
St100	1	IPE450	IPE450	IPE450	HEB360	HEB450	HEB450	HEB360	5	0.93	6.50	0.197	46.61	0.166	4.812
	2	IPE450	IPE450	IPE450	HEB360	HEB450	HEB450	HEB360				0.273	46.61	0.198	
	3	IPE360	IPE360	IPE360	HEB340	HEB400	HEB400	HEB340				0.326	46.61	0.197	
	4	IPE300	IPE300	IPE300	HEB340	HEB400	HEB400	HEB340				0.361	46.61	0.188	
	5	IPE300	IPE300	IPE300	HEB320	HEB360	HEB360	HEB320				0.31	37.06	0.151	
St101	1	IPE400	IPE400	IPE400	HEB320	HEB360	HEB360	HEB320	5	1.16	4.00	0.222	46.61	0.161	3.108
	2	IPE360	IPE360	IPE360	HEB320	HEB360	HEB360	HEB320				0.32	46.61	0.197	
	3	IPE330	IPE330	IPE330	HEB320	HEB340	HEB340	HEB320				0.344	46.61	0.183	
	4	IPE300	IPE300	IPE300	HEB320	HEB340	HEB340	HEB320				0.314	46.61	0.148	
	5	IPE300	IPE300	IPE300	HEB300	HEB320	HEB320	HEB300				0.235	37.06	0.103	
St102	1	IPE330	IPE330	IPE330	HEB260	HEB320	HEB320	HEB260	5	1.49	2.34	0.357	46.61	0.159	1.000
	2	IPE300	IPE300	IPE300	HEB260	HEB320	HEB320	HEB260				0.521	46.61	0.198	
	3	IPE300	IPE300	IPE300	HEB240	HEB300	HEB300	HEB240				0.515	46.61	0.172	
	4	IPE300	IPE300	IPE300	HEB240	HEB300	HEB300	HEB240				0.388	46.61	0.118	
	5	IPE300	IPE300	IPE300	HEB220	HEB280	HEB280	HEB220				0.237	37.06	0.068	
St103	1	IPE550	IPE550	IPE550	HEB450	HEB550	HEB550	HEB450	8	1.11	6.50	0.176	46.61	0.151	5.000
	2	IPE550	IPE550	IPE550	HEB450	HEB550	HEB550	HEB450				0.241	46.61	0.189	
	3	IPE500	IPE500	IPE500	HEB450	HEB550	HEB550	HEB450				0.262	46.61	0.182	
	4	IPE500	IPE500	IPE500	HEB400	HEB500	HEB500	HEB400				0.291	46.61	0.179	
	5	IPE450	IPE450	IPE450	HEB400	HEB500	HEB500	HEB400				0.309	46.61	0.172	
	6	IPE360	IPE360	IPE360	HEB400	HEB500	HEB500	HEB400				0.359	46.61	0.181	
	7	IPE300	IPE300	IPE300	HEB360	HEB450	HEB450	HEB360				0.396	46.61	0.178	
	8	IPE300	IPE300	IPE300	HEB360	HEB450	HEB450	HEB360				0.348	37.06	0.155	

Table C.8: Frames - Lisbon Configuration 1

ID	Floor	B1	B2	B3	C1	C2	C3	C4	St.	T_1	q	ISD	Mass	θ_{EC8}	Ω
St104	1	IPE500	IPE500	IPE500	HEB400	HEB450	HEB450	HEB400	8	1.42	4.00	0.181	46.61	0.138	3.056
	2	IPE450	IPE450	IPE450	HEB400	HEB450	HEB450	HEB400				0.271	46.61	0.186	
	3	IPE400	IPE400	IPE400	HEB400	HEB450	HEB450	HEB400				0.324	46.61	0.199	
	4	IPE400	IPE400	IPE400	HEB360	HEB400	HEB400	HEB360				0.359	46.61	0.198	
	5	IPE400	IPE400	IPE400	HEB360	HEB400	HEB400	HEB360				0.336	46.61	0.17	
	6	IPE330	IPE330	IPE330	HEB360	HEB400	HEB400	HEB360				0.327	46.61	0.154	
	7	IPE330	IPE330	IPE330	HEB340	HEB360	HEB360	HEB340				0.295	46.61	0.129	
	8	IPE300	IPE300	IPE300	HEB340	HEB360	HEB360	HEB340				0.22	37.06	0.094	
St105	1	IPE360	IPE360	IPE360	HEB300	HEB360	HEB360	HEB300	8	2.04	1.97	0.288	46.61	0.153	1.000
	2	IPE360	IPE360	IPE360	HEB300	HEB360	HEB360	HEB300				0.42	46.61	0.199	
	3	IPE330	IPE330	IPE330	HEB300	HEB360	HEB360	HEB300				0.454	46.61	0.195	
	4	IPE330	IPE330	IPE330	HEB280	HEB340	HEB340	HEB280				0.479	46.61	0.189	
	5	IPE300	IPE300	IPE300	HEB280	HEB340	HEB340	HEB280				0.464	46.61	0.169	
	6	IPE300	IPE300	IPE300	HEB280	HEB340	HEB340	HEB280				0.413	46.61	0.141	
	7	IPE300	IPE300	IPE300	HEB260	HEB320	HEB320	HEB260				0.306	46.61	0.1	
	8	IPE300	IPE300	IPE300	HEB260	HEB320	HEB320	HEB260				0.19	37.06	0.06	

Table C.9: Frames - Lisbon Configuration 2

ID	Floor	B1	B2	B3	C1	C2	C3	C4	St.	T_1	q	ISD	Mass	θ_{EC8}	Ω
St106	1	IPE300	IPE360	IPE300	HEB240	HEB300	HEB300	HEB240	2	0.68	6.50	0.293	51.784	0.2	4.175
	2	IPE270	IPE330	IPE270	HEB240	HEB300	HEB300	HEB240				0.314	41.182	0.176	
St107	1	IPE300	IPE360	IPE300	HEB220	HEB260	HEB260	HEB220	2	0.77	4.00	0.349	51.784	0.164	2.554
	2	IPE270	IPE330	IPE270	HEB220	HEB260	HEB260	HEB220				0.311	41.182	0.117	
St108	1	IPE300	IPE360	IPE300	HEB220	HEB260	HEB260	HEB220	2	0.77	1.57	0.349	51.784	0.063	1.310
	2	IPE270	IPE330	IPE270	HEB220	HEB260	HEB260	HEB220				0.311	41.182	0.043	
St109	1	IPE360	IPE400	IPE360	HEB300	HEB360	HEB360	HEB300	3	0.77	6.50	0.241	51.784	0.188	5.659
	2	IPE330	IPE400	IPE300	HEB300	HEB360	HEB360	HEB300				0.307	51.784	0.194	
	3	IPE270	IPE330	IPE270	HEB300	HEB360	HEB360	HEB300				0.264	41.182	0.146	
St110	1	IPE330	IPE360	IPE330	HEB240	HEB300	HEB300	HEB240	3	0.95	4.00	0.323	51.784	0.189	2.680
	2	IPE300	IPE360	IPE300	HEB240	HEB300	HEB300	HEB240				0.367	51.784	0.175	
	3	IPE270	IPE330	IPE270	HEB240	HEB300	HEB300	HEB240				0.27	41.182	0.112	
St111	1	IPE330	IPE360	IPE330	HEB220	HEB280	HEB280	HEB220	3	1.01	1.58	0.363	51.784	0.082	1.000
	2	IPE300	IPE360	IPE300	HEB220	HEB280	HEB280	HEB220				0.375	51.784	0.069	
	3	IPE270	IPE330	IPE270	HEB220	HEB280	HEB280	HEB220				0.26	41.182	0.041	
St112	1	IPE400	IPE450	IPE400	HEB360	HEB450	HEB450	HEB360	4	0.83	6.50	0.197	51.784	0.163	5.354
	2	IPE400	IPE450	IPE400	HEB360	HEB450	HEB450	HEB360				0.284	51.784	0.199	
	3	IPE330	IPE360	IPE330	HEB320	HEB400	HEB400	HEB320				0.296	51.784	0.168	
	4	IPE270	IPE330	IPE270	HEB320	HEB400	HEB400	HEB320				0.281	41.182	0.148	
St113	1	IPE360	IPE400	IPE360	HEB240	HEB340	HEB340	HEB240	4	1.07	4.00	0.296	51.784	0.199	3.200
	2	IPE360	IPE400	IPE360	HEB240	HEB340	HEB340	HEB240				0.35	51.784	0.198	
	3	IPE330	IPE360	IPE330	HEB220	HEB320	HEB320	HEB220				0.303	51.784	0.148	
	4	IPE270	IPE330	IPE270	HEB220	HEB320	HEB320	HEB220				0.231	41.182	0.104	
St114	1	IPE330	IPE360	IPE330	HEB220	HEB300	HEB300	HEB220	4	1.30	2.11	0.417	51.784	0.145	1.000
	2	IPE300	IPE360	IPE300	HEB220	HEB300	HEB300	HEB220				0.51	51.784	0.148	
	3	IPE300	IPE360	IPE300	HEB200	HEB260	HEB260	HEB200				0.434	51.784	0.111	
	4	IPE270	IPE330	IPE270	HEB200	HEB260	HEB260	HEB200				0.273	41.182	0.063	

Table C.9: Frames - Lisbon Configuration 2

ID	Floor	B1	B2	B3	C1	C2	C3	C4	St.	T_1	q	ISD	Mass	θ_{EC8}	Ω
St115	1	IPE450	IPE500	IPE450	HEB360	HEB500	HEB500	HEB360	5	0.91	6.50	0.192	51.784	0.161	5.490
	2	IPE450	IPE500	IPE450	HEB360	HEB500	HEB500	HEB360				0.274	51.784	0.2	
	3	IPE400	IPE450	IPE400	HEB340	HEB450	HEB450	HEB340				0.294	51.784	0.179	
	4	IPE330	IPE360	IPE330	HEB340	HEB450	HEB450	HEB340				0.307	51.784	0.162	
	5	IPE270	IPE330	IPE270	HEB320	HEB400	HEB400	HEB320				0.297	41.182	0.149	
St116	1	IPE400	IPE450	IPE400	HEB280	HEB360	HEB360	HEB280	5	1.20	4.00	0.294	51.784	0.188	2.372
	2	IPE400	IPE450	IPE400	HEB280	HEB360	HEB360	HEB280				0.362	51.784	0.198	
	3	IPE330	IPE360	IPE330	HEB260	HEB340	HEB340	HEB260				0.397	51.784	0.187	
	4	IPE300	IPE360	IPE300	HEB260	HEB340	HEB340	HEB260				0.387	51.784	0.162	
	5	IPE270	IPE330	IPE270	HEB220	HEB300	HEB300	HEB220				0.301	41.182	0.116	
St117	1	IPE330	IPE360	IPE330	HEB220	HEB320	HEB320	HEB220	5	1.53	2.10	0.411	51.784	0.169	1.000
	2	IPE330	IPE360	IPE330	HEB220	HEB320	HEB320	HEB220				0.521	51.784	0.184	
	3	IPE330	IPE360	IPE330	HEB200	HEB280	HEB280	HEB200				0.494	51.784	0.155	
	4	IPE300	IPE360	IPE300	HEB200	HEB280	HEB280	HEB200				0.371	51.784	0.107	
	5	IPE270	IPE330	IPE270	HEB200	HEB260	HEB260	HEB200				0.248	41.182	0.066	
St118	1	IPE550	IPE600	IPE550	HEB500	HEB600	HEB600	HEB500	8	1.12	6.50	0.169	51.784	0.144	5.180
	2	IPE550	IPE600	IPE550	HEB500	HEB600	HEB600	HEB500				0.25	51.784	0.196	
	3	IPE500	IPE550	IPE500	HEB500	HEB600	HEB600	HEB500				0.276	51.784	0.19	
	4	IPE500	IPE550	IPE500	HEB450	HEB550	HEB550	HEB450				0.304	51.784	0.186	
	5	IPE450	IPE500	IPE450	HEB450	HEB550	HEB550	HEB450				0.323	51.784	0.18	
	6	IPE360	IPE400	IPE360	HEB450	HEB550	HEB550	HEB450				0.37	51.784	0.186	
	7	IPE330	IPE360	IPE330	HEB400	HEB450	HEB450	HEB400				0.395	51.784	0.177	
	8	IPE270	IPE330	IPE270	HEB400	HEB450	HEB450	HEB400				0.363	41.182	0.164	

Table C.9: Frames - Lisbon Configuration 2

ID	Floor	B1	B2	B3	C1	C2	C3	C4	St.	T_1	q	ISD	Mass	θ_{EC8}	Ω
St119	1	IPE500	IPE500	IPE500	HEB360	HEB450	HEB450	HEB360	8	1.43	4.00	0.213	51.784	0.164	2.514
	2	IPE500	IPE500	IPE500	HEB360	HEB450	HEB450	HEB360				0.278	51.784	0.193	
	3	IPE450	IPE500	IPE450	HEB360	HEB450	HEB450	HEB360				0.289	51.784	0.18	
	4	IPE450	IPE500	IPE450	HEB340	HEB400	HEB400	HEB340				0.31	51.784	0.174	
	5	IPE400	IPE450	IPE400	HEB340	HEB400	HEB400	HEB340				0.318	51.784	0.163	
	6	IPE330	IPE360	IPE330	HEB340	HEB400	HEB400	HEB340				0.354	51.784	0.167	
	7	IPE300	IPE360	IPE300	HEB320	HEB360	HEB360	HEB320				0.348	51.784	0.151	
	8	IPE270	IPE330	IPE270	HEB320	HEB360	HEB360	HEB320				0.282	41.182	0.118	
St120	1	IPE360	IPE400	IPE360	HEB320	HEB360	HEB360	HEB320	8	2.03	1.89	0.305	51.784	0.152	1.000
	2	IPE360	IPE400	IPE360	HEB320	HEB360	HEB360	HEB320				0.445	51.784	0.199	
	3	IPE360	IPE400	IPE360	HEB320	HEB360	HEB360	HEB320				0.443	51.784	0.18	
	4	IPE330	IPE360	IPE330	HEB300	HEB340	HEB340	HEB300				0.459	51.784	0.171	
	5	IPE330	IPE360	IPE330	HEB300	HEB340	HEB340	HEB300				0.44	51.784	0.152	
	6	IPE300	IPE360	IPE300	HEB300	HEB340	HEB340	HEB300				0.381	51.784	0.124	
	7	IPE300	IPE360	IPE300	HEB280	HEB320	HEB320	HEB280				0.295	51.784	0.092	
	8	IPE270	IPE330	IPE270	HEB280	HEB320	HEB320	HEB280				0.205	41.182	0.061	

Table C.10: Frames - Lisbon Configuration 3

ID	Floor	B1	B2	B3	C1	C2	C3	C4	St.	T_1	q	ISD	Mass	θ_{EC8}	Ω
St121	1	IPE450	IPE450	IPE450	HEB260	HEB400	HEB400	HEB260	2	0.57	6.50	0.248	82.854	0.146	5.890
	2	IPE400	IPE400	IPE400	HEB260	HEB400	HEB400	HEB260				0.245	65.892	0.126	
St122	1	IPE450	IPE450	IPE450	HEB260	HEB400	HEB400	HEB260	2	0.57	4.00	0.248	82.854	0.089	3.620
	2	IPE400	IPE400	IPE400	HEB260	HEB400	HEB400	HEB260				0.245	65.892	0.071	
St123	1	IPE450	IPE450	IPE450	HEB260	HEB400	HEB400	HEB260	2	0.57	1.50	0.248	82.854	0.033	1.000
	2	IPE400	IPE400	IPE400	HEB260	HEB400	HEB400	HEB260				0.245	65.892	0.023	
St124	1	IPE450	IPE450	IPE450	HEB300	HEB450	HEB450	HEB300	3	0.75	6.50	0.252	82.854	0.192	4.680
	2	IPE450	IPE450	IPE450	HEB300	HEB450	HEB450	HEB300				0.299	82.854	0.191	
	3	IPE400	IPE400	IPE400	HEB300	HEB450	HEB450	HEB300				0.218	65.892	0.127	
St125	1	IPE450	IPE450	IPE450	HEB260	HEB400	HEB400	HEB260	3	0.81	4.00	0.292	82.854	0.147	2.881
	2	IPE450	IPE450	IPE450	HEB260	HEB400	HEB400	HEB260				0.309	82.854	0.129	
	3	IPE400	IPE400	IPE400	HEB260	HEB400	HEB400	HEB260				0.208	65.892	0.078	
St126	1	IPE450	IPE450	IPE450	HEB260	HEB400	HEB400	HEB260	3	0.81	1.50	0.292	82.854	0.053	1.000
	2	IPE450	IPE450	IPE450	HEB260	HEB400	HEB400	HEB260				0.309	82.854	0.045	
	3	IPE400	IPE400	IPE400	HEB260	HEB400	HEB400	HEB260				0.208	65.892	0.025	
St127	1	IPE500	IPE500	IPE500	HEB450	HEB550	HEB550	HEB450	4	0.83	6.50	0.189	82.854	0.154	6.000
	2	IPE450	IPE450	IPE450	HEB450	HEB550	HEB550	HEB450				0.282	82.854	0.199	
	3	IPE450	IPE450	IPE450	HEB400	HEB450	HEB450	HEB400				0.268	82.854	0.153	
	4	IPE400	IPE400	IPE400	HEB400	HEB450	HEB450	HEB400				0.221	65.892	0.125	
St128	1	IPE450	IPE450	IPE450	HEB300	HEB400	HEB400	HEB300	4	1.04	4.00	0.29	82.854	0.19	2.690
	2	IPE450	IPE450	IPE450	HEB300	HEB400	HEB400	HEB300				0.358	82.854	0.2	
	3	IPE450	IPE450	IPE450	HEB260	HEB340	HEB340	HEB260				0.298	82.854	0.143	
	4	IPE400	IPE400	IPE400	HEB260	HEB340	HEB340	HEB260				0.188	65.892	0.086	
St129	1	IPE450	IPE450	IPE450	HEB280	HEB400	HEB400	HEB280	4	1.06	1.59	0.301	82.854	0.074	1.000
	2	IPE450	IPE450	IPE450	HEB280	HEB400	HEB400	HEB280				0.36	82.854	0.073	
	3	IPE450	IPE450	IPE450	HEB260	HEB340	HEB340	HEB260				0.294	82.854	0.054	
	4	IPE400	IPE400	IPE400	HEB260	HEB340	HEB340	HEB260				0.184	65.892	0.029	

Table C.10: Frames - Lisbon Configuration 3

ID	Floor	B1	B2	B3	C1	C2	C3	C4	St.	T_1	q	ISD	Mass	θ_{EC8}	Ω
St130	1	IPE600	IPE600	IPE600	HEB500	HEB600	HEB600	HEB500	5	0.89	6.50	0.166	82.854	0.137	4.920
	2	IPE550	IPE550	IPE550	HEB500	HEB600	HEB600	HEB500				0.266	82.854	0.193	
	3	IPE450	IPE450	IPE450	HEB450	HEB500	HEB500	HEB450				0.332	82.854	0.197	
	4	IPE450	IPE450	IPE450	HEB450	HEB500	HEB500	HEB450				0.325	82.854	0.171	
	5	IPE400	IPE400	IPE400	HEB340	HEB400	HEB400	HEB340				0.262	65.892	0.133	
St131	1	IPE500	IPE500	IPE500	HEB400	HEB500	HEB500	HEB400	5	1.11	4.00	0.213	82.854	0.147	2.730
	2	IPE450	IPE450	IPE450	HEB400	HEB500	HEB500	HEB400				0.334	82.854	0.199	
	3	IPE450	IPE450	IPE450	HEB360	HEB400	HEB400	HEB360				0.335	82.854	0.172	
	4	IPE450	IPE450	IPE450	HEB360	HEB400	HEB400	HEB360				0.26	82.854	0.121	
	5	IPE400	IPE400	IPE400	HEB320	HEB360	HEB360	HEB320				0.192	65.892	0.086	
St132	1	IPE450	IPE450	IPE450	HEB320	HEB450	HEB450	HEB320	5	1.23	1.83	0.316	82.854	0.091	1.000
	2	IPE450	IPE450	IPE450	HEB320	HEB450	HEB450	HEB320				0.437	82.854	0.107	
	3	IPE450	IPE450	IPE450	HEB300	HEB400	HEB400	HEB300				0.396	82.854	0.087	
	4	IPE450	IPE450	IPE450	HEB300	HEB400	HEB400	HEB300				0.289	82.854	0.058	
	5	IPE400	IPE400	IPE400	HEB280	HEB360	HEB360	HEB280				0.194	65.892	0.036	
St133	1	HEA600	HEA600	HEA600	HEM500	HEM650	HEM650	HEM500	8	1.11	6.50	0.169	82.854	0.143	4.520
	2	HEA600	HEA600	HEA600	HEM500	HEM650	HEM650	HEM500				0.247	82.854	0.194	
	3	HEA600	HEA600	HEA600	HEM500	HEM650	HEM650	HEM500				0.254	82.854	0.175	
	4	IPE600	IPE600	IPE600	HEM450	HEM600	HEM600	HEM450				0.293	82.854	0.18	
	5	IPE500	IPE500	IPE500	HEM450	HEM600	HEM600	HEM450				0.356	82.854	0.196	
	6	IPE500	IPE500	IPE500	HEM450	HEM600	HEM600	HEM450				0.382	82.854	0.191	
	7	IPE400	IPE400	IPE400	HEB450	HEB600	HEB600	HEB450				0.379	82.854	0.169	
	8	IPE360	IPE360	IPE360	HEB450	HEB600	HEB600	HEB450				0.355	65.892	0.167	

Table C.10: Frames - Lisbon Configuration 3

ID	Floor	B1	B2	B3	C1	C2	C3	C4	St.	T_1	q	ISD	Mass	θ_{EC8}	Ω
St134	1	IPE600	IPE600	IPE600	HEB400	HEB600	HEB600	HEB400	8	1.43	4.00	0.195	82.854	0.152	2.054
	2	IPE600	IPE600	IPE600	HEB400	HEB600	HEB600	HEB400				0.272	82.854	0.191	
	3	IPE550	IPE550	IPE550	HEB400	HEB600	HEB600	HEB400				0.297	82.854	0.186	
	4	IPE500	IPE500	IPE500	HEB360	HEB550	HEB550	HEB360				0.349	82.854	0.197	
	5	IPE500	IPE500	IPE500	HEB360	HEB550	HEB550	HEB360				0.359	82.854	0.185	
	6	IPE400	IPE400	IPE400	HEB360	HEB550	HEB550	HEB360				0.366	82.854	0.173	
	7	IPE400	IPE400	IPE400	HEB340	HEB500	HEB500	HEB340				0.337	82.854	0.147	
	8	IPE360	IPE360	IPE360	HEB340	HEB500	HEB500	HEB340				0.267	65.892	0.115	
St135	1	IPE450	IPE450	IPE450	HEB450	HEB550	HEB550	HEB450	8	1.82	2.00	0.256	82.854	0.119	1.000
	2	IPE450	IPE450	IPE450	HEB450	HEB550	HEB550	HEB450				0.436	82.854	0.181	
	3	IPE450	IPE450	IPE450	HEB450	HEB550	HEB550	HEB450				0.45	82.854	0.17	
	4	IPE450	IPE450	IPE450	HEB400	HEB500	HEB500	HEB400				0.432	82.854	0.15	
	5	IPE450	IPE450	IPE450	HEB400	HEB500	HEB500	HEB400				0.382	82.854	0.124	
	6	IPE400	IPE400	IPE400	HEB400	HEB500	HEB500	HEB400				0.34	82.854	0.103	
	7	IPE400	IPE400	IPE400	HEB340	HEB450	HEB450	HEB340				0.277	82.854	0.081	
	8	IPE360	IPE360	IPE360	HEB340	HEB450	HEB450	HEB340				0.21	65.892	0.057	

Table C.11: Frames - Lisbon Configuration 4

ID	Floor	B1	B2	B3	B4	C1	C2	C3	C4	C5	St.	T_1	q	ISD	Mass	θ_{EC8}	Ω
St136	1	IPE330	IPE330	IPE330	IPE330	HEB260	HEB280	HEB280	HEB280	HEB260	2	0.66	6.50	0.303	69.91	0.178	5.733
	2	IPE330	IPE330	IPE330	IPE330	HEB260	HEB280	HEB280	HEB280	HEB260				0.261	55.59	0.13	
St137	1	IPE330	IPE330	IPE330	IPE330	HEB240	HEB260	HEB260	HEB260	HEB240	2	0.71	4.00	0.335	69.91	0.13	3.612
	2	IPE330	IPE330	IPE330	IPE330	HEB240	HEB260	HEB260	HEB260	HEB240				0.26	55.59	0.082	
St138	1	IPE330	IPE330	IPE330	IPE330	HEB240	HEB260	HEB260	HEB260	HEB240	2	0.71	1.50	0.335	69.91	0.047	1.350
	2	IPE330	IPE330	IPE330	IPE330	HEB240	HEB260	HEB260	HEB260	HEB240				0.26	55.59	0.027	
St139	1	IPE360	IPE360	IPE360	IPE360	HEB300	HEB320	HEB320	HEB320	HEB300	3	0.79	6.50	0.27	69.91	0.196	5.789
	2	IPE360	IPE360	IPE360	IPE360	HEB300	HEB320	HEB320	HEB320	HEB300				0.305	69.91	0.182	
	3	IPE300	IPE300	IPE300	IPE300	HEB280	HEB280	HEB280	HEB280	HEB280				0.244	55.59	0.128	
St140	1	IPE330	IPE330	IPE330	IPE330	HEB240	HEB280	HEB280	HEB280	HEB240	3	0.98	4.00	0.354	69.91	0.191	2.844
	2	IPE330	IPE330	IPE330	IPE330	HEB240	HEB280	HEB280	HEB280	HEB240				0.361	69.91	0.161	
	3	IPE300	IPE300	IPE300	IPE300	HEB220	HEB260	HEB260	HEB260	HEB220				0.243	55.59	0.095	
St141	1	IPE330	IPE330	IPE330	IPE330	HEB240	HEB280	HEB280	HEB280	HEB240	3	0.98	1.50	0.354	69.91	0.067	1.000
	2	IPE330	IPE330	IPE330	IPE330	HEB240	HEB280	HEB280	HEB280	HEB240				0.361	69.91	0.056	
	3	IPE300	IPE300	IPE300	IPE300	HEB220	HEB260	HEB260	HEB260	HEB220				0.243	55.59	0.032	
St142	1	IPE400	IPE400	IPE400	IPE400	HEB360	HEB400	HEB400	HEB400	HEB360	4	0.85	6.50	0.229	69.91	0.167	6.420
	2	IPE400	IPE400	IPE400	IPE400	HEB360	HEB400	HEB400	HEB400	HEB360				0.306	69.91	0.191	
	3	IPE360	IPE360	IPE360	IPE360	HEB340	HEB340	HEB340	HEB340	HEB340				0.287	69.91	0.149	
	4	IPE300	IPE300	IPE300	IPE300	HEB340	HEB340	HEB340	HEB340	HEB340				0.238	55.59	0.118	
St143	1	IPE360	IPE360	IPE360	IPE360	HEB280	HEB300	HEB300	HEB300	HEB280	4	1.11	4.00	0.312	69.91	0.191	3.290
	2	IPE360	IPE360	IPE360	IPE360	HEB280	HEB300	HEB300	HEB300	HEB280				0.36	69.91	0.187	
	3	IPE330	IPE330	IPE330	IPE330	HEB260	HEB280	HEB280	HEB280	HEB260				0.309	69.91	0.139	
	4	IPE300	IPE300	IPE300	IPE300	HEB260	HEB280	HEB280	HEB280	HEB260				0.216	55.59	0.091	
St144	1	IPE330	IPE330	IPE330	IPE330	HEB240	HEB280	HEB280	HEB280	HEB240	4	1.30	1.81	0.437	69.91	0.117	1.000
	2	IPE330	IPE330	IPE330	IPE330	HEB240	HEB280	HEB280	HEB280	HEB240				0.495	69.91	0.111	
	3	IPE300	IPE300	IPE300	IPE300	HEB220	HEB260	HEB260	HEB260	HEB220				0.426	69.91	0.083	
	4	IPE300	IPE300	IPE300	IPE300	HEB220	HEB260	HEB260	HEB260	HEB220				0.268	55.59	0.048	

Table C.11: Frames - Lisbon Configuration 4

ID	Floor	B1	B2	B3	B4	C1	C2	C3	C4	C5	St.	T_1	q	ISD	Mass	θ_{EC8}	Ω
St145	1	IPE450	IPE450	IPE450	IPE450	HEB360	HEB450	HEB450	HEB450	HEB360	5	0.97	6.50	0.219	69.91	0.164	5.770
	2	IPE450	IPE450	IPE450	IPE450	HEB360	HEB450	HEB450	HEB450	HEB360				0.304	69.91	0.196	
	3	IPE360	IPE360	IPE360	IPE360	HEB340	HEB400	HEB400	HEB400	HEB340				0.356	69.91	0.192	
	4	IPE330	IPE330	IPE330	IPE330	HEB340	HEB400	HEB400	HEB400	HEB340				0.366	69.91	0.172	
	5	IPE300	IPE300	IPE300	IPE300	HEB320	HEB360	HEB360	HEB360	HEB320				0.304	55.59	0.137	
St146	1	IPE400	IPE400	IPE400	IPE400	HEB280	HEB340	HEB340	HEB340	HEB280	5	1.24	4.00	0.311	69.91	0.182	2.610
	2	IPE400	IPE400	IPE400	IPE400	HEB280	HEB340	HEB340	HEB340	HEB280				0.372	69.91	0.188	
	3	IPE330	IPE330	IPE330	IPE330	HEB260	HEB320	HEB320	HEB320	HEB260				0.408	69.91	0.177	
	4	IPE300	IPE300	IPE300	IPE300	HEB260	HEB320	HEB320	HEB320	HEB260				0.399	69.91	0.154	
	5	IPE300	IPE300	IPE300	IPE300	HEB240	HEB300	HEB300	HEB300	HEB240				0.285	55.59	0.103	
St147	1	IPE330	IPE330	IPE330	IPE330	HEB260	HEB320	HEB320	HEB320	HEB260	5	1.52	2.00	0.379	69.91	0.13	1.000
	2	IPE330	IPE330	IPE330	IPE330	HEB260	HEB320	HEB320	HEB320	HEB260				0.511	69.91	0.15	
	3	IPE300	IPE300	IPE300	IPE300	HEB240	HEB300	HEB300	HEB300	HEB240				0.504	69.91	0.13	
	4	IPE300	IPE300	IPE300	IPE300	HEB240	HEB280	HEB280	HEB280	HEB240				0.41	69.91	0.096	
	5	IPE300	IPE300	IPE300	IPE300	HEB220	HEB280	HEB280	HEB280	HEB220				0.255	55.59	0.056	
St148	1	IPE550	IPE550	IPE550	IPE550	HEB400	HEB500	HEB500	HEB500	HEB400	8	1.21	6.50	0.231	69.91	0.173	4.236
	2	IPE550	IPE550	IPE550	IPE550	HEB400	HEB500	HEB500	HEB500	HEB400				0.291	69.91	0.2	
	3	IPE500	IPE500	IPE500	IPE500	HEB400	HEB500	HEB500	HEB500	HEB400				0.31	69.91	0.189	
	4	IPE500	IPE500	IPE500	IPE500	HEB360	HEB450	HEB450	HEB450	HEB360				0.344	69.91	0.187	
	5	IPE450	IPE450	IPE450	IPE450	HEB360	HEB450	HEB450	HEB450	HEB360				0.359	69.91	0.178	
	6	IPE360	IPE360	IPE360	IPE360	HEB360	HEB450	HEB450	HEB450	HEB360				0.419	69.91	0.187	
	7	IPE300	IPE300	IPE300	IPE300	HEB340	HEB400	HEB400	HEB400	HEB340				0.464	69.91	0.187	
	8	IPE300	IPE300	IPE300	IPE300	HEB340	HEB400	HEB400	HEB400	HEB340				0.391	55.59	0.157	

Table C.11: Frames - Lisbon Configuration 4

ID	Floor	B1	B2	B3	B4	C1	C2	C3	C4	C5	St.	T_1	q	ISD	Mass	θ_{EC8}	Ω
St149	1	IPE500	IPE500	IPE500	IPE500	HEB300	HEB450	HEB450	HEB450	HEB300	8	1.54	4.00	0.218	69.91	0.158	2.559
	2	IPE450	IPE450	IPE450	IPE450	HEB300	HEB450	HEB450	HEB450	HEB300				0.295	69.91	0.191	
	3	IPE450	IPE450	IPE450	IPE450	HEB300	HEB450	HEB450	HEB450	HEB300				0.32	69.91	0.186	
	4	IPE400	IPE400	IPE400	IPE400	HEB280	HEB400	HEB400	HEB400	HEB280				0.368	69.91	0.192	
	5	IPE360	IPE360	IPE360	IPE360	HEB280	HEB400	HEB400	HEB400	HEB280				0.408	69.91	0.194	
	6	IPE330	IPE330	IPE330	IPE330	HEB280	HEB400	HEB400	HEB400	HEB280				0.417	69.91	0.182	
	7	IPE300	IPE300	IPE300	IPE300	HEB260	HEB360	HEB360	HEB360	HEB260				0.38	69.91	0.153	
	8	IPE300	IPE300	IPE300	IPE300	HEB260	HEB360	HEB360	HEB360	HEB260				0.274	55.59	0.107	
St150	1	IPE360	IPE360	IPE360	IPE360	HEB300	HEB360	HEB360	HEB360	HEB300	8	2.11	2.03	0.299	69.91	0.157	1.000
	2	IPE360	IPE360	IPE360	IPE360	HEB300	HEB360	HEB360	HEB360	HEB300				0.427	69.91	0.2	
	3	IPE360	IPE360	IPE360	IPE360	HEB300	HEB360	HEB360	HEB360	HEB300				0.426	69.91	0.181	
	4	IPE330	IPE330	IPE330	IPE330	HEB280	HEB340	HEB340	HEB340	HEB280				0.451	69.91	0.176	
	5	IPE300	IPE300	IPE300	IPE300	HEB280	HEB340	HEB340	HEB340	HEB280				0.47	69.91	0.169	
	6	IPE300	IPE300	IPE300	IPE300	HEB280	HEB340	HEB340	HEB340	HEB280				0.426	69.91	0.143	
	7	IPE300	IPE300	IPE300	IPE300	HEB260	HEB320	HEB320	HEB320	HEB260				0.316	69.91	0.101	
	8	IPE300	IPE300	IPE300	IPE300	HEB260	HEB320	HEB320	HEB320	HEB260				0.198	55.59	0.06	

Table C.12: Frames - Lisbon Configuration 5

ID	Floor	B1	B2	B3	C1	C2	C3	C4	St.	T_1	q	ISD	Mass	θ_{EC8}	Ω
St151	1	IPE360	IPE300	IPE360	HEB260	HEB300	HEB300	HEB260	2	0.67	6.50	0.292	56.96	0.195	4.696
	2	IPE330	IPE300	IPE330	HEB260	HEB300	HEB300	HEB260				0.303	45.3	0.171	
St152	1	IPE360	IPE300	IPE360	HEB240	HEB260	HEB260	HEB240	2	0.75	4.00	0.343	56.96	0.05	3.000
	2	IPE330	IPE300	IPE330	HEB240	HEB260	HEB260	HEB240				0.302	45.3	0.033	
St153	1	IPE360	IPE300	IPE360	HEB240	HEB260	HEB260	HEB240	2	0.75	1.50	0.343	56.96	0.057	1.153
	2	IPE330	IPE300	IPE330	HEB240	HEB260	HEB260	HEB240				0.302	45.3	0.036	
St154	1	IPE400	IPE360	IPE400	HEB320	HEB360	HEB360	HEB320	3	0.76	6.50	0.246	56.96	0.192	5.740
	2	IPE400	IPE360	IPE400	HEB320	HEB360	HEB360	HEB320				0.304	56.96	0.196	
	3	IPE330	IPE300	IPE330	HEB280	HEB300	HEB300	HEB280				0.258	45.3	0.145	
St155	1	IPE360	IPE300	IPE360	HEB260	HEB300	HEB300	HEB260	3	0.98	4.00	0.332	56.96	0.188	2.373
	2	IPE360	IPE300	IPE360	HEB260	HEB300	HEB300	HEB260				0.383	56.96	0.171	
	3	IPE330	IPE300	IPE330	HEB220	HEB260	HEB260	HEB220				0.279	45.3	0.107	
St156	1	IPE360	IPE300	IPE360	HEB260	HEB280	HEB280	HEB260	3	1.01	1.65	0.353	56.96	0.085	1.000
	2	IPE360	IPE300	IPE360	HEB260	HEB280	HEB280	HEB260				0.389	56.96	0.075	
	3	IPE330	IPE300	IPE330	HEB220	HEB240	HEB240	HEB220				0.281	45.3	0.046	
St157	1	IPE450	IPE450	IPE450	HEB340	HEB450	HEB450	HEB340	4	0.83	6.50	0.207	56.96	0.171	5.260
	2	IPE450	IPE450	IPE450	HEB340	HEB450	HEB450	HEB340				0.284	56.96	0.2	
	3	IPE360	IPE330	IPE360	HEB320	HEB400	HEB400	HEB320				0.296	56.96	0.168	
	4	IPE330	IPE300	IPE330	HEB320	HEB400	HEB400	HEB320				0.274	45.3	0.148	
St158	1	IPE400	IPE360	IPE400	HEB320	HEB340	HEB340	HEB320	4	1.06	4.00	0.265	56.96	0.175	3.320
	2	IPE400	IPE360	IPE400	HEB320	HEB340	HEB340	HEB320				0.355	56.96	0.197	
	3	IPE360	IPE300	IPE360	HEB260	HEB280	HEB280	HEB260				0.352	56.96	0.164	
	4	IPE330	IPE300	IPE330	HEB260	HEB280	HEB280	HEB260				0.259	45.3	0.112	
St159	1	IPE360	IPE300	IPE360	HEB260	HEB280	HEB280	HEB260	4	1.34	2.14	0.442	56.96	0.161	1.000
	2	IPE360	IPE300	IPE360	HEB260	HEB280	HEB280	HEB260				0.532	56.96	0.163	
	3	IPE360	IPE300	IPE360	HEB220	HEB260	HEB260	HEB220				0.432	56.96	0.117	
	4	IPE330	IPE300	IPE330	HEB220	HEB260	HEB260	HEB220				0.257	45.3	0.064	

Table C.12: Frames - Lisbon Configuration 5

ID	Floor	B1	B2	B3	C1	C2	C3	C4	St.	T_1	q	ISD	Mass	θ_{EC8}	Ω
St160	1	IPE500	IPE500	IPE500	HEB340	HEB450	HEB450	HEB340	5	0.94	6.50	0.228	56.96	0.174	5.626
	2	IPE500	IPE500	IPE500	HEB340	HEB450	HEB450	HEB340				0.289	56.96	0.184	
	3	IPE450	IPE450	IPE450	HEB320	HEB400	HEB400	HEB320				0.304	56.96	0.171	
	4	IPE360	IPE330	IPE360	HEB320	HEB400	HEB400	HEB320				0.318	56.96	0.158	
	5	IPE330	IPE300	IPE330	HEB300	HEB360	HEB360	HEB300				0.294	45.3	0.125	
St161	1	IPE450	IPE400	IPE450	HEB320	HEB400	HEB400	HEB320	5	1.18	4.00	0.265	56.96	0.156	2.061
	2	IPE450	IPE400	IPE450	HEB320	HEB400	HEB400	HEB320				0.372	56.96	0.183	
	3	IPE360	IPE300	IPE360	HEB300	HEB360	HEB360	HEB300				0.426	56.96	0.184	
	4	IPE360	IPE300	IPE360	HEB300	HEB360	HEB360	HEB300				0.4	56.96	0.154	
	5	IPE330	IPE300	IPE330	HEB280	HEB320	HEB320	HEB280				0.293	45.3	0.099	
St162	1	IPE360	IPE330	IPE360	HEB260	HEB300	HEB300	HEB260	5	1.57	2.21	0.426	56.96	0.179	1.000
	2	IPE360	IPE330	IPE360	HEB260	HEB300	HEB300	HEB260				0.544	56.96	0.194	
	3	IPE360	IPE300	IPE360	HEB240	HEB280	HEB280	HEB240				0.498	56.96	0.161	
	4	IPE360	IPE300	IPE360	HEB240	HEB280	HEB280	HEB240				0.369	56.96	0.11	
	5	IPE330	IPE300	IPE330	HEB220	HEB260	HEB260	HEB220				0.233	45.3	0.063	
St163	1	IPE600	IPE600	IPE600	HEB500	HEB600	HEB600	HEB500	8	1.12	6.50	0.174	56.96	0.149	4.811
	2	IPE600	IPE600	IPE600	HEB500	HEB600	HEB600	HEB500				0.247	56.96	0.195	
	3	IPE600	IPE550	IPE600	HEB500	HEB600	HEB600	HEB500				0.257	56.96	0.177	
	4	IPE550	IPE500	IPE550	HEB450	HEB550	HEB550	HEB450				0.295	56.96	0.18	
	5	IPE500	IPE450	IPE500	HEB450	HEB550	HEB550	HEB450				0.339	56.96	0.187	
	6	IPE400	IPE360	IPE400	HEB450	HEB550	HEB550	HEB450				0.396	56.96	0.197	
	7	IPE360	IPE300	IPE360	HEB400	HEB500	HEB500	HEB400				0.42	56.96	0.186	
	8	IPE330	IPE300	IPE330	HEB400	HEB500	HEB500	HEB400				0.378	45.3	0.169	

Table C.12: Frames - Lisbon Configuration 5

ID	Floor	B1	B2	B3	C1	C2	C3	C4	St.	T_1	q	ISD	Mass	θ_{EC8}	Ω
St164	1	IPE550	IPE500	IPE550	HEB360	HEB500	HEB500	HEB360	8	1.44	4.00	0.197	56.96	0.153	2.320
	2	IPE550	IPE500	IPE550	HEB360	HEB500	HEB500	HEB360				0.264	56.96	0.185	
	3	IPE500	IPE450	IPE500	HEB360	HEB500	HEB500	HEB360				0.286	56.96	0.179	
	4	IPE500	IPE450	IPE500	HEB340	HEB450	HEB450	HEB340				0.32	56.96	0.18	
	5	IPE400	IPE360	IPE400	HEB340	HEB450	HEB450	HEB340				0.365	56.96	0.186	
	6	IPE360	IPE330	IPE360	HEB340	HEB450	HEB450	HEB340				0.408	56.96	0.189	
	7	IPE360	IPE300	IPE360	HEB320	HEB400	HEB400	HEB320				0.365	56.96	0.156	
	8	IPE330	IPE300	IPE330	HEB320	HEB400	HEB400	HEB320				0.277	45.3	0.115	
St165	1	IPE450	IPE400	IPE450	HEB320	HEB400	HEB400	HEB320	8	1.99	2.10	0.271	56.96	0.146	1.000
	2	IPE400	IPE400	IPE400	HEB320	HEB400	HEB400	HEB320				0.408	56.96	0.197	
	3	IPE400	IPE360	IPE400	HEB320	HEB400	HEB400	HEB320				0.45	56.96	0.196	
	4	IPE360	IPE330	IPE360	HEB300	HEB360	HEB360	HEB300				0.499	56.96	0.198	
	5	IPE360	IPE330	IPE360	HEB300	HEB360	HEB360	HEB300				0.485	56.96	0.178	
	6	IPE360	IPE300	IPE360	HEB300	HEB360	HEB360	HEB300				0.415	56.96	0.143	
	7	IPE360	IPE300	IPE360	HEB260	HEB320	HEB320	HEB260				0.316	56.96	0.104	
	8	IPE330	IPE300	IPE330	HEB260	HEB320	HEB320	HEB260				0.204	45.3	0.064	

Table C.13: Frames - Lisbon Configuration 6

ID	Floor	B1	B2	B3	B4	B5	C1=C6	C2=C5	C3=C4	St.	T_1	q	ISD	Mass	θ_{EC8}	Ω
St166	1	IPE450	IPE450	IPE450	IPE450	IPE450	HEB300	HEB360	HEB340	2	0.64	6.50	0.307	165.708	0.163	5.031
	2	IPE400	IPE400	IPE400	IPE400	IPE400	HEB300	HEB360	HEB340				0.297	131.784	0.144	
St167	1	IPE450	IPE450	IPE450	IPE450	IPE450	HEB300	HEB360	HEB340	2	0.64	4.00	0.307	165.708	0.1	3.096
	2	IPE400	IPE400	IPE400	IPE400	IPE400	HEB300	HEB360	HEB340				0.297	131.784	0.08	
St168	1	IPE450	IPE450	IPE450	IPE450	IPE450	HEB300	HEB360	HEB340	2	0.64	1.50	0.307	165.708	0.037	1.161
	2	IPE400	IPE400	IPE400	IPE400	IPE400	HEB300	HEB360	HEB340				0.297	131.784	0.025	
St169	1	IPE450	IPE450	IPE450	IPE450	IPE450	HEB360	HEB450	HEB400	3	0.81	6.50	0.282	165.708	0.188	4.212
	2	IPE450	IPE450	IPE450	IPE450	IPE450	HEB360	HEB450	HEB400				0.348	165.708	0.198	
	3	IPE400	IPE400	IPE400	IPE400	IPE400	HEB340	HEB400	HEB360				0.266	131.784	0.14	
St170	1	IPE450	IPE450	IPE450	IPE450	IPE450	HEB340	HEB400	HEB360	3	0.86	4.00	0.306	165.708	0.135	2.580
	2	IPE450	IPE450	IPE450	IPE450	IPE450	HEB340	HEB400	HEB360				0.346	165.708	0.127	
	3	IPE400	IPE400	IPE400	IPE400	IPE400	HEB340	HEB400	HEB360				0.248	131.784	0.082	
St171	1	IPE450	IPE450	IPE450	IPE450	IPE450	HEB340	HEB400	HEB360	3	0.86	1.60	0.306	165.708	0.053	1.000
	2	IPE450	IPE450	IPE450	IPE450	IPE450	HEB340	HEB400	HEB360				0.346	165.708	0.048	
	3	IPE400	IPE400	IPE400	IPE400	IPE400	HEB340	HEB400	HEB360				0.248	131.784	0.029	
St172	1	IPE550	IPE550	IPE550	IPE550	IPE550	HEB400	HEB600	HEB500	4	0.84	6.50	0.215	165.708	0.144	5.320
	2	IPE500	IPE500	IPE500	IPE500	IPE500	HEB400	HEB600	HEB500				0.32	165.708	0.186	
	3	IPE450	IPE450	IPE450	IPE450	IPE450	HEB360	HEB550	HEB450				0.321	165.708	0.153	
	4	IPE400	IPE400	IPE400	IPE400	IPE400	HEB360	HEB550	HEB450				0.269	131.784	0.128	
St173	1	IPE450	IPE450	IPE450	IPE450	IPE450	HEB360	HEB400	HEB360	4	1.12	4.00	0.317	165.708	0.185	2.380
	2	IPE450	IPE450	IPE450	IPE450	IPE450	HEB360	HEB400	HEB360				0.399	165.708	0.2	
	3	IPE450	IPE450	IPE450	IPE450	IPE450	HEB340	HEB360	HEB340				0.31	165.708	0.134	
	4	IPE400	IPE400	IPE400	IPE400	IPE400	HEB340	HEB360	HEB340				0.211	131.784	0.089	
St174	1	IPE450	IPE450	IPE450	IPE450	IPE450	HEB340	HEB400	HEB360	4	1.15	1.71	0.318	165.708	0.079	1.000
	2	IPE450	IPE450	IPE450	IPE450	IPE450	HEB340	HEB400	HEB360				0.401	165.708	0.082	
	3	IPE400	IPE400	IPE400	IPE400	IPE400	HEB320	HEB360	HEB340				0.342	165.708	0.062	
	4	IPE400	IPE400	IPE400	IPE400	IPE400	HEB320	HEB360	HEB340				0.239	131.784	0.038	

Table C.13: Frames - Lisbon Configuration 6

ID	Floor	B1	B2	B3	B4	B5	C1=C6	C2=C5	C3=C4	St.	T_1	q	ISD	Mass	θ_{EC8}	Ω
St175	1	IPE550	IPE550	IPE550	IPE550	IPE550	HEB450	HEB700	HEB650	5	0.93	6.50	0.206	165.708	0.139	5.529
	2	IPE550	IPE550	IPE550	IPE550	IPE550	HEB450	HEB700	HEB650				0.326	165.708	0.198	
	3	IPE500	IPE500	IPE500	IPE500	IPE500	HEB400	HEB650	HEB550				0.349	165.708	0.175	
	4	IPE450	IPE450	IPE450	IPE450	IPE450	HEB400	HEB650	HEB550				0.333	165.708	0.149	
	5	IPE400	IPE400	IPE400	IPE400	IPE400	HEB360	HEB600	HEB500				0.284	131.784	0.129	
St176	1	IPE500	IPE500	IPE500	IPE500	IPE500	HEB400	HEB500	HEB450	5	1.21	4.00	0.28	165.708	0.15	2.360
	2	IPE500	IPE500	IPE500	IPE500	IPE500	HEB400	HEB500	HEB450				0.398	165.708	0.185	
	3	IPE450	IPE450	IPE450	IPE450	IPE450	HEB340	HEB400	HEB360				0.437	165.708	0.173	
	4	IPE400	IPE400	IPE400	IPE400	IPE400	HEB340	HEB400	HEB360				0.396	165.708	0.14	
	5	IPE400	IPE400	IPE400	IPE400	IPE400	HEB340	HEB360	HEB340				0.287	131.784	0.097	
St177	1	IPE450	IPE450	IPE450	IPE450	IPE450	HEB360	HEB400	HEB400	5	1.43	2.22	0.357	165.708	0.122	1.000
	2	IPE450	IPE450	IPE450	IPE450	IPE450	HEB360	HEB400	HEB400				0.491	165.708	0.143	
	3	IPE400	IPE400	IPE400	IPE400	IPE400	HEB340	HEB360	HEB360				0.487	165.708	0.125	
	4	IPE400	IPE400	IPE400	IPE400	IPE400	HEB340	HEB360	HEB360				0.397	165.708	0.092	
	5	IPE400	IPE400	IPE400	IPE400	IPE400	HEB320	HEB360	HEB340				0.252	131.784	0.055	
St178	1	HEA600	HEA600	HEA600	HEA600	HEA600	HEM600	HEM700	HEM700	8	1.20	6.50	0.187	165.708	0.129	3.978
	2	HEA550	HEA550	HEA550	HEA550	HEA550	HEM600	HEM700	HEM700				0.308	165.708	0.197	
	3	HEA550	HEA550	HEA550	HEA550	HEA550	HEM600	HEM700	HEM700				0.334	165.708	0.189	
	4	HEA550	HEA550	HEA550	HEA550	HEA550	HEM550	HEM600	HEM600				0.357	165.708	0.179	
	5	IPE500	IPE500	IPE500	IPE500	IPE500	HEM550	HEM600	HEM600				0.421	165.708	0.19	
	6	IPE450	IPE450	IPE450	IPE450	IPE450	HEM550	HEM600	HEM600				0.473	165.708	0.194	
	7	IPE450	IPE450	IPE450	IPE450	IPE450	HEB550	HEB600	HEB600				0.433	165.708	0.164	
	8	IPE400	IPE400	IPE400	IPE400	IPE400	HEB550	HEB600	HEB600				0.356	131.784	0.144	

Table C.13: Frames - Lisbon Configuration 6

ID	Floor	B1	B2	B3	B4	B5	C1=C6	C2=C5	C3=C4	St.	T_1	q	ISD	Mass	θ_{EC8}	Ω
St179	1	IPE600	IPE600	IPE600	IPE600	IPE600	HEB500	HEB600	HEB600	8	1.52	4.00	0.201	165.708	0.135	2.156
	2	IPE600	IPE600	IPE600	IPE600	IPE600	HEB500	HEB600	HEB600				0.298	165.708	0.181	
	3	IPE550	IPE550	IPE550	IPE550	IPE550	HEB500	HEB600	HEB600				0.331	165.708	0.18	
	4	IPE500	IPE500	IPE500	IPE500	IPE500	HEB450	HEB550	HEB550				0.393	165.708	0.191	
	5	IPE450	IPE450	IPE450	IPE450	IPE450	HEB450	HEB550	HEB550				0.43	165.708	0.19	
	6	IPE450	IPE450	IPE450	IPE450	IPE450	HEB450	HEB550	HEB550				0.408	165.708	0.167	
	7	IPE400	IPE400	IPE400	IPE400	IPE400	HEB400	HEB500	HEB500				0.343	165.708	0.131	
	8	IPE400	IPE400	IPE400	IPE400	IPE400	HEB400	HEB500	HEB500				0.261	131.784	0.1	
St180	1	IPE500	IPE500	IPE500	IPE500	IPE500	HEB400	HEB550	HEB550	8	1.98	2.36	0.251	165.708	0.132	1.000
	2	IPE450	IPE450	IPE450	IPE450	IPE450	HEB400	HEB550	HEB550				0.432	165.708	0.2	
	3	IPE450	IPE450	IPE450	IPE450	IPE450	HEB400	HEB550	HEB550				0.478	165.708	0.2	
	4	IPE450	IPE450	IPE450	IPE450	IPE450	HEB360	HEB500	HEB500				0.477	165.708	0.184	
	5	IPE400	IPE400	IPE400	IPE400	IPE400	HEB360	HEB500	HEB500				0.462	165.708	0.165	
	6	IPE400	IPE400	IPE400	IPE400	IPE400	HEB360	HEB500	HEB500				0.414	165.708	0.138	
	7	IPE400	IPE400	IPE400	IPE400	IPE400	HEB340	HEB450	HEB450				0.31	165.708	0.099	
	8	IPE400	IPE400	IPE400	IPE400	IPE400	HEB340	HEB450	HEB450				0.208	131.784	0.064	

Table C.14: Frames - Lagos Configuration 1

ID	Floor	B1	B2	B3	C1	C2	C3	C4	St.	T_1	q	ISD	Mass	θ_{EC8}	Ω
St181	1	IPE300	IPE300	IPE300	HEB240	HEB300	HEB300	HEB240	2	0.65	6.50	0.426	46.61	0.189	2.929
	2	IPE300	IPE300	IPE300	HEB240	HEB300	HEB300	HEB240				0.424	37.06	0.157	
St182	1	IPE300	IPE300	IPE300	HEB200	HEB240	HEB240	HEB200	2	0.80	4.00	0.569	46.61	0.193	1.842
	2	IPE300	IPE300	IPE300	HEB200	HEB240	HEB240	HEB200				0.422	37.06	0.119	
St183	1	IPE300	IPE300	IPE300	HEB200	HEB240	HEB240	HEB200	2	0.80	2.17	0.569	46.61	0.099	1.000
	2	IPE300	IPE300	IPE300	HEB200	HEB240	HEB240	HEB200				0.422	37.06	0.058	
St184	1	IPE330	IPE330	IPE330	HEB320	HEB360	HEB360	HEB320	3	0.76	6.50	0.355	46.61	0.183	3.356
	2	IPE330	IPE330	IPE330	HEB320	HEB360	HEB360	HEB320				0.471	46.61	0.197	
	3	IPE300	IPE300	IPE300	HEB300	HEB340	HEB340	HEB300				0.367	37.06	0.134	
St185	1	IPE300	IPE300	IPE300	HEB240	HEB300	HEB300	HEB240	3	0.96	4.00	0.485	46.61	0.193	1.452
	2	IPE300	IPE300	IPE300	HEB240	HEB300	HEB300	HEB240				0.573	46.61	0.186	
	3	IPE300	IPE300	IPE300	HEB220	HEB280	HEB280	HEB220				0.381	37.06	0.108	
St186	1	IPE300	IPE300	IPE300	HEB200	HEB260	HEB260	HEB200	3	1.10	2.84	0.607	46.61	0.183	1.000
	2	IPE300	IPE300	IPE300	HEB200	HEB260	HEB260	HEB200				0.599	46.61	0.148	
	3	IPE300	IPE300	IPE300	HEB200	HEB240	HEB240	HEB200				0.359	37.06	0.078	
St187	1	IPE400	IPE400	IPE400	HEB360	HEB400	HEB400	HEB360	4	0.83	6.50	0.289	46.61	0.168	3.299
	2	IPE400	IPE400	IPE400	HEB360	HEB400	HEB400	HEB360				0.402	46.61	0.196	
	3	IPE300	IPE300	IPE300	HEB320	HEB360	HEB360	HEB320				0.439	46.61	0.174	
	4	IPE300	IPE300	IPE300	HEB320	HEB360	HEB360	HEB320				0.388	37.06	0.142	
St188	1	IPE330	IPE330	IPE330	HEB300	HEB360	HEB360	HEB300	4	1.05	4.00	0.382	46.61	0.167	1.876
	2	IPE330	IPE330	IPE330	HEB300	HEB360	HEB360	HEB300				0.546	46.61	0.199	
	3	IPE300	IPE300	IPE300	HEB280	HEB320	HEB320	HEB280				0.501	46.61	0.154	
	4	IPE300	IPE300	IPE300	HEB280	HEB320	HEB320	HEB280				0.354	37.06	0.101	
St189	1	IPE330	IPE330	IPE330	HEB240	HEB300	HEB300	HEB240	4	1.23	3.15	0.56	46.61	0.179	1.000
	2	IPE300	IPE300	IPE300	HEB240	HEB300	HEB300	HEB240				0.733	46.61	0.193	
	3	IPE300	IPE300	IPE300	HEB220	HEB260	HEB260	HEB220				0.681	46.61	0.158	
	4	IPE300	IPE300	IPE300	HEB220	HEB260	HEB260	HEB220				0.396	37.06	0.082	

Table C.14: Frames - Lagos Configuration 1

ID	Floor	B1	B2	B3	C1	C2	C3	C4	St.	T_1	q	ISD	Mass	θ_{EC8}	Ω
St190	1	IPE450	IPE450	IPE450	HEB360	HEB450	HEB450	HEB360	5	0.93	6.50	0.251	46.61	0.166	3.174
	2	IPE450	IPE450	IPE450	HEB360	HEB450	HEB450	HEB360				0.347	46.61	0.198	
	3	IPE360	IPE360	IPE360	HEB340	HEB400	HEB400	HEB340				0.416	46.61	0.197	
	4	IPE300	IPE300	IPE300	HEB340	HEB400	HEB400	HEB340				0.461	46.61	0.188	
	5	IPE300	IPE300	IPE300	HEB320	HEB360	HEB360	HEB320				0.393	37.06	0.151	
St191	1	IPE400	IPE400	IPE400	HEB320	HEB360	HEB360	HEB320	5	1.16	4.00	0.331	46.61	0.161	3.050
	2	IPE360	IPE360	IPE360	HEB320	HEB360	HEB360	HEB320				0.475	46.61	0.197	
	3	IPE330	IPE330	IPE330	HEB320	HEB340	HEB340	HEB320				0.514	46.61	0.183	
	4	IPE300	IPE300	IPE300	HEB320	HEB340	HEB340	HEB320				0.469	46.61	0.148	
	5	IPE300	IPE300	IPE300	HEB300	HEB320	HEB320	HEB300				0.348	37.06	0.103	
St192	1	IPE330	IPE330	IPE330	HEB280	HEB340	HEB340	HEB280	5	1.38	2.88	0.494	46.61	0.162	1.000
	2	IPE330	IPE330	IPE330	HEB280	HEB340	HEB340	HEB280				0.699	46.61	0.193	
	3	IPE300	IPE300	IPE300	HEB260	HEB320	HEB320	HEB260				0.698	46.61	0.171	
	4	IPE300	IPE300	IPE300	HEB260	HEB320	HEB320	HEB260				0.574	46.61	0.127	
	5	IPE300	IPE300	IPE300	HEB240	HEB300	HEB300	HEB240				0.364	37.06	0.074	
St193	1	IPE550	IPE550	IPE550	HEB450	HEB550	HEB550	HEB450	8	1.11	6.50	0.187	46.61	0.151	3.400
	2	IPE550	IPE550	IPE550	HEB450	HEB550	HEB550	HEB450				0.258	46.61	0.189	
	3	IPE500	IPE500	IPE500	HEB450	HEB550	HEB550	HEB450				0.28	46.61	0.182	
	4	IPE500	IPE500	IPE500	HEB400	HEB500	HEB500	HEB400				0.31	46.61	0.179	
	5	IPE450	IPE450	IPE450	HEB400	HEB500	HEB500	HEB400				0.329	46.61	0.172	
	6	IPE360	IPE360	IPE360	HEB400	HEB500	HEB500	HEB400				0.383	46.61	0.181	
	7	IPE300	IPE300	IPE300	HEB360	HEB450	HEB450	HEB360				0.423	46.61	0.178	
	8	IPE300	IPE300	IPE300	HEB360	HEB450	HEB450	HEB360				0.371	37.06	0.155	

Table C.14: Frames - Lagos Configuration 1

ID	Floor	B1	B2	B3	C1	C2	C3	C4	St.	T_1	q	ISD	Mass	θ_{EC8}	Ω
St194	1	IPE500	IPE500	IPE500	HEB400	HEB450	HEB450	HEB400	8	1.42	4.00	0.27	46.61	0.138	2.016
	2	IPE450	IPE450	IPE450	HEB400	HEB450	HEB450	HEB400				0.402	46.61	0.186	
	3	IPE400	IPE400	IPE400	HEB400	HEB450	HEB450	HEB400				0.483	46.61	0.199	
	4	IPE400	IPE400	IPE400	HEB360	HEB400	HEB400	HEB360				0.535	46.61	0.198	
	5	IPE400	IPE400	IPE400	HEB360	HEB400	HEB400	HEB360				0.501	46.61	0.17	
	6	IPE330	IPE330	IPE330	HEB360	HEB400	HEB400	HEB360				0.488	46.61	0.154	
	7	IPE330	IPE330	IPE330	HEB340	HEB360	HEB360	HEB340				0.442	46.61	0.129	
	8	IPE300	IPE300	IPE300	HEB340	HEB360	HEB360	HEB340				0.325	37.06	0.094	
St195	1	IPE400	IPE400	IPE400	HEB300	HEB360	HEB360	HEB300	8	1.88	1.92	0.418	46.61	0.156	1.000
	2	IPE360	IPE360	IPE360	HEB300	HEB360	HEB360	HEB300				0.602	46.61	0.2	
	3	IPE360	IPE360	IPE360	HEB300	HEB360	HEB360	HEB300				0.643	46.61	0.195	
	4	IPE360	IPE360	IPE360	HEB280	HEB340	HEB340	HEB280				0.633	46.61	0.177	
	5	IPE330	IPE330	IPE330	HEB280	HEB340	HEB340	HEB280				0.611	46.61	0.158	
	6	IPE300	IPE300	IPE300	HEB280	HEB340	HEB340	HEB280				0.589	46.61	0.143	
	7	IPE300	IPE300	IPE300	HEB260	HEB320	HEB320	HEB260				0.482	46.61	0.112	
	8	IPE300	IPE300	IPE300	HEB260	HEB320	HEB320	HEB260				0.304	37.06	0.065	

Table C.15: Frames - Lagos Configuration 2

ID	Floor	B1	B2	B3	C1	C2	C3	C4	St.	T_1	q	ISD	Mass	θ_{EC8}	Ω
St196	1	IPE300	IPE360	IPE300	HEB240	HEB300	HEB300	HEB240	2	0.68	6.50	0.442	51.784	0.19	2.754
	2	IPE270	IPE330	IPE270	HEB240	HEB300	HEB300	HEB240				0.464	41.182	0.144	
St197	1	IPE300	IPE360	IPE300	HEB220	HEB260	HEB260	HEB220	2	0.77	4.00	0.525	51.784	0.157	1.684
	2	IPE270	IPE330	IPE270	HEB220	HEB260	HEB260	HEB220				0.459	41.182	0.103	
St198	1	IPE300	IPE360	IPE300	HEB220	HEB260	HEB260	HEB220	2	0.77	2.37	0.525	51.784	0.093	1.310
	2	IPE270	IPE330	IPE270	HEB220	HEB260	HEB260	HEB220				0.459	41.182	0.061	
St199	1	IPE360	IPE400	IPE360	HEB300	HEB360	HEB360	HEB300	3	0.77	6.50	0.362	51.784	0.175	3.733
	2	IPE330	IPE400	IPE300	HEB300	HEB360	HEB360	HEB300				0.459	51.784	0.175	
	3	IPE270	IPE330	IPE270	HEB300	HEB360	HEB360	HEB300				0.39	41.182	0.122	
St200	1	IPE330	IPE360	IPE330	HEB240	HEB300	HEB300	HEB240	3	0.95	4.00	0.484	51.784	0.178	1.767
	2	IPE300	IPE360	IPE300	HEB240	HEB300	HEB300	HEB240				0.547	51.784	0.161	
	3	IPE270	IPE330	IPE270	HEB240	HEB300	HEB300	HEB240				0.398	41.182	0.099	
St201	1	IPE330	IPE360	IPE330	HEB200	HEB280	HEB280	HEB200	3	1.04	2.28	0.566	51.784	0.13	1.000
	2	IPE300	IPE360	IPE300	HEB200	HEB280	HEB280	HEB200				0.565	51.784	0.106	
	3	IPE270	IPE330	IPE270	HEB200	HEB280	HEB280	HEB200				0.379	41.182	0.061	
St202	1	IPE400	IPE450	IPE400	HEB360	HEB450	HEB450	HEB360	4	0.83	6.50	0.286	51.784	0.15	3.520
	2	IPE400	IPE450	IPE400	HEB360	HEB450	HEB450	HEB360				0.41	51.784	0.174	
	3	IPE330	IPE360	IPE330	HEB320	HEB400	HEB400	HEB320				0.415	51.784	0.152	
	4	IPE270	IPE330	IPE270	HEB320	HEB400	HEB400	HEB320				0.393	41.182	0.12	
St203	1	IPE360	IPE400	IPE360	HEB240	HEB340	HEB340	HEB240	4	1.07	4.00	0.442	51.784	0.184	2.100
	2	IPE360	IPE400	IPE360	HEB240	HEB340	HEB340	HEB240				0.52	51.784	0.179	
	3	IPE330	IPE360	IPE330	HEB220	HEB320	HEB320	HEB220				0.454	51.784	0.139	
	4	IPE270	IPE330	IPE270	HEB220	HEB320	HEB320	HEB220				0.34	41.182	0.091	
St204	1	IPE360	IPE360	IPE360	HEB220	HEB300	HEB300	HEB220	4	1.24	2.66	0.598	51.784	0.18	1.000
	2	IPE330	IPE360	IPE330	HEB220	HEB300	HEB300	HEB220				0.692	51.784	0.173	
	3	IPE300	IPE360	IPE300	HEB200	HEB260	HEB260	HEB200				0.661	51.784	0.146	
	4	IPE270	IPE330	IPE270	HEB200	HEB260	HEB260	HEB200				0.427	41.182	0.083	

Table C.15: Frames - Lagos Configuration 2

ID	Floor	B1	B2	B3	C1	C2	C3	C4	St.	T_1	q	ISD	Mass	θ_{EC8}	Ω
St205	1	IPE450	IPE500	IPE450	HEB360	HEB500	HEB500	HEB360	5	0.91	6.50	0.253	51.784	0.147	3.620
	2	IPE450	IPE500	IPE450	HEB360	HEB500	HEB500	HEB360				0.358	51.784	0.174	
	3	IPE400	IPE450	IPE400	HEB340	HEB450	HEB450	HEB340				0.387	51.784	0.164	
	4	IPE330	IPE360	IPE330	HEB340	HEB450	HEB450	HEB340				0.403	51.784	0.15	
	5	IPE270	IPE330	IPE270	HEB320	HEB400	HEB400	HEB320				0.386	41.182	0.124	
St206	1	IPE400	IPE450	IPE400	HEB280	HEB360	HEB360	HEB280	5	1.20	4.00	0.439	51.784	0.174	1.565
	2	IPE400	IPE450	IPE400	HEB280	HEB360	HEB360	HEB280				0.538	51.784	0.181	
	3	IPE330	IPE360	IPE330	HEB260	HEB340	HEB340	HEB260				0.594	51.784	0.176	
	4	IPE300	IPE360	IPE300	HEB260	HEB340	HEB340	HEB260				0.579	51.784	0.152	
	5	IPE270	IPE330	IPE270	HEB220	HEB300	HEB300	HEB220				0.447	41.182	0.105	
St207	1	IPE360	IPE360	IPE360	HEB220	HEB320	HEB320	HEB220	5	1.47	2.87	0.587	51.784	0.2	1.000
	2	IPE360	IPE360	IPE360	HEB220	HEB320	HEB320	HEB220				0.705	51.784	0.2	
	3	IPE330	IPE360	IPE330	HEB200	HEB280	HEB280	HEB200				0.714	51.784	0.188	
	4	IPE300	IPE360	IPE300	HEB200	HEB280	HEB280	HEB200				0.572	51.784	0.137	
	5	IPE270	IPE330	IPE270	HEB200	HEB260	HEB260	HEB200				0.382	41.182	0.083	
St208	1	IPE550	IPE600	IPE550	HEB500	HEB600	HEB600	HEB500	8	1.12	6.50	0.179	51.784	0.129	3.560
	2	IPE550	IPE600	IPE550	HEB500	HEB600	HEB600	HEB500				0.264	51.784	0.167	
	3	IPE500	IPE550	IPE500	HEB500	HEB600	HEB600	HEB500				0.291	51.784	0.167	
	4	IPE500	IPE550	IPE500	HEB450	HEB550	HEB550	HEB450				0.321	51.784	0.167	
	5	IPE450	IPE500	IPE450	HEB450	HEB550	HEB550	HEB450				0.342	51.784	0.161	
	6	IPE360	IPE400	IPE360	HEB450	HEB550	HEB550	HEB450				0.39	51.784	0.168	
	7	IPE330	IPE360	IPE330	HEB400	HEB450	HEB450	HEB400				0.417	51.784	0.165	
	8	IPE270	IPE330	IPE270	HEB400	HEB450	HEB450	HEB400				0.383	41.182	0.134	

Table C.15: Frames - Lagos Configuration 2

ID	Floor	B1	B2	B3	C1	C2	C3	C4	St.	T_1	q	ISD	Mass	θ_{EC8}	Ω
St209	1	IPE500	IPE500	IPE500	HEB360	HEB450	HEB450	HEB360	8	1.43	4.00	0.317	51.784	0.15	1.658
	2	IPE500	IPE500	IPE500	HEB360	HEB450	HEB450	HEB360				0.412	51.784	0.173	
	3	IPE450	IPE500	IPE450	HEB360	HEB450	HEB450	HEB360				0.43	51.784	0.164	
	4	IPE450	IPE500	IPE450	HEB340	HEB400	HEB400	HEB340				0.461	51.784	0.161	
	5	IPE400	IPE450	IPE400	HEB340	HEB400	HEB400	HEB340				0.474	51.784	0.151	
	6	IPE330	IPE360	IPE330	HEB340	HEB400	HEB400	HEB340				0.528	51.784	0.155	
	7	IPE300	IPE360	IPE300	HEB320	HEB360	HEB360	HEB320				0.521	51.784	0.143	
	8	IPE270	IPE330	IPE270	HEB320	HEB360	HEB360	HEB320				0.415	41.182	0.103	
St210	1	IPE400	IPE450	IPE400	HEB340	HEB400	HEB400	HEB340	8	1.79	2.80	0.388	51.784	0.158	1.000
	2	IPE400	IPE450	IPE400	HEB340	HEB400	HEB400	HEB340				0.548	51.784	0.199	
	3	IPE400	IPE450	IPE400	HEB340	HEB400	HEB400	HEB340				0.55	51.784	0.182	
	4	IPE360	IPE400	IPE360	HEB320	HEB360	HEB360	HEB320				0.604	51.784	0.182	
	5	IPE330	IPE360	IPE330	HEB320	HEB360	HEB360	HEB320				0.649	51.784	0.18	
	6	IPE300	IPE360	IPE300	HEB320	HEB360	HEB360	HEB320				0.629	51.784	0.162	
	7	IPE300	IPE360	IPE300	HEB300	HEB320	HEB320	HEB300				0.516	51.784	0.127	
	8	IPE270	IPE330	IPE270	HEB300	HEB320	HEB320	HEB300				0.36	41.182	0.081	

Table C.16: Frames - Lagos Configuration 3

ID	Floor	B1	B2	B3	C1	C2	C3	C4	St.	T_1	q	ISD	Mass	θ_{EC8}	Ω
St211	1	IPE450	IPE450	IPE450	HEB260	HEB400	HEB400	HEB260	2	0.57	6.50	0.374	82.854	0.142	3.886
	2	IPE400	IPE400	IPE400	HEB260	HEB400	HEB400	HEB260				0.361	65.892	0.099	
St212	1	IPE450	IPE450	IPE450	HEB260	HEB400	HEB400	HEB260	2	0.57	4.00	0.374	82.854	0.087	2.391
	2	IPE400	IPE400	IPE400	HEB260	HEB400	HEB400	HEB260				0.361	65.892	0.061	
St213	1	IPE450	IPE450	IPE450	HEB260	HEB400	HEB400	HEB260	2	0.57	1.68	0.374	82.854	0.037	1.000
	2	IPE400	IPE400	IPE400	HEB260	HEB400	HEB400	HEB260				0.361	65.892	0.026	
St214	1	IPE450	IPE450	IPE450	HEB300	HEB450	HEB450	HEB300	3	0.75	6.50	0.378	82.854	0.181	3.140
	2	IPE450	IPE450	IPE450	HEB300	HEB450	HEB450	HEB300				0.446	82.854	0.169	
	3	IPE400	IPE400	IPE400	HEB300	HEB450	HEB450	HEB300				0.321	65.892	0.102	
St215	1	IPE450	IPE450	IPE450	HEB260	HEB400	HEB400	HEB260	3	0.81	4.00	0.438	82.854	0.14	1.900
	2	IPE450	IPE450	IPE450	HEB260	HEB400	HEB400	HEB260				0.461	82.854	0.119	
	3	IPE400	IPE400	IPE400	HEB260	HEB400	HEB400	HEB260				0.306	65.892	0.067	
St216	1	IPE450	IPE450	IPE450	HEB260	HEB400	HEB400	HEB260	3	0.81	2.10	0.438	82.854	0.074	1.000
	2	IPE450	IPE450	IPE450	HEB260	HEB400	HEB400	HEB260				0.461	82.854	0.063	
	3	IPE400	IPE400	IPE400	HEB260	HEB400	HEB400	HEB260				0.306	65.892	0.035	
St217	1	IPE500	IPE500	IPE500	HEB450	HEB550	HEB550	HEB450	4	0.83	6.50	0.282	82.854	0.151	3.201
	2	IPE450	IPE450	IPE450	HEB450	HEB550	HEB550	HEB450				0.45	82.854	0.193	
	3	IPE450	IPE450	IPE450	HEB400	HEB450	HEB450	HEB400				0.432	82.854	0.161	
	4	IPE400	IPE400	IPE400	HEB400	HEB450	HEB450	HEB400				0.325	65.892	0.102	
St218	1	IPE450	IPE450	IPE450	HEB300	HEB400	HEB400	HEB300	4	1.04	4.00	0.434	82.854	0.178	1.774
	2	IPE450	IPE450	IPE450	HEB300	HEB400	HEB400	HEB300				0.529	82.854	0.178	
	3	IPE450	IPE450	IPE450	HEB260	HEB340	HEB340	HEB260				0.447	82.854	0.136	
	4	IPE400	IPE400	IPE400	HEB260	HEB340	HEB340	HEB260				0.275	65.892	0.073	
St219	1	IPE450	IPE450	IPE450	HEB280	HEB400	HEB400	HEB280	4	1.06	2.40	0.45	82.854	0.112	1.000
	2	IPE450	IPE450	IPE450	HEB280	HEB400	HEB400	HEB280				0.534	82.854	0.11	
	3	IPE450	IPE450	IPE450	HEB260	HEB340	HEB340	HEB260				0.44	82.854	0.082	
	4	IPE400	IPE400	IPE400	HEB260	HEB340	HEB340	HEB260				0.27	65.892	0.044	

Table C.16: Frames - Lagos Configuration 3

ID	Floor	B1	B2	B3	C1	C2	C3	C4	St.	T_1	q	ISD	Mass	θ_{EC8}	Ω
St220	1	IPE600	IPE600	IPE600	HEB500	HEB600	HEB600	HEB500	5	0.89	6.50	0.222	82.854	0.128	3.249
	2	IPE550	IPE550	IPE550	HEB500	HEB600	HEB600	HEB500				0.351	82.854	0.167	
	3	IPE450	IPE450	IPE450	HEB450	HEB500	HEB500	HEB450				0.441	82.854	0.181	
	4	IPE450	IPE450	IPE450	HEB450	HEB500	HEB500	HEB450				0.432	82.854	0.155	
	5	IPE400	IPE400	IPE400	HEB340	HEB400	HEB400	HEB340				0.345	65.892	0.108	
St221	1	IPE500	IPE500	IPE500	HEB400	HEB500	HEB500	HEB400	5	1.11	4.00	0.318	82.854	0.138	1.801
	2	IPE450	IPE450	IPE450	HEB400	HEB500	HEB500	HEB400				0.494	82.854	0.178	
	3	IPE450	IPE450	IPE450	HEB360	HEB400	HEB400	HEB360				0.5	82.854	0.16	
	4	IPE450	IPE450	IPE450	HEB360	HEB400	HEB400	HEB360				0.389	82.854	0.113	
	5	IPE400	IPE400	IPE400	HEB320	HEB360	HEB360	HEB320				0.28	65.892	0.072	
St222	1	IPE450	IPE450	IPE450	HEB300	HEB450	HEB450	HEB300	5	1.24	2.82	0.485	82.854	0.141	1.000
	2	IPE450	IPE450	IPE450	HEB300	HEB450	HEB450	HEB300				0.653	82.854	0.16	
	3	IPE450	IPE450	IPE450	HEB300	HEB400	HEB400	HEB300				0.586	82.854	0.129	
	4	IPE450	IPE450	IPE450	HEB300	HEB400	HEB400	HEB300				0.427	82.854	0.087	
	5	IPE400	IPE400	IPE400	HEB280	HEB360	HEB360	HEB280				0.281	65.892	0.051	
St223	1	HEA600	HEA600	HEA600	HEM500	HEM650	HEM650	HEM500	8	1.11	6.50	0.179	82.854	0.129	3.095
	2	HEA600	HEA600	HEA600	HEM500	HEM650	HEM650	HEM500				0.261	82.854	0.165	
	3	HEA600	HEA600	HEA600	HEM500	HEM650	HEM650	HEM500				0.269	82.854	0.154	
	4	IPE600	IPE600	IPE600	HEM450	HEM600	HEM600	HEM450				0.311	82.854	0.161	
	5	IPE500	IPE500	IPE500	HEM450	HEM600	HEM600	HEM450				0.378	82.854	0.177	
	6	IPE500	IPE500	IPE500	HEM450	HEM600	HEM600	HEM450				0.405	82.854	0.172	
	7	IPE400	IPE400	IPE400	HEB450	HEB600	HEB600	HEB450				0.403	82.854	0.159	
	8	IPE360	IPE360	IPE360	HEB450	HEB600	HEB600	HEB450				0.376	65.892	0.129	

Table C.16: Frames - Lagos Configuration 3

ID	Floor	B1	B2	B3	C1	C2	C3	C4	St.	T_1	q	ISD	Mass	θ_{EC8}	Ω
St224	1	IPE600	IPE600	IPE600	HEB400	HEB600	HEB600	HEB400	8	1.43	4.00	0.291	82.854	0.14	1.355
	2	IPE600	IPE600	IPE600	HEB400	HEB600	HEB600	HEB400				0.402	82.854	0.17	
	3	IPE550	IPE550	IPE550	HEB400	HEB600	HEB600	HEB400				0.442	82.854	0.17	
	4	IPE500	IPE500	IPE500	HEB360	HEB550	HEB550	HEB360				0.52	82.854	0.182	
	5	IPE500	IPE500	IPE500	HEB360	HEB550	HEB550	HEB360				0.535	82.854	0.171	
	6	IPE400	IPE400	IPE400	HEB360	HEB550	HEB550	HEB360				0.546	82.854	0.161	
	7	IPE400	IPE400	IPE400	HEB340	HEB500	HEB500	HEB340				0.505	82.854	0.139	
	8	IPE360	IPE360	IPE360	HEB340	HEB500	HEB500	HEB340				0.391	65.892	0.097	
St225	1	IPE500	IPE500	IPE500	HEB450	HEB550	HEB550	HEB450	8	1.73	2.90	0.339	82.854	0.141	1.000
	2	IPE500	IPE500	IPE500	HEB450	HEB550	HEB550	HEB450				0.548	82.854	0.199	
	3	IPE450	IPE450	IPE450	HEB450	HEB550	HEB550	HEB450				0.612	82.854	0.203	
	4	IPE450	IPE450	IPE450	HEB400	HEB500	HEB500	HEB400				0.65	82.854	0.198	
	5	IPE450	IPE450	IPE450	HEB400	HEB500	HEB500	HEB400				0.597	82.854	0.168	
	6	IPE400	IPE400	IPE400	HEB400	HEB500	HEB500	HEB400				0.538	82.854	0.142	
	7	IPE400	IPE400	IPE400	HEB340	HEB450	HEB450	HEB340				0.446	82.854	0.113	
	8	IPE360	IPE360	IPE360	HEB340	HEB450	HEB450	HEB340				0.325	65.892	0.073	

Table C.17: Frames - Lagos Configuration 4

ID	Floor	B1	B2	B3	B4	C1	C2	C3	C4	C5	St.	T_1	q	ISD	Mass	θ_{EC8}	Ω
St226	1	IPE330	IPE330	IPE330	IPE330	HEB260	HEB280	HEB280	HEB280	HEB260	2	0.66	6.50	0.456	69.91	0.17	3.781
	2	IPE330	IPE330	IPE330	IPE330	HEB260	HEB280	HEB280	HEB280	HEB260				0.386	55.59	0.109	
St227	1	IPE330	IPE330	IPE330	IPE330	HEB240	HEB260	HEB260	HEB260	HEB240	2	0.71	4.00	0.505	69.91	0.125	2.382
	2	IPE330	IPE330	IPE330	IPE330	HEB240	HEB260	HEB260	HEB260	HEB240				0.385	55.59	0.073	
St228	1	IPE330	IPE330	IPE330	IPE330	HEB240	HEB260	HEB260	HEB260	HEB240	2	0.71	1.68	0.505	69.91	0.052	1.000
	2	IPE330	IPE330	IPE330	IPE330	HEB240	HEB260	HEB260	HEB260	HEB240				0.385	55.59	0.031	
St229	1	IPE360	IPE360	IPE360	IPE360	HEB300	HEB320	HEB320	HEB320	HEB300	3	0.79	6.50	0.405	69.91	0.183	3.819
	2	IPE360	IPE360	IPE360	IPE360	HEB300	HEB320	HEB320	HEB320	HEB300				0.455	69.91	0.164	
	3	IPE300	IPE300	IPE300	IPE300	HEB280	HEB280	HEB280	HEB280	HEB280				0.361	55.59	0.109	
St230	1	IPE330	IPE330	IPE330	IPE330	HEB240	HEB280	HEB280	HEB280	HEB240	3	0.98	4.00	0.532	69.91	0.18	1.872
	2	IPE330	IPE330	IPE330	IPE330	HEB240	HEB280	HEB280	HEB280	HEB240				0.535	69.91	0.148	
	3	IPE300	IPE300	IPE300	IPE300	HEB220	HEB260	HEB260	HEB260	HEB220				0.339	55.59	0.081	
St231	1	IPE300	IPE300	IPE300	IPE300	HEB220	HEB260	HEB260	HEB260	HEB220	3	1.13	2.95	0.62	69.91	0.179	1.000
	2	IPE300	IPE300	IPE300	IPE300	HEB220	HEB260	HEB260	HEB260	HEB220				0.63	69.91	0.148	
	3	IPE300	IPE300	IPE300	IPE300	HEB220	HEB260	HEB260	HEB260	HEB220				0.367	55.59	0.076	
St232	1	IPE400	IPE400	IPE400	IPE400	HEB360	HEB400	HEB400	HEB400	HEB360	4	0.85	6.50	0.321	69.91	0.156	4.230
	2	IPE400	IPE400	IPE400	IPE400	HEB360	HEB400	HEB400	HEB400	HEB360				0.427	69.91	0.17	
	3	IPE360	IPE360	IPE360	IPE360	HEB340	HEB340	HEB340	HEB340	HEB340				0.402	69.91	0.139	
	4	IPE300	IPE300	IPE300	IPE300	HEB340	HEB340	HEB340	HEB340	HEB340				0.329	55.59	0.098	
St233	1	IPE360	IPE360	IPE360	IPE360	HEB280	HEB300	HEB300	HEB300	HEB280	4	1.11	4.00	0.466	69.91	0.179	2.169
	2	IPE360	IPE360	IPE360	IPE360	HEB280	HEB300	HEB300	HEB300	HEB280				0.535	69.91	0.171	
	3	IPE330	IPE330	IPE330	IPE330	HEB260	HEB280	HEB280	HEB280	HEB260				0.463	69.91	0.131	
	4	IPE300	IPE300	IPE300	IPE300	HEB260	HEB280	HEB280	HEB280	HEB260				0.319	55.59	0.079	
St234	1	IPE330	IPE330	IPE330	IPE330	HEB240	HEB280	HEB280	HEB280	HEB240	4	1.30	2.79	0.686	69.91	0.184	1.000
	2	IPE330	IPE330	IPE330	IPE330	HEB240	HEB280	HEB280	HEB280	HEB240				0.741	69.91	0.167	
	3	IPE300	IPE300	IPE300	IPE300	HEB220	HEB260	HEB260	HEB260	HEB220				0.574	69.91	0.116	
	4	IPE300	IPE300	IPE300	IPE300	HEB220	HEB260	HEB260	HEB260	HEB220				0.336	55.59	0.062	

Table C.17: Frames - Lagos Configuration 4

ID	Floor	B1	B2	B3	B4	C1	C2	C3	C4	C5	St.	T_1	q	ISD	Mass	θ_{EC8}	Ω
St235	1	IPE450	IPE450	IPE450	IPE450	HEB360	HEB450	HEB450	HEB450	HEB360	5	0.97	6.50	0.271	69.91	0.15	3.808
	2	IPE450	IPE450	IPE450	IPE450	HEB360	HEB450	HEB450	HEB450	HEB360				0.372	69.91	0.173	
	3	IPE360	IPE360	IPE360	IPE360	HEB340	HEB400	HEB400	HEB400	HEB340				0.437	69.91	0.176	
	4	IPE330	IPE330	IPE330	IPE330	HEB340	HEB400	HEB400	HEB400	HEB340				0.45	69.91	0.159	
	5	IPE300	IPE300	IPE300	IPE300	HEB320	HEB360	HEB360	HEB360	HEB320				0.372	55.59	0.115	
St236	1	IPE400	IPE400	IPE400	IPE400	HEB280	HEB340	HEB340	HEB340	HEB280	5	1.24	4.00	0.465	69.91	0.17	1.720
	2	IPE400	IPE400	IPE400	IPE400	HEB280	HEB340	HEB340	HEB340	HEB280				0.554	69.91	0.172	
	3	IPE330	IPE330	IPE330	IPE330	HEB260	HEB320	HEB320	HEB320	HEB260				0.61	69.91	0.167	
	4	IPE300	IPE300	IPE300	IPE300	HEB260	HEB320	HEB320	HEB320	HEB260				0.597	69.91	0.145	
	5	IPE300	IPE300	IPE300	IPE300	HEB240	HEB300	HEB300	HEB300	HEB240				0.423	55.59	0.093	
St237	1	IPE360	IPE360	IPE360	IPE360	HEB260	HEB320	HEB320	HEB320	HEB260	5	1.47	3.13	0.523	69.91	0.176	1.000
	2	IPE330	IPE330	IPE330	IPE330	HEB260	HEB320	HEB320	HEB320	HEB260				0.711	69.91	0.2	
	3	IPE300	IPE300	IPE300	IPE300	HEB240	HEB300	HEB300	HEB300	HEB240				0.767	69.91	0.192	
	4	IPE300	IPE300	IPE300	IPE300	HEB240	HEB280	HEB280	HEB280	HEB240				0.637	69.91	0.144	
	5	IPE300	IPE300	IPE300	IPE300	HEB220	HEB280	HEB280	HEB280	HEB220				0.396	55.59	0.082	
St238	1	IPE550	IPE550	IPE550	IPE550	HEB400	HEB500	HEB500	HEB500	HEB400	8	1.21	6.50	0.263	69.91	0.156	2.794
	2	IPE550	IPE550	IPE550	IPE550	HEB400	HEB500	HEB500	HEB500	HEB400				0.332	69.91	0.175	
	3	IPE500	IPE500	IPE500	IPE500	HEB400	HEB500	HEB500	HEB500	HEB400				0.354	69.91	0.169	
	4	IPE500	IPE500	IPE500	IPE500	HEB360	HEB450	HEB450	HEB450	HEB360				0.392	69.91	0.171	
	5	IPE450	IPE450	IPE450	IPE450	HEB360	HEB450	HEB450	HEB450	HEB360				0.41	69.91	0.162	
	6	IPE360	IPE360	IPE360	IPE360	HEB360	HEB450	HEB450	HEB450	HEB360				0.479	69.91	0.172	
	7	IPE300	IPE300	IPE300	IPE300	HEB340	HEB400	HEB400	HEB400	HEB340				0.531	69.91	0.176	
	8	IPE300	IPE300	IPE300	IPE300	HEB340	HEB400	HEB400	HEB400	HEB340				0.445	55.59	0.132	

Table C.17: Frames - Lagos Configuration 4

ID	Floor	B1	B2	B3	B4	C1	C2	C3	C4	C5	St.	T_1	q	ISD	Mass	θ_{EC8}	Ω
St239	1	IPE500	IPE500	IPE500	IPE500	HEB300	HEB450	HEB450	HEB450	HEB300	8	1.54	4.00	0.316	69.91	0.144	1.688
	2	IPE450	IPE450	IPE450	IPE450	HEB300	HEB450	HEB450	HEB450	HEB300				0.426	69.91	0.173	
	3	IPE450	IPE450	IPE450	IPE450	HEB300	HEB450	HEB450	HEB450	HEB300				0.463	69.91	0.17	
	4	IPE400	IPE400	IPE400	IPE400	HEB280	HEB400	HEB400	HEB400	HEB280				0.534	69.91	0.178	
	5	IPE360	IPE360	IPE360	IPE360	HEB280	HEB400	HEB400	HEB400	HEB280				0.593	69.91	0.18	
	6	IPE330	IPE330	IPE330	IPE330	HEB280	HEB400	HEB400	HEB400	HEB280				0.607	69.91	0.17	
	7	IPE300	IPE300	IPE300	IPE300	HEB260	HEB360	HEB360	HEB360	HEB260				0.555	69.91	0.145	
	8	IPE300	IPE300	IPE300	IPE300	HEB260	HEB360	HEB360	HEB360	HEB260				0.394	55.59	0.095	
St240	1	IPE400	IPE400	IPE400	IPE400	HEB300	HEB360	HEB360	HEB360	HEB300	8	1.96	2.43	0.445	69.91	0.156	1.000
	2	IPE360	IPE360	IPE360	IPE360	HEB300	HEB360	HEB360	HEB360	HEB300				0.639	69.91	0.199	
	3	IPE360	IPE360	IPE360	IPE360	HEB300	HEB360	HEB360	HEB360	HEB300				0.68	69.91	0.193	
	4	IPE360	IPE360	IPE360	IPE360	HEB280	HEB340	HEB340	HEB340	HEB280				0.664	69.91	0.174	
	5	IPE330	IPE330	IPE330	IPE330	HEB280	HEB340	HEB340	HEB340	HEB280				0.627	69.91	0.153	
	6	IPE330	IPE330	IPE330	IPE330	HEB280	HEB340	HEB340	HEB340	HEB280				0.558	69.91	0.128	
	7	IPE300	IPE300	IPE300	IPE300	HEB260	HEB320	HEB320	HEB320	HEB260				0.445	69.91	0.098	
	8	IPE300	IPE300	IPE300	IPE300	HEB260	HEB320	HEB320	HEB320	HEB260				0.297	55.59	0.061	

Table C.18: Frames - Lagos Configuration 5

ID	Floor	B1	B2	B3	C1	C2	C3	C4	St.	T_1	q	ISD	Mass	θ_{EC8}	Ω
St241	1	IPE360	IPE300	IPE360	HEB260	HEB300	HEB300	HEB260	2	0.67	6.50	0.44	56.96	0.187	3.098
	2	IPE330	IPE300	IPE330	HEB260	HEB300	HEB300	HEB260				0.446	45.3	0.137	
St242	1	IPE360	IPE300	IPE360	HEB240	HEB260	HEB260	HEB240	2	0.75	4.00	0.516	56.96	0.151	2.029
	2	IPE330	IPE300	IPE330	HEB240	HEB260	HEB260	HEB240				0.444	45.3	0.097	
St243	1	IPE360	IPE300	IPE360	HEB240	HEB260	HEB260	HEB240	2	0.75	1.97	0.516	56.96	0.075	1.000
	2	IPE330	IPE300	IPE330	HEB240	HEB260	HEB260	HEB240				0.444	45.3	0.048	
St244	1	IPE400	IPE360	IPE400	HEB320	HEB360	HEB360	HEB320	3	0.76	6.50	0.369	56.96	0.179	3.788
	2	IPE400	IPE360	IPE400	HEB320	HEB360	HEB360	HEB320				0.454	56.96	0.173	
	3	IPE330	IPE300	IPE330	HEB280	HEB300	HEB300	HEB280				0.381	45.3	0.12	
St245	1	IPE360	IPE300	IPE360	HEB260	HEB300	HEB300	HEB260	3	0.98	4.00	0.495	56.96	0.188	1.567
	2	IPE360	IPE300	IPE360	HEB260	HEB300	HEB300	HEB260				0.569	56.96	0.172	
	3	IPE330	IPE300	IPE330	HEB220	HEB260	HEB260	HEB220				0.436	45.3	0.112	
St246	1	IPE360	IPE300	IPE360	HEB260	HEB280	HEB280	HEB260	3	1.01	2.47	0.528	56.96	0.128	1.000
	2	IPE360	IPE300	IPE360	HEB260	HEB280	HEB280	HEB260				0.577	56.96	0.112	
	3	IPE330	IPE300	IPE330	HEB220	HEB240	HEB240	HEB220				0.416	45.3	0.069	
St247	1	IPE450	IPE450	IPE450	HEB340	HEB450	HEB450	HEB340	4	0.83	6.50	0.297	56.96	0.158	3.469
	2	IPE450	IPE450	IPE450	HEB340	HEB450	HEB450	HEB340				0.404	56.96	0.175	
	3	IPE360	IPE330	IPE360	HEB320	HEB400	HEB400	HEB320				0.425	56.96	0.158	
	4	IPE330	IPE300	IPE330	HEB320	HEB400	HEB400	HEB320				0.387	45.3	0.12	
St248	1	IPE400	IPE360	IPE400	HEB320	HEB340	HEB340	HEB320	4	1.06	4.00	0.396	56.96	0.164	2.190
	2	IPE400	IPE360	IPE400	HEB320	HEB340	HEB340	HEB320				0.525	56.96	0.176	
	3	IPE360	IPE300	IPE360	HEB260	HEB280	HEB280	HEB260				0.528	56.96	0.156	
	4	IPE330	IPE300	IPE330	HEB260	HEB280	HEB280	HEB260				0.381	45.3	0.096	
St249	1	IPE400	IPE300	IPE400	HEB260	HEB280	HEB280	HEB260	4	1.29	2.81	0.625	56.96	0.187	1.000
	2	IPE360	IPE300	IPE360	HEB260	HEB280	HEB280	HEB260				0.745	56.96	0.184	
	3	IPE360	IPE300	IPE360	HEB220	HEB260	HEB260	HEB220				0.661	56.96	0.146	
	4	IPE330	IPE300	IPE330	HEB220	HEB260	HEB260	HEB220				0.393	45.3	0.077	

Table C.18: Frames - Lagos Configuration 5

ID	Floor	B1	B2	B3	C1	C2	C3	C4	St.	T_1	q	ISD	Mass	θ_{EC8}	Ω
St250	1	IPE500	IPE500	IPE500	HEB340	HEB450	HEB450	HEB340	5	0.94	6.50	0.288	56.96	0.174	3.711
	2	IPE500	IPE500	IPE500	HEB340	HEB450	HEB450	HEB340				0.364	56.96	0.184	
	3	IPE450	IPE450	IPE450	HEB320	HEB400	HEB400	HEB320				0.384	56.96	0.171	
	4	IPE360	IPE330	IPE360	HEB320	HEB400	HEB400	HEB320				0.402	56.96	0.158	
	5	IPE330	IPE300	IPE330	HEB300	HEB360	HEB360	HEB300				0.368	45.3	0.125	
St251	1	IPE450	IPE400	IPE450	HEB320	HEB400	HEB400	HEB320	5	1.19	4.00	0.395	56.96	0.156	1.360
	2	IPE450	IPE360	IPE450	HEB320	HEB400	HEB400	HEB320				0.553	56.96	0.183	
	3	IPE360	IPE300	IPE360	HEB300	HEB360	HEB360	HEB300				0.638	56.96	0.184	
	4	IPE360	IPE300	IPE360	HEB300	HEB360	HEB360	HEB300				0.598	56.96	0.154	
	5	IPE330	IPE300	IPE330	HEB280	HEB320	HEB320	HEB280				0.433	45.3	0.099	
St252	1	IPE400	IPE330	IPE400	HEB300	HEB340	HEB340	HEB300	5	1.39	2.97	0.506	56.96	0.171	1.000
	2	IPE400	IPE300	IPE400	HEB300	HEB340	HEB340	HEB300				0.699	56.96	0.2	
	3	IPE360	IPE300	IPE360	HEB280	HEB320	HEB320	HEB280				0.693	56.96	0.176	
	4	IPE360	IPE300	IPE360	HEB280	HEB320	HEB320	HEB280				0.562	56.96	0.13	
	5	IPE330	IPE300	IPE330	HEB260	HEB280	HEB280	HEB260				0.381	45.3	0.079	
St253	1	IPE600	IPE600	IPE600	HEB500	HEB600	HEB600	HEB500	8	1.12	6.50	0.184	56.96	0.133	3.320
	2	IPE600	IPE600	IPE600	HEB500	HEB600	HEB600	HEB500				0.26	56.96	0.165	
	3	IPE600	IPE550	IPE600	HEB500	HEB600	HEB600	HEB500				0.27	56.96	0.155	
	4	IPE550	IPE500	IPE550	HEB450	HEB550	HEB550	HEB450				0.31	56.96	0.162	
	5	IPE500	IPE450	IPE500	HEB450	HEB550	HEB550	HEB450				0.357	56.96	0.168	
	6	IPE400	IPE360	IPE400	HEB450	HEB550	HEB550	HEB450				0.417	56.96	0.178	
	7	IPE360	IPE300	IPE360	HEB400	HEB500	HEB500	HEB400				0.443	56.96	0.173	
	8	IPE330	IPE300	IPE330	HEB400	HEB500	HEB500	HEB400				0.397	45.3	0.137	

Table C.18: Frames - Lagos Configuration 5

ID	Floor	B1	B2	B3	C1	C2	C3	C4	St.	T_1	q	ISD	Mass	θ_{EC8}	Ω
St254	1	IPE550	IPE500	IPE550	HEB360	HEB500	HEB500	HEB360	8	1.44	4.00	0.293	56.96	0.14	1.530
	2	IPE550	IPE500	IPE550	HEB360	HEB500	HEB500	HEB360				0.392	56.96	0.166	
	3	IPE500	IPE450	IPE500	HEB360	HEB500	HEB500	HEB360				0.425	56.96	0.163	
	4	IPE500	IPE450	IPE500	HEB340	HEB450	HEB450	HEB340				0.477	56.96	0.166	
	5	IPE400	IPE360	IPE400	HEB340	HEB450	HEB450	HEB340				0.545	56.96	0.173	
	6	IPE360	IPE330	IPE360	HEB340	HEB450	HEB450	HEB340				0.608	56.96	0.176	
	7	IPE360	IPE300	IPE360	HEB320	HEB400	HEB400	HEB320				0.546	56.96	0.148	
	8	IPE330	IPE300	IPE330	HEB320	HEB400	HEB400	HEB320				0.407	45.3	0.1	
St255	1	IPE450	IPE400	IPE450	HEB320	HEB400	HEB400	HEB320	8	1.86	2.58	0.42	56.96	0.163	1.000
	2	IPE450	IPE400	IPE450	HEB320	HEB400	HEB400	HEB320				0.58	56.96	0.2	
	3	IPE450	IPE360	IPE450	HEB320	HEB400	HEB400	HEB320				0.591	56.96	0.186	
	4	IPE400	IPE330	IPE400	HEB300	HEB360	HEB360	HEB300				0.653	56.96	0.189	
	5	IPE400	IPE330	IPE400	HEB300	HEB360	HEB360	HEB300				0.644	56.96	0.172	
	6	IPE360	IPE300	IPE360	HEB300	HEB360	HEB360	HEB300				0.586	56.96	0.146	
	7	IPE360	IPE300	IPE360	HEB260	HEB320	HEB320	HEB260				0.487	56.96	0.117	
	8	IPE330	IPE300	IPE330	HEB260	HEB320	HEB320	HEB260				0.314	45.3	0.069	

Table C.19: Frames - Lagos Configuration 6

ID	Floor	B1	B2	B3	B4	B5	C1=C6	C2=C5	C3=C4	St.	T_1	q	ISD	Mass	θ_{EC8}	Ω
St256	1	IPE450	IPE450	IPE450	IPE450	IPE450	HEB300	HEB360	HEB340	2	0.64	6.50	0.465	165.708	0.162	3.318
	2	IPE400	IPE400	IPE400	IPE400	IPE400	HEB300	HEB360	HEB340				0.433	131.784	0.108	
St257	1	IPE450	IPE450	IPE450	IPE450	IPE450	HEB300	HEB360	HEB340	2	0.64	4.00	0.465	165.708	0.1	2.042
	2	IPE400	IPE400	IPE400	IPE400	IPE400	HEB300	HEB360	HEB340				0.433	131.784	0.067	
St258	1	IPE450	IPE450	IPE450	IPE450	IPE450	HEB300	HEB360	HEB340	2	0.64	2.00	0.465	165.708	0.051	1.000
	2	IPE400	IPE400	IPE400	IPE400	IPE400	HEB300	HEB360	HEB340				0.433	131.784	0.034	
St259	1	IPE450	IPE450	IPE450	IPE450	IPE450	HEB360	HEB450	HEB400	3	0.81	6.50	0.418	165.708	0.183	2.778
	2	IPE450	IPE450	IPE450	IPE450	IPE450	HEB360	HEB450	HEB400				0.509	165.708	0.175	
	3	IPE400	IPE400	IPE400	IPE400	IPE400	HEB340	HEB400	HEB360				0.382	131.784	0.108	
St260	1	IPE450	IPE450	IPE450	IPE450	IPE450	HEB340	HEB400	HEB360	3	0.86	4.00	0.462	165.708	0.132	1.700
	2	IPE450	IPE450	IPE450	IPE450	IPE450	HEB340	HEB400	HEB360				0.516	165.708	0.117	
	3	IPE400	IPE400	IPE400	IPE400	IPE400	HEB340	HEB400	HEB360				0.362	131.784	0.068	
St261	1	IPE450	IPE450	IPE450	IPE450	IPE450	HEB340	HEB400	HEB360	3	0.86	2.47	0.462	165.708	0.082	1.000
	2	IPE450	IPE450	IPE450	IPE450	IPE450	HEB340	HEB400	HEB360				0.516	165.708	0.072	
	3	IPE400	IPE400	IPE400	IPE400	IPE400	HEB340	HEB400	HEB360				0.362	131.784	0.042	
St262	1	IPE550	IPE550	IPE550	IPE550	IPE550	HEB400	HEB600	HEB500	4	0.84	6.50	0.304	165.708	0.139	3.510
	2	IPE500	IPE500	IPE500	IPE500	IPE500	HEB400	HEB600	HEB500				0.447	165.708	0.165	
	3	IPE450	IPE450	IPE450	IPE450	IPE450	HEB360	HEB550	HEB450				0.452	165.708	0.144	
	4	IPE400	IPE400	IPE400	IPE400	IPE400	HEB360	HEB550	HEB450				0.37	131.784	0.098	
St263	1	IPE450	IPE450	IPE450	IPE450	IPE450	HEB340	HEB400	HEB360	4	1.13	4.00	0.477	165.708	0.182	1.575
	2	IPE450	IPE450	IPE450	IPE450	IPE450	HEB340	HEB400	HEB360				0.595	165.708	0.185	
	3	IPE450	IPE450	IPE450	IPE450	IPE450	HEB320	HEB360	HEB340				0.512	165.708	0.142	
	4	IPE400	IPE400	IPE400	IPE400	IPE400	HEB320	HEB360	HEB340				0.346	131.784	0.082	
St264	1	IPE450	IPE450	IPE450	IPE450	IPE450	HEB320	HEB400	HEB360	4	1.16	2.68	0.487	165.708	0.125	1.000
	2	IPE450	IPE450	IPE450	IPE450	IPE450	HEB320	HEB400	HEB360				0.595	165.708	0.125	
	3	IPE400	IPE400	IPE400	IPE400	IPE400	HEB320	HEB360	HEB340				0.508	165.708	0.095	
	4	IPE400	IPE400	IPE400	IPE400	IPE400	HEB320	HEB360	HEB340				0.343	131.784	0.055	

Table C.19: Frames - Lagos Configuration 6

ID	Floor	B1	B2	B3	B4	B5	C1=C6	C2=C5	C3=C4	St.	T_1	q	ISD	Mass	θ_{EC8}	Ω
St265	1	IPE550	IPE550	IPE550	IPE550	IPE550	HEB450	HEB700	HEB650	5	0.93	6.50	0.259	165.708	0.133	3.647
	2	IPE550	IPE550	IPE550	IPE550	IPE550	HEB450	HEB700	HEB650				0.408	165.708	0.172	
	3	IPE500	IPE500	IPE500	IPE500	IPE500	HEB400	HEB650	HEB550				0.439	165.708	0.163	
	4	IPE450	IPE450	IPE450	IPE450	IPE450	HEB400	HEB650	HEB550				0.418	165.708	0.137	
	5	IPE400	IPE400	IPE400	IPE400	IPE400	HEB360	HEB600	HEB500				0.352	131.784	0.099	
St266	1	IPE500	IPE500	IPE500	IPE500	IPE500	HEB400	HEB500	HEB450	5	1.21	4.00	0.42	165.708	0.144	1.557
	2	IPE500	IPE500	IPE500	IPE500	IPE500	HEB400	HEB500	HEB450				0.592	165.708	0.168	
	3	IPE450	IPE450	IPE450	IPE450	IPE450	HEB340	HEB400	HEB360				0.656	165.708	0.165	
	4	IPE400	IPE400	IPE400	IPE400	IPE400	HEB340	HEB400	HEB360				0.595	165.708	0.133	
	5	IPE400	IPE400	IPE400	IPE400	IPE400	HEB340	HEB360	HEB340				0.419	131.784	0.082	
St267	1	IPE450	IPE450	IPE450	IPE450	IPE450	HEB360	HEB400	HEB400	5	1.43	3.30	0.535	165.708	0.177	1.000
	2	IPE450	IPE450	IPE450	IPE450	IPE450	HEB360	HEB400	HEB400				0.728	165.708	0.2	
	3	IPE400	IPE400	IPE400	IPE400	IPE400	HEB340	HEB360	HEB360				0.729	165.708	0.18	
	4	IPE400	IPE400	IPE400	IPE400	IPE400	HEB340	HEB360	HEB360				0.593	165.708	0.133	
	5	IPE400	IPE400	IPE400	IPE400	IPE400	HEB320	HEB360	HEB340				0.367	131.784	0.073	
St268	1	HEA600	HEA600	HEA600	HEA600	HEA600	HEM600	HEM700	HEM700	8	1.20	6.50	0.213	165.708	0.12	2.623
	2	HEA550	HEA550	HEA550	HEA550	HEA550	HEM600	HEM700	HEM700				0.35	165.708	0.173	
	3	HEA550	HEA550	HEA550	HEA550	HEA550	HEM600	HEM700	HEM700				0.381	165.708	0.17	
	4	HEA550	HEA550	HEA550	HEA550	HEA550	HEM550	HEM600	HEM600				0.406	165.708	0.164	
	5	IPE500	IPE500	IPE500	IPE500	IPE500	HEM550	HEM600	HEM600				0.48	165.708	0.176	
	6	IPE450	IPE450	IPE450	IPE450	IPE450	HEM550	HEM600	HEM600				0.539	165.708	0.18	
	7	IPE450	IPE450	IPE450	IPE450	IPE450	HEB550	HEB600	HEB600				0.494	165.708	0.152	
	8	IPE400	IPE400	IPE400	IPE400	IPE400	HEB550	HEB600	HEB600				0.403	131.784	0.11	
St269	1	IPE600	IPE600	IPE600	IPE600	IPE600	HEB500	HEB600	HEB600	8	1.52	4.00	0.294	165.708	0.127	1.422
	2	IPE600	IPE600	IPE600	IPE600	IPE600	HEB500	HEB600	HEB600				0.431	165.708	0.163	
	3	IPE550	IPE550	IPE550	IPE550	IPE550	HEB500	HEB600	HEB600				0.48	165.708	0.165	
	4	IPE500	IPE500	IPE500	IPE500	IPE500	HEB450	HEB550	HEB550				0.573	165.708	0.179	

Table C.19: Frames - Lagos Configuration 6

ID	Floor	B1	B2	B3	B4	B5	C1=C6	C2=C5	C3=C4	St.	T_1	q	ISD	Mass	θ_{EC8}	Ω
	5	IPE450	IPE450	IPE450	IPE450	IPE450	HEB450	HEB550	HEB550				0.627	165.708	0.179	
	6	IPE450	IPE450	IPE450	IPE450	IPE450	HEB450	HEB550	HEB550				0.595	165.708	0.156	
	7	IPE400	IPE400	IPE400	IPE400	IPE400	HEB400	HEB500	HEB500				0.502	165.708	0.125	
	8	IPE400	IPE400	IPE400	IPE400	IPE400	HEB400	HEB500	HEB500				0.371	131.784	0.081	
St270	1	IPE550	IPE550	IPE550	IPE550	IPE550	HEB450	HEB550	HEB550	8	1.79	3.19	0.345	165.708	0.138	1.000
	2	IPE500	IPE500	IPE500	IPE500	IPE500	HEB450	HEB550	HEB550				0.555	165.708	0.194	
	3	IPE500	IPE500	IPE500	IPE500	IPE500	HEB450	HEB550	HEB550				0.615	165.708	0.195	
	4	IPE450	IPE450	IPE450	IPE450	IPE450	HEB400	HEB500	HEB500				0.671	165.708	0.195	
	5	IPE450	IPE450	IPE450	IPE450	IPE450	HEB400	HEB500	HEB500				0.666	165.708	0.178	
	6	IPE400	IPE400	IPE400	IPE400	IPE400	HEB400	HEB500	HEB500				0.614	165.708	0.153	
	7	IPE400	IPE400	IPE400	IPE400	IPE400	HEB360	HEB450	HEB450				0.501	165.708	0.119	
	8	IPE400	IPE400	IPE400	IPE400	IPE400	HEB360	HEB450	HEB450				0.334	131.784	0.07	

Table C.20: Frames - Lagos (Soil Type C) Configuration 1

ID	Floor	B1	B2	B3	C1	C2	C3	C4	St.	T_1	q	ISD	Mass	θ_{EC8}	Ω
St271	1	IPE300	IPE300	IPE300	HEB240	HEB300	HEB300	HEB240	2	0.65	6.50	0.47	46.61	0.189	2.648
	2	IPE300	IPE300	IPE300	HEB240	HEB300	HEB300	HEB240				0.467	37.06	0.157	
St272	1	IPE300	IPE300	IPE300	HEB200	HEB240	HEB240	HEB200	2	0.80	4.00	0.628	46.61	0.193	1.665
	2	IPE300	IPE300	IPE300	HEB200	HEB240	HEB240	HEB200				0.465	37.06	0.119	
St273	1	IPE300	IPE300	IPE300	HEB200	HEB240	HEB240	HEB200	2	0.80	2.40	0.628	46.61	0.109	1.000
	2	IPE300	IPE300	IPE300	HEB200	HEB240	HEB240	HEB200				0.465	37.06	0.064	
St274	1	IPE330	IPE330	IPE330	HEB320	HEB360	HEB360	HEB320	3	0.76	6.50	0.392	46.61	0.183	3.033
	2	IPE330	IPE330	IPE330	HEB320	HEB360	HEB360	HEB320				0.519	46.61	0.197	
	3	IPE300	IPE300	IPE300	HEB300	HEB340	HEB340	HEB300				0.404	37.06	0.134	
St275	1	IPE300	IPE300	IPE300	HEB240	HEB300	HEB300	HEB240	3	0.96	4.00	0.536	46.61	0.193	1.312
	2	IPE300	IPE300	IPE300	HEB240	HEB300	HEB300	HEB240				0.631	46.61	0.186	
	3	IPE300	IPE300	IPE300	HEB220	HEB280	HEB280	HEB220				0.42	37.06	0.108	
St276	1	IPE300	IPE300	IPE300	HEB200	HEB260	HEB260	HEB200	3	1.10	3.14	0.669	46.61	0.2	1.000
	2	IPE300	IPE300	IPE300	HEB200	HEB260	HEB260	HEB200				0.661	46.61	0.164	
	3	IPE300	IPE300	IPE300	HEB200	HEB240	HEB240	HEB200				0.396	37.06	0.086	
St277	1	IPE400	IPE400	IPE400	HEB360	HEB400	HEB400	HEB360	4	0.83	6.50	0.319	46.61	0.168	2.981
	2	IPE400	IPE400	IPE400	HEB360	HEB400	HEB400	HEB360				0.443	46.61	0.196	
	3	IPE300	IPE300	IPE300	HEB320	HEB360	HEB360	HEB320				0.485	46.61	0.174	
	4	IPE300	IPE300	IPE300	HEB320	HEB360	HEB360	HEB320				0.427	37.06	0.142	
St278	1	IPE330	IPE330	IPE330	HEB300	HEB360	HEB360	HEB300	4	1.05	4.00	0.422	46.61	0.167	1.696
	2	IPE330	IPE330	IPE330	HEB300	HEB360	HEB360	HEB300				0.601	46.61	0.199	
	3	IPE300	IPE300	IPE300	HEB280	HEB320	HEB320	HEB280				0.553	46.61	0.154	
	4	IPE300	IPE300	IPE300	HEB280	HEB320	HEB320	HEB280				0.39	37.06	0.101	
St279	1	IPE330	IPE330	IPE330	HEB260	HEB300	HEB300	HEB260	4	1.21	3.44	0.596	46.61	0.185	1.000
	2	IPE300	IPE300	IPE300	HEB260	HEB300	HEB300	HEB260				0.802	46.61	0.2	
	3	IPE300	IPE300	IPE300	HEB240	HEB260	HEB260	HEB240				0.742	46.61	0.167	
	4	IPE300	IPE300	IPE300	HEB240	HEB260	HEB260	HEB240				0.442	37.06	0.089	

Table C.20: Frames - Lagos (Soil Type C) Configuration 1

ID	Floor	B1	B2	B3	C1	C2	C3	C4	St.	T_1	q	ISD	Mass	θ_{EC8}	Ω
St280	1	IPE450	IPE450	IPE450	HEB360	HEB450	HEB450	HEB360	5	0.93	6.50	0.277	46.61	0.166	2.869
	2	IPE450	IPE450	IPE450	HEB360	HEB450	HEB450	HEB360				0.383	46.61	0.198	
	3	IPE360	IPE360	IPE360	HEB340	HEB400	HEB400	HEB340				0.459	46.61	0.197	
	4	IPE300	IPE300	IPE300	HEB340	HEB400	HEB400	HEB340				0.509	46.61	0.188	
	5	IPE300	IPE300	IPE300	HEB320	HEB360	HEB360	HEB320				0.434	37.06	0.151	
St281	1	IPE400	IPE400	IPE400	HEB320	HEB360	HEB360	HEB320	5	1.16	4.00	0.365	46.61	0.161	1.853
	2	IPE360	IPE360	IPE360	HEB320	HEB360	HEB360	HEB320				0.523	46.61	0.197	
	3	IPE330	IPE330	IPE330	HEB320	HEB340	HEB340	HEB320				0.567	46.61	0.183	
	4	IPE300	IPE300	IPE300	HEB320	HEB340	HEB340	HEB320				0.518	46.61	0.148	
	5	IPE300	IPE300	IPE300	HEB300	HEB320	HEB320	HEB300				0.383	37.06	0.103	
St282	1	IPE330	IPE330	IPE330	HEB300	HEB360	HEB360	HEB300	5	1.34	3.20	0.505	46.61	0.163	1.000
	2	IPE330	IPE330	IPE330	HEB300	HEB360	HEB360	HEB300				0.753	46.61	0.2	
	3	IPE300	IPE300	IPE300	HEB280	HEB340	HEB340	HEB280				0.761	46.61	0.182	
	4	IPE300	IPE300	IPE300	HEB280	HEB340	HEB340	HEB280				0.633	46.61	0.137	
	5	IPE300	IPE300	IPE300	HEB260	HEB320	HEB320	HEB260				0.413	37.06	0.082	
St283	1	IPE550	IPE550	IPE550	HEB450	HEB550	HEB550	HEB450	8	1.11	6.50	0.207	46.61	0.151	3.070
	2	IPE550	IPE550	IPE550	HEB450	HEB550	HEB550	HEB450				0.284	46.61	0.189	
	3	IPE500	IPE500	IPE500	HEB450	HEB550	HEB550	HEB450				0.309	46.61	0.182	
	4	IPE500	IPE500	IPE500	HEB400	HEB500	HEB500	HEB400				0.343	46.61	0.179	
	5	IPE450	IPE450	IPE450	HEB400	HEB500	HEB500	HEB400				0.363	46.61	0.172	
	6	IPE360	IPE360	IPE360	HEB400	HEB500	HEB500	HEB400				0.423	46.61	0.181	
	7	IPE300	IPE300	IPE300	HEB360	HEB450	HEB450	HEB360				0.467	46.61	0.178	
	8	IPE300	IPE300	IPE300	HEB360	HEB450	HEB450	HEB360				0.408	37.06	0.155	

Table C.20: Frames - Lagos (Soil Type C) Configuration 1

ID	Floor	B1	B2	B3	C1	C2	C3	C4	St.	T_1	q	ISD	Mass	θ_{EC8}	Ω
St284	1	IPE500	IPE500	IPE500	HEB400	HEB450	HEB450	HEB400	8	1.42	4.00	0.297	46.61	0.138	1.822
	2	IPE450	IPE450	IPE450	HEB400	HEB450	HEB450	HEB400				0.443	46.61	0.186	
	3	IPE400	IPE400	IPE400	HEB400	HEB450	HEB450	HEB400				0.532	46.61	0.199	
	4	IPE400	IPE400	IPE400	HEB360	HEB400	HEB400	HEB360				0.59	46.61	0.198	
	5	IPE400	IPE400	IPE400	HEB360	HEB400	HEB400	HEB360				0.553	46.61	0.17	
	6	IPE330	IPE330	IPE330	HEB360	HEB400	HEB400	HEB360				0.539	46.61	0.154	
	7	IPE330	IPE330	IPE330	HEB340	HEB360	HEB360	HEB340				0.488	46.61	0.129	
	8	IPE300	IPE300	IPE300	HEB340	HEB360	HEB360	HEB340				0.357	37.06	0.094	
St285	1	IPE400	IPE400	IPE400	HEB300	HEB400	HEB400	HEB300	8	1.79	2.89	0.421	46.61	0.161	1.000
	2	IPE400	IPE400	IPE400	HEB300	HEB400	HEB400	HEB300				0.587	46.61	0.2	
	3	IPE360	IPE360	IPE360	HEB300	HEB400	HEB400	HEB300				0.641	46.61	0.198	
	4	IPE360	IPE360	IPE360	HEB280	HEB360	HEB360	HEB280				0.7	46.61	0.198	
	5	IPE330	IPE330	IPE330	HEB280	HEB360	HEB360	HEB280				0.695	46.61	0.181	
	6	IPE300	IPE300	IPE300	HEB280	HEB360	HEB360	HEB280				0.677	46.61	0.164	
	7	IPE300	IPE300	IPE300	HEB260	HEB340	HEB340	HEB260				0.558	46.61	0.129	
	8	IPE300	IPE300	IPE300	HEB260	HEB340	HEB340	HEB260				0.357	37.06	0.077	

Table C.21: Frames - Lagos (Soil Type C) Configuration 2

ID	Floor	B1	B2	B3	C1	C2	C3	C4	St.	T_1	q	ISD	Mass	θ_{EC8}	Ω
St286	1	IPE300	IPE360	IPE300	HEB240	HEB300	HEB300	HEB240	2	0.68	6.50	0.488	51.784	0.19	2.489
	2	IPE270	IPE330	IPE270	HEB240	HEB300	HEB300	HEB240				0.51	41.182	0.144	
St287	1	IPE300	IPE360	IPE300	HEB220	HEB260	HEB260	HEB220	2	0.77	4.00	0.58	51.784	0.157	1.522
	2	IPE270	IPE330	IPE270	HEB220	HEB260	HEB260	HEB220				0.505	41.182	0.103	
St288	1	IPE300	IPE360	IPE300	HEB220	HEB260	HEB260	HEB220	2	0.77	2.63	0.58	51.784	0.103	1.310
	2	IPE270	IPE330	IPE270	HEB220	HEB260	HEB260	HEB220				0.505	41.182	0.068	
St289	1	IPE360	IPE400	IPE360	HEB300	HEB360	HEB360	HEB300	3	0.77	6.50	0.4	51.784	0.175	3.374
	2	IPE330	IPE400	IPE300	HEB300	HEB360	HEB360	HEB300				0.506	51.784	0.175	
	3	IPE270	IPE330	IPE270	HEB300	HEB360	HEB360	HEB300				0.429	41.182	0.122	
St290	1	IPE330	IPE360	IPE330	HEB240	HEB300	HEB300	HEB240	3	0.95	4.00	0.534	51.784	0.178	1.598
	2	IPE300	IPE360	IPE300	HEB240	HEB300	HEB300	HEB240				0.604	51.784	0.161	
	3	IPE270	IPE330	IPE270	HEB240	HEB300	HEB300	HEB240				0.438	41.182	0.099	
St291	1	IPE330	IPE360	IPE330	HEB200	HEB280	HEB280	HEB200	3	1.04	2.53	0.624	51.784	0.144	1.000
	2	IPE300	IPE360	IPE300	HEB200	HEB280	HEB280	HEB200				0.623	51.784	0.117	
	3	IPE270	IPE330	IPE270	HEB200	HEB280	HEB280	HEB200				0.417	41.182	0.068	
St292	1	IPE400	IPE450	IPE400	HEB360	HEB450	HEB450	HEB360	4	0.83	6.50	0.316	51.784	0.15	3.187
	2	IPE400	IPE450	IPE400	HEB360	HEB450	HEB450	HEB360				0.452	51.784	0.174	
	3	IPE330	IPE360	IPE330	HEB320	HEB400	HEB400	HEB320				0.458	51.784	0.152	
	4	IPE270	IPE330	IPE270	HEB320	HEB400	HEB400	HEB320				0.433	41.182	0.12	
St293	1	IPE360	IPE400	IPE360	HEB240	HEB340	HEB340	HEB240	4	1.07	4.00	0.488	51.784	0.184	1.899
	2	IPE360	IPE400	IPE360	HEB240	HEB340	HEB340	HEB240				0.573	51.784	0.179	
	3	IPE330	IPE360	IPE330	HEB220	HEB320	HEB320	HEB220				0.501	51.784	0.139	
	4	IPE270	IPE330	IPE270	HEB220	HEB320	HEB320	HEB220				0.374	41.182	0.091	
St294	1	IPE330	IPE360	IPE330	HEB220	HEB300	HEB300	HEB220	4	1.30	2.95	0.66	51.784	0.18	1.000
	2	IPE300	IPE360	IPE300	HEB220	HEB300	HEB300	HEB220				0.763	51.784	0.173	
	3	IPE300	IPE360	IPE300	HEB200	HEB260	HEB260	HEB200				0.73	51.784	0.146	
	4	IPE270	IPE330	IPE270	HEB200	HEB260	HEB260	HEB200				0.47	41.182	0.083	

Table C.21: Frames - Lagos (Soil Type C) Configuration 2

ID	Floor	B1	B2	B3	C1	C2	C3	C4	St.	T_1	q	ISD	Mass	θ_{EC8}	Ω
St295	1	IPE450	IPE500	IPE450	HEB360	HEB500	HEB500	HEB360	5	0.91	6.50	0.279	51.784	0.147	3.271
	2	IPE450	IPE500	IPE450	HEB360	HEB500	HEB500	HEB360				0.395	51.784	0.174	
	3	IPE400	IPE450	IPE400	HEB340	HEB450	HEB450	HEB340				0.427	51.784	0.164	
	4	IPE330	IPE360	IPE330	HEB340	HEB450	HEB450	HEB340				0.445	51.784	0.15	
	5	IPE270	IPE330	IPE270	HEB320	HEB400	HEB400	HEB320				0.425	41.182	0.124	
St296	1	IPE400	IPE450	IPE400	HEB280	HEB360	HEB360	HEB280	5	1.20	4.00	0.484	51.784	0.174	1.414
	2	IPE400	IPE450	IPE400	HEB280	HEB360	HEB360	HEB280				0.593	51.784	0.181	
	3	IPE330	IPE360	IPE330	HEB260	HEB340	HEB340	HEB260				0.656	51.784	0.176	
	4	IPE300	IPE360	IPE300	HEB260	HEB340	HEB340	HEB260				0.639	51.784	0.152	
	5	IPE270	IPE330	IPE270	HEB220	HEB300	HEB300	HEB220				0.492	41.182	0.105	
St297	1	IPE360	IPE360	IPE360	HEB240	HEB320	HEB320	HEB240	5	1.45	3.00	0.618	51.784	0.2	1.000
	2	IPE360	IPE360	IPE360	HEB240	HEB320	HEB320	HEB240				0.758	51.784	0.2	
	3	IPE330	IPE360	IPE330	HEB200	HEB280	HEB280	HEB200				0.799	51.784	0.196	
	4	IPE300	IPE360	IPE300	HEB200	HEB280	HEB280	HEB200				0.646	51.784	0.144	
	5	IPE270	IPE330	IPE270	HEB200	HEB260	HEB260	HEB200				0.431	41.182	0.087	
St298	1	IPE550	IPE600	IPE550	HEB500	HEB600	HEB600	HEB500	8	1.12	6.50	0.197	51.784	0.129	3.220
	2	IPE550	IPE600	IPE550	HEB500	HEB600	HEB600	HEB500				0.291	51.784	0.167	
	3	IPE500	IPE550	IPE500	HEB500	HEB600	HEB600	HEB500				0.321	51.784	0.167	
	4	IPE500	IPE550	IPE500	HEB450	HEB550	HEB550	HEB450				0.354	51.784	0.167	
	5	IPE450	IPE500	IPE450	HEB450	HEB550	HEB550	HEB450				0.377	51.784	0.161	
	6	IPE360	IPE400	IPE360	HEB450	HEB550	HEB550	HEB450				0.431	51.784	0.168	
	7	IPE330	IPE360	IPE330	HEB400	HEB450	HEB450	HEB400				0.461	51.784	0.165	
	8	IPE270	IPE330	IPE270	HEB400	HEB450	HEB450	HEB400				0.421	41.182	0.134	

Table C.21: Frames - Lagos (Soil Type C) Configuration 2

ID	Floor	B1	B2	B3	C1	C2	C3	C4	St.	T_1	q	ISD	Mass	θ_{EC8}	Ω
St299	1	IPE500	IPE500	IPE500	HEB360	HEB450	HEB450	HEB360	8	1.43	4.00	0.35	51.784	0.15	1.499
	2	IPE500	IPE500	IPE500	HEB360	HEB450	HEB450	HEB360				0.454	51.784	0.173	
	3	IPE450	IPE500	IPE450	HEB360	HEB450	HEB450	HEB360				0.474	51.784	0.164	
	4	IPE450	IPE500	IPE450	HEB340	HEB400	HEB400	HEB340				0.509	51.784	0.161	
	5	IPE400	IPE450	IPE400	HEB340	HEB400	HEB400	HEB340				0.523	51.784	0.151	
	6	IPE330	IPE360	IPE330	HEB340	HEB400	HEB400	HEB340				0.582	51.784	0.155	
	7	IPE300	IPE360	IPE300	HEB320	HEB360	HEB360	HEB320				0.575	51.784	0.143	
	8	IPE270	IPE330	IPE270	HEB320	HEB360	HEB360	HEB320				0.457	41.182	0.103	
St300	1	IPE450	IPE450	IPE450	HEB360	HEB400	HEB400	HEB360	8	1.69	3.20	0.389	51.784	0.157	1.000
	2	IPE450	IPE450	IPE450	HEB360	HEB400	HEB400	HEB360				0.536	51.784	0.191	
	3	IPE400	IPE400	IPE400	HEB360	HEB400	HEB400	HEB360				0.587	51.784	0.19	
	4	IPE400	IPE400	IPE400	HEB340	HEB400	HEB400	HEB340				0.636	51.784	0.187	
	5	IPE330	IPE360	IPE330	HEB340	HEB400	HEB400	HEB340				0.679	51.784	0.184	
	6	IPE300	IPE360	IPE300	HEB340	HEB400	HEB400	HEB340				0.699	51.784	0.174	
	7	IPE300	IPE360	IPE300	HEB300	HEB320	HEB320	HEB300				0.603	51.784	0.142	
	8	IPE270	IPE330	IPE270	HEB300	HEB320	HEB320	HEB300				0.423	41.182	0.091	

Table C.22: Frames - Lagos (Soil Type C) Configuration 3

ID	Floor	B1	B2	B3	C1	C2	C3	C4	St.	T_1	q	ISD	Mass	θ_{EC8}	Ω
St301	1	IPE450	IPE450	IPE450	HEB260	HEB400	HEB400	HEB260	2	0.57	6.50	0.413	82.854	0.142	3.512
	2	IPE400	IPE400	IPE400	HEB260	HEB400	HEB400	HEB260				0.396	65.892	0.099	
St302	1	IPE450	IPE450	IPE450	HEB260	HEB400	HEB400	HEB260	2	0.57	4.00	0.413	82.854	0.087	2.161
	2	IPE400	IPE400	IPE400	HEB260	HEB400	HEB400	HEB260				0.396	65.892	0.061	
St303	1	IPE450	IPE450	IPE450	HEB260	HEB400	HEB400	HEB260	2	0.57	1.85	0.413	82.854	0.04	1.000
	2	IPE400	IPE400	IPE400	HEB260	HEB400	HEB400	HEB260				0.396	65.892	0.028	
St304	1	IPE450	IPE450	IPE450	HEB300	HEB450	HEB450	HEB300	3	0.75	6.50	0.418	82.854	0.181	2.838
	2	IPE450	IPE450	IPE450	HEB300	HEB450	HEB450	HEB300				0.492	82.854	0.169	
	3	IPE400	IPE400	IPE400	HEB300	HEB450	HEB450	HEB300				0.353	65.892	0.102	
St305	1	IPE450	IPE450	IPE450	HEB260	HEB400	HEB400	HEB260	3	0.81	4.00	0.483	82.854	0.14	1.717
	2	IPE450	IPE450	IPE450	HEB260	HEB400	HEB400	HEB260				0.508	82.854	0.119	
	3	IPE400	IPE400	IPE400	HEB260	HEB400	HEB400	HEB260				0.336	65.892	0.067	
St306	1	IPE450	IPE450	IPE450	HEB260	HEB400	HEB400	HEB260	3	0.81	2.33	0.483	82.854	0.082	1.000
	2	IPE450	IPE450	IPE450	HEB260	HEB400	HEB400	HEB260				0.508	82.854	0.069	
	3	IPE400	IPE400	IPE400	HEB260	HEB400	HEB400	HEB260				0.336	65.892	0.039	
St307	1	IPE500	IPE500	IPE500	HEB450	HEB550	HEB550	HEB450	4	0.83	6.50	0.311	82.854	0.151	2.897
	2	IPE450	IPE450	IPE450	HEB450	HEB550	HEB550	HEB450				0.496	82.854	0.193	
	3	IPE450	IPE450	IPE450	HEB400	HEB450	HEB450	HEB400				0.477	82.854	0.161	
	4	IPE400	IPE400	IPE400	HEB400	HEB450	HEB450	HEB400				0.357	65.892	0.102	
St308	1	IPE450	IPE450	IPE450	HEB300	HEB400	HEB400	HEB300	4	1.04	4.00	0.479	82.854	0.178	1.604
	2	IPE450	IPE450	IPE450	HEB300	HEB400	HEB400	HEB300				0.583	82.854	0.178	
	3	IPE450	IPE450	IPE450	HEB260	HEB340	HEB340	HEB260				0.494	82.854	0.136	
	4	IPE400	IPE400	IPE400	HEB260	HEB340	HEB340	HEB260				0.302	65.892	0.073	
St309	1	IPE450	IPE450	IPE450	HEB280	HEB400	HEB400	HEB280	4	1.06	2.66	0.496	82.854	0.124	1.000
	2	IPE450	IPE450	IPE450	HEB280	HEB400	HEB400	HEB280				0.588	82.854	0.122	
	3	IPE450	IPE450	IPE450	HEB260	HEB340	HEB340	HEB260				0.486	82.854	0.091	
	4	IPE400	IPE400	IPE400	HEB260	HEB340	HEB340	HEB260				0.296	65.892	0.048	

Table C.22: Frames - Lagos (Soil Type C) Configuration 3

ID	Floor	B1	B2	B3	C1	C2	C3	C4	St.	T_1	q	ISD	Mass	θ_{EC8}	Ω
St310	1	IPE600	IPE600	IPE600	HEB500	HEB600	HEB600	HEB500	5	0.89	6.50	0.245	82.854	0.128	2.937
	2	IPE550	IPE550	IPE550	HEB500	HEB600	HEB600	HEB500				0.387	82.854	0.167	
	3	IPE450	IPE450	IPE450	HEB450	HEB500	HEB500	HEB450				0.487	82.854	0.181	
	4	IPE450	IPE450	IPE450	HEB450	HEB500	HEB500	HEB450				0.477	82.854	0.155	
	5	IPE400	IPE400	IPE400	HEB340	HEB400	HEB400	HEB340				0.38	65.892	0.108	
St311	1	IPE500	IPE500	IPE500	HEB400	HEB500	HEB500	HEB400	5	1.11	4.00	0.351	82.854	0.138	1.630
	2	IPE450	IPE450	IPE450	HEB400	HEB500	HEB500	HEB400				0.544	82.854	0.178	
	3	IPE450	IPE450	IPE450	HEB360	HEB400	HEB400	HEB360				0.551	82.854	0.16	
	4	IPE450	IPE450	IPE450	HEB360	HEB400	HEB400	HEB360				0.429	82.854	0.113	
	5	IPE400	IPE400	IPE400	HEB320	HEB360	HEB360	HEB320				0.307	65.892	0.072	
St312	1	IPE450	IPE450	IPE450	HEB300	HEB450	HEB450	HEB300	5	1.24	3.12	0.536	82.854	0.156	1.000
	2	IPE450	IPE450	IPE450	HEB330	HEB450	HEB450	HEB300				0.719	82.854	0.177	
	3	IPE450	IPE450	IPE450	HEB300	HEB400	HEB400	HEB300				0.647	82.854	0.143	
	4	IPE450	IPE450	IPE450	HEB300	HEB400	HEB400	HEB300				0.471	82.854	0.096	
	5	IPE400	IPE400	IPE400	HEB280	HEB360	HEB360	HEB280				0.308	65.892	0.057	
St313	1	HEA600	HEA600	HEA600	HEM500	HEM650	HEM650	HEM500	8	1.11	6.50	0.198	82.854	0.129	2.798
	2	HEA600	HEA600	HEA600	HEM500	HEM650	HEM650	HEM500				0.288	82.854	0.165	
	3	HEA600	HEA600	HEA600	HEM500	HEM650	HEM650	HEM500				0.297	82.854	0.154	
	4	IPE600	IPE600	IPE600	HEM450	HEM600	HEM600	HEM450				0.344	82.854	0.161	
	5	IPE500	IPE500	IPE500	HEM450	HEM600	HEM600	HEM450				0.417	82.854	0.177	
	6	IPE500	IPE500	IPE500	HEM450	HEM600	HEM600	HEM450				0.447	82.854	0.172	
	7	IPE400	IPE400	IPE400	HEB450	HEB600	HEB600	HEB450				0.445	82.854	0.159	
	8	IPE360	IPE360	IPE360	HEB450	HEB600	HEB600	HEB450				0.413	65.892	0.129	

Table C.22: Frames - Lagos (Soil Type C) Configuration 3

ID	Floor	B1	B2	B3	C1	C2	C3	C4	St.	T_1	q	ISD	Mass	θ_{EC8}	Ω
St314	1	IPE600	IPE600	IPE600	HEB400	HEB600	HEB600	HEB400	8	1.43	4.00	0.321	82.854	0.14	1.224
	2	IPE600	IPE600	IPE600	HEB400	HEB600	HEB600	HEB400				0.443	82.854	0.17	
	3	IPE550	IPE550	IPE550	HEB400	HEB600	HEB600	HEB400				0.487	82.854	0.17	
	4	IPE500	IPE500	IPE500	HEB360	HEB550	HEB550	HEB360				0.574	82.854	0.182	
	5	IPE500	IPE500	IPE500	HEB360	HEB550	HEB550	HEB360				0.59	82.854	0.171	
	6	IPE400	IPE400	IPE400	HEB360	HEB550	HEB550	HEB360				0.602	82.854	0.161	
	7	IPE400	IPE400	IPE400	HEB340	HEB500	HEB500	HEB340				0.557	82.854	0.139	
	8	IPE360	IPE360	IPE360	HEB340	HEB500	HEB500	HEB340				0.429	65.892	0.097	
St315	1	IPE500	IPE500	IPE500	HEB450	HEB550	HEB550	HEB450	8	1.68	3.00	0.379	82.854	0.145	1.000
	2	IPE500	IPE500	IPE500	HEB450	HEB550	HEB550	HEB450				0.597	82.854	0.2	
	3	IPE500	IPE500	IPE500	HEB450	HEB550	HEB550	HEB450				0.617	82.854	0.19	
	4	IPE450	IPE450	IPE450	HEB400	HEB500	HEB500	HEB400				0.661	82.854	0.186	
	5	IPE450	IPE450	IPE450	HEB400	HEB500	HEB500	HEB400				0.653	82.854	0.17	
	6	IPE400	IPE400	IPE400	HEB400	HEB500	HEB500	HEB400				0.603	82.854	0.146	
	7	IPE400	IPE400	IPE400	HEB340	HEB450	HEB450	HEB340				0.504	82.854	0.117	
	8	IPE360	IPE360	IPE360	HEB340	HEB450	HEB450	HEB340				0.366	65.892	0.076	

Table C.23: Frames - Lagos (Soil Type C) Configuration 4

ID	Floor	B1	B2	B3	B4	C1	C2	C3	C4	C5	St.	T_1	q	ISD	Mass	θ_{EC8}	Ω
St316	1	IPE330	IPE330	IPE330	IPE330	HEB260	HEB280	HEB280	HEB280	HEB260	2	0.66	6.50	0.504	69.91	0.170	3.418
	2	IPE330	IPE330	IPE330	IPE330	HEB260	HEB280	HEB280	HEB280	HEB260				0.426	55.59	0.109	
St317	1	IPE330	IPE330	IPE330	IPE330	HEB240	HEB260	HEB260	HEB260	HEB240	2	0.71	4.00	0.557	69.91	0.125	2.153
	2	IPE330	IPE330	IPE330	IPE330	HEB240	HEB260	HEB260	HEB260	HEB240				0.424	55.59	0.073	
St318	1	IPE330	IPE330	IPE330	IPE330	HEB240	HEB260	HEB260	HEB260	HEB240	2	0.71	1.86	0.557	69.91	0.058	1.000
	2	IPE330	IPE330	IPE330	IPE330	HEB240	HEB260	HEB260	HEB260	HEB240				0.424	55.59	0.034	
St319	1	IPE360	IPE360	IPE360	IPE360	HEB300	HEB320	HEB320	HEB320	HEB300	3	0.79	6.50	0.448	69.91	0.183	3.451
	2	IPE360	IPE360	IPE360	IPE360	HEB300	HEB320	HEB320	HEB320	HEB300				0.503	69.91	0.164	
	3	IPE300	IPE300	IPE300	IPE300	HEB280	HEB280	HEB280	HEB280	HEB280				0.398	55.59	0.109	
St320	1	IPE330	IPE330	IPE330	IPE330	HEB240	HEB280	HEB280	HEB280	HEB240	3	0.98	4.00	0.587	69.91	0.180	1.692
	2	IPE330	IPE330	IPE330	IPE330	HEB240	HEB280	HEB280	HEB280	HEB240				0.590	69.91	0.148	
	3	IPE300	IPE300	IPE300	IPE300	HEB220	HEB260	HEB260	HEB260	HEB220				0.374	55.59	0.081	
St321	1	IPE300	IPE300	IPE300	IPE300	HEB220	HEB260	HEB260	HEB260	HEB220	3	1.13	3.27	0.684	69.91	0.198	1.000
	2	IPE300	IPE300	IPE300	IPE300	HEB220	HEB260	HEB260	HEB260	HEB220				0.694	69.91	0.164	
	3	IPE300	IPE300	IPE300	IPE300	HEB220	HEB260	HEB260	HEB260	HEB220				0.404	55.59	0.084	
St322	1	IPE400	IPE400	IPE400	IPE400	HEB360	HEB400	HEB400	HEB400	HEB360	4	0.85	6.50	0.354	69.91	0.156	3.827
	2	IPE400	IPE400	IPE400	IPE400	HEB360	HEB400	HEB400	HEB400	HEB360				0.471	69.91	0.170	
	3	IPE360	IPE360	IPE360	IPE360	HEB340	HEB340	HEB340	HEB340	HEB340				0.444	69.91	0.139	
	4	IPE300	IPE300	IPE300	IPE300	HEB340	HEB340	HEB340	HEB340	HEB340				0.363	55.59	0.098	
St323	1	IPE360	IPE360	IPE360	IPE360	HEB280	HEB300	HEB300	HEB300	HEB280	4	1.11	4.00	0.515	69.91	0.179	1.960
	2	IPE360	IPE360	IPE360	IPE360	HEB280	HEB300	HEB300	HEB300	HEB280				0.590	69.91	0.171	
	3	IPE330	IPE330	IPE330	IPE330	HEB260	HEB280	HEB280	HEB280	HEB260				0.511	69.91	0.131	
	4	IPE300	IPE300	IPE300	IPE300	HEB260	HEB280	HEB280	HEB280	HEB260				0.351	55.59	0.079	
St324	1	IPE330	IPE330	IPE330	IPE330	HEB240	HEB280	HEB280	HEB280	HEB240	4	1.30	3.10	0.757	69.91	0.200	1.000
	2	IPE330	IPE330	IPE330	IPE330	HEB240	HEB280	HEB280	HEB280	HEB240				0.818	69.91	0.185	
	3	IPE300	IPE300	IPE300	IPE300	HEB220	HEB260	HEB260	HEB260	HEB220				0.634	69.91	0.129	
	4	IPE300	IPE300	IPE300	IPE300	HEB220	HEB260	HEB260	HEB260	HEB220				0.370	55.59	0.068	

Table C.23: Frames - Lagos (Soil Type C) Configuration 4

ID	Floor	B1	B2	B3	B4	C1	C2	C3	C4	C5	St.	T_1	q	ISD	Mass	θ_{EC8}	Ω
St325	1	IPE450	IPE450	IPE450	IPE450	HEB360	HEB450	HEB450	HEB450	HEB360	5	0.97	6.50	0.299	69.91	0.150	3.442
	2	IPE450	IPE450	IPE450	IPE450	HEB360	HEB450	HEB450	HEB450	HEB360				0.410	69.91	0.173	
	3	IPE360	IPE360	IPE360	IPE360	HEB340	HEB400	HEB400	HEB400	HEB340				0.483	69.91	0.176	
	4	IPE330	IPE330	IPE330	IPE330	HEB340	HEB400	HEB400	HEB400	HEB340				0.497	69.91	0.159	
	5	IPE300	IPE300	IPE300	IPE300	HEB320	HEB360	HEB360	HEB360	HEB320				0.409	55.59	0.115	
St326	1	IPE400	IPE400	IPE400	IPE400	HEB280	HEB340	HEB340	HEB340	HEB280	5	1.24	4.00	0.513	69.91	0.170	1.555
	2	IPE400	IPE400	IPE400	IPE400	HEB280	HEB340	HEB340	HEB340	HEB280				0.611	69.91	0.172	
	3	IPE330	IPE330	IPE330	IPE330	HEB260	HEB320	HEB320	HEB320	HEB260				0.673	69.91	0.167	
	4	IPE300	IPE300	IPE300	IPE300	HEB260	HEB320	HEB320	HEB320	HEB260				0.659	69.91	0.145	
	5	IPE300	IPE300	IPE300	IPE300	HEB240	HEB300	HEB300	HEB300	HEB240				0.466	55.59	0.093	
St327	1	IPE360	IPE360	IPE360	IPE360	HEB260	HEB320	HEB320	HEB320	HEB260	5	1.42	3.40	0.583	69.91	0.187	1.000
	2	IPE360	IPE360	IPE360	IPE360	HEB260	HEB320	HEB320	HEB320	HEB260				0.725	69.91	0.197	
	3	IPE300	IPE300	IPE300	IPE300	HEB240	HEB300	HEB300	HEB300	HEB240				0.789	69.91	0.189	
	4	IPE300	IPE300	IPE300	IPE300	HEB240	HEB280	HEB280	HEB280	HEB240				0.705	69.91	0.152	
	5	IPE300	IPE300	IPE300	IPE300	HEB220	HEB280	HEB280	HEB280	HEB220				0.446	55.59	0.088	
St328	1	IPE550	IPE550	IPE550	IPE550	HEB400	HEB500	HEB500	HEB500	HEB400	8	1.21	6.50	0.291	69.91	0.156	2.525
	2	IPE550	IPE550	IPE550	IPE550	HEB400	HEB500	HEB500	HEB500	HEB400				0.366	69.91	0.175	
	3	IPE500	IPE500	IPE500	IPE500	HEB400	HEB500	HEB500	HEB500	HEB400				0.390	69.91	0.169	
	4	IPE500	IPE500	IPE500	IPE500	HEB360	HEB450	HEB450	HEB450	HEB360				0.434	69.91	0.170	
	5	IPE450	IPE450	IPE450	IPE450	HEB360	HEB450	HEB450	HEB450	HEB360				0.453	69.91	0.162	
	6	IPE360	IPE360	IPE360	IPE360	HEB360	HEB450	HEB450	HEB450	HEB360				0.528	69.91	0.172	
	7	IPE300	IPE300	IPE300	IPE300	HEB340	HEB400	HEB400	HEB400	HEB340				0.587	69.91	0.176	
	8	IPE300	IPE300	IPE300	IPE300	HEB340	HEB400	HEB400	HEB400	HEB340				0.490	55.59	0.132	

Table C.23: Frames - Lagos (Soil Type C) Configuration 4

ID	Floor	B1	B2	B3	B4	C1	C2	C3	C4	C5	St.	T_1	q	ISD	Mass	θ_{EC8}	Ω
St329	1	IPE500	IPE500	IPE500	IPE500	HEB300	HEB450	HEB450	HEB450	HEB300	8	1.54	4.00	0.348	69.91	0.144	1.526
	2	IPE450	IPE450	IPE450	IPE450	HEB300	HEB450	HEB450	HEB450	HEB300				0.469	69.91	0.173	
	3	IPE450	IPE450	IPE450	IPE450	HEB300	HEB450	HEB450	HEB450	HEB300				0.511	69.91	0.170	
	4	IPE400	IPE400	IPE400	IPE400	HEB280	HEB400	HEB400	HEB400	HEB280				0.589	69.91	0.178	
	5	IPE360	IPE360	IPE360	IPE360	HEB280	HEB400	HEB400	HEB400	HEB280				0.654	69.91	0.180	
	6	IPE330	IPE330	IPE330	IPE330	HEB280	HEB400	HEB400	HEB400	HEB280				0.669	69.91	0.170	
	7	IPE300	IPE300	IPE300	IPE300	HEB260	HEB360	HEB360	HEB360	HEB260				0.613	69.91	0.145	
	8	IPE300	IPE300	IPE300	IPE300	HEB260	HEB360	HEB360	HEB360	HEB260				0.433	55.59	0.095	
St330	1	IPE400	IPE400	IPE400	IPE400	HEB300	HEB360	HEB360	HEB360	HEB300	8	1.92	2.67	0.493	69.91	0.167	1.000
	2	IPE400	IPE400	IPE400	IPE400	HEB300	HEB360	HEB360	HEB360	HEB300				0.648	69.91	0.195	
	3	IPE360	IPE360	IPE360	IPE360	HEB300	HEB360	HEB360	HEB360	HEB300				0.693	69.91	0.190	
	4	IPE360	IPE360	IPE360	IPE360	HEB280	HEB340	HEB340	HEB340	HEB280				0.739	69.91	0.186	
	5	IPE330	IPE330	IPE330	IPE330	HEB280	HEB340	HEB340	HEB340	HEB280				0.714	69.91	0.167	
	6	IPE330	IPE330	IPE330	IPE330	HEB280	HEB340	HEB340	HEB340	HEB280				0.639	69.91	0.140	
	7	IPE300	IPE300	IPE300	IPE300	HEB260	HEB320	HEB320	HEB320	HEB260				0.512	69.91	0.107	
	8	IPE300	IPE300	IPE300	IPE300	HEB260	HEB320	HEB320	HEB320	HEB260				0.341	55.59	0.066	

Table C.24: Frames - Lagos (Soil Type C) Configuration 5

ID	Floor	B1	B2	B3	C1	C2	C3	C4	St.	T_1	q	ISD	Mass	θ_{EC8}	Ω
St331	1	IPE360	IPE300	IPE360	HEB260	HEB300	HEB300	HEB260	2	0.67	6.50	0.486	56.96	0.187	3.098
	2	IPE330	IPE300	IPE330	HEB260	HEB300	HEB300	HEB260				0.49	45.3	0.137	
St332	1	IPE360	IPE300	IPE360	HEB240	HEB260	HEB260	HEB240	2	0.75	4.00	0.57	56.96	0.151	2.029
	2	IPE330	IPE300	IPE330	HEB240	HEB260	HEB260	HEB240				0.488	45.3	0.097	
St333	1	IPE360	IPE300	IPE360	HEB240	HEB260	HEB260	HEB240	2	0.75	2.18	0.57	56.96	0.083	1.000
	2	IPE330	IPE300	IPE330	HEB240	HEB260	HEB260	HEB240				0.488	45.3	0.053	
St334	1	IPE400	IPE360	IPE400	HEB320	HEB360	HEB360	HEB320	3	0.76	6.50	0.408	56.96	0.179	3.230
	2	IPE400	IPE360	IPE400	HEB320	HEB360	HEB360	HEB320				0.501	56.96	0.173	
	3	IPE330	IPE300	IPE330	HEB280	HEB300	HEB300	HEB280				0.42	45.3	0.12	
St335	1	IPE360	IPE300	IPE360	HEB260	HEB300	HEB300	HEB260	3	0.98	4.00	0.546	56.96	0.188	1.416
	2	IPE360	IPE300	IPE360	HEB260	HEB300	HEB300	HEB260				0.627	56.96	0.172	
	3	IPE330	IPE300	IPE330	HEB220	HEB260	HEB260	HEB220				0.48	45.3	0.112	
St336	1	IPE360	IPE300	IPE360	HEB260	HEB280	HEB280	HEB260	3	1.01	2.73	0.582	56.96	0.142	1.000
	2	IPE360	IPE300	IPE360	HEB260	HEB280	HEB280	HEB260				0.636	56.96	0.124	
	3	IPE330	IPE300	IPE330	HEB220	HEB240	HEB240	HEB220				0.458	45.3	0.077	
St337	1	IPE450	IPE450	IPE450	HEB340	HEB450	HEB450	HEB340	4	0.83	6.50	0.328	56.96	0.158	3.135
	2	IPE450	IPE450	IPE450	HEB340	HEB450	HEB450	HEB340				0.446	56.96	0.175	
	3	IPE360	IPE330	IPE360	HEB320	HEB400	HEB400	HEB320				0.469	56.96	0.158	
	4	IPE330	IPE300	IPE330	HEB320	HEB400	HEB400	HEB320				0.426	45.3	0.12	
St338	1	IPE400	IPE360	IPE400	HEB320	HEB340	HEB340	HEB320	4	1.06	4.00	0.437	56.96	0.164	1.979
	2	IPE400	IPE360	IPE400	HEB320	HEB340	HEB340	HEB320				0.579	56.96	0.176	
	3	IPE360	IPE300	IPE360	HEB260	HEB280	HEB280	HEB260				0.584	56.96	0.156	
	4	IPE330	IPE300	IPE330	HEB260	HEB280	HEB280	HEB260				0.419	45.3	0.096	
St339	1	IPE400	IPE300	IPE400	HEB260	HEB300	HEB300	HEB260	4	1.25	3.25	0.647	56.96	0.196	1.000
	2	IPE360	IPE300	IPE360	HEB260	HEB300	HEB300	HEB260				0.807	56.96	0.2	
	3	IPE360	IPE300	IPE360	HEB220	HEB280	HEB280	HEB220				0.722	56.96	0.16	
	4	IPE330	IPE300	IPE330	HEB220	HEB280	HEB280	HEB220				0.437	45.3	0.086	

Table C.24: Frames - Lagos (Soil Type C) Configuration 5

ID	Floor	B1	B2	B3	C1	C2	C3	C4	St.	T_1	q	ISD	Mass	θ_{EC8}	Ω
St340	1	IPE500	IPE500	IPE500	HEB340	HEB450	HEB450	HEB340	5	0.94	6.50	0.318	56.96	0.174	3.354
	2	IPE500	IPE500	IPE500	HEB340	HEB450	HEB450	HEB340				0.401	56.96	0.184	
	3	IPE450	IPE450	IPE450	HEB320	HEB400	HEB400	HEB320				0.424	56.96	0.171	
	4	IPE360	IPE330	IPE360	HEB320	HEB400	HEB400	HEB320				0.444	56.96	0.158	
	5	IPE330	IPE300	IPE330	HEB300	HEB360	HEB360	HEB300				0.405	45.3	0.125	
St341	1	IPE450	IPE400	IPE450	HEB320	HEB400	HEB400	HEB320	5	1.19	4.00	0.436	56.96	0.156	1.229
	2	IPE450	IPE360	IPE450	HEB320	HEB400	HEB400	HEB320				0.609	56.96	0.183	
	3	IPE360	IPE300	IPE360	HEB300	HEB360	HEB360	HEB300				0.704	56.96	0.184	
	4	IPE360	IPE300	IPE360	HEB300	HEB360	HEB360	HEB300				0.66	56.96	0.154	
	5	IPE330	IPE300	IPE330	HEB280	HEB320	HEB320	HEB280				0.476	45.3	0.099	
St342	1	IPE400	IPE330	IPE400	HEB300	HEB340	HEB340	HEB300	5	1.38	3.00	0.558	56.96	0.176	1.000
	2	IPE400	IPE330	IPE400	HEB300	HEB340	HEB340	HEB300				0.757	56.96	0.2	
	3	IPE360	IPE300	IPE360	HEB280	HEB320	HEB320	HEB280				0.751	56.96	0.178	
	4	IPE360	IPE300	IPE360	HEB280	HEB320	HEB320	HEB280				0.619	56.96	0.133	
	5	IPE330	IPE300	IPE330	HEB260	HEB280	HEB280	HEB260				0.422	45.3	0.082	
St343	1	IPE600	IPE600	IPE600	HEB500	HEB600	HEB600	HEB500	8	1.12	6.50	0.203	56.96	0.133	3.000
	2	IPE600	IPE600	IPE600	HEB500	HEB600	HEB600	HEB500				0.286	56.96	0.165	
	3	IPE600	IPE550	IPE600	HEB500	HEB600	HEB600	HEB500				0.298	56.96	0.155	
	4	IPE550	IPE500	IPE550	HEB450	HEB550	HEB550	HEB450				0.342	56.96	0.163	
	5	IPE500	IPE450	IPE500	HEB450	HEB550	HEB550	HEB450				0.394	56.96	0.168	
	6	IPE400	IPE360	IPE400	HEB450	HEB550	HEB550	HEB450				0.46	56.96	0.178	
	7	IPE360	IPE300	IPE360	HEB400	HEB500	HEB500	HEB400				0.489	56.96	0.173	
	8	IPE330	IPE300	IPE330	HEB400	HEB500	HEB500	HEB400				0.437	45.3	0.137	

Table C.24: Frames - Lagos (Soil Type C) Configuration 5

ID	Floor	B1	B2	B3	C1	C2	C3	C4	St.	T_1	q	ISD	Mass	θ_{EC8}	Ω
St344	1	IPE550	IPE500	IPE550	HEB360	HEB500	HEB500	HEB360	8	1.44	4.00	0.323	56.96	0.14	1.383
	2	IPE550	IPE500	IPE550	HEB360	HEB500	HEB500	HEB360				0.431	56.96	0.166	
	3	IPE500	IPE450	IPE500	HEB360	HEB500	HEB500	HEB360				0.469	56.96	0.163	
	4	IPE500	IPE450	IPE500	HEB340	HEB450	HEB450	HEB340				0.526	56.96	0.166	
	5	IPE400	IPE360	IPE400	HEB340	HEB450	HEB450	HEB340				0.601	56.96	0.173	
	6	IPE360	IPE330	IPE360	HEB340	HEB450	HEB450	HEB340				0.671	56.96	0.176	
	7	IPE360	IPE300	IPE360	HEB320	HEB400	HEB400	HEB320				0.603	56.96	0.148	
	8	IPE330	IPE300	IPE330	HEB320	HEB400	HEB400	HEB320				0.448	45.3	0.1	
St345	1	IPE450	IPE450	IPE450	HEB320	HEB400	HEB400	HEB320	8	1.80	2.80	0.449	56.96	0.168	1.000
	2	IPE450	IPE450	IPE450	HEB320	HEB400	HEB400	HEB320				0.6	56.96	0.199	
	3	IPE450	IPE400	IPE450	HEB320	HEB400	HEB400	HEB320				0.613	56.96	0.186	
	4	IPE400	IPE360	IPE400	HEB300	HEB360	HEB360	HEB300				0.693	56.96	0.192	
	5	IPE400	IPE330	IPE400	HEB300	HEB360	HEB360	HEB300				0.706	56.96	0.181	
	6	IPE360	IPE300	IPE360	HEB300	HEB360	HEB360	HEB300				0.661	56.96	0.157	
	7	IPE360	IPE300	IPE360	HEB260	HEB320	HEB320	HEB260				0.556	56.96	0.127	
	8	IPE330	IPE300	IPE330	HEB260	HEB320	HEB320	HEB260				0.357	45.3	0.074	

Table C.25: Frames - Lagos (Soil Type C) Configuration 6

ID	Floor	B1	B2	B3	B4	B5	C1=C6	C2=C5	C3=C4	St.	T_1	q	ISD	Mass	θ_{EC8}	Ω
St346	1	IPE450	IPE450	IPE450	IPE450	IPE450	HEB300	HEB360	HEB340	2	0.64	6.50	0.514	165.708	0.162	3.000
	2	IPE400	IPE400	IPE400	IPE400	IPE400	HEB300	HEB360	HEB340				0.476	131.784	0.108	
St347	1	IPE450	IPE450	IPE450	IPE450	IPE450	HEB300	HEB360	HEB340	2	0.64	4.00	0.514	165.708	0.1	1.846
	2	IPE400	IPE400	IPE400	IPE400	IPE400	HEB300	HEB360	HEB340				0.476	131.784	0.067	
St348	1	IPE450	IPE450	IPE450	IPE450	IPE450	HEB300	HEB360	HEB340	2	0.64	2.28	0.514	165.708	0.057	1.000
	2	IPE400	IPE400	IPE400	IPE400	IPE400	HEB300	HEB360	HEB340				0.476	131.784	0.038	
St349	1	IPE450	IPE450	IPE450	IPE450	IPE450	HEB360	HEB450	HEB400	3	0.81	6.50	0.462	165.708	0.183	2.511
	2	IPE450	IPE450	IPE450	IPE450	IPE450	HEB360	HEB450	HEB400				0.562	165.708	0.175	
	3	IPE400	IPE400	IPE400	IPE400	IPE400	HEB340	HEB400	HEB360				0.42	131.784	0.108	
St350	1	IPE450	IPE450	IPE450	IPE450	IPE450	HEB340	HEB400	HEB360	3	0.86	4.00	0.511	165.708	0.132	1.537
	2	IPE450	IPE450	IPE450	IPE450	IPE450	HEB340	HEB400	HEB360				0.569	165.708	0.117	
	3	IPE400	IPE400	IPE400	IPE400	IPE400	HEB340	HEB400	HEB360				0.397	131.784	0.068	
St351	1	IPE450	IPE450	IPE450	IPE450	IPE450	HEB340	HEB400	HEB360	3	0.86	2.73	0.511	165.708	0.09	1.000
	2	IPE450	IPE450	IPE450	IPE450	IPE450	HEB340	HEB400	HEB360				0.569	165.708	0.08	
	3	IPE400	IPE400	IPE400	IPE400	IPE400	HEB340	HEB400	HEB360				0.397	131.784	0.046	
St352	1	IPE550	IPE550	IPE550	IPE550	IPE550	HEB400	HEB600	HEB500	4	0.84	6.50	0.336	165.708	0.139	3.173
	2	IPE500	IPE500	IPE500	IPE500	IPE500	HEB400	HEB600	HEB500				0.493	165.708	0.165	
	3	IPE450	IPE450	IPE450	IPE450	IPE450	HEB360	HEB550	HEB450				0.5	165.708	0.144	
	4	IPE400	IPE400	IPE400	IPE400	IPE400	HEB360	HEB550	HEB450				0.407	131.784	0.098	
St353	1	IPE450	IPE450	IPE450	IPE450	IPE450	HEB340	HEB400	HEB360	4	1.15	4.00	0.527	165.708	0.182	1.424
	2	IPE450	IPE450	IPE450	IPE450	IPE450	HEB340	HEB400	HEB360				0.655	165.708	0.185	
	3	IPE400	IPE400	IPE400	IPE400	IPE400	HEB320	HEB360	HEB340				0.566	165.708	0.142	
	4	IPE400	IPE400	IPE400	IPE400	IPE400	HEB320	HEB360	HEB340				0.38	131.784	0.089	
St354	1	IPE450	IPE450	IPE450	IPE450	IPE450	HEB320	HEB400	HEB360	4	1.16	2.97	0.537	165.708	0.138	1.000
	2	IPE450	IPE450	IPE450	IPE450	IPE450	HEB320	HEB400	HEB360				0.655	165.708	0.139	
	3	IPE400	IPE400	IPE400	IPE400	IPE400	HEB320	HEB360	HEB340				0.561	165.708	0.106	
	4	IPE400	IPE400	IPE400	IPE400	IPE400	HEB320	HEB360	HEB340				0.376	131.784	0.061	

Table C.25: Frames - Lagos (Soil Type C) Configuration 6

ID	Floor	B1	B2	B3	B4	B5	C1=C6	C2=C5	C3=C4	St.	T_1	q	ISD	Mass	θ_{EC8}	Ω
St355	1	IPE550	IPE550	IPE550	IPE550	IPE550	HEB450	HEB700	HEB650	5	0.93	6.50	0.286	165.708	0.133	3.296
	2	IPE550	IPE550	IPE550	IPE550	IPE550	HEB450	HEB700	HEB650				0.449	165.708	0.172	
	3	IPE500	IPE500	IPE500	IPE500	IPE500	HEB400	HEB650	HEB550				0.485	165.708	0.163	
	4	IPE450	IPE450	IPE450	IPE450	IPE450	HEB400	HEB650	HEB550				0.462	165.708	0.137	
	5	IPE400	IPE400	IPE400	IPE400	IPE400	HEB360	HEB600	HEB500				0.387	131.784	0.099	
St356	1	IPE500	IPE500	IPE500	IPE500	IPE500	HEB400	HEB500	HEB450	5	1.21	4.00	0.464	165.708	0.144	1.407
	2	IPE500	IPE500	IPE500	IPE500	IPE500	HEB400	HEB500	HEB450				0.652	165.708	0.168	
	3	IPE450	IPE450	IPE450	IPE450	IPE450	HEB340	HEB400	HEB360				0.724	165.708	0.165	
	4	IPE400	IPE400	IPE400	IPE400	IPE400	HEB340	HEB400	HEB360				0.657	165.708	0.133	
	5	IPE400	IPE400	IPE400	IPE400	IPE400	HEB340	HEB360	HEB340				0.46	131.784	0.082	
St357	1	IPE450	IPE450	IPE450	IPE450	IPE450	HEB360	HEB450	HEB450	5	1.37	3.88	0.496	165.708	0.156	1.000
	2	IPE450	IPE450	IPE450	IPE450	IPE450	HEB360	HEB450	HEB450				0.665	165.708	0.175	
	3	IPE400	IPE400	IPE400	IPE400	IPE400	HEB340	HEB400	HEB400				0.758	165.708	0.175	
	4	IPE400	IPE400	IPE400	IPE400	IPE400	HEB340	HEB400	HEB400				0.696	165.708	0.143	
	5	IPE400	IPE400	IPE400	IPE400	IPE400	HEB320	HEB360	HEB340				0.461	131.784	0.084	
St358	1	HEA600	HEA600	HEA600	HEA600	HEA600	HEM600	HEM700	HEM700	8	1.20	6.50	0.236	165.708	0.12	2.371
	2	HEA550	HEA550	HEA550	HEA550	HEA550	HEM600	HEM700	HEM700				0.386	165.708	0.173	
	3	HEA550	HEA550	HEA550	HEA550	HEA550	HEM600	HEM700	HEM700				0.42	165.708	0.17	
	4	HEA550	HEA550	HEA550	HEA550	HEA550	HEM550	HEM600	HEM600				0.449	165.708	0.164	
	5	IPE500	IPE500	IPE500	IPE500	IPE500	HEM550	HEM600	HEM600				0.53	165.708	0.176	
	6	IPE450	IPE450	IPE450	IPE450	IPE450	HEM550	HEM600	HEM600				0.596	165.708	0.18	
	7	IPE450	IPE450	IPE450	IPE450	IPE450	HEB550	HEB600	HEB600				0.546	165.708	0.152	
	8	IPE400	IPE400	IPE400	IPE400	IPE400	HEB550	HEB600	HEB600				0.442	131.784	0.11	

Table C.25: Frames - Lagos (Soil Type C) Configuration 6

ID	Floor	B1	B2	B3	B4	B5	C1=C6	C2=C5	C3=C4	St.	T_1	q	ISD	Mass	θ_{EC8}	Ω
St359	1	IPE600	IPE600	IPE600	IPE600	IPE600	HEB500	HEB600	HEB600	8	1.52	4.00	0.324	165.708	0.127	1.285
	2	IPE600	IPE600	IPE600	IPE600	IPE600	HEB500	HEB600	HEB600				0.475	165.708	0.163	
	3	IPE550	IPE550	IPE550	IPE550	IPE550	HEB500	HEB600	HEB600				0.53	165.708	0.165	
	4	IPE500	IPE500	IPE500	IPE500	IPE500	HEB450	HEB550	HEB550				0.632	165.708	0.179	
	5	IPE450	IPE450	IPE450	IPE450	IPE450	HEB450	HEB550	HEB550				0.692	165.708	0.179	
	6	IPE450	IPE450	IPE450	IPE450	IPE450	HEB450	HEB550	HEB550				0.656	165.708	0.156	
	7	IPE400	IPE400	IPE400	IPE400	IPE400	HEB400	HEB500	HEB500				0.554	165.708	0.125	
	8	IPE400	IPE400	IPE400	IPE400	IPE400	HEB400	HEB500	HEB500				0.407	131.784	0.081	
St360	1	IPE550	IPE550	IPE550	IPE550	IPE550	HEB450	HEB550	HEB550	8	1.70	3.61	0.385	165.708	0.151	1.000
	2	IPE550	IPE550	IPE550	IPE550	IPE550	HEB450	HEB550	HEB550				0.57	165.708	0.196	
	3	IPE500	IPE500	IPE500	IPE500	IPE500	HEB450	HEB550	HEB550				0.623	165.708	0.195	
	4	IPE500	IPE500	IPE500	IPE500	IPE500	HEB400	HEB500	HEB500				0.674	165.708	0.193	
	5	IPE450	IPE450	IPE450	IPE450	IPE450	HEB400	HEB500	HEB500				0.685	165.708	0.18	
	6	IPE400	IPE400	IPE400	IPE400	IPE400	HEB400	HEB500	HEB500				0.684	165.708	0.167	
	7	IPE400	IPE400	IPE400	IPE400	IPE400	HEB360	HEB450	HEB450				0.573	165.708	0.133	
	8	IPE400	IPE400	IPE400	IPE400	IPE400	HEB360	HEB450	HEB450				0.382	131.784	0.079	

Appendix D

Ground Motion Record Selection

This appendix provides a detailed presentation of the ground motion records used in the response-history analysis conducted in the thesis.

D.1 Ground Motion Records Groups

Table D.1: Ground Motion Records Porto

Event	Year	Mag.	Epicentral Distance [km]	Hypocenter Distance [km]	Campbell Distance [km]	Closest Distance to Fault Rupture [km]	Joyner-Boore Distance [km]	V_{s30} [m/s]	Lowest Useable Freq. [Hz]	Rake Angle [^{o}]	PGA [g]
Parkfield	1966	6.19	34.01	35.45	13.24	12.90	12.90	256.80	0.25	180.00	0.25
San Fernando	1971	6.61	39.49	41.57	25.89	22.77	22.77	316.50	0.25	83.00	0.17
Coyote Lake	1979	5.74	10.94	13.55	9.02	9.02	8.47	270.80	0.25	176.00	0.21
Imperial Valley-06	1979	6.53	22.43	24.55	15.34	15.30	13.52	274.50	0.25	180.00	0.19
Imperial Valley-06	1979	6.53	43.90	45.02	32.23	31.92	31.92	274.50	0.25	180.00	0.12
Imperial Valley-06	1979	6.53	35.18	36.56	21.68	21.68	19.76	237.30	0.13	180.00	0.13
Imperial Valley-06	1979	6.53	22.43	24.55	15.34	15.30	13.52	274.50	0.25	180.00	0.15
Livermore-01	1980	5.80	26.79	29.35	-	-	-	338.50	0.19	160.00	0.23
Irpinia, Italy-01	1980	6.90	46.16	47.13	23.35	22.56	22.54	500.00	0.25	-90.00	0.20
Irpinia, Italy-01	1980	6.90	46.16	47.13	23.35	22.56	22.54	500.00	0.25	-90.00	0.22
Taiwan SMART1(5)	1981	5.90	30.50	32.46	0.00	0.00	0.00	274.50	0.13	64.00	0.11
Coalinga-01	1983	6.36	44.66	44.89	34.00	34.00	32.81	376.10	0.25	90.00	0.11
Coalinga-05	1983	5.77	11.09	13.33	-	-	-	376.10	0.11	102.00	0.29
Coalinga-05	1983	5.77	16.17	17.79	-	-	-	257.40	0.13	102.00	0.41
Morgan Hill	1984	6.19	38.10	39.04	14.00	13.69	13.68	270.80	0.25	180.00	0.16
Morgan Hill	1984	6.19	38.10	39.04	14.00	13.69	13.68	270.80	0.25	180.00	0.21
N. Palm Springs	1986	6.06	21.14	23.83	10.84	10.84	10.08	207.50	0.25	150.00	0.19
N. Palm Springs	1986	6.06	18.17	21.24	7.84	7.84	6.74	345.40	0.19	150.00	0.22
Whittier Narrows-01	1987	5.99	14.64	20.67	17.91	17.91	10.50	308.60	0.18	150.00	0.17
Whittier Narrows-01	1987	5.99	12.00	18.90	16.32	16.32	6.42	308.60	0.23	150.00	0.14

Table D.1: Ground Motion Records Porto

Event	Year	Mag.	Epicentral Distance [km]	Hypocenter Distance [km]	Campbell Distance [km]	Closest Distance to Fault Rupture [km]	Joyner-Boore Distance [km]	V_{s30} [m/s]	Lowest Useable Freq. [Hz]	Rake Angle [^{o}]	PGA [g]
Whittier Narrows-01	1987	5.99	43.92	46.28	41.69	41.69	38.04	280.90	0.23	150.00	0.12
Loma Prieta	1989	6.93	35.47	39.54	18.33	18.33	17.92	663.30	0.25	140.00	0.13
Loma Prieta	1989	6.93	54.54	57.27	39.51	39.51	39.32	367.60	0.25	140.00	0.11
Loma Prieta	1989	6.93	28.98	33.84	9.96	9.96	9.19	729.70	0.25	140.00	0.36
Northridge-01	1994	6.69	18.22	25.26	24.08	24.08	13.34	446.00	0.06	103.00	0.20
Northridge-01	1994	6.69	22.45	28.47	26.45	26.45	17.28	336.20	0.14	103.00	0.37
Northridge-01	1994	6.69	47.48	50.61	46.74	46.74	43.20	271.90	0.20	103.00	0.16
Northridge-01	1994	6.69	44.32	47.65	39.31	39.31	38.86	401.40	0.16	103.00	0.26
Northridge-01	1994	6.69	19.19	25.97	25.59	25.59	15.46	659.60	0.12	103.00	0.18
Northridge-01	1994	6.69	18.62	25.55	22.49	22.49	13.80	398.40	0.08	103.00	0.28
Northridge-01	1994	6.69	18.62	25.55	22.49	22.49	13.80	398.40	0.08	103.00	0.47
Northridge-01	1994	6.69	57.98	60.57	56.92	56.92	53.57	234.90	0.25	103.00	0.12
Northridge-01	1994	6.69	14.66	22.83	16.74	16.74	1.69	715.10	0.12	103.00	0.29
Northridge-01	1994	6.69	28.20	33.18	29.88	29.88	23.51	297.10	0.16	103.00	0.17
Northridge-01	1994	6.69	47.11	50.25	45.03	45.03	43.22	405.20	0.25	103.00	0.13
Northridge-01	1994	6.69	36.47	40.45	34.20	34.20	32.39	376.10	0.20	103.00	0.21
Chi-Chi, Taiwan	1999	7.62	88.84	89.20	38.49	38.43	38.36	375.30	0.06	55.00	0.31
Hector Mine	1999	7.13	83.79	85.09	65.89	65.89	65.04	345.40	0.07	179.00	0.11
Chi-Chi, Taiwan-05	1999	6.20	62.76	63.56	60.33	60.33	54.91	215.00	0.25	100.00	0.17
Chi-Chi, Taiwan-06	1999	6.30	42.99	45.87	31.14	31.14	29.49	427.70	0.25	100.00	0.14

Table D.2: Ground Motion Records Lisbon

Event	Year	Mag.	Epicentral Distance [km]	Hypocenter Distance [km]	Campbell Distance [km]	Closest Distance to Fault Rupture [km]	Joyner-Boore Distance [km]	V_{s30} [m/s]	Lowest Useable Freq. [Hz]	Rake Angle [°]	PGA [g]
Imperial Valley-02	1940	6.95	12.99	15.69	7.51	6.09	6.09	213.40	0.25	180.00	0.31
Imperial Valley-02	1940	6.95	12.99	15.69	7.51	6.09	6.09	213.40	0.25	180.00	0.21
Kern County	1952	7.36	43.49	46.21	38.89	38.89	38.42	385.40	0.06	61.00	0.16
Kern County	1952	7.36	43.49	46.21	38.89	38.89	38.42	385.40	0.06	61.00	0.18
Coyote Lake	1979	5.74	23.24	24.58	19.70	19.70	19.46	370.80	0.25	176.00	0.11
Imperial Valley-06	1979	6.53	43.15	44.29	10.57	10.42	8.54	208.70	0.13	180.00	0.22
Imperial Valley-06	1979	6.53	24.82	26.74	16.06	15.19	15.19	659.60	0.13	180.00	0.16
Imperial Valley-06	1979	6.53	33.73	35.17	22.54	22.03	22.03	274.50	0.06	180.00	0.35
Imperial Valley-06	1979	6.53	31.99	33.50	18.85	17.94	17.94	196.90	0.13	180.00	0.14
Irpinia, Italy-01	1980	6.90	22.65	24.56	10.76	8.18	8.14	1000.00	0.13	-90.00	0.14
Coalinga-01	1983	6.36	37.97	38.25	29.38	29.38	28.00	376.10	0.25	90.00	0.12
Morgan Hill	1984	6.19	38.20	39.13	13.35	13.02	13.01	349.90	0.13	180.00	0.20
Taiwan SMART1(40)	1986	6.32	65.48	67.36	-	-	-	274.50	0.25	100.00	0.18
N. Palm Springs	1986	6.06	21.14	23.83	10.84	10.84	10.08	207.50	0.25	150.00	0.16
Superstition Hills-02	1987	6.54	29.91	31.24	17.37	17.03	17.03	208.70	0.16	180.00	0.16
Superstition Hills-02	1987	6.54	19.28	21.27	18.79	18.48	18.48	207.50	0.19	180.00	0.12
Loma Prieta	1989	6.93	30.78	35.40	20.34	20.34	19.97	597.10	0.13	140.00	0.15
Loma Prieta	1989	6.93	54.54	57.27	39.51	39.51	39.32	367.60	0.25	140.00	0.12
Loma Prieta	1989	6.93	20.13	26.66	14.69	14.69	14.18	671.80	0.06	140.00	0.23
Loma Prieta	1989	6.93	27.23	32.35	8.50	8.50	7.58	370.80	0.13	140.00	0.51

Table D.2: Ground Motion Records Lisbon

Event	Year	Mag.	Epicentral Distance [km]	Hypocenter Distance [km]	Campbell Distance [km]	Closest Distance to Fault Rupture [km]	Joyner-Boore Distance [km]	V_{s30} [m/s]	Lowest Useable Freq. [Hz]	Rake Angle [^{o}]	PGA [g]
Landers	1992	7.28	27.33	28.21	21.98	21.78	21.78	345.40	0.07	180.00	0.17
Landers	1992	7.28	59.68	60.09	54.34	54.25	54.25	345.40	0.10	180.00	0.10
Northridge-01	1994	6.69	48.32	51.40	40.34	40.34	34.78	234.90	0.10	103.00	0.12
Northridge-01	1994	6.69	48.32	51.40	40.34	40.34	34.78	234.90	0.10	103.00	0.12
Northridge-01	1994	6.69	17.95	25.07	22.50	22.50	12.92	416.60	0.12	103.00	0.19
Northridge-01	1994	6.69	23.61	29.39	24.03	24.03	19.73	316.50	0.20	103.00	0.23
Northridge-01	1994	6.69	31.73	36.24	31.33	31.33	27.82	270.20	0.20	103.00	0.19
Northridge-01	1994	6.69	32.72	37.11	31.48	31.48	28.82	376.10	0.20	103.00	0.13
Northridge-01	1994	6.69	32.72	37.11	31.48	31.48	28.82	376.10	0.20	103.00	0.18
Northridge-01	1994	6.69	29.59	34.38	29.74	29.74	25.60	405.20	0.16	103.00	0.16
Northridge-01	1994	6.69	19.55	26.24	23.60	23.60	14.55	392.20	0.12	103.00	0.25
Northridge-01	1994	6.69	22.45	28.47	26.45	26.45	17.28	336.20	0.14	103.00	0.37
Northridge-01	1994	6.69	24.13	29.81	13.35	13.35	12.38	446.00	0.06	103.00	0.13
Chi-Chi, Taiwan	1999	7.62	55.23	55.80	25.88	24.11	24.11	442.20	0.05	55.00	0.18
Chi-Chi, Taiwan	1999	7.62	68.78	69.24	37.92	37.48	37.48	272.60	0.05	55.00	0.14
Chi-Chi, Taiwan	1999	7.62	69.29	69.75	49.15	49.15	44.89	473.90	0.03	55.00	0.12
Hector Mine	1999	7.13	47.97	50.20	43.05	43.05	41.82	271.40	0.08	179.00	0.15
Chi-Chi, Taiwan-03	1999	6.20	31.85	32.79	24.38	24.38	23.44	542.60	0.10	80.00	0.14
Chi-Chi, Taiwan-04	1999	6.20	50.36	53.48	50.14	50.04	50.02	228.70	0.25	15.00	0.10
Chi-Chi, Taiwan-06	1999	6.30	58.32	60.47	41.58	41.58	40.36	473.90	0.25	100.00	0.16

Table D.3: Ground Motion Records Lagos Soil B

Event	Year	Mag.	Epicentral Distance [km]	Hypocenter Distance [km]	Campbell Distance [km]	Closest Distance to Fault Rupture [km]	Joyner-Boore Distance [km]	V_{s30} [m/s]	Lowest Useable Freq. [Hz]	Rake Angle [^{o}]	PGA [g]
Imperial Valley-02	1940	6.95	12.99	15.69	7.51	6.09	6.09	213.40	0.25	180.00	0.21
Imperial Valley-02	1940	6.95	12.99	15.69	7.51	6.09	6.09	213.40	0.25	180.00	0.31
Kern County	1952	7.36	43.49	46.21	38.89	38.89	38.42	385.40	0.06	61.00	0.16
Kern County	1952	7.36	43.49	46.21	38.89	38.89	38.42	385.40	0.06	61.00	0.18
Imperial Valley-06	1979	6.53	33.73	35.17	22.54	22.03	22.03	274.50	0.06	180.00	0.24
Imperial Valley-06	1979	6.53	27.13	28.90	7.38	7.05	4.90	208.90	0.13	180.00	0.49
Imperial Valley-06	1979	6.53	24.82	26.74	16.06	15.19	15.19	659.60	0.13	180.00	0.16
Imperial Valley-06	1979	6.53	43.15	44.29	10.57	10.42	8.54	208.70	0.13	180.00	0.22
Irpinia, Italy-02	1980	6.20	11.97	13.87	10.55	8.83	8.81	600.00	0.25	-90.00	0.16
Coalinga-01	1983	6.36	55.67	55.86	44.72	44.72	43.83	184.80	0.25	90.00	0.11
Coalinga-01	1983	6.36	37.97	38.25	29.38	29.38	28.00	376.10	0.25	90.00	0.12
Morgan Hill	1984	6.19	38.20	39.13	13.35	13.02	13.01	349.90	0.13	180.00	0.20
Taiwan SMART1(40)	1986	6.32	65.48	67.36	-	-	-	274.50	0.25	100.00	0.18
Superstition Hills-02	1987	6.54	29.91	31.24	17.37	17.03	17.03	208.70	0.16	180.00	0.16
Superstition Hills-02	1987	6.54	35.83	36.94	18.52	18.20	18.20	192.10	0.13	180.00	0.36
Superstition Hills-02	1987	6.54	19.28	21.27	18.79	18.48	18.48	207.50	0.19	180.00	0.12
Loma Prieta	1989	6.93	55.16	57.86	39.85	39.85	39.66	284.80	0.13	140.00	0.19
Loma Prieta	1989	6.93	54.54	57.27	39.51	39.51	39.32	367.60	0.25	140.00	0.12
Loma Prieta	1989	6.93	20.13	26.66	14.69	14.69	14.18	671.80	0.06	140.00	0.23
Loma Prieta	1989	6.93	18.46	25.42	3.88	3.88	0.00	477.70	0.13	140.00	0.59

Table D.3: Ground Motion Records Lagos Soil B

Event	Year	Mag.	Epicentral Distance [km]	Hypocenter Distance [km]	Campbell Distance [km]	Closest Distance to Fault Rupture [km]	Joyner-Boore Distance [km]	V_{s30} [m/s]	Lowest Useable Freq. [Hz]	Rake Angle [^{o}]	PGA [g]
Loma Prieta	1989	6.93	35.47	39.54	18.33	18.33	17.92	663.30	0.25	140.00	0.13
Loma Prieta	1989	6.93	30.78	35.40	20.34	20.34	19.97	597.10	0.13	140.00	0.15
Landers	1992	7.28	75.20	75.53	69.27	69.21	69.21	271.40	0.10	180.00	0.15
Landers	1992	7.28	27.33	28.21	21.98	21.78	21.78	345.40	0.07	180.00	0.17
Northridge-01	1994	6.69	24.13	29.81	13.35	13.35	12.38	446.00	0.06	103.00	0.13
Northridge-01	1994	6.69	29.59	34.38	29.74	29.74	25.60	405.20	0.16	103.00	0.16
Northridge-01	1994	6.69	19.55	26.24	23.60	23.60	14.55	392.20	0.12	103.00	0.25
Northridge-01	1994	6.69	20.22	26.74	23.41	23.41	15.54	278.00	0.14	103.00	0.22
Northridge-01	1994	6.69	48.32	51.40	40.34	40.34	34.78	234.90	0.10	103.00	0.12
Northridge-01	1994	6.69	25.44	30.88	28.30	28.30	20.36	234.90	0.25	103.00	0.32
Northridge-01	1994	6.69	17.95	25.07	22.50	22.50	12.92	416.60	0.12	103.00	0.19
Northridge-01	1994	6.69	31.73	36.24	31.33	31.33	27.82	270.20	0.20	103.00	0.10
Northridge-01	1994	6.69	31.73	36.24	31.33	31.33	27.82	270.20	0.20	103.00	0.19
Kobe, Japan	1995	6.90	45.97	49.33	28.49	19.15	19.14	256.00	0.13	180.00	0.21
Chi-Chi, Taiwan	1999	7.62	55.23	55.80	25.88	24.11	24.11	442.20	0.05	55.00	0.18
Chi-Chi, Taiwan	1999	7.62	68.78	69.24	37.92	37.48	37.48	272.60	0.05	55.00	0.14
Chi-Chi, Taiwan	1999	7.62	38.91	39.73	9.45	3.78	3.78	487.30	0.03	55.00	0.29
Hector Mine	1999	7.13	47.97	50.20	43.05	43.05	41.82	271.40	0.08	179.00	0.15
Chi-Chi, Taiwan-04	1999	6.20	38.91	42.87	38.25	38.14	38.11	442.20	0.25	15.00	0.12
Chi-Chi, Taiwan-06	1999	6.30	58.32	60.47	41.58	41.58	40.36	473.90	0.25	100.00	0.16

Table D.4: Ground Motion Records Lagos Soil C

Event	Year	Mag.	Epicentral Distance [km]	Hypocenter Distance [km]	Campbell Distance [km]	Closest Distance to Fault Rupture [km]	Joyner-Boore Distance [km]	V_{s30} [m/s]	Lowest Useable Freq. [Hz]	Rake Angle [^{o}]	PGA [g]
Imperial Valley-02	1940	6.95	12.99	15.69	7.51	6.09	6.09	213.40	0.25	180.00	0.21
Imperial Valley-02	1940	6.95	12.99	15.69	7.51	6.09	6.09	213.40	0.25	180.00	0.31
Kern County	1952	7.36	43.49	46.21	38.89	38.89	38.42	385.40	0.06	61.00	0.18
Kern County	1952	7.36	43.49	46.21	38.89	38.89	38.42	385.40	0.06	61.00	0.16
Imperial Valley-06	1979	6.53	31.99	33.50	18.85	17.94	17.94	196.90	0.13	180.00	0.14
Imperial Valley-06	1979	6.53	33.73	35.17	22.54	22.03	22.03	274.50	0.06	180.00	0.24
Imperial Valley-06	1979	6.53	24.82	26.74	16.06	15.19	15.19	659.60	0.13	180.00	0.16
Imperial Valley-06	1979	6.53	43.15	44.29	10.57	10.42	8.54	208.70	0.13	180.00	0.22
Irpinia, Italy-02	1980	6.20	11.97	13.87	10.55	8.83	8.81	600.00	0.25	-90.00	0.16
Coalinga-01	1983	6.36	37.97	38.25	29.38	29.38	28.00	376.10	0.25	90.00	0.12
Taiwan SMART1(40)	1986	6.32	65.48	67.36	-	-	-	274.50	0.25	100.00	0.18
N. Palm Springs	1986	6.06	21.14	23.83	10.84	10.84	10.08	207.50	0.25	150.00	0.16
Superstition Hills-02	1987	6.54	19.28	21.27	18.79	18.48	18.48	207.50	0.19	180.00	0.12
Superstition Hills-02	1987	6.54	35.83	36.94	18.52	18.20	18.20	192.10	0.13	180.00	0.36
Loma Prieta	1989	6.93	55.16	57.86	39.85	39.85	39.66	284.80	0.13	140.00	0.19
Loma Prieta	1989	6.93	30.78	35.40	20.34	20.34	19.97	597.10	0.13	140.00	0.15
Loma Prieta	1989	6.93	70.81	72.93	52.68	52.68	52.53	271.10	0.25	140.00	0.14
Loma Prieta	1989	6.93	20.13	26.66	14.69	14.69	14.18	671.80	0.06	140.00	0.23
Loma Prieta	1989	6.93	54.54	57.27	39.51	39.51	39.32	367.60	0.25	140.00	0.12
Loma Prieta	1989	6.93	18.46	25.42	3.88	3.88	0.00	477.70	0.13	140.00	0.59

Table D.4: Ground Motion Records Lagos Soil C

Event	Year	Mag.	Epicentral Distance [km]	Hypocenter Distance [km]	Campbell Distance [km]	Closest Distance to Fault Rupture [km]	Joyner-Boore Distance [km]	V_{s30} [m/s]	Lowest Useable Freq. [Hz]	Rake Angle [^{o}]	PGA [g]
Loma Prieta	1989	6.93	35.47	39.54	18.33	18.33	17.92	663.30	0.25	140.00	0.13
Landers	1992	7.28	27.33	28.21	21.98	21.78	21.78	345.40	0.07	180.00	0.17
Northridge-01	1994	6.69	17.95	25.07	22.50	22.50	12.92	416.60	0.12	103.00	0.19
Northridge-01	1994	6.69	23.61	29.39	24.03	24.03	19.73	316.50	0.20	103.00	0.23
Northridge-01	1994	6.69	32.72	37.11	31.48	31.48	28.82	376.10	0.20	103.00	0.13
Northridge-01	1994	6.69	24.13	29.81	13.35	13.35	12.38	446.00	0.06	103.00	0.13
Northridge-01	1994	6.69	31.73	36.24	31.33	31.33	27.82	270.20	0.20	103.00	0.19
Northridge-01	1994	6.69	31.73	36.24	31.33	31.33	27.82	270.20	0.20	103.00	0.10
Northridge-01	1994	6.69	48.32	51.40	40.34	40.34	34.78	234.90	0.10	103.00	0.12
Northridge-01	1994	6.69	32.72	37.11	31.48	31.48	28.82	376.10	0.20	103.00	0.18
Northridge-01	1994	6.69	29.59	34.38	29.74	29.74	25.60	405.20	0.16	103.00	0.16
Northridge-01	1994	6.69	20.22	26.74	23.41	23.41	15.54	278.00	0.14	103.00	0.22
Northridge-01	1994	6.69	19.55	26.24	23.60	23.60	14.55	392.20	0.12	103.00	0.25
Chi-Chi, Taiwan	1999	7.62	68.78	69.24	37.92	37.48	37.48	272.60	0.05	55.00	0.14
Chi-Chi, Taiwan	1999	7.62	74.12	74.55	53.56	53.56	49.69	272.60	0.03	55.00	0.17
Chi-Chi, Taiwan	1999	7.62	45.37	46.07	14.08	8.53	8.53	272.60	0.04	55.00	0.20
Chi-Chi, Taiwan	1999	7.62	55.23	55.80	25.88	24.11	24.11	442.20	0.05	55.00	0.18
Hector Mine	1999	7.13	47.97	50.20	43.05	43.05	41.82	271.40	0.08	179.00	0.15
Chi-Chi, Taiwan-04	1999	6.20	38.91	42.87	38.25	38.14	38.11	442.20	0.25	15.00	0.12
Chi-Chi, Taiwan-06	1999	6.30	58.32	60.47	41.58	41.58	40.36	473.90	0.25	100.00	0.16

Appendix E

Detailed results for the steel MRFs archetypes

This appendix includes documentation and details regarding the collapse assessment according to FEMA (2009). The results for the 360 archetype buildings are presented.

E.1 Key archetype design parameters

Table E.1: Key Archetype Design Parameters

Archetype Design ID Number	*No. of Stories*	*Key Archetype Design Parameters*						
		Gravity Loads	*Seismic Design Criteria*					$S_{MT}(T_1)[g]$
			$S_a(T_1)[g]$	$S_d(T_1)[g]$	q	$T_1[sec]$	$M[ton]$	
Performance Group No. PG-1/PG-25/PG-49								
St1/St2/St3	2	Residential	0.11/0.09/0.09	0.02/0.02/0.06	6.5/4/1.5	0.65/0.8/0.8	82.78	0.19/0.15/0.15
St4/St5/St6	3	Residential	0.1/0.08/0.06	0.01/0.02/0.04	6.5/4/1.5	0.76/0.96/1.16	130.28	0.16/0.13/0.11
St7/St8/St9	4	Residential	0.09/0.07/0.05	0.01/0.02/0.03	6.5/4/1.5	0.83/1.05/1.42	176.89	0.15/0.12/0.09
St10/St11/St12	5	Residential	0.08/0.06/0.04	0.01/0.02/0.03	6.5/4/1.5	0.93/1.16/1.77	223.5	0.13/0.11/0.07
St13/St14/St15	8	Residential	0.07/0.05/0.02	0.01/0.01/0.01	6.5/4/1.5	1.11/1.42/2.55	363.33	0.11/0.09/0.04
Performance Group No. PG-2/PG-26/PG-50								
St91/St92/St93	2	Residential	0.46/0.37/0.37	0.07/0.09/0.25	6.5/4/1.5	0.65/0.8/0.8	92.97	0.78/0.63/0.63
St94/St95/St96	3	Residential	0.39/0.31/0.26	0.06/0.08/0.14	6.5/4/1.83	0.76/0.96/1.16	144.75	0.67/0.53/0.44
St97/St98/St99	4	Residential	0.36/0.28/0.22	0.05/0.07/0.09	6.5/4/2.41	0.83/1.05/1.37	196.53	0.61/0.48/0.37
St100/St101/St102	5	Residential	0.32/0.26/0.2	0.05/0.06/0.08	6.5/4/2.34	0.93/1.16/1.49	248.32	0.54/0.44/0.34
St103/St104/St105	8	Residential	0.27/0.21/0.14	0.04/0.05/0.07	6.5/4/1.97	1.11/1.42/2.04	403.67	0.46/0.36/0.24
Performance Group No. PG-3/PG-27/PG-51								
St181/St182/St183	2	Residential	0.69/0.56/0.56	0.11/0.14/0.26	6.5/4/2.17	0.65/0.8/0.8	148.75	1.18/0.96/0.96
St184/St185/St186	3	Residential	0.59/0.47/0.41	0.09/0.12/0.14	6.5/4/2.84	0.76/0.96/1.1	231.6	1.01/0.8/0.7
St187/St188/St189	4	Residential	0.54/0.43/0.37	0.08/0.11/0.12	6.5/4/3.15	0.83/1.05/1.23	314.45	0.93/0.73/0.62
St190/St191/St192	5	Residential	0.48/0.39/0.33	0.07/0.1/0.11	6.5/4/2.88	0.93/1.16/1.38	397.31	0.83/0.66/0.56
St193/St194/St195	8	Residential	0.4/0.32/0.24	0.06/0.08/0.12	6.5/4/1.92	1.11/1.42/1.88	645.85	0.69/0.54/0.41
Performance Group No. PG-4/PG-28/PG-52								
St271/St272/St273	2	Residential	0.76/0.62/0.62	0.12/0.16/0.26	6.5/4/2.4	0.65/0.8/0.8	125.5	1.31/1.06/1.06
St274/St275/St276	3	Residential	0.65/0.52/0.45	0.1/0.13/0.14	6.5/4/3.14	0.76/0.96/1.1	195.41	1.12/0.89/0.77
St277/St278/St279	4	Residential	0.6/0.47/0.41	0.09/0.12/0.12	6.5/4/3.44	0.83/1.05/1.21	265.32	1.02/0.81/0.7
St280/St281/St282	5	Residential	0.53/0.43/0.37	0.08/0.11/0.12	6.5/4/3.2	0.93/1.16/1.34	335.23	0.91/0.73/0.63
St283/St284/St285	8	Residential	0.45/0.35/0.28	0.07/0.09/0.1	6.5/4/2.89	1.11/1.42/1.79	544.95	0.77/0.6/0.47

Table E.1: Key Archetype Design Parameters

Archetype Design ID Number	*No. of Stories*	*Key Archetype Design Parameters*							
		Gravity Loads	*Seismic Design Criteria*						$S_{MT}(T_1)[g]$
			$S_a(T_1)[g]$	$S_d(T_1)[g]$	q	$T_1[sec]$	$M[ton]$		
Performance Group No. PG-5/PG-29/PG-53									
St16/St17/St18	2	Residential	0.11/0.09/0.09	0.02/0.02/0.06	6.5/4/1.5	0.68/0.77/0.77	102.26	0.18/0.16/0.16	
St19/St20/St21	3	Residential	0.09/0.08/0.07	0.01/0.02/0.05	6.5/4/1.5	0.77/0.95/1.01	159.23	0.16/0.13/0.12	
St22/St23/St24	4	Residential	0.09/0.07/0.05	0.01/0.02/0.04	6.5/4/1.5	0.83/1.07/1.37	216.19	0.15/0.12/0.09	
St25/St26/St27	5	Residential	0.08/0.06/0.04	0.01/0.02/0.03	6.5/4/1.5	0.91/1.2/1.64	273.15	0.14/0.1/0.08	
St28/St29/St30	8	Residential	0.06/0.05/0.02	0.01/0.01/0.02	6.5/4/1.5	1.12/1.43/2.43	444.04	0.11/0.09/0.04	
Performance Group No. PG-6/PG-30/PG54									
St106/St107/St108	2	Residential	0.44/0.38/0.38	0.07/0.1/0.25	6.5/4/1.57	0.68/0.77/0.77	297.49	0.74/0.66/0.66	
St109/St110/St111	3	Residential	0.38/0.31/0.29	0.06/0.08/0.19	6.5/4/1.58	0.77/0.95/1.01	463.2	0.66/0.53/0.5	
St112/St113/St114	4	Residential	0.36/0.28/0.23	0.05/0.07/0.11	6.5/4/2.11	0.83/1.07/1.3	628.91	0.61/0.47/0.39	
St115/St116/St117	5	Residential	0.33/0.25/0.19	0.05/0.06/0.09	6.5/4/2.1	0.91/1.2/1.53	794.62	0.56/0.42/0.33	
St118/St119/St120	8	Residential	0.26/0.21/0.14	0.04/0.05/0.08	6.5/4/1.89	1.12/1.43/2.03	1291.74	0.45/0.35/0.25	
Performance Group No. PG-7/PG-31/PG-55									
St196/St197/St198	2	Residential	0.66/0.58/0.58	0.1/0.15/0.25	6.5/4/2.37	0.68/0.77/0.77	82.78	1.13/1/1	
St199/St200/St201	3	Residential	0.58/0.47/0.43	0.09/0.12/0.19	6.5/4/2.28	0.77/0.95/1.04	130.28	1/0.81/0.74	
St202/St203/St204	4	Residential	0.54/0.42/0.36	0.08/0.1/0.14	6.5/4/2.66	0.83/1.07/1.24	176.89	0.93/0.72/0.62	
St205/St206/St207	5	Residential	0.49/0.37/0.31	0.08/0.09/0.11	6.5/4/2.87	0.91/1.2/1.47	223.5	0.84/0.64/0.52	
St208/St209/St210	8	Residential	0.4/0.31/0.25	0.06/0.08/0.09	6.5/4/2.8	1.12/1.43/1.79	363.33	0.69/0.54/0.43	
Performance Group No. PG-8/PG-32/PG-56									
St286/St287/St288	2	Residential	0.73/0.65/0.65	0.11/0.16/0.25	6.5/4/2.63	0.68/0.77/0.77	92.97	1.25/1.1/1.1	
St289/St290/St291	3	Residential	0.65/0.52/0.48	0.1/0.13/0.19	6.5/4/2.53	0.77/0.95/1.04	144.75	1.1/0.89/0.82	
St292/St293/St294	4	Residential	0.6/0.46/0.38	0.09/0.12/0.13	6.5/4/2.95	0.83/1.07/1.3	196.53	1.02/0.79/0.65	
St295/St296/St297	5	Residential	0.55/0.41/0.34	0.08/0.1/0.11	6.5/4/3	0.91/1.2/1.45	248.32	0.93/0.71/0.59	
St298/St299/St300	8	Residential	0.44/0.35/0.29	0.07/0.09/0.09	6.5/4/3.2	1.12/1.43/1.69	403.67	0.76/0.59/0.5	

Table E.1: Key Archetype Design Parameters

Archetype Design ID Number	*No. of Stories*	*Key Archetype Design Parameters*						
		Gravity Loads	*Seismic Design Criteria*					$S_{MT}(T_1)[g]$
			$S_a(T_1)[g]$	$S_d(T_1)[g]$	q	$T_1[sec]$	$M[ton]$	
Performance Group No. PG-9/PG-33/PG-57								
St31/St32/St33	2	Residential	0.12/0.12/0.12	0.02/0.03/0.08	6.5/4/1.5	0.57/0.57/0.57	148.75	0.21/0.21/0.21
St34/St35/St36	3	Residential	0.1/0.09/0.09	0.01/0.02/0.06	6.5/4/1.5	0.75/0.81/0.81	231.6	0.16/0.15/0.15
St37/St38/St39	4	Residential	0.09/0.07/0.07	0.01/0.02/0.05	6.5/4/1.5	0.83/1.04/1.06	314.45	0.15/0.12/0.12
St40/St41/St42	5	Residential	0.08/0.07/0.06	0.01/0.02/0.04	6.5/4/1.5	0.89/1.11/1.24	397.31	0.14/0.11/0.1
St43/St44/St45	8	Residential	0.07/0.05/0.04	0.01/0.01/0.03	6.5/4/1.5	1.11/1.43/1.84	645.85	0.11/0.09/0.07
Performance Group No. PG-10/PG-34/PG-58								
St121/St122/St123	2	Residential	0.49/0.49/0.49	0.08/0.12/0.33	6.5/4/1.5	0.57/0.57/0.57	125.5	0.84/0.84/0.84
St124/St125/St126	3	Residential	0.4/0.37/0.37	0.06/0.09/0.24	6.5/4/1.5	0.75/0.81/0.81	195.41	0.68/0.63/0.63
St127/St128/St129	4	Residential	0.36/0.28/0.28	0.05/0.07/0.18	6.5/4/1.59	0.83/1.04/1.06	265.32	0.61/0.49/0.48
St130/St131/St132	5	Residential	0.33/0.27/0.24	0.05/0.07/0.13	6.5/4/1.83	0.89/1.11/1.23	335.23	0.57/0.46/0.41
St133/St134/St135	8	Residential	0.27/0.21/0.16	0.04/0.05/0.08	6.5/4/2	1.11/1.43/1.82	544.95	0.46/0.35/0.28
Performance Group No. PG-11/PG-35/PG-59								
St211/St212/St213	2	Residential	0.75/0.75/0.75	0.12/0.19/0.45	6.5/4/1.68	0.57/0.57/0.57	102.26	1.28/1.28/1.28
St214/St215/St216	3	Residential	0.6/0.55/0.55	0.09/0.14/0.26	6.5/4/2.1	0.75/0.81/0.81	159.23	1.02/0.95/0.95
St217/St218/St219	4	Residential	0.54/0.43/0.42	0.08/0.11/0.18	6.5/4/2.4	0.83/1.04/1.06	216.19	0.93/0.74/0.72
St220/St221/St222	5	Residential	0.5/0.4/0.36	0.08/0.1/0.13	6.5/4/2.82	0.89/1.11/1.24	273.15	0.86/0.69/0.62
St223/St224/St225	8	Residential	0.4/0.31/0.26	0.06/0.08/0.09	6.5/4/2.9	1.11/1.43/1.73	444.04	0.69/0.54/0.44
Performance Group No. PG-12/PG-36/PG-60								
St301/St302/St303	2	Residential	0.83/0.83/0.83	0.13/0.21/0.45	6.5/4/1.85	0.57/0.57/0.57	297.49	1.42/1.42/1.42
St304/St305/St306	3	Residential	0.66/0.61/0.61	0.1/0.15/0.26	6.5/4/2.33	0.75/0.81/0.81	463.2	1.13/1.05/1.05
St307/St308/St309	4	Residential	0.6/0.48/0.47	0.09/0.12/0.18	6.5/4/2.66	0.83/1.04/1.06	628.91	1.02/0.82/0.8
St310/St311/St312	5	Residential	0.56/0.45/0.4	0.09/0.11/0.13	6.5/4/3.12	0.89/1.11/1.24	794.62	0.95/0.77/0.69
St313/St314/St315	8	Residential	0.45/0.35/0.3	0.07/0.09/0.1	6.5/4/3	1.11/1.43/1.68	1291.74	0.77/0.59/0.51

Table E.1: Key Archetype Design Parameters

Archetype Design ID Number	*No. of Stories*	*Key Archetype Design Parameters*						
		Gravity Loads	*Seismic Design Criteria*					$S_{MT}(T_1)[g]$
			$S_a(T_1)[g]$	$S_d(T_1)[g]$	q	$T_1[sec]$	$M[ton]$	
Performance Group No. PG-13/PG-37/PG-61								
St46/St47/St48	2	Residential	0.11/0.1/0.1	0.02/0.03/0.07	6.5/4/1.5	0.66/0.71/0.71	82.78	0.19/0.17/0.17
St49/St50/St51	3	Residential	0.09/0.07/0.07	0.01/0.02/0.05	6.5/4/1.5	0.79/0.98/0.98	130.28	0.16/0.13/0.13
St52/St53/St54	4	Residential	0.08/0.07/0.06	0.01/0.02/0.04	6.5/4/1.5	0.85/1.11/1.3	176.89	0.15/0.11/0.1
St55/St56/St57	5	Residential	0.07/0.06/0.04	0.01/0.01/0.03	6.5/4/1.5	0.97/1.24/1.64	223.5	0.13/0.1/0.08
St58/St59/St60	8	Residential	0.06/0.05/0.02	0.01/0.01/0.01	6.5/4/1.5	1.21/1.54/2.57	363.33	0.1/0.08/0.04
Performance Group No. PG-14/PG-38/PG-62								
St136/St137/St138	2	Residential	0.45/0.42/0.42	0.07/0.1/0.28	6.5/4/1.5	0.66/0.71/0.71	92.97	0.77/0.71/0.71
St139/St140/St141	3	Residential	0.38/0.3/0.3	0.06/0.08/0.2	6.5/4/1.5	0.79/0.98/0.98	144.75	0.64/0.52/0.52
St142/St143/St144	4	Residential	0.35/0.27/0.23	0.05/0.07/0.13	6.5/4/1.81	0.85/1.11/1.3	196.53	0.6/0.46/0.39
St145/St146/St147	5	Residential	0.31/0.24/0.19	0.05/0.06/0.1	6.5/4/2	0.97/1.24/1.52	248.32	0.52/0.41/0.33
St148/St149/St150	8	Residential	0.24/0.19/0.13	0.04/0.05/0.07	6.5/4/2.03	1.21/1.54/2.11	403.67	0.42/0.33/0.23
Performance Group No. PG-15/PG-39/PG-63								
St226/St227/St228	2	Residential	0.68/0.63/0.63	0.1/0.16/0.38	6.5/4/1.68	0.66/0.71/0.71	148.75	1.16/1.08/1.08
St229/St230/St231	3	Residential	0.57/0.46/0.4	0.09/0.11/0.13	6.5/4/2.95	0.79/0.98/1.13	231.6	0.97/0.78/0.68
St232/St233/St234	4	Residential	0.53/0.4/0.35	0.08/0.1/0.12	6.5/4/2.79	0.85/1.11/1.3	314.45	0.9/0.69/0.59
St235/St236/St237	5	Residential	0.46/0.36/0.31	0.07/0.09/0.1	6.5/4/3.13	0.97/1.24/1.47	397.31	0.79/0.62/0.52
St238/St239/St240	8	Residential	0.37/0.29/0.23	0.06/0.07/0.09	6.5/4/2.43	1.21/1.54/1.96	645.85	0.63/0.5/0.39
Performance Group No. PG-16/PG-40/PG-64								
St316/St317/St318	2	Residential	0.75/0.7/0.7	0.12/0.17/0.38	6.5/4/1.86	0.66/0.71/0.71	125.5	1.29/1.2/1.2
St319/St320/St321	3	Residential	0.63/0.51/0.44	0.1/0.13/0.13	6.5/4/3.27	0.79/0.98/1.13	195.41	1.08/0.87/0.75
St322/St323/St324	4	Residential	0.58/0.45/0.38	0.09/0.11/0.12	6.5/4/3.1	0.85/1.11/1.3	265.32	1/0.77/0.65
St325/St326/St327	5	Residential	0.51/0.4/0.35	0.08/0.1/0.1	6.5/4/3.4	0.97/1.24/1.42	335.23	0.88/0.69/0.6
St328/St329/St330	8	Residential	0.41/0.32/0.26	0.06/0.08/0.1	6.5/4/2.67	1.21/1.54/1.92	544.95	0.7/0.55/0.44

Table E.1: Key Archetype Design Parameters

Archetype Design ID Number	*No. of Stories*	*Key Archetype Design Parameters*						
		Gravity Loads	*Seismic Design Criteria*					$S_{MT}(T_1)[g]$
			$S_a(T_1)[g]$	$S_d(T_1)[g]$	q	$T_1[sec]$	$M[ton]$	
Performance Group No. PG-17/PG-41/PG-65								
St61/St62/St63	2	Residential	0.11/0.1/0.1	0.02/0.02/0.06	6.5/4/1.5	0.67/0.75/0.75	102.26	0.18/0.16/0.16
St64/St65/St66	3	Residential	0.1/0.07/0.07	0.01/0.02/0.05	6.5/4/1.5	0.76/0.98/1.01	159.23	0.16/0.13/0.12
St67/St68/St69	4	Residential	0.09/0.07/0.05	0.01/0.02/0.04	6.5/4/1.5	0.83/1.06/1.34	216.19	0.15/0.12/0.09
St70/St71/St72	5	Residential	0.08/0.06/0.04	0.01/0.02/0.03	6.5/4/1.5	0.94/1.19/1.66	273.15	0.13/0.1/0.07
St73/St74/St75	8	Residential	0.06/0.05/0.03	0.01/0.01/0.02	6.5/4/1.5	1.12/1.44/2.29	444.04	0.11/0.09/0.05
Performance Group No. PG-18/PG-42/PG-66								
St151/St152/St153	2	Residential	0.44/0.4/0.4	0.07/0.1/0.26	6.5/4/1.5	0.67/0.75/0.75	297.49	0.76/0.68/0.68
St154/St155/St156	3	Residential	0.39/0.3/0.29	0.06/0.08/0.18	6.5/4/1.65	0.76/0.98/1.01	463.2	0.67/0.52/0.5
St157/St158/St159	4	Residential	0.36/0.28/0.22	0.05/0.07/0.1	6.5/4/2.14	0.83/1.06/1.34	628.91	0.61/0.48/0.38
St160/St161/St162	5	Residential	0.32/0.25/0.19	0.05/0.06/0.09	6.5/4/2.21	0.94/1.18/1.57	794.62	0.54/0.43/0.32
St163/St164/St165	8	Residential	0.26/0.21/0.15	0.04/0.05/0.07	6.5/4/2.1	1.12/1.44/1.99	1291.74	0.45/0.35/0.25
Performance Group No. PG-19/PG-43/PG-67								
St241/St242/St243	2	Residential	0.67/0.6/0.6	0.1/0.15/0.3	6.5/4/1.97	0.67/0.75/0.75	82.78	1.15/1.02/1.02
St244/St245/St246	3	Residential	0.59/0.46/0.44	0.09/0.11/0.18	6.5/4/2.47	0.76/0.98/1.01	130.28	1.01/0.78/0.76
St247/St248/St249	4	Residential	0.54/0.42/0.35	0.08/0.11/0.12	6.5/4/2.81	0.83/1.06/1.29	176.89	0.93/0.72/0.6
St250/St251/St252	5	Residential	0.48/0.38/0.32	0.07/0.09/0.11	6.5/4/2.97	0.94/1.19/1.39	223.5	0.82/0.65/0.55
St253/St254/St255	8	Residential	0.4/0.31/0.24	0.06/0.08/0.09	6.5/4/2.58	1.12/1.44/1.86	363.33	0.69/0.53/0.41
Performance Group No. PG-20/PG-44/PG-68								
St331/St332/St333	2	Residential	0.74/0.66/0.66	0.11/0.17/0.3	6.5/4/2.18	0.67/0.75/0.75	92.97	1.27/1.13/1.13
St334/St335/St336	3	Residential	0.65/0.51/0.49	0.1/0.13/0.18	6.5/4/2.73	0.76/0.98/1.01	144.75	1.12/0.87/0.84
St337/St338/St339	4	Residential	0.6/0.47/0.4	0.09/0.12/0.12	6.5/4/3.25	0.83/1.06/1.25	196.53	1.02/0.8/0.68
St340/St341/St342	5	Residential	0.53/0.42/0.36	0.08/0.1/0.12	6.5/4/3	0.94/1.19/1.38	248.32	0.9/0.71/0.62
St343/St344/St345	8	Residential	0.44/0.35/0.28	0.07/0.09/0.1	6.5/4/2.8	1.12/1.44/1.8	403.67	0.76/0.59/0.47

Table E.1: Key Archetype Design Parameters

Archetype Design ID Number	*No. of Stories*	*Key Archetype Design Parameters*							
		Gravity Loads	*Seismic Design Criteria*						$S_{MT}(T_1)[g]$
			$S_a(T_1)[g]$	$S_d(T_1)[g]$	q	$T_1[sec]$	$M[ton]$		
Performance Group No. PG-21/PG-45/PG-69									
St76/St77/St78	2	Residential	0.11/0.11/0.11	0.02/0.03/0.08	6.5/4/1.5	0.64/0.64/0.64	148.75	0.19/0.19/0.19	
St79/St80/St81	3	Residential	0.09/0.08/0.08	0.01/0.02/0.06	6.5/4/1.5	0.81/0.86/0.86	231.6	0.15/0.14/0.14	
St82/St83/St84	4	Residential	0.09/0.06/0.06	0.01/0.02/0.04	6.5/4/1.5	0.84/1.13/1.16	314.45	0.15/0.11/0.11	
St85/St86/St87	5	Residential	0.08/0.06/0.05	0.01/0.01/0.03	6.5/4/1.5	0.93/1.21/1.43	397.31	0.13/0.1/0.09	
St88/St89/St90	8	Residential	0.06/0.05/0.04	0.01/0.01/0.02	6.5/4/1.5	1.2/1.52/2.03	645.85	0.1/0.08/0.06	
Performance Group No. PG-22/PG-46/PG-70									
St166/St167/St168	2	Residential	0.46/0.46/0.46	0.07/0.12/0.31	6.5/4/1.5	0.64/0.64/0.64	125.5	0.79/0.79/0.79	
St169/St170/St171	3	Residential	0.37/0.34/0.34	0.06/0.09/0.22	6.5/4/1.6	0.81/0.86/0.86	195.41	0.63/0.59/0.59	
St172/St173/St174	4	Residential	0.35/0.26/0.26	0.05/0.07/0.15	6.5/4/1.71	0.84/1.12/1.15	265.32	0.6/0.45/0.44	
St175/St176/St177	5	Residential	0.32/0.24/0.21	0.05/0.06/0.09	6.5/4/2.22	0.93/1.21/1.43	335.23	0.54/0.42/0.35	
St178/St179/St180	8	Residential	0.25/0.19/0.15	0.04/0.05/0.06	6.5/4/2.36	1.2/1.52/1.98	544.95	0.42/0.33/0.26	
Performance Group No. PG-23/PG-47/PG-71									
St256/St257/St258	2	Residential	0.7/0.7/0.7	0.11/0.18/0.35	6.5/4/2	0.64/0.64/0.64	102.26	1.2/1.2/1.2	
St259/St260/St261	3	Residential	0.55/0.52/0.52	0.09/0.13/0.21	6.5/4/2.47	0.81/0.86/0.86	159.23	0.95/0.89/0.89	
St262/St263/St264	4	Residential	0.53/0.4/0.39	0.08/0.1/0.14	6.5/4/2.68	0.84/1.13/1.16	216.19	0.91/0.68/0.66	
St265/St266/St267	5	Residential	0.48/0.37/0.31	0.07/0.09/0.1	6.5/4/3.3	0.93/1.21/1.43	273.15	0.83/0.63/0.54	
St268/St269/St270	8	Residential	0.37/0.3/0.25	0.06/0.07/0.08	6.5/4/3.19	1.2/1.52/1.79	444.04	0.64/0.51/0.43	
Performance Group No. PG-24/PG-48/PG-72									
St346/St347/St348	2	Residential	0.78/0.78/0.78	0.12/0.19/0.34	6.5/4/2.28	0.64/0.64/0.64	297.49	1.33/1.33/1.33	
St349/St350/St351	3	Residential	0.61/0.58/0.58	0.09/0.14/0.21	6.5/4/2.73	0.81/0.86/0.86	463.2	1.05/0.99/0.99	
St352/St353/St354	4	Residential	0.59/0.43/0.43	0.09/0.11/0.14	6.5/4/2.97	0.84/1.15/1.16	628.91	1.01/0.74/0.73	
St355/St356/St357	5	Residential	0.53/0.41/0.36	0.08/0.1/0.09	6.5/4/3.88	0.93/1.21/1.37	794.62	0.91/0.7/0.62	
St358/St359/St360	8	Residential	0.41/0.33/0.29	0.06/0.08/0.08	6.5/4/3.61	1.2/1.52/1.7	1291.74	0.71/0.56/0.5	

E.2 FEMA P695 Results

Table E.2: FEMA695 results for each archetype

ID	*St.*	$T_1[sec]$	$V_{elast}[kN]$	$V_{des}[kN]$	Δ_y	μ_T	Ω	$V_{max}[kN]$	$S_{CT}[g]$	*CMR*	*SSF*	*ACMR*
St1	2	0.65	90.26	13.89	1.14	8.71	40.15	557.51	3.23	17.00	1.16	19.72
St2	2	0.80	73.34	18.33	1.22	5.94	21.32	390.96	2.16	14.01	1.17	16.40
St3	2	0.80	73.34	48.89	1.22	5.94	8.00	390.96	2.16	14.01	1.17	16.40
St4	3	0.76	121.49	18.69	1.01	8.70	38.97	728.40	3.24	19.93	1.20	23.92
St5	3	0.96	96.18	24.05	1.13	8.00	20.95	503.68	2.08	16.15	1.25	20.19
St6	3	1.16	79.60	53.07	1.10	4.58	6.53	346.40	0.97	9.12	1.20	10.95
St7	4	0.83	151.05	23.24	0.92	8.38	38.33	890.66	3.06	20.55	1.20	24.66
St8	4	1.05	119.40	29.85	1.01	7.88	21.08	629.29	1.99	16.91	1.27	21.47
St9	4	1.42	88.29	58.86	1.01	5.32	5.96	350.98	0.86	9.92	1.30	12.89
St10	5	0.93	170.33	26.20	0.89	8.01	38.34	1004.63	2.72	20.49	1.22	25.00
St11	5	1.16	136.56	34.14	0.94	7.59	20.99	716.66	1.91	17.98	1.30	23.37
St12	5	1.77	89.49	59.66	0.96	4.27	5.32	317.38	0.47	6.79	1.25	8.49
St13	8	1.11	231.99	35.69	0.79	7.78	41.64	1486.20	2.67	23.99	1.27	30.47
St14	8	1.42	181.35	45.34	0.83	6.44	22.04	999.00	1.58	18.21	1.30	23.68
St15	8	2.55	79.20	52.80	0.85	3.26	6.06	320.03	0.31	8.17	1.21	9.89
St16	2	0.68	96.90	14.91	1.16	8.53	38.74	577.46	3.30	18.18	1.18	21.45
St17	2	0.77	85.57	21.39	1.23	6.64	22.58	483.09	2.54	15.84	1.17	18.54
St18	2	0.77	85.57	57.05	1.23	6.64	8.47	483.09	2.54	15.84	1.17	18.54
St19	3	0.77	133.24	20.50	1.01	8.45	38.03	779.58	3.02	18.82	1.20	22.59
St20	3	0.95	107.99	27.00	1.10	7.85	20.92	564.69	2.08	16.02	1.22	19.54
St21	3	1.01	101.58	67.72	1.10	5.52	7.39	500.13	1.47	11.99	1.21	14.51
St22	4	0.83	167.82	25.82	0.92	8.27	38.81	1002.02	2.89	19.40	1.20	23.28
St23	4	1.07	130.18	32.55	0.99	6.07	20.47	666.07	1.65	14.26	1.23	17.54
St24	4	1.37	101.67	67.78	1.02	4.21	6.21	421.03	0.70	7.73	1.23	9.51
St25	5	0.91	193.40	29.75	0.86	8.00	39.23	1167.36	2.63	19.37	1.22	23.63
St26	5	1.20	146.66	36.67	0.97	6.75	20.58	754.42	1.62	15.76	1.25	19.71
St27	5	1.64	107.31	71.54	0.96	4.79	5.75	411.69	0.56	7.45	1.25	9.31
St28	8	1.12	255.45	39.30	0.80	7.59	41.98	1649.64	1.63	14.80	1.27	18.80
St29	8	1.43	200.07	50.02	0.87	5.66	22.40	1120.54	1.25	14.52	1.30	18.87
St30	8	2.43	96.90	64.60	0.87	3.72	6.25	403.63	0.38	9.12	1.25	11.40
St31	2	0.57	175.71	27.03	0.97	6.89	41.44	1120.26	3.56	17.30	1.13	19.55
St32	2	0.57	175.71	43.93	0.97	6.89	25.50	1120.26	3.56	17.30	1.13	19.55
St33	2	0.57	175.71	117.14	0.97	6.89	9.56	1120.26	3.56	17.30	1.13	19.55
St34	3	0.75	218.86	33.67	0.93	7.07	37.36	1257.97	3.10	18.82	1.18	22.21
St35	3	0.81	202.65	50.66	0.92	4.83	20.85	1056.46	2.06	13.51	1.14	15.40
St36	3	0.81	202.65	135.10	0.92	4.83	7.82	1056.46	2.06	13.51	1.14	15.40
St37	4	0.83	268.52	41.31	0.87	7.97	37.51	1549.38	3.16	21.22	1.20	25.46
St38	4	1.04	214.30	53.57	0.87	6.07	19.01	1018.58	1.40	11.77	1.21	14.24
St39	4	1.06	210.25	140.17	0.87	5.30	7.10	994.57	1.22	10.44	1.23	12.84
St40	5	0.89	316.40	48.68	0.84	7.58	39.00	1898.58	2.77	19.93	1.22	24.31
St41	5	1.11	253.69	63.42	0.85	5.73	20.43	1295.82	1.72	15.48	1.23	19.05

Table E.2: FEMA695 results for each archetype

ID	*St.*	$T_1[sec]$	$V_{elast}[kN]$	$V_{des}[kN]$	Δ_y	μ_T	Ω	$V_{max}[kN]$	$S_{CT}[g]$	*CMR*	*SSF*	*ACMR*
St42	5	1.24	227.09	151.39	0.83	5.43	6.85	1037.18	1.22	12.27	1.25	15.34
St43	8	1.11	412.40	63.45	0.83	8.06	43.38	2752.16	2.43	21.84	1.27	27.73
St44	8	1.43	320.11	80.03	0.83	5.75	21.22	1698.12	1.09	12.64	1.30	16.43
St45	8	1.84	248.78	165.86	0.79	5.32	6.26	1037.66	0.70	10.38	1.32	13.70
St46	2	0.66	134.77	20.73	1.30	7.71	33.43	693.03	3.22	17.22	1.18	20.32
St47	2	0.71	125.28	31.32	1.29	5.70	18.86	590.72	2.87	16.52	1.15	18.99
St48	2	0.71	125.28	83.52	1.29	5.70	7.07	590.72	2.87	16.52	1.15	18.99
St49	3	0.79	175.31	26.97	1.13	7.63	30.66	826.97	2.98	19.07	1.20	22.89
St50	3	0.98	141.32	35.33	1.22	5.79	17.08	603.38	1.83	14.49	1.21	17.53
St51	3	0.98	141.32	94.21	1.22	5.79	6.40	603.38	1.83	14.49	1.21	17.53
St52	4	0.85	221.23	34.04	0.97	7.88	30.96	1053.82	3.04	20.92	1.22	25.52
St53	4	1.11	169.41	42.35	1.10	5.44	16.59	702.77	1.55	13.93	1.23	17.14
St54	4	1.30	144.65	96.43	1.15	4.90	5.44	524.85	1.08	11.36	1.22	13.86
St55	5	0.97	244.94	37.68	0.92	7.60	31.15	1173.79	2.50	19.60	1.25	24.49
St56	5	1.24	191.61	47.90	1.05	6.32	16.94	811.29	1.57	15.81	1.25	19.76
St57	5	1.64	144.87	96.58	1.12	4.38	4.87	470.04	0.67	8.84	1.25	11.04
St58	8	1.21	319.20	49.11	0.86	6.81	33.61	1650.68	1.99	19.45	1.25	24.31
St59	8	1.54	250.80	62.70	0.91	5.92	18.14	1137.54	1.32	16.41	1.32	21.66
St60	8	2.57	116.95	77.97	1.09	2.85	5.41	421.75	0.32	8.45	1.21	10.22
St61	2	0.67	108.18	16.64	1.17	8.34	40.20	669.06	3.16	17.11	1.18	20.19
St62	2	0.75	96.64	24.16	1.18	6.25	22.35	539.99	2.59	15.72	1.15	18.08
St63	2	0.75	96.64	64.43	1.18	6.25	8.38	539.99	2.59	15.72	1.15	18.08
St64	3	0.76	148.49	22.84	1.03	8.14	39.13	893.96	3.17	19.50	1.20	23.40
St65	3	0.98	115.15	28.79	1.11	6.90	20.50	590.25	1.78	14.09	1.21	17.05
St66	3	1.01	111.73	74.49	1.11	6.36	7.35	547.44	1.59	13.01	1.21	15.74
St67	4	0.83	184.61	28.40	0.91	8.00	38.29	1087.61	3.05	20.52	1.20	24.63
St68	4	1.06	144.55	36.14	1.01	6.40	20.64	745.81	1.78	15.29	1.23	18.81
St69	4	1.34	114.35	76.23	0.96	5.18	6.07	462.85	0.90	9.73	1.27	12.36
St70	5	0.94	205.95	31.68	0.87	7.38	38.27	1212.63	2.80	21.30	1.22	25.98
St71	5	1.19	162.68	40.67	0.95	6.89	20.46	831.98	1.78	17.13	1.25	21.41
St72	5	1.66	116.62	77.75	0.85	3.11	5.16	400.81	0.55	7.41	1.21	8.96
St73	8	1.12	280.99	43.23	0.81	7.09	42.03	1816.78	2.66	24.08	1.27	30.59
St74	8	1.44	218.55	54.64	0.87	5.60	21.89	1195.93	1.44	16.78	1.30	21.81
St75	8	2.29	120.02	80.02	0.79	4.17	5.67	453.44	0.47	10.00	1.25	12.50
St76	2	0.64	329.45	50.68	1.21	5.26	22.99	1165.14	2.93	15.20	1.13	17.17
St77	2	0.64	329.45	82.36	1.21	5.26	14.15	1165.14	2.93	15.20	1.13	17.17
St78	2	0.64	329.45	219.63	1.21	5.26	5.30	1165.14	2.93	15.20	1.13	17.17
St79	3	0.81	405.30	62.35	1.16	6.04	22.79	1420.76	2.67	17.51	1.17	20.49
St80	3	0.86	381.74	95.43	1.15	5.44	13.26	1265.58	2.08	14.49	1.19	17.24
St81	3	0.86	381.74	254.49	1.15	5.44	4.97	1265.58	2.08	14.49	1.19	17.24
St82	4	0.84	530.64	81.64	0.98	7.03	23.59	1925.45	2.93	19.94	1.20	23.92
St83	4	1.13	394.46	98.61	1.08	4.41	11.69	1152.85	1.17	10.66	1.18	12.58
St84	4	1.16	384.26	256.17	1.11	4.47	4.39	1124.39	1.12	10.50	1.20	12.60

Table E.2: FEMA695 results for each archetype

ID	*St.*	$T_1[sec]$	$V_{elast}[kN]$	$V_{des}[kN]$	Δ_y	μ_T	Ω	$V_{max}[kN]$	$S_{CT}[g]$	*CMR*	*SSF*	*ACMR*
St85	5	0.93	605.57	93.17	0.90	7.25	23.94	2230.11	2.68	20.15	1.22	24.59
St86	5	1.21	465.44	116.36	1.06	4.74	12.48	1451.71	1.43	14.00	1.20	16.80
St87	5	1.43	393.84	262.56	1.10	4.51	4.17	1095.37	0.91	10.52	1.23	12.94
St88	8	1.20	762.93	117.37	0.92	7.25	27.54	3232.87	2.06	19.99	1.30	25.99
St89	8	1.52	602.32	150.58	0.93	5.46	13.41	2020.01	1.12	13.83	1.32	18.26
St90	8	2.03	444.33	296.22	0.98	4.39	3.95	1170.20	0.61	10.25	1.25	12.82
St91	2	0.65	370.12	56.94	1.14	8.71	9.79	557.51	3.25	4.18	1.16	4.84
St92	2	0.80	300.72	75.18	1.20	5.97	5.10	383.25	2.16	3.41	1.17	4.00
St93	2	0.80	300.72	200.48	1.20	5.97	1.91	383.25	2.16	3.41	1.17	4.00
St94	3	0.76	498.19	76.64	1.01	8.70	9.50	728.40	3.16	4.74	1.20	5.69
St95	3	0.96	394.40	98.60	1.11	8.10	5.02	495.27	2.05	3.89	1.25	4.86
St96	3	1.16	326.40	178.36	1.03	4.00	1.80	321.64	0.97	2.22	1.20	2.67
St97	4	0.83	619.38	95.29	0.92	8.39	9.29	885.63	2.91	4.77	1.20	5.72
St98	4	1.05	489.61	122.40	0.99	7.95	5.05	617.96	1.95	4.04	1.27	5.14
St99	4	1.37	375.25	155.70	0.95	6.04	2.26	351.24	1.01	2.72	1.30	3.54
St100	5	0.93	698.44	107.45	0.88	8.03	9.23	991.58	2.75	5.05	1.22	6.16
St101	5	1.16	559.95	139.99	0.92	7.64	4.98	696.84	1.75	4.01	1.30	5.21
St102	5	1.49	435.94	186.30	0.92	6.01	2.31	429.61	1.10	3.22	1.32	4.26
St103	8	1.11	951.29	146.35	0.77	7.59	9.94	1454.29	2.68	5.87	1.27	7.45
St104	8	1.42	743.61	185.90	0.79	6.21	5.17	960.76	1.60	4.50	1.30	5.85
St105	8	2.04	507.46	257.60	0.84	4.63	1.90	490.34	0.70	2.87	1.25	3.58
St106	2	0.68	397.33	61.13	1.16	8.53	9.45	577.46	3.21	4.30	1.18	5.08
St107	2	0.77	350.89	87.72	1.20	6.57	5.39	472.91	2.54	3.86	1.17	4.51
St108	2	0.77	350.89	223.49	1.20	6.57	2.12	472.91	2.54	3.86	1.17	4.51
St109	3	0.77	546.34	84.05	1.00	8.49	9.21	774.31	3.13	4.76	1.20	5.71
St110	3	0.95	442.82	110.71	1.07	7.96	4.99	552.02	1.99	3.72	1.22	4.54
St111	3	1.01	416.51	263.62	1.04	4.84	1.79	472.18	1.42	2.84	1.17	3.32
St112	4	0.83	688.16	105.87	0.91	8.29	9.42	996.89	2.79	4.57	1.20	5.49
St113	4	1.07	533.81	133.45	0.95	5.83	4.81	641.24	1.60	3.39	1.23	4.17
St114	4	1.30	439.37	208.23	0.97	5.90	2.12	441.22	1.07	2.75	1.27	3.49
St115	5	0.91	793.05	122.01	0.85	8.04	9.42	1148.79	2.80	5.03	1.22	6.13
St116	5	1.20	601.40	150.35	0.93	6.22	4.81	722.74	1.54	3.64	1.25	4.55
St117	5	1.53	471.68	224.61	0.88	4.91	1.92	432.06	0.85	2.55	1.25	3.19
St118	8	1.12	1047.47	161.15	0.78	7.45	9.99	1609.36	1.69	3.73	1.27	4.73
St119	8	1.43	820.40	205.10	0.82	4.88	5.19	1064.87	1.33	3.76	1.23	4.63
St120	8	2.03	569.37	301.26	0.81	4.40	1.78	537.58	0.64	2.60	1.25	3.25
St121	2	0.57	720.49	110.84	0.97	6.87	10.05	1114.26	3.62	4.29	1.13	4.85
St122	2	0.57	720.49	180.12	0.97	6.87	6.19	1114.26	3.62	4.29	1.13	4.85
St123	2	0.57	720.49	480.33	0.97	6.87	2.32	1114.26	3.62	4.29	1.13	4.85
St124	3	0.75	897.45	138.07	0.91	7.12	8.92	1230.91	3.04	4.50	1.18	5.31
St125	3	0.81	830.97	207.74	0.85	4.80	4.73	983.07	2.05	3.27	1.14	3.73
St126	3	0.81	830.97	553.98	0.87	4.86	1.80	999.42	2.08	3.33	1.14	3.79
St127	4	0.83	1101.06	169.39	0.85	8.09	8.96	1518.53	3.17	5.19	1.20	6.23

Table E.2: FEMA695 results for each archetype

ID	*St.*	$T_1[sec]$	$V_{elast}[kN]$	$V_{des}[kN]$	Δ_y	μ_T	Ω	$V_{max}[kN]$	$S_{CT}[g]$	*CMR*	*SSF*	*ACMR*
St128	4	1.04	878.73	219.68	0.82	4.74	4.35	956.28	1.37	2.82	1.17	3.29
St129	4	1.06	862.15	542.23	0.81	4.07	1.70	920.36	1.30	2.72	1.18	3.21
St130	5	0.89	1297.39	199.60	0.82	7.67	9.27	1849.60	2.87	5.03	1.22	6.14
St131	5	1.11	1040.25	260.06	0.81	5.77	4.72	1226.35	1.73	3.80	1.23	4.67
St132	5	1.23	938.76	512.98	0.76	5.19	1.89	969.36	1.28	3.11	1.25	3.89
St133	8	1.11	1691.04	260.16	0.80	7.88	10.32	2684.55	2.39	5.25	1.27	6.66
St134	8	1.43	1312.63	328.16	0.77	2.80	4.83	1585.60	1.08	3.05	1.19	3.63
St135	8	1.82	1031.35	515.68	0.71	5.18	1.85	954.21	0.73	2.63	1.32	3.48
St136	2	0.66	552.62	85.02	1.30	7.71	8.15	693.03	3.22	4.20	1.18	4.96
St137	2	0.71	513.71	128.43	1.28	5.71	4.56	586.26	2.88	4.03	1.15	4.63
St138	2	0.71	513.71	342.47	1.27	5.71	1.70	581.62	2.88	4.03	1.15	4.64
St139	3	0.79	718.87	110.59	1.12	7.69	7.40	818.56	2.95	4.60	1.20	5.53
St140	3	0.98	579.49	144.87	1.19	5.79	4.04	585.20	1.79	3.46	1.21	4.19
St141	3	0.98	579.49	386.33	1.19	5.79	1.51	585.20	1.79	3.46	1.21	4.19
St142	4	0.85	907.15	139.56	0.96	7.91	7.50	1046.85	2.89	4.86	1.22	5.92
St143	4	1.11	694.66	173.67	1.06	5.31	3.89	675.52	1.58	3.47	1.23	4.26
St144	4	1.30	593.14	327.70	1.09	4.74	1.51	493.52	1.08	2.76	1.22	3.37
St145	5	0.97	1004.38	154.52	0.91	7.62	7.52	1162.51	2.30	4.41	1.25	5.51
St146	5	1.24	785.69	196.42	1.02	5.70	4.00	785.16	1.57	3.84	1.25	4.80
St147	5	1.52	640.95	320.48	1.04	5.52	1.62	518.09	1.09	3.28	1.32	4.32
St148	8	1.21	1308.90	201.37	0.84	6.43	8.07	1625.96	2.06	4.91	1.25	6.14
St149	8	1.54	1028.42	257.11	0.89	5.65	4.30	1106.34	1.29	3.94	1.32	5.20
St150	8	2.11	711.47	350.48	0.95	4.20	1.62	566.18	0.62	2.73	1.25	3.41
St151	2	0.67	443.58	68.24	1.17	8.34	9.80	669.06	3.16	4.17	1.18	4.92
St152	2	0.75	396.27	99.07	1.17	6.25	5.43	538.16	2.59	3.83	1.15	4.41
St153	2	0.75	396.27	264.18	1.17	6.25	2.04	538.16	2.59	3.83	1.15	4.41
St154	3	0.76	608.88	93.67	1.03	8.14	9.54	893.94	3.17	4.76	1.20	5.71
St155	3	0.98	472.19	118.05	1.11	6.91	4.99	588.54	1.78	3.44	1.21	4.16
St156	3	1.01	458.17	277.68	1.11	6.35	1.97	546.35	1.59	3.17	1.21	3.84
St157	4	0.83	756.98	116.46	0.91	8.00	9.33	1086.54	3.05	5.01	1.20	6.01
St158	4	1.06	592.73	148.18	1.00	6.41	5.03	745.11	1.78	3.73	1.23	4.59
St159	4	1.34	468.88	219.10	0.96	3.90	2.11	461.22	0.90	2.37	1.22	2.90
St160	5	0.94	844.51	129.92	0.88	7.39	9.37	1217.66	2.80	5.19	1.22	6.34
St161	5	1.18	672.75	168.19	0.95	6.88	5.03	846.36	1.78	4.14	1.25	5.18
St162	5	1.57	505.63	228.79	0.90	4.70	2.04	466.28	0.84	2.59	1.25	3.24
St163	8	1.12	1152.21	177.26	0.81	7.09	10.24	1814.83	2.66	5.87	1.27	7.46
St164	8	1.44	896.16	224.04	0.86	5.59	5.34	1195.32	1.44	4.09	1.30	5.32
St165	8	1.99	648.48	308.80	0.85	4.59	2.08	641.78	0.64	2.50	1.25	3.12
St166	2	0.64	1350.92	207.83	1.18	5.23	5.44	1130.79	3.01	3.81	1.13	4.30
St167	2	0.64	1350.92	337.73	1.18	5.23	3.35	1130.79	3.01	3.81	1.13	4.30
St168	2	0.64	1350.92	900.61	1.18	5.23	1.26	1130.79	3.01	3.81	1.13	4.30
St169	3	0.81	1661.94	255.68	1.13	6.10	5.42	1384.84	2.67	4.26	1.17	4.99
St170	3	0.86	1565.32	391.33	1.08	4.48	3.03	1187.28	2.04	3.47	1.15	3.99

Table E.2: FEMA695 results for each archetype

ID	*St.*	$T_1[sec]$	$V_{elast}[kN]$	$V_{des}[kN]$	Δ_y	μ_T	Ω	$V_{max}[kN]$	$S_{CT}[g]$	*CMR*	*SSF*	*ACMR*
St171	3	0.86	1565.32	978.32	1.08	4.48	1.21	1187.28	2.04	3.47	1.15	3.99
St172	4	0.84	2175.91	334.76	0.95	7.17	5.60	1874.86	2.95	4.90	1.20	5.88
St173	4	1.12	1631.93	407.98	1.00	3.76	2.56	1044.40	1.22	2.69	1.18	3.18
St174	4	1.15	1589.36	929.45	1.03	3.62	1.09	1013.85	1.16	2.63	1.20	3.16
St175	5	0.93	2483.18	382.03	0.89	7.33	5.71	2180.46	2.59	4.76	1.22	5.81
St176	5	1.21	1908.56	477.14	0.99	4.75	2.83	1351.94	1.42	3.40	1.20	4.08
St177	5	1.43	1614.93	727.45	1.01	3.53	1.36	989.08	0.91	2.57	1.23	3.16
St178	8	1.20	3128.43	481.30	0.91	7.23	6.59	3169.62	2.01	4.75	1.30	6.18
St179	8	1.52	2469.82	617.45	0.89	4.78	3.09	1905.86	1.09	3.28	1.25	4.10
St180	8	1.98	1896.02	803.40	0.90	4.21	1.39	1113.92	0.63	2.48	1.25	3.10
St181	2	0.65	561.15	86.33	1.14	8.71	6.46	557.51	3.25	2.75	1.16	3.19
St182	2	0.80	455.94	113.98	1.22	5.94	3.43	390.96	2.15	2.24	1.17	2.62
St183	2	0.80	455.94	210.11	1.22	5.94	1.86	390.96	2.15	2.24	1.17	2.62
St184	3	0.76	755.32	116.20	1.01	8.70	6.27	728.40	3.17	3.13	1.20	3.76
St185	3	0.96	597.96	149.49	1.13	8.00	3.37	503.68	2.06	2.58	1.25	3.22
St186	3	1.10	521.86	183.75	1.11	5.86	2.09	384.63	1.24	1.77	1.23	2.18
St187	4	0.83	939.06	144.47	0.92	8.38	6.16	890.66	3.17	3.43	1.20	4.12
St188	4	1.05	742.31	185.58	1.01	7.88	3.39	629.29	1.93	2.64	1.27	3.36
St189	4	1.23	633.68	201.17	1.02	6.18	2.29	461.41	1.44	2.30	1.25	2.88
St190	5	0.93	1058.92	162.91	0.89	8.01	6.17	1004.63	2.77	3.35	1.22	4.09
St191	5	1.16	848.96	212.24	0.94	7.59	3.38	716.66	1.93	2.91	1.30	3.79
St192	5	1.38	713.62	247.79	0.97	6.89	2.10	520.41	1.35	2.42	1.30	3.14
St193	8	1.11	1442.27	221.89	0.79	7.78	6.70	1486.20	2.55	3.68	1.27	4.67
St194	8	1.42	1127.41	281.85	0.83	6.44	3.54	999.00	1.64	3.04	1.30	3.95
St195	8	1.88	851.55	443.52	0.88	4.90	1.37	607.25	0.74	1.80	1.25	2.26
St196	2	0.68	602.40	92.68	1.16	8.53	6.23	577.46	3.31	2.93	1.18	3.45
St197	2	0.77	531.99	133.00	1.23	6.64	3.63	483.09	2.52	2.53	1.17	2.96
St198	2	0.77	531.99	224.47	1.23	6.64	2.15	483.09	2.52	2.53	1.17	2.96
St199	3	0.77	828.32	127.43	1.01	8.45	6.12	779.58	3.10	3.11	1.20	3.74
St200	3	0.95	671.37	167.84	1.10	7.85	3.36	564.69	1.99	2.46	1.22	3.00
St201	3	1.04	613.27	268.98	1.10	4.64	1.76	474.46	1.26	1.71	1.17	2.00
St202	4	0.83	1043.35	160.51	0.92	8.27	6.24	1002.02	2.97	3.21	1.20	3.85
St203	4	1.07	809.33	202.33	0.99	6.07	3.29	666.07	1.61	2.24	1.23	2.76
St204	4	1.24	698.37	262.54	1.03	5.85	1.96	513.99	1.04	1.68	1.25	2.10
St205	5	0.91	1202.36	184.98	0.86	8.00	6.31	1167.36	2.75	3.26	1.22	3.98
St206	5	1.20	911.79	227.95	0.97	6.75	3.31	754.42	1.63	2.55	1.25	3.18
St207	5	1.47	744.32	259.35	0.98	4.88	2.00	518.15	0.83	1.58	1.25	1.97
St208	8	1.12	1588.10	244.32	0.80	7.59	6.75	1649.64	1.65	2.40	1.27	3.05
St209	8	1.43	1243.83	310.96	0.87	5.66	3.60	1120.54	1.29	2.41	1.30	3.13
St210	8	1.79	993.67	354.88	0.91	5.20	2.14	760.33	0.83	1.94	1.32	2.56
St211	2	0.57	1092.35	168.05	0.97	6.89	6.67	1120.26	3.58	2.80	1.13	3.16
St212	2	0.57	1092.35	273.09	0.97	6.89	4.10	1120.26	3.58	2.80	1.13	3.16
St213	2	0.57	1092.35	650.21	0.97	6.89	1.72	1120.26	3.58	2.80	1.13	3.16

Table E.2: FEMA695 results for each archetype

ID	*St.*	$T_1[sec]$	$V_{elast}[kN]$	$V_{des}[kN]$	Δ_y	μ_T	Ω	$V_{max}[kN]$	$S_{CT}[g]$	*CMR*	*SSF*	*ACMR*
St214	3	0.75	1360.65	209.33	0.93	7.07	6.01	1257.97	3.16	3.09	1.18	3.64
St215	3	0.81	1259.86	314.97	0.92	4.83	3.35	1056.46	2.06	2.17	1.14	2.47
St216	3	0.81	1259.86	599.93	0.92	4.83	1.76	1056.46	2.06	2.17	1.14	2.47
St217	4	0.83	1669.35	256.82	0.87	7.97	6.03	1549.38	3.10	3.36	1.20	4.03
St218	4	1.04	1332.27	333.07	0.87	6.07	3.06	1018.58	1.38	1.87	1.21	2.26
St219	4	1.06	1307.13	544.64	0.87	5.30	1.83	994.57	1.22	1.69	1.23	2.08
St220	5	0.89	1967.01	302.62	0.84	7.58	6.27	1898.58	2.75	3.19	1.22	3.89
St221	5	1.11	1577.15	394.29	0.85	5.73	3.29	1295.82	1.73	2.50	1.23	3.07
St222	5	1.24	1411.81	500.64	0.83	5.43	2.07	1037.18	1.22	1.97	1.25	2.47
St223	8	1.11	2563.84	394.44	0.83	8.06	6.98	2752.16	2.24	3.23	1.27	4.11
St224	8	1.43	1990.12	497.53	0.83	5.75	3.41	1698.12	1.08	2.02	1.30	2.63
St225	8	1.73	1645.01	567.24	0.81	5.51	2.10	1191.67	0.85	1.92	1.32	2.53
St226	2	0.66	837.85	128.90	1.30	7.71	5.38	693.03	3.38	2.90	1.18	3.42
St227	2	0.71	778.85	194.71	1.29	5.70	3.03	590.72	2.88	2.66	1.15	3.06
St228	2	0.71	778.85	463.60	1.29	5.70	1.27	590.72	2.88	2.66	1.15	3.06
St229	3	0.79	1089.89	167.68	1.13	7.63	4.93	826.97	3.03	3.12	1.20	3.75
St230	3	0.98	878.59	219.65	1.22	5.79	2.75	603.38	1.81	2.31	1.21	2.79
St231	3	1.13	761.96	258.29	1.31	5.22	1.82	469.76	1.30	1.92	1.23	2.36
St232	4	0.85	1375.36	211.59	0.97	7.88	4.98	1053.82	2.92	3.24	1.22	3.95
St233	4	1.11	1053.20	263.30	1.10	5.44	2.67	702.77	1.59	2.29	1.23	2.82
St234	4	1.30	899.27	322.32	1.15	4.90	1.63	524.85	1.08	1.82	1.22	2.22
St235	5	0.97	1522.77	234.27	0.92	7.60	5.01	1173.79	2.48	3.13	1.25	3.91
St236	5	1.24	1191.20	297.80	1.05	6.32	2.72	811.29	1.59	2.57	1.25	3.22
St237	5	1.47	1004.82	321.03	1.10	5.66	1.85	595.23	1.20	2.30	1.32	3.04
St238	8	1.21	1984.46	305.30	0.86	6.81	5.41	1650.68	1.90	3.00	1.25	3.75
St239	8	1.54	1559.22	389.81	0.91	5.92	2.92	1137.54	1.29	2.58	1.32	3.40
St240	8	1.96	1225.10	504.16	0.97	4.35	1.39	701.27	0.60	1.53	1.25	1.92
St241	2	0.67	672.53	103.47	1.17	8.34	6.47	669.06	3.16	2.75	1.18	3.25
St242	2	0.75	600.80	150.20	1.20	6.25	3.66	549.68	2.59	2.53	1.15	2.91
St243	2	0.75	600.80	304.97	1.20	6.25	1.80	549.68	2.59	2.53	1.15	2.91
St244	3	0.76	923.14	142.02	1.03	8.11	6.33	899.42	3.17	3.14	1.20	3.76
St245	3	0.98	715.90	178.98	1.14	6.85	3.37	603.71	1.78	2.27	1.21	2.74
St246	3	1.01	694.64	281.23	1.14	6.32	2.01	564.72	1.59	2.09	1.21	2.53
St247	4	0.83	1147.68	176.57	0.93	7.94	6.24	1102.39	3.05	3.30	1.20	3.96
St248	4	1.06	898.65	224.66	1.04	6.31	3.42	768.44	1.78	2.46	1.23	3.03
St249	4	1.29	738.43	262.79	1.04	5.66	2.04	535.28	0.84	1.41	1.27	1.80
St250	5	0.94	1280.39	196.98	0.90	7.35	6.32	1244.84	2.80	3.43	1.22	4.18
St251	5	1.19	1011.40	252.85	0.99	6.81	3.40	860.37	1.78	2.76	1.25	3.44
St252	5	1.39	865.87	291.54	0.99	5.93	2.22	648.30	1.16	2.10	1.30	2.73
St253	8	1.12	1746.90	268.75	0.84	7.28	6.94	1865.63	2.66	3.87	1.27	4.92
St254	8	1.44	1358.70	339.68	0.91	5.83	3.69	1251.79	1.44	2.70	1.30	3.51
St255	8	1.86	1051.90	407.71	0.91	4.60	1.94	789.37	0.63	1.53	1.25	1.92
St256	2	0.64	2048.16	315.10	1.21	5.26	3.70	1165.14	2.93	2.44	1.13	2.76

Table E.2: FEMA695 results for each archetype

ID	*St.*	$T_1[sec]$	$V_{elast}[kN]$	$V_{des}[kN]$	Δ_y	μ_T	Ω	$V_{max}[kN]$	$S_{CT}[g]$	*CMR*	*SSF*	*ACMR*
St257	2	0.64	2048.16	512.04	1.21	5.26	2.28	1165.14	2.93	2.44	1.13	2.76
St258	2	0.64	2048.16	1024.08	1.21	5.26	1.14	1165.14	2.98	2.48	1.13	2.81
St259	3	0.81	2519.72	387.65	1.16	6.04	3.67	1420.76	2.67	2.82	1.17	3.30
St260	3	0.86	2373.23	593.31	1.15	5.44	2.13	1265.58	2.08	2.33	1.19	2.77
St261	3	0.86	2373.23	960.82	1.15	5.44	1.32	1265.58	2.04	2.29	1.19	2.72
St262	4	0.84	3298.96	507.53	0.98	7.03	3.79	1925.45	2.93	3.21	1.20	3.85
St263	4	1.13	2452.32	613.08	1.08	4.41	1.88	1152.85	1.17	1.71	1.18	2.02
St264	4	1.16	2388.90	891.38	1.11	4.47	1.26	1124.39	1.11	1.67	1.20	2.01
St265	5	0.93	3764.81	579.20	0.90	7.25	3.85	2230.11	2.68	3.24	1.22	3.95
St266	5	1.21	2893.62	723.40	1.06	4.74	2.01	1451.71	1.43	2.25	1.20	2.70
St267	5	1.43	2448.45	741.95	1.10	4.51	1.48	1095.37	0.93	1.73	1.23	2.12
St268	8	1.20	4743.11	729.71	0.92	7.25	4.43	3232.87	2.06	3.22	1.30	4.18
St269	8	1.52	3744.56	936.14	0.93	5.46	2.16	2020.01	1.12	2.22	1.32	2.94
St270	8	1.79	3179.74	996.78	0.97	4.74	1.51	1504.63	0.71	1.67	1.25	2.08
St271	2	0.65	620.85	95.52	1.14	8.71	5.84	557.51	3.25	2.49	1.16	2.89
St272	2	0.80	504.44	126.11	1.22	5.94	3.10	390.96	2.14	2.02	1.17	2.36
St273	2	0.80	504.44	210.18	1.22	5.94	1.86	390.96	2.14	2.02	1.17	2.36
St274	3	0.76	835.68	128.57	1.01	8.70	5.67	728.40	3.16	2.83	1.20	3.39
St275	3	0.96	661.58	165.39	1.13	8.00	3.05	503.68	2.10	2.37	1.25	2.97
St276	3	1.10	577.38	183.88	1.11	5.86	2.09	384.63	1.24	1.61	1.23	1.98
St277	4	0.83	1038.96	159.84	0.92	8.38	5.57	890.66	3.14	3.07	1.20	3.68
St278	4	1.05	821.28	205.32	1.01	7.88	3.06	629.29	1.98	2.45	1.27	3.11
St279	4	1.21	712.68	207.17	1.03	6.39	2.34	484.12	1.49	2.12	1.25	2.65
St280	5	0.93	1171.57	180.24	0.89	8.01	5.57	1004.63	2.79	3.06	1.22	3.73
St281	5	1.16	939.28	234.82	0.94	7.59	3.05	716.66	1.79	2.44	1.30	3.17
St282	5	1.34	813.11	254.10	0.98	7.26	2.21	561.53	1.47	2.32	1.32	3.07
St283	8	1.11	1595.71	245.49	0.79	7.78	6.05	1486.20	2.67	3.49	1.27	4.43
St284	8	1.42	1247.35	311.84	0.83	6.44	3.20	999.00	1.68	2.81	1.30	3.65
St285	8	1.79	989.52	342.39	0.88	5.29	1.94	663.13	0.86	1.82	1.32	2.40
St286	2	0.68	666.48	102.54	1.16	8.53	5.63	577.46	3.25	2.60	1.18	3.07
St287	2	0.77	588.58	147.15	1.23	6.64	3.28	483.09	2.53	2.29	1.17	2.68
St288	2	0.77	588.58	223.80	1.23	6.64	2.16	483.09	2.53	2.29	1.17	2.68
St289	3	0.77	916.44	140.99	1.01	8.45	5.53	779.58	3.15	2.86	1.20	3.43
St290	3	0.95	742.80	185.70	1.10	7.85	3.04	564.69	2.07	2.31	1.22	2.82
St291	3	1.04	678.52	268.19	1.10	4.64	1.77	474.46	1.26	1.55	1.17	1.81
St292	4	0.83	1154.34	177.59	0.92	8.27	5.64	1002.02	2.97	2.90	1.20	3.48
St293	4	1.07	895.42	223.86	0.99	6.07	2.98	666.07	1.59	2.00	1.23	2.45
St294	4	1.30	737.00	249.83	1.03	5.78	1.87	467.38	1.07	1.63	1.27	2.07
St295	5	0.91	1330.28	204.66	0.86	8.00	5.70	1167.36	2.74	2.94	1.22	3.59
St296	5	1.20	1008.79	252.20	0.97	6.75	2.99	754.42	1.59	2.25	1.25	2.81
St297	5	1.45	834.86	278.29	0.98	4.90	1.92	535.25	0.94	1.60	1.23	1.96
St298	8	1.12	1757.05	270.31	0.80	7.59	6.10	1649.64	1.56	2.06	1.27	2.61
St299	8	1.43	1376.15	344.04	0.87	5.66	3.26	1120.54	1.25	2.11	1.30	2.74

Table E.2: FEMA695 results for each archetype

ID	*St.*	$T_1[sec]$	$V_{elast}[kN]$	$V_{des}[kN]$	Δ_y	μ_T	Ω	$V_{max}[kN]$	$S_{CT}[g]$	*CMR*	*SSF*	*ACMR*
St300	8	1.69	1164.43	363.89	0.91	5.66	2.29	833.60	0.96	1.91	1.32	2.52
St301	2	0.57	1208.56	185.93	0.97	6.89	6.03	1120.26	3.51	2.48	1.13	2.80
St302	2	0.57	1208.56	302.14	0.97	6.89	3.71	1120.26	3.51	2.48	1.13	2.80
St303	2	0.57	1208.56	653.28	0.97	6.89	1.71	1120.26	3.51	2.48	1.13	2.80
St304	3	0.75	1505.40	231.60	0.93	7.07	5.43	1257.97	3.19	2.82	1.18	3.32
St305	3	0.81	1393.89	348.47	0.92	4.83	3.03	1056.46	2.06	1.96	1.14	2.23
St306	3	0.81	1393.89	598.24	0.92	4.83	1.77	1056.46	2.06	1.96	1.14	2.23
St307	4	0.83	1846.94	284.15	0.87	7.97	5.45	1549.38	3.14	3.07	1.20	3.68
St308	4	1.04	1474.00	368.50	0.87	6.07	2.76	1018.58	1.39	1.70	1.21	2.06
St309	4	1.06	1446.19	543.68	0.87	5.30	1.83	994.57	1.21	1.51	1.23	1.86
St310	5	0.89	2176.27	334.81	0.84	7.58	5.67	1898.58	2.78	2.91	1.22	3.55
St311	5	1.11	1744.93	436.23	0.85	5.73	2.97	1295.82	1.76	2.30	1.23	2.83
St312	5	1.24	1562.00	500.64	0.83	5.43	2.07	1037.18	1.22	1.78	1.25	2.23
St313	8	1.11	2836.59	436.40	0.83	8.06	6.31	2752.16	2.24	2.92	1.27	3.71
St314	8	1.43	2201.83	550.46	0.83	5.75	3.08	1698.12	1.09	1.84	1.30	2.39
St315	8	1.68	1874.18	624.73	0.81	5.60	1.99	1241.02	0.87	1.72	1.32	2.27
St316	2	0.66	926.98	142.61	1.30	7.71	4.86	693.03	3.22	2.50	1.18	2.95
St317	2	0.71	861.70	215.43	1.29	5.70	2.74	590.72	2.91	2.43	1.15	2.80
St318	2	0.71	861.70	463.28	1.29	5.70	1.28	590.72	2.91	2.43	1.15	2.80
St319	3	0.79	1205.84	185.51	1.13	7.63	4.46	826.97	2.98	2.77	1.20	3.33
St320	3	0.98	972.06	243.01	1.22	5.79	2.48	603.38	1.81	2.08	1.21	2.52
St321	3	1.13	843.02	257.80	1.31	5.22	1.82	469.76	1.32	1.75	1.23	2.15
St322	4	0.85	1521.67	234.10	0.97	7.88	4.50	1053.82	2.94	2.94	1.22	3.58
St323	4	1.11	1165.24	291.31	1.10	5.44	2.41	702.77	1.59	2.08	1.23	2.55
St324	4	1.30	994.94	320.95	1.15	4.90	1.64	524.85	1.09	1.66	1.22	2.03
St325	5	0.97	1684.77	259.20	0.92	7.60	4.53	1173.79	2.50	2.86	1.25	3.57
St326	5	1.24	1317.92	329.48	1.05	6.32	2.46	811.29	1.51	2.21	1.25	2.76
St327	5	1.42	1150.86	338.49	1.09	5.77	1.87	632.81	1.23	2.06	1.30	2.68
St328	8	1.21	2195.58	337.78	0.86	6.81	4.89	1650.68	1.97	2.81	1.25	3.51
St329	8	1.54	1725.09	431.27	0.91	5.92	2.64	1137.54	1.33	2.41	1.32	3.19
St330	8	1.92	1383.67	518.23	0.97	4.43	1.43	741.41	0.66	1.48	1.25	1.85
St331	2	0.67	744.08	114.47	1.17	8.34	5.84	669.06	3.16	2.49	1.18	2.94
St332	2	0.75	664.71	166.18	1.20	6.25	3.31	549.68	2.59	2.29	1.15	2.63
St333	2	0.75	664.71	304.91	1.20	6.25	1.80	549.68	2.59	2.29	1.15	2.63
St334	3	0.76	1021.34	157.13	1.03	8.11	5.72	899.42	3.17	2.84	1.20	3.40
St335	3	0.98	792.06	198.02	1.14	6.85	3.05	603.71	1.78	2.05	1.21	2.48
St336	3	1.01	768.54	281.52	1.14	6.32	2.01	564.72	1.59	1.89	1.21	2.29
St337	4	0.83	1269.77	195.35	0.93	7.94	5.64	1102.39	3.05	2.98	1.20	3.58
St338	4	1.06	994.26	248.56	1.04	6.31	3.09	768.44	1.78	2.22	1.23	2.73
St339	4	1.25	843.13	259.42	1.04	5.85	2.20	570.17	1.15	1.69	1.25	2.12
St340	5	0.94	1416.60	217.94	0.90	7.35	5.71	1244.84	2.80	3.10	1.22	3.78
St341	5	1.19	1118.99	279.75	0.99	6.81	3.08	860.37	1.78	2.49	1.25	3.11
St342	5	1.38	964.93	321.64	0.98	5.98	2.04	656.78	1.18	1.91	1.30	2.48

Table E.2: FEMA695 results for each archetype

ID	*St.*	$T_1[sec]$	$V_{elast}[kN]$	$V_{des}[kN]$	Δ_y	μ_T	Ω	$V_{max}[kN]$	$S_{CT}[g]$	*CMR*	*SSF*	*ACMR*
St343	8	1.12	1932.74	297.34	0.84	7.28	6.27	1865.63	2.66	3.50	1.27	4.45
St344	8	1.44	1503.24	375.81	0.91	5.83	3.33	1251.79	1.44	2.44	1.30	3.17
St345	8	1.80	1202.59	429.50	0.92	4.64	1.95	835.97	0.68	1.43	1.25	1.79
St346	2	0.64	2266.05	348.62	1.21	5.26	3.34	1165.14	2.98	2.25	1.13	2.54
St347	2	0.64	2266.05	566.51	1.21	5.26	2.06	1165.14	2.98	2.25	1.13	2.54
St348	2	0.64	2266.05	993.88	1.21	5.26	1.17	1165.14	2.98	2.25	1.13	2.54
St349	3	0.81	2787.78	428.89	1.16	6.04	3.31	1420.76	2.66	2.54	1.17	2.97
St350	3	0.86	2625.70	656.42	1.15	5.44	1.93	1265.58	2.07	2.10	1.19	2.50
St351	3	0.86	2625.70	961.79	1.15	5.44	1.32	1265.58	2.07	2.10	1.19	2.50
St352	4	0.84	3649.91	561.53	0.98	7.03	3.43	1925.45	2.92	2.88	1.20	3.46
St353	4	1.15	2666.02	666.51	1.13	4.51	1.70	1132.74	1.18	1.59	1.20	1.91
St354	4	1.16	2643.04	889.91	1.11	4.47	1.26	1124.39	1.12	1.53	1.20	1.84
St355	5	0.93	4165.33	640.82	0.90	7.25	3.48	2230.11	2.57	2.81	1.22	3.43
St356	5	1.21	3201.45	800.36	1.06	4.74	1.81	1451.71	1.48	2.11	1.20	2.53
St357	5	1.37	2827.56	728.75	1.09	4.83	1.65	1200.24	1.18	1.90	1.23	2.33
St358	8	1.20	5247.69	807.34	0.92	7.25	4.00	3232.87	2.04	2.88	1.30	3.75
St359	8	1.52	4142.92	1035.73	0.93	5.46	1.95	2020.01	1.09	1.94	1.32	2.56
St360	8	1.70	3704.25	1026.11	0.96	4.64	1.60	1641.70	0.73	1.47	1.25	1.83

Appendix F

Seismic Structural Performance Summary

This appendix describes in detail the seismic structural performance for all the archetype structures analysed in the thesis. Due to space limitation, the seismic structural performance summary is only presented for 5 buldings. The results for other buildings are available in Seismic Structural Performance Summary.

Building Type: Steel Moment Resisting Frame, designed according EC8

Building Design ID: *St1*

Location: *Porto - Soil Type B*

Number of Stories: *2*

Fundamental Period (sec): *0.65*

Behaviour Factor: *6.50*

Elastic Base Shear (kN): *90.26*

Design Base Shear (kN): *13.89*

Mass (ton): *82.78*

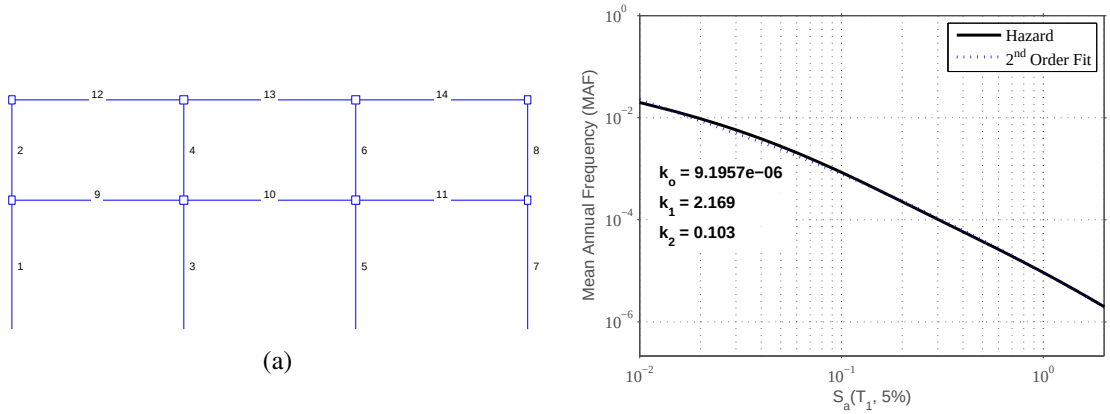

(a) (b)

Figure F.1: (a) Structure Configuration and (b) Hazard Curve

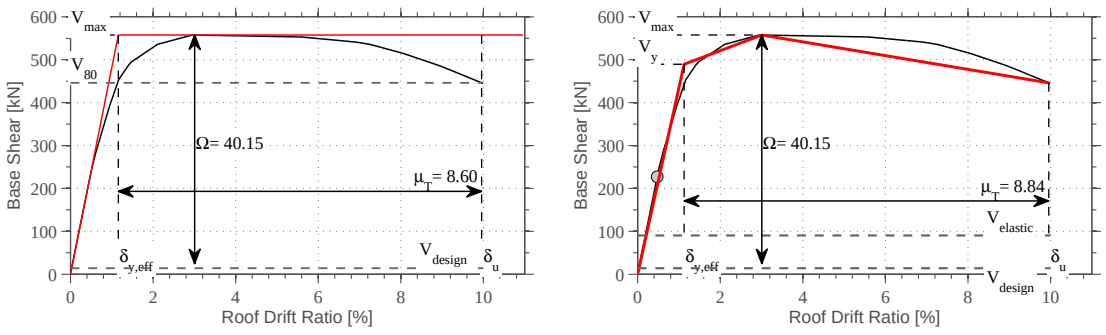

(a) (b)

Figure F.2: Nonlinear static pushover results.

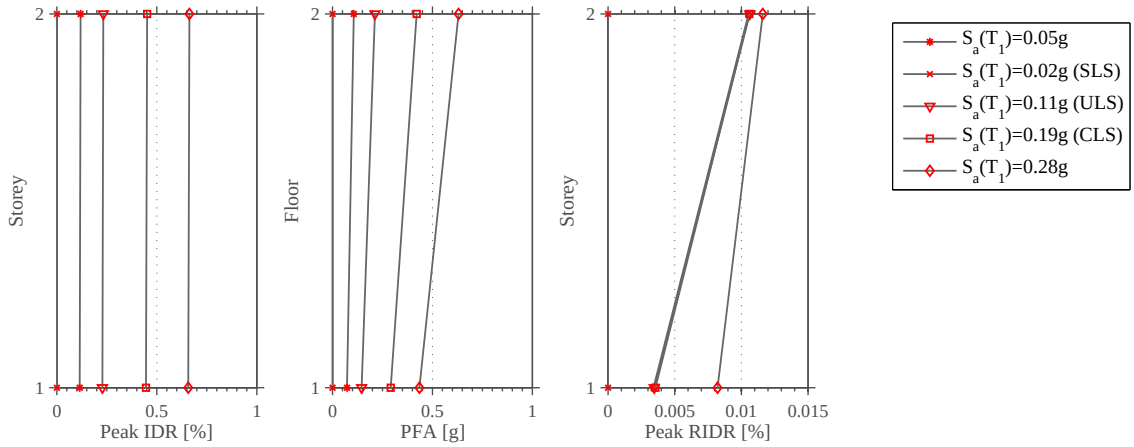

Figure F.3: Maximum ISDR, PFA and RISDR along building height.

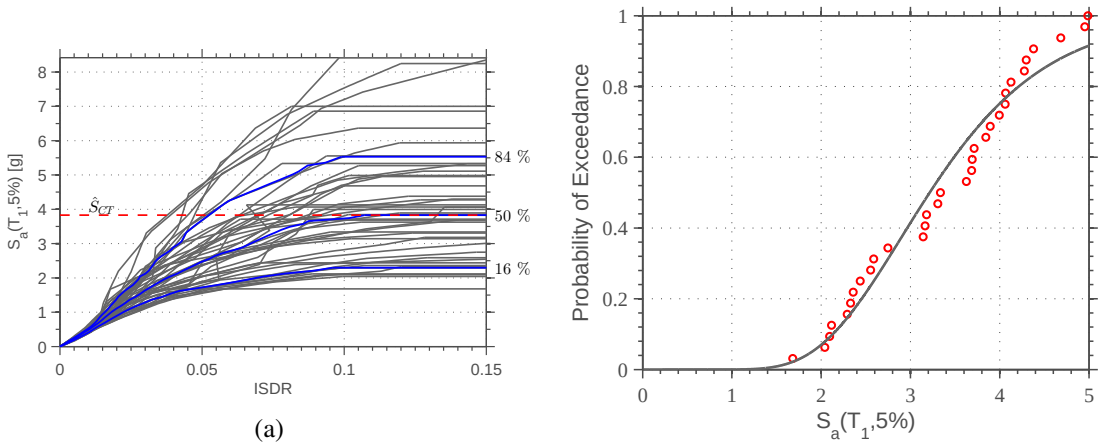

(a) (b)

Figure F.4: IDA curves and collapse fragility curves (FEMA 695).

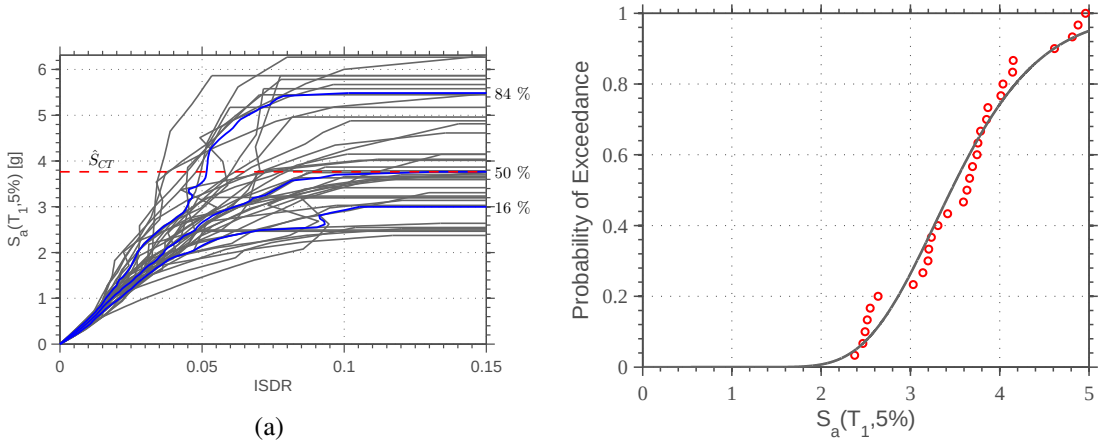

(a) (b)

Figure F.5: IDA curves and collapse fragility curves.

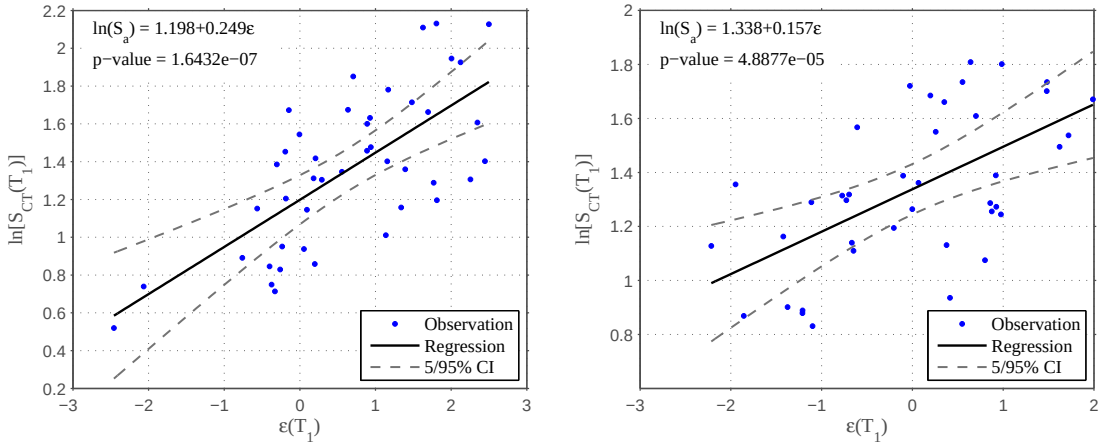

(a) (b)

Figure F.6: Relationship between collapse capacity and ε: (a) FEMA GM set and (b) Hazard set

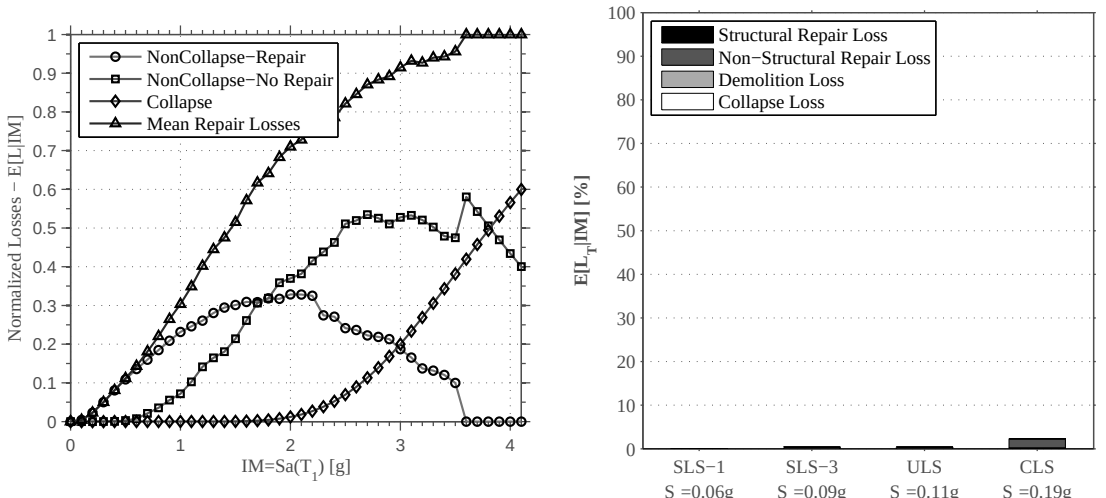

(a) (b)

Figure F.7: Vulnerability curves and corresponding normalized expected losses at several intensity levels.

Building Type: Steel Moment Resisting Frame, designed according EC8

Building Design ID: *St4*

Location: *Porto - Soil Type B*

Number of Stories: *3*

Fundamental Period (sec): *0.76*

Behaviour Factor: *6.50*

Elastic Base Shear (kN): *121.49*

Design Base Shear (kN): *20.84*

Mass (ton): *130.28*

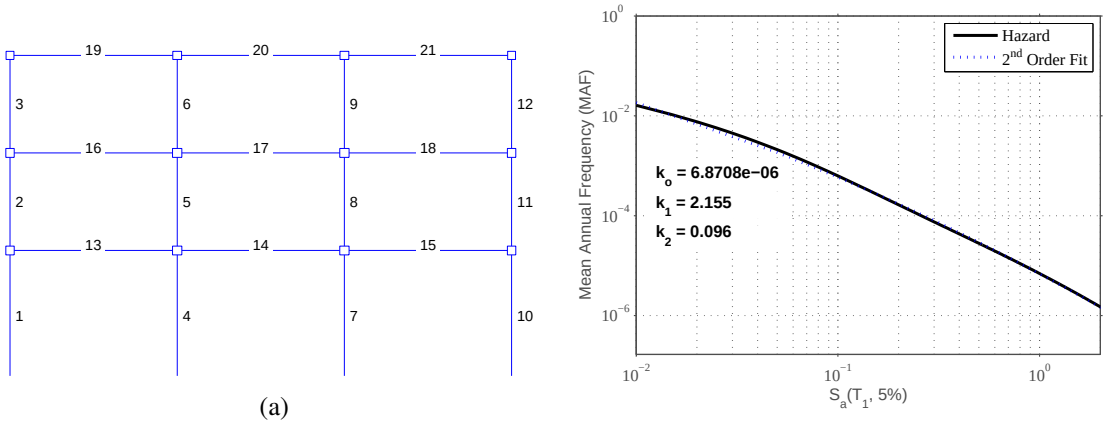

(a) (b)

Figure F.8: (a) Structure Configuration and (b) Hazard Curve

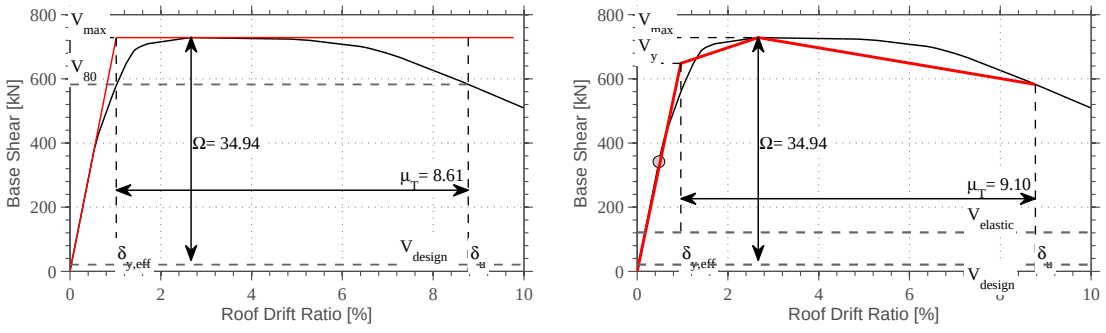

(a) (b)

Figure F.9: Nonlinear static pushover results.

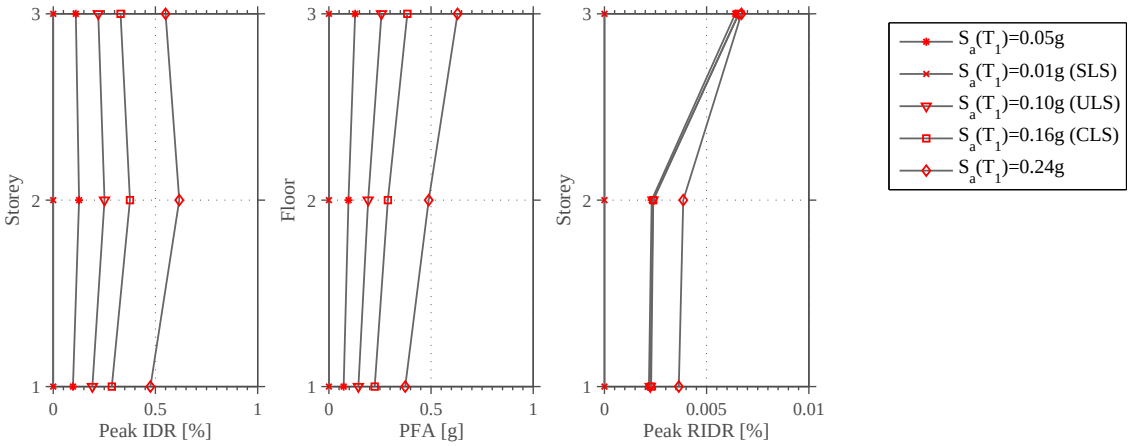

Figure F.10: Maximum ISDR, PFA and RISDR along building height.

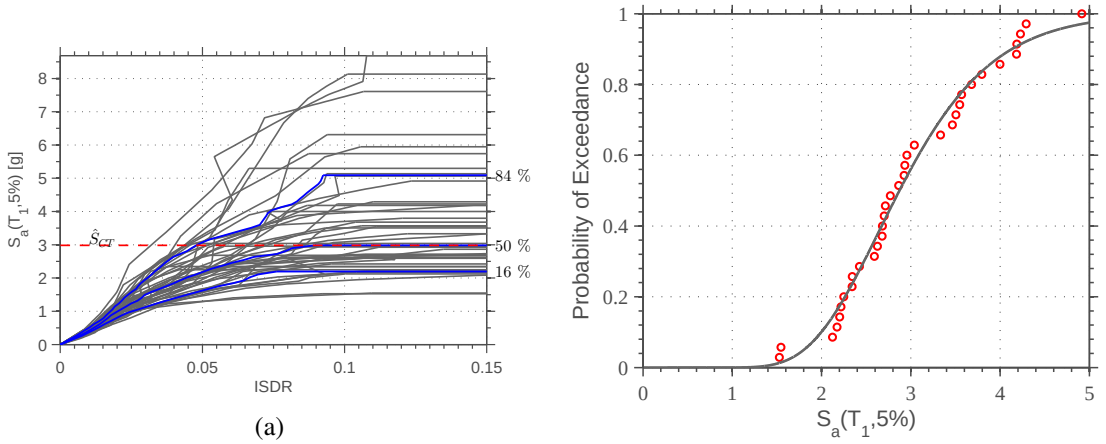

(a) (b)

Figure F.11: IDA curves and collapse fragility curves (FEMA 695).

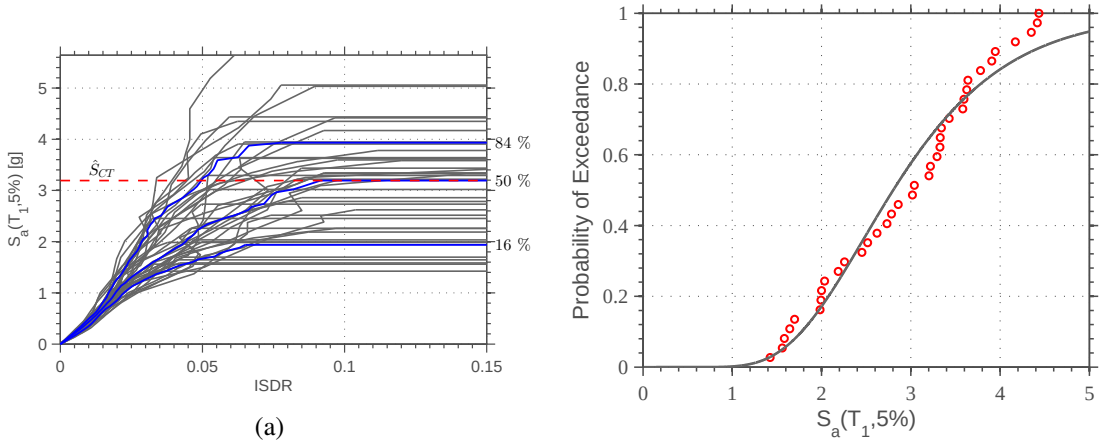

(a) (b)

Figure F.12: IDA curves and collapse fragility curves.

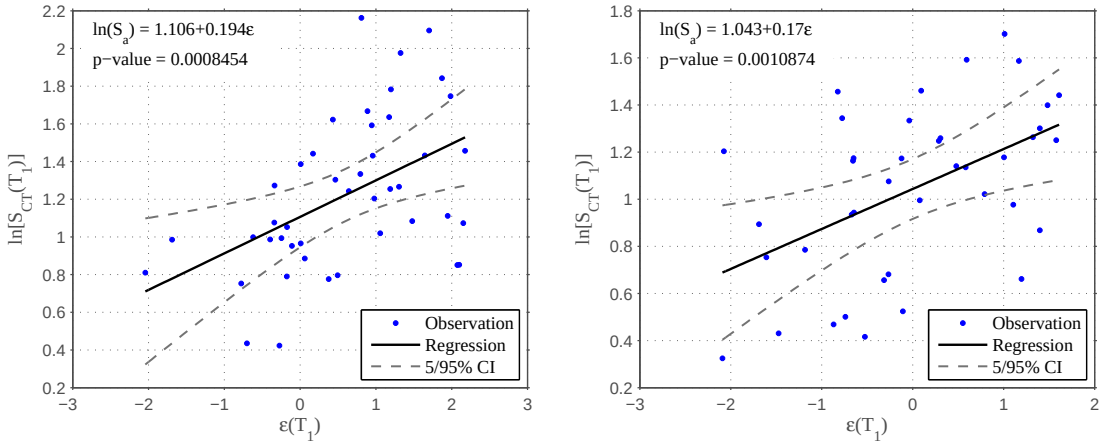

(a) (b)

Figure F.13: Relationship between collapse capacity and ε: (a) FEMA GM set and (b) Hazard set

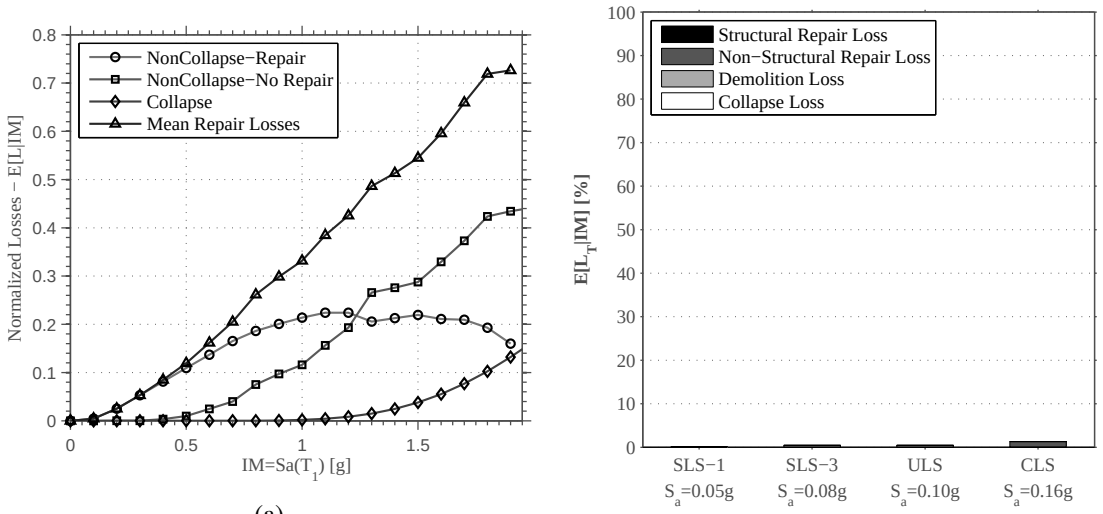

(a) (b)

Figure F.14: Vulnerability curves and corresponding normalized expected losses at several intensity levels.

Building Type: Steel Moment Resisting Frame, designed according EC8

Building Design ID: *St7*

Location: *Porto - Soil Type B*

Number of Stories: *4*

Fundamental Period (sec): *0.83*

Behaviour Factor: *6.50*

Elastic Base Shear (kN): *151.05*

Design Base Shear (kN): *28.30*

Mass (ton): *176.89*

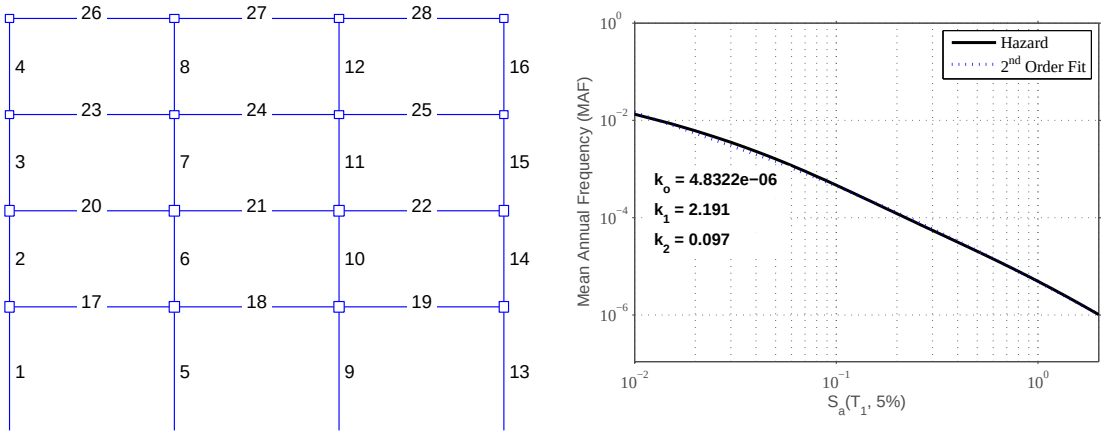

(a) (b)

Figure F.15: (a) Structure Configuration and (b) Hazard Curve

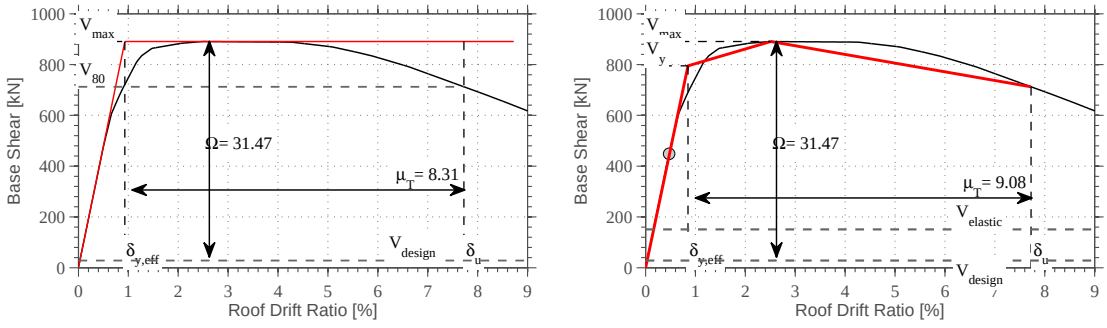

(a) (b)

Figure F.16: Nonlinear static pushover results.

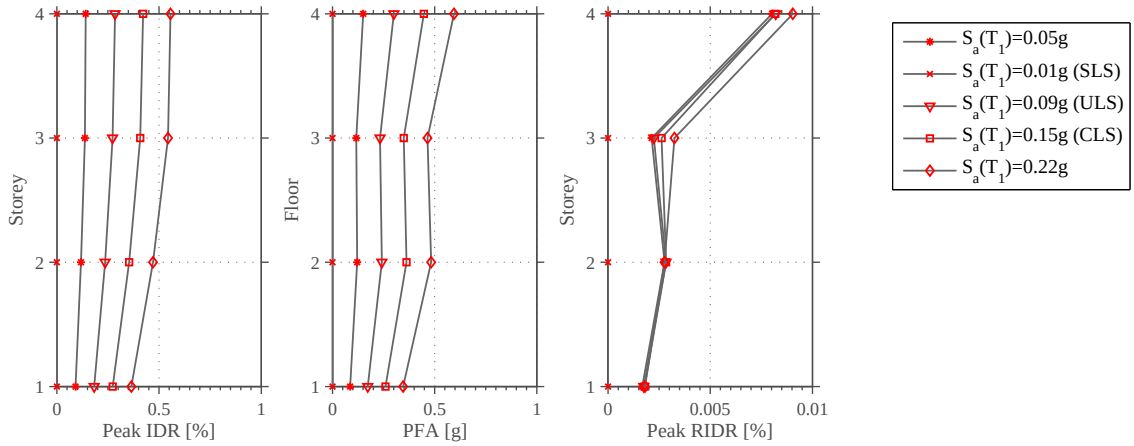

Figure F.17: Maximum ISDR, PFA and RISDR along building height.

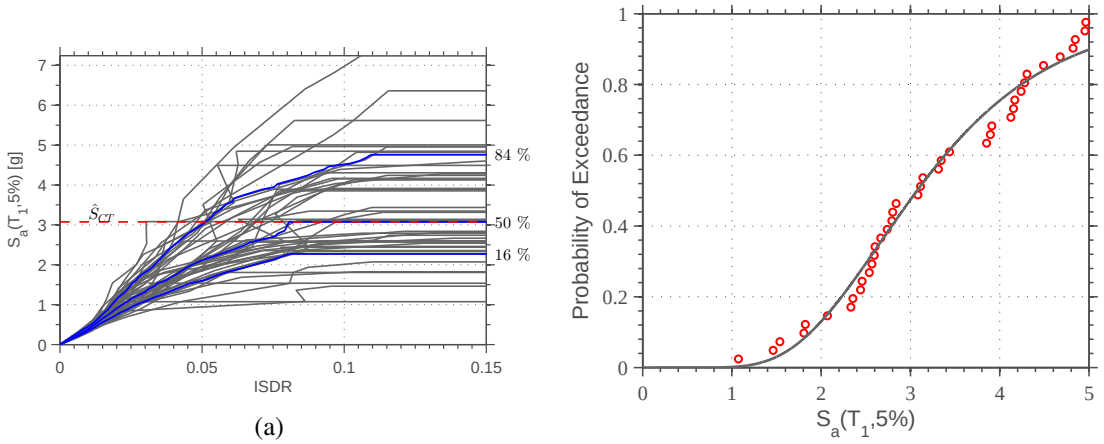

(a) (b)

Figure F.18: IDA curves and collapse fragility curves (FEMA 695).

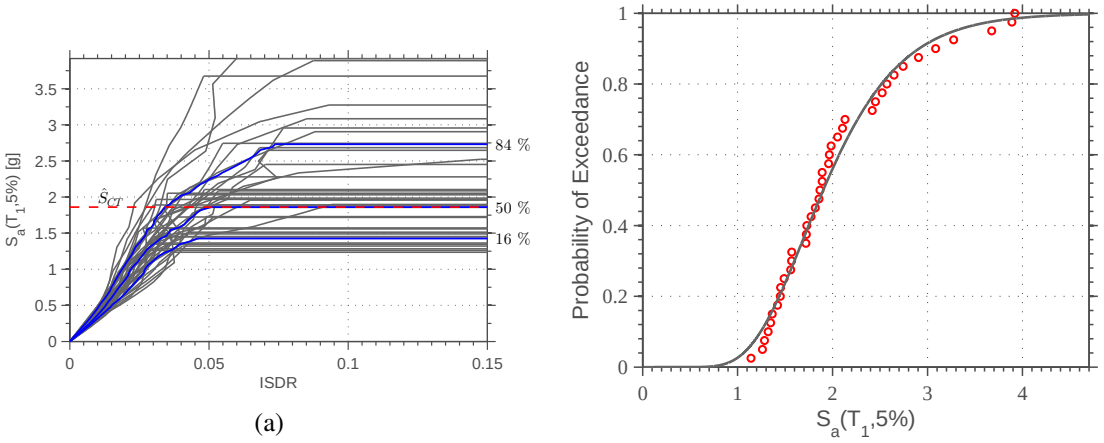

(a) (b)

Figure F.19: IDA curves and collapse fragility curves.

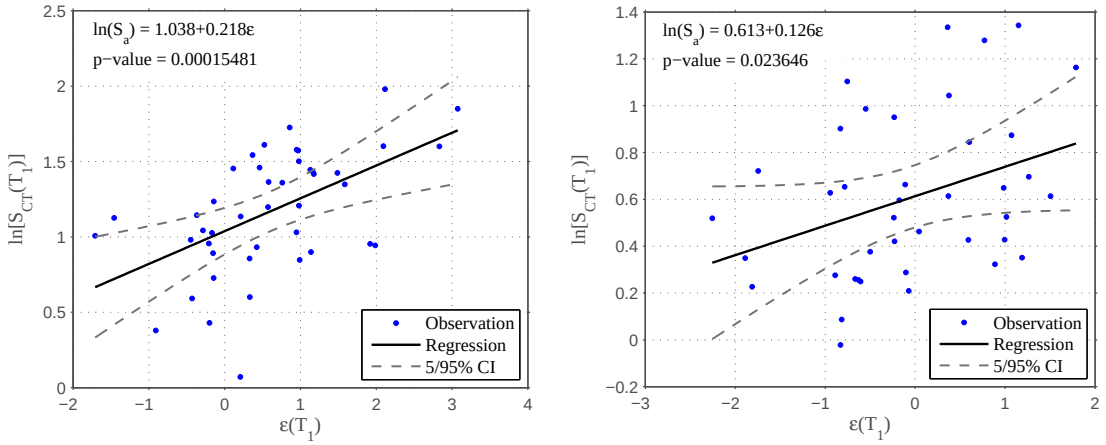

Figure F.20: Relationship between collapse capacity and ε: (a) FEMA GM set and (b) Hazard set

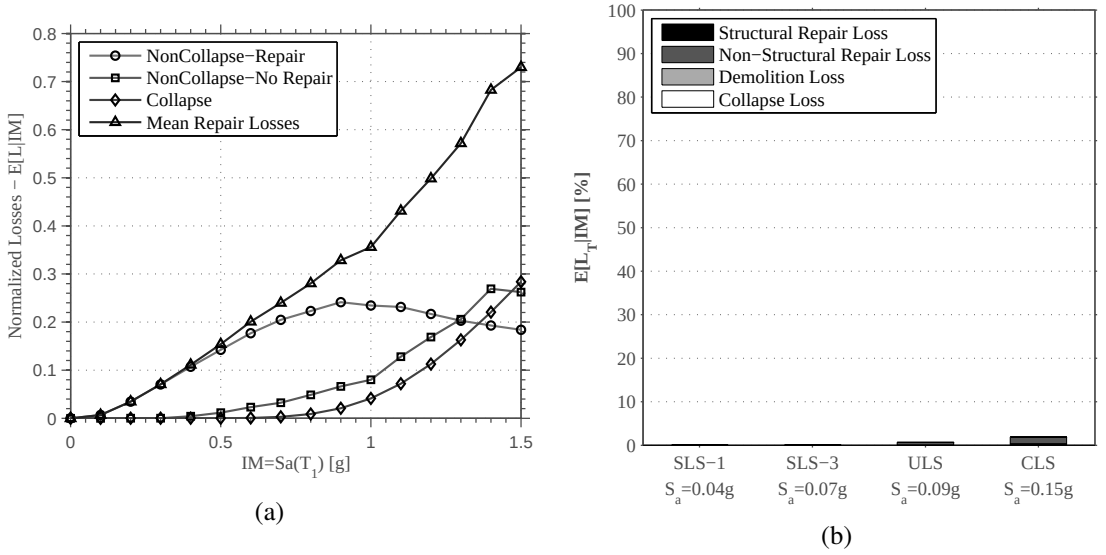

Figure F.21: Vulnerability curves and corresponding normalized expected losses at several intensity levels.

Building Type: Steel Moment Resisting Frame, designed according EC8

Building Design ID: *St10*

Location: *Porto - Soil Type B*

Number of Stories: *5*

Fundamental Period (sec): *0.93*

Behaviour Factor: *6.50*

Elastic Base Shear (kN): *170.33*

Design Base Shear (kN): *35.76*

Mass (ton): *223.50*

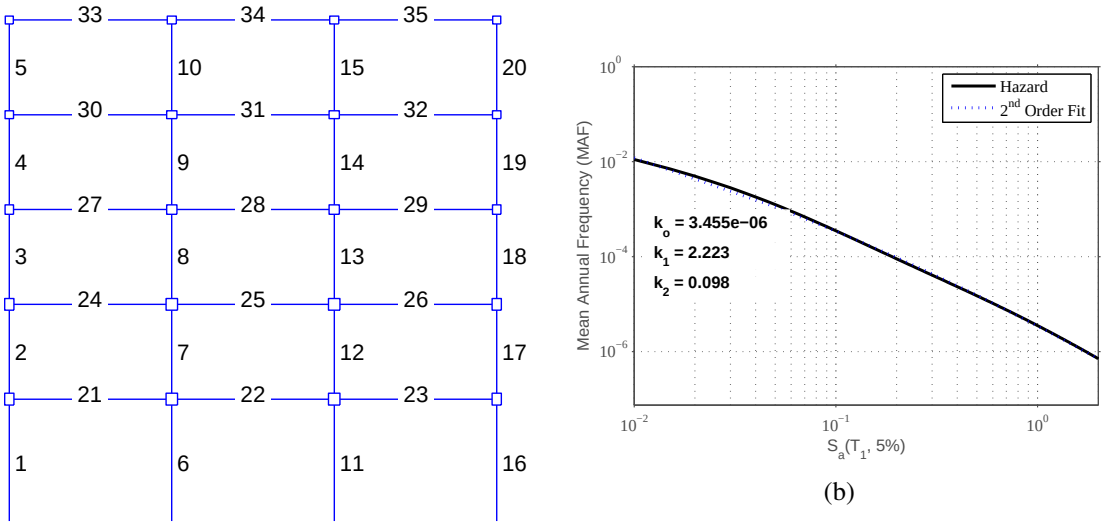

(a) (b)

Figure F.22: (a) Structure Configuration and (b) Hazard Curve

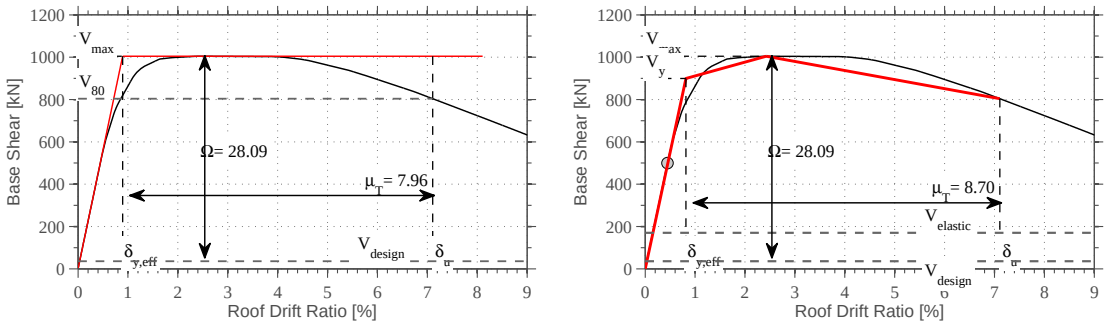

(a) (b)

Figure F.23: Nonlinear static pushover results.

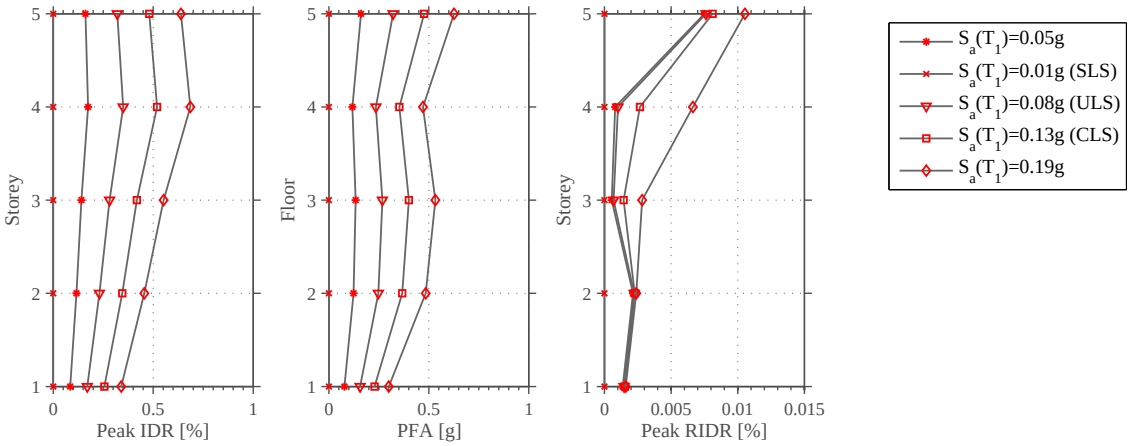

Figure F.24: Maximum ISDR, PFA and RISDR along building height.

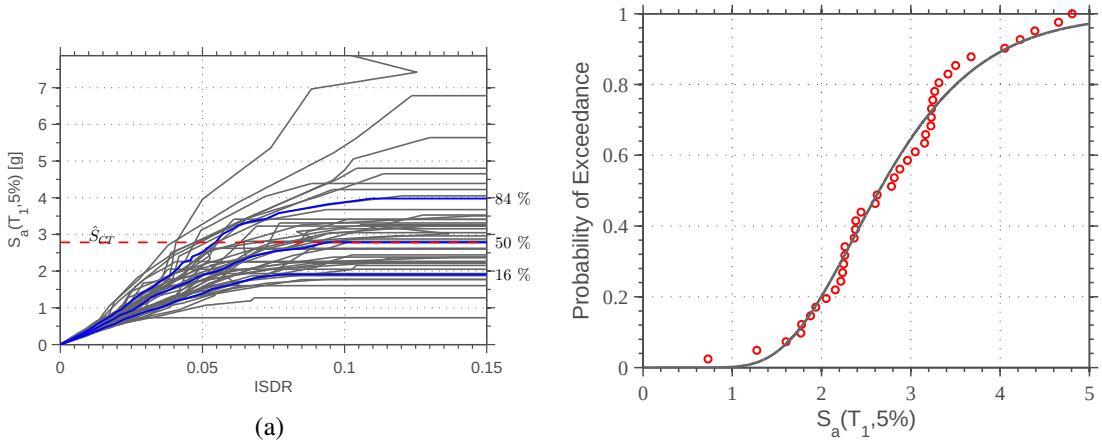

(a) (b)

Figure F.25: IDA curves and collapse fragility curves (FEMA 695).

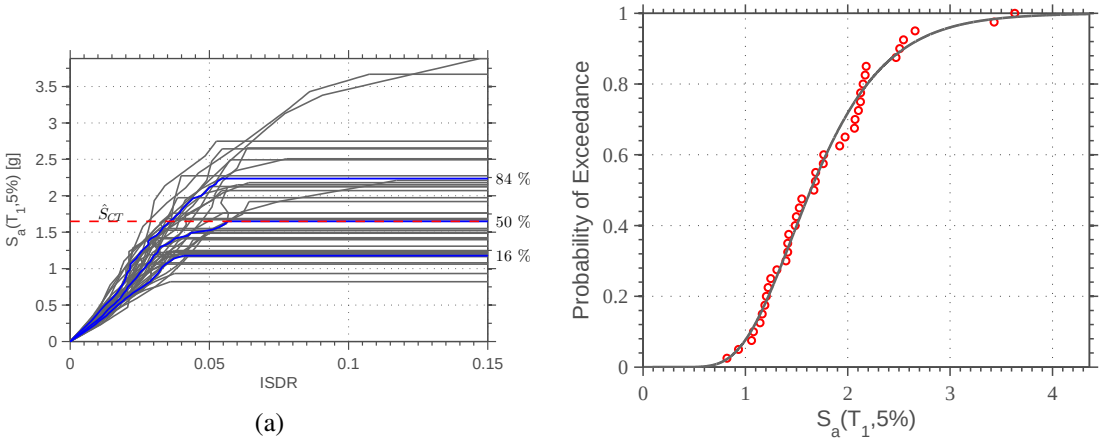

(a) (b)

Figure F.26: IDA curves and collapse fragility curves.

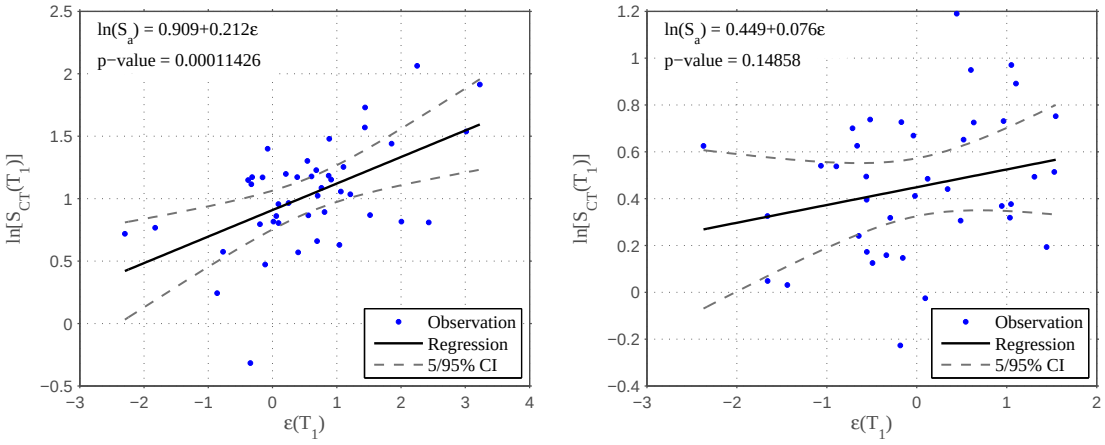

Figure F.27: Relationship between collapse capacity and ε: (a) FEMA GM set and (b) Hazard set

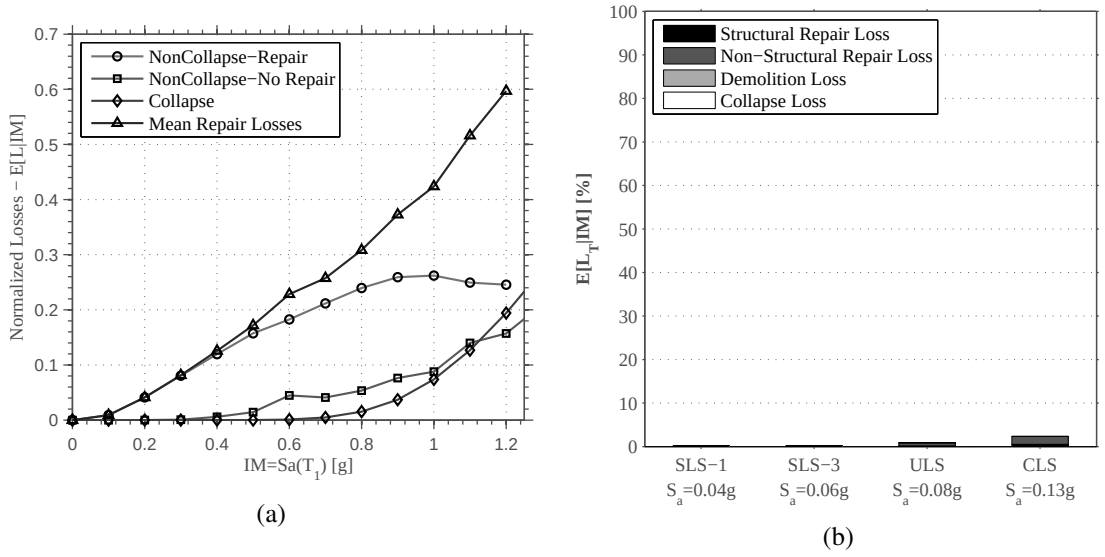

Figure F.28: Vulnerability curves and corresponding normalized expected losses at several intensity levels.

Building Type: Steel Moment Resisting Frame, designed according EC8

Building Design ID: *St13*

Location: *Porto - Soil Type B*

Number of Stories: *8*

Fundamental Period (sec): *1.11*

Behaviour Factor: *6.50*

Elastic Base Shear (kN): *231.99*

Design Base Shear (kN): *58.13*

Mass (ton): *363.33*

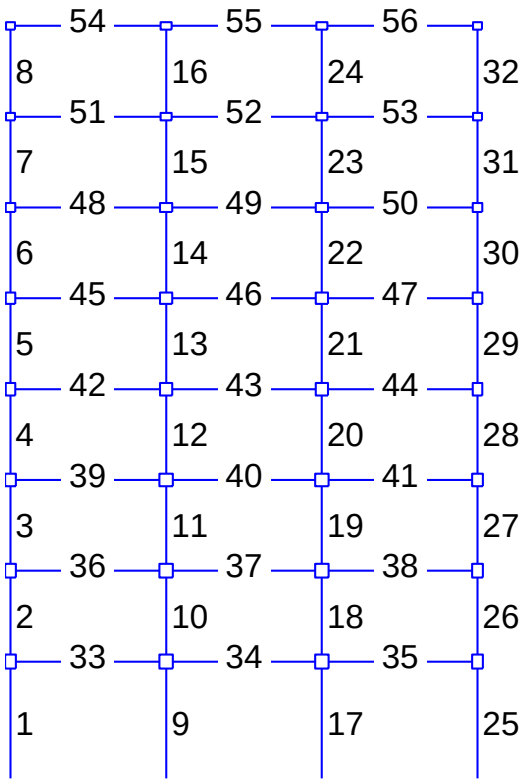

(a)

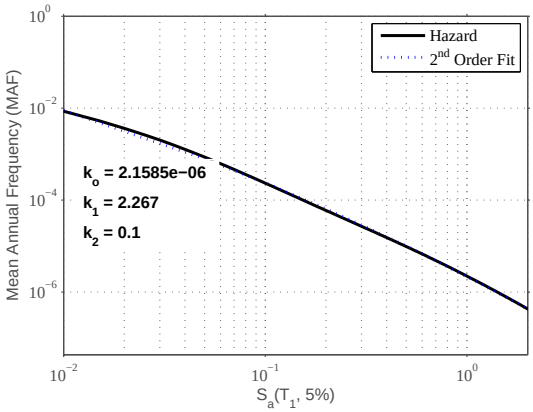

(b)

Figure F.29: (a) Structure Configuration and (b) Hazard Curve

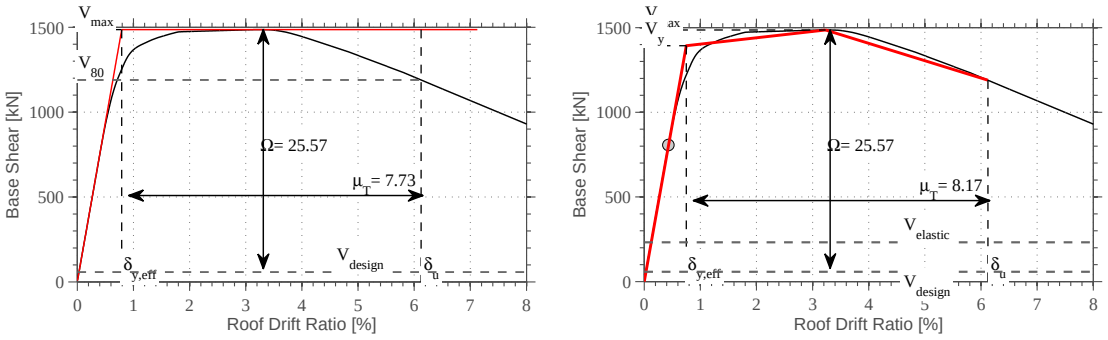

Figure F.30: Nonlinear static pushover results.

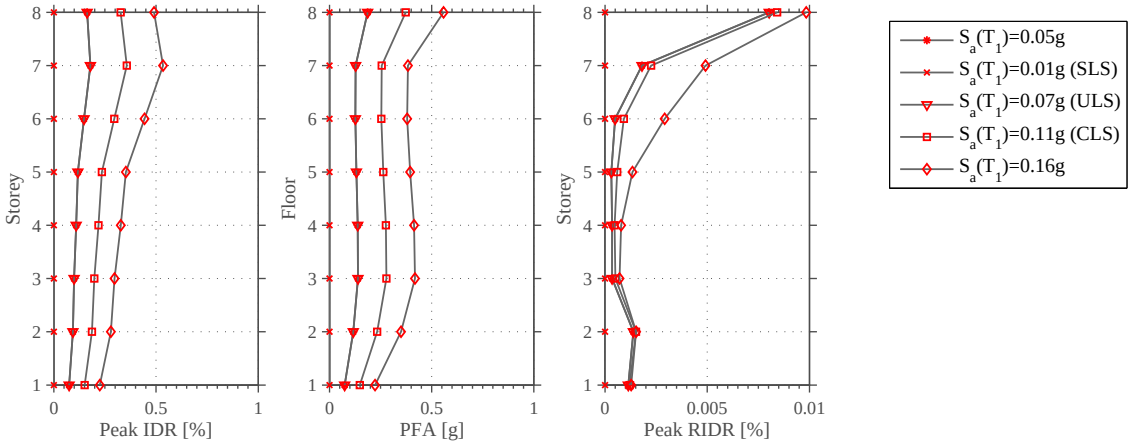

Figure F.31: Maximum ISDR, PFA and RISDR along building height.

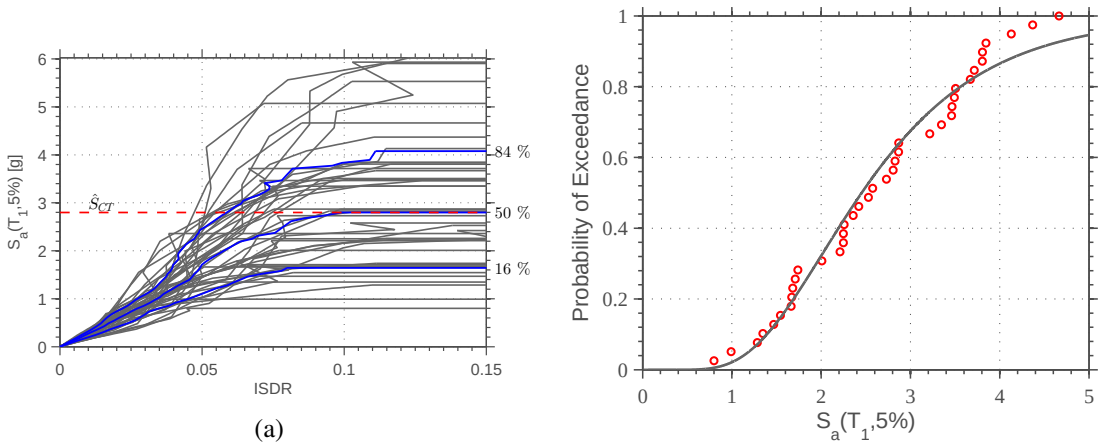

Figure F.32: IDA curves and collapse fragility curves (FEMA 695).

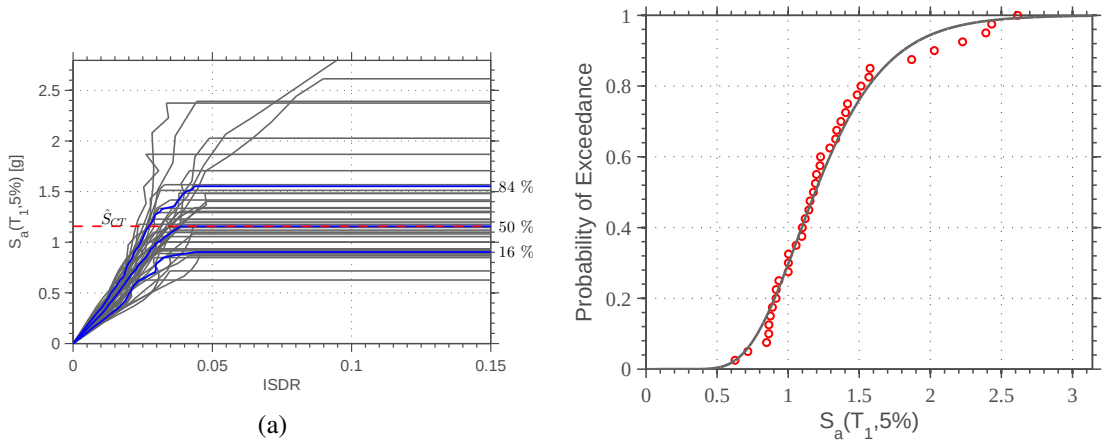

(a) (b)

Figure F.33: IDA curves and collapse fragility curves.

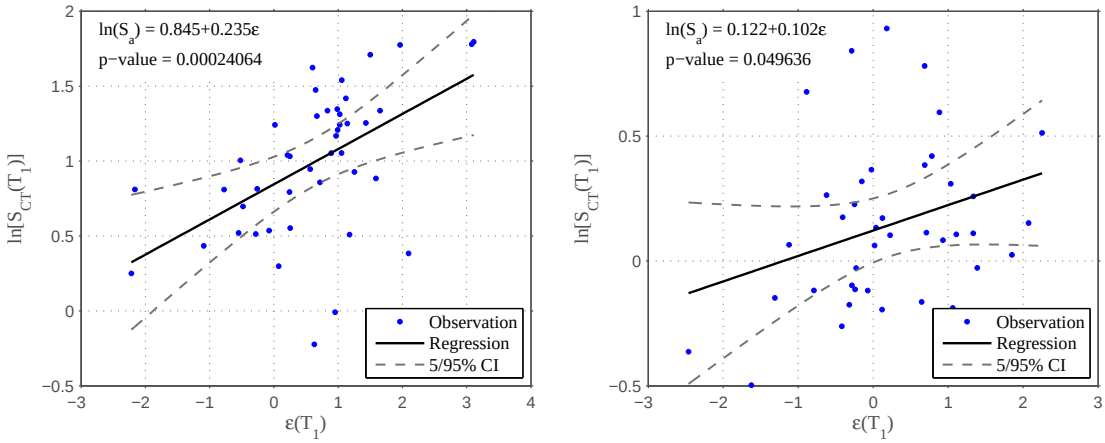

(a) (b)

Figure F.34: Relationship between collapse capacity and ε: (a) FEMA GM set and (b) Hazard set

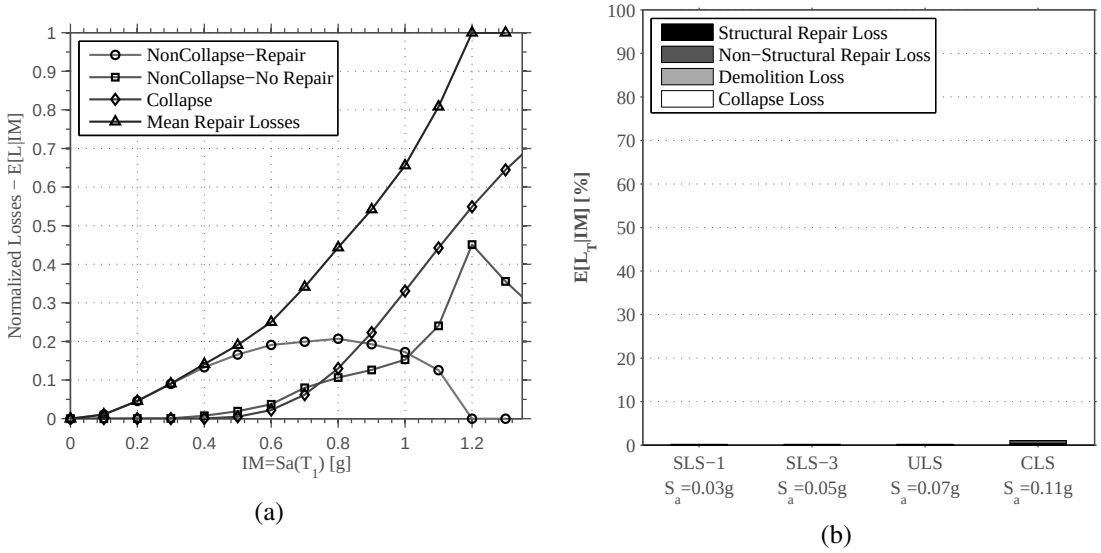

(a) (b)

Figure F.35: Vulnerability curves and corresponding normalized expected losses at several intensity levels.

References

Akkar, S. and Bommer, J. J. (2010). Empirical equations for the prediction of PGA, PGV, and spectral accelerations in europe, the mediterranean region, and the middle east, *Seismological Research Letters* **81**(2): 195–206.

Akkar, S., Sandıkkaya, M., Şenyurt, M., Sisi, A. A., Ay, B., Traversa, P., Douglas, J., Cotton, F., Luzi, L., Hernandez, B. et al. (2014). Reference database for seismic ground-motion in europe (RESORCE), *Bulletin of earthquake engineering* **12**(1): 311–339.

Alberdi, R. and Khandelwal, K. (2015). Comparison of robustness of metaheuristic algorithms for steel frame optimization, *Engineering Structures* **102**: 40–60.

Altoontash, A. (2004). *Simulation and damage models for performance assessment of reinforced concrete beam-column joints*, PhD thesis, Stanford University.

Ambraseys, N., Smit, P., Douglas, J., Margaris, B., Sigbjörnsson, R., Olafsson, S., Suhadolc, P. and Costa, G. (2004). Internet site for european strong-motion data, *Bollettino di Geofisica Teorica ed Applicata* **45**(3): 113–129.

Amiri, G. G., Abdolahi Rad, A., Aghajari, S. and Khanmohamadi Hazaveh, N. (2012). Generation of near-field artificial ground motions compatible with median-predicted spectra using pso-based neural network and wavelet analysis, *Computer-Aided Civil and Infrastructure Engineering* **27**(9): 711–730.

Ancheta, T. D., Darragh, R. B., Stewart, J. P., Seyhan, E., Silva, W. J., Chiou, B. S.-J., Wooddell, K. E., Graves, R. W., Kottke, A. R., Boore, D. M. et al. (2014). NGA-West2 database, *Earthquake Spectra* **30**(3): 989–1005.

Ancheta, T., Darragh, R., Stewart, J., Seyhan, E., Silva, W., Chiou, B., Wooddell, K., Graves, R., Kottke, A., Boore, D. et al. (2013). PEER NGA-West2 database, PEER Report 2013/03, *Berkeley, CA: Pacific Earthquake Engineering Research Center* .

ANSI, A. (2005). *ANSI/AISC 341-05. Seismic provisions for structural steel buildings*, American Institute of Steel Construction, Inc.: Chicago, IL.

ANSI, A. (2010). *ANSI/AISC 360-10. Specification for structural steel buildings*, American Institute of Steel Construction, Inc.: Chicago, IL.

ANSI, A. (2016). *ANSI/AISC 341-16. Seismic provisions for structural steel buildings*, American Institute of Steel Construction, Inc.: Chicago, IL.

ANSYS (2013). *Ansys structural analysis guide*, ANSYS, Inc., Canonsburg.

Araújo, M. and Castro, J. M. (2013). Numerical assessment of the deformation capacity of steel members subjected to monotonic and cyclic loading, *Proceedings of the HSS-SERF international workshop—high strength steel in seismic resistant structures*.

Araújo, M. and Castro, J. M. (2016). On the quantification of local deformation demands and adequacy of linear analysis procedures for the seismic assessment of existing steel buildings to EC8-3, *Bulletin of Earthquake Engineering* **14**(6): 1613–1642.

Araújo, M. and Castro, J. M. (2017). A critical review of european and american provisions for the seismic assessment of existing steel moment-resisting frame buildings, *Journal of Earthquake Engineering* pp. 1–29.

Araújo, M., Macedo, L. and Castro, J. M. (2017). Evaluation of the rotation capacity limits of steel members defined in EC8-3, *Journal of Constructional Steel Research* **135**: 11 – 29.

Araújo, M., Macedo, L., Marques, M. and Castro, J. M. (2016). Code-based record selection methods for seismic performance assessment of buildings, *Earthquake Engineering & Structural Dynamics* **45**(1): 129–148.

ASCE/SEI (2005). *ASCE 7-05 - Minimum design loads for buildings and other structures*, American Society of Civil Engineers / Structural Engineering Institute, Reston, VA.

ASCE/SEI (2010). *ASCE 7-10 - Minimum design loads for buildings and other structures*, American Society of Civil Engineers / Structural Engineering Institute, Reston, VA.

ASCE/SEI (2013). *ASCE 41-13 - Seismic evaluation and upgrade of existing buildings*, American Society of Civil Engineers / Structural Engineering Institute, Reston, VA.

Aschheim, M. and Black, E. F. (2000). Yield point spectra for seismic design and rehabilitation, *Earthquake Spectra* **16**(2): 317–336.

Aslani, H. and Miranda, E. (2005). *Probabilistic earthquake loss estimation and loss disaggregation in buildings*, PhD thesis, Stanford University.

ATC (1996). *ATC-40: The seismic evaluation and retrofit of concrete buildings*, Applied Tecnnology Council, Redwood City, CA.

ATC (2010). *PEER/ATC-72-1 Modeling and Acceptance Criteria for Seismic Design and Analysis of Tall Buildings*, Pacific Earthquake Engineering Research Center (PEER), Redwood City, CA.

Atkinson, G. M. and Boore, D. M. (2006). Earthquake ground-motion prediction equations for eastern north america, *Bulletin of the Seismological Society of America* **96**(6): 2181–2205.

Ay, B. Ö. and Akkar, S. (2014). Evaluation of a recently proposed record selection and scaling procedure for low-rise to mid-rise reinforced concrete buildings and its use for probabilistic risk assessment studies, *Earthquake Engineering & Structural Dynamics* **43**(6): 889–908.

Aydoğdu, İ., Akın, A. and Saka, M. P. (2016). Design optimization of real world steel space frames using artificial bee colony algorithm with levy flight distribution, *Advances in Engineering Software* **92**: 1–14.

Azad, S. K. and Hasançebi, O. (2013). Upper bound strategy for metaheuristic based design optimization of steel frames, *Advances in Engineering Software* **57**: 19–32.

Baker, J. W. (2010). Conditional mean spectrum: Tool for ground-motion selection, *Journal of Structural Engineering* **137**(3): 322–331.

Baker, J. W. (2015). Efficient analytical fragility function fitting using dynamic structural analysis, *Earthquake Spectra* **31**(1): 579–599.

Baker, J. W. and Cornell, C. A. (2005). A vector-valued ground motion intensity measure consisting of spectral acceleration and epsilon, *Earthquake Engineering & Structural Dynamics* **34**(10): 1193–1217.

Baker, J. W. and Cornell, C. A. (2006a). Spectral shape, epsilon and record selection, *Earthquake Engineering & Structural Dynamics* **35**(9): 1077–1095.

Baker, J. W. and Cornell, C. A. (2006b). Which spectral acceleration are you using?, *Earthquake Spectra* **22**(2): 293–312.

Barbosa, A. R., Ribeiro, F. L. and Neves, L. A. (2017). Influence of earthquake ground-motion duration on damage estimation: application to steel moment resisting frames, *Earthquake Engineering & Structural Dynamics* **46**(1): 27–49.

Bazzurro, P. and Cornell, C. A. (1999). Disaggregation of seismic hazard, *Bulletin of the Seismological Society of America* **89**(2): 501–520.

Beck, J. L., Porter, K. A. and Shaikhutdinov, R. V. (2004). *Simplified estimation of seismic lifecycle costs*, ASCE Library, pp. 229–237.

Bertero, V., Krawinkler, H. and Popov, E. (1973). Further studies on seismic behaviour of steel beam-column subassemblages, report no. eerc 73-27, *Earthquake Engineering Reseaarch Centre, College of Engineering, University of California, Berkeley, California* .

Bertero, V. V., Popov, E. P. and Krawinkler, H. (1972). Beam-column subassemblages under repeated loading, *Journal of the Structural Division* **98**(5): 1137–1159.

Beyer, K. and Bommer, J. J. (2007). Selection and scaling of real accelerograms for bi-directional loading: a review of current practice and code provisions, *Journal of Earthquake Engineering* **11**(S1): 13–45.

Bojórquez, E. and Ruiz-García, J. (2013). Residual drift demands in moment-resisting steel frames subjected to narrow-band earthquake ground motions, *Earthquake Engineering & Structural Dynamics* **42**(11): 1583–1598.

Bommer, J. J. and Acevedo, A. B. (2004). The use of real earthquake accelerograms as input to dynamic analysis, *Journal of Earthquake Engineering* **8**(spec01): 43–91.

Bommer, J. J., Stafford, P. J. and Akkar, S. (2010). Current empirical ground-motion prediction equations for europe and their application to eurocode 8, *Bulletin of Earthquake Engineering* **8**(1): 5–26.

Boroschek, R., Bonelli, P., Restrepo, J., Retamales, R. and Contreras, C. (2014). Lessons from the 2010 chile earthquake for performance based design and code development, *Geotechnical, Geological and Earthquake Engineering* **32**: 143–157.

Bradley, B. A. (2010). A generalized conditional intensity measure approach and holistic ground-motion selection, *Earthquake Engineering & Structural Dynamics* **39**(12): 1321–1342.

Brandonisio, G., De Luca, A. and Mele, E. (2011). Shear instability of panel zone in beam-to-column connections, *Journal of Constructional Steel Research* **67**(5): 891–903.

Brandonisio, G., De Luca, A. and Mele, E. (2012). Shear strength of panel zone in beam-to-column connections, *Journal of Constructional Steel Research* **71**: 129–142.

Buratti, N., Stafford, P. J. and Bommer, J. J. (2010). Earthquake accelerogram selection and scaling procedures for estimating the distribution of drift response, *Journal of Structural Engineering* **137**(3): 345–357.

Cannavó, F. (2012). Sensitivity analysis for volcanic source modeling quality assessment and model selection, *Computers & Geosciences* **44**: 52–59.

Casarotti, C. and Pinho, R. (2007). An adaptive capacity spectrum method for assessment of bridges subjected to earthquake action, *Bulletin of Earthquake Engineering* **5**(3): 377–390.

Castro, J. M. (2006). *Seismic behaviour of composite moment-resisting frames*, PhD thesis, Imperial College London (University of London).

Castro, J. M., Davila-Arbona, F. and Elghazouli, A. Y. (2008). Seismic design approaches for panel zones in steel moment frames, *Journal of Earthquake Engineering* **12**(S1): 34–51.

Castro, J. M., Elghazouli, A. Y. and Izzuddin, B. (2005). Modelling of the panel zone in steel and composite moment frames, *Engineering structures* **27**(1): 129–144.

CEN (1993). *EN 10034, Structural steel I and H sections - Tolerances on shape and dimensions*, European Committee for Standardization, Brussels.

CEN (2005a). *EN 1993-1-1, Eurocode 3: Design of steel structures - Part 1.1: General rules and rules for buildings*, European Committee for Standardization, Brussels.

CEN (2005b). *EN 1993-1-8, Eurocode 3: Design of steel structures - Part 1.8: Design of joints*, European Committee for Standardization, Brussels.

CEN (2005c). *EN 1998-1, Eurocode 8: Design of structures for earthquake resistance, Part 1: General rules, seismic actions and rules for buildings*, European Committee for Standardization, Brussels.

CEN (2005d). *EN 1998-2, Eurocode 8: Design of structures for earthquake resistance, Part 2: Bridges*, European Committee for Standardization, Brussels.

CEN (2005e). *EN 1998-3, Eurocode 8: Design of structures for earthquake resistance, Part 2: Assessment and retrofitting of buildings*, European Committee for Standardization, Brussels.

CEN (2010). *NP ENV 1998-1, Portuguese national annex to Eurocode 8: Design of structures for earthquake resistance, Part 1: General rules, seismic actions and rules for buildings*, Instituto Português da Qualidade, Lisboa.

Chaboche, J. (2008). A review of some plasticity and viscoplasticity constitutive theories, *International Journal of Plasticity* **24**(10): 1642–1693.

Charney, F. A. and Downs, W. M. (2004). Modeling procedures for panel zone deformations in moment resisting frames, *Proceedings*.

Chiou, B., Darragh, R., Gregor, N. and Silva, W. (2008). Nga project strong-motion database, *Earthquake Spectra* **24**(1): 23–44.

Committee, S. et al. (1959). Recommended lateral force requirements and commentary, *Structural Engineers Association of California* .

Cornell, C. A. (1968). Engineering seismic risk analysis, *Bulletin of the Seismological Society of America* **58**(5): 1583–1606.

Cornell, C. A. (2004). Hazard, ground motions and probabilistic assessment for pbsd, *Performance based seismic design concepts and implementation. PEER report* **5**: 39–52.

Cornell, C. A. and Krawinkler, H. (2000). Progress and challenges in seismic performance assessment, *PEER Center News* **3**(2): 1–3.

D'Aniello, M., Landolfo, R., Piluso, V. and Rizzano, G. (2012). Ultimate behavior of steel beams under non-uniform bending, *Journal of Constructional Steel Research* **78**: 144–158.

Davila-Arbona, F. J. (2007). *Panel zone behaviour in steel moment resisting frames*, Master's thesis, Università deglo Studi di Pavia.

dei Lavori Pubblici (CS. LL. PP.), C. S. (2008). *DM 14 Gennaio 2008. Norme tecniche per le costruzioni*, Vol. 29, Gazzetta Ufficiale della Repubblica Italiana, Brussels.

Denavit, M. D., Hajjar, J. F., Perea, T. and Leon, R. T. (2016). Seismic performance factors for moment frames with steel-concrete composite columns and steel beams, *Earthquake Engineering & Structural Dynamics* **45**(10): 1685–1703.

Dias, J., Castro, J. M., Romão, X., Gonçalves, M. and Lopes, J. C. (2010). Seleq: a web-based application for the selection of earthquake ground motions for structural analysis, *14th European Conference on Earthquake Engineering*.

Doğan, E. and Saka, M. P. (2012). Optimum design of unbraced steel frames to lrfd–aisc using particle swarm optimization, *Advances in Engineering Software* **46**(1): 27–34.

Dong, Y., Tang, J., Xu, B. and Wang, D. (2005). An application of swarm optimization to nonlinear programming, *Computers & Mathematics with Applications* **49**(11-12): 1655–1668.

Eads, L., Miranda, E., Krawinkler, H. and Lignos, D. G. (2013). An efficient method for estimating the collapse risk of structures in seismic regions, *Earthquake Engineering & Structural Dynamics* **42**(1): 25–41.

El-Tawil, S. (2000). Panel zone yielding in steel moment connections, *Engineering Journal-American Institute of Steel Construction* **37**(3): 120–131.

El-Tawil, S., Vidarsson, E., Mikesell, T. and Kunnath, S. K. (1999). Inelastic behavior and design of steel panel zones, *Journal of Structural Engineering* **125**(2): 183–193.

Elghazouli, A. Y. (2005). Assessment of capacity design approaches for steel framed structures, *Journal of steel structures* **5**(5): 465–475.

Elghazouli, A. Y. (2009). *Seismic Design of Buildings to Eurocode 8*, CRC Press.

Elghazouli, A. Y. (2010). Assessment of european seismic design procedures for steel framed structures, *Bulletin of earthquake engineering* **8**(1): 65–89.

Elghazouli, A. Y. and Castro, J. M. (2009). Design of steel structures, *Seismic Design of Buildings to Eurocode 8*, CRC Press, pp. 158–189.

Elkady, A. and Lignos, D. G. (2015). Analytical investigation of the cyclic behavior and plastic hinge formation in deep wide-flange steel beam-columns, *Bulletin of Earthquake Engineering* **13**(4): 1097–1118.

Elwood, K. J., Pampanin, S., Kam, W. Y. and Priestley, M. N. (2014). Performance-based issues from the 22 february 2011 christchurch earthquake christchurch earthquake christchurch earthquake christchurch earthquake christchurch earthquake, *Performance-Based Seismic Engineering: Vision for an Earthquake Resilient Society*, Springer, pp. 159–175.

Fardis, M. N. (2009). *Seismic design, assessment and retrofitting of concrete buildings: based on EN-Eurocode 8*, Vol. 8, Springer Science & Business Media.

FEMA (1999). *HAZUS - Earthquake loss estimation methodology*, Federal Emergency Management Agency, Washington, DC.

FEMA (2000). *FEMA 350 - Recommended seismic design criteria for new steel moment-frame buildings*, Federal Emergency Management Agency, Washington, DC.

FEMA (2006). *FEMA 445 - Next-generation of performance-based seismic design guidelines. Program plan for new and existing buildings*, Federal Emergency Management Agency, Washington, DC.

FEMA (2009). *FEMA 695 - Quantification of building seismic performance factors*, Federal Emergency Management Agency, Washington, DC.

FEMA (2012a). *FEMA P58-1 - Seismic performance assessment of buildings Volume 1 – Methodology*, Federal Emergency Management Agency, Washington, DC.

FEMA (2012b). *FEMA P58-2 - Seismic performance assessment of buildings Volume 2 - Implementation Guide*, Federal Emergency Management Agency, Washington, DC.

Ferraioli, M., Lavino, A. and Mandara, A. (2014). Behaviour factor of code-designed steel moment-resisting frames, *International journal of steel structures* **14**(2): 243–254.

Fielding, D. and Huang, J. (1971). Shear in steel beam-to-column connections, *Welding Journal* **50**(7): 313–326.

Fragiadakis, M. and Papadrakakis, M. (2008). Modeling, analysis and reliability of seismically excited structures: computational issues, *International journal of computational methods* **5**(04): 483–511.

Geem, Z. W. (2000). *Optimal design of water distribution networks using harmony search*, PhD thesis, Korea University.

Geem, Z. W., Kim, J. H. and Loganathan, G. V. (2001). A new heuristic optimization algorithm: harmony search, *Simulation* **76**(2): 60–68.

Ghafory-Ashtiany, M., Azarbakht, A. and Mousavi, M. (2012). State of the art: Structure-specific strong ground motion selection by emphasizing on spectral shape indicators, *15th World Conference on Earthquake Engineering, Lisbon, Portugal*, pp. 24–28.

Goulet, C. A., Haselton, C. B., Mitrani-Reiser, J., Beck, J. L., Deierlein, G. G., Porter, K. A. and Stewart, J. P. (2007). Evaluation of the seismic performance of a code-conforming reinforced-concrete frame building—from seismic hazard to collapse safety and economic losses, *Earthquake Engineering & Structural Dynamics* **36**(13): 1973–1997.

Guin, J. and Saxena, V. (2000). Extreme losses from natural disasters-earthquakes, tropical cyclones and extratropical cyclones, *Boston, MA: Applied Insurance Research Inc* .

Gupta, A. and Krawinkler, H. (2000). Estimation of seismic drift demands for frame structures, *Earthquake Engineering & Structural Dynamics* **29**(9): 1287–1305.

Hare, W., Nutini, J. and Tesfamariam, S. (2013). A survey of non-gradient optimization methods in structural engineering, *Advances in Engineering Software* **59**: 19–28.

Hasançebi, O. and Carbas, S. (2014). Bat inspired algorithm for discrete size optimization of steel frames, *Advances in Engineering Software* **67**: 173–185.

Hasançebi, O., Erdal, F. and Saka, M. P. (2009). Adaptive harmony search method for structural optimization, *Journal of Structural Engineering* **136**(4): 419–431.

Haselton, C. B., Baker, J. W., Liel, A. B. and Deierlein, G. G. (2009). Accounting for ground-motion spectral shape characteristics in structural collapse assessment through an adjustment for epsilon, *Journal of Structural Engineering* **137**(3): 332–344.

Haselton, C. B., Liel, A. B., Deierlein, G. G., Dean, B. S. and Chou, J. H. (2010). Seismic collapse safety of reinforced concrete buildings. i: Assessment of ductile moment frames, *Journal of Structural Engineering* **137**(4): 481–491.

Haselton, C. B., Whittaker, A. S., Hortacsu, A., Baker, J. W., Bray, J. D. and Grant, D. N. (2012). Selecting and scaling earthquake ground motions for performing response-history analyses, *Proceedings of the 15th World Conference on Earthquake Engineering*.

Hejazi, F., Toloue, I., Jaafar, M. S. and Noorzaei, J. (2013). Optimization of earthquake energy dissipation system by genetic algorithm, *Computer-Aided Civil and Infrastructure Engineering* **28**(10): 796–810.

Homma, T. and Saltelli, A. (1996). Importance measures in global sensitivity analysis of nonlinear models, *Reliability Engineering & System Safety* **52**(1): 1–17.

Hwang, S.-H., Elkady, A., Bardaweel, S. A. and Lignos, D. G. (2015). Earthquake loss assessment of steel frame buildings designed in highly seismic regions, *Proceedings of 5th ECCOMAS Thematic Conference on Computational Methods in Structural Dynamics and Earthquake Engineering (COMPDYN 2015)*, pp. 25–27.

Hwang, S. and Lignos, D. G. (2017). Earthquake-induced loss assessment of steel frame buildings with special moment frames designed in highly seismic regions, *Earthquake Engineering & Structural Dynamics* **46**(13): 2141–2162.

Ibarra, L. F., Medina, R. A. and Krawinkler, H. (2005). Hysteretic models that incorporate strength and stiffness deterioration, *Earthquake engineering & structural dynamics* **34**(12): 1489–1511.

ICBO (1927). *Uniform Building Code*, International conference of building officials, Whittier, CA.

ICBO (1988). *Uniform Building Code*, International conference of building officials, Whittier, CA.

Iervolino, I. and Cornell, C. A. (2005). Record selection for nonlinear seismic analysis of structures, *Earthquake Spectra* **21**(3): 685–713.

Iervolino, I., Galasso, C. and Cosenza, E. (2010). Rexel: computer aided record selection for code-based seismic structural analysis, *Bulletin of Earthquake Engineering* **8**(2): 339–362.

Iervolino, I., Manfredi, G., Polese, M., Prota, A. and Verderame, G. M. (2014). L'aquila earthquake: A wake-up call for european research and codes, *Performance-Based Seismic Engineering: Vision for an Earthquake Resilient Society*, Springer, pp. 129–142.

Inselberg, A. and Dimsdale, B. (1991). *Parallel Coordinates*, Springer US, Boston, MA, pp. 199–233.

Jayaram, N. and Baker, J. W. (2008). Statistical tests of the joint distribution of spectral acceleration values, *Bulletin of the Seismological Society of America* **98**(5): 2231–2243.

Jayaram, N., Lin, T. and Baker, J. W. (2011). A computationally efficient ground-motion selection algorithm for matching a target response spectrum mean and variance, *Earthquake Spectra* **27**(3): 797–815.

Jayaram, N., Shome, N. and Rahnama, M. (2012). Development of earthquake vulnerability functions for tall buildings, *Earthquake Engineering & Structural Dynamics* **41**(11): 1495–1514.

Jiao, Y., Yamada, S., Kishiki, S. and Shimada, Y. (2011). Evaluation of plastic energy dissipation capacity of steel beams suffering ductile fracture under various loading histories, *Earthquake Engineering & Structural Dynamics* **40**(14): 1553–1570.

Jin, J. and El-Tawil, S. (2005). Evaluation of fema-350 seismic provisions for steel panel zones, *Journal of Structural Engineering* **131**(2): 250–258.

Karavasilis, T. L., Dimopoulos, A. I., Tzimas, A. S., Kamaris, G. S. and Vamvatsikos, D. (2015). Estimation of economic losses in seismic-resistant post-tensioned steel frames with viscous dampers, *Proceedings of the 8th International Conference on Advances in Steel Structures, Lisbon, Portugal*.

Katsanos, E. I. and Sextos, A. G. (2013). Issars: An integrated software environment for structure-specific earthquake ground motion selection, *Advances in Engineering Software* **58**: 70–85.

Katsanos, E. I., Sextos, A. G. and Manolis, G. D. (2010). Selection of earthquake ground motion records: a state-of-the-art review from a structural engineering perspective, *Soil Dynamics and Earthquake Engineering* **30**(4): 157–169.

Kayhan, A. H. (2016). Scaled and unscaled ground motion sets for uni-directional and bi-directional dynamic analysis, *Earthquakes and Structures* **10**(3): 563–588.

Kayhan, A. H., Korkmaz, K. A. and Irfanoglu, A. (2011). Selecting and scaling real ground motion records using harmony search algorithm, *Soil Dynamics and Earthquake Engineering* **31**(7): 941–953.

Kim, K. D. and Engelhardt, M. D. (2002). Monotonic and cyclic loading models for panel zones in steel moment frames, *Journal of Constructional Steel Research* **58**(5): 605–635.

Kitayama, S. and Constantinou, M. C. (2016). Probabilistic collapse resistance and residual drift assessment of buildings with fluidic self-centering systems, *Earthquake Engineering & Structural Dynamics* **45**(12): 1935–1953.

Kottke, A. and Rathje, E. M. (2008). A semi-automated procedure for selecting and scaling recorded earthquake motions for dynamic analysis, *Earthquake Spectra* **24**(4): 911–932.

Krawinkler, H. (1971). *Inelastic behavior of steel beam-to-column subassemblages*, Vol. 71-7, University of California, Berkeley.

Krawinkler, H. (1978). Shear in beam-column joints in seismic design of steel frames, *Engineering Journal* **15**(3).

Krawinkler, H. and Al-Ali, A. (1996). Seismic demand evaluation for a 4-story steel frame structure damaged in the northridge earthquake, *The Structural Design of Tall and Special Buildings* **5**(1): 1–27.

Krawinkler, H. and Bertero, V. (1975). Shear behavior of steel frame joints, *Journal of the Structural Division* **101**(11): 2317–2336.

Krawinkler, H. and Mohasseb, S. (1987). Effects of panel zone deformations on seismic response, *Journal of Constructional Steel Research* **8**: 233 – 250.

Krawinkler, H., Zareian, F., Medina, R. A. and Ibarra, L. F. (2006). Decision support for conceptual performance-based design, *Earthquake Engineering & Structural Dynamics* **35**(1): 115–133.

Kuwamura, H. (1998). Fracture of steel during an earthquake—state-of-the-art in japan, *Engineering Structures* **20**(4-6): 310–322.

Lagaros, N. D. and Karlaftis, M. G. (2011). A critical assessment of metaheuristics for scheduling emergency infrastructure inspections, *Swarm and Evolutionary Computation* **1**(3): 147–163.

Lee, D., Cotton, S. C., Dexter, R. J., Hajjar, J. F., Ye, Y. and Ojard, S. D. (2002). *Column stiffener detailing and panel zone behavior of steel moment frame connections*, Citeseer.

Liel, A. B., Haselton, C. B., Deierlein, G. G. and Baker, J. W. (2009). Incorporating modeling uncertainties in the assessment of seismic collapse risk of buildings, *Structural Safety* **31**(2): 197–211.

Lignos, D. G. and Krawinkler, H. (2010). Deterioration modeling of steel components in support of collapse prediction of steel moment frames under earthquake loading, *Journal of Structural Engineering* **137**(11): 1291–1302.

Lignos, D. G. and Krawinkler, H. (2012). Development and utilization of structural component databases for performance-based earthquake engineering, *Journal of Structural Engineering* **139**(8): 1382–1394.

Lin, T., Harmsen, S. C., Baker, J. W. and Luco, N. (2013). Conditional spectrum computation incorporating multiple causal earthquakes and ground-motion prediction models, *Bulletin of the Seismological Society of America* **103**(2A): 1103–1116.

Lin, T., Haselton, C. B. and Baker, J. W. (2013a). Conditional spectrum-based ground motion selection. part i: Hazard consistency for risk-based assessments, *Earthquake engineering & structural dynamics* **42**(12): 1847–1865.

Lin, T., Haselton, C. B. and Baker, J. W. (2013b). Conditional spectrum-based ground motion selection. part ii: Intensity-based assessments and evaluation of alternative target spectra, *Earthquake Engineering & Structural Dynamics* **42**(12): 1867–1884.

Luzi, L., Hailemikael, S., Bindi, D., Pacor, F., Mele, F. and Sabetta, F. (2008). Itaca (italian accelerometric archive): a web portal for the dissemination of italian strong-motion data, *Seismological Research Letters* **79**(5): 716–722.

Macedo, L., Araújo, M. and Castro, J. M. (2013). Assessment and calibration of the harmony search algorithm for earthquake record selection, *Proceedings of the Vienna Congress on Recent Advances in Earthquake Engineering and Structural Dynamics*.

Macedo, L., Araújo, M. and Castro, J. M. (2015). Comparison of modelling strategies for steel structures under cyclic loads, *Proceedings of the 8th International Conference Stessa-2015, Behaviour of Steel Structures in Seismic Areas*, pp. 12–16.

Macedo, L. and Castro, J. M. (2017). SelEQ: An advanced ground motion record selection and scaling framework, *Advances in Engineering Software* **114**: 32–47.

Mahdavi, M., Fesanghary, M. and Damangir, E. (2007). An improved harmony search algorithm for solving optimization problems, *Applied mathematics and computation* **188**(2): 1567–1579.

Mahin, S. A. (1998). Lessons from damage to steel buildings during the northridge earthquake, *Engineering structures* **20**(4-6): 261–270.

McCormick, J., Aburano, H., Ikenaga, M. and Nakashima, M. (2008). Permissible residual deformation levels for building structures considering both safety and human elements, *Proceedings of the 14th world conference on earthquake engineering*, pp. 12–17.

McKenna, F. (2011). Opensees: a framework for earthquake engineering simulation, *Computing in Science & Engineering* **13**(4): 58–66.

Miller, D. K. (1998). Lessons learned from the northridge earthquake, *Engineering structures* **20**(4-6): 249–260.

Miranda, E. (2014). Lessons learned from the 2010 haiti earthquake for performance-based design, *Performance-Based Seismic Engineering: Vision for an Earthquake Resilient Society*, Springer, pp. 117–127.

Mukhopadhyay, A., Roy, A., Das, S., Das, S. and Abraham, A. (2008). Population-variance and explorative power of harmony search: an analysis, *Digital Information Management, 2008. ICDIM 2008. Third International Conference on*, pp. 775–781.

Naeim, F., Alimoradi, A. and Pezeshk, S. (2004). Selection and scaling of ground motion time histories for structural design using genetic algorithms, *Earthquake spectra* **20**(2): 413–426.

Naeim, F. and Lew, M. (1995). On the use of design spectrum compatible time histories, *Earthquake Spectra* **11**(1): 111–127.

Nakashima, M., Inoue, K. and Tada, M. (1998). Classification of damage to steel buildings observed in the 1995 hyogoken-nanbu earthquake, *Engineering Structures* **20**(4-6): 271–281.

Nossent, J., Elsen, P. and Bauwens, W. (2011). Sobol'sensitivity analysis of a complex environmental model, *Environmental Modelling & Software* **26**(12): 1515–1525.

Omran, M. G. and Mahdavi, M. (2008). Global-best harmony search, *Applied mathematics and computation* **198**(2): 643–656.

Owen, A. B. (1994). Controlling correlations in latin hypercube samples, *Journal of the American Statistical Association* **89**(428): 1517–1522.

Pacor, F., Paolucci, R., Luzi, L., Sabetta, F., Spinelli, A., Gorini, A., Nicoletti, M., Marcucci, S., Filippi, L. and Dolce, M. (2011). Overview of the italian strong motion database itaca 1.0, *Bulletin of Earthquake Engineering* **9**(6): 1723–1739.

Padgett, J. E. and DesRoches, R. (2007). Sensitivity of seismic response and fragility to parameter uncertainty, *Journal of Structural Engineering* **133**(12): 1710–1718.

Pagani, M., Monelli, D., Weatherill, G., Danciu, L., Crowley, H., Silva, V., Henshaw, P., Butler, L., Nastasi, M., Panzeri, L. et al. (2014). Openquake engine: An open hazard (and risk) software for the global earthquake model, *Seismological Research Letters* **85**(3): 692–702.

Pan, Q.-K., Suganthan, P. N., Tasgetiren, M. F. and Liang, J. J. (2010). A self-adaptive global best harmony search algorithm for continuous optimization problems, *Applied Mathematics and Computation* **216**(3): 830–848.

Paulay, T. and Priestley, M. N. (1992). *Seismic design of reinforced concrete and masonry buildings*, Wiley New York.

Peres, R. and Castro, J. M. (2010). Comparison of european and american approaches for consideration of p-δ effects in seismic design, *Proceedings of the 14th European Conference on Earthquake Engineering, Ohrid (Rep. of Macedonia)*.

Peres, R., Castro, J. M. and Bento, R. (2016). An extension of an improved forced based design procedure for 3D steel structures, *Steel and Composite Structures* **22**(5): 1115–1140.

Pinto, P. E. and Franchin, P. (2014). Existing buildings: The new italian provisions for probabilistic seismic assessment, *Perspectives on European earthquake engineering and seismology*, Springer, pp. 97–130.

Popov, E. (1987). Panel zone flexibility in seismic moment joints, *Journal of Constructional Steel Research* **8**: 91–118.

Porter, K. A. (2003). An overview of peer's performance-based earthquake engineering methodology, *Proceedings of Ninth International Conference on Applications of Statistics and Probability in Civil Engineering*.

Priestley, M. N., Calvi, G. M. and Kowalsky, M. J. (2007). *Displacement-based Seismic Design of Structures*, IUSS Press.

Ramirez, C. M. and Miranda, E. (2009). *Building-specific loss estimation methods & tools for simplified performance-based earthquake engineering*, PhD thesis, Stanford University.

Ramirez, C. M. and Miranda, E. (2012). Significance of residual drifts in building earthquake loss estimation, *Earthquake Engineering & Structural Dynamics* **41**(11): 1477–1493.

Romão, X. (2012). *Deterministic and probabilistic methods for structural seismic safety assessment*, PhD thesis, Faculdade de Engenharia da Universidade do Porto.

Romão, X., Delgado, R. and Costa, A. (2012a). Statistical characterization of structural demand under earthquake loading. part 1: Robust estimation of the central value of the data, *Journal of Earthquake Engineering* **16**(5): 686–718.

Romão, X., Delgado, R. and Costa, A. (2012b). Statistical characterization of structural demand under earthquake loading. part 2: Robust estimation of the dispersion of the data, *Journal of Earthquake Engineering* **16**(6): 864–896.

Ryu, H.-S., Oh, S.-H. and Lee, M.-S. (2011). Seismic performance evaluation of moment resisting frames using high performance steel, *International Journal of Steel Structures* **11**(2): 235–246.

Saka, M. and Hasancebi, O. (2009). Adaptive harmony search algorithm for design code optimization of steel structures, *Harmony search algorithms for structural design optimization*, Springer, pp. 79–120.

Saka, M. P., Hasançebi, O. and Geem, Z. W. (2016). Metaheuristics in structural optimization and discussions on harmony search algorithm, *Swarm and Evolutionary Computation* **28**: 88–97.

Saltelli, A., Annoni, P., Azzini, I., Campolongo, F., Ratto, M. and Tarantola, S. (2010). Variance based sensitivity analysis of model output. design and estimator for the total sensitivity index, *Computer Physics Communications* **181**(2): 259–270.

Saltelli, A., Tarantola, S., Campolongo, F. and Ratto, M. (2004). *Sensitivity analysis in practice: a guide to assessing scientific models*, John Wiley & Sons.

Sato, A. and Uang, C.-M. (2013). A fema p695 study for the proposed seismic performance factors for cold-formed steel special bolted moment frames, *Earthquake Spectra* **29**(1): 259–282.

Schneider, S. P. and Amidi, A. (1998). Seismic behavior of steel frames with deformable panel zones, *Journal of Structural Engineering* **124**(1): 35–42.

Sextos, A. G. (2014). *Selection of Ground Motions for Response History Analysis*, Springer Berlin Heidelberg, Berlin, Heidelberg, pp. 1–10.

Shibata, A. and Sozen, M. A. (1976). Substitute-structure method for seismic design in r/c, *Journal of the structural division* **102**(ASCE# 11824).

Shome, N., Cornell, C. A., Bazzurro, P. and Carballo, J. E. (1998). Earthquakes, records, and nonlinear responses, *Earthquake Spectra* **14**(3): 469–500.

Silva, V., Crowley, H., Varum, H. and Pinho, R. (2015). Seismic risk assessment for mainland portugal, *Bulletin of Earthquake Engineering* **13**(2): 429–457.

Sobol, I. M. (1993). Sensitivity estimates for nonlinear mathematical models, *Mathematical Modelling and Computational Experiments* **1**(4): 407–414.

Standard, N. Z. (2004). *NZS 1170.5: 2004 Structural Design Actions Part 5: Earthquake actions–New Zealand*, Standards New Zealand, Wellington, NZ.

Stewart, J. P., Chiou, S.-J., Bray, J. D., Graves, R. W., Somerville, P. G. and Abrahamson, N. A. (2002). Ground motion evaluation procedures for performance-based design, *Soil dynamics and earthquake engineering* **22**(9): 765–772.

Sullivan, T. J. (2002). *The current limitations of displacement based design*, Master's thesis, Università deglo Studi di Pavia.

Tremblay, R., Filiatrault, A., Timler, P. and Bruneau, M. (1995). Performance of steel structures during the 1994 northridge earthquake, *Canadian Journal of Civil Engineering* **22**(2): 338–360.

Tukey, J. W. (1949). Comparing individual means in the analysis of variance, *Biometrics* **5**(2): 99–114.

Tzimas, A. S., Kamaris, G., Karavasilis, T. L. and Galasso, C. (2016). Collapse risk and residual drift performance of steel buildings using post-tensioned MRFs and viscous dampers in near-fault regions, *Bulletin of Earthquake Engineering* **14**(6): 1643–1662.

Uang, C.-M. (1991). Establishing *r* (or *rw*) and *cd* factors for building seismic provisions, *Journal of Structural Engineering* **117**(1): 19–28.

Vamvatsikos, D. and Cornell, C. A. (2002). Incremental dynamic analysis, *Earthquake Engineering & Structural Dynamics* **31**(3): 491–514.

Vilanova, S. P. and Fonseca, J. F. (2007). Probabilistic seismic-hazard assessment for portugal, *Bulletin of the Seismological Society of America* **97**(5): 1702–1717.

Villani, A., Castro, J. M. and Elghazouli, A. Y. (2009). Improved seismic design procedure for steel moment frames, *Proceedings of the 6th International Conference Stessa-2009, Behaviour of Steel Structures in Seismic Areas*, pp. 12–16.

Vision, S. (1995). Performance based seismic engineering of buildings, *Structural Engineers Association of California, Sacramento, Calif* .

Wang, Y. C. (1988). *Ultimate strength analysis of three dimensional structures with flexible restraints.*, PhD thesis, University of Sheffield.

Welch, D. P., Sullivan, T. J. and Calvi, G. M. (2014). Developing direct displacement-based procedures for simplified loss assessment in performance-based earthquake engineering, *Journal of Earthquake Engineering* **18**(2): 290–322.

Woessner, J., Laurentiu, D., Giardini, D., Crowley, H., Cotton, F., Grünthal, G., Valensise, G., Arvidsson, R., Basili, R., Demircioglu, M. B. et al. (2015). The 2013 european seismic hazard model: key components and results, *Bulletin of Earthquake Engineering* **13**(12): 3553–3596.

Ye, K., Chen, Z. and Zhu, H. (2012). Proposed strategy for the application of the modified harmony search algorithm to code-based selection and scaling of ground motions, *Journal of Computing in Civil Engineering* **28**(6): 04014019.

Zareian, F. and Krawinkler, H. (2006). *Simplified performance-based earthquake engineering*, PhD thesis, Stanford University.

Zareian, F., Lignos, D. G. and Krawinkler, H. (2010). Evaluation of seismic collapse performance of steel special moment resisting frames using FEMA P695 (ATC-63) methodology, *Structures Congress 2010*, pp. 1275–1286.

Zareian, F. and Medina, R. A. (2010). A practical method for proper modeling of structural damping in inelastic plane structural systems, *Computers & structures* **88**(1): 45–53.